Les effets protecteurs de la spadine et ses analogues dans la récupération motrice et cognitive post-AVC

Mariel Pietri

UNIVERSITÉ CÔTE D'AZUR

ÉCOLE DOCTORALE
SCIENCES DE LA VIE ET DE LA SANTÉ

THÈSE DE DOCTORAT

Les effets protecteurs de la Spadine et ses analogues dans la récupération motrice et cognitive post-AVC

Mariel PIETRI

Institut de Pharmacologie Moléculaire et Cellulaire

Présentée en vue de l'obtention du grade de docteur en Sciences de la Vie d'Université Côte d'Azur
Dirigée par : Catherine Heurteaux/Marc Borsotto
Soutenue le : 21 juin 2019

Devant le jury, composé de :
Marc Borsotto, Dr, IPMC
Lorenz Hirt, Pr, CHU Vaudois (Lausanne)
Jean-Marc Muller, Pr, Université de Poitiers
Brigitte Onteniente, Dr, PHENOCELL
Serge Richard, Dr, CERB
Jean-Marie Vaugeois, Pr, Université de Rouen

CERB Together a step forward for mankind

LABEX ICST ION CHANNEL SCIENCE AND THERAPEUTICS

Agence Nationale de la Recherche ANR

Les effets protecteurs de la Spadine et de ses analogues dans la récupération motrice et cognitive post-AVC

Jury :

Président du jury

Serge Richard, Dr, CERB

Rapporteurs

Lorenz Hirt, Pr, CHU Vaudois (Lausanne)
Jean-Marie Vaugeois, Pr, Université de Rouen

Examinateurs

Brigitte Onteniente, Dr, PHENOCELL
Jean-Marc Muller, Pr, Université de Poitiers

Invité (tuteur)

Marc Borsotto, Dr, IPMC

Les effets protecteurs de la spadine et ses analogues dans la récupération motrice et cognitive post-AVC

Les Accidents Vasculaires Cérébraux (AVC) sont la deuxième cause de décès dans le monde (environ 500 000 par an en Europe). A ce jour, il n'existe pas de traitement neuroprotecteur efficace. Dans 20 à 60% des cas, les patients ayant subi un AVC développent un état dépressif dans les semaines qui suivent le trauma et, malgré leur efficacité, les traitements antidépresseurs (AD) actuels présentent des limites et des inconvénients. Il existe donc un besoin urgent de mettre au point de nouvelles approches thérapeutiques contre ces maladies.

Il y a un peu plus de 10 ans, notre laboratoire a identifié le canal potassique TREK-1 comme étant une nouvelle cible face à l'AVC et face à la dépression. En 2010, le laboratoire a découvert la Spadine (PE 12-28), un peptide naturel issu de la maturation post-traductionnelle de la Sortiline. La spadine un bloqueur spécifique du canal TREK-1 qui possède des propriétés antidépressives particulières notamment sa rapidité d'action et son absence d'effets secondaires. Récemment, un essai clinique réalisé sur plus de 1000 patients a montré que la Fluoxétine, un antidépresseur couramment utilisé, administrée pendant plusieurs semaines à des personnes ayant subi un AVC permet une meilleure récupération neurologique. Nous avons donc formulé l'hypothèse que la Spadine pouvait correspondre à un nouveau concept de neuroprotection.

Les tests *in vivo* ont démontré que les effets AD de la Spadine disparaissaient 6 heures après l'injection. Nous avons alors recherché et identifié des analogues possédant les mêmes propriétés mais ayant une efficacité et une durée d'effet *in vivo* plus supérieures. Plusieurs analogues plus courts de la Spadine ont été synthétisés. La première partie de ma thèse a été dédiée à mettre en évidence leurs effets AD grâce à des modèles animaux de comportement. Ce criblage, associé à un criblage électrophysiologique, a permis l'identification de 3 analogues de la Spadine manifestant une efficacité et une biodisponibilité supérieures à celles de la Spadine. Le chef de file de ces peptides est la Mini-Spadine ou PE 22-28. Les autres analogues ont été construits en utilisant le PE 22-28 comme peptide de base, le G/A-PE 22-28 et le G/A-PE 22-28 Biotinylé, où la Glycine en position N-terminale a été remplacée par une Alanine.

Les premiers résultats confirmaient les effets AD des ces analogues courts. Par conséquent, j'ai pu entreprendre les études concernant leurs éventuelles capacités neuroprotectrices, avec une attention particulière sur la récupération post AVC. Nous avons choisi pour mimer un AVC d'utiliser le modèle de la MCAO (occlusion de l'artère cérébrale moyenne) sur souris adultes. Nous avons confirmé l'apparition d'un état dépressif 10 semaines après le trauma. Grâce à ce modèle, nous avons établi qu'un traitement par injection intrapéritonéale de Mini-Spadine avait des propriétés neuroprotectrices face au choc ischémique et permettait une meilleure récupération fonctionnelle des animaux. La mini Spadine réduit le taux de mortalité et prévient la perte de poids et les dysfonctionnements moteurs et cognitifs induits par l'ischémie. Par ailleurs, nous avons constaté grâce aux modèles FST (test de la nage forcée) et en NSF (Suppression de l'Alimentation induite par la Nouveauté) que la mini Spadine empêche le développement de la dépression post-AVC qui s'observe chez des souris non traitées. Enfin, le traitement mini Spadine augmente la neurogenèse et la synaptogenèse, et prévient la dégénération des neurones dopaminergiques de la *substantia nigra.*
Ces résultats confirment que la mini Spadine représente un concept novateur en neuroprotection contre les AVC et les dépressions associées.

Mots clés : AVC, Dépression post-AVC, TREK-1, Spadine, Neurogenèse, Comportement

Protective effects of Spadin and its analogs in motor and cognitive recovery after stroke

Stroke is the second leading cause of death in the world (about 500,000 per year in Europe). To date, there is no effective neuroprotective treatment. In 20 to 60% of cases, stroke patients develop depression within weeks of trauma and, despite their efficacy, current antidepressant (AD) treatments have limitations and deleterious side effects. There is therefore an urgent need to develop new therapeutic approaches against these diseases.

About 10 years ago, our laboratory identified the potassium channel TREK-1 as a new target for stroke and depression. In 2010, the laboratory discovered Spadin (PE 12-28), a natural peptide derived from the post-translational maturation of Sortilin. Spadin is a specific blocker of the TREK-1 channel that has particular antidepressant properties mainly its rapid action and its absence of side effects. Recently, a clinical trial involving more than 1000 patients showed that Fluoxetine, an antidepressant commonly used, administered for several weeks to people who have suffered from stroke, improves neurological recovery. We therefore hypothesized that Spadin could correspond to a new concept of neuroprotection.

In vivo tests showed that the AD effects of Spadin disappeared 6 hours after injection. We then researched and identified analogues with the same properties but with greater efficacy and *in vivo* bioavailability. Several analogues shorter than Spadin have been synthesized. The first part of my thesis was dedicated to highlight their AD effects using animal behavioural models. This screening, combined with electrophysiological screening, allowed the identification of 3 Spadin analogues with greater efficacy and bioavailability than Spadin itself. The leader peptide is Mini-Spadin or PE 22-28. The other two were designed from this sequence, G/A-PE 22-28 and G/A-PE 22-28 Biotinylated, where the Glycine residue in the N-terminal position has been replaced by an Alanine residue.

Our first results confirmed the AD effects of these short analogues. Consequently, I started to study their possible neuroprotective properties, with a particular focus on post-stroke recovery. We chose to use the MCAO (middle cerebral artery occlusion) model in adult mice to mimic stroke. We confirmed the onset of a depressive state 10 weeks after the trauma. Using this model, we have established that intraperitoneal injection of Mini-Spadin had neuroprotective properties against ischemic shock. The Mini-Spadin treatment also allows a better functional recovery of the animals. Mini-Spadin reduces the mortality rate, prevents weight loss and reduced motor and cognitive dysfunctions induced by ischemia. In addition, we showed by using FST (forced swimming test) and NSF (Novelty-Induced Feeding Suppression) models that mini Spadin prevents the development of a depressive behaviour that occurs in untreated mice. Finally, the Mini-Spadin treatment increases neurogenesis and synaptogenesis, and prevents the degeneration of dopaminergic neurons of the *substantia nigra.*

These results confirmed that Mini-Spadin open the possibility of developing an innovative concept in neuroprotection against stroke and associated depression.

Keywords: Stroke, Post-stroke depression, TREK-1, Spadin, Neurogenesis, Behaviour

Remerciements :

Un grand merci à vous Catherine, pour m'avoir donné l'opportunité de travailler dans votre équipe. Merci de votre écoute et de votre soutien face aux divers problèmes que nous avons rencontrés (et que nous rencontrons toujours pour certains).

Je tiens à remercier chaleureusement les membres du jury qui ont permis l'évaluation de ce travail de thèse, merci aux rapporteurs, les P^r^ Jean-Marie VAUGEOIS et Lorenz HIRT, et merci au D^r^ Brigitte ONTENIENTE et au P^r^ Jean-Marc MULLER. Un merci tout particulier au D^r^ Serge RICHARD d'avoir accepté de présider ce jury et d'avoir permis de financer mon Doctorat grâce à un contrat CIFRE.

Merci à vous Jean, je suis sûre que les statistiques sur le comportement vont vous manquer.

Marc, merci de m'avoir supportée pendant ces trois années. Il y a de l'amélioration niveau confiance en soi, mais je pense que pour les associations d'idées je vais encore avoir besoin de quelques années. Je vous suis reconnaissante de votre patience face à mon caractère parfois buté, ces trois années ont été pleines d'enrichissement et de leçons de vie. Vous avez toujours été à l'écoute et ne vous êtes jamais départi de votre humour. Vous avez également pris le parti de me forcer à réfléchir plus posément et cela m'a permis d'avancer tant au niveau professionnel que personnel.

Un grand merci à Carine pour ton écoute et tes conseils. J'aurais été bien en mal sans une chirurgienne du petit animal vers qui me tourner. Merci à Cathy, la culture primaire n'aurait pas été la même sans toi, et les commandes de dernière minute non plus. Merci aussi à toutes les deux de m'avoir forcée à prendre l'air de temps en temps, quand reprend-t-on l'Aquattack ?

Merci aux excités du B09 (je suis sûre que vous vous reconnaissez, mais dans le doute : Jojo et Dazou). L'ambiance n'aurait pas été la même sans vous. Je cherche encore à comprendre d'où vous vient cette énergie, ainsi que toutes ces idées… particulières. Ne changez pas ! Merci à Ninon qui a dû supporter avec moi ces deux énergumènes. Merci à Seb, l'exilé, même si tu n'as jamais « logé » dans notre boîte à sardines, tu y as tout à fait ta place. Merci à Veronika, j'espère que nous aurons l'occasion de nous revoir malgré la distance.

Merci aux résidents du « bureau des chefs » : Thierry, Sophie, Nicolas (Nature-Fonction !) et Patricia. Jamais avares en conseils et réponses.

Merci à mes camarades d'infortune, ceux qui sont déjà diplômés et les autres. Merci pour les heures passées à discuter et à partager les hauts et les bas d'une thèse, à l'Institut comme à l'extérieur. Katharina, Shockea, Marie, Alexandre, Audrey, …

Je voulais également remercier les anciens de l'équipe Heurteaux, Sarah et Miled, mais aussi Joëlle, Alice et Agnès.

Un grand merci à la plateforme animalerie, Thomas, Nicolas, Lucien, Alain, Benjamin, Véronique et Jessica. Pour votre aide concernant le suivi des animaux, vos conseils quant à l'analyse comportementale, et votre bonne volonté pour le changement des bouteilles d'air.

Merci également à Sophie et Fréderic pour leur aide avec les confocaux et l'analyse d'images.

Merci à Gauthier pour les étagères et l'installation électrique du bureau, mais il en manque encore (et oui je parle des deux) !

Enfin, merci à ma famille. Tout particulièrement mes parents qui n'ont jamais douté de moi. Merci de m'avoir écoutée, pendant des heures parfois, ressasser mes erreurs ou les doutes que j'avais. Avoir une famille telle que la nôtre derrière moi a été d'un grand réconfort.

Je ne pense pas que j'en serais arrivée là sans vous, alors encore une fois merci à tous.

Abréviations :

5-HIAA : Acide 5-HydroxyIndolAcétique

5-HT : 5-HydroxyTryptamine, sérotonine

AA : Acide Arachidonique

ADN : Acide DésoxyriboNucléique

AGPI : Acides Gras PolyInsaturés

AKAP150 : *A-Kinase Anchoring Protein*

ALA : Acide α-Linolénique

AMPA : α-Amino-3-hydroxy-5-Méthylisoazol-4-Propionate

AMPc : Adénosine MonoPhosphate cyclique

ARNm : Acide RiboNucléique messager

ATP : Adénosine TriPhosphate

AVC : Accident Vasculaire Cérébral

BDNF : *Brain Derived Neurotrophic Factor* (facteur neurotrophique cerebral)

BHE : Barrière Hémato-Encéphalique

BrdU : 5-Bromo-2'-deoxyUridine

CMST *: Conditioned Motility Suppression Test*

COX : Cyclo-oxygénase

CPF : Cortex PréFrontal

CREB : *cAMP Response Element Binding protein*

DALY : Disability Adjusted Life Years

FST : *Forced Swimming Test* (test de la nage forcée)

GABA : Acide γ-AminoButyrique

GFAP : *Glial Fribillary Acidic Protein*

HDAC : Histone DéACétylase

HDL : *High Density Lipoprotein*

HPLC : *High-Performance Liquid Chromatography* (Chromatographie en phase liquide à haute performance)

HTR1B : *5-HydroxyTryptamine Receptor 1B* (gène du récepteur 5-HT1B)

HTR2A : *5-HydroxyTryptamine Receptor 2A (*gène du récepteur 5-HT2A)

i.p. : intra-péritonéal

i.v. : intra-veineux

i.c.v. : IntraCérébroVentriculaire

IL : Interleukine

IMAO : Inhibiteurs de la MonoAmine Oxydase

IMC : Indice de Masse Corporelle

iNOS : forme inductible de l'oxyde nitrate synthase

IRM : Imagerie par Résonnance Magnétique

K2P : Canaux potassiques à deux domaines pore

LCR : Liquide Céphalo-Rachidien

LDL : *Low Density Lipoprotein*

LH : *Learned Helplessness* (test de la résignation apprise)

MABP : *Mean Arterial Blood Pressure*

MAO : MonoAmine Oxydase

MCAO *: Middle Cerebral Artery Occlusion (*occlusion de l'artère cérébrale moyenne*)*

MCP-1 : *Monocyte chemoattractant protein-1*

MDD : *Major Depressive Disorder*

MEC : Matrice ExtraCellulaire

MMPs : métalloprotéases matricielles

MnD : Minor Depressive Disorder

Mtap2 : *Microtubule-associated protein*

MWM : Morris Water Maze

NA : Noradrénaline

NeuN*: Neuronal Nuclei* (marqueur des neurons matures)

NIHSS : National Institute of Health Stroke Scale

NMDA : N-Méthyl-D-Aspartate

NO : Monoxyde d'azote

NOS : NO Synthase

NSF : *Novelty Suppressed Feeding* (test de la suppression de nourriture)

OH : hydroxyle

OMS : Organisation Mondiale de la Santé

PBS : Phosphate Buffered Saline

PE : Propeptide

PFA : ParaFormAldéhyde

PKA : Protéine Kinase A

PKC : Protéine Kinase C

PLC : PhosphoLipase C

RAP : *Receptor Associated Protein*

RCPG : Récepteurs Couplés aux Protéines G

RNS : *Reactive Nitrogen Species*

ROS : *Reactive Oxygen Species*

rt-PA : Activateur recombinant du plasminogène

s.c. : sous-cutané

SEM : *Standard Error of the Mean* (Erreur standard à la moyenne)

SERT : *SERotonin Transporter* (Transporteur de la sérotonine)

SGZ : *SubGranular Zone* (Zone sous-granulaire)

SNC : Système Nerveux Central

SNP : *Single Nucleotide Polymorphism*

SNRI : *Serotonin/Noradrenaline Reuptake Inhibitors*

SOD : Superoxyde dismutase

SSRI *: Specific Serotonin Reuptake Inhibitor*

SVZ *: SubVentricular Zone* (Zone sous-ventriculaire)

t-PA : activateur tissulaire du plasminogène (*tissue-type plasminogen activator*)

TASK : *TWIK-related Acid Sensing K+ channel*

TCAs : *TriCyclic Antidepressants* (antidépresseurs tricycliques)

TCE : 2,2,2-trichloréthanol

TEP : Tomographie par Emission de Positons

TGF-b : *Transforming Growth Factor*-b

TH : Tyrosine Hydroxylase

TMZ : Témozolomide

TNF *: Tumor Necrosis Factor*

TRAAK : *TWIK-Related Arachidonic Acid activated K+ channel*

TREK : *Twik RElated K+ channel*

TRESK : *TWIK-RElated Spinal cord K+ channel*

TrkB *: Tyrosine receptor kinase B*

TST : *Tail Suspension Test* (test de la suspension par la queue)

TWIK : *Weak Inwardly rectifying channel*

Liste des figures et tableaux :

Préambule :

L'équipe des Docteurs C. Heurteaux et J. Mazella travaille depuis des années sur le développement de nouvelles thérapies pour faire face à l'AVC et à la dépression, deux pathologies encore mal comprises, et surtout dont les traitements sont soit absents ou presque (AVC) soit pas toujours très bien adaptés (dépression). Il y a plusieurs années, le laboratoire a identifié pour ces deux pathologies le canal TREK-1 comme une cible importante. Par conséquent le laboratoire a recherché des molécules modulatrices de ce canal. C'est ainsi que la Spadine a été identifiée comme étant un modulateur spécifique de TREK-1. La Spadine est un peptide conçu à partir de la séquence du peptide de 44 acides aminés issu de la maturation post-traductionnelle de la Sortiline appelé propeptide ou PE. La sortiline est une protéine impliquée dans de nombreux processus physiologiques car c'est à la fois un récepteur et une protéine partenaire pour l'adressage à la membrane. La Spadine bloque le canal TREK-1 avec une forte affinité, or l'inhibition de ce canal entraîne le développement d'un phénotype de résistance face à la dépression. Cette capacité à inhiber TREK-1 a conduit le laboratoire à étudier le potentiel thérapeutique de la spadine dans le cadre de la dépression. A mon arrivée au laboratoire les propriétés antidépressives de la Spadine avaient déjà été largement caractérisées. Sa rapidité d'action (4 jours) et son absence d'effets secondaires avaient été clairement démontrées. Toutefois avec pour but de faire de la spadine un médicament utilisable en médecine humaine, la stabilité *in vivo* de la Spadine qui n'est que de 6 heures nécessitait, si possible, d'être améliorée.

De nouveaux projets portant sur la recherche d'analogues de la Spadine, plus stables que la spadine ont été initiés. Une première stratégie a consisté en la conception d'analogues retro-inverso, c'est-à-dire de peptides dont la séquence est inversée et dont les acides aminés sont en conformation D. Cependant, malgré des premiers résultats intéressants, sur des cultures de neurones, ces analogues se sont avérés délétères à fortes concentrations. C'est la raison pour laquelle le laboratoire s'est orienté vers une autre stratégie, celle de concevoir des analogues courts. La première partie de mon travail de doctorat a consisté à caractériser ces analogues. L'objectif était d'identifier ceux qui avaient conservé les propriétés antidépressives de la Spadine, mais surtout qui étaient beaucoup plus stables.. Les résultats obtenus supportent l'hypothèse que ces analogues courts de la Spadine pourraient un jour devenir des antidépresseurs de nouvelle génération.

La deuxième partie de mon projet a été établi à la suite d'une observation assez récemment mise en lumière qui indique que traiter les patients ayant subi un AVC améliore la récupération sur le long terme. L'activation de TREK-1 est protectrice face au choc ischémique. Nous avons démontré par des mesures électrophysiologiques que la spadine et surtout ses dérivés plus courts avaient un effet biphasique sur TREK-1 : activation à basses concentrations et inhibitrices à fortes concentrations. Nous nous sommes alors intéressés aux potentiels effets neuroprotecteurs de la Spadine et de ses analogues face à l'AVC et ses conséquences. Notamment, notre attention s'est portée sur la récupération post AVC du point de vue moteur mais aussi du point de vue cognitif. Nous avons également étudié les effets d'un traitement avec la spadine ou ses analogues sur la dépression post-AVC. Cette deuxième partie de mon doctorat a mis en avant les effets bénéfiques d'un traitement avec la spadine ou ses analogues dans la protection vis-à-vis de l'AVC et de ses conséquences aussi bien termes de récupération que de dépression. Ces analogues pourraient donc non seulement être développés en tant qu'antidépresseurs, mais également en tant que neuroprotecteurs.

Table des matières :

Introduction

I- AVC

A- Introduction

Malgré le taux d'incidence des Accidents Vasculaires Cérébraux (AVC) qui est resté stable au cours de ces deux dernières décennies, la mortalité était en baisse. Malheureusement aujourd'hui ces taux repartent à la hausse, entraînant une augmentation du nombre de survivants handicapés à vie (Feigin and Krishnamurthi, 2010). En effet en 2010, on dénombrait 16,9 millions d'AVC, chiffre auquel il convient d'additionner les 33 millions de survivants et les 5,9 millions de morts. Tout cela correspond approximativement à 102 millions d'années perdues pour cause d'incapacité ou de décès (mesurée par EVCI pour « Espérance de Vie Corrigée par l'Incapacité » ou DALY pour « Disabilty Adjusted Life Years ») (Krishnamurthi et al., 2013). De tels chiffres placent les AVC en deuxième position des causes de mortalité dans le monde et en troisième concernant les invalidités. Il s'agit donc indéniablement d'un enjeu sociétal majeur, et malgré toutes les avancées récentes qui ont pu être faites, une thérapie adaptée reste à trouver (Hankey, 2017).

La pathologie de l'AVC se définit cliniquement par la perte de fonctions neurologiques à la suite d'un infarctus ou d'une hémorragie cérébrale. Il peut également correspondre à un épisode de dysfonctionnement focal aigu du cerveau suffisamment important ou long pour qu'il soit possible d'en observer les conséquences par imagerie ou, bien évidemment, après autopsie.
Cette pathologie est divisée en deux sous-types majeurs : les AVC ischémiques, qui représente 80% des cas observés, et les AVC hémorragiques, les 20% restants. Les AVC ischémiques sont classés selon leur cause (maladie des petits vaisseaux, embolie cardiaque, …) (Amarenco et al., 2013) (Ay et al., 2007), et les AVC hémorragiques selon leur cause et l'aire cérébrale qu'ils affectent (hypertension, anti coagulation, zone supratentoriale, …) (Rannikmae et al., 2016). Mais malgré ces classifications, 30% des AVC ischémiques et 20% des AVC hémorragiques ont des causes indéterminées.

Un AVC hémorragique est dû à la rupture d'un vaisseau sanguin à l'intérieur du cerveau. Alors, non seulement le sang ne rejoint plus les zones à irriguer, mais de surcroît l'hématome provoqué comprime la zone impliquée **(Figure 1).** A l'inverse, lors d'un AVC ischémique il y a obstruction d'un vaisseau, qui peut être due à l'apparition d'un caillot sanguin ou à des plaques d'athérome (**Figure 1).** Dans un cas comme dans l'autre, il s'agit d'une perte d'afflux sanguin dans une zone plus ou moins étendue du cerveau qui entraîne une privation en oxygène et en glucose. La zone la plus atteinte s'appelle le cœur ischémique **(Figure 1)**.

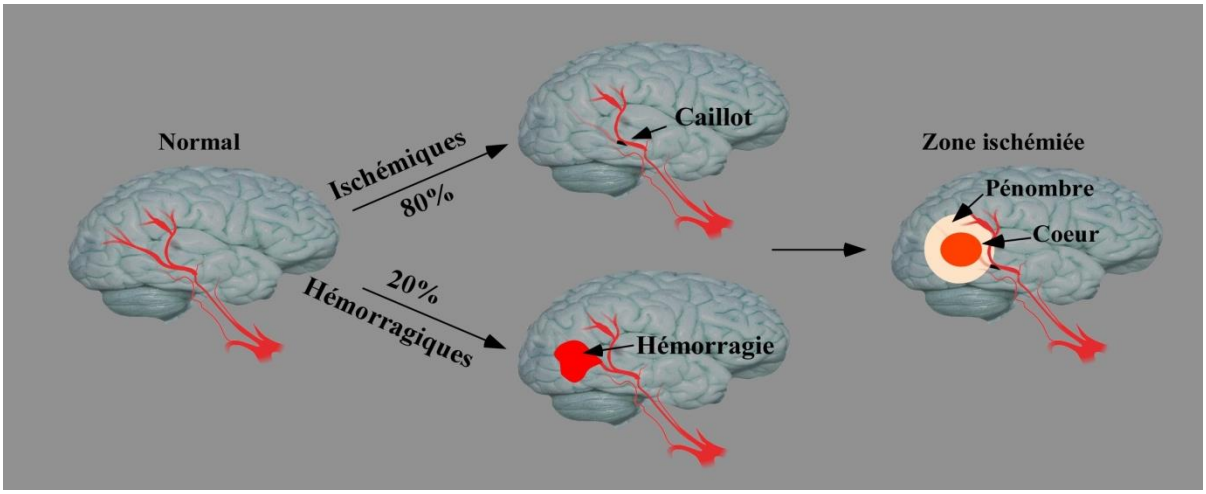

Figure 1 : Les différents types d'AVC

Dans le cas d'un AVC ischémique, l'étendue de cette zone est influencée par la taille et l'aire d'irrigation du vaisseau sanguin concerné, mais également par la possibilité de reperfusion (autrement dit de retour du flux sanguin). En effet, si le flux sanguin est interrompu au niveau des régions d'adressage du vaisseau touché, il existe tout autour une zone dans laquelle il est suffisamment maintenu, grâce à de petits vaisseaux sanguins collatéraux. Cela permet aux neurones de conserver leur intégrité (Liebeskind, 2010)**.** Dans cette région appelée « pénombre ischémique » ou « zone de péri-infarctus » **(Figure 1)** le déficit énergétique provoqué par l'AVC est tel qu'il n'y a plus d'activité neuronale mais sans être suffisant pour que le désordre ionique provoqué entraîne une destruction des membranes cellulaires. Les neurones de cette zone, bien que non stimulables, sont donc toujours physiquement intacts. (Astrup et al., 1981)**.** Leur destin dépend alors de la possibilité de reperfusion potentielle de la pénombre ischémique. S'il y a rapidement reperfusion, les dégâts seront réduits. Mais si au contraire l'insuffisance sanguine persiste, la pénombre subira le même sort que le « cœur ischémique » et le tissu

neuronal sera lésé de manière irréversible (Weinstein et al., 1986) (Selman et al., 1990) **(Figure 1)**.

B- Mécanismes impliqués

L'ischémie cérébrale entraînée par l'AVC prive les zones concernées d'apports en oxygène et en nutriments. Or le cerveau est énergétiquement l'organe le plus gourmand du corps. Comme le reste du corps, il consomme cette énergie sous forme d'Adénosine Triphosphate (ATP) qui est en majeure partie issue de la glycolyse en condition aérobie et du cycle de Krebs.
Cependant, pour faire face à une pénurie de glucose, le cerveau ne dispose que de très peu de réserves en glycogène, réserves exclusivement présentes dans les astrocytes (Iadecola, 2004). Plus dramatique pour les neurones si à cette pénurie s'ajoute une absence d'oxygène, ces réserves seront alors transformées en lactate par glycolyse anaérobie, et les quantités d'ATP que pourront ainsi fournir les mitochondries ne seront pas suffisantes pour répondre aux réels besoins énergétiques du cerveau. Il est donc impératif que les apports en oxygène et glucose soient parfaitement régulés, leur absence prolongée entraînant la mort du tissu cérébral.

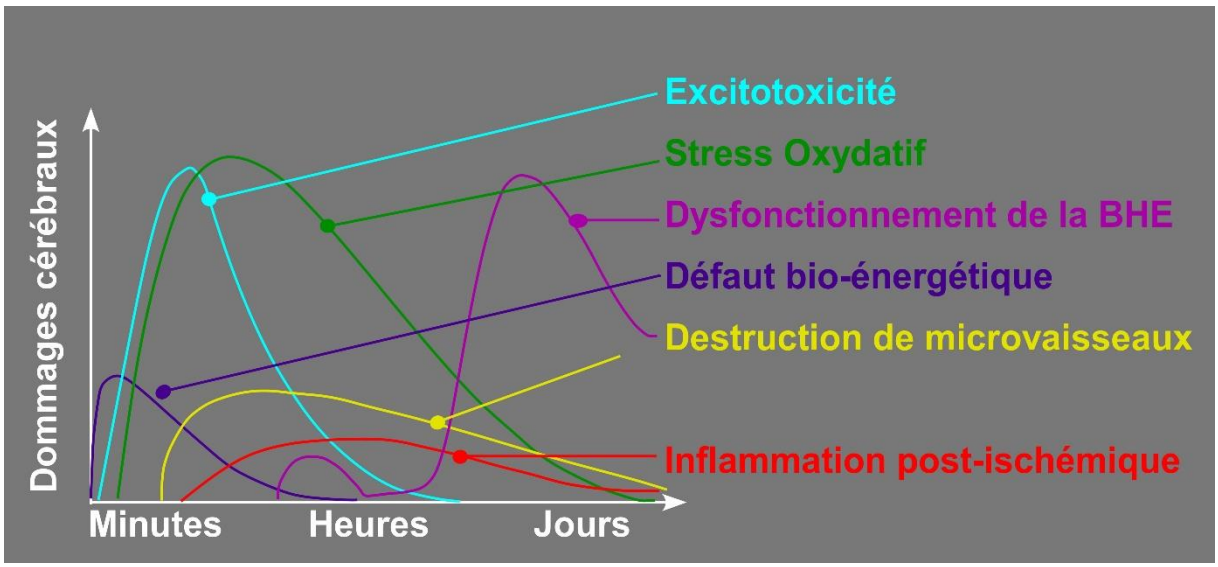

Figure 2 : les différents processus de l'AVC d'après (Brouns and De Deyn, 2009)

Les processus se mettant en place à la suite de l'ischémie sont nombreux et suivent une organisation dans le temps bien précise. Ainsi se succèdent et se chevauchent : le déficit

énergétique, l'excitotoxicité, le stress oxydatif et l'inflammation (Brouns and De Deyn, 2009) **(Figure 2)**.

1- Déficit Energétique / Exitotoxicité

En conditions normales, la phosphorylation oxydative du glucose apporte la majeure partie de l'énergie utilisée par le cerveau, l'ATP. Cette énergie est en grande partie utilisée afin de faire fonctionner différentes pompes ioniques (Na^+ et K^+) qui permettent de conserver une répartition physiologique des ions entre l'intérieur et l'extérieur de la cellule nerveuse. C'est cette répartition différentielle qui permet l'établissement du potentiel de membrane et donc le fonctionnement du neurone. Les concentrations en Na^+, Ca^{2+} et Cl^- doivent rester supérieures dans le milieu extracellulaire alors que la concentration en K^+ est au contraire supérieure à l'intérieur de la cellule. Ce n'est que dans ces conditions que l'influx nerveux (potentiel d'action) peut être transmis d'un neurone à l'autre **(Figure 3)**.
En effet, la première phase (ou dépolarisation) d'un potentiel d'action se traduit par une entrée de Na^+ dans la cellule, suivie par la repolarisation (sortie du K^+) et enfin l'hyperpolarisation (résultante de la sortie massive de K^+ en phase 2). Le retour à la normale se fait grâce aux pompes ioniques qui utilisent l'ATP pour rétablir les gradients ioniques à leurs niveaux physiologiques **(Figure 3)**.

La perte d'apports en oxygène et en glucose entraîne, en quelques minutes seulement, un déficit en énergie suffisante pour empêcher le maintien de l'équilibre ionique. Les gradients électrochimiques font qu'il y a une entrée massive des Na^+, Ca^{2+} et Cl^- dans la cellule et une sortie de K^+, mouvements qui entraînent une dépolarisation neuronale générale. En réponse à ce phénomène les neurotransmetteurs sont libérés dans la fente synaptique où ils activent leurs récepteurs spécifiques de manière continue car, en effet, en l'absence d'ATP il n'y a pas de recapture possible (Katsura et al., 1994). Cette suractivation, notamment celle médiée par le glutamate (principal neurotransmetteur excitateur) sur les récepteurs de type alpha-amino-3-hydroxy-5- methylisoxazole-4-propionate (AMPA) ou N-methyl-D-aspartate (NMDA), ou encore du kaïnate, conduit à une entrée massive de Ca^{2+} dans la cellule, contribuant ainsi à la mise en place du phénomène d'excitotoxicité (Rossi et al., 2000). En effet, l'activation des récepteurs AMPA induit dans un premier temps une entrée de Na^+ dans la cellule conduisant à une dépolarisation de la membrane qui, associée à la présence du Glutamate, active les

récepteurs NMDA. Ces derniers provoquent un influx important de Ca^{2+} dans la cellule. L'augmentation du Na^{+} cellulaire génère alors une importante entrée d'eau dans les cellules, provoquant leur gonflement (Olney et al., 1986). A plus long terme (24h), cette entrée d'eau est à l'origine de l'œdème cérébral et l'accumulation du Ca^{2+} est impliquée dans la mort neuronale (Choi, 1985) (Moskowitz et al., 2010). En effet, cette hausse de concentration (facteur 500 à 1000) provoque l'activation de mécanismes cataboliques médiés par les lipases, les nucléases et les protéases qui entraînent les processus physiologiques cités précédemment : stress oxydatif (caractérisé par une accumulation d'Espèces Réactives Oxygénées) et inflammation (marquée par la sécrétion de cytokines pro-inflammatoires).

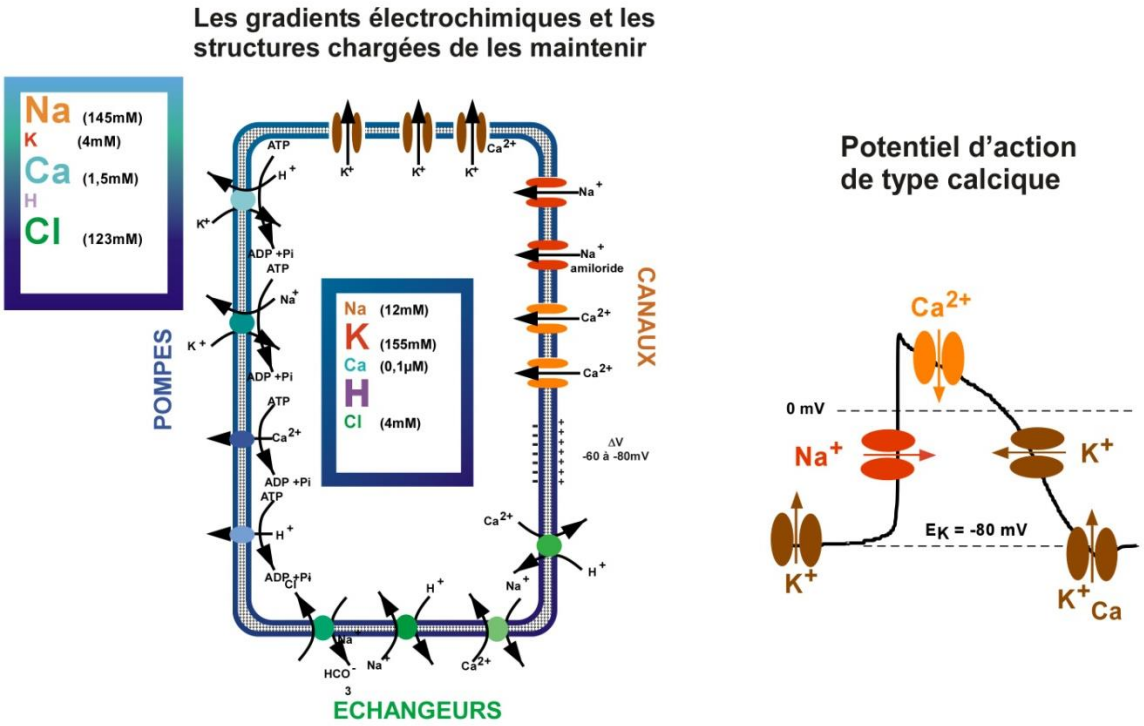

Figure 3 : Pompes ioniques et Potentiel d'action

In fine, tous ces processus conduisent à la détérioration de l'ADN et à la désorganisation du cytosquelette, phénomène conduisant à la mort cellulaire.

2- Stress Oxydatif

En conditions physiologiques les Espèces Réactives Oxygénées (ROS pour « Reactive Oxygen Species ») ont un rôle important dans le maintien de l'homéostasie du neurone. Leur production est étroitement régulée par les antioxydants endogènes de la cellule. En effet, ces antioxydants agissent comme des seconds messagers et sont impliqués dans l'apoptose, la détoxification ou encore la signalisation cellulaire (Bergendi et al., 1999). Cependant, une régulation altérée ou insuffisante face aux concentrations en ROS de la cellule entraîne un phénomène de stress oxydatif. Cela peut s'avérer particulièrement délétère pour la cellule du fait de son influence sur des processus tels que la dysfonction mitochondriale, la peroxydation lipidique et l'inflammation (Crack and Taylor, 2005).

On compte parmi les ROS des espèces telles que les radicaux libres (atomes ou molécules avec au moins un électron libre dans leur orbite externe) ainsi que les ions oxygénés et peroxydes, par exemple l'anion superoxyde O_2^-, l'oxygène singulet ·O, le radical hydroxyle ·HO ou encore le peroxyde d'hydrogène H_2O_2 et l'ozone O_3.

Ces ROS peuvent aussi se conjuguer avec d'autres atomes ou molécules plus grosses pour former des radicaux alkyl- ou peroxyl- (par exemple dans les lipides). Lorsque ces espèces chimiques oxygénées se lient à au moins un atome d'Azote, on parle alors « d'Espèces Réactives Azotées » (RNS pour « Reactive Nitrogen Species »), telles que l'oxyde nitrique ·NO, le peroxynitrite $ONOO^-$ et le dioxyde d'azote ·NO2 (Bergendi et al., 1999). Tout comme les ROS, ces derniers sont également produits en conditions physiologiques et sont impliqués dans des processus tels que la régulation de la pression sanguine, la signalisation neuronale ou encore la réponse immunitaire (Ridnour et al., 2004).

Si la surproduction des ROS entraîne un stress oxydatif, celle des RNS donne lieu à un stress nitrosatif.

En cas d'ischémie, il y a production excessive de RONS (ROS et RNS). En effet, l'activation par l'augmentation du Ca^{2+} d'enzymes telles que les Oxyde Nitrique Synthases (NOS), la phospholipase A2 et la cyclooxygénase, génère des radicaux libres dont la présence surcharge les mécanismes endogènes de piégeage. Cela a pour conséquences une peroxydation lipidique et une oxydation protéique qui, par la suite, altèrent l'ADN (Dirnagl et al., 1999) (Ahmadinejad et al., 2017).

Le cerveau est un organe particulièrement sensible aux dommages infligés par le stress oxydatif, et cela pour plusieurs raisons. Tout d'abord, il est abondamment composé d'acides gras

polyinsaturés facilement peroxydables. Ensuite, il n'est pas particulièrement riche en enzymes antioxydantes (superoxyde dismutase – SOD, glutathion péroxydase – GPx, catalase) ou autres molécules de même vocation (glutathion sous forme réduite, vitamine E, vitamine C, β-carotène) (Saeed et al., 2007). S'ajoutent aussi à cela la faible capacité de régénération des neurones et leur métabolisme élevé ainsi que la quantité importante de fer (dont de fortes concentrations favorisent la production de ROS et la peroxydation lipidique) se trouvant dans le cerveau (Smith et al., 2013).

Les dommages membranaires dus aux RONS sont le résultat de l'oxydation des acides gras polyinsaturés. Si en conditions physiologiques, ces réactions permettent le renouvellement de la membrane lipidique, en cas de stress oxydatif et nitrosatif, elles altèrent la structure même de la membrane et la fragilisent. En effet, l'activation de la phospholipase A2 entraîne l'hydrolyse des phospholipides de la membrane, relarguant ainsi des acides gras libres tels que l'acide arachidonique (AA). L'hydrolyse de l'AA par la cyclooxygénase et la lipoxygénase (COX/LOP) génère des métabolites et des ROS. Les métabolites se lient aux protéines et lipides membranaires, provoquant ainsi une modification des propriétés physiques de la membrane cellulaire, laquelle ne permet plus le bon fonctionnement des enzymes, et modifie grandement les interactions cellulaires (Braughler and Hall, 1989)**.**

Les effets délétères des RONS induisent également une dégradation protéique. Lorsque les protéines sont oxydées, de nombreux changements chimiques ont lieu, notamment la fragmentation ou l'agrégation ou encore le mauvais repliement des protéines, ainsi que la modification des chaînes latérales des acides aminés (Radak et al., 2011). Il s'agit d'une réaction en chaîne complexe par la variété des mécanismes impliqués et par la production de différents métabolites. Ainsi, les protéines peuvent être hydrolysées ou au contraire réticulées, et enfin l'oxydation des chaînes latérales d'acides aminés génère des dérivés d'oxydation spécifiques à chaque amine (Dean et al., 1997)**.** L'accumulation de ces modifications oxydatives sur les acides aminés entraîne un dérèglement des fonctions cellulaires. En effet, la carbonylation et toutes les autres modifications post-traductionnelles médiées par les ROS provoquent l'inactivation des protéines concernées. Ce qui, dans le cas d'enzymes, les rend incapables de catalyser les réactions biochimiques pour lesquelles elles sont synthétisées. Cette inhibition de processus biologiques est responsable en majeure partie de la mort cellulaire (Radak et al., 2011).

Enfin, le dernier niveau d'action cellulaire des RONS est la molécule d'ADN, laquelle peut subir des dommages tels que la modification de ses bases nucléotidiques, une formation de sites

apurinique/apyrimidique (AP) ou une fragmentation (rupture de l'hélice). Par son faible potentiel réducteur comparé aux autres bases azotées, la Guanine est très sujette à l'oxydation. Aujourd'hui plus de 20 résidus d'oxydation de la Guanine ont déjà pu être identifiés, le plus courant est la 8-oxo-7,8-dihydroguanine (8-oxoG). Lorsque cette 8-oxoG n'est pas réparée, elle devient mutagène, car s'associant à l'adénine (A) au lieu de la cytosine (C), elle induit des transversions de G à T (Radak et al., 2011)**.** Cette apparition de mutations entraîne l'activation de systèmes de réparation de la cellule par excision de base, et par la suite la génération de « sites vacants » (où il manque une base), aussi appelés sites AP. Il a également été démontré que les ROS réagissent avec les sucres des nucléotides, et tout particulièrement les radicaux hydroxyles qui ciblent les positions C1 et C4 du pentose du désoxyribose. Là encore, les modifications générées sur les bases touchées peuvent entraîner l'activation des systèmes de réparation de la cellule par excision de base, et donc la formation de sites AP (Demple and DeMott, 2002). Ces interactions des radicaux hydroxyles avec le désoxyribose peuvent aboutir à des ruptures simple brin ou double brin de l'ADN. En effet, les radicaux peroxyles ($ROO^{\bullet -}$) générés endommagent les liaisons phosphodiester du squelette de la molécule d'ADN et provoquent ainsi sa rupture (Dedon, 2008).

Les radicaux libres ont également un impact au niveau extracellulaire où ils activent les métalloprotéases matricielles qui sont à l'origine de la dégradation du collagène et de la laminine, constituant la lame basale. Les conséquences sont l'altération de la perméabilité de la barrière hémato-encéphalique (BHE).

3- Barrière Hémato-Encéphalique

La BHE est une membrane qui isole le liquide cérébro-spinal (LCS), dans lequel est immergé le système nerveux central (SNC), de la circulation sanguine. Elle filtre de façon très sélective toutes les molécules arrivant au cerveau ou à la moelle épinière. Elle empêche par exemple le passage d'agents pathogènes, de toxines ou encore d'hormones nocives mais ne fait pas obstacle à l'entrée de molécules nécessaires au bon fonctionnement du SNC. Au niveau anatomique, de la circulation sanguine vers le LCS, la BHE est composée de cellules endothéliales, de péricytes et de matrice extracellulaire (lame basale) auxquels s'associent astrocytes et neurones (Hawkins and Davis, 2005) **(Figure 4)**. Ce sont les cellules endothéliales qui composent la première couche de la BHE. En effet, elles recouvrent les vaisseaux cérébraux et, du fait de leurs

jonctions serrées qui rendent le transport para-cellulaire presque impossible, sont à l'origine de l'étanchéité de la BHE. Ainsi, les molécules sont pour la plupart contraintes de passer de la circulation sanguine au LCS par transport actif au travers des cellules (transport trans-cellulaire). Cela permet le filtrage sélectif des substances pouvant pénétrer le SNC.

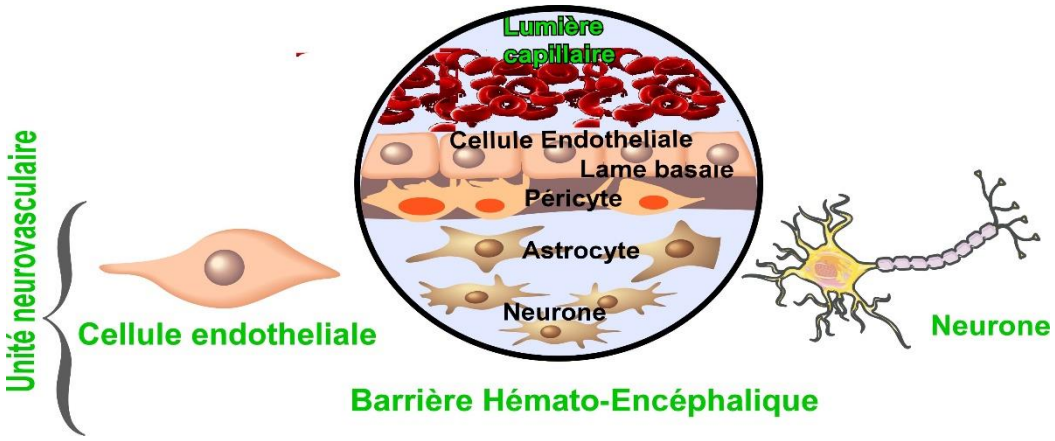

Figure 4 : Organisation de la BHE

Les péricytes sont localisés au contact des cellules endothéliales (25 à 50% des cellules endothéliales sont ainsi associées à un péricyte) (Pardridge, 2005). Ils jouent un rôle important dans le développement des vaisseaux, le maintien de la BHE, la régulation des entrées de cellules immunitaires dans le SNC et dans le contrôle du flux sanguin cérébral (Attwell et al., 2016). Ils sont également impliqués dans différentes pathologies, comme par exemple l'AVC ischémique durant lequel ils compriment les capillaires, empêchant ainsi le passage des globules rouges et gênant ainsi la reperfusion à la suite du retrait du caillot (Yemisci et al., 2009).

La lame basale recouvre ensuite l'ensemble des cellules endothéliales et des péricytes sur 30 à 40nm d'épaisseur. Elle est composée de molécules de soutien telles que le glycogène de type IV, le sulfate d'héparine, les laminines, les protéoglycanes ou la fibronectine. Des cellules immunitaires, comme les macrophages périvasculaires et la microglie, sont également présentes (Serlin et al., 2015) (Sharif et al., 2018).

Les astrocytes, se greffent sur la lame basale grâce à des extensions membranaires appelées pieds astrocytaires. Ils ont un rôle crucial non seulement dans le support de la BHE mais aussi dans l'interaction de cette dernière avec les neurones (Rodriguez-Arellano et al., 2016).

Le dysfonctionnement des transporteurs ioniques au niveau de la BHE lors d'un AVC est un processus décisif menant à l'œdème cérébral. En effet, peu après l'ischémie, l'augmentation de l'activité des échangeurs Na^+/H^+, des co-transporteurs Na^+-K^+-Cl^- ou du canal potassium KCa3.1 induite par le calcium amplifie le transport trans-cellulaire du Na^+ et du Cl^- vers le cerveau à travers la BHE**.** La dérégulation homéostasique qui en résulte (particulièrement l'augmentation de l'absorption de Na^+) contribue alors grandement à la formation d'œdème. (Chen et al., 2015c) (O'Donnell, 2014). De plus, le stress hypoxique conduit à une augmentation de la perméabilité de la BHE en altérant les jonctions serrées (Fischer et al., 1999)**.** Si une reperfusion précoce peut limiter les lésions, une reperfusion trop tardive ou un traitement thrombolytique différé ont, en revanche, des conséquences délétères (Hjort et al., 2008).

La perméabilisation de la BHE est également fortement impliquée dans l'augmentation de la mortalité due à une hémorragie après un traitement par le tPA (tissue-type plasminogen activator), une enzyme qui catalyse la conversion du plasminogène en plasmine au niveau du thrombus, ce qui induit la rupture de ce dernier (Jickling et al., 2014). Le traitement par tPA augmente également les taux de métalloprotéinase 9 (MMP-9), enzyme responsable de la dégradation de l'occludine et de la claudine-5, et donc responsable de la perte d'intégrité des jonctions serrées (Kelly et al., 2006) (Qi et al., 2016). En effet, à la suite de l'effondrement des jonctions serrées dû, entre autres, à la phosphorylation de la connexine43, l'hémorragie associée au tPA résulte souvent d'une rupture importante de la BHE (Yang et al., 2016). Des études effectuées sur des patients sous traitement thrombolytique ont permis de constater par IRM que l'ouverture précoce de la BHE est un prédicteur de processus hémorragique final (Latour et al., 2004). A noter cependant que, même sans traitement, les taux plasmatiques et cérébraux des MMP chez les victimes d'AVC sont augmentés (Montaner et al., 2001), et par conséquent certainement responsables des dégâts induits par l'ischémie.

Cette perméabilisation de la BHE permet alors l'infiltration de cellules immunitaires périphériques et de molécules associées dans le parenchyme cérébral. Ces phénomènes contribuent grandement à aggraver non seulement l'état de la BHE, mais aussi du tissu cérébral dans son ensemble (Gelderblom et al., 2009).

4- Inflammation

a- Leucocytes

Bien que de nombreux aspects de l'inflammation ne se manifestent que plusieurs jours après l'AVC, la cascade inflammatoire est activée immédiatement après occlusion du vaisseau (De Meyer et al., 2016) **(Figure 3).** Ainsi, il y a production de cytokines et de médiateurs proinflammatoires par les cellules neuronales endommagées dans les premières heures suivant l'ischémie, parmi lesquels sont présents, entre autres, le facteur de nécrose tumorale (TNF-α) et les interleukines 1b et 6 (IL- 1b et IL-6). Ces derniers sont décrits comme étant délétères dans les modèles d'ischémie expérimentale, d'ailleurs leurs niveaux augmentent dans le fluide cérébrospinal et dans le sang des patients victimes d'AVC ischémiques (Basic Kes et al., 2008) (McCoy and Tansey, 2008).

Ces sécrétions d'IL-1 et d'IL-6 entraînent l'augmentation de l'expression de molécules d'adhésion par les cellules endothéliales, notamment ICAM-1, la P-selectine et la E-selectine. Ces molécules permettent, entre autre, l'adhérence, l'accumulation et la transmigration des leucocytes à travers l'endothélium et servent de médiateurs dans les cascades inflammatoires, aggravant l'impact de l'infarctus (McColl et al., 2008) (Wang and Doerschuk, 2002)**.** En effet, ces molécules induisent l'adhésion des neutrophiles aux cellules endothéliales (Choi et al., 2009) (Schnoor and Parkos, 2008)**,** condition indispensable à leur infiltration (l'absence de ces molécules d'adhésion chez l'animal a un effet neuroprotecteur (Denes et al., 2010)). Ces cellules qui sont une source majeure de MMP-9 au niveau du cœur de l'infarctus, favorisent la dégradation de la BHE, et contribuent ainsi aux lésions neuronales (Justicia et al., 2003) (Rosell et al., 2006). La MMP-9 facilite également le recrutement de leucocytes supplémentaires ainsi que l'activation de cellules immunitaires résidentes (Amantea et al., 2009). Son élimination réduit considérablement l'accumulation leucocytaire post-ischémique dans le tissu cérébral (Gidday et al., 2005) en diminuant la taille de la lésion cérébrale, et conduit à un meilleur pronostic fonctionnel (Barone and Feuerstein, 1999).

En plus de la MMP-9, les neutrophiles, après avoir pénétré dans le parenchyme cérébral, libérent des ROS et des enzymes protéolytiques. En effet, à la suite de l'infiltration leucocytaire il y a augmentation de la forme inductible de l'oxyde nitrique synthase (iNOS) ou encore de COX-2. La première produit du NO en quantité délétères (Forster et al., 1999), et la seconde de l'ion superoxyde et des prostaglandines (métabolites de l'AA) dans la pénombre ischémique (Iadecola et al., 1999). Dans des modèles murins, l'inhibition de ces deux enzymes, et celle de

la MMP-9 permet de réduire la taille de l'infarctus cérébral (Iadecola et al., 1997) (Iadecola et al., 2001)**.**

Il est important de noter que, outre les conséquences liées à la sécrétion de molécules dangereuses, le recrutement important de neutrophiles peut obstruer la microcirculation, et ainsi empêcher la reperfusion sanguine (del Zoppo et al., 1991).

Les neutrophiles sont les premières cellules de la circulation à pénétrer dans la zone ischémiée, leur invasion se poursuit jusqu'à 2 jours après l'AVC avant que leur nombre ne décline peu à peu (Gelderblom et al., 2009)**.** Ils ne sont en revanche pas les seuls leucocytes à passer la BHE. Les monocytes eux aussi infiltrent le parenchyme cérébral. Ils sont d'ailleurs la population cellulaire présente en plus grand nombre dans les stades avancés de l'infarctus (Iadecola, 1997).

L'ensemble de ces résultats démontre clairement que l'inflammation cérébrale induite par l'ischémie est associée à l'activation de différentes populations cellulaires, telles que les microglies/macrophages et les astrocytes. Cependant d'autres types cellulaires comme les lymphocytes T régulateurs (Tregs) et les lymphocytes B, en limitant le traumatisme, jouent également un rôle protecteur (Li et al., 2015) (Liesz et al., 2015) (Offner and Hurn, 2012).

b- Microglie

Bien que l'inflammation intravasculaire ouvre la voie à la dégradation de la BHE et à l'invasion leucocytaire du tissu ischémique, des processus inflammatoires sont également initiés dans le parenchyme cérébral. En effet, l'un des premiers événements à prendre place serait la libération de « motifs moléculaires associés au danger/dommages » (DAMP) par des neurones blessés ou mourants. Les lésions tissulaires génèrent une multitude de ces DAMPs (parmi eux des protéines, des lipides complexes et des acides nucléiques provenant de cellules mortes, ainsi que des peptides issus de la protéolyse matricielle) qui activent alors des récepteurs sur la microglie et les astrocytes (Garcia-Bonilla and Iadecola, 2012) (Benakis et al., 2014). Dans les premières heures suivant l'ischémie, la microglie réagit à l'altération de l'environnement, la morphologie de ces cellules change alors et les rapproche de manière préférentielle des neurones qui présentent des signes de surcharge en calcium (Szalay et al., 2016). Cette microglie activée prend alors un aspect amiboïde similaire à celui des macrophages (Patel et al., 2013)**,** et exprime certains de leurs marqueurs de surface comme CD11b, IB4 (*Isolectin B-4*), Iba-1 (*ionized calcium-binding adapter molecule 1*), F4/80 ou encore ED-1 (CD68 chez

l'humain) (Ginhoux et al., 2010; Taylor and Sansing, 2013). La microglie sécrète alors des molécules telles que l'IL-1β ou le TNFα, qui influent sur la cascade inflammatoire en induisant la production de cytokines et de chimiokines dans les cellules endothéliales et les astrocytes.

Cependant, bien que l'activation de la microglie entraîne la libération de cytokines pro-inflammatoires, de ROS et de MMPs (implication néfaste face à l'AVC) (Gregersen et al., 2000) (Iadecola and Anrather, 2011), contrarier cette activation ou la prolifération de ces cellules, entraîne une augmentation du volume de l'infarctus et du nombre de neurones à destin apoptotique de la zone touchée (Lalancette-Hebert et al., 2012).

L'activation de la microglie à la suite d'un AVC aurait ainsi un double rôle, délétère et protecteur.

Une contradiction qui s'explique par le fait qu'après son activation, la microglie peut évoluer vers deux phénotypes différents. La microglie de type M1 (ou classique) est pro-inflammatoire, elle sécrète de nombreux médiateurs pro-inflammatoires, tels que l'IL-1b, le TNF-a, iNOS, MCP-1 (CCL-2) et l'interféron-γ (INF-γ) (Starossom et al., 2012) (Ransohoff and Brown, 2012). *A contrario,* la microglie de type M2, qui sécrète des médiateurs anti-inflammatoires tels que l'IL-4, l'IL-10, l'IL-13 ou encore le facteur de croissance transformant β (TGF-β) ainsi que d'autres facteurs neurotropiques (Hanisch and Kettenmann, 2007) (Liu et al., 2012) (Taylor and Sansing, 2013) (Zhou et al., 2012) (Shin et al., 2004), serait plutôt impliquée dans la neuroprotection et la récupération (Starossom et al., 2012) (Kawanokuchi et al., 2008).

La microglie M2, bien qu'elle soit plus présente au niveau de la lésion ischémique dans les premiers temps suivant l'AVC, est rapidement supplantée par le type M1, faisant ainsi place aux effets délétères (Hu et al., 2012).

c- Astrocytes

En cas d'AVC les astrocytes, bien que moins sensibles à la privation en oxygène et en glucose que les neurones, subissent d'importantes modifications morphologiques, qui se caractérisent par une hypertrophie qui peut se transformer en hyperplasie. Dans les minutes qui suivent la blessure, l'activation des astrocytes est déclenchée par des cytokines, comme TGFα (Rabchevsky et al., 1998), l'IL-1 (Herx and Yong, 2001) ou l'IL-6 (Brunello et al., 2000), qui sont produites par les neurones et les cellules gliales du cœur ischémique et par les neurones blessés de la pénombre. Ces cellules, également appelées astrocytes réactifs (Sofroniew, 2009), présentent une hypertrophie cellulaire, un degré de prolifération plus important, une expression

accrue des protéines filamenteuses intermédiaires (comme la protéine fibrillaire gliale acide (GFAP), la vimentine et la nestine), et une expression altérée de nombreuses autres molécules (impliquées dans la structure cellulaire, la transcription génétique, le métabolisme énergétique, la signalisation intracellulaire et les transporteurs de membranes) (Fuchs and Cleveland, 1998) (Li and Chopp, 1999) (Ridet et al., 1997) (Liu and Chopp, 2016).

In vitro en l'absence d'oxygène et de glucose, l'activité et l'expression des transporteurs du glutamate, la capacité de recapture du glutamate, et l'expression intracellulaire du glutathion des astrocytes matures sont diminuées (Gouix et al., 2014). Or plus de 80 % des transporteurs de glutamate, en particulier EAAT2, sont situés sur les astrocytes, faisant de ces cellules le principal site d'absorption du glutamate (Dallerac and Rouach, 2016) (Petr et al., 2015). Après l'ischémie, l'une des premières réactions dues à l'absorption accrue de glutamate et de lactate est le gonflement des astrocytes (Landis, 1994) (Kimelberg, 2005). Ces cellules hypertrophiques peuvent comprimer les vaisseaux dans les régions ischémiques et exacerber l'hypoperfusion vasculaire (Sykova, 2001). Les astrocytes sont également une source de MMP, et donc accroissent la dégradation des jonctions serrées et de la matrice extra-cellulaire après une ischémie (Mun-Bryce and Rosenberg, 1998)**.** Par leur production de cytokines et d'iNOS**,** ils sont également impliqués dans la réponse inflammatoire (Endoh et al., 1994).

Cette chaîne d'événements provoquée par l'ischémie conduit finalement à la mort cellulaire.

d- Mort cellulaire

A la suite d'un AVC, deux processus de mort cellulaire se mettent en place, la nécrose et l'apoptose. C'est majoritairement l'amplitude du déficit énergétique qui va faire basculer les cellules vers l'un ou l'autre de ces processus. En effet, la nécrose est importante dans les régions les plus pauvres en ATP, telles que le cœur ischémique (Dirnagl et al., 1999), alors que l'apoptose a plutôt lieu dans la pénombre ischémique où, bien qu'en quantité inférieure à la norme, il y a toujours de l'ATP (Leist et al., 1997). Cependant, le degré de sévérité de l'ischémie est aussi primordial, ainsi en cas d'ischémie permanente c'est la nécrose qui prend le pas, alors que dans le cas d'une occlusion transitoire c'est l'apoptose le processus principal.

La nécrose est considérée comme une mort cellulaire « accidentelle » et majoritairement pathologique, alors que l'apoptose est une mort cellulaire « programmée » et physiologique.

Dans le cas de la nécrose, c'est la déficience énergétique provoquée par l'ischémie qui entraîne une rupture de la membrane plasmique et le relargage des composants cytoplasmiques de la cellule. Ce relargage d'enzymes de dégradation, de glutamate, mais aussi certaines de toxines induit la nécrose des neurones avoisinants (Zong and Thompson, 2006).

Au contraire de la nécrose, l'apoptose répond à un programme génétique bien précis. Lorsque la cellule est soumise à un stress délétère, comme une production de ROS importante (Dugan et al., 1995) ou une diminution de K^+ de grande ampleur (Yu et al., 1997), il y a activation des gènes codant certaines protéines (Bax et Trp53 par exemple) et certaines enzymes (Caspases) impliquées dans les processus de mort cellulaire programmée. Des études ont montré que l'expression de ces gènes est surtout augmentée dans la pénombre (Mitsios et al., 2007) (Sairanen et al., 2006). Les caspases sont des enzymes de clivage qui dégradent les protéines du cytosquelette et détruisent les composants cytoplasmiques (Marsden and Strasser, 2003) (Strasser, 2005), ce sont majoritairement les caspases 1 et 3 qui sont impliquées dans l'apoptose provoquée par une ischémie cérébrale. La membrane cellulaire reste ainsi intacte jusqu'au terme du processus, ce qui limite la libération des constituants cytoplasmiques et réduit l'inflammation environnante (Choi, 1996) (Lee et al., 1999) (Namura et al., 1998). Les neurones aux alentours ne sont donc pas affectés par la mort de leurs voisins.
A noter que l'inhibition de ces caspases (Thornberry and Lazebnik, 1998) a un effet neuroprotecteur (Fink et al., 1998).

Cette perte neuronale provoque des lésions cérébrales qui ont de nombreuses conséquences pour les patients qui survivent à l'AVC.

C-Séquelles de l'AVC

A la suite d'un AVC le taux de mortalité varie de 15% dans les premiers mois à 50% après plusieurs années (Luengo-Fernandez et al., 2013). Cependant, dans la plupart des cas, les survivants présentent des séquelles. En effet, d'après l'INSERM si 60% récupèrent une « indépendance fonctionnelle » suffisante pour réintégrer leur domicile, 40% gardent des séquelles assez importantes pour remettre en cause leur autonomie quotidienne, sans mentionner les risques de récidive ou de développement d'un état dépressif.

Le cerveau étant un organe complexe et structuré en zones correspondant la plupart du temps à des fonctions différentes, les séquelles d'un AVC dépendent non seulement de la sévérité de l'ischémie mais aussi de la zone lésée. Elles peuvent ainsi aussi bien être d'ordre moteur que cognitif, voire émotionnel.

1- Motrices

La plupart des patients survivant à un AVC développent des séquelles motrices, c'est-à-dire une perte totale ou partielle de mobilité (Jorgensen et al., 1995). Chez 80% d'entre eux cela se traduit par une incapacité à contrôler les muscles du côté contralatéral du corps, phénomène appelé l'hémiparésie (Langhorne et al., 2009) (Hatem et al., 2016). Généralement cette paralysie de l'hémicorps est totale immédiatement après l'AVC mais dès quelques jours les muscles sont de nouveau capables de se contracter. Cependant cette récupération n'est que partielle, les patients sont incapables de faire des mouvements précis et leur force musculaire est très réduite. A cela s'ajoutent les problèmes de tonicité qui entraînent de nombreux handicaps dans la réalisation de tâches simples, et qui sont bien souvent à l'origine de la dépendance des patients dans leur vie quotidienne.
Souvent les patients victimes d'AVC présentent des troubles de la coordination (ataxie) ainsi qu'une incapacité à réaliser certains mouvements particuliers adaptés à une situation donnée (apraxie) (Heilman et al., 1997). Dans le cas de l'apraxie c'est la conceptualisation même du geste qui est affectée.
Cette prévalence des déficits moteurs s'explique du fait que, dans 80% des cas, l'AVC ischémique est une conséquence de l'obstruction de l'une des trois artères principales du cerveau, l'artère cérébrale moyenne (artère Sylvienne). Cette dernière irrigue la capsule interne ainsi que les ganglions de la base, mais aussi, en partie, les lobes frontal, pariétal et temporal. Des structures qui sont toutes impliquées dans la fonction motrice et dans le contrôle des mouvements.

Bien qu'étant les plus communes, les séquelles motrices ne sont généralement pas les seules associées à l'AVC. Un autre type de troubles fréquents sont ceux d'ordre cognitif.

2- Cognitives

Tout comme les déficits moteurs, les troubles cognitifs après un AVC peuvent avoir un impact important sur la qualité de vie et l'indépendance des patients (Tatemichi et al., 1994). Le terme cognition regroupe de nombreux processus tels que la mémoire, l'attention, le langage ou encore la fonction exécutive (planification, organisation, contrôle). Ces processus sont généralement associés pour mener à bien même la plus simple des tâches intellectuelles, comme par exemple se rappeler d'une liste de course, qui fait appel non seulement à la mémoire mais aussi au langage et à l'attention. Les troubles cognitifs sont déterminés au travers de tests neuropsychologiques variés, également utilisés pour évaluer les dégâts dans la maladie d'Alzheimer, qui permettent d'identifier le type d'atteinte que manifeste le patient. Près de 30% des patients ayant subi un AVC développent une démence (dite vasculaire) dans les 12 mois (Cullen et al., 2007). Ce qui classe l'AVC en deuxième position, immédiatement après la maladie d'Alzheimer, des causes de démence (OMS).

Tout comme dans le cas des troubles moteurs, l'obstruction de l'artère cérébrale moyenne est associée à un risque plus important de développer des atteintes cognitives (Jaillard et al., 2010). En clinique, les deux séquelles cognitives les plus fréquentes sont l'héminégligence spatiale aujourd'hui appelée négligence spatiale unilatérale, et l'aphasie (Cumming et al., 2013). 85% des patients ayant subi un AVC dans l'hémisphère droit, présentent une négligence visuelle gauche dans les premiers temps suivant l'AVC (Azouvi et al., 2006). Le patient « ignore » les signaux envoyés et ne considère pas ce qui se trouve à sa gauche. Par exemple, il ne mangera que ce qui se trouve à gauche dans son assiette, ou il se heurtera aux obstacles à sa gauche. Cette héminégligence s'atténue généralement de manière spontanée (Ringman et al., 2004), cependant elle persiste chez au moins un tiers des patients qui manifestent une négligence spatiale unilatérale importante même plusieurs mois après l'AVC (Karnath et al., 2011).

Un AVC peut également entraîner une incapacité partielle ou totale à communiquer et à comprendre bien que les sons soient perçus correctement, c'est l'aphasie. Ce trouble est présent chez 10 à 38% des patients et est un facteur majeur dans la dépendance post ischémie (Pedersen et al., 1995) (Yoon et al., 2015) (Hilari et al., 2003). Cette incapacité à communiquer est un handicap majeur dans le développement de relations sociales, c'est pourquoi l'aphasie va souvent de pair avec les troubles émotionnels et psychosociaux (Hemsley and Code, 1996). Elle est d'ailleurs considérée comme un marqueur prédictif des désordres émotionnels et d'isolation sociale (Thomas and Lincoln, 2008).

3- Emotionnelles

A la suite d'un AVC, les victimes font souvent preuve d'anxiété et ont une inclination à l'isolement. Cliniquement, l'atteinte émotionnelle avec la plus grande incidence est la dépression post-AVC. En effet, moins de 12 mois après l'AVC, un tiers des survivants développe un état dépressif (Hackett et al., 2005b) (Hackett and Pickles, 2014) (Robinson, 2003). Ce trouble se traduit principalement par une incapacité à ressentir du plaisir (l'anhédonie). D'autres symptômes fréquemment rencontrés sont la fatigue, les insomnies, des difficultés de concentration et la perte d'appétit.

Si contrairement aux séquelles motrices et cognitives, la dépression n'est pas liée à la zone cérébrale touchée (Carson et al., 2000), elle est d'autant plus favorisée par la gravité des autres troubles développés par le patient (Kouwenhoven et al., 2011).

Le développement d'une dépression post-AVC est signe de mauvais pronostic (Hadidi et al., 2009). On rapporte en effet une mortalité plus de 3 fois supérieure chez les patients atteints de dépression. Il faut également ajouter à cela que la récupération est plus lente et les séquelles plus importantes, ce qui impacte grandement la qualité de vie du patient et de ses proches.

La dépression post-AVC qui a constitué une part importante de mes recherches fait l'objet du chapitre II de ce manuscrit.

II- Dépression Post-AVC

A- Généralités

De nos jours près de la moitié des survivants d'un AVC souffrent de handicap permanent et doivent être placés en institution pour soins et réhabilitation (Bonita et al., 1997) (Go et al., 2013). Pour compliquer plus encore le processus déjà complexe de réhabilitation, près d'un tiers des survivants souffre de dépression post-AVC (PSD).

La PSD est le principal prédicteur de mauvais pronostics fonctionnels à la suite d'un AVC, car elle est associée à de nombreux troubles comme les insomnies, les difficultés de réadaptation, les déficits cognitifs, le retrait social et l'isolement, et surtout, une mortalité accrue (Hadidi et al., 2009).
La prévalence de la PSD varie selon les études (Paolucci, 2008) (Robinson, 2003) (Truelsen et al., 2006). Dans leur méta-analyse de 43 études, Ayerbe et al, ont rapporté une prévalence totale de 29% durant les 10 années post-AVC (Ayerbe et al., 2013). Puis, une méta-analyse de 61 études par Hackett et Pickles a rapporté une fréquence de dépression stable de 31% à tout moment durant les cinq années suivant l'AVC, ce qui corrobore avec les résultats obtenus dans l'étude menée 10 ans plus tôt, qui avait déterminé une fréquence de 33% (Hackett and Anderson, 2005; Hackett and Pickles, 2014).

La PSD reste assez mal diagnostiquée, sous traitée et peu étudiée. Une des limites de la plupart des études est le manque de critères pour diagnostiquer de manière spécifique les différents troubles de l'humeur, faisant ainsi disparaître d'importantes variables cliniques. Une revue écrite par Robinson sur la compilation de données d'études cliniques avait fait part d'une prévalence de 19,3% pour les troubles dépressifs majeurs (MDD) et de 18,5% pour les troubles dépressifs mineurs (MnD) (Robinson, 2003). Plus récemment, une méta-analyse de 108 études sur les troubles de l'humeur observant 147 patients sur une durée de 2 jours à 7 ans après AVC a déterminé une prévalence de 33,5% tout troubles dépressifs confondus. Avec la MDD représentant 17,7%, la MnD 13.1%, et la dysthymie (trouble de l'huleur chronique modéré) 3,1%. Les troubles de l'adaptation étaient présent chez 6,9% des patients et les troubles de l'anxiété chez 9,8% (Mitchell et al., 2017).

Les études longitudinales ont offert des résultats contradictoires quant à l'évolution de la PSD au cours du temps. Si l'on en croit les méta-analyses de Ayerbe, et de Hackett et Pickles, le taux de prévalence reste stable durant la première année puis décline (Ayerbe et al., 2013) (Hackett and Pickles, 2014). Cependant, la revue de Werheid, basée sur 10 études longitudinales prospectives, a observé une évolution variant en fonction du temps : une augmentation des symptômes dépressifs durant les premiers 6 mois, une légère diminution environ 1 an après l'AVC et une nouvelle augmentation durant la deuxième année (Werheid, 2015).

La PSD est également un facteur de risque de récidive précoce de l'AVC : 8,15 ans chez des patients atteints de PSD contre 9,63–9,75 ans chez des patients sans PSD (Sibolt et al., 2013). Sans surprise, la PSD est aussi associée à l'augmentation du coût de l'hospitalisation après un AVC (Husaini et al., 2013).

L'augmentation de la mortalité est l'événement clinique le plus marquant chez les personnes souffrant de PSD. Une étude récente menée sur 10 ans chez une population de personnes ayant subi un AVC regroupées par tranche d'âge, a révélé un risque relatif (hazard ratio ou HR) de 1,56 dans la tranche 25 à 74 ans, et de 2,28 dans la tranche 65 à 74 ans (Razmara et al., 2017). L'augmentation de la mortalité chez les patients atteints de PSD pourrait résulter de dysfonctionnements cardiovasculaires, notamment des troubles du rythme cardiaque résultants de l'altération des fonctions autonomes (Robinson et al., 2008).

Les indicateurs les plus fréquemment mentionnés dans la littérature (parfois contradictoires) sont le genre féminin, les antécédents de PSD, les troubles physiques, l'anxiété, l'aphasie, la sévérité de l'AVC, les handicaps physiques et cognitifs, la dysphagie et les facteurs psychosociaux comme les événements antérieurs à l'AVC et le manque de support familial et social (De Ryck et al., 2014) (Hackett and Anderson, 2005; Kutlubaev and Hackett, 2014; Shi et al., 2017).

B- Hypothèses

La pathophysiologie de la PSD est complexe et multifactorielle. Elle est le résultat de la combinaison de dysfonctions neurologiques induites par l'ischémie et d'une détresse psychologique. En effet, les données actuelles établissent les facteurs neurobiologiques (plutôt que la réponse psychologique au handicap) comme principaux éléments à associer avec la PSD. Cette hétérogénéité pourrait s'expliquer par les différent sous-types de dépression (majeur, mineur), la survenue de la reperfusion (précoce, tardive), la zone cérébrale touchée (gauche, droite) (Wei et al., 2015) et les facteurs de causalité (Provinciali and Coccia, 2002).

De nombreux mécanismes pathogéniques ont été proposés concernant la PSD, notamment des processus semblables à ceux de la dépression primaire (Penninx et al., 2013)

Basée sur l'hypothèse monoaminergique de la dépression, la PSD pourrait être liée à l'interruption de la transmission aminergique des axones reliant le tronc cérébral au cortex à la suite de la lésion ischémique. Cette lésion entraînerait une diminution de la synthèse de 5-HT et de noradrénaline (Robinson et al., 1984) (Santos et al., 2009) (Terroni et al., 2011) (Narushima et al., 2003). Ce déséquilibre de la neurotransmission 5-HT est supporté par la présence de concentrations plus faibles de métabolites de la sérotonine (l'acide 5-hydroxy-indol-acétique) dans le LCS (Bryer et al., 1992) et par la régulation à la hausse des récepteurs 5-HT2A mesurée par PET (tomographie par émission de positrons) (Mayberg et al., 1988) (Moller et al., 2007). Cependant cette hypothèse monoaminergique seule n'est plus communément acceptée.

L'hypothèse de l'excitoxicité médiée par le glutamate (Sanacora et al., 2012) a été proposée du fait de l'augmentation transitoire du ratio glutamate+glutamine/créatinine dans les régions préfrontales de l'hémisphère contralatéral qui disparaît après 4 mois (Glodzik-Sobanska et al., 2006). De plus, le risque de développement d'une PSD à 3 mois a également été mis en corrélation avec de hauts niveaux plasmatiques de glutamate et une faible concentration de « glutamate oxalacetate transaminase » (GOT) pendant l'AVC (Cheng et al., 2014).

La PSD pourrait être liée à des facteurs vasculaires, tels que les lésions de la matière blanche (observées par IRM) qui pourraient affecter les projections monoaminergiques entre le cerveau moyen et le tronc cérébral. Cette hypothèse rejoint celle de la "dépression vasculaire" tardive (Naarding and Beekman, 2011) (Provinciali and Coccia, 2002) (Taylor et al., 2013).

Une autre hypothèse d'intérêt grandissant est l'implication du métabolisme mitochondrial (Klinedinst and Regenold, 2015). Une étude (Renshaw et al., 2001) indique que l'utilisation de molécules augmentant la disponibilité de l'ATP a des effets antidépresseurs. De plus, des déficiences mitochondriales ont été observées chez un modèle animal de dépression (CMS ou Chronic Mild Stress, qui consiste à infliger aux animaux un stress chronique pendant plusieurs semaines) (Bansal and Kuhad, 2016) (Ferrari and Villa, 2017) (Gardner and Boles, 2011) (Rezin et al., 2009).

Certaines recherches suggèrent également un rôle de l'inflammation. Les cytokines relarguées lors de la réponse pro-inflammatoire sont impliquées à la fois dans l'AVC aigu

(Ferrarese et al., 1999) (Ferrari et al., 2016) (Spalletta et al., 2006), et dans la dépression (Ferrari and Villa, 2017). Ces cytokines pourraient avoir un rôle dans le développement de la PSD (Spalletta et al., 2013) (Li et al., 2014b). Cette hypothèse est appuyée par le fait que l'activation microgliale serait impliquée dans le développement de la PSD (Jawaid et al., 2016). Cependant, une revue de 37 études souligne la controverse de l'association entre les cytokines et le développement de la PSD (Pietra Pedroso et al., 2016). S'il venait à s'avérer que les cytokines sont réellement impliquées dans le développement de la PSD, elles pourraient interagir à de nombreux niveaux : le métabolisme des neurotransmetteurs (métabolisation du Tryptophane en Kynurénine et non plus en sérotonine) (Maes et al., 2011), la fonction endocrine (altération de l'axe hypothalamo-hypophyso-surrénalien) (Szczudlik et al., 2004) (Barugh et al., 2014) ou encore la plasticité synaptique.

L'altération de la plasticité neuronale est également considérée comme une hypothèse. Il existe de nombreuses preuves reliant la neurogenèse hippocampique, la ramification axonale, la dendritogenèse et la synaptogenèse au stress chronique, aux troubles affectifs et à l'activité antidépressive, tout particulièrement dans la PSD (Ferrari and Villa, 2017) (Masi and Brovedani, 2011). Par exemple, en réponse à l'ischémie focale, la neurogenèse spontanée observée dans le gyrus dentelé de l'hippocampe est altérée chez des rats exposés à un stress chronique léger (Wang et al., 2008).

Le BDNF joue un rôle crucial dans la PSD, et l'utilisation d'antidépresseurs chez des patients atteints ramène la neurogenèse au même niveau que celle des patients n'ayant pas subi d'AVC (Ferrari and Villa, 2017). Plusieurs études ont révélé une diminution du taux de BDNF chez les patients déprimés, qui est rétabli par un traitement antidépresseur (Molendijk et al., 2014)**.** Yang et ses collaborateurs ont démontré qu'une concentration sérique de BDNF inférieure à 5,86 ng/ml le premier jour après l'AVC était associée à la PSD (Yang et al., 2011). Dans le même cadre, une autre étude a montré une corrélation négative entre les niveaux de BDNF et la gravité de l'AVC (définie selon le score de l'échelle NIHSS (National Institutes of Health Stroke Scale)). Le taux de BDNF sérique est plus faible chez les patients souffrant de dépression à l'admission en service d'urgences, et d'autre part le risque de développer une PSD à 3 mois est 11,5 fois plus élevé pour des taux de BDNF inférieurs à 10,2 ng/ml (Li et al., 2014a).

Chez l'animal, il y a également une diminution du taux de BDNF dans l'hippocampe des rongeurs ayant subi un AVC et soumis à un stress chronique pour induire un état dépressif

(O'Keefe et al., 2014) (Zhang et al., 2012). La surexpression du BDNF permet d'atténuer le comportement dépressif (Chen et al., 2015b).

C- Thérapies - Plasticité synaptique

Les patients victimes d'un AVC présentent généralement une récupération spontanée durant la phase sub-aiguë. Cette amélioration des résultats fonctionnels semble correspondre à la « réparation » partielle des réseaux neuronaux survivants, et au recrutement de synapses intactes (Alia et al., 2017) (Askim et al., 2010) (Cramer, 2008) (Harrison et al., 2013).

Le cerveau est très plastique au cours du développement. De nouvelles connexions sont formées et éliminées par des processus dépendants de leur utilisation. Ainsi, l'expérience environnementale au cours de cette période peut avoir une incidence marquée sur les propriétés et les fonctions subséquentes du cerveau adulte. Par exemple, des études ont montré qu'une privation visuelle pendant une " période critique " du début de la vie modifie de façon permanente les propriétés physiologiques des neurones du cortex visuel (Hubel and Wiesel, 1970) (Mataga et al., 2002).
La réorganisation cérébrale après une lésion ou un AVC peut être comparée à celle qui se produit pendant le développement normal. Par exemple, le rétablissement du comportement alimentaire après des lésions bilatérales de l'hypothalamus latéral suit les quatre processus distincts qui caractérisent également le développement du comportement alimentaire chez les jeunes rats (Teitelbaum et al., 1969). De même, un parallèle entre la récupération motrice après un AVC et l'acquisition d'habiletés motrices chez les nourrissons humains a été établi (Cramer and Chopp, 2000).
Les connaissances fondées sur cette analogie pourraient avoir un impact crucial sur le rétablissement des personnes touchées par un AVC. Cependant, il est important de prendre en compte que les circuits neuronaux de patients avec « facteurs aggravants », comme l'âge ou l'hypertension, sont probablement moins réceptifs au remodelage neuronal que ceux d'un cerveau en développement. Cette anomalie est très certainement due à une microvascularisation altérée, une inflammation chronique ou tout autre processus entravant la plasticité.

Des études sur l'animal indiquent que de nombreux gènes et protéines importants pour la croissance neuronale, la synaptogenèse et la prolifération des épines dendritiques sont exprimés

à leur niveau le plus élevé au cours du développement précoce du cerveau puis diminuent sensiblement avec le vieillissement (Hattiangady et al., 2005). Ces gènes sont régulés à la hausse après un AVC (Carmichael et al., 2005) (Carmichael, 2006) (Cramer, 2000). Cette variation d'expression crée une période critique pour la neuroplasticité à la suite de l'AVC. Les répercussions sur le rétablissement fonctionnel sont énormes, car les délais d'amorce d'une thérapie de récupération après un AVC varient considérablement et, pour de nombreux patients, le traitement est appliqué en dehors de cette période cruciale. Dans une expérience importante, des rats ont été soumis à une thérapie de récupération qui a débuté 5, 14 ou 30 jours après l'occlusion de l'artère cérébrale moyenne. Les animaux ayant reçu un traitement précoce ou semi-précoce (5 ou 14 jours après l'AVC) se sont rétablis de façon significative, tandis que les rats ayant reçu un traitement tardif (30 jours après l'AVC) ont montré peu d'amélioration (Biernaskie et al., 2004). Le traitement précoce a également augmenté le nombre de ramifications dendritiques des neurones corticaux de la couche V, alors que celui entamé 30 jours après l'AVC n'a eu aucun effet sur les ramifications. Associés aux résultats cliniques (Horn et al., 2005) (Salter et al., 2006), ces données fournissent des preuves solides concernant l'existence d'une période critique après l'AVC, au cours de laquelle le cerveau est le plus réceptif à la réadaptation, et suggèrent que le traitement appliqué de façon précoce est le plus bénéfique.

Bien que l'entraînement précoce soit plus efficace, de nombreux patients d'AVC continuent de s'améliorer longtemps après leur lésion initiale en raison d'une récupération spontanée, d'une réadaptation à domicile ou à la suite d'une thérapie par mouvement contraint. Cela indique que la fenêtre temporelle de la réadaptation post-AVC, comme celle de l'apprentissage normal, ne se ferme jamais vraiment. Cependant, les processus plastiques qui caractérisent le développement précoce du cerveau et la phase semi-aiguë après l'AVC diminuent et ralentissent avec le temps. Un défi important consisterait à trouver des moyens d'élargir cette fenêtre et de la garder ouverte plus longtemps afin d'optimiser la récupération post-AVC. Par exemple, l'hydrolyse des protéoglycanes sulfates chondroïtines extracellulaires (il s'agit de composants jouant un rôle important dans le développement neuronal et la formation de cicatrices gliales, et dont l'augmentation provoquée par une lésion cérébrale inhibe la croissance axonale (Siebert et al., 2014)) entraîne une réouverture de la fenêtre de plasticité du système visuel chez les animaux adultes (Pizzorusso et al., 2006) et favorise le rétablissement à la suite d'une lésion de

la moelle épinière (Silver and Miller, 2004) (Massey et al., 2006). On ne sait cependant pas si ces facteurs pourraient avoir un effet sur la récupération après un AVC.

De nombreuses recherches ont également été conduites sur l'utilisation d'antidépresseurs pour traiter la PSD. Cependant, très peu d'études portent sur des essais contrôlés et randomisés, et utilisent des critères normalisés pour le diagnostic de la dépression, ce qui pourrait expliquer des résultats parfois contradictoires (Lipsey et al., 1984) (Robinson et al., 2000) (Wiart et al., 2000). Néanmoins, ces études ont permis d'établir que la PSD répondait bien à l'utilisation d'antidépresseurs tels que les TCA (Tricyclic Antidepressant) ou les SSRI (Selective Serotonine Reuptake Inhibitor). Les antidépresseurs utilisés étaient la fluoxétine (Prozac), la nortriptyline et le citalopram.

La fluoxétine, un puissant inhibiteur du CYP2D6 (un type de cytochrome P450, impliqués dans le métabolisme de nombreuses molécules médicamenteuses) interagit avec plusieurs médicaments cardiaques, et la nortriptyline augmente le risque de délire. Il faut donc faire preuve de prudence dans la posologie en fonction des patients (DeVane and Markowitz, 2000) (Fullerton and Agerhom, 1984). En comparaison, l'Escitalopram est considéré comme un antidépresseur sûr et efficace. Certaines données indiquent que le taux de récupération chez les patients traités avec des psychotropes est de 65 % contre 40 % chez les patients traités avec un placebo (Starkstein et al., 2008). Une méta-analyse récente a confirmé que les antidépresseurs étaient plus efficaces que le placebo pour réduire les symptômes dépressifs chez les patients atteints de PSD (Xu et al., 2016).

En France, une étude menée sur 113 patients durant trois mois a également démontré l'intérêt d'un traitement précoce (5 à 10 jours après l'AVC) avec de la fluoxétine dans la récupération post-AVC. Elle a cependant de nouveau souligné les effets secondaires engendrés par le traitement antidépressif (comme les troubles digestifs ou les crises épileptiques). Cette étude démontre la nécessité d'utiliser des antidépresseurs n'ayant pas d'effets secondaires.

III- Thérapies actuelles

A- AVC ischémique

Lors d'un AVC ischémique, c'est l'apparition d'un caillot qui est à l'origine de la perte d'afflux sanguin dans le cerveau. Le traitement employé est l'administration intraveineuse d'activateur tissulaire du plasminogène, comme l'alteplase (rtPA). Toutefois ce traitement doit être administré dans les 4 à 5h qui suivent le trauma. Il a pour but de dissoudre le caillot et rétablir dès que possible la circulation dans la zone ischémiée (Emberson et al., 2014**).** Sa principale limite est que cette méthode n'est applicable que chez 10% des patients. Si elle est utilisée dans la fenêtre de temps adaptée, elle permet de diminuer d'environ 30% le risque de handicap chez le patient. Il s'agit là du seul traitement médicamenteux utilisable et autorisé. Il a cependant des limites, notamment il peut entraîner des hémorragies sévères.

Une autre approche, chirurgicale cette fois et qui peut s'ajouter à l'administration d'alteplase, est la thrombectomie endovasculaire. Elle consiste en le retrait du caillot par voie endovasculaire. Si l'opération est effectuée durant les 6h suivant l'AVC, elle double les chances de reperfusion à 24h, et augmente la récupération fonctionnelle à 90 jours (Badhiwala et al., 2015). Cette approche récente n'est cependant pas encore totalement démocratisée. De plus, elle nécessite des équipements spécialisés et la mise en place de procédures particulières pour la sélection des patients éligibles, notamment que la zone de l'infarctus soit accessible. De ce fait, ce protocole n'est applicable qu'à seulement 10% des patients (Goyal et al., 2016).

En plus de ces protocoles curatifs il existe deux protocoles préventifs lorsque les artères sont fragilisées par de l'athérosclérose : l'endatériectomie de la carotide, qui consiste en l'élimination des résidus d'athérome sur paroi de l'artère touchée, et l'angioplastie, qui consiste à placer un ballonnet dans l'artère pour rétablir le flux le plus proche possible de la normale. Ces deux interventions nécessitent que l'AVC soit sous contrôle et ne peuvent servir de traitements curatifs.

B- AVC hémorragique

En cas d'AVC hémorragique, donc de rupture de vaisseau, la première étape est de faire baisser la pression sanguine pour limiter la propagation de l'hémorragie, mais ce n'est pas sans danger pour tous les patients (Tsivgoulis et al., 2014). Si l'hémorragie n'est pas liée à la prise d'antithrombique, l'administration de facteur recombinant d'activation VII (rFVIIa), comme l'eptacog alfa, atténue la croissance des hématomes en stimulant les processus de coagulation sanguine, mais augmente le risque d'accidents thromboemboliques ce qui est, évidemment, plus délétère pour les patients (Yuan et al., 2010).

Si, au contraire, l'hémorragie est due à un traitement anticoagulant, c'est l'utilisation d'agents hémostatiques comme le concentré de complexe de la photothrombine qui permet une réduction de l'expansion de l'hématome (Steiner et al., 2016).

A noter que la transfusion de plaquettes après hémorragie intracérébrale liée à l'utilisation de traitements antiplaquettaires entraîne une augmentation de la dépendance à 3 mois post-AVC et voire augmente la mortalité à ce même stade (Baharoglu et al., 2016).

Le drainage par cathéter, peu invasif, est également une technique prometteuse dans le traitement des hématomes profonds (Mould et al., 2013). Il réduit la mortalité mais n'a pas d'effet sur la dépendance fonctionnelle en cas d'hémorragie intraventriculaire et d'hydrocéphalie (Ziai et al., 2014).

Comme on le voit les traitements contre les AVC, et leurs conséquences, sont peu nombreux et ne sont pas applicables à tous les patients. Cela démontre la nécessité impérieuse de mettre au point de nouveaux protocoles de soin de cette pathologie.

Il est cependant important de noter que la mise en place d'Unités Mobiles Neurovasculaires a permis une diminution du temps de prise en charge des patients, et ainsi entraîné une augmentation du nombre de personnes pouvant être traitées dans les premières heures suivant l'AVC (Walter et al., 2010) (Walter et al., 2012).

C- Dépression

Les traitements de la dépression se divisent en deux groupes, la psychothérapie et la pharmacothérapie.

La psychothérapie est organisée selon plusieurs approches (la thérapie cognitivo-comportementale, la thérapie psychodynamique, la thérapie interpersonnelle, la thérapie de la pleine conscience,…), mais si son efficacité a été largement prouvée, il n'existe aucune donnée indiquant que les résultats obtenus chez les patients varient en fonction de l'approche choisie (Luborsky and Singer, 1975). Une des hypothèses pour expliquer cela est que les bases de ces différentes approches sont les mêmes : un encadrement bienveillant, positif et à l'écoute (Martin et al., 2000), et la présence du psychothérapeute (Kim et al., 2006). La psychothérapie seule n'est conseillée qu'en cas de syndrome dépressif léger ou modéré (National Institute for Health and Care Excellence. Depression in adults: recognition and management. *NICE* https://www.nice.org.uk/guidance/cg90 (2018).) (Otte et al., 2016) et ne peut excéder deux semaines. Si elle n'est pas suffisante pour permettre la récupération du patient elle doit être remplacée, ou complétée, par de la pharmacothérapie (Harter et al., 2010)**.**

La principale hypothèse sur laquelle se base le développement de traitements pharmacologiques contre la dépression est l'hypothèse monoaminergique, qui postule que la dépression a pour origine un déséquilibre en monoamines (McHenry, 2006). L'optique de ces traitements est d'augmenter la quantité de monoamines dans la fente synaptique, par inhibition de leur recapture, ou de leur dégradation. Il existe pour cela trois classes d'antidépresseurs : les SSRI (inhibiteurs sélectifs de la recapture de la sérotonine) et NSRI (inhibiteurs de la recapture de la noradrénaline et de la sérotonine), les TCA (tricycliques) et les IMAO (inhibiteurs de la monoamine oxydase). Les TCA, SSRI et NSRI empêchent la recapture des monoamines par le neurone présynaptique en antagonisant leurs transporteurs, et les IMAO, comme leur nom l'indique, inhibent la mono amine oxydase, enzyme responsable de la dégradation des monoamines (Otte et al., 2016) (**Figure 5)**.

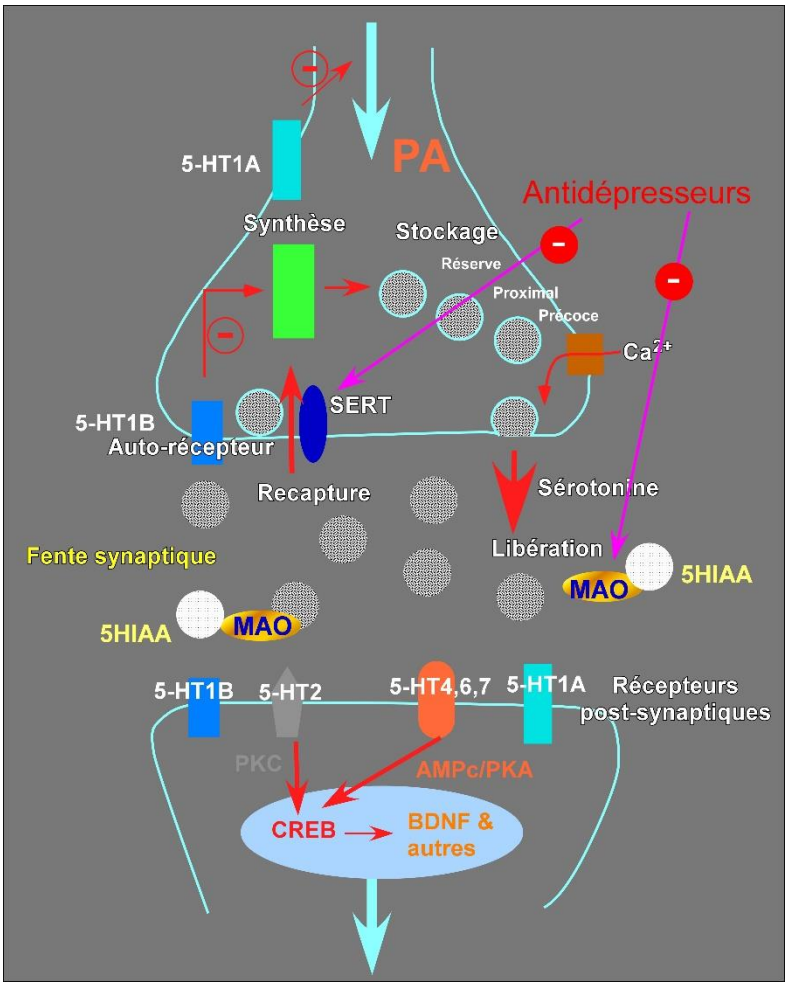

Figure 5 : les voies de la sérotonine

Cette hypothèse monoaminergique est cependant grandement qualifiée de simpliste, et insuffisante pour la compréhension de la dépression. Les antidépresseurs sont des molécules dont les effets ne sont visibles qu'après plusieurs semaines alors que leurs actions sur les monoamines sont immédiates. De plus, des études ont également montré que l'utilisation de molécules entraînant une diminution des monoamines n'avait pas d'effet sur l'humeur de patients sains (Krishnan and Nestler, 2008) (Hirschfeld, 2000). L'hypothèse serait que ce sont les changements dans l'expression génique induits par l'utilisation de ces antidépresseurs qui pourraient être réellement à l'origine des effets observés (Wong and Licinio, 2001). Ces molécules ont malheureusement de nombreux effets secondaires comme des nausées ou une fatigue importante pour les plus bénins, ou des tendances suicidaires et des troubles cardiaques pour les plus sévères. Cela pousse 7 à 15% des patients à arrêter leur traitement (Locher et al., 2017). Elles n'ont pas non plus une efficacité totale puisque la proportion de patients répondant

positivement aux traitements est inférieure à 50% (Rush et al., 2006) (Fava and Davidson, 1996).

C'est la raison pour laquelle au cours de ces deux dernières décennies, de nombreux efforts ont été déployés pour mettre au point des antidépresseurs non basés sur l'hypothèse monoaminergique, dépourvus d'effets secondaires, et de délais d'action plus courts. Par exemple, en prônant l'utilisation des antagonistes de la neurokinine 1 (Ratti et al., 2013), des modulateurs du système glutamatergique (Sanacora et al., 2008), des stimulant de la neurogenèse hippocampique (Fava et al., 2016) ou des antiglucocorticoïdes (Gallagher et al., 2015). Aujourd'hui la Kétamine (antagoniste des récepteurs NMDA) et la Spadine (inhibiteur des canaux TREK-1), sont les seules molécules dont les effets, rapidement observables, passent par des voies différentes. Elles pourraient offrir une alternative aux traitements classiques et éventuellement soulager les patients atteints de « dépression résistante » (sur laquelle les antidépresseurs classiques n'ont pas d'effet) (Pham and Gardier, 2019). La Kétamine et la Spadine ne sont pas au même point de développement : phase III pour la Kétamine et phase préclinique pour la Spadine. La Kétamine a également des effets secondaires très importants comme la déréalisation et la dépersonnalisation (Palucha-Poniewiera, 2018)**.** Les effets antidépresseurs de la Spadine seront détaillés au chapitre V.

IV- TREK-1

A-Généralités

TREK-1, pour "TWIK-related K+ channel-1", qui a été le premier canal K_{2P} cloné, et avec lequel TREK-1 partage 28% d'homologie (Lesage et al., 1996)**,** fait partie de la grande famille des canaux K_{2P} (ou canaux potassiques à deux domaines P) qui regroupe 15 membres, eux-mêmes réunis en 6 sous-familles **(Figure 6)**. Il s'agit de la classe de canaux potassiques la plus récemment découverte. Ils sont constitués d'un tandem de 4 segments transmembranaires (S1-

S4) contenant deux pores (P1 and P2), selon la séquence S1-P1-S2-S3-P2-S4. Leurs extrémités N- et C-terminales sont cytosoliques. Ces canaux sont modulés par différents stimuli tels que la température, le pH ou l'étirement membranaire (Cohen et al., 2009) (Franks and Honore, 2004) (Patel and Honore, 2001) (Maingret et al., 1999). Les sous-familles sont classées en fonction de leurs réponses à ces différents stimuli (Gonzalez et al., 2012) **(Figure 5).** Tout comme les autres membres de cette famille, le canal TREK-1 est responsable du maintien du potentiel de repos des neurones, et du contrôle de la durée du potentiel d'action. Les canaux K_{2P} participent également à la sécrétion de neurotransmetteurs.

TREK-1 est, avec TREK-2 et TRAAK (les deux autres membres de la même sous-famille), un canal K_{2P} mécano- et thermo-sensible (Honore, 2007). Tous trois sont ouverts par l'étirement de la membrane et par le gonflement cellulaire.

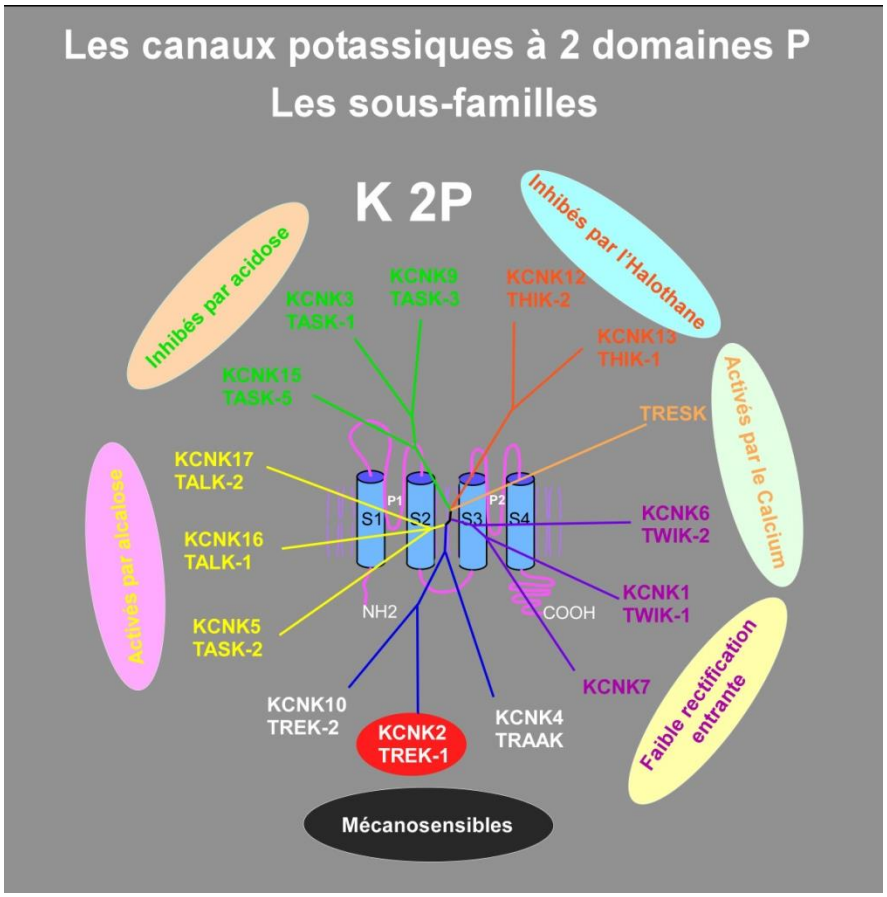

Figure 6 : La famille des K_{2P}

Les souris TREK-$1^{-/-}$, TREK-$2^{-/-}$ et TRAAK$^{-/-}$ sont hypersensibles à la force mécanique, expriment une allodynie mécanique et sont hyperalgésiques à la suite d'un processus

inflammatoire (Brohawn, 2015). Il a été démontré que la force mécanique est directement transmise à TREK-1 et TRAAK au travers de la membrane lipidique (Brohawn et al., 2014). Ces canaux s'ouvrent ainsi rapidement en réponse à une tension avec un seuil d'activation bas et une importante gamme de tension d'activation (Brohawn, 2015) (Buckler and Honore, 2005) (Chemin et al., 2005).

TREK-1 est très exprimé dans le cerveau, particulièrement dans des régions telles que les bulbes olfactifs, l'hippocampe, le cervelet ou le cortex. Ce canal est également très exprimé dans les tissus périphériques comme les poumons, les reins, le cœur et les muscles squelettiques (Fink et al., 1996).

B- Régulation

Comme indiqué plus haut, TREK-1 est régulé par une série de stimuli physiques et chimiques. Par exemple, dans des cellules COS transfectées (ou dans des oocytes de Xénopes), en configuration cellule attachée ou en configuration « inside-out », TREK-1 est ouvert par l'étirement mécanique (Patel et al., 1998b; Patel et al., 1998a)**.** Cette ouverture peut avoir lieu à des potentiels positifs ou négatifs de manière indifférente. En revanche, lorsque l'organisation du cytosquelette est perturbée par des colchicines ou de la cytochalasine D, l'activation de TREK-1 par étirement disparaît (Patel et al., 1998b) (Maingret et al., 1999)**.**

TREK-1 est également sensible aux variations de température. En effet, la chaleur active TREK-1 de façon graduelle et réversible, avec un pic à 37°C, alors que des températures approchant les 12° C abolissent son courant basal, cela fait de TREK-1 un senseur de la douleur par le froid (Maingret et al., 2000)**.** A noter que dans la configuration patch excisé cette activation par la température disparaît, démontrant que l'activation de TREK-1 par la chaleur nécessite les composants cytosoliques (Maingret et al., 2000)**.**

TREK-1 est également activé par les lipides (Kim, 2003) (Patel and Honore, 2001) comme les acides gras polyinsaturés (AGPI) tels que l'acide arachidonique (AA) (Patel et al., 1998b; Patel et al., 1998a). L'AA active TREK-1 de manière dose dépendante et requiert l'extrémité C-terminale du canal, laquelle est nécessaire pour l'inhibition induite par phosphorylation par la protéine kinase A (PKA).

Le Phosphatidylinositol bisphosphate (PIP_2), en configuration « inside-out », stimule le courant striatal natif de TREK-1 (Chemin et al., 2005)**.** Parallèlement sur les oocytes de Xénopes son hydrolyse inhibe le canal TREK-1 en modifiant sa dépendance au voltage (Lopes et al., 2005).

Une acidose cytosolique active TREK-1 en agissant sur son extrémité C-terminale (Maingret et al., 1999) (Honore et al., 2002)**.**

L'activité de TREK-1 est diminuée par la stimulation de récepteurs couplés aux protéines Gs- and Gq, de récepteurs de la 5-HT (5-HT4) (Fink et al., 1996) (Patel et al., 1998b) ou celle de récepteurs du glutamate (mGluR1 et mGluR5 (Chemin et al., 2003) (Lopes et al., 2005) ainsi que mGluR2 et mGluR3 (Moha Ou Maati et al., 2014)) **(Figure 7).**

Enfin, les SSRI tels que la fluoxétine (Kennard et al., 2005) (Heurteaux et al., 2006b) ou, beaucoup plus spécifiquement, la Spadine (Mazella et al., 2010)**, s**ont des inhibiteurs de TREK-1 **(Figure 7)**. Les effets de la Spadine et de ses dérivés seront discutés au chapitre V.

L'ouverture pharmacologique de ce canal est aussi médiée par des anesthésiques volatils (Patel et al., 1999)**.** L'ouverture des canaux potassiques est responsable de leur action anesthésique (Heurteaux et al., 2004)**.** Les analgésiques tels que la morphine, par l'activation des récepteurs aux opoïdes (Devilliers et al., 2013), sont également capables d'activer le canal TREK-1, confirmant son implication dans les phénomènes de douleur.

1- Hétérodimérisation

Les canaux K_{2P} ne sont fonctionnels que sous forme dimérisée. Cela est dû au fait qu'il faille quatre domaines P pour former un pore. Il s'agit la plupart du temps d'homodimères (les mêmes sous-unités), mais les hétérodimères existent aussi dans certaines sous-familles.

Des études récentes ont rapporté que des hétérodimères fonctionnels de TREK-1 peuvent se former avec TREK-2 et TRAAK, les deux autres membres de la sous famille TREK (Blin et al., 2016) (Levitz et al., 2016)**.** Bien que TREK-1 et TREK-2 présentent une homologie de 78% (Lesage and Lazdunski, 2000)**,** ils ne sont pas régulés de la même façon. Ainsi, l'hétérodimère TREK-1/TREK-2 partage des propriétés des deux sous-unités, par exemple son activité est minimale à pH physiologique, alors que le complexe est actif aussi bien dans environnement alcalin qu'acide. Il en est de même pour l'hétérodimère TREK-1/TRAAK (Levitz et al., 2016)**.** Cependant, ce complexe a des propriétés biophysiques uniques et est régulé de façon différente. En effet, si TREK-1 est inhibé à la fois par la PKA et la PKC, seule la PKA est capable d'inhiber TREK/TRAAK (Blin et al., 2016)**.** Cette hétérodimérisation de la sous-famille TREK augmente la diversité fonctionnelle des canaux K_{2P} et offre ainsi la possibilité de réguler leur activité de manière beaucoup plus fine.

2- Protéines partenaires

Une protéine d'architecture (scaffold protein) AKAP150 (pour A-kinase anchoring protein) a été identifiée grâce à une approche protéomique basée sur de l'immunoprécipitation et de l'analyse par spéctrométrie de masse des complexes obtenus (Sandoz et al., 2006). AKAP150 se fixe à la sous-unité régulatrice de la PKA quand elle est à proximité de ses substrats. AKAP150 s'assemble en complexes de signalisation à l'intérieur des neurones avec PKA, PKC, PP2B (protéine phosphatase 2B), PSD-95, SAP97 et plusieurs canaux ioniques (Esseltine and Scott, 2013). Quand AKAP150 se fixe au niveau de sa région post-M4, TREK-1 devient un canal de fuite actif, insensible à l'acidification interne, à l'AA, ou à l'étirement mécanique (Sandoz et al., 2006).

Mtap2 (Microtubule-associated protein 2), dont le rôle est de stabiliser les microtubules en s'y liant, est également un partenaire de TREK-1 dans le cerveau (Sandoz et al., 2008). Cette protéine colocalise avec TREK-1 dans de nombreuses régions cérébrales telles que l'hippocampe, le cervelet, le bulbe olfactif, le striatum et le cortex. Tout comme AKAP150, la fixation de Mtap2 à TREK-1 augmente son activité (Sandoz et al., 2008). En revanche cette augmentation de l'amplitude du courant de TREK-1 n'est pas due à son interaction directe avec Mtap2 mais résulte de l'augmentation de ses niveaux d'expression à la membrane plasmique. En effet, à l'intérieur du neurone les complexes de signalisation formés par TREK-1, AKAP150 et Mtap2 permettent de réguler l'activité de TREK-1 et son trafic à la membrane plasmique au niveau des terminaisons post-synaptiques.

Il a aussi été possible de constater une interaction directe entre β-COP et TREK-1 (Kim et al., 2010). β-COP est une sous unité du « Coat Protein Complex I » (COPI) dont le rôle est de former des vésicules enrobées et de gérer le trafic rétrograde du Golgi vers le réticulum endoplasmique (RE) ou entre différents compartiments à l'intérieur du Golgi lui-même (Gomez-Navarro and Miller, 2016). La déplétion de β-COP entraîne une diminution du canal chlorure « cystic fibrosis transmembrane conductance regulator » (CFTR), dont les mutations provoquent des fibroses kystiques dans les poumons (Rennolds et al., 2008). β-COP augmente l'expression de TREK-1 à la surface cellulaire. Le transport de TREK-1 est direct et passe par une interaction avec sa région N-terminale.

La protéine partenaire de TREK-1 la plus récemment découverte est la Sortiline, ou encore appelée récepteur à la Neurotensine 3 ($NTSR_3$) (Mazella et al., 2010). La Sortiline est synthétisée sous la forme d'un précurseur appelé Pro-sortiline qui est clivé dans le trans-Golgi

par la Furine pour donner la Sortiline mature (**Figure 10)**. Ce clivage relargue un peptide de 44 acides aminés appelé Propeptide (PE). $NTSR_3$ se compose d'un imposant domaine luminal, d'un seul segment transmembranaire et d'une courte extrémité C-terminale. La quantité de $NTSR_3$ à la membrane ne dépasse pas les 10%, ce récepteur étant majoritairement exprimé de façon intracellulaire et grandement impliqué dans le trafic intracellulaire. $NTSR_3$ et TREK-1 sont tous deux fortement exprimés dans les zones cérébrales qui contrôlent les émotions comme les cortex préfrontal (CPF) et cingulaire, ainsi que dans l'amygdale, l'hippocampe, le noyau accumbens, le noyau raphé dorsal et l'hypothalamus.

3- Pharmacologie

Depuis la découverte de l'implication de TREK-1 dans de nombreuses pathologies du Système Nerveux Central (SNC), l'intérêt porté à la recherche de molécules modulatrices de son activité a considérablement augmenté. En effet, TREK-1 est impliqué dans la dépression (Chen et al., 2015a) (Heurteaux et al., 2006b), l'ischémie (Wang et al., 2012), la perception de la douleur (Han et al., 2016) (Alloui et al., 2006) ou encore la dépression post AVC (Lin et al., 2015).
De nombreux antagonistes (**Figure 7**), et de beaucoup moins nombreux agonistes (**Figure 8)** de TREK-1 ont été identifiés et développés.

a- Antagonistes de TREK-1

La recherche de bloqueurs de l'activité de TREK-1 a commencé avec la découverte de son rôle dans les processus de dépression. En effet, les souches murines avec une mutation du gène *kncnk2*, codant pour TREK-1, manifestent un phénotype de résistance face au développement de la dépression (Heurteaux et al., 2006b).
La Spadine est la première molécule développée dans le seul but de bloquer TREK-1 et ainsi reproduire ce phénotype de résistance observé chez les souris *kncnk2*$^{-/-}$ (Mazella et al., 2010). Il s'agit d'un peptide dessiné à partir du PE, lui-même issu de la maturation post-traductionnelle de la Sortiline par la Furine. De nombreux analogues de la Spadine ont été conçus depuis afin d'en améliorer son activité antidépressive et sa stabilité *in vivo* (Veyssiere et al., 2015) (Article 1). La Spadine et ses analogues seront détaillés au chapitre V et chapitre 1 des résultats.

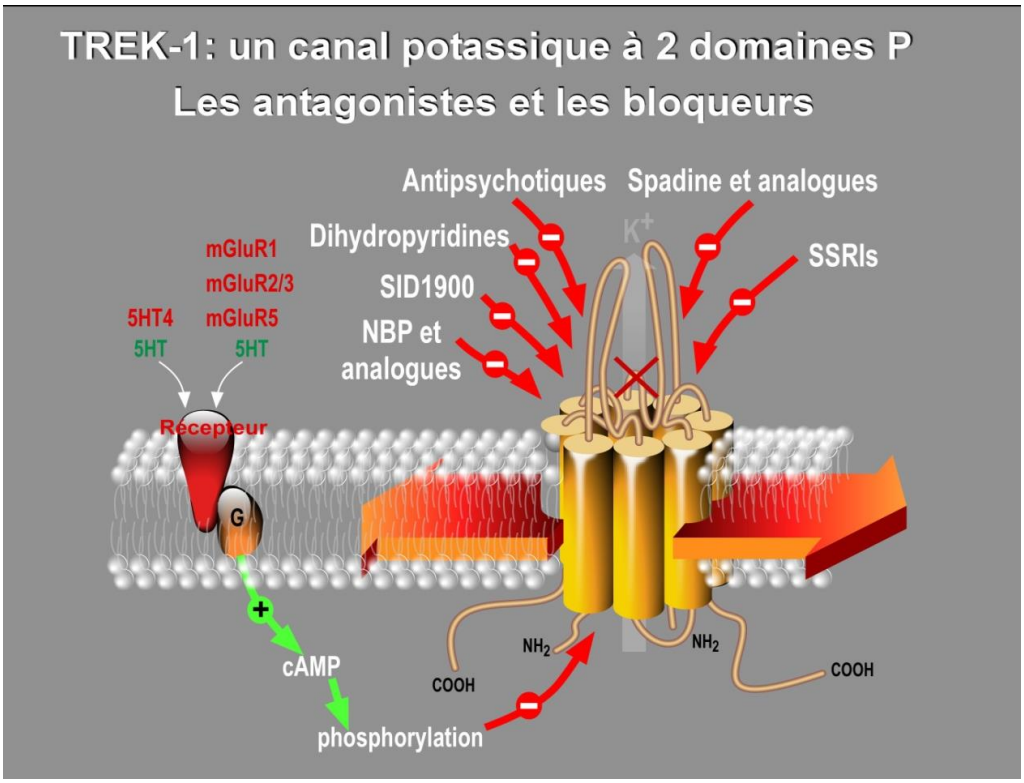

Figure 7 : Les antagonistes et les bloqueurs de TREK-1

Les antidépresseurs les plus utilisés comme les inhibiteurs spécifiques de la recapture de la Sérotonine (SSRI) sont également des inhibiteurs de l'activité de TREK-1. En concentrations cliniques, les SSRIs comme la Fluoxétine, la Norfluoxétine, la Paroxétine, le Citalopram ou l'Escitalopram bloquent l'activité de TREK-1 de manière plus ou moins spécifique et efficace, IC_{50}=19µM et IC_{50}=9µM pour la Fluoxétine et la Norfluoxétine par exemple (Kennard et al., 2005). Les SSRI ne sont pas spécifiques, et ciblent également TREK-2, Nav1.5 et les canaux Ca^{2+} de type L (Wong et al., 2005) (Poulin et al., 2014) (McClenaghan et al., 2016).

Les antipsychotiques utilisés pour le traitement de psychoses telles que la schizophrénie et le trouble bipolaire, (par exemple la fluphenazine, la chlorpromazine ou le pimozide), sont eux aussi de puissants bloqueurs de TREK-1 (avec des IC_{50} de 4.7 ± 1.6 µM, 2.7 ± 0.3 µM, *et* 1.8 ± 0.3 µM, respectivement). Cependant, bien que sans effet saur TRAAK, ils antagonisent également TREK-2 (Thummler et al., 2007).

Des Dihydropyridines telles que l'Amlodipine ou la Niguldipine, qui sont des bloqueurs de canaux Ca^{2+} de type L (souvent utilisés comme antihypertenseurs), bloquent aussi TREK-1 avec une bonne affinité (IC_{50}=0.43µM pour l'Amlodipine et 0.75µM pour la Niguldipine). Les souris mutantes n'exprimant pas le canal de type L Cav1.3 manifestent un phénotype de

résistance à la dépression (Busquet et al., 2010), démontrant son implication dans le processus de dépression.

Le composé SID1900 qui bloque TREK-1 avec une IC_{50}~30µM a démontré des propriétés antidépressives dans un modèle de « chronic unpredictable mild stress » (CUMS) sur rat (Ye et al., 2015). Son effet est comparable à celui de la Spadine, cependant il n'y a aucune preuve que le SID1900 n'agisse pas sur d'autres cibles, et des données manquent pour pouvoir tirer des conclusions, quant à sa spécificité.

Enfin, d'autres molécules ont été rapportées comme bloquant TREK-1, comme par exemple le NBP et son analogue, lig4-4 (Ji et al., 2011) (Wang et al., 2018). Cependant, s'il n'y a aucune information concernant la spécificité de NBP, il est confirmé que lig4-4 modifie les courants de type hERG (un des canaux potassiques responsables de troubles graves au niveau cardiaque comme la mort subite), des canaux K^+ voltage-dépendants (K_v), et des canaux neuronaux Na^+ et Ca^{2+}, ce qui est assurément une limite à son développement thérapeutique.

b- Agonistes de TREK-1

Le canal TREK-1 est activé par les anesthésiques volatils tels que le chloroforme, le diethyl ether, l'halothane ou l'isoflurane. Sa partie C-terminale joue un rôle crucial dans cette activation (Patel et al., 1999). En revanche, les anesthésiques locaux tels que la bupivacaïne (anesthésique local actuel le plus utilisé) se comportent eux comme des inhibiteurs de TREK-1 (IC_{50} = 41 µM) (Kindler et al., 1999).

L'AA et d'autres AGPI (Acides Gras PolyInsaturé) ouvrent le canal TREK-1 de façon dose-dépendante (Patel et al., 1998b). Il a été montré que l'ouverture du canal par l'AA, l'acide α-linolenique (ALA) ou l'acide docosahexaenoique (DHA) correspond à la mise en place d'un processus de neuroprotection (Lauritzen et al., 2000).

Si les SSRI et les antipsychotiques agissent comme des bloqueurs de TREK-1, les stabilisateurs de l'humeur (psychorégulateurs) tels que le chlorure de lithium et les antiépileptiques comme la gabapentine, le valproate ou la carbamazepine, sont décrits comme des activateurs de TREK-1 (Kim et al., 2017).

Le composant BL-1249, un dérivé du tétrazole, active également TREK-1 avec une bonne affinité ; EC_{50}~1,5µM sur culture de monocytes de vessie humaine (Tertyshnikova et al., 2005), et EC_{50}=2 ± 2 µM sur une lignée de carcinome de pancréas (Sauter et al., 2016).

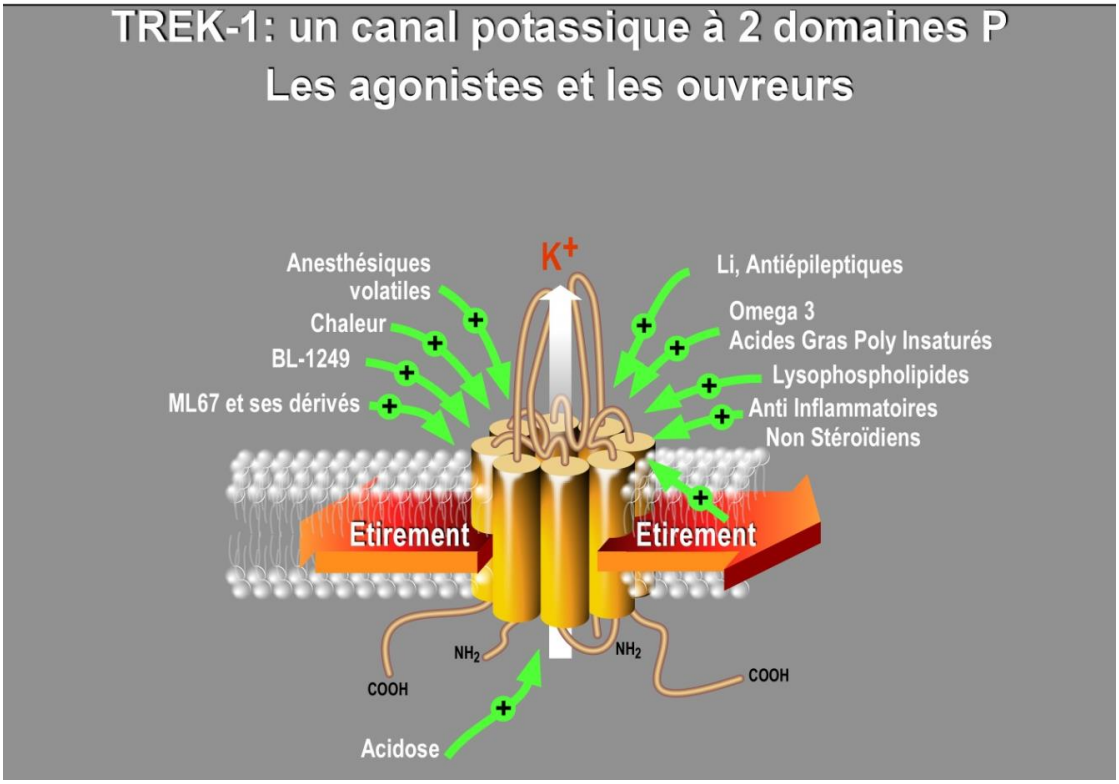

Figure 8 : Les agonistes et les ouvreurs de TREK-1

Un criblage à haut débit de plus de 106 000 molécules a permis l'identification d'un activateur de TREK-1, le ML67, et de son analogue optimisé, le ML67-33 (Bagriantsev et al., 2013). Ces molécules ont servi de bases pour le développement de deux composés au potentiel plus important, le ML335 et le ML402. Ceux-ci modulent l'activité de TREK-1 avec une EC_{50} de 5.2 ± 0.8 µM et 5.9 ± 1.6 µM respectivement (Lolicato et al., 2017).

Les anti-inflammatoires non stéroïdiens (AINS) comme l'acide flufénamique, l'acide niflumique et l'acide méfénamique sont des activateurs de TREK-1, propriétés indépendantes de leur capacité à inhiber la cyclooxygénase COX (Veale et al., 2014).

c- Modulateurs de TREK-1

Le Riluzole est une molécule neuroprotectrice principalement utilisée en clinique humaine comme anticonvulsant. Son mécanisme d'action implique le blocage des récepteurs au glutamate. Il est aussi prescrit pour prolonger la survie de patients atteints de sclérose latérale amyotrophique. Il a été démontré que le Riluzole agit comme un activateur transitoire de TREK-1 pendant 30 secondes puis comme un puissant inhibiteur pendant 90 secondes (Duprat et al., 2000), une double activité qui pourrait être engendrée par l'activation de la PKA par l'AMPc (Adénosine MonoPhosphate cyclique). En revanche, le Riluzole entraîne une activation durable de TRAAK sans une inhibition subséquente.

C- Implication dans les pathologies

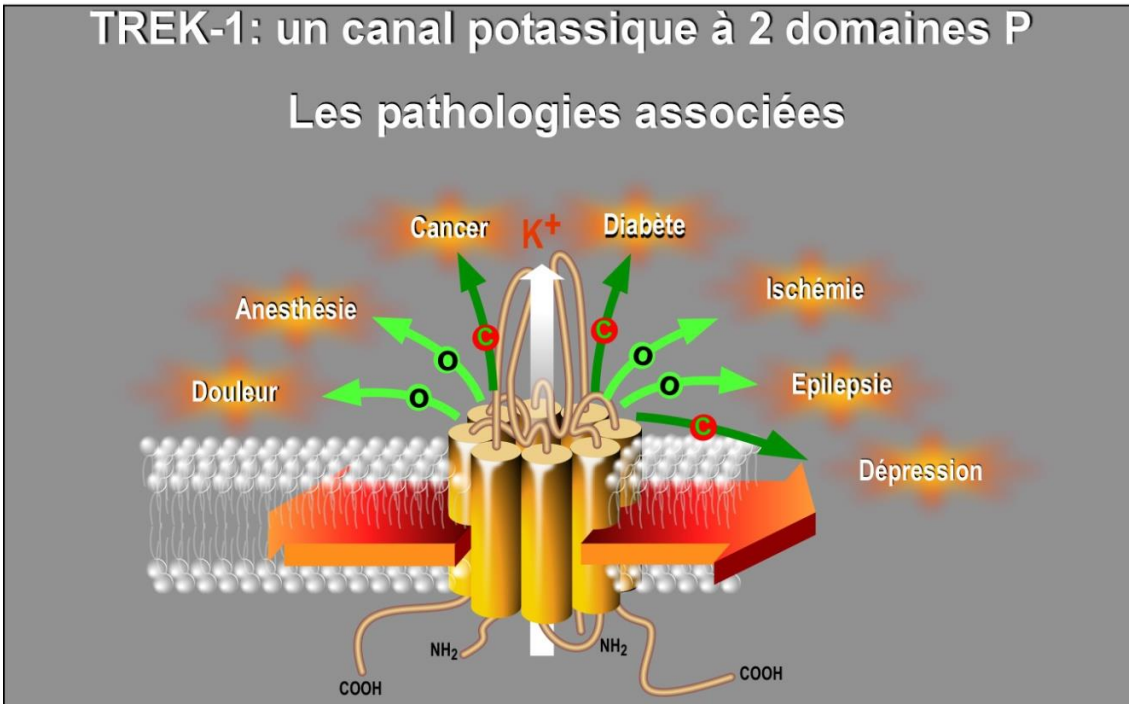

Figure 9 : Les pathologies associées à TREK-1

TREK-1 est un canal impliqué dans de nombreux processus pathologiques. En effet, son ouverture (activation) et sa fermeture (inhibition) ont toutes deux des propriétés protectrices dans diverses maladies, tant neurologiques que cardiovasculaires ou métaboliques **(Figure 9)**.

1- Niveau Central

a- TREK-1 et la dépression

Le rôle de TREK-1 dans la dépression a été démontré grâce à des souris invalidées pour le gène *kcnk2*, codant TREK-1 (souris *kcnk2*$^{-/-}$ ou TREK-1$^{-/-}$ ou TREK-1 KO) (Heurteaux et al., 2006b). Ces souris manifestent un phénotype de résistance à la dépression dans 5 modèles murins de dépression différents : le Test de la Nage Forcée de Porsolt (FST: Forced Swimming Test), le Test de Suspension par la Queue (TST: Tail Suspension Test), le Test de Suppression Conditionnée de Mobilité (CSMT: Conditioned Suppressed Motility Test), le Test de Résignation Apprise (LH: Learned Helplessness) et le Test de Suppression de l'Alimentation induite par la Nouveauté (NSF: Novelty Suppressed Feeding) (Heurteaux et al., 2006b). En effet, le comportement des souris *kcnk2*$^{-/-}$ est alors similaire à celui de souris traitées avec des antidépresseurs classiques comme la fluoxétine (Heurteaux et al., 2006b). Ces souris manifestent aussi une augmentation de la neurotransmission sérotoninergique (5-HT) dans les neurones du noyau raphé dorsal (DRN), et une augmentation de la neurogenèse comparable à celle observée à la suite d'un traitement chronique avec des antidépresseurs (Heurteaux et al., 2006b).

Bloquer TREK-1 est devenu récemment la stratégie de design pour la synthèse de nouveaux antidépresseurs. De plus, cela corrobore les observations selon lesquelles il a été montré qu'en concentrations cliniques les SSRI inhibent TREK-1 (cf : chapitre IV, B, 3, a) (Kennard et al., 2005). Ces observations chez la souris ont également été confortées par des études chez l'humain. Perliss et ses collaborateurs ont en effet observé un lien entre les variants génétiques de *kcnk2* et la résistance aux traitements antidépressifs. Par exemple, les patients possédant les SNP (Single Nucleotide Polymorphism) de TREK-1 rs10494996, rs2841608, et rs2841616, manifestent une meilleure réponse aux traitements antidépressifs (Perlis et al., 2008) (Dillon et al., 2010).

b- TREK-1 et l'épilepsie

TREK-1 est présent dans les interneurones GABAergiques du cortex et de l'hippocampe (Hervieu et al., 2001). *In vivo*, il a été montré que les AGPI tels que l'acide α-linolénique, protègent les rats traités avec un agoniste du récepteur au glutamate, l'acide kaïnique (KA), contre les convulsions et les dommages hippocampiques qui en résultent (Lauritzen et al., 2000). Ces mêmes effets sont constatés dans un autre modèle de convulsions mettant en jeu les neurones glutamatergiques (Lauritzen et al., 2000). Cet effet est associé à l'inhibition de la neurotransmission glutamatergique (Lauritzen et al., 2000). A la suite d'un traitement au KA, l'expression de *c-fos*, un marqueur d'excitabilité neuronale, augmente dans les neurones pyramidaux du CA3 (Heurteaux et al., 2004). L'acide linolénique et la lysophosphatidylcholine (LPC) diminuent le nombre de convulsions provoquées par le KA chez des souris sauvages alors qu'il n'y a aucun effet observable chez les souris TREK-$1^{-/-}$. Ces dernières sont aussi plus vulnérables au développement de crises épileptiques provoquées par le KA et le pentylènetétrazole (PTZ, antagoniste du récepteur $GABA_A$) (Heurteaux et al., 2004). Clairement, les effets protecteurs de l'acide α-linolénique et de la LPC nécessitent la présence de TREK-1.

Le mutant de TREK-1, TREK-M qui est un canal TREK-1 constitutivement ouvert, montre une résistance face à la régulation négative des PKA et PKC. En culture, la présence de TREK-M entraîne une hyperpolarisation de la membrane plasmique et une diminution des décharges spontanées des neurones hippocampaux (Dey et al., 2014). *In vivo*, la présence de TREK-M induite par l'administration d'un adénovirus recombinant (AAV-TREK-M) dans le cortex entorhinal et dans la région CA3 de l'hippocampe réduit de 50% la durée du *Status epilepticus* (état de convulsions répétées persistant plus de 5 minutes) chez un modèle murin dans lequel l'état épileptique est induit par du lithium et de la pilocarpine (Dey et al., 2014). AAV-TREK-M prévient donc la mort neuronale dans le cortex entorhinal et dans le CA3 (Dey et al., 2014). Contrairement à ce qui a pu être observé dans le cadre de la dépression, dans le phénomène épileptique c'est l'ouverture de TREK-1 qui engendre la neuroprotection.

c- TREK-1 et l'ischémie

Un modèle d'ischémie globale, induit par l'occlusion transitoire des deux artères carotides communes pendant un épisode d'hypotension (MABP (Mean Arterial Blood Pressure)

maintenu à 30±3 mmHg), a montré que 3 jours après l'opération 74% des souris *kcnk2*$^{-/-}$ décédaient contre seulement 34% dans le groupe contrôle (Heurteaux et al., 2004). Comme dans le cas de convulsions épileptiques, un prétraitement à l'ALA ou à la LPC se montre inefficace chez les souris TREK-1$^{-/-}$ alors que ce même traitement augmente de façon significative le taux de survie chez les souris sauvages (Heurteaux et al., 2004).

Chez les souris, dans le modèle d'ischémie de la moelle épinière obtenu en obstruant à la fois l'arc aortique et l'artère sous-clavière gauche, seules 25% des souris *kcnk2*$^{-/-}$ survivent 3h après une ischémie de 10 minutes alors que 86% des souris sauvages sont encore en vie 24h après l'ischémie (Heurteaux et al., 2004). De plus, les souris TREK-1$^{-/-}$ survivantes développent une paralysie sévère des membres inférieurs alors qu'aucun déficit neurologique n'a été observé chez les animaux sauvages soumis à la même opération (Heurteaux et al., 2004).

Dans les astrocytes, qui sont fortement impliqués dans l'ischémie cérébrale, l'ouverture des canaux TREK-1 contribue au maintien d'un potentiel de membrane fortement négatif, processus crucial pour contrôler l'excitabilité cellulaire (Zhou et al., 2009). L'expression des canaux TREK-1 hippocampiques et corticaux est augmentée lors de l'astrogliose survenant après l'ischémie (Wang et al., 2012). Cette augmentation transitoire du canal TREK-1 en conditions hypoxiques accroît les processus d'élimination du glutamate et diminue la sécrétion par les astrocytes de S100β (protéine inflammatoire jouant un rôle délétère dans diverses pathologies cérébrales (Matsui et al., 2002)). Ces phénomènes contribuent à réduire la mort neuronale (Wu et al., 2013).

d- TREK-1 et l'anesthésie générale

Les doses d'isoflurane, de diéthyl éther, d'halothane et de chloroforme utilisées en clinique dans le cadre d'anesthésie générale sont suffisantes pour activer TREK-1 (Patel et al., 1999). Cette activation entraîne une hyperpolarisation membranaire et une diminution des décharges de potentiel d'action, conduisant ainsi à un effet neuroprotecteur.

Le gaz hilarant (ou protoxyde d'azote) et le xénon exercent majoritairement leurs effets anesthésiques en antagonisant les récepteurs NMDA. Ils assurent l'analgésie (et l'euphorie) et sont responsables de la neuroprotection. En revanche, ils ne potentialisent pas les récepteurs $GABA_A$ (Gruss et al., 2004). Il a été montré que ces deux gaz ouvraient le canal TREK-1 par un processus (protonation) passant par le résidu Glu306 (Gruss et al., 2004).

Une fois administré, l'hydrate de chloral, utilisé en pédiatrie pour certaines formes d'épilepsies telles que la myoclonie évolutive ou les épilepsies juvéniles réfractaires, est rapidement métabolisé en sa supposée forme active , le 2,2,2-trichloréthanol (TCE) (Harinath and Sikdar, 2004). Le TCE induit une « dépression » du SNC en potentialisant les récepteurs $GABA_A$ et en inhibant les récepteurs NMDA, AMPA et au Kaïnate. Il active les canaux TREK-1 et TRAAK, contribuant ainsi à augmenter l'effet anesthésique central (Harinath and Sikdar, 2004). *In vivo,* les souris TREK-$1^{-/-}$ manifestent une sensibilité modérée face aux anesthésiques comme le sevoflurane, le desflurane et l'isoflurane mais aussi face au chloroforme et à l'halothane (Heurteaux et al., 2004) (Noel et al., 2011). En effet, le temps nécessaire à l'endormissement des animaux est plus long et les doses minimales d'anesthésique sont plus importantes.
En revanche, le phénobarbital, un anesthésique général qui n'active pas TREK-1, est toujours efficace chez les souris *kcnk2*$^{-/-}$. Ainsi, le phénotype de résistance observé est spécifiquement imputable à l'absence de TREK-1. Le préconditionnement *in vitro* et *in vivo* avec du sévoflurane offre une protection neuronale par activation de TREK-1 (Tong et al., 2014). Des résultats confirmés, par l'observation qu'après une ischémie focale (modèle MCAO) des rats traités avec du sévoflurane présentent une meilleure neuroprotection laquelle semble être médiée par TREK-1 (Pan et al., 2017).

e- TREK-1 et la perception de la douleur

Comme indiqué plus haut, la température est un modulateur de l'activité des canaux TREK-1. Ces canaux sont fermés à 12°C et s'ouvrent graduellement jusqu'à un pic à 37°C. A noter que cette ouverture de TREK-1 est reversée par l'AMPc et la prostaglandine E2, deux senseurs des thermorécepteurs centraux et périphériques. Le blocage de TREK-1 est dû à la phosphorylation de son extrémité C-terminale sur son résidu Ser333. TREK-1 est très exprimé dans les neurones des ganglions de la racine dorsale (DRG) ainsi que dans les neurones de l'hypothalamus, régions fortement impliquées dans la sensation de douleur (Maingret et al., 2000). 60% des neurones sensoriels expriment TREK-1 et la plupart d'entre eux sont en lien avec la substance P. Plus de 40% des neurones des DRG exprimant TREK-1 expriment aussi le canal nociceptif thermal TRPV1. *In vivo,* les souris TREK-$1^{-/-}$ ont un seuil thermal de douleur plus bas et sont plus sensibles aux stimuli mécaniques que des souris sauvages (Alloui et al., 2006) (Noel et al., 2009). Ces souris manifestent une réponse inflammatoire focale exacerbée après une lésion de la moelle épinière (LME). De plus, l'absence de TREK-1 augmente l'astrogliose, l'apoptose

neuronale, la démyélinisation et le temps de récupération motrice (Fang et al., 2017). Le blocage de TREK-1 est donc fortement handicapant en ce cas.

Toutefois, d'autres études rapportent qu'en cas de douleur neuropathique induite par une constriction lésionnelle chronique du nerf sciatique (CLC), l'expression du microRNA miR-183 (un microRNA fortement exprimé dans les organes sensoriels du SNC, et impliqué dans les processus de douleur neuropathiques (Xie et al., 2017)) est diminuée et l'expression de TREK-1 augmente dans les DRG (Han et al., 2016) (Shi et al., 2018). Inversement, l'injection sous arachnoïdienne (intrathécale) de ce miR-183 atténue la douleur dans un modèle de CLC chez le rat et réduit l'expression de TREK-1 (Shi et al., 2018).

Il a été récemment rapporté que le riluzole, un modulateur de TREK-1, prévient non seulement les déficits sensoriels mais aussi les déficits moteurs dans les cas de douleur neuropathique induite par l'oxaliplatine, une molécule chemiothérapique (Poupon et al., 2018). Cependant cette étude considère le riluzole comme un activateur de TREK-1, alors qu'il a été montré que le riluzole n'active TREK-1 que pendant 30 secondes avant de l'inhiber. Il semble bien curieux que le Riluzole puisse être à la fois neuroprotecteur et antidépresseur en tant qu'activateur puisqu'il a été montré que les souris TREK-1 KO manifestent un phénotype de résistance à la dépression. Les résultats publiés dans cet article sont pour le moins discutables.

2- Niveau Périphérique

En plus de ses rôles au niveau central (cerveau), il était rationnel de supposer que la modulation de TREK-1 pouvait aussi avoir un rôle au niveau périphérique. TREK-1 est exprimé dans de nombreux tissus périphériques comme le pancréas, la prostate ou les cellules des muscles lisses (Medhurst et al., 2001).

a- TREK-1 et le pancréas

Le pancréas, et tout particulièrement les cellules β sécrétant l'insuline, constitue l'un des tissus périphériques où le canal TREK-1 (et d'autres K_{2P}) jouent un rôle important dans l'homéostasie du glucose (Dadi et al., 2014) (Kang et al., 2004) (Mazella et al., 2010) (Vierra et al., 2015). Grâce à la Spadine, le rôle de TREK-1 dans l'homéostasie du glucose a pu être étudié (Hivelin et al., 2016). TREK-1 est exprimé dans la lignée cellulaire β-pancréatique β-TC3 (Mazella et

al., 2010). La régulation de la sécrétion d'insuline par les cellules β-pancréatiques est finement contrôlée par plusieurs hormones comme le glucagon like-peptide-1 (GLP-1), la leptine, les œstrogènes, la mélatonine et les hormones de croissance (Fu et al., 2013), et les canaux K^+ sensibles à l'ATP (K_{ATP}) jouent un rôle critique dans le maintien de l'homéostasie du glucose (McTaggart et al., 2010). Les canaux K_{ATP} servent de senseurs métaboliques pour les cellules β-pancréatiques. Quand les niveaux de glucose augmentent, les K_{ATP} se ferment, ce qui induit une dépolarisation de la membrane qui, à son tour, entraîne une ouverture des canaux Ca^{2+}, qui provoque la sécrétion d'insuline (McTaggart et al., 2010). Le blocage de TREK-1 par la Spadine n'induit une sécrétion d'insuline que s'il y a stimulation par le glucose. Par contre, à l'inverse des incrétines, la Spadine entraîne une augmentation de Ca^{2+} et un relargage d'insuline grâce à un mécanisme indépendant de la PKA (Hivelin et al., 2016). TREK-1 est inhibé par la phosphorylation du résidu Ser333 sur son extrémité C-terminale par la PKA (Murbartian et al., 2005). Cette phosphorylation est la conséquence de l'activation de différents récepteurs couplés aux protéines G à la membrane plasmique **(Figure 11)**. En se fixant sur leur récepteur, GLP-1 (« Glucagon-like peptide », une hormone de la satiété) et ses analogues tels que l'exendine-4 sont capables de provoquer la synthèse d'AMPc et donc d'induire l'activation de la PKA, responsable de la sécrétion d'insuline (Goke et al., 1993). Ici, la Spadine ou ses analogues pourraient se substituer aux incrétines et ainsi proposer une thérapie alternative en cas d'inefficacité de traitement basé sur la reproduction des effets de GLP-1.

Bien que la plupart des travaux s'intéressant au lien entre les K_{2P} et le cancer aient été conduits sur TASK-3, TREK-1 a également été défini comme un acteur important dans le cancer du pancréas. En effet, dans ce type de cancer son activation par BL1249 permettrait d'inhiber la prolifération et la migration cancéreuses et donc d'en réduire l'impact délétère (Sauter et al., 2016).

b- TREK-1 et la prostate

Dans le cancer de la prostate, où il est d'ailleurs surexprimé, TREK-1 a été décrit comme ayant un rôle pro-prolifératif (Voloshyna et al., 2008). Le même laboratoire a également démontré qu'en cas de surexpression d'un dominant négatif de ce canal dans les cellules PC3 (lignée cancéreuse de la prostate), la prolifération cellulaire était diminuée. A noter que sa surexpression dans des cellules de la lignée, cette fois non cancéreuse, NPE (« Non Pigmented Epithelial cells » dérivées de cellules épithéliales bovines) entraîne elle-aussi une augmentation

de la prolifération (Voloshyna et al., 2008)**.** La surexpression de TREK-1 dans ce type de cancer est donc largement désavantageuse et par conséquent le blocage de l'activité de TREK-1 peut être envisagé pour traiter ces cancers.

c- TREK-1 et le cœur

Au niveau cardiaque, les canaux K^+ activés par l'étirement (KAE) repolarisent la membrane cellulaire et contrebalancent l'activité des canaux cationiques activés par l'étirement (CAE) qui, au contraire, augmentent la dépolarisation membranaire. TREK-1 est un candidat de choix pour les KAE dans le cœur, avec les canaux K^+ activés par le Ca^{2+} de grande conductance (K_{Ca}) et les canaux K_{ATP} (Decher et al., 2017b; a). Chez le rat, tous les gènes des canaux K_{2P} ont pu être détectés dans au moins une des cavités cardiaques, avec une prévalence de l'expression de TWIK-2, TASK-1 et TREK-1. TREK-1 est très fortement exprimé dans le ventricule droit (Liu and Saint, 2004). Dans les myocytes auriculaires néonataux de rat, il a été mesuré par patch-clamp en configuration inside-out qu'un courant potassique qui était activé par l'AA et l'acidose interne (Kim and Clapham, 1989). Ce courant TREK-1-like peut également être réversiblement activé par les anesthésiques volatils tels que le chloroforme, l'halothane et l'isoflurane. Ce courant est diminué par des analogues des AMPc et des agonistes des récepteurs β-adrenergiques (Terrenoire et al., 2001). Il apparaît donc que les courants KAE ont les mêmes propriétés biophysiques que le courant TREK-1, notamment la conductance, l'indépendance au voltage et la sensibilité face aux anesthésiques volatils. Dans les cardiomyocytes ventriculaires, deux variants de TREK-1 ont été découverts, un de haute conductance (132 ± 5 pS), et de basse conductance (41 ± 5 pS), à potentiels positifs (Xian Tao et al., 2006). Le variant TREK-1 de basse conductance est ouvert par l'étirement mécanique, l'acidification interne et l'AA. Les propriétés biophysiques de ces deux canaux TREK-1 sont similaires à celles de TREK-1 exprimé dans les cellules HEK293.

De même, dans le cœur du poisson zèbre, il a été identifié deux orthologues de TREK-1, TREK-1a et TREK-1b, qui possèdent des propriétés biophysiques similaires mais toutefois suffisamment distinctes pour qu'ils puissent être différenciés (Nasr et al., 2018).

D- TREK-1 dans la dépression post-AVC

La dépression post-AVC (PSD) est un désordre neuropsychiatrique de haute prévalence qui survient à la suite d'un AVC. Il a été montré dans un modèle de PSD chez le rat que les niveaux d'expression de TREK-1 étaient élevés dans l'hippocampe et le CPF (Lin et al., 2015). Ce modèle particulier de PSD reproduit les principaux acteurs responsables du développement de cette pathologie chez l'humain. Par exemple, l'opération chirurgicale de « middle cerebral artery occlusion » (MCAO) est utilisée pour reproduire l'AVC, alors que le « chronic mild stress » (CMS) et l'élevage en isolement permettent de mimer respectivement le stress et les conditions psychologiques (Lin et al., 2015). A noter que la régulation positive de TREK-1 observée dans ce modèle est abolie en cas de traitement chronique avec des bloqueurs du canal ainsi qu'avec le SSRI Escitalopram. Il nous a donc semblé naturel d'étudier le rôle de TREK-1 dans le processus de la dépression post-AVC (PSD). Cette étude est décrite dans la Partie 2 de la Section Résultats.

V- La Spadine et ses analogues

A- Spadine

1- Origines – La Sortiline

Le canal TREK-1 interagit avec plusieurs protéines, telles que l'AKAP150 (Sandoz et al., 2006) ou Mtap2 (Sandoz et al., 2008), qui régulent l'adressage de TREK-1 à la membrane plasmique. En 2010, une autre protéine interagissant avec TREK-1 a été identifiée, la Sortiline, également appelée récepteur 3 de la Neurotensine. Cette dernière régule, transporte et adresse le canal TREK-1 à la membrane plasmique (Mazella et al., 2010).

La Sortiline est une protéine membranaire de 95 kDa, avec un large domaine luminal, un seul segment transmembranaire et une courte extrémité C-terminale cytoplasmique **(Figure 10)**. Elle est exprimée dans le SNC et le système nerveux périphérique.

La Sortiline a d'abord été identifiée comme molécule d'adressage dans le cerveau humain (Petersen et al., 1997), puis a été décrite comme étant le récepteur 3 de la Neurotensine (NTSR-3) (Mazella et al., 1998). La Sortiline/NTSR-3 a de nombreux ligands, comme la Neurotensine (NT), le « precursor of the nerve growth factor » (proNGF) (Nykjaer et al., 2004), la lipoprotéine lipase (Nielsen et al., 1999), et le propeptide (PE) (Munck Petersen et al., 1999).

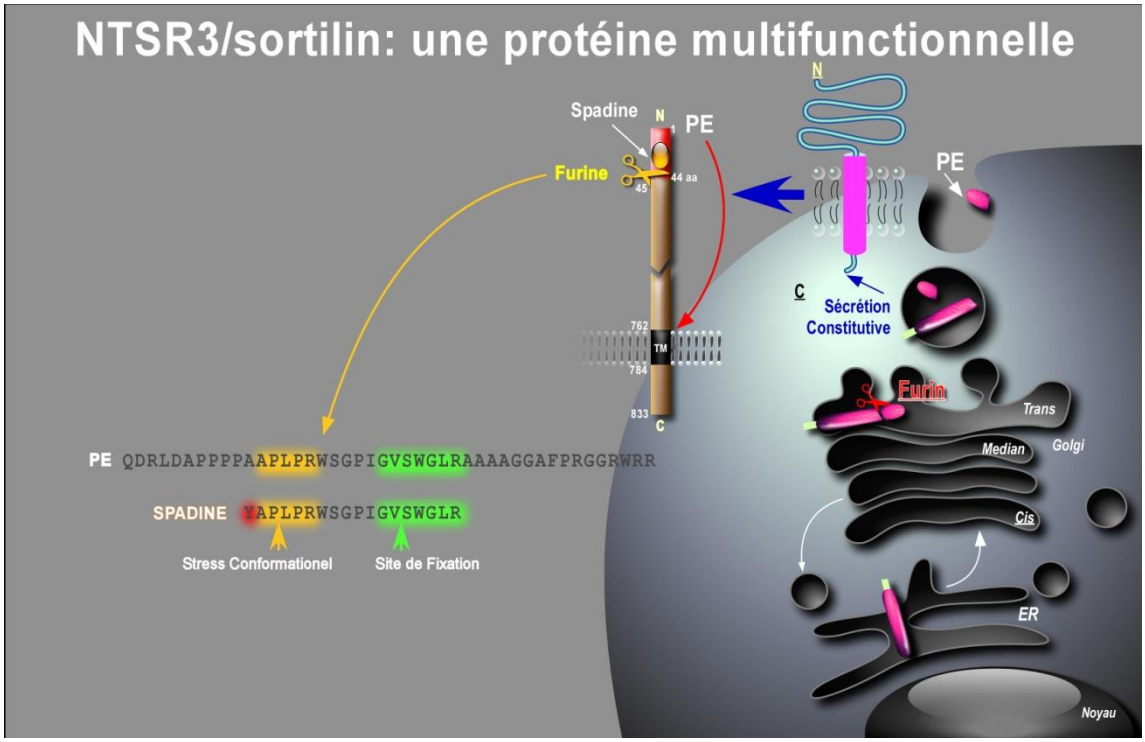

Figure 10 : Maturation de la Sortiline et design de la Spadine

La Sortiline/NTSR-3 co-localise avec TREK-1 dans de nombreuses régions du cerveau impliquées dans la gestion de l'humeur comme le cortex préfrontal, l'hippocampe, le striatum, l'amygdale et l'hypothalamus (Mazella et al., 2010). L'interaction physique entre TREK-1 et la Sortiline/NTSR-3 a été caractérisée par co-immunoprécipitation. Il a également été montré que l'expression de TREK-1 à la membrane plasmique augmente en présence de Sortiline/NTSR-3 (Mazella et al., 2010) et qu'au contraire en l'absence de Sortiline TREK-1 n'est présent qu'en faible quantité à la membrane. Les souris déficientes pour la La

Sortiline/NTSR-3 manifestent également un phénotype de résistance à la dépression, similaire à celui des souris *kcnk2*$^{-/-}$ (Moreno et al., 2018).

La Sortiline/NTSR-3 est également impliquée dans le contrôle de la sécrétion du précurseur du BDNF, dont la diminution provoque des dysfonctionnements synaptiques pouvant se traduire par des difficultés de mémorisation (Martinowich et al., 2007) (Egan et al., 2003).
Ces observations sont autant d'arguments dans le sens d'une implication de TREK-1 et de la Sortiline/NTSR-3 dans la physiopathologie de la dépression.
A noter que dans un autre modèle de souris KO pour le gène de la Sortiline, une tendance accrue au développement de plaques amyloïdes a été observée (Carlo, 2013). La Sortiline serait donc potentiellement impliquée dans la maladie d'Alzheimer.

La Sortiline est synthétisée sous la forme d'une protéine précurseur (la Prosortiline) qui, après un clivage post-traductionnel par la convertase Furine dans le réseau du Golgi, donne naissance à une Sortiline mature et fonctionnelle et libère un peptide de 44 acides aminés, le Propeptide (PE) (Gln1-Arg44) (Munck Petersen et al., 1999).
Ce PE se lie à la Sortiline mature avec une forte affinité (Kd ~20–30 nM) (Munck Petersen et al., 1999). Notre laboratoire a également montré que le PE se lie au canal TREK-1, avec une forte affinité (100nM).
C'est à partir d'une étude structure-fonction, qui a permis d'identifier les acides aminés responsables de la liaison de ce peptide à son récepteur, que la Spadine a été dessinée **(Figure 10)**.

2- La Spadine

La Spadine, pour "Sortilin-derived Peptide with Antidepressant properties", est un peptide de 17 acides aminés correspondant à la séquence Ala12-Arg28, ou PE 12-28 (Mazella et al., 2010) **(Figure 10)**.

a- Inhibiteur spécifique de TREK-1

La Spadine se lie avec une très forte affinité (IC_{50}=40-70 nM) au complexe TREK-1/sortiline à la surface cellulaire (Mazella et al., 2010) (Article 1), et induit une endocytose du canal et une

dégradation lysosomale. Cette internalisation reproduit en quelque sorte les conditions des KO de TREK-1. En présence de la Spadine la quantité de TREK-1 à la membrane ne serait plus suffisante pour s'opposer à la dépolarisation membranaire et par conséquent rendrait plus excitables les cellules **(Figure 11)** (Mazella et al., 2010).

La Spadine a d'abord été testée par patch-clamp en configuration cellule entière sur la lignée cellulaire COS-7 exprimant TREK-1. Le courant basal de TREK-1 étant très faible, il a été mis à profit la capacité de l'AA d'activer le canal. TREK-1 activé par l'AA est bloqué par la Spadine avec une IC_{50} de 70.7 nM (Mazella et al., 2010). Le blocage de TREK-1 a été confirmé sur d'autres types cellulaires comme les hTREK-1/HEK (IC_{50} = 40 nM) (Moha ou Maati et al., 2011) ou la lignée pancréatique β-TC3 (Mazella et al., 2010) (Article 1), mais également sur tranches de cerveau, dans les neurones pyramidaux du CA3 de l'hippocampe (Mazella et al., 2010).

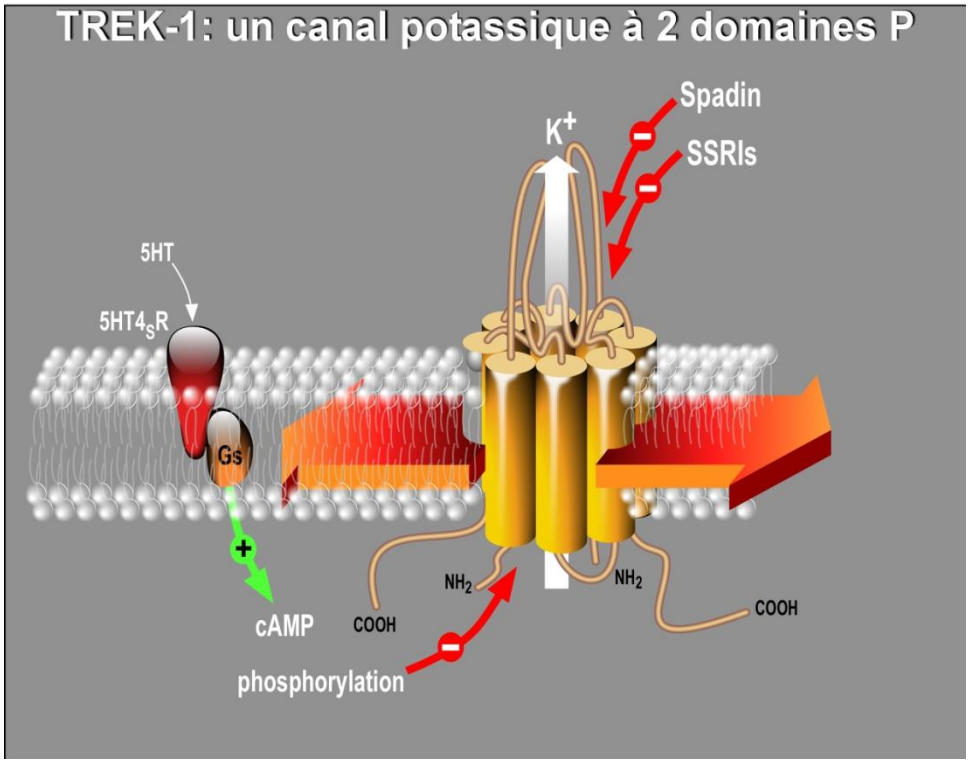

Figure 11 : TREK-1 et la Spadine

De façon très intéressante, l'effet de la Spadine disparaît totalement quand elle est utilisée sur des coupes d'hippocampe de souris TREK-$1^{-/-}$, ce qui confirme solidement que la Spadine cible ce canal (Mazella et al., 2010). En effet, malgré une forte homologie dans la structure, la

fonction et la régulation entre TREK-1, TREK-2 et TRAAK (Lesage and Lazdunski, 2000), la Spadine bloque TREK-1 de manière spécifique. Aucun effet n'a pu être observé sur TREK-2 et TRAAK, les 2 autres membres de la sous-famille TREK, eux aussi activés par l'étirement. TASK-1 et TRESK, deux autres K_{2P} très largement représentés dans le cerveau, sont eux aussi insensibles à la Spadine (Moha Ou Maati et al., 2012b). Cette absence d'effet de la Spadine sur TASK-1, qui est impliqué dans l'inflammation (Bittner et al., 2009) et l'apoptose (Lauritzen et al., 2003) (Leithner et al., 2016), et sur TRESK, qui est impliqué dans les processus de migraine (Lafreniere and Rouleau, 2011) et de douleur (Tulleuda et al., 2011) (Marsh et al., 2012), est très intéressante car cela réduit considérablement les éventuels effets secondaires de ce peptide.

b- Stimulation de la transmission 5-HT

TREK-1 est fortement exprimé dans le DRN (Medhurst et al., 2001), et les souris *kcnk2*$^{-/-}$ ont une neurotransmission sérotoninergique augmentée (Heurteaux et al., 2006b). Ainsi, pour savoir si le blocage pharmacologique de TREK-1 par la Spadine affecte ou non la neurotransmission 5-HT, des souris ont reçu une injection intrapéritonéale de 10 µM de Spadine. L'activité extracellulaire unitaire des neurones sérotoninergiques a ensuite été enregistrée sur animaux anesthésiés dans les noyaux du raphé dorsal, c'est-à-dire en un point éloigné de la zone d'injection du peptide. Les données montrent que la Spadine potentialise par un facteur 2 les décharges de neurotransmission 5-HT *in vivo* (Mazella et al., 2010), pour donner un niveau similaire à celui observé chez les neurones 5-HT des souris *kcnk2*$^{-/-}$ avec 3,1 Hertz contre 1,26 Hertz chez des contrôles non traitées (Heurteaux et al., 2006b).

c- Neurogenèse et synaptogenèse

Les effets de la Spadine sur la neurogenèse sont remarquables du fait qu'ils surviennent après seulement 4 jours de traitement, alors qu'un délai de 3 à 4 semaines doit être observé avec les SSRI (Mazella et al., 2010). De plus, *in vitro* (sur neurones corticaux) et *in vivo* (dans l'hippocampe), la Spadine augmente non seulement l'expression des ARNm mais aussi celle des marqueurs protéiques de la synaptogenèse, tels que la « post-synaptic density protein-95 » (PSD-95) ou la Synapsine (Devader et al., 2015). Cette augmentation est associée avec une augmentation transitoire de BDNF après seulement 5h. Ces données indiquent que la Spadine augmente le nombre de neurones fonctionnels. Observation supportée par le fait que le

traitement avec la Spadine augmente aussi significativement les nombre d'épines dendritiques matures et d'axones (Devader et al., 2015). *In vivo*, l'administration quotidienne de Spadine pendant 4 jours augmente dans l'hippocampe l'expression des ARNm de BDNF, de PSD-95 et de la Synapsine après seulement 7 jours. Cependant, dans le cortex préfrontal après 3 semaines, seul l'ARNm du BDNF est augmenté (Devader et al., 2015).
Combinées, ces données confirment que les neurones nouvellement générés par le traitement Spadine sont non seulement fonctionnels mais aussi capables d'interagir au sein d'un réseau neuronal complexe. Le traitement subchronique (4 jours) avec la Spadine résulte aussi en l'augmentation de l'activation de CREB (C-AMP Response Element-binding protein) (Mazella et al., 2010), un facteur de transcription important dans le remodelage synaptique.

Le traitement avec la Spadine engendre donc deux effets « canoniques » des antidépresseurs : l'augmentation de la transmission 5-HT et l'induction de neurogenèse (Mazella et al., 2010). Ces résultats confirment les données précédentes obtenues chez les souris *kcnk2*$^{-/-}$ dont la principale caractéristique phénotypique est leur résistance à la dépression (Heurteaux et al., 2006b). Il fallait donc confirmer l'hypothèse selon laquelle la Spadine pourrait être un antidépresseur par l'utilisation de modèles animaux de dépression.

d- Propriétés antidépressives

Les propriétés antidépressives de la Spadine ont été étudiées dans les mêmes tests comportementaux que ceux préalablement utilisés pour la caractérisation des souris *kcnk2*$^{-/-}$.
La Spadine a donc été administrée aux souris en traitements aigu et subchronique avant que son activité antidépressive ne soit mesurée par différents tests : FST, TST, CSMT, LHT et NSF.
Dans les tests du FST et du TST, de la même façon que le KO de TREK-1, le traitement avec la Spadine induit une diminution du temps d'immobilité, peu importe le mode d'administration (i.p., i.v., i.c.v., s.c. ou par voie orale).
Dans le CMST, le traitement avec la Spadine atténue la résignation, traduite par une immobilité croissante, qui s'observe chez les contrôles non traités (Heurteaux et al., 2006b). A noter que la Spadine n'a aucun effet sur la mobilité des souris qui ne sont pas soumises aux chocs électriques, ce traitement n'a donc aucun effet moteur en conditions normales.

Dans le test du LH, les animaux traités avec la Spadine ont une latence d'échappement plus faible que celle des contrôles non traités. Tout comme dans le CMST, les souris traitées sont moins résignées.
Enfin, dans le test du NSF, étroitement lié à la neurogenèse, le traitement avec la Spadine diminue la latence des souris avant d'aller se nourrir. Les animaux sont donc moins anxieux.
En bloquant TREK-1, la Spadine génère des souris avec un phénotype de résistance à la dépression dans cinq tests régulièrement utilisés dans le screening de molécules antidépressives, après un traitement de seulement 4 jours contre 3 semaines pour d'autres molécules telles que les SSRI. Ces résultats sont en parfait accord avec ceux obtenus chez les souris TREK-1 KO.

e- Mécanismes et effets secondaires

In vitro, la Spadine stimule les voies des MAPK et de PI3K en fonction du temps et de façon dose-dépendante. A 100nM la Spadine augmente la phosphorylation d'ERK1/2 et d'Akt mais n'a aucun effet sur mTOR, ce qui suggère que le mécanisme d'action de la Spadine est différent de celui de la Kétamine, un autre antidépresseur à action rapide dont les effets passent par la voie mTOR (Devader et al., 2015). La Spadine a des effets neuroprotecteurs face à l'apoptose induite par la Caspase 3 provoquée par la Staurosporine à travers l'activation de la voie PI3K.

Etant donné que l'ouverture de TREK-1 engendre une neuroprotection face aux épisodes épileptiques, bloquer ce canal K_{2P} devrait avoir des conséquences délétères. Mais de façon surprenante, chez la souris la Spadine n'augmente pas les convulsions induites par un traitement au KA ou PTZ. Plus intéressant encore, les souris traitées avec la Spadine manifestent même une résistance face au développement de convulsions. Le groupe d'animaux traité avec la Spadine ne récence aucune mort en opposition aux deux morts du groupe injecté avec une solution saline (Moha Ou Maati et al., 2012b). De plus, un traitement de 3 semaines avec la Spadine n'augmente pas non plus la taille des infarctus après ischémie focale (Moha Ou Maati et al., 2012b).

TREK-1 joue également un rôle important dans la perception de la douleur (Alloui et al., 2006). Les souris *kcnk2*$^{-/-}$ sont plus sensibles à la douleur induite par un stimulus thermique (Alloui et al., 2006). Cependant, la Spadine n'entraîne pas de modification dans la perception de la

douleur dans les tests de retrait de la queue ou de la plaque chauffante (Moha Ou Maati et al., 2012b).

Enfin, un des enjeux majeurs lors du développement de nouvelles molécules médicamenteuses est l'absence d'effet que le traitement doit avoir sur l'intervalle QT d'un électrocardiogramme. En effet, un allongement de cet intervalle entraîne la formation de torsades de pointes (une forme sévère du trouble du réflexe cardiaque). Les molécules ayant cet effet bloquent deux types de courants potassiques : les courants potassiques sortants à composante rapide (IKr) ou à composante lente (IKs) (Cheng and Kodama, 2004) (Sanguinetti and Jurkiewicz, 1990). Le courant IKr est produit par le canal hERG seul, et l'activité de IKs requiert l'association des canaux KCNQ1avec la sous-unité régulatrice KCNE1 (Sanguinetti et al., 1996) (Barhanin et al., 1996). Ces courants sont des composantes essentielles de la fonction cardiaque normale, et la prolongation de l'intervalle QT induite par des molécules médicamenteuses entraîne une augmentation du risque de mort subite (Brown, 2004). Les effets de certaines molécules sur ces canaux ont eu pour conséquence leur retrait des études voire du marché (Finlayson et al., 2004). Toute molécule candidate doit d'abord être testée *in vitro* pour s'assurer de son inocuité sur les canaux hERG (Chen et al., 2016). Le but final étant d'amener la Spadine au stade de molécule antidépressive approuvée, ce peptide a donc été testé sur hERG. La Spadine, même à forte concentration (10 μM), n'affecte pas les propriétés biophysiques des courants IKr et IKs (Moha Ou Maati et al., 2012b) (Article 1). Tout ceci confirme que la Spadine est une molécule éligible à l'utilisation en clinique.
Les puissantes propriétés antidépressives de la Spadine ont donné lieu à un brevet publié sous le N° US8252748B2 (Mazella et al., 2012).

Dans le FST l'activité antidépressive de la Spadine disparaît au bout de 6h après l'injection intrapéritonéale (Veyssiere et al., 2015). Plusieurs stratégies ont été considérées afin d'améliorer cette stabilité *in vivo* et de prolonger l'activité antidépressive de la Spadine. Parmi celles-ci il y eut tout d'abord la stratégie des retro-inverso (RI) puis la stratégie des peptides courts.

B- Analogues Retro-Inverso

La stratégie des Retro Inverso (RI) consiste à changer la configuration L naturelle des acides aminés en une configuration D, tout en inversant la séquence de ces derniers.
De nombreuses études ont montré que cette technologie RI permettait d'augmenter la résistance des peptides face à la protéolyse, et donc d'augmenter leur biodisponibilité (Chorev et al., 1979) (Chorev and Goodman, 1995).
Onze analogues RI ont été synthétisés et ont été criblés sur la lignée cellulaire hTREK-1/HEK par patch-clamp. Ce criblage a identifié deux peptides : l'analogue 3 (Ac-RI-PE 12-28, le RI de la Spadine) et l'analogue 8 (Ac-RI-PE 1-28, le RI de la séquence 1 à 28 du PE) manifestant un fort potentiel inhibiteur pour l'activité de TREK-1 (IC_{50} = 11.5±0.59 nM et 9.95 ±0.85 nM respectivement, contre 56.39± 0.01 nM pour la Spadine) (Veyssiere et al., 2015) **(Figure 12)**.
Ces deux analogues conservent les propriétés antidépressives de la Spadine après traitements aigu ou subchronique. Ils diminuent par exemple significativement le temps d'immobilité dans le FST (Veyssiere et al., 2015) et la latence avant d'aller se nourrir dans le test du NSF. Ils induisent également une augmentation de la neurogenèse. L'un des enjeux en terme de développement était d'améliorer la stabilité *in vivo* de la Spadine et les analogues 3 et 8 manifestent une activité antidépressive durant 16 heures, c'est-à-dire un temps presque 3 fois plus long que la Spadine (Veyssiere et al., 2015).
A noter que l'analogue 3 n'a aucun effet secondaire sur la perception de la douleur, l'épilepsie et l'arythmie. La totalité des analogues RI, y compris le 3 et le 8, ont été brevetés pour le traitement de la dépression sous le N° WO2015110915A2 (Gaudriault et al., 2015).

D'autres analogues ont été conçus grâce à cette stratégie RI comme l'analogue 13 (même séquence que la Spadine mais dans laquelle les trois résidus Glycine (qui n'a pas de carbone asymétrique, donc pas de conformation L ou D) ont été remplacés par des Alanines : G/A-PE 12-28) et son RI, l'analogue 14 (RI-G/A-PE 12-28) **(Figure 12)**. Les analogues 13 et 14 sont capables de fortement inhiber TREK-1 (83.50% ± 9.76% et 72.15% ± 11.75% respectivement), comparés à la Spadine (87.08% ± 7.32%, n = 8). Plus intéressant encore, ces analogues 13 et 14 conservent leur activité antidépressive dans le FST quand injectés par intraveineuse (i.v.). En effet le temps d'immobilité est réduit de manière significative (120.4±9.7 s et 127.7 ±8.32 s, respectivement) **(Figure 13)**.

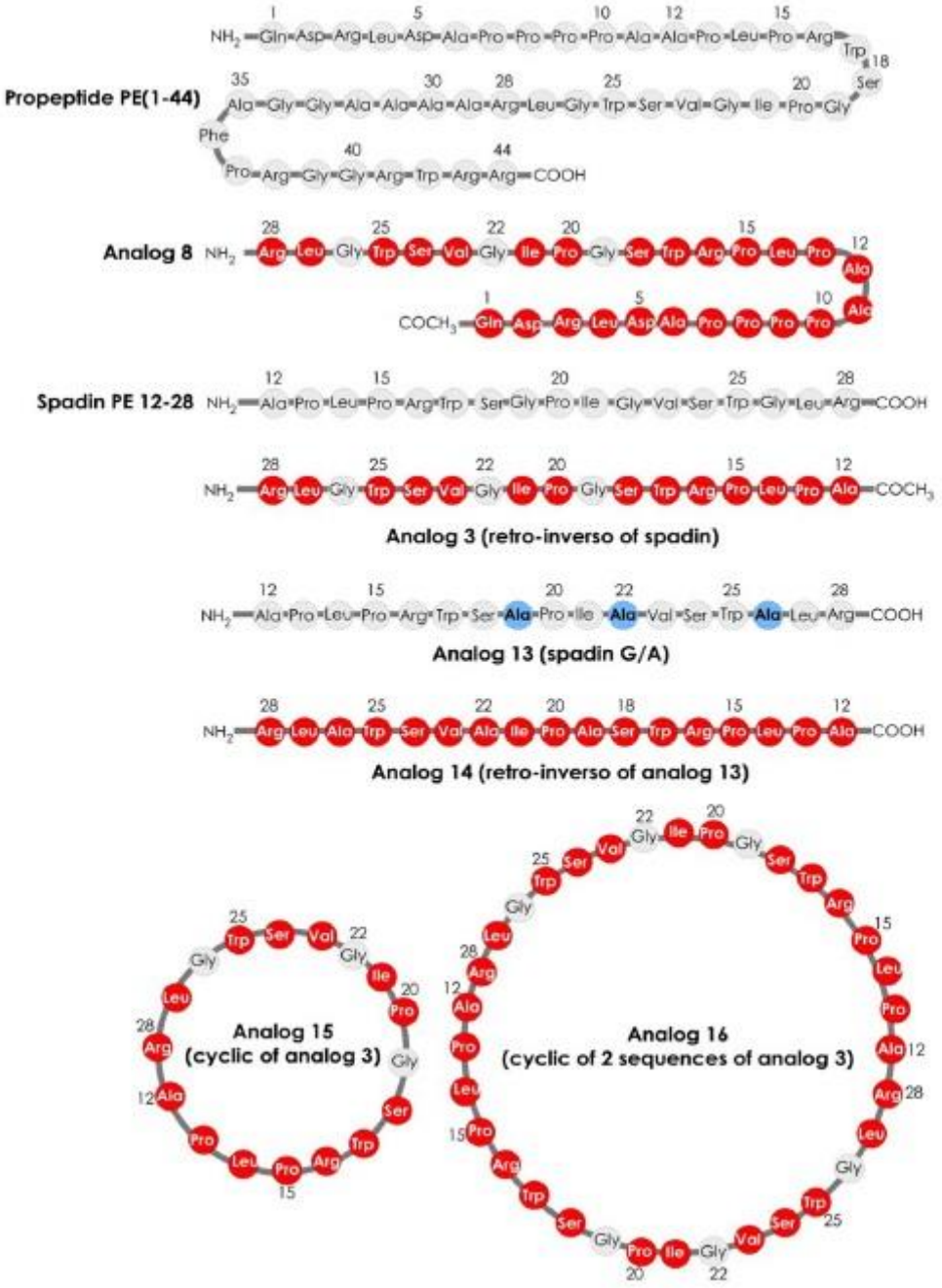

Figure 12 : Les analogues retro-inverso de la Spadine

La cyclisation est également une des stratégies les plus communément utilisées pour augmenter la stabilité et l'efficacité des peptides (Adessi and Soto, 2002) **(Figure 12)**. Il a été démontré que cette cyclisation permet d'augmenter la résistance des peptides face à la dégradation protéolytique, et par conséquent leur biodisponibilité (Wang et al., 2014). Cette stratégie a consisté à mettre sous forme cyclique l'analogue 3, soit en séquence unique (analogue 15 : c(RI-PE 12-28)), soit en tandem (analogue 16) afin d'étudier l'impact de la cyclisation des peptides sur le franchissement de la BHE. En Patch clamp sur cellule entière, ces analogues inhibent le

courant de TREK-1 avec des potentiels différents (67.24% ± 3.41% et 91.25%±8.14%, respectivement). En revanche, quand ces deux analogues sont administrés par i.v., aucun n'induit de diminution significative du temps d'immobilité dans le FST (157 ± 8.09 s et 146.7 ± 12.99 s, respectivement). Il apparaît que ce manque d'activité est dû à leur incapacité à franchir la BHE, étant donné qu'ils manifestent des propriétés antidépressives quand ils sont directement injectés dans le cerveau de façon intracérébroventriculaire **(Figure 13).**

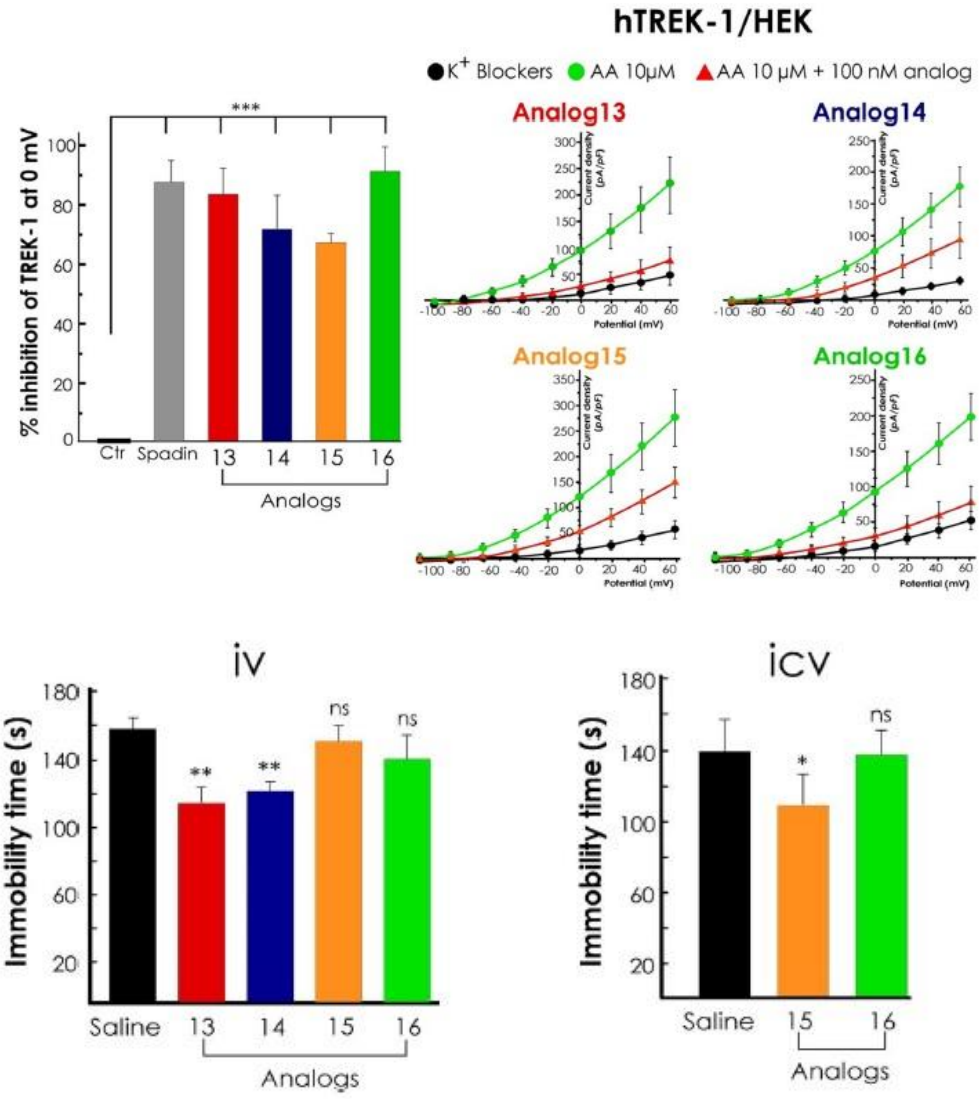

Figure 13 : Propriétés inhibitrices et antidépressives des analogues 13 à 16 de la Spadine

Cette stratégie des RI qui semblait prometteuse a été abandonnée, car des effets délétères ont été observés. *In vitro*, dans des cultures cellulaires, l'utilisation des analogues RI à forte concentration provoque une mort cellulaire accrue. Une autre stratégie de synthèse d'analogues de la Spadine a alors été envisagée : les analogues courts.

C- Analogues courts

Ce chapitre fait l'objet de la Première partie de la section Résultats.

Comportement

Dans la recherche sur les pathologies, une des contraintes est de rendre comparable l'état des modèles animaux utilisés à celui de l'être humain. Il faut pour cela être capable d'évaluer de nombreux aspects du comportement de ces animaux, comme par exemple les capacités motrices, la mémorisation, ou encore l'état émotionnel. De nombreux modèles comportementaux ont été développés dans cette optique, comme par exemple les tests du mât, du rotarod ou du retrait de l'adhésif pour la coordination motrice, mais également les tests de la piscine de Morris ou du labyrinthe circulaire pour la mémorisation. Il existe également des modèles développés pour évaluer l'état émotionnel des animaux, tels que les tests de la nage forcée, de la résignation apprise, de la suppression de l'alimentation induite par la nouveauté, de la suspension par la queue ou de l'interaction sociale (Engel et al., 2011).
Il est cependant important de prendre en compte le fait qu'un seul protocole ne permet pas de tirer de conclusion sur le phénotype des animaux. Il est donc nécessaire d'utiliser une variété de tests : dans le cadre de notre étude, nous avons par exemple choisi d'utiliser les tests du mât et du Rotarod pour évaluer la condition physique des animaux. Nous avons également choisi les modèles de la nage forcée, de la suppression de l'alimentation induite par la nouveauté, et de la résignation apprise pour estimer leur état émotionnel. Ainsi que la Piscine de Morris dans le but d'évaluer leurs capacités de mémorisation.
Je ne décrirai ici que les tests utilisés pendant mon Doctorat.

I- Tests d'anxiété/résignation

Ces tests sont habituellement utilisés pour le criblage de molécules antidépressives.

A-Learned Helplessness (LH)

Le test de la résignation apprise consiste à placer les animaux dans une enceinte close où ils vont recevoir des chocs électriques auxquels ils ne peuvent échapper. Ce protocole est répété durant quatre jours consécutifs, c'est le conditionnement. Le cinquième jour, le jour test, les

souris ont cette fois la possibilité de s'échapper après avoir reçu le choc électrique. La mesure de la latence à cette fuite du stimulus douloureux permet de dissocier les animaux résignés des autres. En effet, un animal résigné aura beaucoup moins tendance à tenter de fuir après les quatre jours de conditionnement. Il restera prostré et subira passivement le protocole.
Dans ce test, un traitement avec des antidépresseurs fait diminuer la latence à l'échappement.

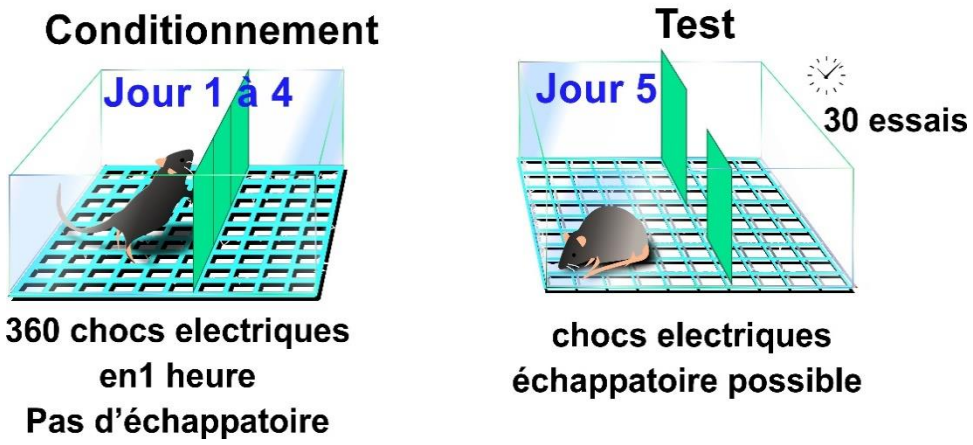

Figure 14 : Représentation du conditionnement et du test dans le modèle du LH

Le protocole que nous avons utilisé est le suivant.
Lors du conditionnement les souris reçoivent 360 chocs électriques non évitables de 0.3mA, durant une heure (la porte, séparant les deux compartiments, reste fermée). Les chocs sont d'une durée de 2 secondes et un intervalle de 8 secondes est respecté entre chaque choc. Cette étape de conditionnement permet d'induire un phénomène de résignation chez les animaux.
Le jour du test, les souris sont placées dans les mêmes compartiments mais avec une possibilité d'échapper au choc. Le test compte 30 essais. Lors de l'administration du choc la porte séparant les deux compartiments s'ouvre, permettant aux animaux de fuir. Lorsque l'animal change de compartiment l'essai est terminé et une nouvelle séquence choc/ouverture de porte est initiée. Si la souris ne change pas de compartiment, la porte se referme au bout de 24 secondes et une autre séquence est lancée. Ce test permet d'enregistrer les latences d'échappement des animaux.

B- Porsolt Forced Swimming Test (FST)

Le test de la nage forcée a été mis au point par Porsolt vers la fin des années 70 (Porsolt et al., 1977). Dans ce test, les animaux sont placés dans un cylindre partiellement rempli d'eau à 21-23°C, sans aucune échappatoire, pendant 6 minutes.

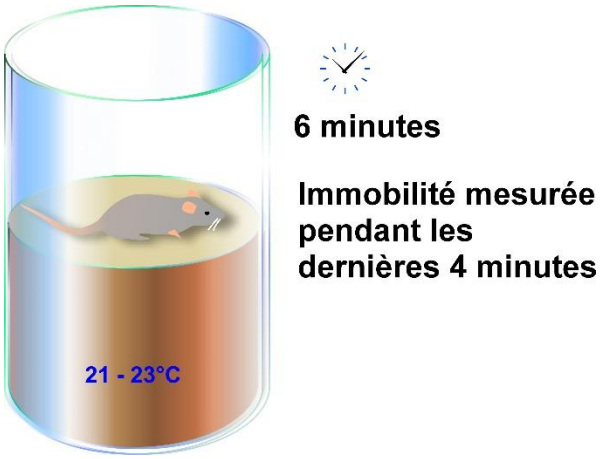

Figure 15 : Représentation du FST

L'idée de base est que dans une situation de stress (ici l'immersion) l'animal va tenter de fuir, et pour cela il va nager énergiquement pour trouver une sortie. Or il n'y en a aucune. Un animal qui continue à nager bien qu'il ne trouve pas de sortie est considéré comme combatif, ce qui est un comportement normal pour une souris. En revanche, un animal qui s'arrêt de nager pour se laisser flotter est « résigné » à son sort. Or la résignation est un des symptômes de la dépression. Ainsi, les temps d'immobilité des animaux est mesuré durant les quatre dernières minutes du test, les 2 premières minutes servent de conditionnement. Plus le temps d'immobilité est important, plus l'animal est résigné.

Dans ce test, l'administration d'antidépresseurs fait diminuer ce temps d'immobilité des animaux.

C- Novelty Suppressed Feeding Test (NSF)

Le test de suppression de l'alimentation induite par la nouveauté se base sur la balance entre le besoin de se nourrir et la peur de s'aventurer en pleine lumière dans un espace inconnu. Dans ce test, les souris sont mises à jeun pendant 24 heures. Elles sont ensuite déposées dans une

enceinte recouverte de sciure placée sous une lumière vive (milieu très anxiogène pour les souris). Une plateforme avec une boulette de nourriture est placée au centre. Les souris sont laissées libres, et le temps nécessaire aux animaux pour aller se nourrir est mesuré.

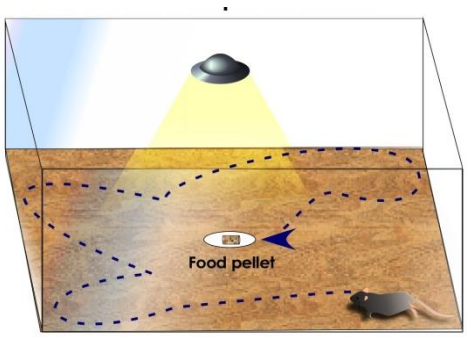

Figure 16 : Représentations du NSF

Plus cette latence est importante, plus la souris est anxieuse (son anxiété est plus importante que sa faim). Le test dure au maximum 10 minutes. Ce test est corrélé à la neurogenèse hippocampique (Santarelli et al., 2003). La diminution de la latence est faible correspond à la mise en place de la neurogenèse.

Dans ce test, l'utilisation d'antidépresseurs fait diminuer le temps nécessaire aux animaux pour aller se nourrir.

II- Test de cognition

A-Morris Water Maze (MWM)

Le test de la piscine de Morris, développé dans les années 80 par Richard Morris, s'intéresse à la capacité de mémorisation spatiale des animaux (Morris, 1984) (Vorhees and Williams, 2006) (Winter et al., 2004). Tout comme le LH, ce test se déroule en deux phases. Durant la première phase, ou l'apprentissage, les animaux sont placés dans un bassin rempli d'eau rendue opaque,

et doivent apprendre à retrouver une plateforme cachée qui leur permettra de se mettre au sec. Pour cela les souris s'aident de repères de couleur disséminés dans la pièce. Chaque souris est placée dans la piscine quatre fois chaque jour (toujours à un endroit différent), et le temps nécessaire pour trouver la plateforme est enregistré. Dans la deuxième phase, le test proprement dit, les animaux sont de nouveau mis dans le bassin, mais cette fois la plateforme est retirée. Cela permet de suivre le parcours des animaux pendant 1 minute et de relever le temps qu'ils passent à chercher la plateforme dans la zone, appelée quadrant (sur l'exemple ci-dessous NW), où cette dernière se trouvait pendant l'apprentissage. Plus les souris passent de temps dans cette zone, meilleure est leur capacité de mémorisation spatiale.

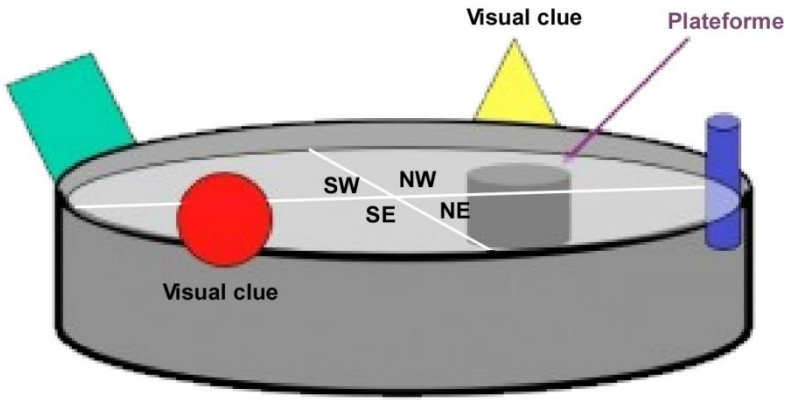

Figure 17 : Représentation de la Piscine de Morris

D'autres paramètres peuvent être mesurés grâce à ce test. La vitesse de nage et la distance parcourue, ces deux mesures peuvent rendre compte de l'absence ou au contraire de la présence de troubles moteurs. Différents types de stratégies peuvent également être analysées, Ces différentes stratégies sont modélisées dans la **figure 18**. Il s'agit i) du thigmotaxis, où l'animal tourne autour de la piscine très près de la paroi ; ii) du « chaining » qui proche du thigmotaxis mais où la zone de nage est comprise entre la paroi et la position de la plateforme ; iii) du balayage ou « scanning » où l'animal nage au hasard dans une zone particulière de la piscine ; iv) au hasard ou « random », où l'animal nage au hasard sur toute la surface de la piscine, et enfin v) la persévérance, où l'animal nage principalement dans la zone où était positionnée la plateforme.

Thigmotaxis

La souris nage tout autour de la piscine collée à la paroi

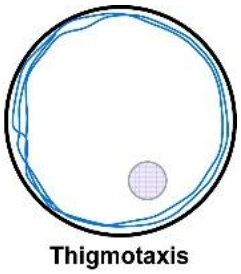

Chaining

La souris nage tout autour de la piscine dans une zone définie par la paroi et la position de la plateforme

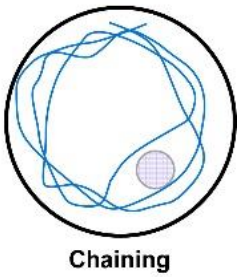

Balayage ou Scanning

La souris nage au hasard dans une seule zone de la piscine

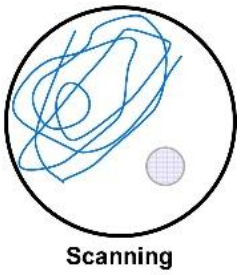

Au hasard ou Random

La souris nage au hasard dans toute la piscine

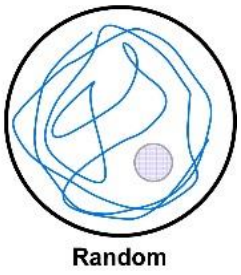

Persévérance

La souris nage dans la zone où il y avait la plateforme

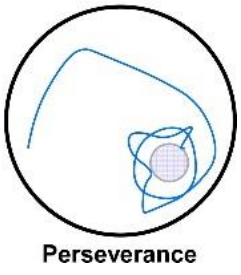

Figure 18 : Récapitulatif des différentes stratégies de recherche dans le MWM

III- Tests moteurs

A-Rotarod

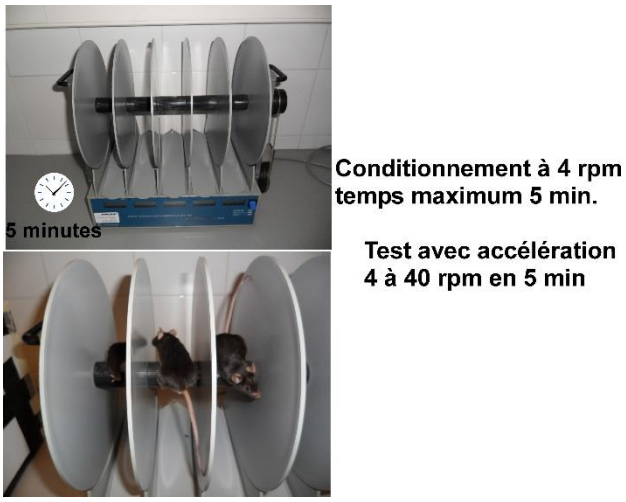

Figure 19 : Représentation du Rotarod

Le test du rotarod permet d'évaluer les fonctions motrices des animaux (Hunter et al., 2000). Le test du rotarod se fait en deux étapes : le conditionnement et le test. Le conditionnement se fait en plaçant les souris sur l'appareil que l'on fait tourner à petite vitesse, 4 rpm, pendant 5 minutes maximum. Après une période de repos de 5 minutes, le même protocole est appliqué, puis renouvelé une troisième fois. Pour le test, les souris sont placées sur l'appareil mais cette fois la vitesse de rotation augmente de façon régulière de 4rpm à 40rpm en 10 minutes. Plus les souris parviennent à rester longtemps sur l'appareil, meilleure est leur coordination motrice, et donc meilleure est leur récupération.

B- Pole Test

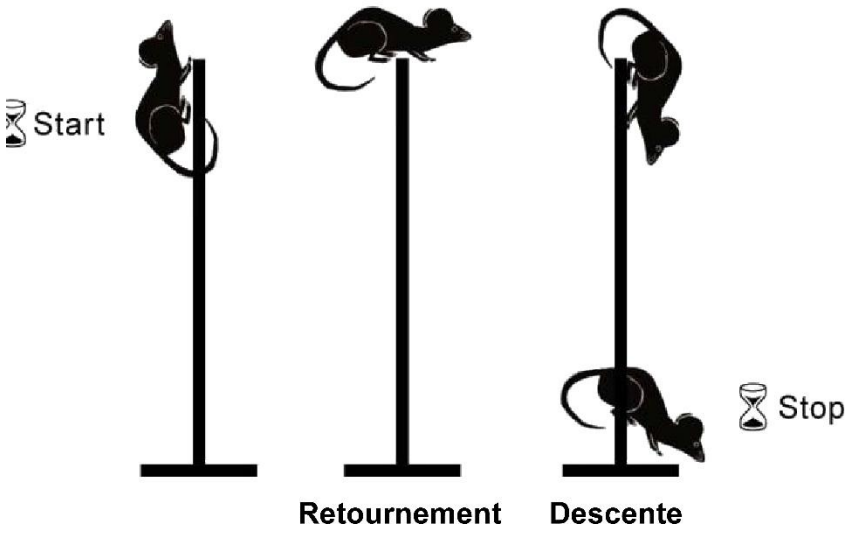

Figure 20 : Représentation du Pole test

Tout comme le rotarod, le test du mât ou pole test s'intéresse aux fonctions motrices des animaux (Bouet et al., 2007) (Matsuura et al., 1997). Les souris sont déposées au sommet d'un mât de 40 cm, la tête vers le haut. Deux variables sont alors mesurées : la latence au retournement (la tête vers le sol), et le temps nécessaire à la descente, la souris est considérée ayant descendu le mât au moment où ses quatre pattes touchent le support sur lequel il est posé. Plus la souris est rapide dans ces deux tâches, meilleure est sa récupération.

Les projets

I-Historique

A mon arrivée, l'équipe des Docteurs Heurteaux et Mazella travaillait depuis longtemps sur le développement de nouvelles stratégies thérapeutiques face à l'AVC et à la dépression. 10 ans auparavant, le laboratoire avait identifié le canal potassique TREK-1 comme étant une nouvelle cible importante face à ces deux pathologies (Heurteaux et al., 2004) (Heurteaux et al., 2006a). Puis, en 2010, la découverte de la Spadine (PE 12-28) et de sa capacité à bloquer l'activité des canaux TREK-1 a inspiré l'hypothèse que la Spadine pourrait être une molécule de choix dans le développement de nouveaux traitements contre la dépression.

La stabilité *in vivo* de la Spadine n'étant que de 6 heures, le laboratoire a cherché à concevoir des analogues afin d'augmenter la biodisponibilité et l'efficacité de cette molécule. Une première stratégie a consisté en la synthèse d'analogues retro-inverso (RI) (Veyssiere et al., 2015). Cette technologie permet de stabiliser les peptides. Elle consiste à utiliser des amino acides en conformation D (les acides aminés sont naturellement en conformation L) et à synthétiser la séquence en inversant l'ordre des amino acides (N vers C devient C vers N). Mais *in vitro,* sur culture cellulaire, ces peptides RI utilisés à haute concentration ont des effets délétères. Le laboratoire s'est alors tourné vers une seconde stratégie : synthétiser des analogues courts.

Mon projet de thèse comporte 2 chapitres. Le premier avait pour but de déterminer si ces analogues courts conservaient les propriétés antidépressives de la Spadine. Le deuxième a consisté à identifier si ces analogues avaient des propriétés neuroprotectrices, notamment face à l'AVC, et plus particulièrement dans le cadre de la dépression post-AVC. En effet il a été montré que l'utilisation d'AD améliorait la récupération des patients ayant subi un AVC (Chollet et al., 2011).

II- Objectifs

A- Partie I : Les propriétés antidépressives des analogues courts de la Spadine (Article 1)

Rappelons ici que le peptide issu de la maturation post-transcriptionnelle de la Sortiline est appelé PE. Ce PE est composé de 44 acides aminés : PE 1-44. Les peptides courts sont identifiés en fonction du PE, ainsi la Spadine devient PE 12-28.

L'analyse par spectrométrie de masse des produits de dégradation de la Spadine dans le sang a permis d'identifier deux peptides, PE 12-27 et PE 14-25. Grâce à une étude structure-fonction, nous avons pu identifier le plus petit peptide issu de la séquence de la Spadine qui en conserve ses propriétés sur TREK-1, le PE 22-28 ou Mini-Spadine. Des études de patch-clamp sur des cellules hTREK-1/HEK ont montré que ce PE 22-28 a une meilleure affinité pour le canal TREK-1 par rapport à la Spadine (IC_{50} de 0,12 nM vs. 40-60 nM), soit une augmentation de plus de 300 fois. Dans le but d'augmenter encore son efficacité, les extrémités de la séquence de cet analogue ont ensuite été modifiées, et 12 autres peptides ont été synthétisés. Un nouveau criblage électrophysiologique de cette cohorte a permis d'identifier, en plus du PE 22-28, le G/A-PE 22-28 et le G/A-PE 22-28 Biotinylé, où l'Alanine en position N-terminale a été remplacée par une Glycine dans la séquence du PE 22-28.

La raison pour laquelle ces analogues ont été conçus était d'améliorer la stabilité *in vivo* de la Spadine. Il s'agit donc du premier paramètre analysé : le test du FST a montré que les effets antidépresseurs de ces analogues étaient toujours visibles jusqu'à 23 heures après leur administration, contre seulement 6 heures pour la Spadine. Nous avons ensuite confirmé ces effets dans d'autres tests comportementaux comme celui du NSF et du LH, réalisés dans un modèle de dépression induite par un traitement chronique avec de la corticostérone (la corticostérone est diluée dans l'eau de boisson à raison de 35mg/L, et les souris sont soumises à ce régime pendant 7 semaines). Tout comme la Spadine, le PE 22-28 et ses analogues sont également capables d'induire une neurogenèse après seulement 4 jours de traitement. *In vitro,* le PE 22-28 et ses dérivés stimulent la synaptogenèse mesurée par l'augmentation du niveau d'expression PSD-95 dans des neurones corticaux de souris.

Ces données démontrent que le PE 22-28 et ses dérivés sont de nouvelles molécules prometteuses qui pourraient constituer une alternative à la Spadine dans le traitement de la dépression, car non seulement ils ont conservé toutes les propriétés de la Spadine, mais ils sont aussi beaucoup plus courts et donc auront un coût de synthèse moindre. Donnée économique importante dans la perspective d'en faire un médicament utilisable chez l'Homme (ou l'animal).

B- Partie II : Les propriétés de la Spadine et de la Mini-Spadine dans l'AVC et la récupération post AVC (Article 2)

Ces résultats concluants quant aux effets AD des analogues de la Spadine m'ont permis d'entreprendre une étude sur leurs éventuelles propriétés neuroprotectrices dans le cadre de l'AVC et de la dépression post-AVC.

TREK-1 est une cible importante dans les pathologies de la dépression et de l'AVC. Dans le cadre de la dépression, c'est son inhibition qui provoque l'effet antidépressif (Heurteaux 2006). En revanche dans le cas de l'ischémie, c'est son activation qui est protectrice (Heurteaux 2004). Il aurait donc à priori un effet paradoxal. Mais des études électrophysiologiques ont mis en évidence que la Mini-Spadine avait une action biphasique sur l'activité TREK-1 en conditions basales. A faibles doses, l'activité du canal est augmentée, tandis qu'à doses élevées, l'activité de TREK-1 est inhibée. A partir de ces résultats nous avons dessiné un protocole expérimental constitué de 2 phases distinctes. Cette étude a été conduite sur le modèle d'AVC murin MCAO où l'ischémie focale est induite par l'occlusion de l'artère cérébrale moyenne, un modèle utilisé en routine dans notre laboratoire. Pour activer TREK-1 et induire un effet neuroprotecteur, les souris ont reçu une injection intrapéritonéale quotidienne de Mini-Spadine à faible concentration (0,03 µg/kg) durant la première semaine suivant l'ischémie. Ensuite, pour inhiber TREK-1 et induire un effet antidépresseur, le peptide est injecté à une concentration plus élevée (3 µg/kg) une fois par jour pendant 4 jours/semaine jusqu'au sacrifice des animaux.

Avant d'appliquer ce protocole expérimental, nous avons vérifié qu'une injection unique (traitement aigu) de Mini-Spadine à faible concentration (0,03 µg/kg) avait un effet protecteur. Cette injection aiguë permet de réduire significativement la taille de l'infarctus généré par la MCAO (volume de l'infarctus plus faible) et augmente le taux de survie).

L’état dépressif mesuré par le test du FST (test de la nage forcée) apparaît clairement après 10 semaines. Nous avons donc suivi les effets du peptide sur 10 semaines en soumettant les animaux à différents tests comportementaux. Le premier paramètre que nous avons mesuré est le poids. Les animaux traités avec la Mini-Spadine perdent moins de poids et moins vite que les animaux non traités. Le deuxième paramètre mesuré est la récupération motrice. Là encore les animaux traités récupèrent plus rapidement que les animaux non traités.

Dans la phase chronique du traitement à concentration plus élevée, la Mini-Spadine réduit les déficits cognitifs mesurés en Piscine de Morris, et empêche le développement d’un état dépressif, analysé dans les tests de FST et NSF (Suppression de l’Alimentation induite par la Nouveauté). Elle freine également la dégénérescence dopaminergique dans la *substantia nigra,* et elle augmente la neurogenèse hippocampique et la synaptogenèse.

Ce travail révèle les premières preuves que la modulation des canaux TREK-1 dans les phases précoces et chroniques de l'AVC, ainsi que la stimulation de la plasticité cérébrale par la Mini-Spadine, pourraient jouer un rôle clé dans ses effets protecteurs du cerveau contre les AVC et ses conséquences délétères comme la dépression post AVC.

Ces résultats ouvrent la possibilité de développer un concept novateur en neuroprotection contre les AVC et les dépressions post-AVC chez l’Homme. C’est d’autant plus important qu’il n’existe aujourd’hui que peu de thérapies pour ces pathologies (voire Introduction Chapitre III).

III- Résultats

A- Partie I : Les propriétés antidépressives des analogues courts de la Spadine (Article 1)

1- Introduction

La dépression est une pathologie complexe et son impact social est important. En effet, 20% de la population mondiale ont déjà fait ou feront un épisode dépressif au cours de leur vie. Un des problèmes majeurs de la dépression est que les mécanismes à l'origine de cette pathologie ne sont pas totalement élucidés. C'est une des raisons pour lesquelles les traitements actuels ne sont pas totalement efficaces : un tiers de la population ne répond pas aux molécules antidépressives (SSRI, TCA, IMAO). Il est donc nécessaire d'en trouver de nouvelles. C'est dans ce but que le laboratoire a dessiné la Spadine, un peptide créé à partir d'un peptide endogène issu de la maturation post-traductionnelle de la Sortiline. La plupart des antidépresseurs actuels cherchent à augmenter la quantité de neurotransmetteurs dans la fente synaptique en inhibant leur recapture ou leur dégradation. La Spadine n'a pas les mêmes cibles, elle agit en tant que bloqueur du canal potassique TREK-1. Notre laboratoire a démontré que ce canal est un acteur important dans le processus de la dépression. Les premières études ont mis en évidence le fort potentiel antidépresseur de la Spadine ainsi que son absence d'effets secondaires. Deux propriétés qui en font un candidat de choix pour le développement d'un nouveau type de traitement contre la dépression. Cependant, la stabilité *in vivo* de la Spadine est de 6h. Dans le cas où la Spadine deviendrait un médicament, ce délai n'autoriserait pas une seule prise journalière. En effet, il faut savoir qu'un tiers des patients ne sont pas traités car ils abandonnent, très souvent par omission, leur médicament, en diminuant le nombre de prises quotidiennes on diminue le risque d'oubli. C'est la raison pour laquelle notre laboratoire a cherché à augmenter cette stabilité. Pour cela il a développé deux stratégies, les rétro-inverso et les analogues courts.

Dans un premier temps, c'est la stratégie des Retro Inverso (RI) qui a été utilisée. Cette technologie consiste à inverser la séquence en acides aminés des peptides (Cterm→Nter devient Nter→Cter) et la synthèse se fait en utilisant des aminoacides en configuration D au lieu de la

configuration L (la naturelle). Bien que certains de ces analogues se soient révélés plus stables et plus afin pour TREK-1 que la Spadine, ils se sont également révélés délétères à fortes concentrations sur des cultures de neurones. Cette approche a donc été écartée et le laboratoire s'est orienté vers une autre stratégie : les analogues courts.

A mon arrivée au laboratoire, l'équipe des Docteurs Heurteaux et Mazella, venait d'identifier le PE 22-28 (Mini-Spadine), le plus petit peptide issu de la séquence de la Spadine qui en a conservé les propriétés d'inhibition des courants TREK-1, et surtout les propriétés antidépressives. Le PE 22-28 a servi de « peptide-squelette » (Core-peptide) pour générer une nouvelle série d'analogues. Toujours dans l'optique d'identifier la molécule issue de la Spadine la plus adaptée à un usage en clinique humaine, j'ai dans la première partie de mon projet déterminé quels analogues avaient conservé les propriétés antidépressives. Une fois identifié, j'ai étudié leur stabilité *in vivo*.

2- Résultats

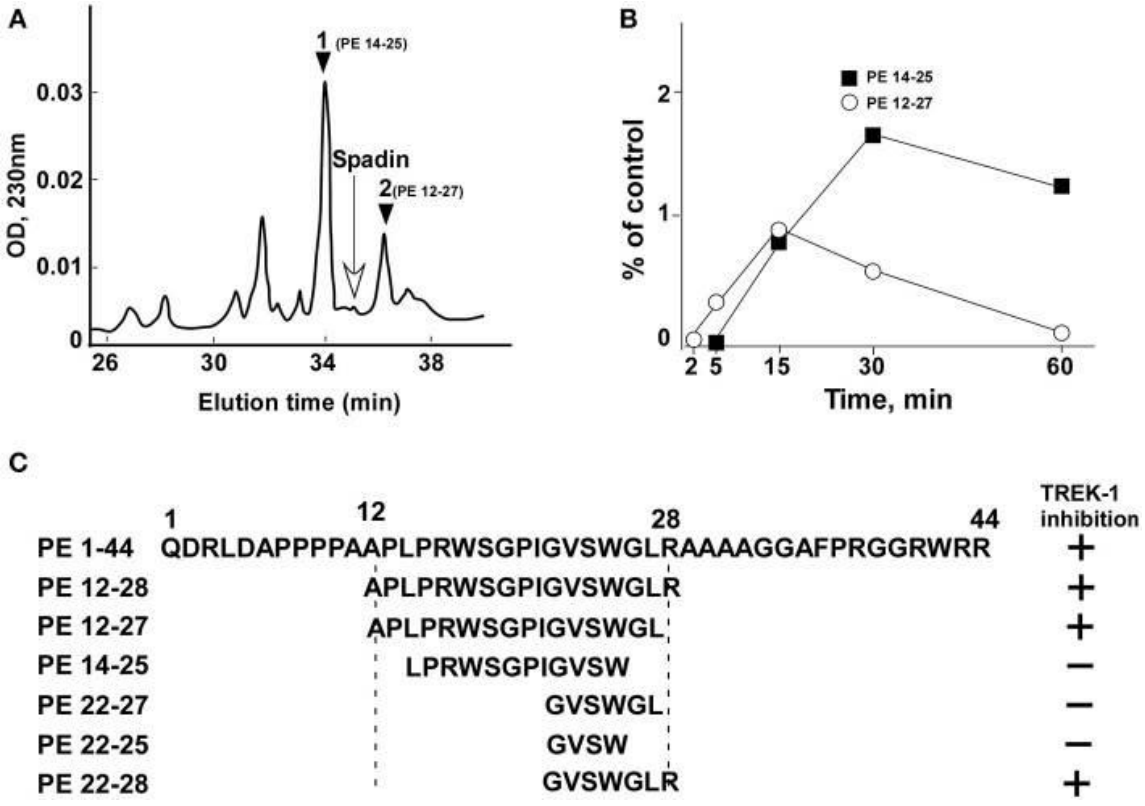

Figure 21 : Profil de dégradation HPLC de la Spadine dans le sérum

L'identification du PE 22-28 avait été obtenue grâce à une étude structure-fonction réalisée à partir de produits de dégradation de la Spadine par du sérum, incubation 30 minutes à 37°C. La spectrométrie de masse a permis d'identifier deux peptides, le PE 14-25 et le PE 12-27 (**Figure 21A- B**).

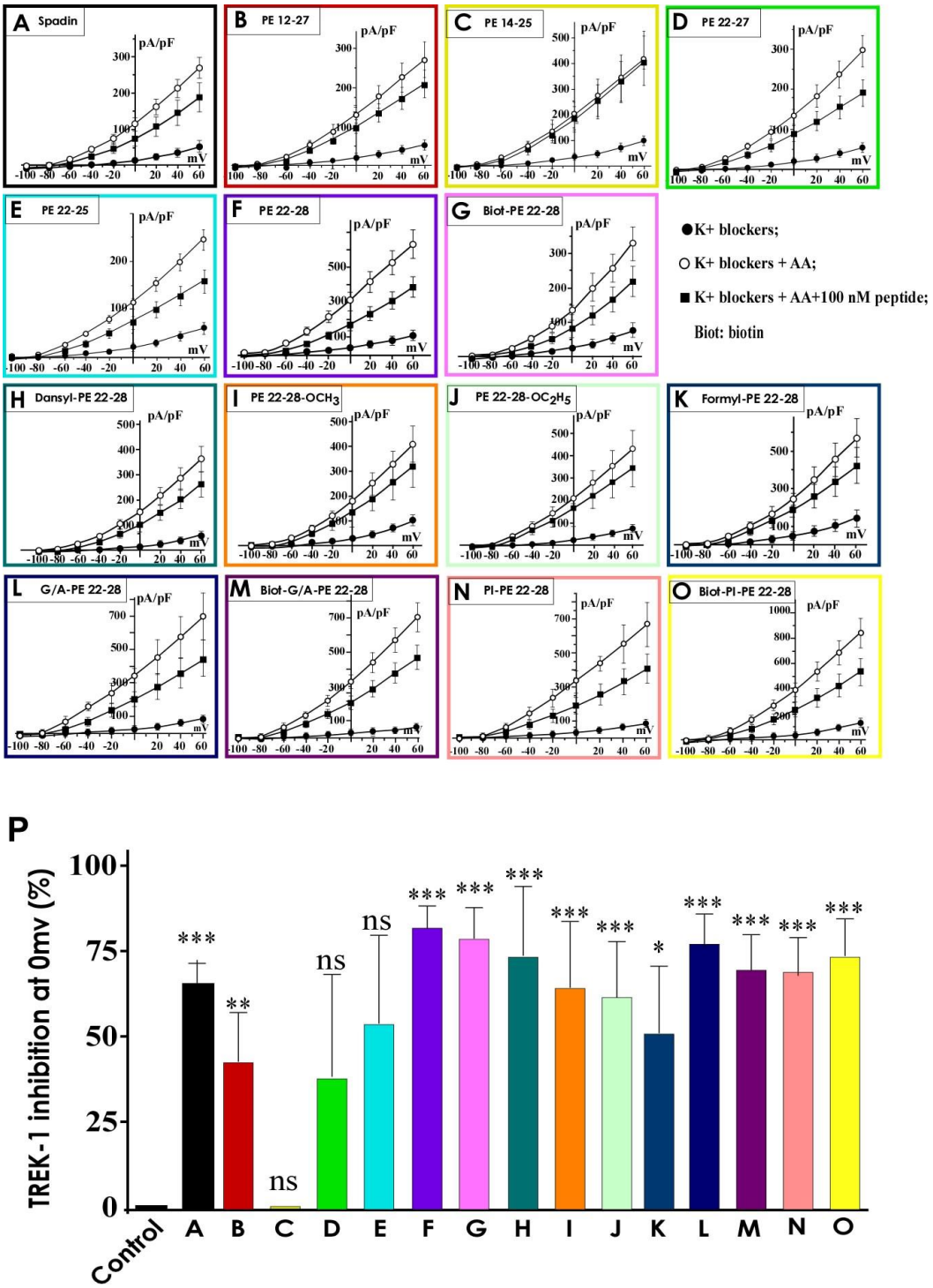

Figure 22 : Inhibition de TREK-1

Ces deux produits de dégradation (PE 14-25 et PE 12-27) ont ensuite été testés individuellement sur la lignée cellulaire hTREK-1/HEK (Moha ou Maati et al., 2011) en utilisant la technique du patch-clamp **(Figure 21C)**. Pour cela, les canaux TREK-1 ont été activés au préalable avec 10 µM AA (Patel et al., 1998b), et une fois l'amplitude maximale atteinte, la capacité à inhiber l'activité du canal TREK-1 de chaque peptide (100 nM) a été mesurée avant de la comparer avec celle de la Spadine (**Figure 22**). L'analogue PE 14-25 n'a aucun effet sur TREK-1 **(Figure 22C et P**). En effet, la densité de courant mesurée à 0 mV et comparée à l'activité AA seule (100 %) était de 114,7 ± 10,6 % (n = 8, p = 0,09). En revanche, le PE 12-27 est capable d'inhiber fortement l'activité du TREK-1 28,4 ± 9,9 % (n = 22, p = 0,03 **(Figure 22B et P).**

Analogues	Noms	Modifications	% d'inhibition de TREK-1	Spécificité	FST en aigu (sec)	Spécificité
1	**PE 12-28 (Spadin)**	**No modification**	**87,08 ± 7,32**	***	**107.40 ± 5.05**	***
2	Ac-PE 12-28	N-acetylation	83,46 ± 8,33	***	nd	nd
3	Ac-RI-PE 12-28	retro-inverso of spadin	94,43 ± 10,87	***	135.10 ± 8.11	**
4	Ac-PE-22-28	N-acetylation	19,29 ± 25,7	ns	nd	nd
5	Ac-PE-21-28	N-acetylation	26,89 ± 14,9	ns	nd	nd
6	Ac-RI-PE-21-28	N-acetylation + retro-inverso	31,19 ± 17,8	ns	nd	nd
7	Ac-PE 1-28	N-acetylation	10,43 ± 28,5	ns	nd	nd
8	Ac-RI-PE 1-28	N-acetylation + retro-inverso	108,59 ± 10	***	83.60 ± 9.01	***
9	Ac-PE 6-28	N-acetylation	71,85 ± 28,12	**	nd	nd
10	Ac-RI-PE 6-28	N-acetylation + retro-inverso	56,47 ± 24,13	*	nd	nd
11	Ac-PE 1-44	N-acetylation	26,97 ± 6,25	ns	nd	nd
12	Ac-RI-PE 1-44	N-acetylation + retro-inverso	37,73 ± 8,77	ns	nd	nd
13	G/A-PE 12-28	aa substitution	83,5 ± 9,76	***	120,4 ± 9,7	**
14	RI-G/A-PE 12-28	retro-inverso +aa substitution	72,15 ± 11,75	***	127,7 ± 8,32	**
15	c(RI-PE 12-28)	cyclization	67,24 ± 3,41	***	157 ± 8,09	ns
16	$c(RI\text{-}PE\ 12\text{-}28)_2$	cyclization	91,25 ± 8,14	***	146,7 ± 12,99	ns
17	PE 12-27	No modification	28,39 ± 9,916	**	100.2 ± 5.0	***
18	PE 14-25	No modification	0	ns	112.2 ± 7.1	**
19	PE 22-27	No modification	25,7 ± 20,01	ns	168.2 ± 4.2	ns
20	PE 22-25	No modification	36,02 ± 17,47	*	100.2 ± 5.0	***
21	**PE 22-28**	**No modification**	**55,46 ± 4,555**	***	**91.8 ± 6.1**	***

22	Biotin-PE 22-28	N-biotinylation	53,03 ± 6,416	***	112.1 ± 4.3	***
23	Dansyl-PE 22-28	N-dansylation	48,78 ± 14,52	**	104.6 ± 11.8	***
24	PE 22-28-O-Methyl	C-methoxylation	42,98 ± 13,47	**	137.1 ± 8.1	*
25	PE 22-28-O-Ethyl	C-ethoxylation	41,39 ± 11,52	**	113.2 ± 8.5	***
26	Formyl-PE 22-28	N-formylation	32,45 ± 12,22	*	nd	nd
27	**G/A-PE 22-28**	**aa substitution**	**50,61 ± 7,935**	***	**110.2 ± 3.6**	***
28	**Biotin-G/A-PE 22-28**	**aa substitution+N-biotinylation**	**46,11 ± 7,743**	***	**140.7 ± 7.1**	*
29	PI-PE 22-28	No modification	46,19 ± 7,565	***	119.7 ± 11.8	**
30	Biotin-PI-PE 22-28	N-biotinylation	49,11 ± 7,454	***	124.1 ± 11.7	**
31	Palmitoyl-PE 22-28	N-palmitoylation	26,69 ± 16,45	ns	nd	nd
32	FITC-PE 22-28	N-FITC group	22,1 ± 12,63	ns	nd	nd
33	Acetyl-PE 22-28	N-acetylation	20,49 ± 8,777	*	nd	nd
34	Myristoyl-PE 22-28	N-myristoylation	18,04 ± 17,77	ns	nd	nd
35	LC biotin-PE 22-28	N-long chain biotinylation	15,86 ± 11,21	ns	nd	nd
36	5'FAM-PE 22-28	N-5'FAM group	6,633 ± 7,065	ns	nd	nd
37	FMoc-PE 22-28	N-Fmoc group	5,826 ± 10,91	ns	nd	nd
38	**Stearic acid-PE 22-28**	**N-stearic acid group**	**5,412 ± 5,496**	**ns**	**nd**	**nd**

Tableau 1 : Récapitulatif des analogues de la Spadine

A partir de ces observations, trois autres peptides plus courts ont été synthétisés : PE 22-25, PE 22-27 et PE 22-28 qui ont, à leur tour, été testés en patch-clamp. Finalement, seul le PE 22-28 (**Figure 21 et Figure 22D-F et P**) bloque efficacement l'activité du TREK-1 (55,46 ± 4,6 %, n = 13, $p < 0,0001$).

Ce criblage a permis d'identifier le PE 22-28 comme l'inhibiteur TREK-1 le plus efficace, son affinité pour TREK-1 très supérieure à celle de la Spadine, 0.1 nM contre 40 nM soit une augmentation de 400 fois **(Figure 23B).** Dans le but d'augmenter encore plus la stabilité et l'efficacité du peptide, nous avons utilisé le PE 22-28 comme peptide central pour la conception de plusieurs analogues, notamment en modifiant ses extrémités N- et C-term **(Tableau 1, lignes 22-38).**

Parce que la capacité d'une molécule à passer à travers la BHE est une propriété cruciale pour un médicament agissant sur des cibles cérébrales. Il a été démontré que la biotinylation augmente l'absorption des peptides par le cerveau (Scherrmann, 2002) (Wu et al., 2002). De fait, à certains de ces analogues un groupement biotine a été ajouté à leur extrémité N-terminale Tous les analogues ont été testés pour leur capacité à inhiber TREK-1, seuls ceux qui inhibaient l'activité de TREK-1 à plus de 35%, ont été retenus, leurs propriétés AD ont été évaluée par FST (**Figure 22G-P**) : le PE 22-28 biotinylé **(Figure 22G**), le dansyl-PE 22-28 (un groupe chimique dansyle a été ajouté en N-terminal) **(Figure 22H)**, le O-méthyl-PE 22-28 et le O-éthyl-PE 22-28 (un groupe chimique O-méthyle ou O-éthyle a été ajouté en C-terminal) (**Figure 22I et J**), le Formyl-PE 22-28 (un groupement formyl est ajouté à la séquence) **(Figure 22K)**, le G/A-PE 22-28 (la séquence PE 22-28 où la Glycine en position 22 est remplacée une Alanine) (**Figure 22L**), G/A-PE 22-28 biotinylé (**Figure 22M**), le PI-PE 22-28 (la séquence PE 20-28 avec un résidu Proline et un résidu Isoleucine en N-terminal) (**Figure 22N**), le PI-PE 22-28 biotinylé (**Figure 22O et Tableau 1).**

Les analogues, dont le pourcentage d'inhibition de TREK-1 était supérieur à 35 ont été testés *in vivo* pour leurs propriétés antidépressives. Le test que nous avons choisi d'utiliser est le FST réalisé en condition aiguë c'est-à-dire 30 minutes après une injection i.p. unique à une concentration unique (3 µg/kg) d'analogue. Grâce à ce test nous avons pu établir que chaque analogue capable d'inhiber TREK-1 est également capable de réduire le temps d'immobilité mesuré dans ce test **(Figure 23A).**

En fonction des performances observées à la fois en électrophysiologie et en comportement, nous avons sélectionné le PE 22-28, le G/A-PE 22-28 et le G/A-PE 22-28 biotinylé. Outre leur pourcentage élevé d'inhibition du courant TREK-1, ces analogues sont également beaucoup plus affins pour le canal (**Figure 23B**). En effet, l'IC_{50} mesurée de la Spadine (PE 12-28) est de 40 nM, alors que celles des PE 22-28 et G/A-PE 22-28 sont de 0,10 et 0,12 nM (soit pratiquement 400 fois supérieure à celle de la Spadine), et celle du biotine-G/A-PE 22-28 est de 1,2 nM (30 fois supérieure à celle de la Spadine).

Par souci de simplification et de clarté, dans la suite de ce manuscrit ces trois peptides seront regroupés sous l'appellation : « analogues de la Spadine ».

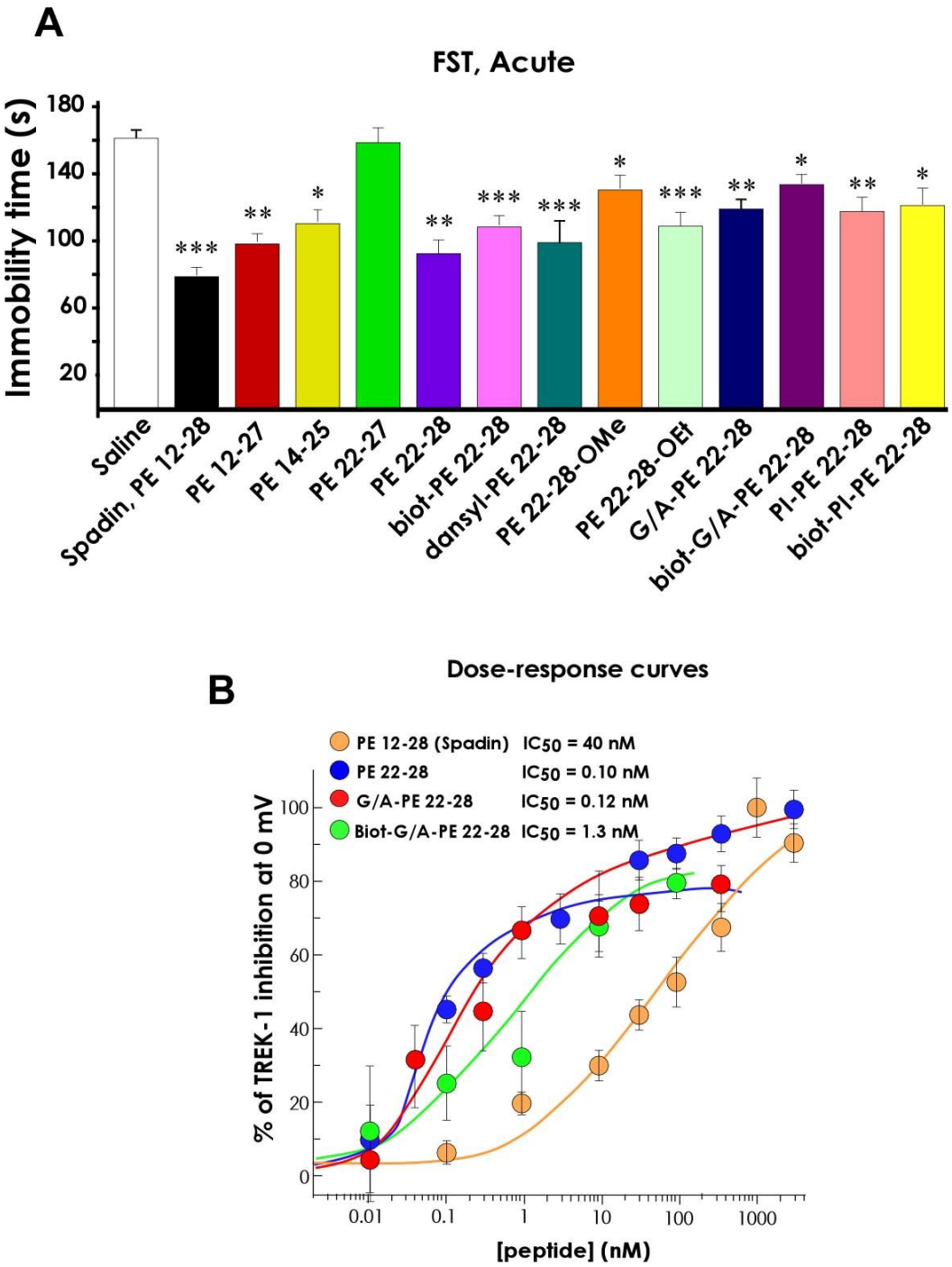

Figure 23 : Effet des analogues en FST et courbe de dose réponse sur TREK-1

Le but principal du laboratoire était de trouver des analogues ayant une meilleure stabilité *in vivo* que la Spadine elle-même. Nous nous sommes donc intéressés à mesurer la durée d'action du G/A-PE 22-28 et du biotine-G/A-PE 22-28. Dans ce but, nous avons injecté en i.p, dans un bolus de 100µL, ces analogues à des souris naïves, à des doses finales de 3,2 µg/kg ou 32 µg/kg pour le G/A-PE 22-28, ou de 4,0 µg/kg ou 40 µg/kg pour le biotine-G/A-PE 22-28. Chaque

groupe de souris (10 par temps) a ensuite été soumis au test du FST 1, 3, 5, 7, 12, 16, 20 ou 24 heures après l'injection (**Figure 24A**). Les groupes contrôles (injectés avec du sérum physiologique) n'ont été soumis au FST qu'à 1 ou 24 h, de façon à constater que le temps d'immobilité des contrôles ne variait pas pendant le temps de l'expérience. De fait, le temps que les souris passent sans nager est similaire pour les deux temps : 171,2 ± 8,2 s au temps 1h, et 175,5 ± 6,8 s au temps 24h (**Figure 24A**).

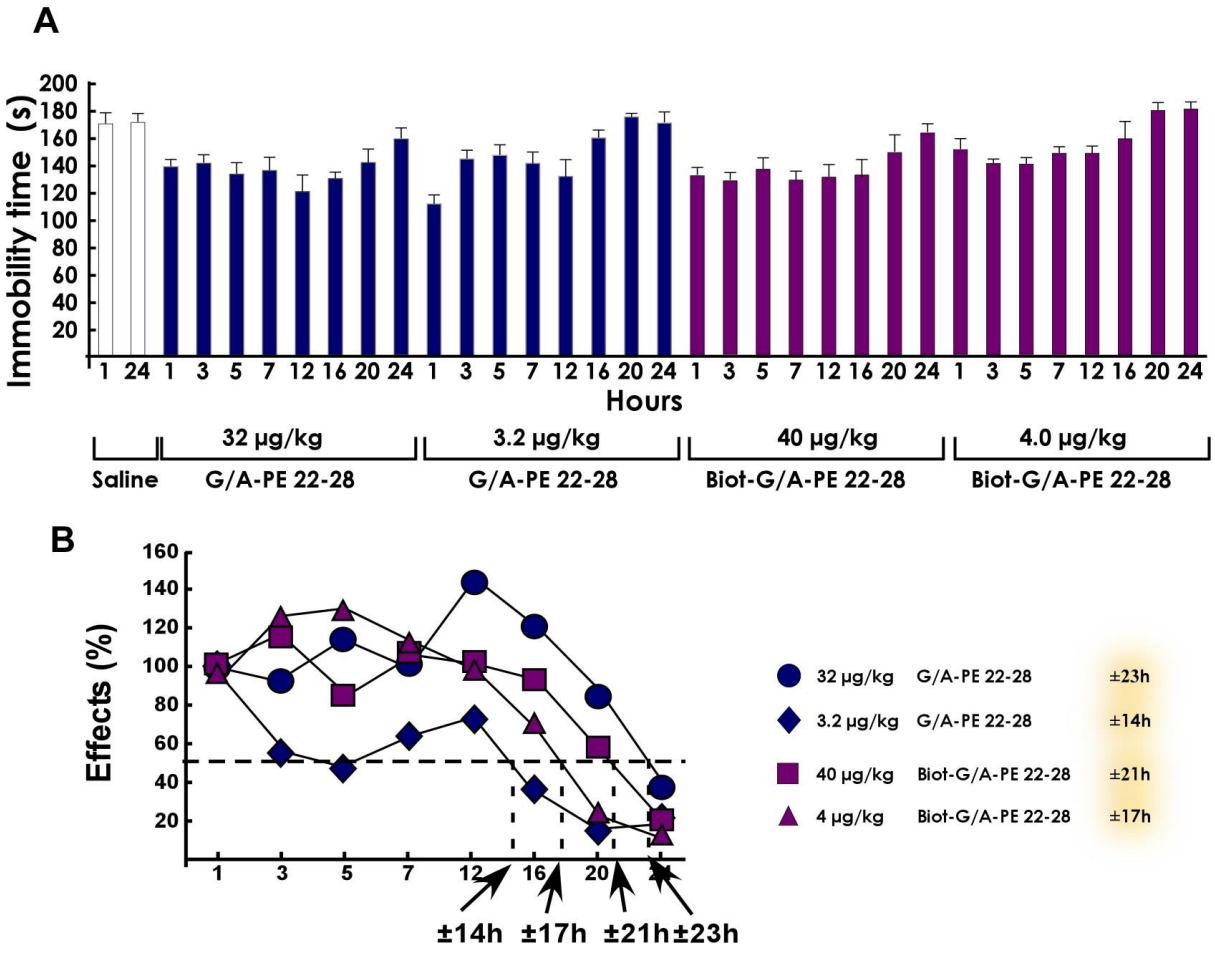

Figure 24 : Stabilité *in vivo* des analogues de la Spadine

Afin de calculer le temps de demi-effet des analogues de la Spadine, nous avons considéré la différence entre le temps d'immobilité mesuré à 1 h chez les souris contrôles et celui mesuré à 1 h chez les analogues de la Spadine comme valant 100%. Nous avons ensuite normalisé les autres mesures à partir de cette valeur (**Figure 24B**). Nous avons ainsi obtenu des valeurs de demi-effet de 14 et 23 h pour le G/A-PE 22-28 (à 3,2 µg/kg et à 32 µg/kg), et de 17 et 21 h pour

le biotine-G/A-PE 22-28 (à 4,0 µg/kg et à 40 µg/kg) (**Figure 24B**). Des valeurs jusqu'à 4 fois supérieures à celles obtenues précédemment avec la Spadine (6 h) (Veyssiere et al., 2015).
Cette stabilité de quasiment 24 h est compatible avec une seule prise quotidienne, pour l'éventuel futur médicament et correspond au but recherché pour ces analogues.

Du fait de leurs propriétés similaires et de leurs séquences très proches, le PE 22-28 a été choisi comme peptide représentatif des analogues de la Spadine pour tester sa spécificité pour TREK-1.
Ainsi, les effets du PE 22-28 ont été enregistrés sur les deux autres membres de la sous-famille TREK : TREK-2 et TRAAK, mais aussi sur deux K_{2P} présents en grande quantité dans le cerveau : TRESK et TASK-1 (Lesage and Lazdunski, 2000) (Kim et al., 2001) (Talley et al., 2001) (Lauritzen et al., 2003) (Lafreniere et al., 2010). Tout comme pour sur TREK-1, TREK-2 et TRAAK ont été activés par 10 µM AA avant l'ajout du PE 22-28 une fois l'amplitude du courant à son maximum. Les mesures effectuées montrent que les courants de ces quatre K_{2P} ne sont pas altérés par le PE 22-28 (**Figure 25A-D**). En d'autres termes, les analogues de la Spadine sont aussi spécifiques que la Spadine elle-même pour le canal TREK-1. Cette spécificité pourrait s'expliquer par les différences de séquence entre les trois canaux.
Plus important encore, les analogues de la Spadine, testés à une concentration élevée (10 µM), n'ont pas d'effet non plus sur le plus important courant repolarisant du cœur, IKr, généré par les canaux hERG (**Figure 25E-G**) (Sanguinetti and Jurkiewicz, 1990) (Cheng and Kodama, 2004). Le dysfonctionnement de ces canaux peut causer la mort par Torsades de Pointes, l'un des effets secondaires les plus redoutés pour les molécules à effets pharmacologiques comme les antidépresseurs (Cheng and Kodama, 2004).

Une fois les propriétés électrophysiologiques établies, nous avons poussé plus avant la caractérisation de leur action antidépressive. Comme nous l'avons mentionné plus haut, une injection i.p. unique de 3,0-4,0 µg/kg de ces analogues réduisait significativement le temps d'immobilité des souris dans le test du FST. En effet, comparées aux valeurs des souris non traitées à 161,7 ± 6,49 s, nous avions obtenu 91,80 ± 6,1 s ($n = 10$, $p < 0,0001$), 110,2 ± 6,6 s ($n = 10$, $p < 0,0001$) et 140.7 ± 7,1 s ($n = 10$, $p = 0,02$) pour le PE 22-28, le G/A-PE 22-28 et le biotine-G/A-PE 22-28, respectivement (**Figure 23A**).

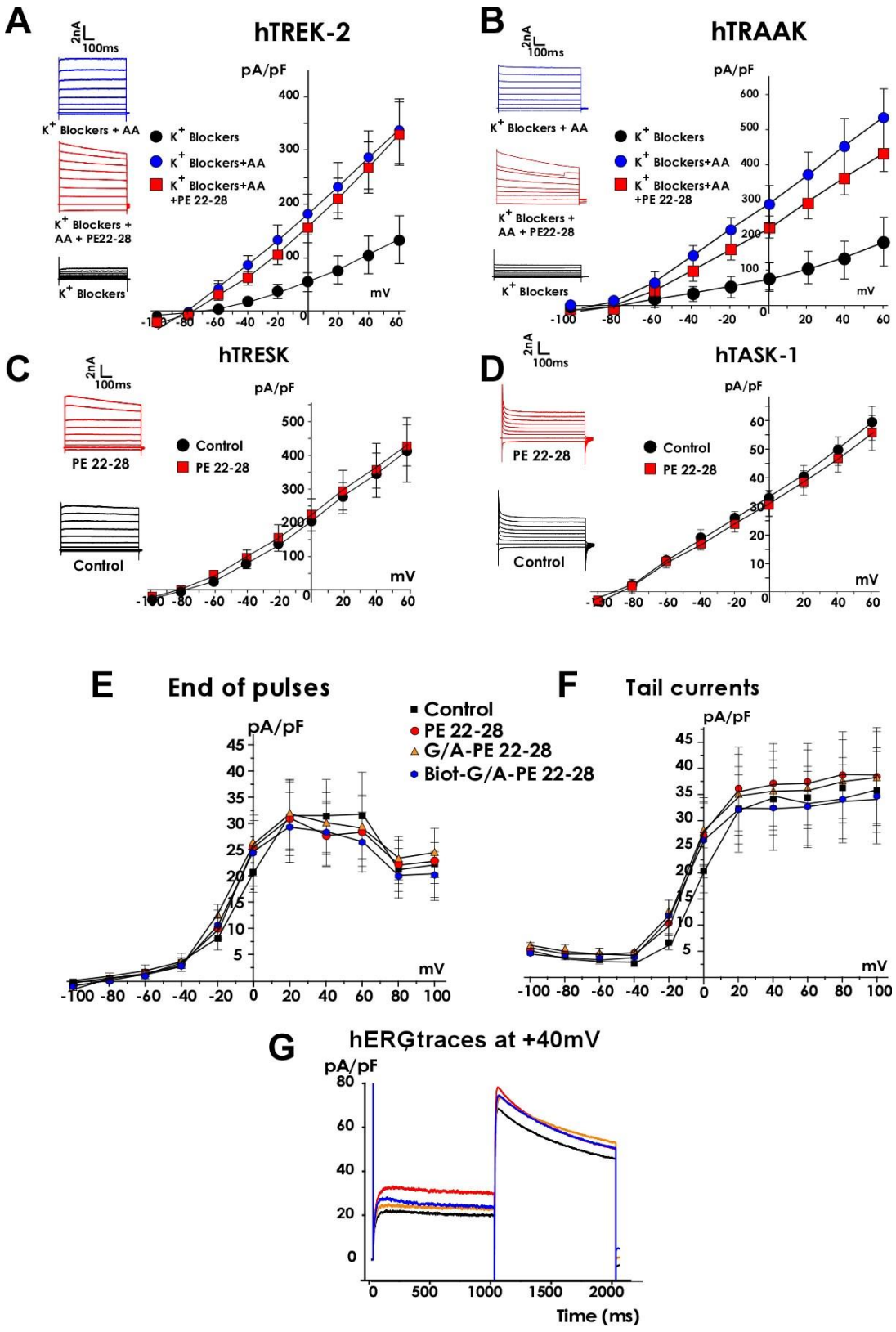

Figure 25 : La spécificité des analogues de la Spadine pour TREK-1

Les analogues de la Spadine en traitement subchronique s'avèrent tout aussi efficaces que la Spadine dans le FST. Cet effet est observé qu'ils soient administrés par injection i.p. (3,0 µg/kg) ou par gavage (1 mg/kg) (**Figure 26A**). Nous avons également soumis les souris à d'autres tests validés pour le criblage de molécules antidépressives. Les animaux ont ainsi été soumis au LH. Un traitement subchronique de 4 jours avec les analogues de la Spadine (3,0 µg/kg, i.p.) réduit de façon significative le temps nécessaire aux souris pour s'échapper après avoir reçu le choc électrique (**Figure 26B**).

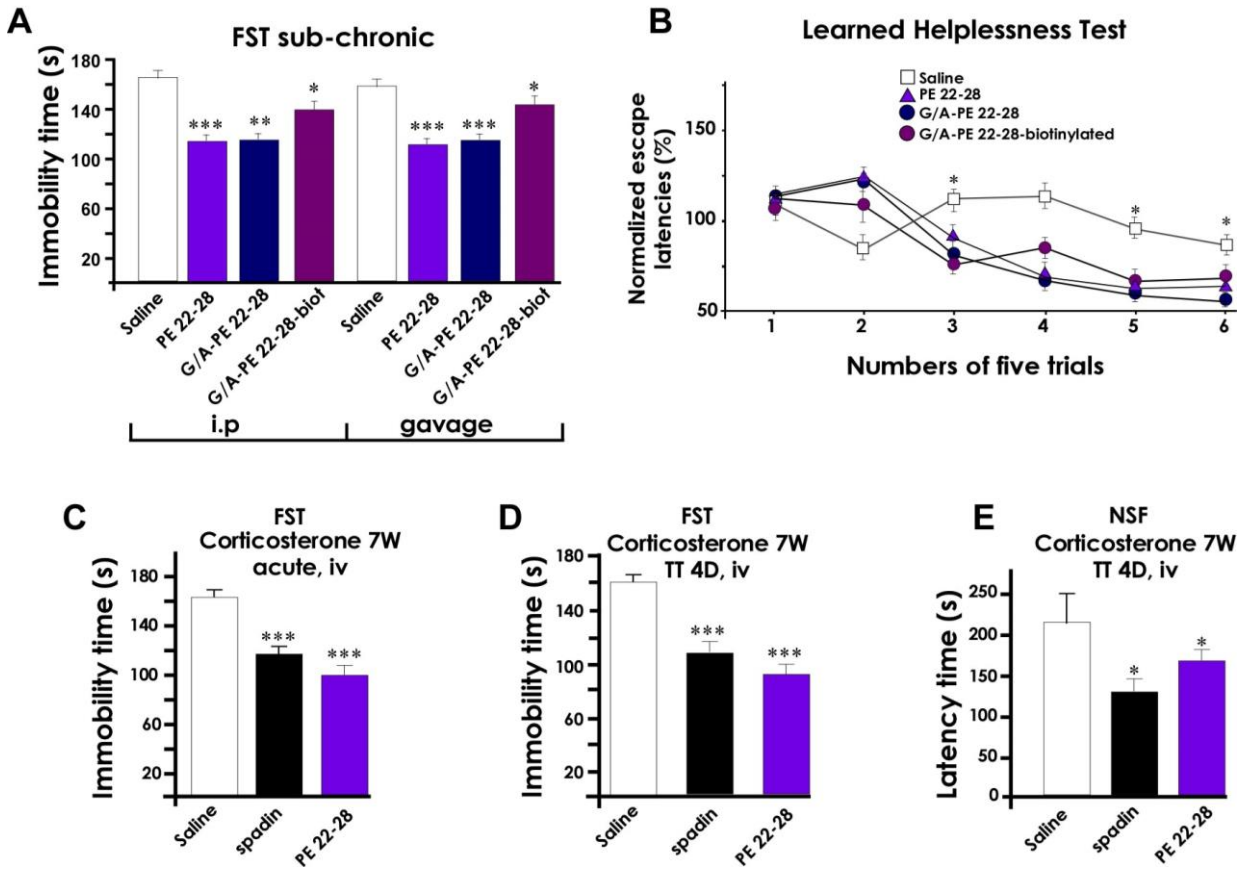

Figure 26 : Effets des analogues de la Spadine dans des modèles de dépression

Nous avons également utilisé un modèle de dépression induite chimiquement par un traitement chronique (7 semaines) avec de la corticostérone (Zhao et al., 2008). Dans ce modèle, que ce soit après un traitement aigu (30 minutes) ou subchronique (4 jours) le PE 22-28 (3,0 µg/kg) manifeste dans les tests du FST et du NSF les mêmes propriétés antidépressives que la Spadine mais avec des doses injectées beaucoup plus faibles (**Figure 26C-E**). En effet, dans le FST, une injection unique de PE 22-28 (3,0 µg/kg, i.v.) a les mêmes effets qu'une injection de Spadine

(100 µg/kg) sur le temps d'immobilité : 98,1 ± 8,78 s (n = 10, p < 0,0001) et 117,4 ± 6,85 s (n = 10, p < 0,0001) respectivement, comparés au témoin (164,9 ± 6,03 s) (**Figure 26C**). Cet effet est tout aussi puissant en cas de traitement subchronique, avec un temps d'immobilité de 89,60 ± 7,7 s (n = 10, p < 0,0001) pour la Mini-Spadine, de 107,5 ± 6,5 s (n = 10, p < 0,0001) pour la Spadine, et de 158,3 ± 7,15 s (n = 10) pour le contrôle (**Figure 26D**).

Enfin, dans le test du NSF, le traitement subchronique avec le PE 22-28 (3 µg/kg) ou la Spadine (100 µg/kg) réduisent significativement le temps nécessaire aux souris pour aller se nourrir : 153,2 ± 5.41 s (n = 10, p < 0,05) pour le PE 22-28, et 129,2 ± 15,28 s (n = 10, p< 0,05) pour la Spadine, par rapport au groupe contrôle : 226,1 ± 34,97 s (n = 10) (**Figure 26E).**

Ces données confirment les propriétés antidépressives de la Spadine et de ses analogues, aussi bien sur des souris sauvages que sur un modèle de souris dépressives. Les effets sont visibles après seulement 4 jours de traitement, caractéristique unique et cruciale, car elle réduit considérablement le temps nécessaire pour confirmer l'efficacité du traitement de la dépression. Cela est d'autant plus intéressant que la majorité des suicides surviennent dans les premières semaines suivant un traitement antidépresseur (Moller, 2003).

Nos résultats indiquent également que la Spadine et/ou ses analogues sont efficaces même administrés par voie orale.

Un fait important est qu'en plus de mesurer l'anxiété, le NSF permet également de mettre en évidence la neurogenèse (Duman et al., 2001) (Santarelli et al., 2003). De plus, plusieurs études ont démontré qu'un traitement antidépressif chronique augmentait la neurogenèse dans l'hippocampe (Duman et al., 2001) (Santarelli et al., 2003), et auparavant, le laboratoire a déjà montré que la Spadine induisait de la neurogenèse et l'activation CREB dans l'hippocampe après un traitement de 4 jours (Mazella et al., 2010). Par conséquent nous avons contrôlé que les analogues de la Spadine augmentaient la neurogenèse dans le cortex et l'hippocampe.

Pour cela les souris ont été injectées en i.p. (3,0-4,0 µg/kg/jour) pendant 4 jours avec des analogues de la Spadine, le dernier jour les animaux sont également injectés avec du BrdU (3 injections espacées de 2 heures avec 500µL d'une solution 10mg/mL de BrdU/0.9% NaCl).Le 5e jour, les animaux sont sacrifiés. Le BrdU est un marqueur des cellules en division. Le traitement subchronique a augmenté significativement le nombre de cellules BrdU positives dans le gyrus dentelé de l'hippocampe : 1736 ± 126 (n = 5, p < 0.0001) pour PE 22-28, 2110 ± 132, (n = 5, p < 0,0001) pour le G/A-PE 22-28, et 1809 ± 267 (n = 5, p < 0,0001) pour le biotine-G/A-PE 22-28, par rapport au contrôle : 899 ± 109 (n = 5) (**Figure 26A**).

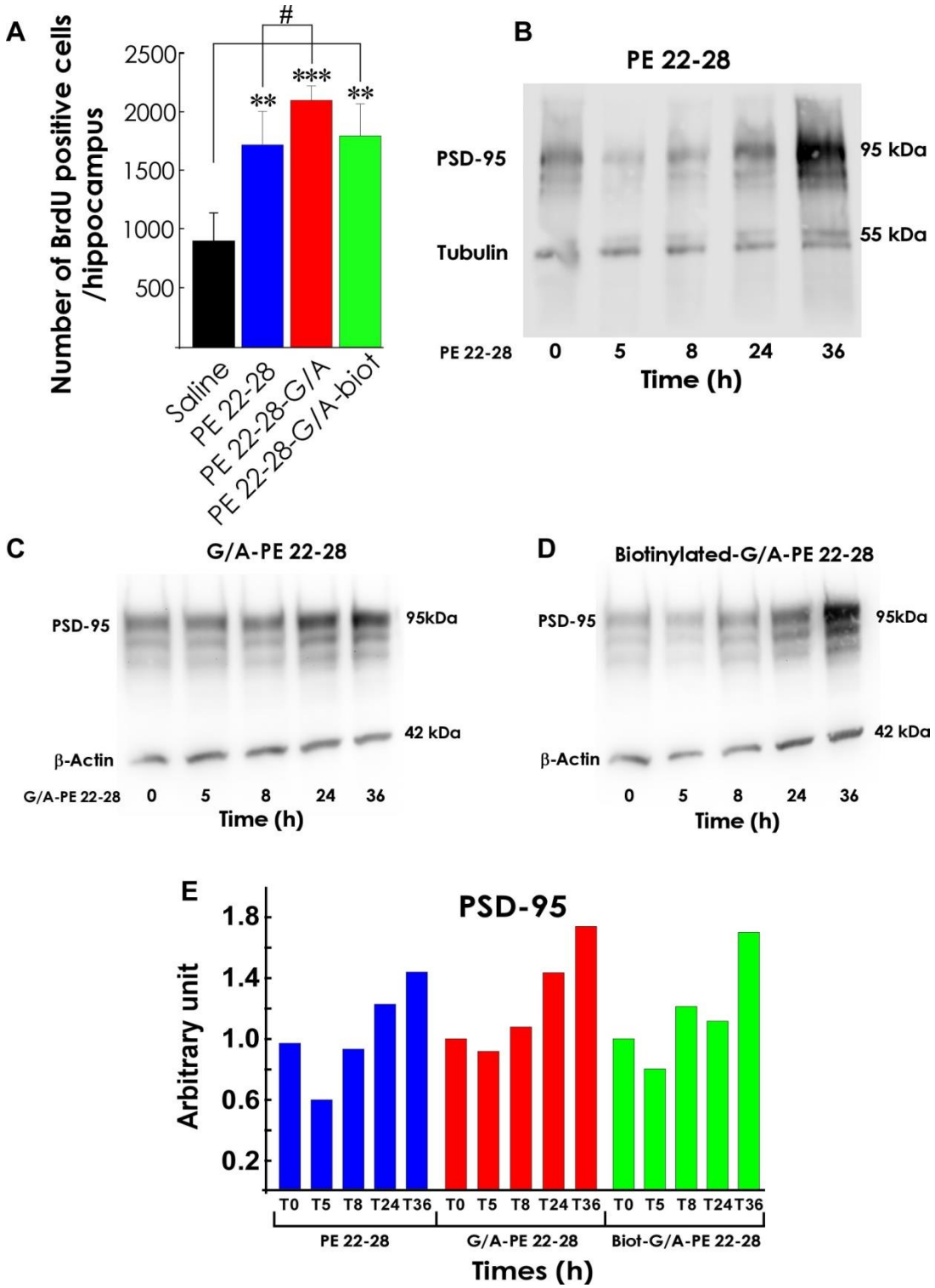

Figure 27 : Neurogenèse et Synaptogenèse

Ces données confirment que, comme la Spadine, les analogues de la Spadine sont capables d'induire de la neurogenèse hippocampique. Les antidépresseurs classiques mettent plusieurs

semaines à produire une activité antidépressive, un mécanisme que l'on pense médié par la neurogenèse (Santarelli et al., 2003) (Malberg and Schechter, 2005).

Une autre fonction importante des antidépresseurs est leur effet sur la synaptogenèse. Nous avons naturellement étudié les effets des analogues de la Spadine sur la synaptogenèse. Pour cela nous avons incubé des neurones corticaux avec 0,1 µM d'analogues de la Spadine et quantifié par Western-Blot les PSD-95 (marqueurs post synaptiques). Une légère diminution observée au cours des 5 premières heures, puis le traitement avec les analogues de la Spadine augmente la quantité de PSD-95 d'autant plus fortement que la durée d'incubation est importante (**Figure 27B-E**).
Ces données montrent qu'en plus d'induire de la neurogenèse, les analogues de la Spadine sont également capables de générer de la synaptogenèse. Cela laisse présager que la plupart des cellules générées à la suite du traitement deviendront des neurones matures.

3- Conclusion

Les données obtenues dans cette étude confirment que ces analogues courts de la Spadine conservent les mêmes propriétés que la Spadine.
En effet, ils sont tout aussi spécifiques que la Spadine et les analogues RI pour TREK-1, mais surtout plus efficaces pour bloquer l'activité du canal (leur affinité est jusqu'à 400 fois supérieure). Le laboratoire a déjà mis en évidence, pour la Spadine et ses analogues RI, l'absence d'effets délétères sur la douleur, l'ischémie ou au niveau cardiaque (Moha Ou Maati et al., 2012a) (Veyssiere et al., 2015). La Spadine et ses analogues constitue une grande famille de peptides qui partagent leur spécificité pour TREK-1 et surtout ne modifient pas l'activité des canaux hERG. Du fait qu'il s'agit de molécules naturelles (certes partielles) nous pouvons considérer que les moyens de dégradation et d'élimination de ces peptides sont présents dans les organismes. Par conséquent, nous pouvons espérer que les analogues Spadine seront également exempts d'effets secondaires chez l'Homme. Cette simple observation différencie positivement les analogues de la Spadine des autres antidépresseurs, comme les SSRI, les NSRI, les TCA (Ferguson, 2001) ou la Kétamine (Katalinic et al., 2013).
A cela il convient d'ajouter le fait que, comme la Spadine, les analogues produisent leurs effets sur la neurogenèse et la synaptogenèse en 4 jours seulement et, plus important encore *in vivo*, ils sont 4 fois plus stables que la Spadine

De plus, un autre point non négligeable est la taille de ces peptides, en effet, la réduction à 7 acides aminés assure un moindre coût pour la fabrication du médicament et *in fine* une diminution de la charge économique pour traiter les patients dépressifs.

Tous nos résultats indiquent que les analogues de la Spadine sont d'excellents candidats pour une utilisation en clinique humaine dans un avenir proche.

frontiers in Pharmacology

ORIGINAL RESEARCH
published: 12 September 2017
doi: 10.3389/fphar.2017.00643

Shortened Spadin Analogs Display Better TREK-1 Inhibition, *In Vivo* Stability and Antidepressant Activity

*Alaeddine Djillani†, Mariel Pietri†, Sébastien Moreno, Catherine Heurteaux, Jean Mazella and Marc Borsotto**

Centre National de la Recherche Scientifique, Institut de Pharmacologie Moléculaire et Cellulaire, UMR7275, Université Côte d'Azur, Valbonne, France

Depression is a devastating mental disorder that affects 20% of the population worldwide. Despite their proven efficacy, antidepressants present a delayed onset of action and serious adverse effects. Seven years ago, we described spadin (PE 12-28) as a promising endogenous peptide with antidepressant activity. Spadin specifically blocks the TREK-1 channel. Previously, we showed *in vivo* that, spadin activity disappeared beyond 7 h after administration. In order to improve *in vivo* spadin stability and bioavailability, we screened spadin analogs and derivatives. From the study of spadin blood degradation products, we designed a 7 amino-acid peptide, PE 22-28. *In vitro* studies on hTREK-1/HEK cells by using patch-clamp technique, showed that PE 22-28 displayed a better specificity and affinity for TREK-1 channel compared to spadin, IC_{50} of 0.12 nM vs. 40–60 nM for spadin. In the same conditions, we also pointed out that different modifications of its N or C-terminal ends maintained or abolished TREK-1 channel activity without affecting PE 22-28 affinity. *In vivo*, the antidepressant properties of PE 22-28 and its derivatives were demonstrated in behavioral models of depression, such as the forced swimming test. Mice treated with spadin-analogs showed a significant reduction of the immobility time. Moreover, in the novelty suppressed feeding test after a 4-day sub-chronic treatment PE 22-28 reduced significantly the latency to eat the food pellet. PE 22-28 and its analogs were able to induce neurogenesis after only a 4-day treatment with a prominent effect of the G/A-PE 22-28. On mouse cortical neurons, PE 22-28 and its derivatives enhanced synaptogenesis measured by the increase of PSD-95 expression level. Finally, the action duration of PE 22-28 and its analogs was largely improved in comparison with that of spadin, up to 23 h instead of 7 h. Taken together, our results demonstrated that PE 22-28 and its derivatives represent other promising molecules that could be an alternative to spadin in the treatment of depression.

Keywords: spadin-analogs, TREK-1 channel, PE 22-28, neurogenesis, synaptogenesis, antidepressant

OPEN ACCESS

Edited by:
Maurizio Taglialatela, University of Naples Federico II, Italy

Reviewed by:
Giulia Maria Camerino, Università degli Studi di Bari Aldo Moro, Italy
Sergei Noskov, University of Calgary, Canada

****Correspondence:***
Marc Borsotto
borsotto@ipmc.cnrs.fr

†These authors have contributed equally to this work.

Specialty section:
This article was submitted to Pharmacology of Ion Channels and Channelopathies, a section of the journal Frontiers in Pharmacology

Received: *16 June 2017*
Accepted: *30 August 2017*
Published: *12 September 2017*

Citation:
Djillani A, Pietri M, Moreno S, Heurteaux C, Mazella J and Borsotto M (2017) Shortened Spadin Analogs Display Better TREK-1 Inhibition, In Vivo Stability and Antidepressant Activity. Front. Pharmacol. 8:643. doi: 10.3389/fphar.2017.00643

INTRODUCTION

Depression is one of the most common mood disorders that represents a heavy economic burden in industrialized countries (Smith, 2014). Severe depression affects 2–5% of US citizens and up to 20% of the population suffer from mild depression (Nestler et al., 2002; Maletic et al., 2007; Krishnan and Nestler, 2008; Kessler et al., 2012). Depression is a complex syndrome with a variety of causes

mostly genetic and environmental (Nestler et al., 2002). One of the main hypotheses proposed to explain the physiopathology of depression is the monoamine hypothesis where depletion of three monoamines serotonin (5-HT), norepinephrine (NA) or dopamine (DA) is thought to cause depression (Hillhouse and Porter, 2015). Later, several antidepressant (AD) drugs were developed in the aim to restore the physiological synaptic levels of the three neurotransmitters (Hillhouse and Porter, 2015). Several types of AD drugs were and are still used in the treatment of depression. Initially, depression was mainly treated by tricyclics family and at lesser extent by monoamine oxidase inhibitors (MAOIs) and serotonin-norepinephrine re-uptake inhibitors (SNRIs). However, these classes of ADs exhibit numerous and serious side effects (Hirschfeld, 2012). To reduce the frequency and occurrence of these side effects, these drugs were replaced by a generation of ADs more specific and with lesser adverse effects. This includes serotonin-selective re-uptake inhibitors (SSRIs) and norepinephrine selective re-uptake inhibitors (NSRIs) that are widely used nowadays and recommended as first-line treatment for depression (Nestler et al., 2002; Cleare et al., 2015). SSRIs and NSRIs are thought to increase monoamine synaptic concentrations by inhibiting the re-uptake of 5-HT or NA by blocking their specific transporters, SERT and NAT, respectively (Kohler et al., 2016). These AD drugs are more tolerated but their efficacy on depressive patients is not really improved. On the other hand, the actual ADs like fluoxetine are only efficient after 3–4 weeks of treatment, a latency period that still remains unexplained (Nestler et al., 2002). Thus, it is necessary to discover and characterize new targets for new AD drugs. Recently, different fast-onset AD drugs have been described like ketamine, scopolamine or GLYX-13 (Ramaker and Dulawa, 2017). Nevertheless, these molecules, particularly ketamine produces a number of adverse effects (Katalinic et al., 2013). Multimodal drugs, such as vortioxetine or vilazodone are a new class of ADs latterly approved by the US Food and Drug Administration for the treatment of major depressive disorders (Wang et al., 2015; Sowa-Kucma et al., 2017). Nevertheless, these drugs have not represented a clear improvement of antidepressant efficacy, but vortioxetine showed beneficial effects in depression-related cognitive impairment whereas vilazodone appeared to induce minor sexual dysfunctions (Deardorff and Grossberg, 2014; Li et al., 2015; Thase et al., 2016). Despite this therapeutic arsenal, more than 30% of depressive patients never remit even after several classical treatments (Rush et al., 2006). An alternate for drug therapy in resistant patients is the electroconvulsive therapy (ECT). ECT is efficient in 50% of pharmacotherapy-resistant patients (Heijnen et al., 2010) but ECT also induces some adverse effects mainly in the cognitive processes (Semkovska and McLoughlin, 2010). Thus, the discovery of new AD drugs is challenging. Ten years ago, we have identified the selective two-pore domain potassium channel TREK-1 (TWIK-related potassium channel-1) as a potential target for depression treatment (Heurteaux et al., 2006; Borsotto et al., 2015). TREK-1 channels are ubiquitous potassium channels that play pivotal role in stabilizing membrane potential and thus prevent cellular excitability (Honore, 2007). TREK-1 channels are very particular K_{2P} channels since they are involved in many physiological and physiopathological processes, such as pain, epilepsy, stroke, and depression (Lauritzen et al., 2000; Alloui et al., 2006; Heurteaux et al., 2006). TREK-1 became also an attractive target in cardiovascular research because it plays an important role in atrial fibrillation, pulmonary arterial hypertension and ventricular arrhythmia (Wiedmann et al., 2016; Decher et al., 2017). In the field of depression, we showed in five different models of depression that deletion of *kcnk2* gene, which encodes for TREK-1 channels results in a depression-resistant phenotype associated with an enhanced serotonergic neurotransmission and an increased neurogenesis in the hippocampus (Heurteaux et al., 2006). These observations led us to search for potent TREK-1 blockers. Then, we identified spadin which derives from a larger peptide called propeptide (PE) (Mazella et al., 2010). PE is a 44 amino-acid that results from the post-translational maturation in the Golgi apparatus of sortilin, also known as the neurotensin receptor-3 (Mazella, 2001). Spadin is a fast-acting AD which does not produce any side effects on functions that are controlled by the TREK-1 channel (Moha Ou Maati et al., 2012). It is able to counteract depression in only 4 days when classical ADs require 3–4 weeks to be efficient (Mazella et al., 2010). Moreover, spadin blocks TREK-1 with higher affinity, $IC_{50} \sim 40$–60 nM vs. $IC_{50} \sim 6\,\mu M$ for the most used SSRI fluoxetine (Mazella et al., 2010; Moha ou Maati et al., 2011). However, in mice, the AD activity of spadin measured by FST disappears beyond 7 h after an acute ip administration (Veyssiere et al., 2015). In order to improve the spadin stability *in vivo*, we decided to search for analogs or derivatives of spadin. In a previous study we have identified two analogs, analogs 3 and 8, that were synthesized by using the retro-inverso technology (Veyssiere et al., 2015). Although the gain in term of affinity and action duration was about 20, it is not sufficient to make these analogs competitive in regard of their synthesis cost in comparison to spadin. Then, we decided to search for shortened analogs. We first studied whether or not spadin is degraded in the blood circulation. We identified two shortened peptides. By comparing their ability to inhibit TREK-1 channel expressed in the hTREK-1/HEK cell line (Moha ou Maati et al., 2011), we identified the shortest efficient sequence that only contained 7 amino-acid called PE 22-28. This peptide was used as a core sequence for preparing analogs by chemical modifications of its N- or C-terminus ends and also by substitution of amino-acids. As PE 22-28, some modified peptide-analogs displayed a better potency in blocking TREK-1 channel and more importantly, they have retained their AD properties when injected in acute or sub-chronic treatments.

Abbreviations: AD, antidepressant; FST, Forced Swim Test; NSF, Novelty-suppressed Feeding; LHT, Learned Helplessness Test; ip, intraperitoneal; PSD-95, Post-Synaptic Density protein 95.

MATERIALS AND METHODS

In Vitro Analysis

Cell Lines

The human TREK-1/HEK cell line (Moha ou Maati et al., 2011) and the native HEK293 cell line were maintained in Dulbecco's

Modified Eagle's Medium (DMEM) supplemented with 10% (v/v) heat-inactivated fetal bovine serum, 1% (v/v) penicillin-streptomycin, 1% Glutamax. For the hTREK-1/HEK cells, 0.5 mg/ml G418 were added to the medium.

Cells were incubated in a humidified atmosphere containing 5% CO_2. For electrophysiological measurements, cells were plated at a density of 20,000 cells per 35 mm dish.

In order to study the effects of shortened spadin analogs on hTREK-2, hTASK-1, hTRAAK and hTRESK, the native HEK293 cells were transfected with DNAs corresponding to the channels using JetPEI (Polyplus-transfection, France) following the provider's instructions.

Electrophysiological Measurements

Cells from the hTREK-1/HEK cell line were seeded at a density of 20,000 cells/35 mm dish. Electrophysiological recordings were performed 24–48 h after plating using the whole-cell configuration of patch-clamp technique. TREK-1 currents (I_{TREK-1}) were recorded using RK400 patch-clamp amplifier (Axon Instrument, USA). They were low-pass filtered at 3 kHz and digitized at 10 kHz using a 12-bit analog-to-digital converter digidata (1322 series, Axon Instrument, USA). I_{TREK-1}amplitudes were expressed as current densities [current amplitude (pA)/membrane capacitance (pF)]. The results were expressed as mean ± SEM (standard error of the mean).

Pipettes were pulled from borosilicate glass capillaries using a dual-stage micropipette puller (PC-10, Narishige); they had a resistance of 1.5–3 MΩ. Cells were continuously perfused using an external bath solution containing in mM: 150 NaCl, 5 KCl, 3 $MgCl_2$, 1 $CaCl_2$, and 10 HEPES. The bath solution was initially adjusted to pH 7.4 with NaOH. The intra-pipette solution contained in mM: 155 KCl, 3 $MgCl_2$, 5 EGTA, and 10 HEPES adjusted to pH 7.2 with KOH. In order to measure I_{TREK-1}, a cocktail of potassium channel blockers was added to the bath solution. This cocktail contained: 3 mM 4-AP (4-aminopyridine), 10 mM TEA (tetraethylammonium), 10 μM Glibenclamide, 100 nM Apamin, and 50 nM Charybdotoxin. Data acquisition was carried out using a computer (Dell Pentium) with pClamp software (Axon Instrument, USA). Whole-cell currents were generated by running a pulse or ramp protocol every 5 s from −100 to +60 mV with a holding potential maintained at −80 mV. To evaluate the inhibitory effect on TREK-1 channels of shortened spadin analogs compared with spadin, cells were first activated by 10 μM arachidonic acid (AA). Dose-response curves were realized to compare spadin-analog effects with spadin using Origin 8.6 (Northampton, MA, USA).

Patch-clamp recording data were analyzed using Clampfit (Molecular Devices, USA). $I = f(V)$ curves were obtained from −100 to +60 mV ramp. Data were presented as mean ± SEM.

In Vivo Analysis

Animals

Naïve male C57Bl/6J mice from 7 to 9 weeks old were used in all experiments (Janvier laboratory, Saint Berthevin, France). Mice were housed (10 animals per cage) under a 12-h light/12-h dark cycle (light on at 8:00 am) in a ventilated room at a temperature of 22 ± 1°C. Animals had free access to water and food (A03; SAFE, Augy, France). All experiments were conducted according to policies on the care and use of laboratory animals of the Society for Neuroscience, and also with respect to national laws on animal use. The local Ethics Committee (CIEPAL, N° 736-02) approved the experiments.

Chemicals

Spadin, PE 22-28 and PE 22-28 analogs were purchased from GeneCust Europe, Luxembourg. G418, Arachidonic acid (AA), 4-AP (4-aminopyridine), TEA (tetraethylammonium), Apamin and Charybdotoxin were purchased from Sigma-Aldrich, France, Glibenclamide was purchased from ICN Biomedicals (USA).

In Vitro Half-Life Time of Spadin in Serum

The half-life time of spadin was measured in serum by incubating 10 nmoles of the peptide with 200 μl of mouse serum in the absence or in the presence of the metalloprotease inhibitor 1–10 phenanthroline (1 mM) for various times (2, 5, 15, 30, and 60 min) at room temperature. Incubations were stopped by direct acidification (5 μl of 2.5 M HCl), loaded in C-18 sepack cartridges, lyophilized, resuspended in 20% acetonitrile before loading onto HPLC for analysis of PE degradation/stability. Elutions of HPLC products were carried out by means of a 50-min linear gradient of acetonitrile from 20 to 70% at a flow rate of 1 ml/min. The amount of the intact PE for each incubation time was expressed as the percent of the initial amount of spadin.

Behavioral Tests

Porsolt Forced Swim Test (FST)

Mice were individually placed for 6 min in a non-escapable cylinder (30 cm height and 15 cm diameter) half-filled with water at 22 ± 1°C. The immobility time was manually measured only during the last 4 min. A mouse was considered immobile when it remained immobile with only slight movements in order to keep its head above water (Porsolt et al., 1977).

Novelty Suppressed Feeding Test (NSF)

Mice were deprived from food for 24 h before the test. A food pellet was placed on a white platform in the center of a highly illuminated area (45 × 45 × 20 cm). The floor was covered with wooden bedding. Mice were placed in the corner of the arena, during a period of 10 min, the latency to start eating the pellet was measured (Santarelli et al., 2003).

Learned Helplessness Test (LHT)

The learned helplessness test consists in a 4-day training session and a single day test.

During the training session mice were exposed to 360 inescapable 2 s foot shocks, with an inter-trial interval of 8 s. A non-shocked group was exposed to the apparatus for the same duration but no shock was delivered.

The test consisted in 30 trials separated by a 30 s interval. One trial was defined as a 5 s period before shock onset and was terminated when the mouse moved to the second compartment or at the end of the shock onset. The latency to escape for each mouse during every trial was recorded (Caldarone et al., 2000).

BrdU Labeling

Twenty hours after the injections of 5-Bromo-2′-deoxyuridine (BrdU) (12 mg per animals administered in three bolus of 100 μL of a solution of 40 mg/mL of BrdU diluted in 0.9% NaCl), mice were anesthetized with isoflurane and transcardially perfused first with NaCl 0.9% and, second with 4% paraformaldehyde. Brains were cut in 40 μm sections, by using a vibratome (Leica), throughout the entire hippocampus. Eight slices, from bregma 3.3 to bregma 5.3, were taken to process the BrdU immunohistochemistry as previously described (Heurteaux et al., 2006). For each BrdU labeling, slices were first incubated with a mouse monoclonal anti-BrdU antibody (1/7,000, Becton Dinckinson). For chromogenic immunodetection, sections were incubated during 2 h in specific biotin-conjugated secondary antibodies (1/400; Vector Laboratories) followed by a peroxidase-avidin complex solution, to amplify the reaction. The peroxidase activity of immune complex was visualized with DAB staining using the VectaStain ABC kit according to the manufacturer's protocol (Vector Laboratories).

Synaptogenesis

Mouse cortical neurons were treated with 0.1 μM of the indicated spadin analog for different times and homogenized in the Laemmli buffer and analyzed onto 10% SDS PAGE gels. Separated proteins were then transferred from gels onto nitrocellulose membranes (VWR, Fontenay-sous-Bois, France) and blocked with either 5% skim milk or 5% BSA as indicated in PBS for 30 min at room temperature. Membranes were incubated with antibodies directed against PSD-95, overnight at 4°C. Tubulin or β-actin contents were determined after stripping using a 1/1,000 dilution anti-tubulin or anti-β-actin antibodies (Sigma-Aldrich, Saint-Quentin Fallavier). After four washes in 0.1% Tween/PBS, secondary anti-mouse or anti-rabbit horseradish peroxidase-conjugated antibodies (1/10000, Amersham Biosciences, Orsay, France) were incubated for 1 h at room temperature. Proteins were detected with the ECL plus detection reagents (Amersham Biosciences, Orsay, France) using a LAS-3000 imaging system (Fujifilm, Düsseldorf, Germany).

Relative intensities of the labeled bands were analyzed by densitometric scanning using ImageJ software (Wayne Rasband, Bethesda, USA). PSD-95 expression was normalized using total tubulin or β-actin labeling.

Statistical Analysis

Data are presented as mean ± SEM of at least 3 independent experiments. In GraphPad Prism (GraphPad software, La Jolla, USA), statistical comparisons were performed using Student's *t*-test or ANOVA one-way. A result is considered as statistically significant when $p < 0.05$.

RESULTS

Spadin Degradation in the Serum

From the analysis of spadin degradation after 30 min of incubation with serum at 37°C, we observed the disappearance of almost all spadin and the appearance of two other peaks, peak 1 and peak 2 (**Figure 1A**). Mass spectroscopy analyses indicated that peak 1 and peak 2 corresponded to sequences PE 14-25 and PE 12-27, respectively (**Figure 1C**). These peaks appeared rapidly and reached a maximal value at 15 min for peak 1 followed by a further degradation (**Figure 1B**). By contrast, peak 2 reached its maximal appearance at 30 min which was maintained up to 60 min (**Figure 1B**).

Identification of the PE 22-28 Sequence as the Most Efficient TREK-1 Blocker with Higher Affinity Compared to Spadin

Spadin shortened analogs were individually screened on the hTREK-1/HEK cell line (Moha ou Maati et al., 2011) using the patch-clamp technique (**Figure 1C**). Shortened PE peptides showed differences in their capacity to inhibit TREK-1 activity in comparison with spadin (PE 12-28) and PE 1-44 sequences. In all experiments (**Figure 2**), TREK-1 channels were prior activated with 10 μM AA (Patel et al., 1998). When the maximal amplitude was reached, we measured the ability of each peptide at 100 nM to inhibit the TREK-1 channel activity induced by AA and we compared them with spadin (**Figure 2** and **Table 1**). We first tested the two peptides identified above (PE 14-25 and PE 12-27) (**Figures 2B,C,P**). No significant effect on TREK-1 channels was observed with the PE 14-25 analog (**Figures 2C,P**). The current density measured at 0 mV and compared with AA activity alone (100%) was 114.7 ± 10.6% ($n = 8$, $p = 0.09$). Interestingly, we found that PE 12-27 was able to strongly inhibit TREK-1 activity (28.4 ± 9.9%, $n = 22$, $p = 0.03$; **Figures 2B,P**).

Then, we designed three other shortened peptides, PE 22-25, PE 22-27 and PE 22-28 (**Table 1**). Neither PE 22-27 (**Figures 2D,P**, **Table 1**) nor PE 22-25 (**Figures 2E,P**, **Table 1**) had significant effect in inhibiting I_{TREK-1} (27.5 ± 20%, $n = 10$, $p = 0.23$) and (36.02 ± 17.5%, $n = 14$, $p = 0.06$), respectively. Only, the PE 22-28 (**Figures 2F,P**, **Table 1**) was able to efficiently block TREK-1 activity (55.46 ± 4.6%, $n = 13$, $p < 0.0001$).

Spadin-Analog Design

After the screening of these analogs with the hTREK-1/HEK cells, PE 22-28 was identified as the most efficient TREK-1 blocker and was retained for further studies. With the aim to increase again the stability and the efficacy of the peptide we used PE 22-28 as core peptide for the design of several analogs. Peptides that were able to block TREK-1 activity were described in the **Figures 2G–P**) and in **Table 1**. They include biotinylated PE 22-28, PI-PE 22-28, corresponding to the PE 20-28 sequence, biotinylated-PI-PE 22-28, G/A-PE 22-28 corresponding to the PE 22-28 sequence where the Glycine at position 22 was replaced by an Alanine residue, biotinylated-G/A-PE 22-28, dansyl-PE 22-28 where a dansyl chemical group was added at the N-terminus of the peptide, O-methyl-PE 22-28 and O-ethyl-PE 22-28 where a O-methyl or a O-ethyl chemical group was added to the C-terminus of the peptides, respectively.

We tested other analogs but they were unable to inhibit TREK-1 current (**Table 1**). Corresponding current-voltage curves are depicted in the Supplementary Figure 1.

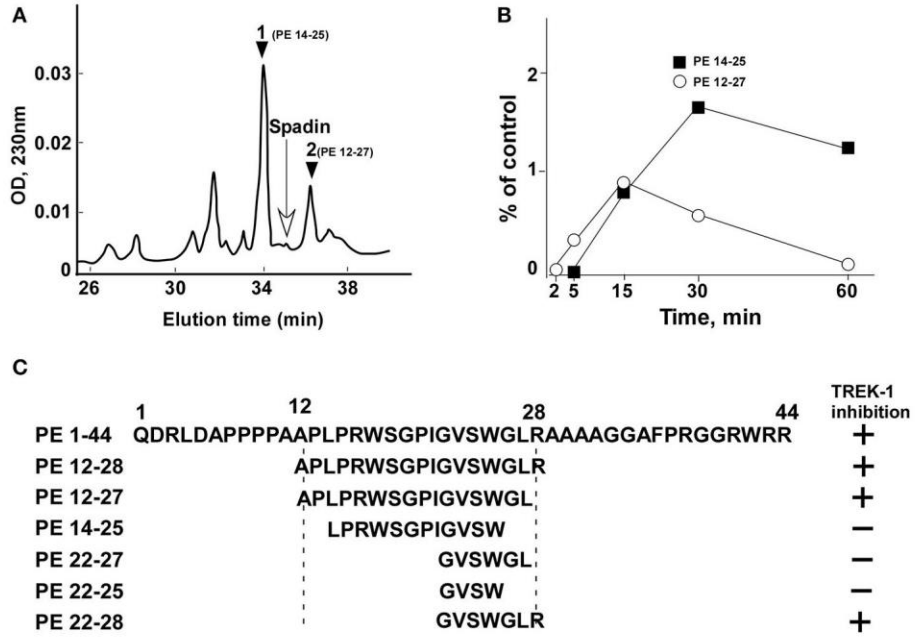

FIGURE 1 | HPLC profiles of spadin degradation products in serum. **(A)** A typical HPLC profile obtained after 30 min incubation of spadin with mouse serum at 37°C. The position of spadin peak is indicated by an arrow. **(B)** Kinetics of appearance of peaks 1 (PE 14-28) and 2 (PE 12-27). **(C)** Sequences of shortened peptides and their capacity to inhibit TREK-1 activity compared with PE and spadin (PE 12-28) sequences.

All screened analogs able to inhibit TREK-1 channel also displayed AD properties measured with the Forced Swim Test (FST) (**Figure 3A**, **Table 1**).

Analyses of electrophysiological and behavioral data allowed us to focus further studies on PE 22-28, G/A-PE 22-28 and biotinylated-G/A-PE 22-28. These three peptides are hereafter called spadin-analogs (bolded in **Table 1**). They shared common AD properties, a high percentage of TREK-1 current inhibition and, they had an affinity for TREK-1 that was largely increased in comparison to spadin (**Figure 3B**). The IC_{50} measured were 40, 0.12, 0.10, and 1.2 nM for PE 12-28 (Spadin), PE 22-28, G/A-PE 22-28 and biotinylated-G/A-PE 22-28, respectively.

Spadin-Analogs Specifically Block TREK-1 Channel Activity

PE 22-28 was chosen as representative peptide among spadin-analogs and was tested on other K_{2P} channels like hTREK-2, hTRAAK, hTRESK, and also hTASK-1 (Lesage and Lazdunski, 2000; Kim et al., 2001; Talley et al., 2001; Lauritzen et al., 2003; Lafreniere et al., 2010). Native HEK cells were transfected by plasmids coding for these channels. TREK-2 and TRAAK were activated by 10 μM AA. Then 100 nM of PE 22-28 combined to AA were applied when current amplitude reached the maximum. PE 22-28 was inefficient in producing any change in the amplitude of the current (**Figures 4A,B**). Similarly, PE 22-28 was unable to modify currents generated by hTRESK and hTASK-1, two important K_{2P} channels in the brain (**Figures 4C,D**). Spadin-analogs represented by PE 22-28 did not inhibit these K_{2P} channels indicating that they are as specific as spadin for blocking TREK-1 channels.

More importantly, spadin-analogs tested at higher concentration (10 μM) did not modify the I_{Kr} current generated by hERG channels (**Figures 4E–G**). I_{Kr} current is the most important repolarizing current in the heart (Sanguinetti and Jurkiewicz, 1990; Cheng and Kodama, 2004). Dysfunction of these channels could cause death by Torsades de Pointes that are one of the most important side effects observed with AD drugs (Cheng and Kodama, 2004).

Spadin-Analogs Display Antidepressant Properties in Depression Tests and in Mouse Model of Depression

After an acute ip administration of 3.0–4.0 μg/kg spadin-analogs, the immobility time of mice was decreased significantly, 91.80 ± 6.1 s ($n = 10$, $p < 0.0001$), 110.2 ± 6.6 s ($n = 10$, $p < 0.0001$), and 140.7 ± 7.1 s ($n = 10$, $p = 0.02$) for PE 22-28, G/A-PE 22-28 and biotinylated-G/A-PE 22-28, respectively, values that have to be compared with that of the saline solution (161.7 ± 6.49 s) (**Figure 3A**).

As spadin, spadin-analogs were efficient after sub-chronic treatments. Whether administered by ip injections (3.0 μg/kg) or gavage (1 mg/kg) (**Figure 5A**), they remained active in the FST. Then, we subjected mice to the Learned Helplessness Test, a validated and efficient test for identifying AD molecules. A 4-day sub-chronic treatment with spadin-analogs (3.0 μg/kg, ip) significantly reduced the escape latencies (**Figure 5B**). In the chemically induced model of depression using long term

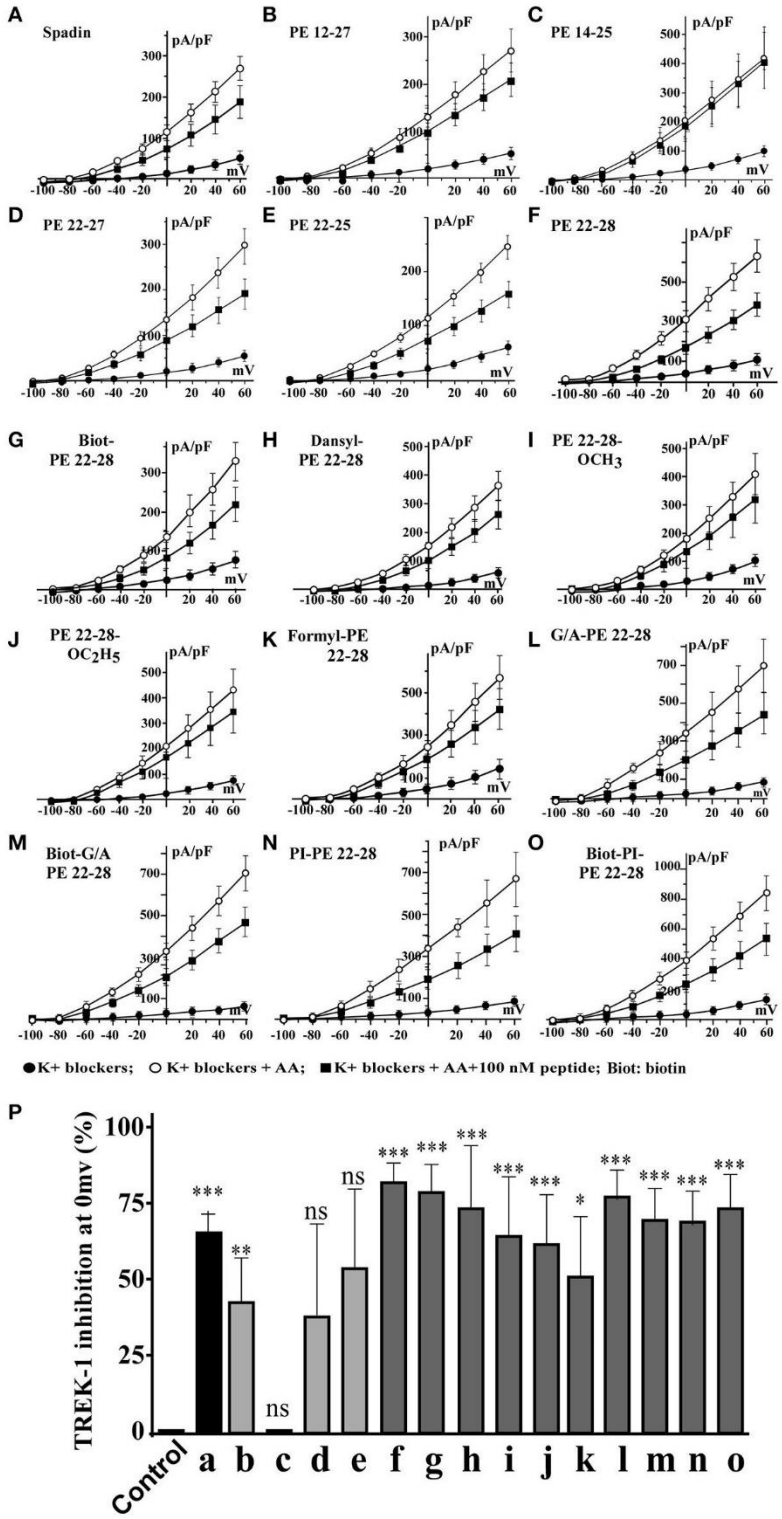

FIGURE 2 | $I = f(V)$ curves and % of TREK-1 inhibition. **(A–F)**, current density curves obtained with spadin and shortened peptides described in **Figure 1C**. **(G–O)**, current density curves obtained with PE 22-28 analogs. **(P)** Inhibition percentages of TREK-1 current measured at 0 mV for corresponding peptides described from "**A**" to "**O**". Control value was obtained by using a solution of 0.9% NaCl. ns, not significant. $^{*}p < 0.05$, $^{**}p < 0.01$, $^{***}p < 0.001$.

TABLE 1 | Spadin analogs and their ability to inhibit TREK-1 channel activity and reduce immobility times in FST.

Figure 2 code	Peptide names	Modifications	% of TREK-1 inhibition	*n*	*P*	FST immobility times (s)	*p*
a	PE 12-28 (Spadin)	Not modified	44.37 ± 8.817	7	0.0024	88.3 ± 7.0	0.0001
b	PE 12-27	Not modified	28.39 ± 9.916	22	0.0093	100.2 ± 5.0	0.0001
c	PE 14-25	Not modified	−14.73 ± 10.6	8	0.2074	112.2 ± 7.1	0.0080
d	PE 22-27	Not modified	25.7 ± 20.01	10	0.2311	168.2 ± 4.2	ns
e	PE 22-25	Not modified	36.02 ± 17.47	14	0.0599	100.2 ± 5.0	0.0001
f	**PE 22-28**	**Not modified**	**55.46 ± 4.555**	**13**	**0.0001**	**91.8 ± 6.1**	**0.0001**
g	Biotinylated-PE 22-28	Addition N-terminus	53.03 ± 6.416	12	0.0001	112.1 ± 4.3	0.0001
h	Dansyl-PE 22-28	Addition N-terminus	48.78 ± 14.52	10	0.0084	104.6 ± 11.8	0.0010
i	PE 22-28-O-Methyl	Addition C-terminus	42.98 ± 13.47	12	0.0086	137.1 ± 8.1	0.0200
j	PE 22-28-O-Ethyl	Addition C-terminus	41.39 ± 11.52	10	0.0058	113.2 ± 8.5	0.0001
k	Formyl-PE 22-28	Addition N-terminus	32.45 ± 12.22	10	0.0262	ND	
l	**G/A-PE 22-28**	**Substitution-N- terminus**	**50.61 ± 7.935**	**10**	**0.0001**	**110.2 ± 3.6**	**0.0001**
m	**Biotinylated G/A-PE 22-28**	**Addition + substitution N-terminus**	**46.11 ± 7.743**	**11**	**0.0001**	**140.7 ± 7.1**	**0.0200**
n	PI-PE 22-28	Addition N-terminus	46.19 ± 7.565	7	0.0009	119.7 ± 11.8	0.0070
o	Biotinylated-PI-PE 22-28	Addition N-terminus	49.11 ± 7.454	10	0.0001	124.1 ± 11.7	0.0080
	Palmitoyl-PE 22-28	Addition N-terminus	26.69 ± 16.45	12	0.133	ND	
	FITC-PE 22-28	Addition N-terminus	22.1 ± 12.63	9	0.1183	ND	
	Acetyl-PE 22-28	Addition N-terminus	20.49 ± 8.777	15	0.035	ND	
	Myristoyl-PE 22-28	Addition N-terminus	18.04 ± 17.77	13	0.3302	ND	
	Long Chain biotinylated-PE 22-28	Addition N-terminus	15.86 ± 11.21	12	0.1847	ND	
	5'FAM-PE 22-28	Addition N-terminus	6.633 ± 7.065	11	0.3699	ND	
	F-Moc-PE 22-28	Addition N-terminus	5.826 ± 10.91	11	0.6051	ND	
	Stearic acid-PE 22-28	Addition N-terminus	5.412 ± 5.496	32	0.3399	ND	

n, numbers of cells. In FST experiments, n, 10 mice for each peptide.
ns, not significant, ND, Not determined, p-values are from Student's t-test.
Bolded values correspond to the spadin-analogs retained for further studies.

(7 weeks) corticosterone treatment (Zhao et al., 2008), PE 22-28 displayed the same AD properties as spadin after acute or sub-chronic treatments (3.0 μg/kg) (**Figures 5C–E**). In the FST, PE 22-28 (3.0 μg/kg, ip) was slightly more efficient in decreasing immobility time (98.1 ± 8.78 s, $n = 10$, $p < 0.0001$) than spadin (100 μg/kg; 117.4 ± 6.85 s, $n = 10$, $p < 0.0001$) in this model of depression in comparison with control (164.9 ± 6.03 s) (**Figure 5C**). Moreover, 4-day sub-chronic administrations of spadin-analogs were significantly efficient in decreasing the immobility time (89.60 ± 7.7 s, $n = 10$, $p < 0.0001$) compared to spadin (107.5 ± 6.5 s, $n = 10$, $p < 0.0001$) or saline (158.3 ± 7.15 s, $n = 10$; **Figure 5D**). These data confirmed the AD action of spadin-analogs on control or corticosterone induced depressive mice.

In the NSF, 4-day sub-chronic treatments with PE 22-28 (3 μg/kg) or spadin (100 μg/kg) significantly reduced the latency to eat the food pellet (129.2 ± 15.28 s, $n = 10$, $p < 0.05$) and (153.2 ± 5.41 s, $n = 10$, $p < 0.05$) in spadin and PE 22-28 groups, respectively in comparison with control (226.1 ± 34.97 s, $n = 10$) in the corticosterone induced model of depression (**Figure 5E**). The NSF test predicts not only depression but also neurogenesis (Duman et al., 2001; Santarelli et al., 2003). We hypothesized that spadin-analogs could increase neurogenesis in the cortex and the hippocampus.

Spadin-Analogs Increase Neurogenesis *in Vivo* in the Hippocampus after 4-Day Treatment

Several studies demonstrated that a chronic AD treatment up-regulates neurogenesis in the hippocampus (Duman et al., 2001; Santarelli et al., 2003). We have previously shown that spadin increased neurogenesis and CREB activation in the hippocampus only after a 4-day treatment (Mazella et al., 2010). We wondered whether spadin-analogs produced the same effects. Mice were ip treated (3.0–4.0 μg/kg/day) for 4 days with spadin-analogs and, on the 5th day, were sacrificed. the 4-day treatment with spadin-analogs significantly increased BrdU positive cells (1736 ± 126 ($n = 5$, $p < 0.0001$), 2110 ± 132, ($n = 5$, $p < 0.0001$), 1809 ± 267 ($n = 5$, $p < 0.0001$), for PE 22-28, G/A-PE 22-28, and biotinylated-G/A-PE 22-28, respectively) in comparison with saline injected mice (899 ± 109, $n = 5$) (**Figure 6A**). These data confirmed that similarly to spadin, spadin-analogs have kept their ability to induce *in vivo* hippocampal neurogenesis.

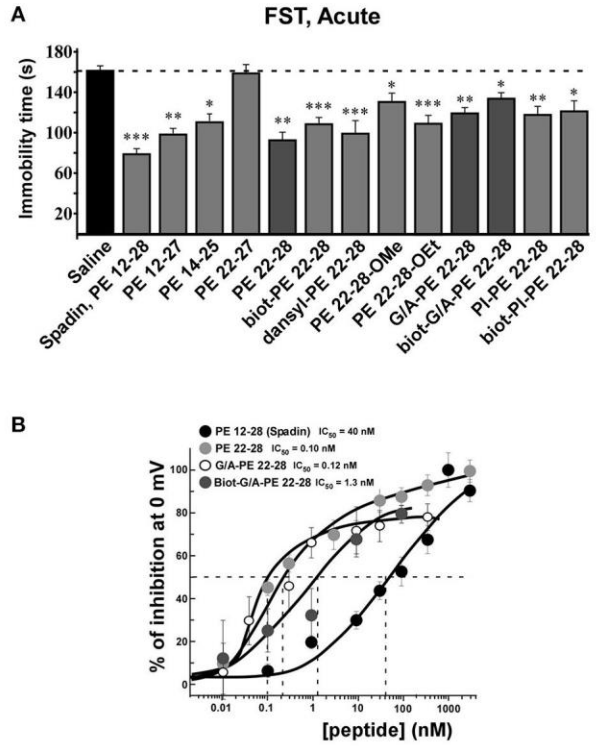

FIGURE 3 | FST and dose-response curves of TREK-1 current inhibition by spadin-analogs. **(A)** Peptides able to inhibit TREK-1 channel activity were tested in the FST. Immobility times were measured 30 min after ip injection and compared with the immobility time obtained with saline injected mice. Spadin was injected at 100 μg/kg and spadin-analogs were injected at 3.2–4.0 μg/kg. $^{*}p < 0.05$, $^{**}p < 0.01$, $^{***}p < 0.001$. **(B)** Dose-response curves of TREK-1 current inhibition at 0 mV obtained with spadin-analogs compared with spadin. IC_{50} were 0.1, 0.12, 1.2, and 40.0 nM for PE 22-28, G/A-PE 22-28, biotinylated-G/A-PE 22-28 and spadin, respectively.

Spadin-Analogs Increase Synaptogenesis *in Vitro* in Cortical Neurons

Incubation of cortical neurons with 0.1 μM of spadin-analogs enhanced synaptogenesis as illustrated by the increase in the expression of PSD-95 36 h after incubation (**Figures 6B–D**). Except a slight decrease during the first 5 h, spadin-analog treatments continuously increased the expression of PSD-95 up to 36 h (**Figure 6E**). These data showed that spadin-analogs not only increased neurogenesis but also synaptogenesis, indicating that the fate of a majority of newborn cells is to generate mature neurons.

Action Duration of Spadin-Analogs

Naïve mice (10 per time groups) were injected once to obtain a dose of 3.2 μg/kg or 32 μg/kg of G/A-PE 22-28 or a dose of 4.0 μg/kg or 40 μg/kg of biotinylated-G/A-PE 22-28. These doses were injected in a bolus of 100 μL of 0.9% NaCl. At times 1, 3, 5, 7, 12, 16, 20, and 24 h after injection, mice were submitted to FST (**Figure 7A**). Immobility times were compared to those obtained with mice injected with the saline solution (0.9% NaCl). FST for saline injected mice were only performed at times 1 and 24 h, immobility times were very similar, 171.2 ± 8.2 s and 175.5 ± 6.8 s, respectively (**Figure 7A**). To calculate the half-effect time, the immobility time measured at 1 h of saline injected mice was subtracted from the immobility time measured at 1 h for spadin-analogs, the difference value was considered as 100%. Other immobility times were normalized to the 100% value (**Figure 7B**). Calculated half-effect time values were 14, 17, 21, and 23 h for G/A-PE 22-28 (3.2 μg/kg), biotinylated-G/A-PE 22-28 (4.0 μg/kg), G/A-PE 22-28 (32 μg/kg) and biotinylated-G/A-PE 22-28 (40 μg/kg), respectively (**Figure 7B**). These values were higher than the one previously obtained with spadin (6 h) (Veyssiere et al., 2015).

DISCUSSION

Spadin-Analogs Are More Potent TREK-1 Blockers than Spadin

Depression is the most devastating and common mood disorder (Wong and Licinio, 2001). Treatments available nowadays target several proteins and undergo different mechanisms of action (Schechter et al., 2005). However, classical ADs are not fully specific and generally lead to side effects with different degree of severity. In order to avoid these adverse effects and improve the selectivity of the AD drugs, our strategy has consisted in focusing on improvement of the affinity, bioavailability and efficacy of the endogenous peptide that we have previously identified and called spadin (Mazella et al., 2010). Spadin was designed from a larger peptide called PE, a 44 aa peptide released in the blood flow following the translational maturation of the sortilin or neurotensin receptor 3 (Munck Petersen et al., 1999; Mazella, 2001). First, we identified degradation products of PE in the blood. From the peptides we identified we have designed a short 7 aa peptide, called PE-22-28. It displayed a better affinity for the TREK-1 potassium channel, a target that we have previously identified in the depression mechanism (Heurteaux et al., 2006). PE 22-28 was used for the design of 16 analogs. Because increasing the drug crossing through the blood brain barrier is a crucial goal for a therapeutic drug acting on brain targets and, because it was shown that biotinylation can increase peptide brain uptake, we synthesized some biotinylated derivatives (Scherrmann, 2002; Wu et al., 2002). By testing the different PE 22-28 derived peptides for their ability to inhibit TREK-1 channels expressed in the hTREK-1/HEK cell line (Moha ou Maati et al., 2011), we only retained those that inhibited more than 35% of TREK-1 activity in order to measure their AD properties by FST. Then, by comparing both abilities, we only retained 3 peptides (that we called spadin-analogs) PE 22-28, G/A-PE 22-28 and biotinylated-G/A-PE 22-28 for further studies.

Here, we showed that spadin-analogs displayed higher potencies in blocking TREK-1 channels when compared with spadin. Their IC_{50} were increased by more than 300 fold, 0.10 nM, and 0.12 nM for PE 22-28 and G/A-PE 22-28, respectively, these values have to be compared with spadin affinity, 40–60 nM (Mazella et al., 2010; Moha Ou Maati et al., 2012).

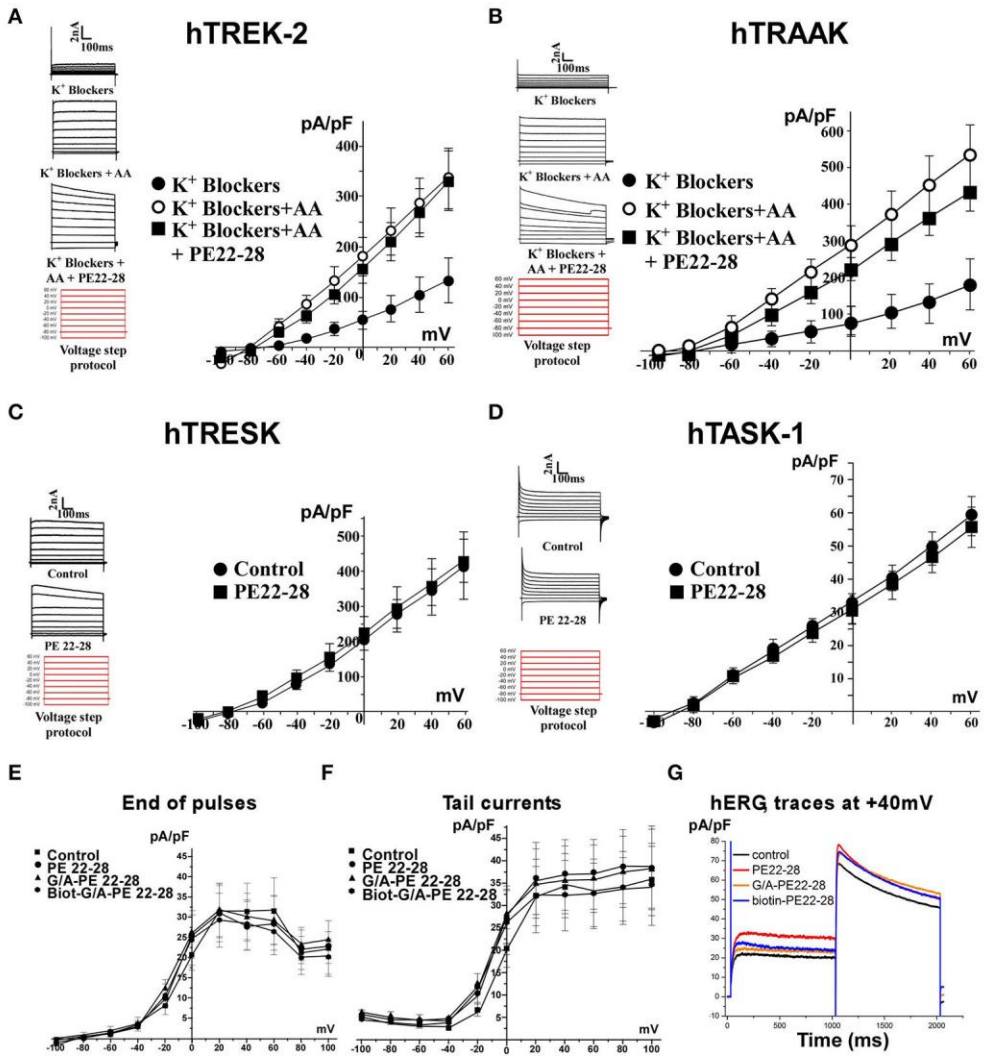

FIGURE 4 | Spadin-analog specificity. **(A–D)** PE 22-28 was used as the representative peptide for testing the specificity of spadin-analogs vs. other K_{2P} channels, TREK-2 **(A)**, TRAAK **(B)**, TRESK **(C)**, and TASK-1 **(D)**. **(E–G)** Spadin-analogs were without effect on hERG channel activity. Current densities at the end of pulses **(E)**, current densities of tail currents **(F)**, and typical traces obtained at +40 mV with spadin-analogs **(G)**.

Spadin-Analogs Are Specific for the TREK-1 Channel

Additionally, spadin-analogs have kept their specificity for TREK-1 channels (Moha Ou Maati et al., 2012). They were unable to inhibit TREK-2 and TRAAK channels, the two other members of the TREK channel sub-family (Kim et al., 2001; Honore, 2007). The specificity of spadin and its analogs for TREK-1 channel could be accounted by the sequence differences between the three channels: TREK-1 and TREK-2 share 63% of identity and only 45% between TREK-1 and TRAAK (Noel et al., 2011). They were also unable to inhibit TRESK (Lafreniere et al., 2010; Wood, 2010) and TASK-1 (Lauritzen et al., 2003) channels, two K_{2P} channels that are important in the brain and, as TREK-1 they are both modulated by volatile anaesthetics (Patel and Honore, 2001). Here again, sequence differences could account for the absence of effects, homologies between TREK-1 and both channels are around 50% (Noel et al., 2011). More noteworthy, spadin-analogs were devoid of effects on hERG channels that are responsible for the cardiac I_{Kr} current, one of the main potassium repolarizing current in the cardiac ventricle (Sanguinetti and Jurkiewicz, 1990; Cheng and Kodama, 2004).

Spadin and its analogs block TREK-1 channels more efficiently when they are activated by arachidonic acid indicating the need of an open-state conformation of the channel. The weak direct inhibition of TREK-1 in basal condition could be due to the necessity for spadin to access the selectivity filter in a closed channel.

The monoamine hypothesis of depression was expanded to other recent hypotheses mainly the neurotrophic and neurogenesis hypothesis that suggest that a decrease in neurotrophic factors, such as the brain-derived neurotrophic factor (BDNF) or in adult hippocampal neurogenesis are

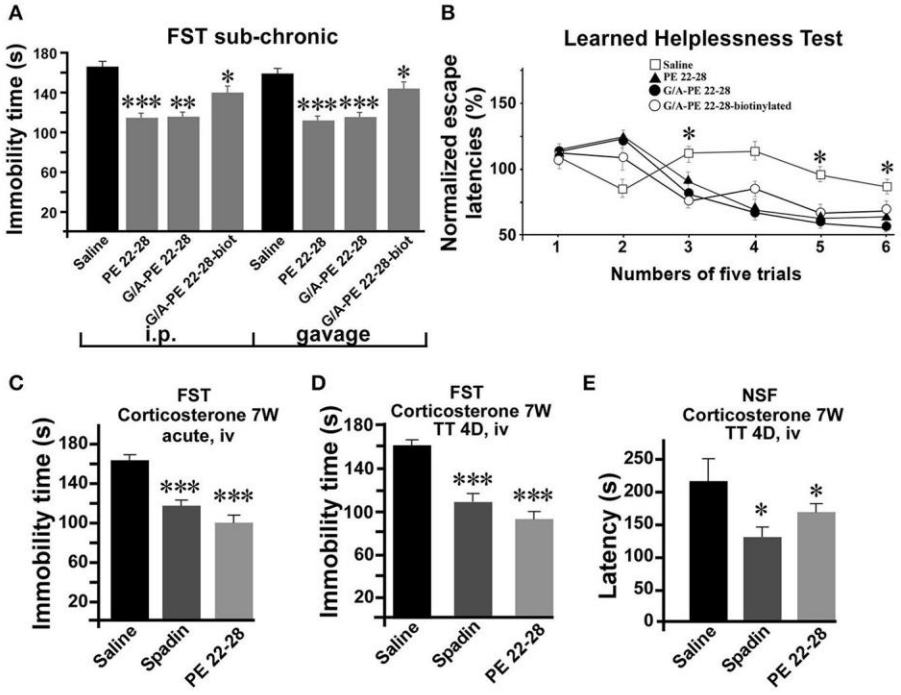

FIGURE 5 | Behavior of spadin-analogs in mouse model of depression. **(A)** FST performed after a sub-chronic (4 days) treatment (3.0–4.0 μg/kg) with each spadin-analog or the 0.9% NaCl saline solution. Treatments were administered either by ip injection (100 μg/kg) or by gavage (1.0 mg/kg). **(B)** The Learned Helplessness test performed with each spadin-analog (3.0–4.0 μg/kg). 30 trials were divided in 6 pools of five trials. $^{*}p < 0.05$. **(C,D)** Corticosterone-induced model of depression. PE 22-28 was used as the representative peptide for spadin-analogs for comparing the effects of spadin-analogs with those of spadin in this chemically-induced mouse model. FST performed after acute (30 min after injection, **(C)** or sub-chronic (4 days treatment, **D**) ip injections of spadin (100 μg/kg) or PE 22-28 (3.0 μg/kg). Sub-chronic treatments administered at the same doses were also used before the NSF **(E)**. $^{*}p < 0.05$, $^{**}p < 0.01$, $^{***}p < 0.001$.

in one way or another associated with depression (Yohn et al., 2017). Classical ADs take several weeks to produce antidepressant activity, a mechanism that is thought to be mediated through neurogenesis (Santarelli et al., 2003; Malberg and Schechter, 2005). Interestingly, spadin and analogs display their antidepressant response within 4-day treatment, this short time correlates with the same period required for hippocampal neurogenesis to develop (Devader et al., 2015). The rapid increase in the BDNF expression in the hippocampus after *in vivo* administration of spadin points out the fact that spadin and derivative peptides induce a fast expression of BDNF to be distinguished from the slow BDNF expression observed with the conventional ADs. Two phases, fast and slow, are also observed with ketamine (Kavalali and Monteggia, 2015). Nevertheless, cellular pathway of neurogenesis activation are different. Ketamine uses the mTOR pathway (Kavalali and Monteggia, 2015) whereas spadin does not interfere with mTOR signaling (Devader et al., 2015).

Spadin-Analogs Are Potent Antidepressants

Spadin-analogs have also kept the AD properties of spadin. We showed that spadin-analogs behaved as an AD drug in the FST but also in the learned helplessness test. Both tests are commonly and widely used by pharmaceutical industries for characterizing new AD drugs. Importantly, we showed that spadin-analogs were also efficient after gavage, indicating that these molecules could be administered *per os*. Interestingly, in a chemically (corticosterone)-induced model of depression spadin-analogs were as efficient as spadin for decreasing depression-like behavior generated by the corticosterone treatment. As expected for spadin derivatives, spadin-analogs were efficient after only 4 days of treatment. This unique property is crucial because it considerably reduces the onset time to observe the efficiency of the AD treatment. That is particularly interesting because the majority of suicides occurs during the first weeks following an AD treatment (Moller, 2003).

Spadin-Analogs Are More Stable than Spadin *in Vivo*

Another remarkable property of spadin-analogs is their prolonged action duration. Despite a relatively short *in vitro* serum half-life time, the *in vivo* antidepressant efficacy measured by FST lasted for almost 24 h. G/A-PE 22-28 or biotinylated-G/A-PE 22-28 injected at doses as low as 32.0 or 40.0 μg/kg, respectively had a half-time of effect of 23 and 21 h after injection. These values represent a huge improvement in comparison with spadin. In the same conditions, the half-time effect of spadin at a dose of 100 μg/kg was only of 6 h (Veyssiere et al., 2015).

Chronic treatments with ADs are known to induce neurogenesis in the hippocampus (Duman et al., 2001; Malberg and Schechter, 2005). However, neurogenesis up-regulation

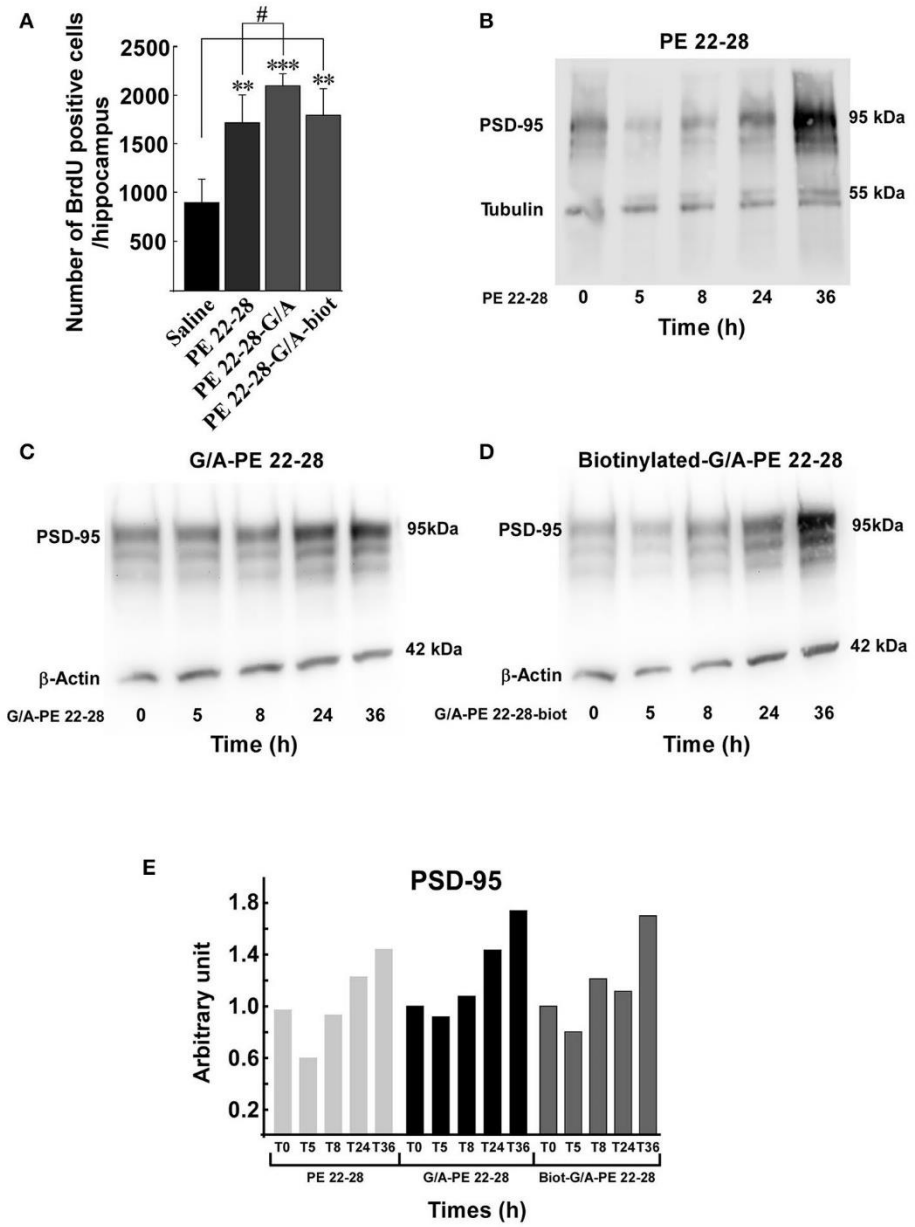

FIGURE 6 | Neurogenesis and synaptogenesis. **(A)** Neurogenesis was assessed by measuring the number of BrdU positive cells per hippocampus after sub-chronic treatments (3.0–4.0 μg/kg, 4 days) with spadin-analogs. The cell number was given for the entirety of hippocampus. $^{**}p < 0.01$, $^{***}p < 0.001$, $^{\#}p < 0.05$. **(B–D)** Synaptogenesis was assessed by measuring the increase in the level of PSD-95 in mouse cortical neuron. Mouse cortical neurons were treated with 0.1 μM of the indicated spadin-analog PE 22-28 **(B)**, G/A-PE 22-28 **(C)** and biotinylated-G/A-PE 22-28 **(D)**. At the indicated times neurons were homogenized in Laemmli buffer and submitted to Western blot analysis. **(E)** Histogram illustration of the PSD-95. For each spadin-analog, the PSD-95 amount at 36 h was about twice than that measured at 5 h.

currently occurs after 2–4 weeks of administration. This is consistent with the fact that classical ADs are efficient only after the same period. Previously, we have shown that spadin was able to increase BrdU incorporation and CREB activation after only 4 days of treatment (Mazella et al., 2010). *In vivo* administration of spadin induces neurogenesis over different time scale through two phases, a rapid increase in the expression of BDNF and a slow spine maturation (Devader et al., 2015). Since targets and specificity for these targets are the same between spadin and its derivatives, we could speculate that spadin analogs could behave identically to spadin. Here, we demonstrated that spadin-analogs were also able to induce neurogenesis in the dentate gyrus. Interestingly, spadin-analog treatments also increased the PSD-95 expression, a biomarker of synaptogenesis. These observations indicated that number of newborn neurons were functional and should participate to

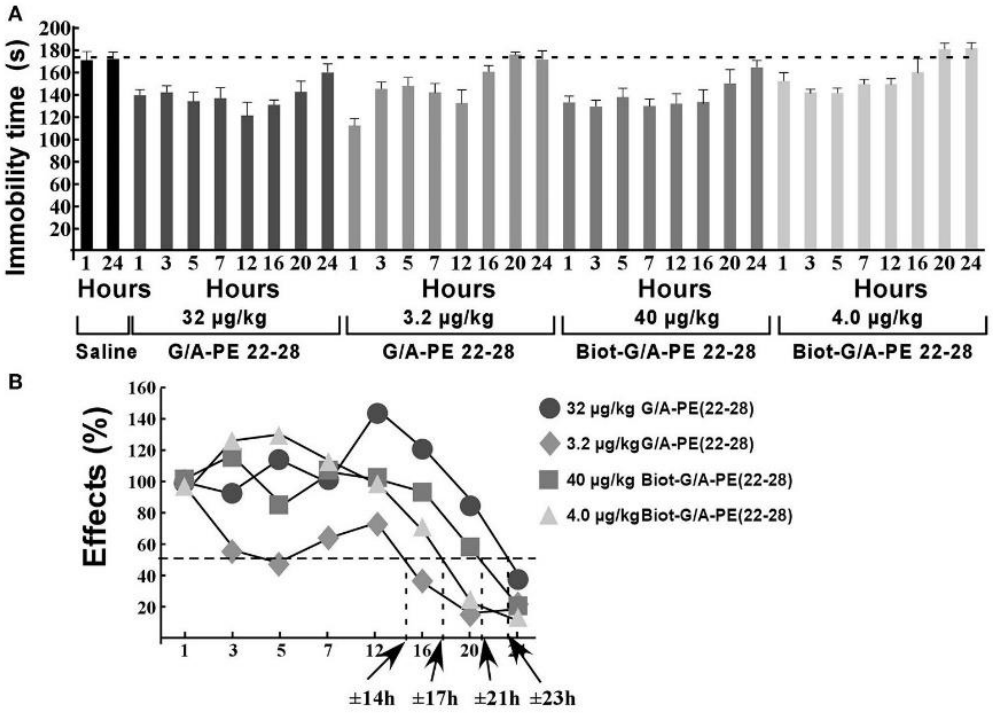

FIGURE 7 | Action duration of G/A-PE 22-28 and biotinylated-G/A-PE 22-28 measured by FST. **(A)** At each time-point, 10 naïve mice were tested for immobility in the FST. Saline injected mice were tested only at two times, 1 and 24 h. For each spadin-analog, at time 1 h the difference between saline and spadin-analog treated mice was considered as 100%, Time-point immobility times were normalized to this 100% value. **(B)** Half-time effects were approximately of 14, 21, 17, and 23 h for 3.2 μg/kg of G/A-PE 22-28, 32 μg/kg of G/A-PE 22-28, 4.0 μg/kg of biotinylated-G/A-PE 22-28 and 40 μg/kg of biotinylated-G/A-PE 22-28, respectively.

the brain network. This property is crucial for the AD action of spadin-analogs.

CONCLUSION

Our final goal is to make spadin-analogs drugs usable in clinics. All our data converge toward this goal. Spadin-analogs are specific for the TREK-1 channel, a target in the depression pathway, and efficient as AD. They induce neurogenesis after only 4 days of treatment. We have demonstrated that spadin and its retro-inverso analogs have no deleterious effects on pain, ischemia or at the cardiac levels (Moha Ou Maati et al., 2012). Since spadin analogs share the same targets (TREK-1 and NTR-3) and, have no effect on the other K_{2P} channels, more importantly they do not modify hERG channel activity then, we could expect that spadin analogs would be devoid of side effects. The absence of adverse effects differentiates spadin-analogs from other antidepressant drugs, such as SSRIs, SNRIs, tricyclics (Ferguson, 2001), or ketamine (Katalinic et al., 2013). Additionally to the shared properties with spadin, spadin-analogs display a largely increased affinity for TREK-1 and, also a largely increased action duration. Another important point concerns the shortening of the peptide that will induce a lower cost for the drug manufacturing and *in fine* a decrease of economic burden to treat depressive patients. All these reasons encourage us to think that in the really near future spadin-analogs will constitute a promising alternative to spadin and become efficient AD drugs usable in clinic.

AUTHOR CONTRIBUTIONS

AD, performed electrophysiological experiments. MP, performed behavioral experiments. SM, performed biochemical experiments. CH, JM, and MB, conceived and designed the experiments. CH, JM, and MB, contributed reagents/materials/analysis tools and wrote the paper.

FUNDING

This work was supported by the Centre National de la Recherche Scientifique and the Agence Nationale de la Recherche (ANR-13-SAMA-0001 and 0002 and ANR-13-RPIB-0001 and 0002). We also thank the French Government for the "Investments for the Future" LabEx ICST # ANR-11 LabEx 0015 and the Fondation de l'Avenir N° AP-RMA-2015-021. MP was supported by a CIFRE fellowship.

SUPPLEMENTARY MATERIAL

The Supplementary Material for this article can be found online at: http://journal.frontiersin.org/article/10.3389/fphar.2017.00643/full#supplementary-material

REFERENCES

Alloui, A., Zimmermann, K., Mamet, J., Duprat, F., Noel, J., Chemin, J., et al. (2006). TREK-1, a K^+ channel involved in polymodal pain perception. *EMBO J.* 25, 2368–2376. doi: 10.1038/sj.emboj.7601116

Borsotto, M., Veyssiere, J., Moha Ou Maati, H., Devader, C., Mazella, J., and Heurteaux, C. (2015). Targeting two-pore domain K^+ channels TREK-1 and TASK-3 for the treatment of depression: a new therapeutic concept. *Br. J. Pharmacol.* 172, 771–784. doi: 10.1111/bph.12953

Caldarone, B. J., George, T. P., Zachariou, V., and Picciotto, M. R. (2000). Gender differences in learned helplessness behavior are influenced by genetic background. *Pharmacol. Biochem. Behav.* 66, 811–817. doi: 10.1016/S0091-3057(00)00271-9

Cheng, J. H., and Kodama, I. (2004). Two components of delayed rectifier K^+ current in heart: molecular basis, functional diversity, and contribution to repolarization. *Acta Pharmacol. Sin.* 25, 137–145.

Cleare, A., Pariante, C. M., Young, A. H., Anderson, I. M., Christmas, D., Cowen, P. J., et al. (2015). Evidence-based guidelines for treating depressive disorders with antidepressants: a revision of the 2008 British Association for Psychopharmacology guidelines. *J. Psychopharmacol.* 29, 459–525. doi: 10.1177/0269881115581093

Deardorff, W. J., and Grossberg, G. T., (2014). A review of the clinical efficacy, safety and tolerability of the antidepressants vilazodone, levomilnacipran and vortioxetine. *Expert Opin. Pharmacother.* 15, 2525–2542. doi: 10.1517/14656566.2014.960842

Decher, N., Kiper, A. K., and Rinne, S. (2017). Stretch-activated potassium currents in the heart: focus on TREK-1 and arrhythmias. *Prog. Biophys. Mol. Biol.* doi: 10.1016/j.pbiomolbio.2017.05.005. [Epub ahead of print].

Devader, C., Khayachi, A., Veyssiere, J., Moha Ou Maati, H., Roulot, M., Moreno, S., et al. (2015). *In vitro* and *in vivo* regulation of synaptogenesis by the novel antidepressant spadin. *Br. J. Pharmacol.* 172, 2604–2617. doi: 10.1111/bph.13083

Duman, R. S., Nakagawa, S., and Malberg, J. (2001). Regulation of adult neurogenesis by antidepressant treatment. *Neuropsychopharmacology* 25, 836–844. doi: 10.1016/S0893-133X(01)00358-X

Ferguson, J. M. (2001). SSRI Antidepressant medications: adverse effects and tolerability. *Prim. Care Companion J. Clin. Psychiatry* 3, 22–27. doi: 10.4088/PCC.v03n0105

Heijnen, W. T., Birkenhager, T. K., Wierdsma, A. I., and van den Broek, W. W. (2010). Antidepressant pharmacotherapy failure and response to subsequent electroconvulsive therapy: a meta-analysis. *J. Clin. Psychopharmacol.* 30, 616–619. doi: 10.1097/JCP.0b013e3181ee0f5f

Heurteaux, C., Lucas, G., Guy, N., El Yacoubi, M., Thümmler, S., Peng, X., et al. (2006). Deletion of TREK-1, a background potassium channel, results in a depression-resistant phenotype. *Nature Neurosci.* 9, 1134–1141. doi: 10.1038/nn1749

Hillhouse, T. M., and Porter, J. H. (2015). A brief history of the development of antidepressant drugs: from monoamines to glutamate. *Exp. Clin. Psychopharmacol.* 23, 1–21. doi: 10.1037/a0038550

Hirschfeld, R. M. (2012). The epidemiology of depression and the evolution of treatment. *J. Clin. Psychiatry* 73(Suppl. 1), 5–9. doi: 10.4088/JCP.11096su1c.01

Honore, E. (2007). The neuronal background K_{2P} channels: focus on TREK1. *Nat. Rev. Neurosci.* 8, 251–261. doi: 10.1038/nrn2117

Katalinic, N., Lai, R., Somogyi, A., Mitchell, P. B., Glue, P., and Loo, C. K. (2013). Ketamine as a new treatment for depression: a review of its efficacy and adverse effects. *Aust. N. Z. J. Psychiatry* 47, 710–727. doi: 10.1177/0004867413486842

Kavalali, E. T., and Monteggia, L. M. (2015). How does ketamine elicit a rapid antidepressant response? *Curr. Opin. Pharmacol.* 20, 35–39. doi: 10.1016/j.coph.2014.11.005

Kessler, R. C., Petukhova, M., Sampson, N. A., Zaslavsky, A. M., and Wittchen, H. U. (2012). Twelve-month and lifetime prevalence and lifetime morbid risk of anxiety and mood disorders in the United States. *Int. J. Methods Psychiatr. Res.* 21, 169–184. doi: 10.1002/mpr.1359

Kim, Y., Gnatenco, C., Bang, H., and Kim, D. (2001). Localization of TREK-2 K^+ channel domains that regulate channel kinetics and sensitivity to pressure, fatty acids and pHi. *Pflugers Arch.* 442, 952–960. doi: 10.1007/s004240100626

Kohler, S., Cierpinsky, K., Kronenberg, G., and Adli, M. (2016). The serotonergic system in the neurobiology of depression: relevance for novel antidepressants. *J. Psychopharmacol.* 30, 13–22. doi: 10.1177/0269881115609072

Krishnan, V., and Nestler, E. J. (2008). The molecular neurobiology of depression. *Nature* 455, 894–902. doi: 10.1038/nature07455

Lafreniere, R. G., Cader, M. Z., Poulin, J. F., Andres-Enguix, I., Simoneau, M., Gupta, N., et al. (2010). A dominant-negative mutation in the TRESK potassium channel is linked to familial migraine with aura. *Nat. Med.* 16, 1157–1160. doi: 10.1038/nm.2216

Lauritzen, I., Blondeau, N., Heurteaux, C., Widmann, C., Romey, G., and Lazdunski, M. (2000). Polyunsaturated fatty acids are potent neuroprotectors. *EMBO J.* 19, 1784–1793. doi: 10.1093/emboj/19.8.1784

Lauritzen, I., Zanzouri, M., Honore, E., Duprat, F., Ehrengruber, M. U., Lazdunski, M., et al. (2003). K^+-dependent cerebellar granule neuron apoptosis. Role of task leak K^+ channels. *J. Biol. Chem.* 278, 32068–32076. doi: 10.1074/jbc.M302631200

Lesage, F., and Lazdunski, M. (2000). Molecular and functional properties of two pore domain potassium channels. *Am. J. Physiol.* 279, 793–801.

Li, Y., Abdourahman, A., Tamm, J. A., Pehrson, A. L., Sanchez, C., and Gulinello, M. (2015). Reversal of age-associated cognitive deficits is accompanied by increased plasticity-related gene expression after chronic antidepressant administration in middle-aged mice. *Pharmacol. Biochem. Behav.* 135, 70–82. doi: 10.1016/j.pbb.2015.05.013

Malberg, J. E., and Schechter, L. E. (2005). Increasing hippocampal neurogenesis: a novel mechanism for antidepressant drugs. *Curr. Pharm. Des.* 11, 145–155. doi: 10.2174/1381612053382223

Maletic, V., Robinson, M., Oakes, T., Iyengar, S., Ball, S. G., and Russell, J. (2007). Neurobiology of depression: an integrated view of key findings. *Int. J. Clin. Pract.* 61, 2030–2040. doi: 10.1111/j.1742-1241.2007.01602.x

Mazella, J. (2001). Sortilin/neurotensin receptor-3: a new tool to investigate neurotensin signaling and cellular trafficking? *Cell. Signal.* 13, 1–6. doi: 10.1016/S0898-6568(00)00130-3

Mazella, J., Petrault, O., Lucas, G., Deval, E., Beraud-Dufour, S., Gandin, C., et al. (2010). Spadin, a sortilin-derived peptide, targeting rodent TREK-1 channels: a new concept in the antidepressant drug design. *PLoS Biol.* 8:e1000355. doi: 10.1371/journal.pbio.1000355

Moha ou Maati, H., Peyronnet, R., Devader, C., Veyssiere, J., Labbal, F., Gandin, C., et al. (2011). A human TREK-1/HEK cell line: a highly efficient screening tool for drug development in neurological diseases. *PLoS ONE* 6:e25602. doi: 10.1371/journal.pone.0025602

Moha Ou Maati, H., Veyssiere, J., Labbal, F., Coppola, T., Gandin, C., Widmann, C., et al. (2012). Spadin as a new antidepressant: absence of TREK-1-related side effects. *Neuropharmacology* 62, 278–288. doi: 10.1016/j.neuropharm.2011.07.019

Moller, H. J. (2003). Suicide, suicidality and suicide prevention in affective disorders. *Acta Psychiatr. Scand. Suppl.* 418, 73–80. doi: 10.1034/j.1600-0447.108.s418.15.x

Munck Petersen, C., Nielsen, M. S., Jacobsen, C., Tauris, J., Jacobsen, L., Gliemann, J., et al. (1999). Propeptide cleavage conditions sortilin/neurotensin receptor-3 for ligand binding. *EMBO J.* 18, 595–604. doi: 10.1093/emboj/18.3.595

Nestler, E. J., Barrot, M., DiLeone, R. J., Eisch, A. J., Gold, S. J., and Monteggia, L. M. (2002). Neurobiology of depression. *Neuron* 34, 13–25. doi: 10.1016/S0896-6273(02)00653-0

Noel, J., Sandoz, G., and Lesage, F. (2011). Molecular regulations governing TREK and TRAAK channel functions. *Channels* 5, 402–409. doi: 10.4161/chan.5.5.16469

Patel, A. J., and Honore, E. (2001). Properties and modulation of mammalian 2P domain K^+ channels. *Trends Neurosci.* 24, 339–346. doi: 10.1016/S0166-2236(00)01810-5

Patel, A. J., Honore, E., Maingret, F., Lesage, F., Fink, M., Duprat, F., et al. (1998). A mammalian two pore domain mechano-gated S-like K^+ channel. *EMBO J.* 17, 4283–4290. doi: 10.1093/emboj/17.15.4283

Porsolt, R. D., Le Pichon, M., and Jalfre, M. (1977). Depression: a new animal model sensitive to antidepressant treatments. *Nature* 266, 730–732. doi: 10.1038/266730a0

Ramaker, M. J., and Dulawa, S. C. (2017). Identifying fast-onset antidepressants using rodent models. *Mol. Psychiatry* 22, 656–665. doi: 10.1038/mp.2017.36

Rush, A. J., Trivedi, M. H., Wisniewski, S. R., Nierenberg, A. A., Stewart, J. W., Warden, D., et al. (2006). Acute and longer-term outcomes in depressed outpatients requiring one or several treatment steps: a STAR*D report. *Am. J. Psychiatry* 163, 1905–1917. doi: 10.1176/ajp.2006.163.11.1905

Sanguinetti, M. C., and Jurkiewicz, N. K. (1990). Two components of cardiac delayed rectifier K^+ current. Differential sensitivity to block by class III antiarrhythmic agents. *J. Gen. Physiol.* 96, 195–215. doi: 10.1085/jgp.96.1.195

Santarelli, L., Saxe, M., Gross, C., Surget, A., Battaglia, F., Dulawa, S., et al. (2003). Requirement of hippocampal neurogenesis for the behavioral effects of antidepressants. *Science*. 301, 805–809. doi: 10.1126/science.1083328

Schechter, L. E., Ring, R. H., Beyer, C. E., Hughes, Z. A., Khawaja, X., Malberg, J. E., et al. (2005). Innovative approaches for the development of antidepressant drugs: current and future strategies. *NeuroRx* 2, 590–611. doi: 10.1602/neurorx.2.4.590

Scherrmann, J. M. (2002). Drug delivery to brain via the blood-brain barrier. *Vascul. Pharmacol.* 38, 349–354. doi: 10.1016/S1537-1891(02)00202-1

Semkovska, M., and McLoughlin, D. M. (2010). Objective cognitive performance associated with electroconvulsive therapy for depression: a systematic review and meta-analysis. *Biol. Psychiatry* 68, 568–577. doi: 10.1016/j.biopsych.2010.06.009

Smith, K. (2014). Mental health: a world of depression. *Nature* 515, 181. doi: 10.1038/515180a

Sowa-Kucma, M., Panczyszyn-Trzewik, P., Misztak, P., Jaeschke, R. R., Sendek, K., Styczen, K., et al. (2017). Vortioxetine: a review of the pharmacology and clinical profile of the novel antidepressant. *Pharmacol. Rep.* 69, 595–601. doi: 10.1016/j.pharep.2017.01.030

Talley, E. M., Solorzano, G., Lei, Q., Kim, D., and Bayliss, D. A. (2001). Cns distribution of members of the two-pore-domain (KCNK) potassium channel family. *J. Neurosci.* 21, 7491–7505.

Thase, M. E., Mahableshwarkar, A. R., Dragheim, M., Loft, H., and Vieta, E. (2016). A meta-analysis of randomized, placebo-controlled trials of vortioxetine for the treatment of major depressive disorder in adults. *Eur. Neuropsychopharmacol.* 26, 979–993. doi: 10.1016/j.euroneuro.2016.03.007

Veyssiere, J., Moha Ou Maati, H., Mazella, J., Gaudriault, G., Moreno, S., Heurteaux, C., et al. (2015). Retroinverso analogs of spadin display increased antidepressant effects. *Psychopharmacology* 232, 561–574. doi: 10.1007/s00213-014-3683-2

Wang, S. M., Han, C., Lee, S. J., Patkar, A. A., Masand, P. S., and Pae, C. U. (2015). Vilazodone for the treatment of major depressive disorder: focusing on its clinical studies and mechanism of action. *Psychiatry Investig.* 12, 155–163. doi: 10.4306/pi.2015.12.2.155

Wiedmann, F., Schmidt, C., Lugenbiel, P., Staudacher, I., Rahm, A. K., Seyler, C., et al. (2016). Therapeutic targeting of two-pore-domain potassium (K_{2P}) channels in the cardiovascular system. *Clin. Sci.* 130, 643–650. doi: 10.1042/CS20150533

Wong, M. L., and Licinio, J. (2001). Research and treatment approaches to depression. *Nat. Rev. Neurosci.* 2, 343–351. doi: 10.1038/35072566

Wood, H. (2010). Migraine: familial migraine with aura is associated with a mutation in the TRESK potassium channel. *Nat. Rev. Neurol.* 6:643. doi: 10.1038/nrneurol.2010.166

Wu, D., Song, B. W., Vinters, H. V., and Pardridge, W. M. (2002). Pharmacokinetics and brain uptake of biotinylated basic fibroblast growth factor conjugated to a blood-brain barrier drug delivery system. *J. Drug Target.* 10, 239–245. doi: 10.1080/10611860290022679

Yohn, C. N., Gergues, M. M., and Samuels, B. A. (2017). The role of 5-HT receptors in depression. *Mol. Brain* 10, 28. doi: 10.1186/s13041-017-0306-y

Zhao, Y., Ma, R., Shen, J., Su, H., Xing, D., and Du, L. (2008). A mouse model of depression induced by repeated corticosterone injections. *Eur. J. Pharmacol.* 581, 113–120. doi: 10.1016/j.ejphar.2007.12.005

Conflict of Interest Statement: The authors declare that the research was conducted in the absence of any commercial or financial relationships that could be construed as a potential conflict of interest.

B- Partie II : Les propriétés de la Spadine et de la Mini-Spadine dans l'AVC et la récupération post AVC (Article 2)

1- Introduction

L'AVC est associé à des troubles neuropsychiatriques comme la dépression et l'anxiété. La dépression post-AVC (PSD) est particulièrement importante sur le plan clinique. Au cours de la première année suivant le début de l'AVC, la PSD entraîne une baisse de l'activité cognitive, une détérioration des résultats de réadaptation et une diminution de la qualité de vie. La mortalité peut être jusqu'à 10 fois plus élevée que chez les patients d'AVC sans PSD (Angelelli et al., 2004) (Esparrago Llorca et al., 2015) (Pohjasvaara et al., 2001). Il est donc essentiel de mettre au point un traitement efficace pour la PSD. Au cours des dernières décennies, différentes cibles ont été impliquées dans le processus de l'AVC. Certaines ont un rôle délétère, comme CCL2 (Chemokine Ligand 2), une chimiokine sécrétée par les cellules endothéliales, et dont les propriétés chimioattractives ciblent de nombreuses cellules immunitaires (Georgakis et al., 2019) (Landreneau et al., 2018) (Huang et al., 2018) alors que d'autres ont un rôle bénéfique, c'est le cas des canaux TREK-1 (Lin et al., 2015) (Mathie and Veale, 2007). D'autre part, dans ce même laps de temps plus d'un millier de molécules a été testé, plus de 200 d'entre elles ont donné lieu à des essais cliniques mais aucun d'entre eux n'a abouti. Plus récemment, des études cliniques ont démontré que les antidépresseurs, en particulier les inhibiteurs sélectifs de la recapture de la sérotonine (SSRI), dont l'Escitalopram, peuvent soulager les symptômes dépressifs chez les patients atteints de PSD (Chen et al., 2006) (Cole et al., 2001) (Hackett et al., 2008) (Hackett et al., 2005a). L'étude clinique la plus convaincante est "fluoxétine in motor recovery of patients with acute ischemic stroke" (FLAME), qui a montré qu'après 90 jours, le traitement avec la fluoxétine améliore la récupération motrice et prévient la PSD (Chollet et al., 2011). La mise en œuvre de stratégies thérapeutiques utilisant les AD pour réduire les troubles de l'humeur et améliorer la récupération post-AVC semble prometteuse. Cependant, les AD entraînent des effets secondaires qui peuvent se révéler dangereux pour une population à risques telle que les victimes d'AVC. C'est dans ce contexte que nous avons choisi d'utiliser la Spadine. En effet, la Spadine dont les propriétés antidépressives ont déjà été prouvées dans plusieurs modèles de dépression, n'a pas d'effets secondaires, tout du moins au niveau cardiaque et sur l'ensemble des fonctions contrôlées par TREK-1 (Article 3) (Mazella et al., 2010) (Moha Ou

Maati et al., 2012b). Cela en fait une molécule de choix pour soulager les complications psychiatriques et réduire les troubles fonctionnels provoqués par l'AVC.
Les résultats que nous avons obtenus avec les analogues de la Spadine (Partie I) ont montré qu'ils étaient des antidépresseurs tout aussi efficaces que la Spadine, et de surcroît plus stables *in vivo* (Article 1). Nous avons donc entrepris, d'une part d'étudier les effets de ces peptides dans la récupération post-AVC et, d'autre part, comparer leurs effets (ceux du PE 22-28 ou Mini-Spadine, que nous avons choisie pour représenter les analogues de la Spadine) avec ceux de la Spadine et de l'Escitalopram (un des SSRI les plus utilisés en clinique et dans les recherches expérimentales sur le traitement post-AVC (Kronenberg et al., 2014)). Le but de cette étude était de caractériser les effets de la Mini-Spadine sur la récupération post-AVC, et les comparer à ceux des SSRI. Une amélioration de la récupération suggèrerait la Mini-Spadine comme nouvelle thérapeutique face à l'AVC en clinique humaine.

Nous avons pour cela utilisé le modèle de la MCAO (Middle Cerebral Artery Occlusion) (**Figure 28A)**. qui est, chez les rongeurs, très largement utilisé et considéré comme une référence (Herson and Traystman, 2014). Nous avons choisi la MCAO car ce protocole permet de mimer le plus fidèlement possible l'AVC humain notamment l'apparition de la pénombre ischémique, le développement de troubles semblables à ceux observés en clinique humaine, et la possibilité d'une reperfusion (Kumar et al., 2016) (Fluri et al., 2015). Le principe est d'insérer un filament dans l'artère cérébrale moyenne afin de bloquer le flux sanguin. Le filament est laissé, selon le protocole, 1 heure pour l'étude de la neuroprotection, ou 30 minutes dans le cas de l'étude de la PSD (**Figure 28A)**. Durant la totalité de l'opération le flux sanguin des animaux dans la zone d'intérêt est mesuré par laser Doppler, afin de s'assurer que l'ischémie est correctement réalisée.

2- Résultats

Lors de travaux précédents, nous avons montré que la Mini-Spadine et la Spadine (à 100 nM) inhibent le canal TREK-1 préalablement activé avec de l'acide arachidonique (AA, 10 µM), avec une IC_{50} de 0,12 nM pour la Mini-Spadine et de 40 nM pour la Spadine (Article 1). Cependant, la Mini-Spadine et la Spadine sont également capables d'interagir sur le courant basal de TREK-1.

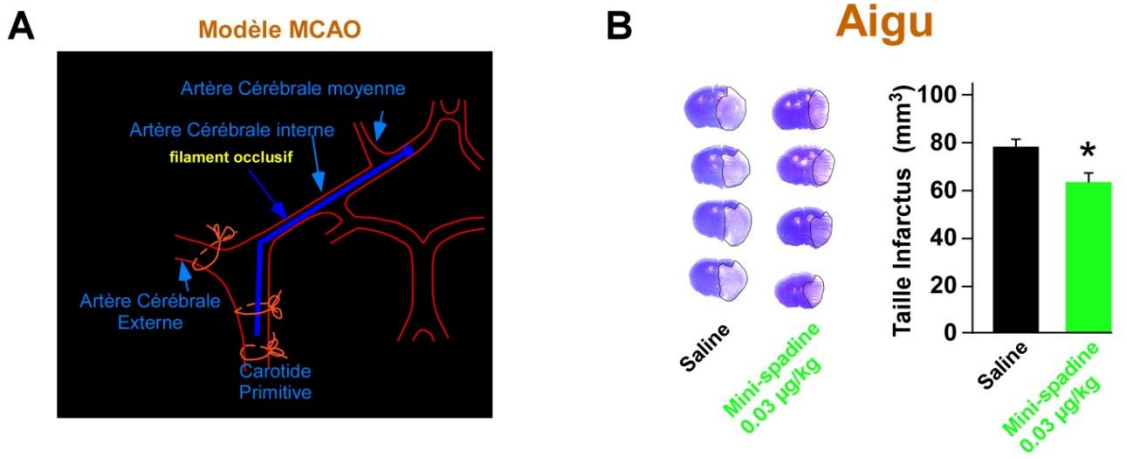

Figure 28 : Effets de la Mini-Spadine dans le modèle de la MCAO

Lors d'une expérience de dose-réponse avec une gamme de concentration de 10^{-11} à 10^{-5} M, nous avons constaté que les faibles concentrations au lieu d'inhiber le canal, l'activaient. En effet, la Mini-Spadine, de 10^{-11} à 10^{-8} M active de manière dose-dépendante le canal TREK-1 avec un pic d'effet à 10^{-8} M (85,3 ± 27,3 %, n=18, P=0,017) et à 10^{-9} M (65,1 ±19,8 %, n=7, P=0,017) (**Figure 29A**). Le même effet a été obtenu avec la Spadine qui active le courant de base de TREK-1 à 10^{-6} M (49,4 ±20,0 3 %, n=9, *P=0,039) (**Figure 29B)**. Les densités de courant mesurées à 0 mV étaient de 149 ± 20,0 % pour la Spadine à 10^{-6} M (n=9, *P=0,038) et de 194,3 ± 27,5 % pour la Mini-Spadine à 10^{-8} M (n=15, **P=0,004) par rapport au contrôle **(Figure 29B**).

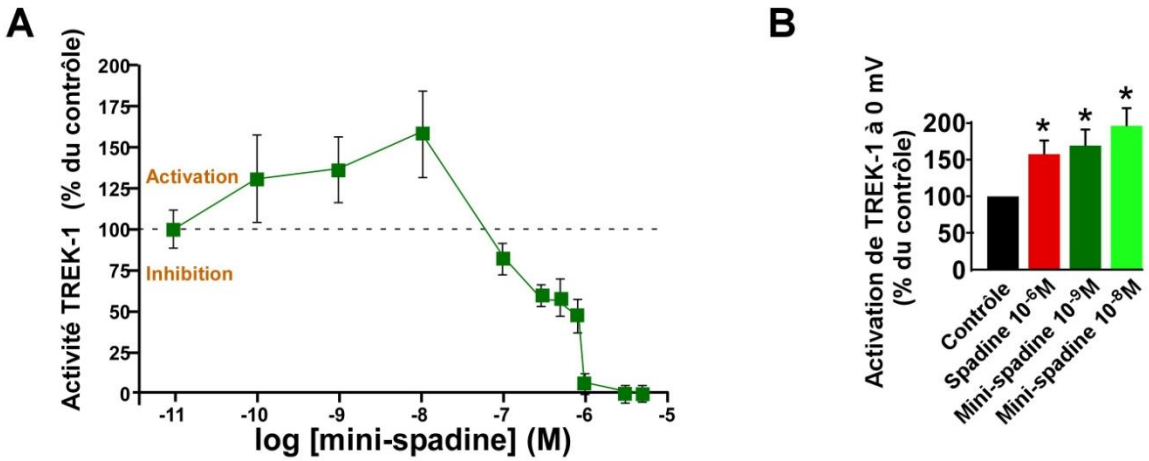

Figure 29 : Effets biphasiques de la Mini-Spadine sur l'activité de TREK-1

L'activation de TREK-1 est neuroprotectrice dans les modèles d'ischémie focale et globale (Blondeau et al., 2002a) (Blondeau et al., 2002b) (Heurteaux et al., 2006a) (Lauritzen et al., 2000) (Quast, 1992), et les données électrophysiologiques indiquent une activation de ce canal par la Mini-Spadine à 10^{-8} et 10^{9} M. Nous avons alors fait l'hypothèse, qu'à ces faibles concentrations, la Mini-Spadine pouvait s'avérer protectrice face au choc ischémique. Cette hypothèse a ensuite été vérifiée *in vivo* dans le modèle de MCAO (**Figure 28)**.

En effet, à la dose de 0,03 µg/kg (correspondant à 10^{-8} M dans les études électrophysiologiques) la Mini-Spadine augmente significativement le pourcentage de survie des animaux 24 et 96 heures après la MCAO en comparaison à des souris non traitées **(Figure 30)**. Alors qu'à une dose plus élevée, 0,3 µg/kg (correspondant à 10^{-7} M dans les études électrophysiologiques), la Mini-Spadine inhibe TREK-1, et devient délétère (**Figure 30**). Ces résultats, *in vivo*, confirment donc bien les mesures électrophysiologiques.

		24 h			96 h		
	Total	Vivante	Morte	% survie	Vivante	Morte	% survie
Saline	26	17	9	65.4	16	10	61.5
Mini-spadine 0.3 µg/kg	19	10	9	52.6	5	14	26.3
Mini-spadine 0.03 µg/kg	20	18	2	90	15	5	75

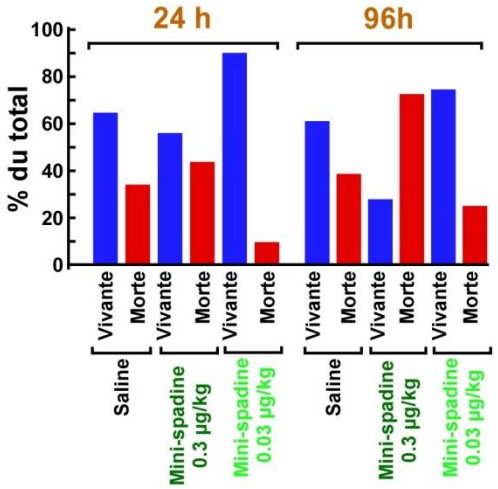

Figure 30 : Effets de la Mini-Spadine sur la survie post-MCAO

De plus, en injection aiguë la Mini-Spadine administrée à 0,03 µg/kg 30 min après une MCAO d'1 heure entraîne également une diminution significative du volume de l'infarctus par rapport aux souris non traitées **(Figure 28B)**. Cela représente un argument de plus en faveur de

l'hypothèse d'un effet protecteur de la Mini-Spadine utilisée à faible concentration pendant la phase aiguë de l'AVC.

La dose de Mini-Spadine de 0,03 µg/kg (10^{-8} M) induit la meilleure activation TREK-1 **(Figure 29B)**, une augmentation de la survie des animaux **(Figure 30)** et une diminution significative du volume de l'infarctus **(Figure 28B)**, nous avons donc décidé d'utiliser cette dose pour toute l'étude.

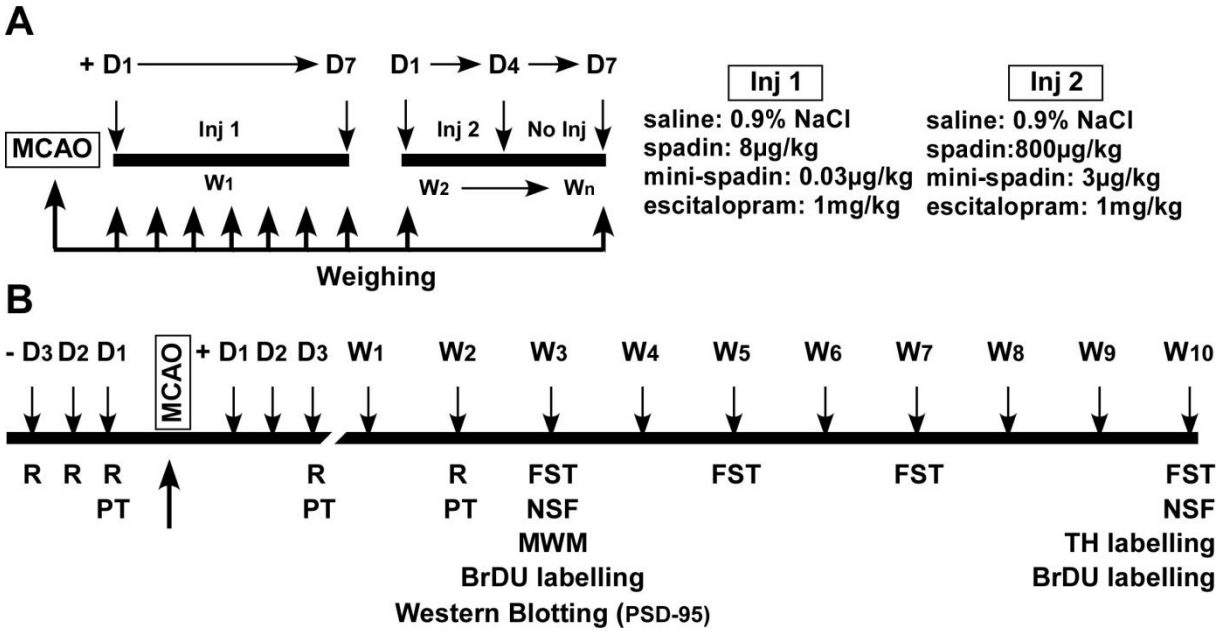

Figure 31 : Protocole expérimental en deux phases pour l'étude des effets de la Mini-Spadine sur l'AVC

Les effets antidépresseurs de ce peptide ont, quant à eux, été rapportés à des concentrations plus élevées (3 µg/kg pour la Mini-Spadine) (Article 1) Les processus de l'AVC et leurs conséquences ne sont pas les mêmes pendant les phases aiguë ou tardive, et doivent être gérées différemment : reperfusion précoce et neuroprotection pour la phase aiguë, rétablissement neuronal par neuroplasticité pour la phase tardive (Chollet et al., 2014). C'est la raison pour laquelle nous avons mis au point un protocole en deux temps :

1/ les 7 jours suivant la MCAO, les souris sont traitées quotidiennement avec la faible concentration de Mini-Spadine (0,03 µg/kg) pour activer TREK-1 **(Figure 31)**

2/ à partir du 8ème jour, les souris reçoivent une injection quotidienne de Mini-Spadine de concentration plus importante (3 µg/kg) pendant 4 jours pour induire un effet antidépresseur

et stimuler la neurogenèse et la synaptogenèse. Aucune injection n'est réalisée lors des trois derniers jours. Ce protocole (4 jours injections puis 3 jours sans injection) est répété jusqu'au sacrifice des animaux **(Figure 31)**.

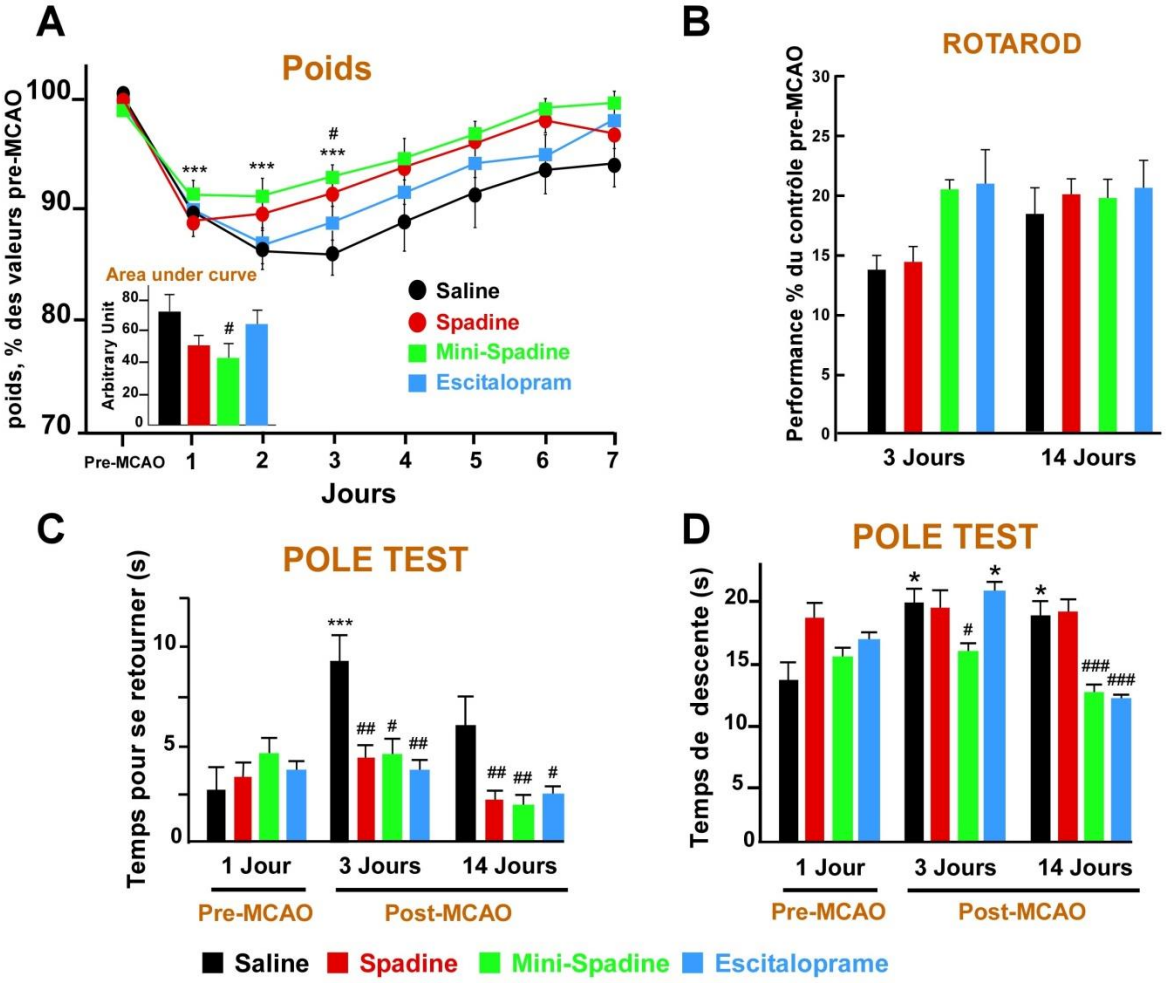

Figure 32 : Variations de poids et analyse des fonctions motrices

En plus des souris traitées au sérum physiologique (véhicule), nous avons également choisi d'utiliser deux molécules témoins : la Spadine et l'Escitalopram. Tout comme la Mini-Spadine, la Spadine a été injectée selon un protocole en deux étapes (8 µg/kg pendant 7 jours et 800 µg/kg pendant 4 jours/semaine). L'Escitalopram a été injecté pendant les deux étapes à la dose de 1 mg/kg **(Figure 31).**

Afin de nous assurer du bien-être général des animaux, nous avons mesuré les variations de poids immédiatement après la MCAO, et ce jusqu'à la fin de l'étude.

Nous avons ainsi constaté que les souris traitées au sérum physiologique soumises à la MCAO présentent une perte de poids significative dans les trois jours suivant l'opération (***P<0,001) **(Figure 32A)** et ne retrouvent leur poids préopératoire qu'après deux semaines. En revanche, la perte de poids des souris traitées avec la Mini-Spadine est plus faible. En effet, alors que la Spadine et l'Escitalopram n'ont pas eu d'effet significatif, la mesure des surfaces sous la courbe a montré que la Mini-Spadine réduit significativement la perte de poids observée chez les souris non traitées ($F_{3, 51}$=2,78, #P=0,029) 3 jours après la MCAO **(Figure 32A, insert).** Les animaux traités avec la Mini-Spadine reprennent également du poids à un rythme plus rapide que les animaux du groupe contrôle, elles reviennent à 95,5 % de leur poids préopératoire seulement 5 jours après la MCAO **(Figure 32A).**

A noter que ces effets ne sont pas dus à des variations du peptide endogène, puisque les niveaux mesurés (en fait le niveau de PE) sont identiques chez les animaux opérés que chez les animaux non opérés (P>0,05, **Figure 33).**

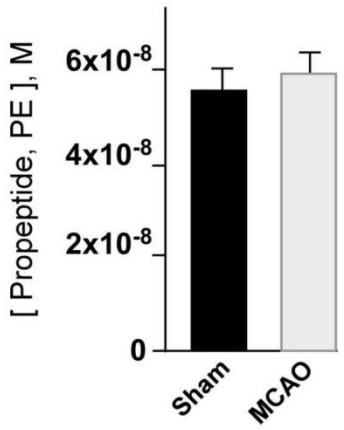

Figure 33 : Concentrations de propeptide

De même, chez des animaux non opérés (groupes sham), il n'y a pas de différence significative sur de la prise de poids entre le groupe de souris non traitées et de souris traitées avec la Mini-Spadine (**Figure 34**), ce qui exclut tout effet métabolique du peptide qui aurait pu rendre compte des différences dans les variations du poids.

De plus, nous avons constaté que les souris traitées à la Spadine présentent le même taux de récupération que les souris traitées à la Mini-Spadine (5 jours), mais les souris traitées à l'Escitalopram ont besoin de deux jours de plus pour retrouver un poids comparable **(Figure 32A).**

Les déficits moteurs et cognitifs sont des séquelles neurologiques courantes chez les patients victimes d'AVC (Cumming et al., 2013) (Langhorne et al., 2009), nous avons donc étudié les effets des traitements peptidiques sur ces déficits.

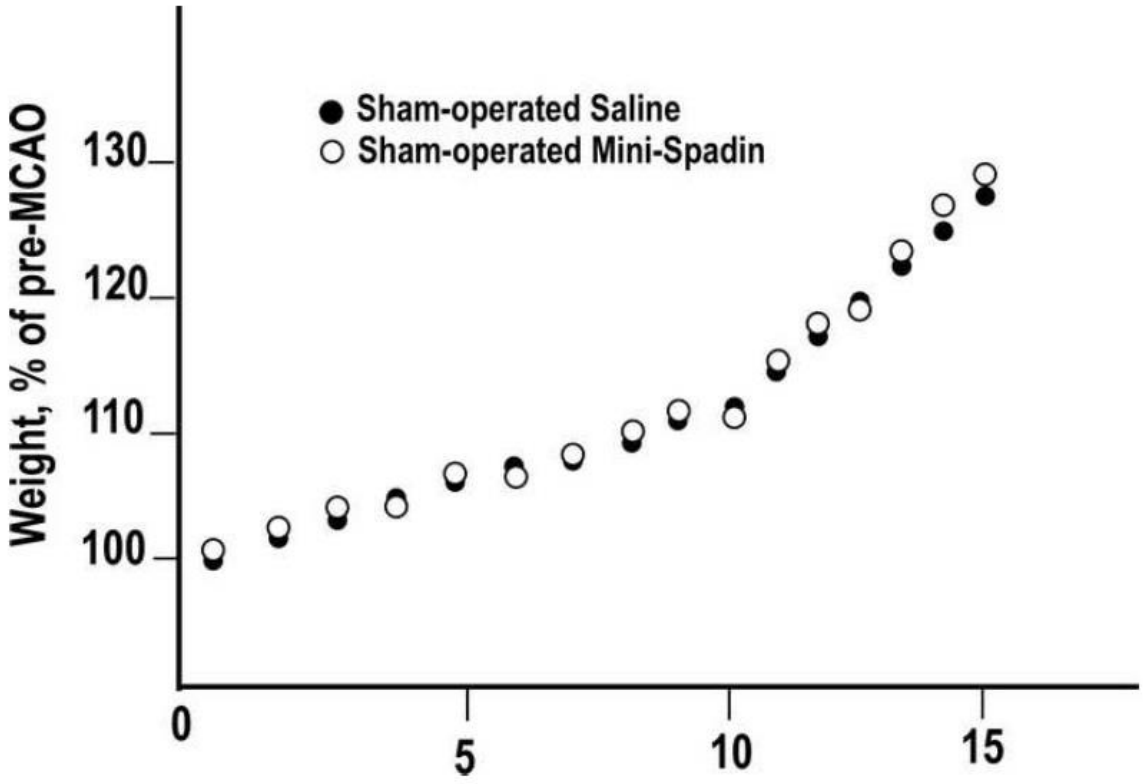

Figure 34 : Courbe de poids d'animaux non opérés, traités ou non avec de la Mini-Spadine

Pour les déficits moteurs, nous avons choisi deux tests : le rotarod et le pole test. Dans chacun de ces tests, les souris ont été évaluées pour leurs performances motrices avant la MCAO pour éviter toute variabilité non imputable à la MCAO ou aux traitements.

Dans le test du rotarod, les données recueillies après opération ont été normalisées pour chaque souris en fonction de ses performances préopératoires (considérées comme étant 100%) **(Figure 32B).** Trois jours après la MCAO, tous les groupes manifestent une forte diminution de leurs performances par rapport aux données pré-ischémiques, mais seul le groupe traité avec la Mini-Spadine présente un déficit moteur moins important que le groupe contrôle (#P=0,032, **Figure**

32B, 3 jours). Deux semaines après la MCAO, tous les groupes ont des performances similaires (**Figure 32B, 14 jours**).

Dans le pole test, il n'y a aucune différence significative dans les performances pré-ischémiques des groupes **(Figure 32C-D, panel pré-MCAO**). Trois jours après la MCAO, on observe une augmentation significative du temps de rotation et de descente le long du pôle dans tous les groupes par rapport aux valeurs pré-MCAO (***P<0,001 pour la rotation et *P<0,05 pour la descente, **Figure 32C-D**, **panel 3 jours**), ce qui suggère des déficits moteurs induits par l'ischémie. Il est intéressant de noter que la Mini-Spadine réduit de façon significative le temps passé dans les deux tâches par rapport au groupe non traité ($F_{3, 42}$=5.004, ##P=0.0044 pour la rotation et #P=0.049 pour la descente, **Figure 32C-D**). La Spadine et l'Escitalopram réduisent également significativement le temps de rotation ($F_{3, 42}$ = 5,004, #P=0,0152 pour la Spadine et #P=0,0159 pour l'Escitalopram, **Figure 32C**), mais pas le temps de descente. Deux semaines après la MCAO, il n'y a plus d'effet des traitements au niveau du temps de rotation, mais la Mini-Spadine conserve son effet sur le temps de descente et, à ce stade, l'Escitalopram induit également une amélioration des performances dans cette tâche ($F_{3, 33}$ = 5,169, #P=0,045 pour la Mini-Spadine et #P=0,025 pour l'Escitalopram, (**Figure 32D**).

Pour les déficits cognitifs, nous avons utilisé le test de la Piscine de Morris réalisé trois semaines après la MCAO. Durant les quatre jours d'apprentissage, tous les groupes opérés ont manifesté de grandes difficultés à trouver la plateforme **(Figure 35A).**
En effet, le temps le temps nécessaire aux souris pour trouver effectuer cette tâche est considérablement plus long chez ces animaux par rapport à ceux du groupe sham (**Figure 35C**). De plus, alors que les souris traitées avec le sérum physiologique ou l'Escitalopram ne présentent pas d'amélioration de leurs performances au fur et à mesure des essais, il est intéressant de constater que les souris traitées avec la Mini-Spadine ont considérablement amélioré le temps nécessaire pour trouver la plate-forme cachée **(Figure 35B)**. En effet, nous avons observé une différence significative de latence dès le troisième jour d'entraînement chez les souris traitées avec la Mini-Spadine (-27,8 %, $F_{3, 56}$=7,538, #P=0,021 vs jour 1 correspondant), et jusqu'au quatrième (-44,4 %, ###P=0,001 vs jour 1 correspondant). De plus, au terme de l'apprentissage (jour 4), la Mini-Spadine induit également une amélioration significative des performances des souris opérées par rapport au groupe MCAO non traité ($F_{3,}$

$_{56}$ = 4,01, $$P=0,0073, **Figure 35A**). L'Escitalopram n'a en revanche aucun effet significatif dans nos conditions (P=0,58).

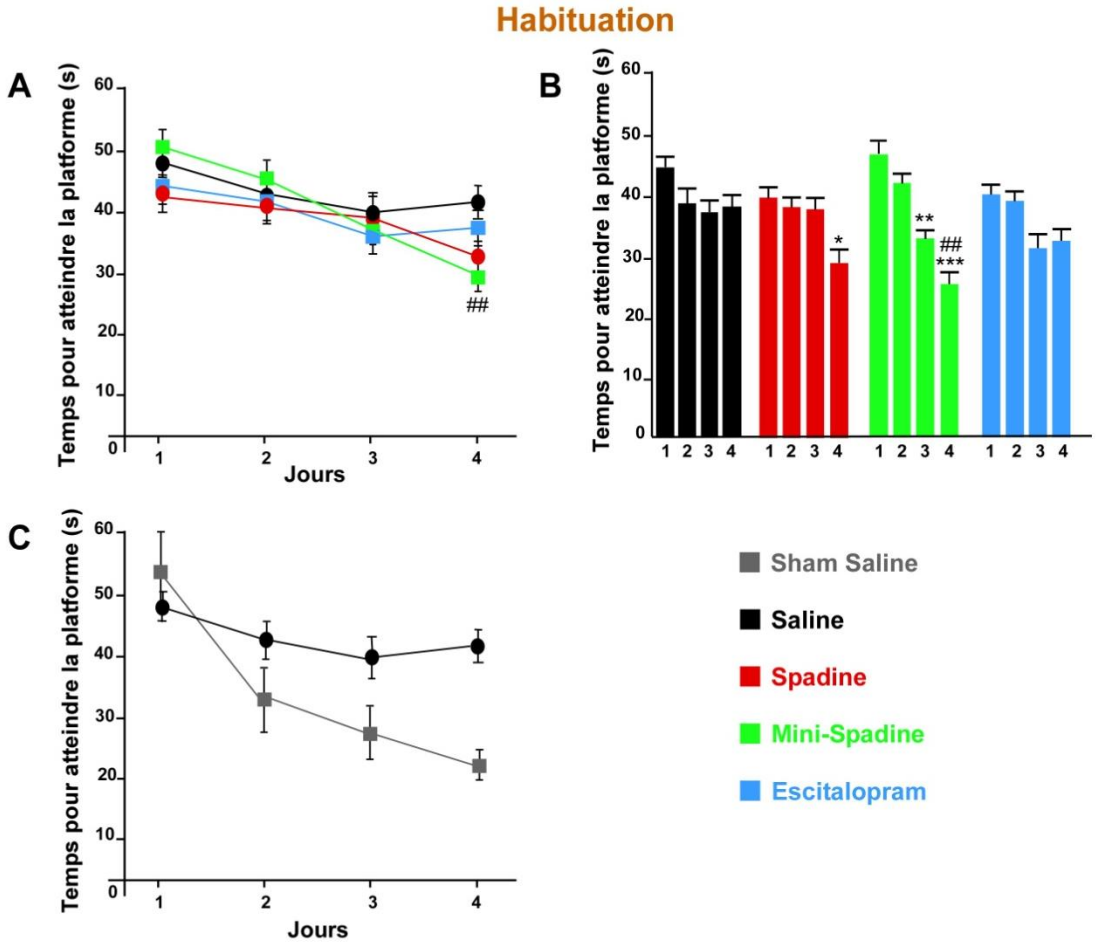

Figure 35 : Apprentissage dans le test de la Piscine de Morris

Au cours du test, le cinquième jour, seules les souris traitées avec la Mini-Spadine ont pénétré significativement plus rapidement dans le quadrant où se trouvait la plate-forme durant l'apprentissage (NW) (**Figure 36A**, **panneau droit,** #P<0,05). Nous avons également observé que les souris opérées traitées avec la Spadine et la Mini-Spadine manifestent une préférence pour le quadrant NW, dans lequel elles ont tendance à passer plus de temps que les souris non traitées. Cela suggère que les animaux se souviennent de la zone où se trouvait la plate-forme au départ, mais le résultat n'a pas atteint la significativité (**Figure 36A, panneau de gauche**, $F_{3, 54}$ = 1,92, P=0,066 vs groupe MCAO-sérum).

L'analyse des stratégies ((Lorivel et al., 2015), **Figure 18**) a montré que par rapport au groupe MCAO non traité et au groupe MCAO Escitalopram, les souris traitées avec la Mini-Spadine

utilisent une stratégie de recherche de la plateforme plus efficace. Nous avons effet observé l'émergence de la persévérance (recherche active dans la zone où se trouvait la plateforme pendant l'entraînement), absente chez les souris MCAO non traitées ou traitées avec l'Escitalopram **(Figure 36B et Figure 18).**

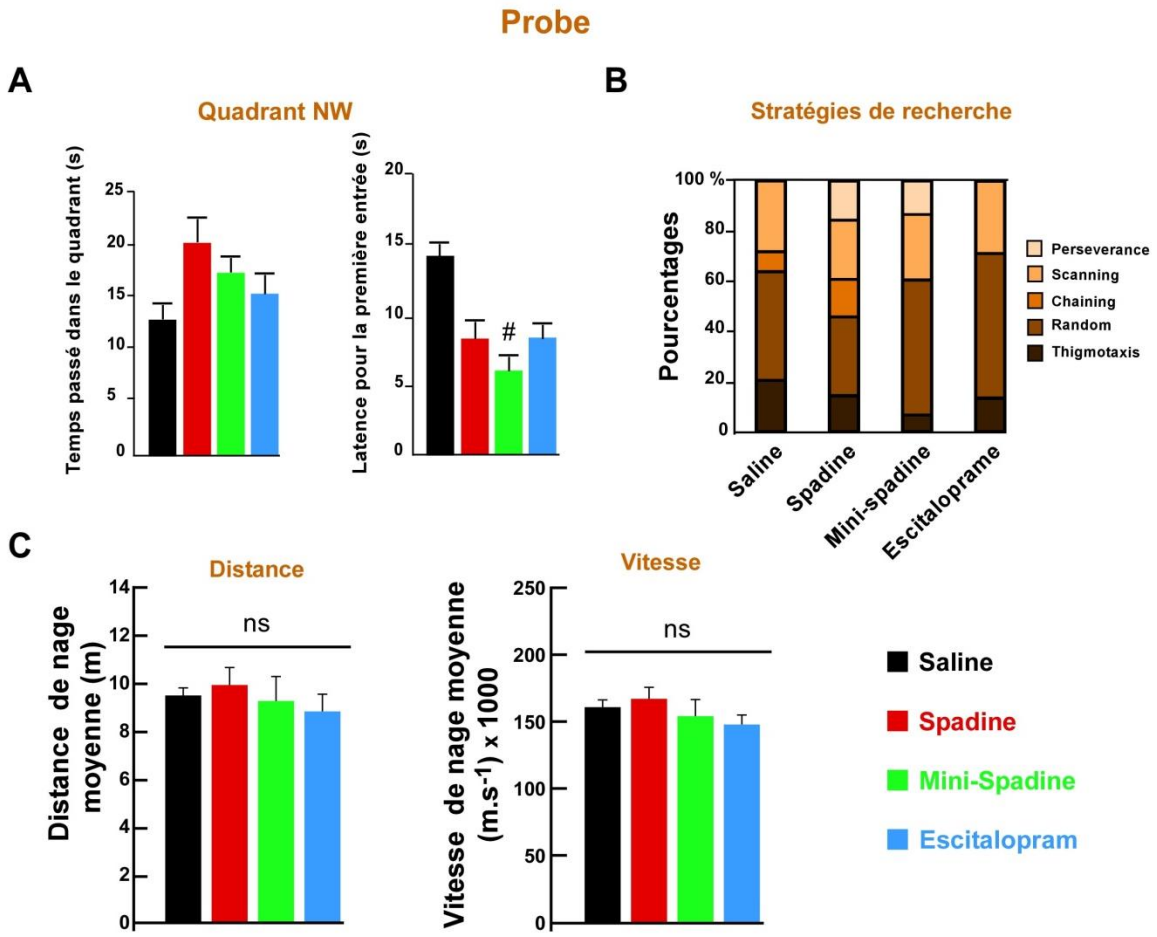

Figure 36 : Mesures jour test de la Piscine de Morris

La distance parcourue et la vitesse moyenne de tous les groupes étant semblables, nous pouvons également affirmer que les différences observées entre les souris traitées avec la Mini-Spadine et les autres ne sont pas dues à des altérations motrices (**Figure 36C**).

Les résultats obtenus dans ces trois premiers tests indiquent que, dans nos conditions, la Mini-Spadine est plus efficace que la Spadine et l'Escitalopram pour diminuer les déficits moteurs et cognitifs induits par l'AVC.

Un autre problème majeur induit par l'AVC est le développement d'une dépression post-AVC. Avant d'étudier les effets antidépresseurs de la Mini-Spadine, nous avons dans un premier temps confirmé l'établissement de l'état dépressif post-AVC dans notre modèle. Pour ne pas induire de biais dans l'expérience nous avons souhaité dans notre protocole ne pas ajouter de stress chronique, comme le CMS qui est souvent utilisé (Kronenberg et al., 2014), en plus de la MCAO.

Pour vérifier si l'état dépressif avait été induit par notre protocole, nous avons choisi les tests du FST et du NSF. Ces deux tests sont couramment utilisés pour le criblage de molécules antidépressives.

Les FST effectués 3, 5, 7 et 10 semaines après la MCAO, nous montrent que les souris traitées avec la Mini-Spadine et la Spadine manifestent une diminution significative du temps d'immobilisation (qui est symptôme de désespoir) par rapport aux souris opérées non traitées et cela dès la cinquième semaine de traitement ($F_{4, 112}$ = 6,097, ##P=0,0013, **Figure 37**). Dans ces mêmes conditions d'expérimentation, l'Escitalopram n'a d'effet antidépresseur significatif qu'après 10 semaines ($F_{3, 113}$ = 10,44, ##P=0,0059, **Figure 37**). Il est important de rappeler que ces différences ne sont pas dues à une perte de locomotion, comme nous l'avons démontré dans le test de la piscine de Morris (**Figure 36C**). Nous avons également mis en évidence une augmentation du temps d'immobilité qui devient significative à 10 semaines post opératoires dans le groupe de souris opérées non traitées par rapport au groupe sham correspondant ($F_{4, 113}$ = 10,44, *P=0,035) (**Figure 37**). Ces résultats confirment l'apparition d'un phénotype « dépressif » associé à la MCAO.

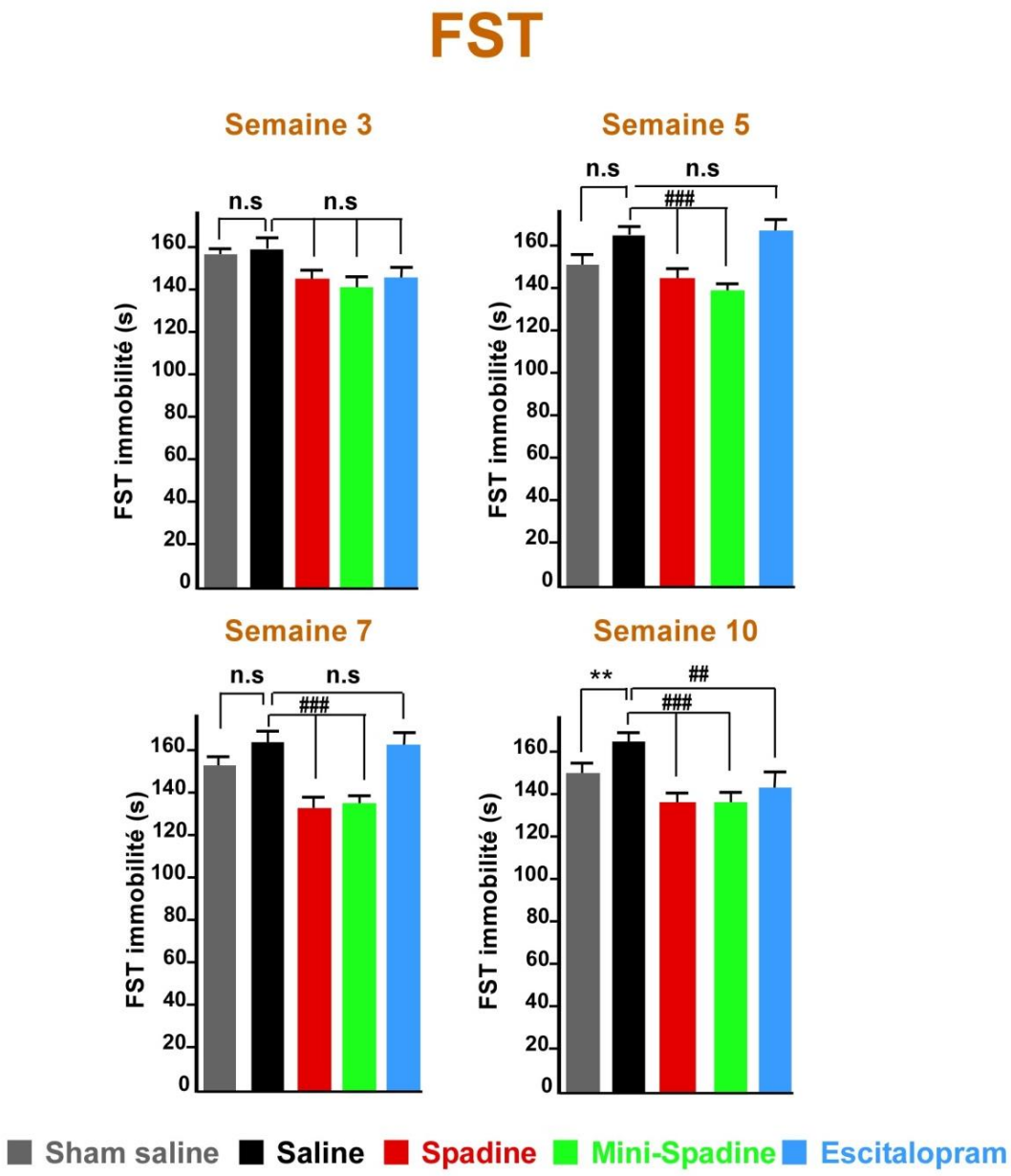

Figure 37 : Etude du phénotype dépressif dans le test du FST

Dans le NSF, le comportement dépressif induit par la MCAO apparaît 3 semaines après l'ischémie mais ne s'établit définitivement qu'après 10 semaines (**Figure 38A**). En effet, la MCAO entraîne une augmentation significative du temps que mettent les animaux pour aller se nourrir par rapport au groupe sham ($F_{4, 63}$ = 5,93, **P=0,0039, **Figure 38B**). Cette latence est 1,9 fois plus élevée 3 semaines après l'ischémie, et 3,8 plus élevée après 10 semaines chez les souris opérées par rapport aux sham (**Figure 38A**). Le traitement avec les trois molécules antidépressives permet d'alléger significativement ces changements comportementaux ($F_{4, 63}$ =

5,93, #P=0,0296 pour la Mini-Spadine, #P=0,0231 pour la Spadine et ###P=0,0007 pour l'Escitalopram, par rapport au groupe contrôle, **Figure 38B-C**). Là encore on peut observer que la Spadine et la Mini-Spadine provoquent une diminution de 40% de la latence dès 3 semaines, alors que l'Escitalopram ne devient efficace de manière significative qu'après 10 semaines.

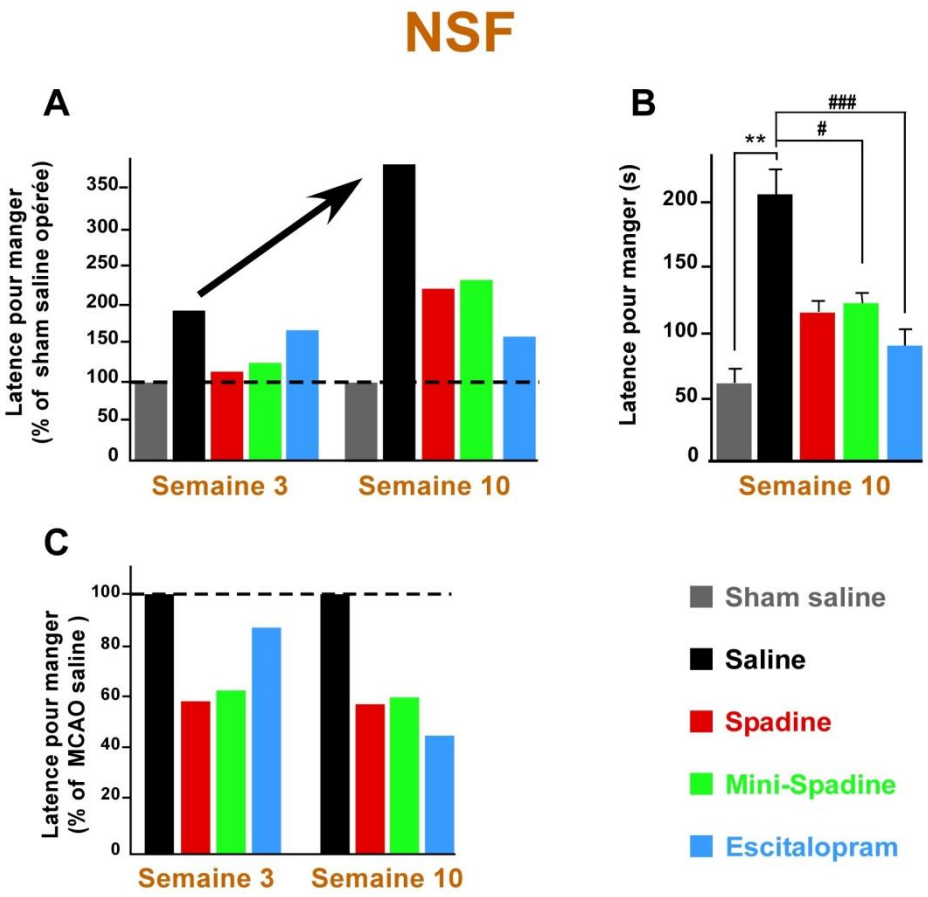

Figure 38 : Etude du phénotype dépressif dans le test du NSF

Ces résultats démontrent qu'un traitement avec une molécule antidépressive, et tout particulièrement la Mini-Spadine, inverse les altérations comportementales de type dépressif induites par un AVC. Ils confirment également le développement d'un phénotype dépressif 10 semaines après la MCAO, un délai comparable à celui observable chez l'humain, qui varie de deux mois à un an après la survenue de l'AVC (Francisco, 1993).

Comme mentionné précédemment, le test du NSF est étroitement corrélé à la neurogenèse hippocampique qui est l'un des effets canoniques des antidépresseurs.

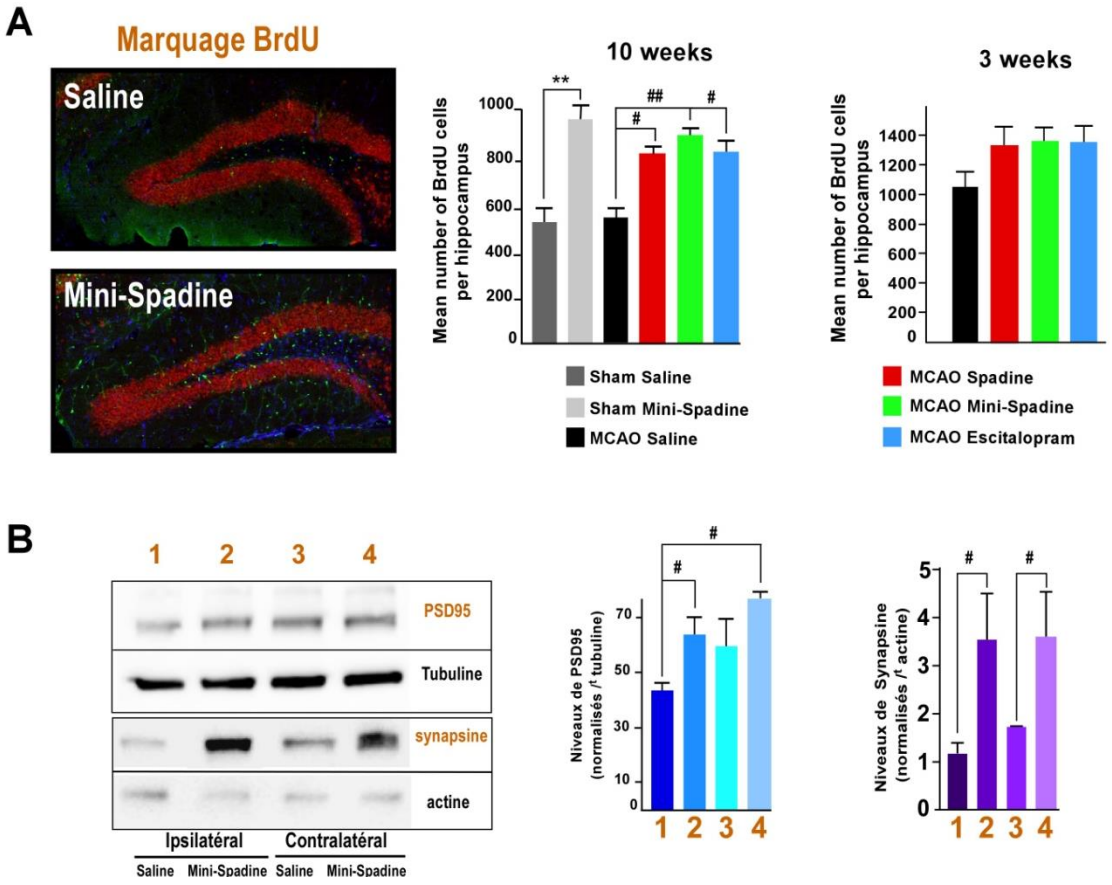

Figure 39 : Neurogenèse et synaptogenèse

Pour mettre en évidence les effets des trois molécules sur la neurogenèse, nous avons utilisé du BrdU. Le BrdU s'incorpore à la molécule d'ADN lors de sa synthèse et ainsi marque les cellules nouvellement formées.

Trois semaines après la MCAO, nous n'avons observé aucune différence dans le nombre de cellules BrdU positives entre les souris non traitées et les souris traitées (**Figure 39A panneau gauche**).

Dix semaines après la MCAO, le nombre de cellules BrdU positives dans la zone sous-granulaire (SGZ) des souris opérées et des sham est comparable ($F_{3, 36} = 3,77$, P=0,21) (**Figure 39A, panneau du milieu**) Cependant, la prolifération cellulaire maximale dans le cerveau adulte se produit une à deux semaines après l'AVC (Arvidsson et al., 2002) (Jin et al., 2001), or dans notre étude, nous avons analysé la neurogenèse à 3 et 10 semaines, mais pas quelques jours après la MCAO. C'est probablement la raison pour laquelle nous n'avons pas pu observer d'augmentation de la neurogenèse qui se produit après une MCAO. A noter que, comme nous

l'avons précédemment montré (**Figure 20A**) (Article 1), un traitement avec de la Mini-Spadine chez des souris non soumises à la MCAO entraîne une augmentation de la prolifération des cellules souches neurales dans la SGZ ($F_{3,36}$ = 3,77, **P=0,0042) (**Figure 39A, panneau du milieu**).

Chez des souris ischémiées, le traitement avec la Mini-Spadine induit une augmentation du nombre de cellules nouvellement formées de 52,5 % ($F_{3,36}$ = 3,77, ##P=0,0054 vs MCAO non traité) (**Figure 39A, panneau du milieu**). Vingt et un jours après la dixième semaine suivant la MCAO, le nombre de cellules co-marquées BrdU/NeuN (un marqueur des neurones matures) dans la SGZ était également plus élevé chez les souris traitées avec la Mini-Spadine que dans le groupe non traité (**Figure 39A, panneau gauche**). Ce résultat montre que la Mini-Spadine stimule la neurogenèse induite par l'ischémie et que la majorité (80%) des nouvelles cellules formées dans la SGZ se différencient en neurones matures.

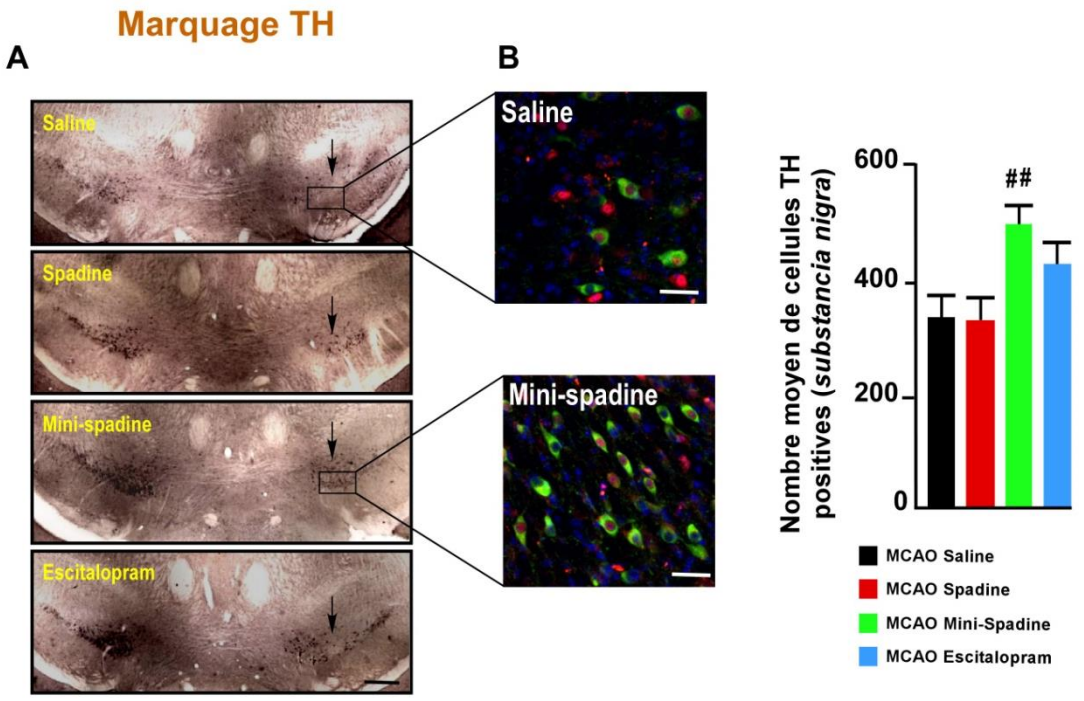

Figure 40 : Marquage TH des neurones GABAergiques

La dépression est également associée à la perte des connexions synaptiques dans les circuits de l'humeur, et les traitements antidépresseurs facilitent la récupération en stimulant la

synaptogenèse (Bambico and Belzung, 2013). L'analyse par Western-Blot du tissu cérébral 3 semaines après l'ischémie a montré que la Mini-Spadine entraîne une augmentation significative des quantités de PSD-95 et de Synapsine, deux marqueurs clés de la synaptogenèse, (de Bartolomeis and Fiore, 2004) (Mirza and Zahid, 2018) dans le cortex ipsilatéral (donc ischémié) des animaux (**Figure 39B**). Ce qui confirme les résultats déjà obtenus dans des études précédentes (Article 4) (Devader et al., 2015).

Enfin, le syndrome dépressif développé après un AVC est associé à des altérations fonctionnelles et structurelles du système dopaminergique mésolimbique (Kronenberg et al., 2012). Un marquage des neurones dopaminergiques de la *substantia nigra* avec la tyrosine hydroxylase (TH) a montré que, dix semaines après la MCAO, l'ischémie induit une forte diminution du nombre de cellules TH-positives (**Figure 40A-B).** Cet effet de la MCAO est atténué de façon significative par le traitement avec la Mini-Spadine ($F_{3, 35}$ = 4,53, ##P=0,0093 par rapport au groupe MCAO sérum). Le traitement avec la Mini-Spadine induit une augmentation de 46 % du nombre de neurones TH-positifs par rapport aux souris non traitées (**Figure 40B**). La Spadine et l'Escitalopram n'ont pas d'effet significatif sur le niveau de TH (P=0,999 pour la Spadine et P=0,957 pour l'Escitalopram).
Le traitement avec la Mini-Spadine stimule donc non seulement la neurogenèse hippocampique mais aussi la synaptogenèse. De plus, il permet également d'atténuer la perte de neurones dopaminergiques induite par l'ischémie. C'est un ensemble de processus bénéfiques pour la récupération post-AVC.

3- Conclusion

Ces résultats montrent clairement que les effets de la Mini-Spadine sur les séquelles de l'AVC (perte de poids, rotarod et pole test, Piscine de Morris, perte de neurones dopaminergiques) et sur la PSD sont plus rapides (5 semaines au lieu de 10 semaines en FST) et plus puissants que ceux obtenus avec l'Escitalopram.
En conclusion, il s'agit de la première étude qui démontre le potentiel thérapeutique de la Mini-Spadine en tant qu'alternative aux AD actuellement utilisées pour soulager les troubles neurologiques et neuropsychiatriques après un AVC.

First evidence of protective effects on stroke recovery and post-stroke depression induced by sortilin-derived peptides

Mariel Pietri, Alaeddine Djillani, Jean Mazella, Marc Borsotto, and Catherine Heurteaux*

Université Côte d'Azur, CNRS, IPMC, UMR7275, 660 route des Lucioles, Sophia Antipolis

06560 Valbonne France

*** Corresponding author:**

Dr Catherine HEURTEAUX; phone: +33 (0)4 93 95 77 84, Fax: +33 (0)4 93 95 77 08;

e-mail: heurteau@ipmc.cnrs.fr

Running title: Mini-spadin prevents post-stroke depression

Post-stroke depression (PSD) is the most common mood disorder following stroke with high relevance for outcome and survival of patients. The TREK-1 channel represents a crucial target in the pathogenesis of stroke and depression. Spadin and its short analog mini-spadin were reported to display potent antidepressant properties. We investigated the therapeutic effects of mini-spadin in a mouse model of focal ischemia and PSD. To activate TREK-1 and induce neuroprotection a single low dose of mini-spadin (0.03 μg/kg) was intraperitoneally injected 30 min after the onset of ischemia, once a day during 7 days post-ischemia. Then, to inhibit TREK-1 and induce antidepressant effect, the peptide was injected at higher concentration (3 μg/kg) once a day for 4 days/week until the sacrifice of animals. Electrophysiological studies showed that mini-spadin had a biphasic action on TREK-1. At low doses, the channel activity was increased whereas at higher doses it was inhibited. Mini-spadin prevented the loss of body weight and the delayed dopaminergic degeneration in *substantia nigra* and improved the motor and cognitive ischemia-induced deficits. Moreover, mini-spadin prevented PSD analyzed in the Forced Swim and Novelty Suppressed Feeding tests. Finally, enhanced neurogenesis and synaptogenesis contributed to the beneficial effects of mini-spadin against stroke and PSD. This work reveals the first evidence that the modulation of TREK-1 channels in the early and chronic phases of stroke as well as the stimulation of brain plasticity by mini-spadin could play a key role in its brain protective effects against stroke and its deleterious consequences such as PSD.

Key words: post-stroke depression, mini-spadin, stroke, TREK-1 channel, antidepressant

Abbreviations

PSD, post-stroke depression, MCAO, middle cerebral artery occlusion, TREK-1, TWIK-related-potassium channel, type 1, SSRI, selective serotonin reuptake inhibitor, BDNF, brain-derived neurotrophic factor; PSD-95, post-synaptic density protein of 95 kDa TH, tyrosine hydroxylase, BrdU, bromodeoxyuridine.

1- Introduction

Stroke is associated with neuropsychiatric disorders such as depression, anxiety and cognitive disorders. Post-stroke depression (PSD) is particularly of high clinical importance with a prevalence varying between 20 to 65% (Carota and Bogousslavsky, 2003) . During the first year after stroke onset, PSD results in poorer cognitive activity and worse rehabilitation outcomes. Mortality may be up to 10 times higher than in stroke patients without PSD

(Pohjasvaara et al., 2001; Angelelli et al., 2004; Esparrago Llorca et al., 2015). Developing effective treatment for this specific population is critical. Few clinical studies have demonstrated that antidepressants (ADs), particularly the Selective Serotonin Reuptake Inhibitors (SSRIs) including escitalopram can alleviate depressive symptoms in patients with PSD (Cole et al., 2001; Hackett et al., 2005a; Chen et al., 2006; Hackett et al., 2008). The most convincing study conducted has been the "fluoxetine in motor recovery of patients with acute ischemic stroke" (FLAME) trial, which showed that fluoxetine enhances motor recovery and prevented PSD (Chollet et al., 2011). In a recent meta-analysis reporting 52 trials SSRIs appeared to improve dependence, disability, neurological impairment, anxiety and depression after stroke(Mead et al., 2013). Interestingly, protective effects of other AD serotoninergic drugs such as $5HT_{1A}$ agonists against neuronal damage induced by stroke have also been demonstrated in rats and humans (Zoli et al., 1993; Peruche et al., 1994; Ramos et al., 2004; Johansen et al., 2014).

Thus, implementing therapeutic strategies by using ADs to reduce the risk of PSD and improve rehabilitation outcomes appears of crucial interest. Nevertheless, regarding their limited tolerability provoking adverse events, they could seriously affect the extremely high-risk stroke population. In this context spadin, a novel peptidic AD can represent a molecule of choice to prevent and relieve psychiatric complications associated to stroke and improve the functional outcomes following stroke. Spadin has been identified as an endogenous and fast-acting AD using several depression tests in rodents (Mazella et al., 2010; Djillani et al., 2018). Spadin corresponds to a partial sequence (Ala^{12}-Arg^{28}, PE12-28) of the 44-aa propeptide (Gln^{1}-Arg^{44}, PE 1-44) issued from the post-translational maturation of sortilin (Munck Petersen et al., 1999). This peptide is a potent and selective antagonist of TREK-1 (Mazella et al., 2010), a crucial target in the treatment of depression (Heurteaux et al., 2006b; Borsotto et al., 2015). Spadin increases the firing activity of serotonergic neurons in the dorsal raphe nucleus (DRN) and activates in only 4 days two specific markers of AD action, the transcription factor cAMP response element-binding protein (CREB) and neurogenesis (Mazella et al., 2010). Interestingly, spadin concentrations are decreased in major depressive disorder (MDD) patients and recover to normal levels following AD treatments in correlation with clinical positive evolution of MDD (Devader et al., 2017). Related to cell survival, spadin enhances brain-derived neurotrophic factor (BDNF) as well as two markers of synaptogenesis, PSD-95 and synapsin (Devader et al., 2015). Spadin increases the proportion of mature spines in cortical neurons (Devader et al., 2015). Spadin depolarizes the cell membrane and activates the MAP

and PI3 kinase pathways, leading to a strong protective effect against staurosporine-induced apoptosis (Devader et al., 2015). The main advantage of spadin over conventional ADs is potentially the absence of adverse effects. Spadin does not induce cardiac dysfunctions and side effects related to TREK-1 inhibition (Moha Ou Maati et al., 2012b). Shortened spadin-analogs such as mini-spadin (PE 22-28) have been recently identified and reported to display a better efficacy and *in vivo* stability compared to spadin (Djillani et al., 2017). From these data, this work aimed to compare the effects of mini-spadin to those of both spadin and the SSRI, escitalopram, one of the most used SSRI in clinic and in experimental researches (Kronenberg et al., 2014), in the treatment of stroke with a particular focus on PSD.

2-Methods

Detailed Materials and methods are indicated in the Supplementary Material.

2-1 Electrophysiology

The electrophysiological recordings were performed on the human cell line hTREK-1/HEK (Moha ou Maati et al., 2011) using the whole-cell configuration of patch-clamp technique as previously described (Djillani et al., 2017). TREK-1 currents (I_{TREK-1}) were recorded using Axopatch 200B amplifier (Axon Instrument, USA). Currents were low-pass filtered at 3 kHz and digitized at 10 kHz. I_{TREK-1} amplitudes were expressed as current densities (current amplitude (*pA*)/membrane capacitance (*pF*)). Cells were continuously perfused using an external bath solution containing (in mM): 150 NaCl, 5 KCl, 3 $MgCl_2$, 1 $CaCl_2$ and 10 HEPES (pH 7.4). The pipette solution contained (in mM): 155 KCl, 3 $MgCl_2$, 5 EGTA and 10 HEPES (pH 7.2). A cocktail of potassium channel blockers (3 mM 4-AP (4-aminopyridine), 10 mM TEA (tetraethylammonium), 10 µM Glibenclamide, 100 nM Apamin and 50 nM Charybdotoxin) was added to the bath solution to specifically record I_{TREK-1}. The effect of mini-spadin on basal TREK-1 current amplitudes was tested with a wide range of concentrations (from 10^{-11} to 10^{-5}M). Data acquisition was carried out using a computer with pClamp software (Axon Instrument, USA). Whole-cell currents were generated by running a pulse or ramp protocol every 5 s from -100 to +60 mV with a holding potential maintained at -80 mV. Data were analyzed using Clampfit (Molecular Devices, USA) and the dose-response curves were drawn using Origin 8.6 (Northampton, MA, USA). Normalized I_{TREK-1} after application of peptides was analyzed using GraphPad Prism.

2-2 Animals

Animal studies were conducted in compliance with the ARRIVE guidelines (Kilkenny et al., 2011). Seven weeks old C57BL/6J male mice (Janvier laboratory, France) were housed under controlled laboratory conditions according to the FELASA guidelines and recommendations; 6 mice/cage with a 12 h dark-light cycle, a temperature of 21 ± 2°C, and 40 – 60% humidity. They have free access to standard rodent diet and tap water. The local Ethics Committee (CIEPAL) and the French ministry of higher education and scientific research approved experimental procedures (protocol number 1314.02). Animal care was in accordance with the policies on the care and use of laboratory animals of European Community legislation 2010/63/EU.

2-3 Drug treatment

2-3-1 Acute treatment

To assess the effect of mini-spadin on infarct volume induced by MCAO in the acute phase of stroke, we injected a single low dose of mini-spadin (0.03 μg/kg) 30 min after the end of MCAO and analyzed the infarct volume on cresyl violet stained brain sections 24 hours post-MCAO.

2-3-2 Chronic treatment

Considering the biphasic effect of mini-spadin on TREK-1 channel activity, we decided to use a two-step treatment for mini-spadin and spadin. A single dose in a bolus of 100 μl of mini-spadin (0.03 μg/kg corresponding to 10^{-8} M) or spadin (8 μg/kg corresponding to 10^{-6} M in electrophysiology studies) diluted in saline (as vehicle) was intraperitoneally injected 30 min after the onset of ischemia and once a day during 7-day reperfusion. Then, mini-spadin or spadin injected doses were increased to 3 μg/kg (corresponding to 10^{-6} M), or 800 μg/kg (corresponding to 10^{-4}M), respectively, once a day for 4 days/week until the sacrifice of animals (Fig.1A). The half-life of exogenously administered mini-spadin and spadin was 23 and 6 hours, as shown in previous works (Veyssière et al., 2014; Djillani et al., 2017). The doses injected and the period of 4 days of treatment opted have been chosen because they have been previously shown to induce neurogenesis and a potent antidepressant effect (Djillani et al., 2017). Escitalopram, a selective SSRI used as control was injected with the same schedule at the same time points at the dose of 1 mg/kg. The dose was opted according to previous positive results

obtained in mouse models of depression (Fish et al., 2004; Zomkowski et al., 2010). Animals were equally and randomly divided into 5 groups as follows: Control (Sham-operated), Saline-MCAO, Spadin-MCAO, Mini-spadin-MCAO and Escitalopram-MCAO. The researchers who carried out the ischemic surgery and all behavioral experiments were blinded to the treatment code. The flowchart illustrating the overall experimental design is shown in Supplementary Fig.1.

2-4 Ischemic stroke model (MCAO)

Focal ischemia was performed on mice by transient (30 min) left middle cerebral artery occlusion (MCAO) using a 6–0 coated filament (Doccol, Redlands, Calif., USA) as previously described (Heurteaux et al., 2010). The regional cerebral blood flow was monitored by laser Doppler flowmetry (Perimed, Craponne, France) to control MCAO severity and reperfusion. Animals presenting with sustained CBF reduction >70% during ischemia or a severe brain hemorrhage after MCAO were excluded from the study (<1%). Mice received mini-spadin, spadin or escitalopram in post-treatment until the sacrifice of animals. Sham-operation was performed by inserting the thread into the common carotid artery without advancing it to occlude MCA.

2-5 Survival rate and evaluation of brain ischemic lesions

The survival rate of mice was observed 24 and 96 hours after MCAO in the following groups: saline (n=26), mini-spadin 0.3 μg/kg (n=19), mini-spadin 0.03 μg/kg (n=20).

The infarct volume was determined 24 hours after MCAO on coronal (20 μm) frozen brain sections (n=12 section per brain) in mice treated by mini-spadin (n=18) or saline (n=13). Sections were stained using a solution of 1% cresyl violet in 0.25% acetic acid. The whole surface of infarction was measured on each section using a computer image analysis system and corrected for brain edema according (Golanov and Reis, 1995). Infarct volume (in mm^3) was calculated by a linear integration of the corrected lesion areas (Bourourou et al., 2016).

2-6 Body weight

The weight gain was calculated according to the following formula: weight gain (%) = [(body weight at measurement point (g) – body weight before MCAO (g)) / body weight before MCAO (g)] x 100. Data are reported as Mean ± SEM in the different experimental groups: saline (n=17), spadin (n=14), mini-spadin (n=15) and escitalopram (n=15).

2-7 Behavioral experiments

In order to avoid acute effect of drugs, all behavioral tests were performed 24 h after the last injection. Data are reported as Mean ± SEM. in the different groups.

2-7-1 Accelerated rotarod test

To assess motor coordination (Bourourou et al., 2016), mice were conditioned to the accelerating rotarod (Ugo Basile, France) for three days before ischemia. Mice were first placed on the apparatus during 30 sec with no rotation and thereafter for 120 sec with a constant low speed (4 rpm). After 10 min rest, each mouse then received a single baseline trial on the accelerating rotarod in which the spindle increased in speed from 4 to 40 rpm during 600 sec. The maximum duration animals were able to walk on the rotarod before falling (latency to fall) was measured (maximum value: 600 sec) during the test trial. Mice were tested over three daily trials in the accelerated condition (4-40 rpm). Data are reported as Mean ± SEM in the different groups: saline (n=16), spadin (n=14), mini-spadin (n=15) and escitalopram (n=14).

2-7-2 Pole test

To analyze sensory motor function (Matsuura et al., 1997), mice were placed head upward at the top of a vertical rough-surfaced pole and then allowed to descend five times during one session. The total time needed to turn completely head downward ("time-to-turn") and the time it took the mouse to reach the floor with all four paws ("time-to-come-down") were recorded. Data are reported as Mean ± SEM in the different groups: saline (n=13), spadin (n=11), mini-spadin (n=14) and escitalopram (n=15).

2-7-3 Morris water maze test

To investigate the spatial learning and memory (Winter et al., 2004; Quintard et al., 2014), mice had to locate a platform hidden under the surface of a circular swimming pool (90 cm in diameter, water at 24 ± 1°C) by referring to visual cues arranged all around the experimental room. The experiment included 2 phases:

Acquisition. Acquisition training consisted of 4 consecutive days of conditioning with 4 trials per day. Animals were placed within one of 4 quadrants and the latency and swimming path until they found the platform were recorded.

Probe test. One day after the last learning trial, the platform was removed and mice were allowed to swim for 60 sec as during acquisition training. The latency for the first entry and the

time spent within the platform quadrant were measured. The strategies used by mice to carry out the task were taken into account (Garthe and Kempermann, 2013). The strategy categories (see Supplementary Figure 1) reached from thigmotaxis and random search, which are inadequate strategies to perseverance, chaining and scanning that correspond to efficient spatial strategies. Recorded trials were analyzed with the tracking software Anymaze (Stoelting,USA). The speed of swimming and the total swum run distance were also measured. Data are reported as Mean ± SEM in the different groups: saline (n=16), spadin (n=13), mini-spadin (n=15) and escitalopram (n=14).

2-7-4 Porsolt forced swim test (FST)

Mice were individually placed for 6 min in a non-escapable cylinder (30 cm height and 15 cm diameter) half-filled with water at 22 ± 1°C. The immobility time was manually measured only during the last 4 min (Porsolt, 2000).

2-7-5 Novelty suppressed feeding test (NSF)

Mice were 24h deprived from food before the test. A food pellet was placed on a white platform in the center of the illuminated arena (50 x 50 x 40 cm). The latency to start eating the pellet was measured during 10 min (Santarelli et al., 2003).

2-8 Immunostaining on perfused brain sections

For neurogenesis studies, mice were treated with 3 injections of BrdU (75 mg/kg, i.p. each, 2 hour interval). Brains were removed 24 hours after the last injection. Serial sections of paraformaldehyde-perfused-brains were cut (40 µm) throughout the entire hippocampus on a vibratome (Leica). Slices were then processed as described in (Heurteaux et al., 2006b). The antibody used was a monoclonal mouse anti-BrdU (1/7000; BD Biosciences, Le Pont de Claix) The same protocol was used to specifically identify TH-positive cells colocalized with neuronal cells (rabbit polyclonal anti-TH; 1/100, Abcam ab51191). For double immunofluorescence labeling of TH, a specific mouse monoclonal NeuN antibody was used (Millipore, #MAB377, 1/300).

2-9 Western Blots

Brain tissues (n=3 per group) were collected after MCAO, and the fresh brains were carefully separated into ipsilateral and contralateral hemispheres, and into cortical and subcortical regions, with respect to the infarct location. Western blots were performed on 10% SDS PAGE.

Membranes were incubated with the rabbit polyclonal antibody directed against PSD-95 or synapsin (dilution 1/1000) overnight at 4°C. Tubulin and actin contents were determined after stripping using an anti-tubulin (1/1000, Clinisciences, Nanterre, France) or anti-actin (1/3000) antibody (Cell Signalling, Leiden, Netherland). Secondary antibodies, were the anti-mouse or anti-rabbit HRP-conjugated antibodies (Amersham Biosciences, Orsay, France; 1/10000).

2-10 Statistical analysis

Data show the mean ± SEM. Analysis was performed using Graphpad Prism software version 6.0. Significant differences between two groups of data were determined using a Mann & Whitney U test for non-parametric data or when necessary by one-way ANOVA with a Dunnett's multiple comparison test for comparing the treatment effect. Level of significance was set at $P < 0.05$. Data and statistical analysis comply with the recommendations on experimental design and analysis in pharmacology (Curtis et al., 2015).

3-Results

3-1 Dose-response of mini-spadin as compared to spadin on TREK-1 basal currents

100 nM of mini-spadin and spadin strongly inhibited TREK-1 channels pre-activated by arachidonic acid (AA, 10 μM) (Djillani et al., 2017). TREK-1 inhibition occurred with IC_{50} of 0.12 nM and 40 nM for mini-spadin and spadin, respectively (Djillani et al., 2017). Mini-spadin and spadin slightly blocked TREK-1 activity without prior AA activation. The effect of mini-spadin on basal TREK-1 current amplitudes was tested with a wide range of concentrations (from 10^{-11} to 10^{-5}M) (Fig.1A). Surprisingly, when tested at low concentrations (from 10^{-11} to 10^{-8} M), mini-spadin activated TREK-1 channels in a dose-dependent manner (Fig.1A). The maximum effect of activation was observed at 10^{-8} M (85.3 ± 27.3 %, n=18, *P*=0.017) (Fig. 1A). In comparison, spadin significantly activated TREK-1 basal current only at 10^{-6} M (49.4 ±20.0 %, n=9, **P*=0.039) (Fig.1B). The current densities at 0 mV compared to unstimulated currents were 149 ± 20.0 % for spadin at 10^{-6} M (n=9, **P*=0.038) and 194.3 ± 27.5 % for mini-spadin at 10^{-8} M (n=15, ***P*=0.004) (Fig.1B).

TREK-1 activation was shown to be neuroprotective in models of focal and global ischemia (Quast, 1992; Lauritzen et al., 2000; Blondeau et al., 2002a; Blondeau et al., 2002b; Heurteaux et al., 2006a). Mini-spadin activates TREK-1 at low concentration (Fig.1A) suggesting a

protective effect. Neuroprotection induced by low concentration of mini-spadin (0.03 μg/kg) was confirmed *in vivo*. The percentage of mice which died 24 or 96 hours after MCAO clearly showed that 0.3 μg/kg of mini-spadin was less protective than 0.03 μg/kg (Supplementary Fig. 2A and Supplementary Table 1). These data confirmed the electrophysiological data. Mini-spadin injected at the dose of 0.03 μg/kg 30 min after MCAO significantly decreased the infarct volume when compared to saline-treated mice (Supplementary Fig. 2B), suggesting a protective effect of low dose of mini-spadin in the acute phase of stroke. Because the dose of 0.03 μg/kg (corresponding to 10^{-8} M) induced the best TREK-1 activation (Fig.1B) and a strong protective effect *in vivo* (Supplementary Fig.2), we decided to administrate mini-spadin at this dose throughout the study. The antidepressant and neurogenic effects of this peptide have been reported at higher concentrations (3 μg/kg for mini-spadin) (Djillani et al., 2017). Because the acute and delayed phases of stroke have to be managed differently (early reperfusion and neuroprotection for the acute phase and neuronal recovery through neuroplasticity for the delayed phase (Chollet et al., 2014), we decided to 1/ treat mice with low concentration of mini-spadin (0.03 μg/kg) during 7 days following MCAO to activate TREK-1 and then 2/ increase the peptide concentration to 3 μg/kg, once a day during 4 days/week to induce AD effect and stimulate neurogenesis and synaptogenesis. Additionally to the saline-treated mice (vehicle), two control molecules were also used, spadin and escitalopram. Spadin was also injected following a two-step protocol (8 μg/kg for 7 days and 800 μg/kg for 4 days); escitalopram was injected during the two steps at the dose of 1 mg/kg (Supplementary Fig.1A).

3-2 Mini-spadin prevented the loss of body weight induced by ischemia

After stroke, animal body weight changes were used as an indicator of their overall well-being. As compared to the pre-MCAO values, saline-treated mice submitted to MCAO showed a significant loss of weight in the first three days following MCAO (***P<0.001) (Fig.2A) and returned to the pre-surgery values after two weeks. In contrast, weight loss in mini-spadin-treated mice was weak. Whereas spadin and escitalopram had no significant effect, the measure of areas under curve showed that mini-spadin significantly prevented weight loss observed in saline-treated mice ($F_{3, 51}$=2.78, $^{\#}P$=0.029) 3 days after MCAO (Fig.2A, Inset). There was no significant difference in body weight gain between the two sham groups treated with saline or mini-spadin (Supplementary Fig. 3), excluding a potential metabolic effect of the peptide. Mini-spadin-treated mice returned to 95.5% of their pre-surgery weight only 5 days after MCAO (Fig.2A). Spadin-treated mice displayed the same recovery rate than mini-spadin but

escitalopram-treated mice needed two more days to reach the same level of body weight (Fig.2A). There were no significant changes in endogenous spadin (measured by PE levels) after stroke (P>0.05, Supplementary Fig. 4).

3-3 Mini-spadin improved the motor and cognitive deficits induced by ischemia

Motor and cognitive deficits are common neurological sequels in stroke patients (Langhorne et al., 2009; Cumming et al., 2013). The beneficial motor effects of mini-spadin were first observed in the accelerated rotarod test, which assessed the motor coordination (Fig. 2B). All mice were identified and their performances were measured in a pre-ischemia test (data not shown). For each mouse the pre-ischemic value was considered as 100%. At Day 3 after MCAO, all groups showed a strong decrease in their performances when compared to the corresponding pre-ischemia group (Fig. 2B). Only the mini-spadin group showed a significant improvement of their performances when compared with the saline-treated ischemic group ($^{\#}P$=0.032, Fig. 2B). Two weeks post-MCAO, animals from all groups have recovered and spent the same time on the rotarod (data not shown).

In the pole test, there were no significant differences in performance between pre-MCAO groups (Fig. 2C-D). Three days post-MCAO, ischemia induced a significant increase in time to rotate and to come down along the pole ($^{***}P$<0.001 for rotation and $^{*}P$<0.05 for descent, Fig. 2C-D), suggesting motor deficits induced by stroke. Interestingly, mini-spadin significantly reduced the times in both tasks when compared to saline-treated group ($F_{3, 42}$=5.004, $^{\#\#}P$=0.0044 for rotation and $^{\#}P$=0.049 for descent, Fig. 2C-D). Contrary to the descent task, mice treated with spadin and escitalopram decreased significantly their time to rotate when compared to saline-treated mice ($F_{3, 42}$ = 5.004, $^{\#}P$=0.0152 for spadin and $^{\#}P$=0.0159 for escitalopram, Fig. 2C). Two weeks post-MCAO, we observed in the descent task but not in the rotation task an improvement of performances when mice were treated with mini-spadin or escitalopram , ($F_{3, 33}$ = 5.169, $^{\#}P$=0.045 for mini-spadin and $^{\#}P$=0.025 for escitalopram, Fig.2D). Three days post-MCAO we observed in the rotation task a significant decrease in time by 82.4, 72.9 and 74.4 % induced by mini-spadin, spadin, and escitalopram, respectively (Fig. 2C, 3 Days post-MCAO panel).

Then, mini-spadin effects on spatial learning and memory were tested in the Morris Water Maze paradigm three weeks after MCAO. During the training, all groups of animals poorly performed in this task. MCAO has a deleterious effect on learning trials (Fig. 3A-B). The latency to find

the platform was significantly increased in MCAO saline-treated mice when compared to saline-sham operated animals (data not shown). Whereas saline- and escitalopram-treated mice did not ameliorate their performance during the learning trials, mice treated with mini-spadin significantly improved the latency to find the platform (Fig.3A-B). Indeed, a significant difference in latency was observed from the third training day in mini-spadin-treated mice (-27.8%, $F_{3, 56}$=7.538, $^{\#}P$=0.021 *vs* corresponding Day 1), which was even increased at the fourth day (-44.4%, $^{\#\#\#}P$=0.001 *vs* corresponding Day 1). Mini-spadin induced a significant increase in performance of ischemic mice when compared to MCAO-saline-treated group ($F_{3, 56}$ = 4.01, $^{\$\$}P$=0.0073, Fig.3a-b). Escitalopram had no significant effect (P=0.58). During the probe testing, only mice treated with mini-spadin penetrated significantly quicker in the platform quadrant (NW) when compared to the MCAO-saline group (Fig. 3C, right panel, $^{\#}P$<0.05). In addition, we observed a tendency to exhibit a preference for the NW quadrant with an increase in time spent in MCAO-spadin- and mini-spadin-treated mice as compared to the MCAO-saline group. These observations suggested that they collectively remembered the area where the platform was initially, but the result did not reach the significativity (Fig. 3C, left panel, $F_{3, 54}$ = 1.92, P=0.066 *vs* MCA0-saline group). The analysis of strategies (Lorivel et al., 2015, Supplementary Fig. 1) showed that mice treated with mini-spadin used a more efficient strategy by the emergence of the perseverance, not observable in the MCAO-saline-treated mice (Fig. 3D and Supplementary Fig. 5). The difference observed between mini-spadin treated mice and other groups were not due to motor deficits because the swim distance and speed average were very similar for each group (Supplementary Fig. 5). Taken together the results obtained in the 3 tests indicated that mini-spadin is more efficacious than spadin and escitalopram by strongly decreasing the motor and cognitive deficits induced by stroke.

3-4 Mini-spadin prevented the depressant-like behaviour induced by ischemia

In FST performed at 3, 5, 7 and 10 weeks post-MCAO, sham-operated mice treated with mini-spadin or spadin displayed a significant decrease in the immobility time, when compared to saline-treated mice (data not shown). The increase in the immobility time observed in MCAO-vehicle group compared to sham-operated-vehicle group became significant 10 weeks after MCAO ($F_{4, 113}$ = 10.44, $^{*}P$=0.035, Fig. 4A) and characterized the despair-related phenotype associated with MCAO. Interestingly, as compared to MCAO-vehicle- group, mini-spadin and spadin significantly decreased the immobility time as early as 5 weeks of treatment ($F_{4, 112}$ =

6.097, $^{\#\#}P$=0.0013, Fig. 4A), Escitalopram only had a significant AD effect after 10 weeks ($F_{3, 113}$ = 10.44, $^{\#\#}P$=0.0059, Fig. 4A). Differences observed are not due to difference in locomotor performance as demonstrated in the Morris water maze experiment (Supplementary Fig. 5B-C).

In NSF, MCAO induced a depressive-like behavior which started to appear 3 weeks following ischemia but was definitively established after 10 weeks (Fig. 4B). MCAO resulted in an increased latency in saline-treated animals when compared to sham-operated-saline group ($F_{4, 63}$ = 5.93, $^{**}P$=0.0039, Fig. 4C). The latency to eat the pellet, which was 1.9-fold higher 3 weeks post-ischemia was increased to 3.8-fold after 10 weeks when compared to sham-operated saline-treated mice (Fig. 4B). The treatment with the three AD drugs significantly prevented the behavioral changes induced by MCAO ($F_{4, 63}$ = 5.93, $^{\#}P$=0.0296 for mini-spadin, $^{\#}P$=0.0231 for spadin and $^{\#\#\#}P$=0.0007 for escitalopram *vs* saline group, Fig. 4C-D). A 40% decrease in latency to eat was observed in mini-spadin- and spadin-treated mice as soon as 3 weeks, when escitalopram only became efficient after 10 weeks post-MCAO. Taken together, these findings demonstrated that a treatment with an AD and, particularly with mini-spadin reverses the depressive-like behavioral alterations induced by stroke.

3-5 Mini-spadin stimulated the hippocampal cell proliferation and synaptogenesis

Three weeks post-MCAO, we observed no difference in the number of BrdU positive cells between saline and mini-spadin-treated mice (data not shown). Ten weeks after MCAO, the number of BrdU positive cells in the subgranular zone (SGZ) of both ischemic and sham-saline mice was comparable ($F_{3, 36}$=3.77, P=0.21) (Fig. 5A, right panel). As already published, mice treated with mini-spadin and not submitted to MCAO (sham group) showed an increase in neural stem cell proliferation in the SGZ ($F_{3,36}$ =3.77, $^{**}P$=0.0042 *vs* sham-operated saline) (Fig. 5A, right panel) (Djillani et al., 2017). The number of newborn cells was increased by 52.5% when ischemic mice were treated with mini-spadin ($F_{3,36}$ = 3.77, $^{\#\#}P$=0.0054 *vs* MCAO saline-treated group). Interestingly, the neurogenic effect of mini-spadin was still observable even at 10 weeks post-MCAO (Fig. 5A, left panel). Twenty-one days after the tenth week post-MCAO, the number of BrdU/NeuN co-labeled cells in the SGZ was still increased in the mini-spadin-treated mice when compared to saline group (Fig. 5A, left panel). However, in the SGZ no GFAP/BrdU colocalization was observed. This result showed that mini-spadin stimulates neurogenesis induced by ischemia and that the majority of newborn cells (80%) in the SGZ differentiate into mature neurons.

Depression is also associated with loss of synaptic connections in mood circuitry. AD therapy facilitates remission by fast induction of synaptogenesis (Bambico and Belzung, 2013). Three weeks after ischemia mini-spadin significantly enhanced the expression of PSD-95 and synapsin, two key markers of synaptogenesis (de Bartolomeis and Fiore, 2004; Mirza and Zahid, 2018) in the ipsi lateral cortice of treated mice when compared to saline group (Fig. 5B).

3-6 Mini-spadin attenuated the loss of dopaminergic neurons induced by ischemia and PSD in midbrain

The depression-like syndrome after stroke is associated with secondary functional and structural alterations of the mesolimbic dopamine system (Kronenberg et al., 2012). Ten weeks post-MCAO, immunolabeling of dopaminergic neurons with tyrosine hydroxylase (TH) in the midbrain showed that MCAO induced a strong loss of TH-positive cells neurons in ipsilateral *substantia nigra* in saline-treated mice (Fig. 6A-B) when compared to the contralateral hemisphere. This MCAO effect was significantly attenuated by mini-spadin ($F_{3,\ 35}$ = 4.53,$^{\#\#}P$=0.0093 *versus* MCAO saline-treated group), but not by spadin or escitalopram. (P=0.999 for spadin and P=0.957 for escitalopram). Relative to saline treatment, mini-spadin induced a 46% increase in the number of TH-positive neurons (Fig. 6B).

4- Discussion

At least one-third of stroke survivors suffer from depression. The development of comorbid depression after stroke is clinically highly significant. Physical disability, stroke severity and cognitive impairment figure especially prominently in the clinical literature (Hackett et al., 2005a). The underlying mechanisms of PSD associated to ischemic damage are complex and difficult to model in rodents. Nevertheless, several reliable PSD models are now available and well-recognized (Kronenberg et al., 2014) to mimick the main stroke and PSD features observed in real-word clinical situations. In this study, we have chosen to use a recognized PSD-like animal model, which has the advantage to only carry out MCAO without inducing PSD by any additional stress like chronic mild stress or isolation rearing, which can induce a bias. Indeed, the combined application of MCAO and unpredictable chronic mild stress (CMS) is often used in preclinical PSD studies(Kronenberg et al., 2014). While CMS induces depressive behaviors, the applied stressors such as cold water and electric shock could also lead to neuronal damage. Social isolation for several weeks before MCAO is also used to induce PSD (Kronenberg et al., 2014). In our model on C57/Bl6J, MCAO induces a depressive-like behavior 10 weeks after reperfusion, a long delay for a mouse but corresponding to real-world

situations where PSD occurs up to one year after the onset of stroke (Francisco, 1993). This model also displays consistent and reliable clinical core features of stroke and associated PSD such as motor and cognitive deficits, neuronal loss and impaired neurogenesis(Kronenberg et al., 2014).

In this study we took advantage that mini-spadin has a rapid effect as AD, only four days when other classical AD drugs need at least 3 weeks. Additionally, mini-spadin is devoid of deleterious side effects. For the first time, this study provides evidence that mini-spadin induced neuroprotection against stroke and subsequent PSD as compared to spadin and escitalopram. In this work, for the first time, we have demonstrated that in the acute phase of stroke recovery mini-spadin increased the survival rate of mice submitted to MCAO, prevented the loss of body weight and decreased the infarct volume. In the chronic phase of stroke, mini-spadin prevented the delayed dopaminergic degeneration in *substantia nigra* and improved the motor and cognitive ischemia-induced deficits. The beneficial effects provided by this peptide could be the result of its biphasic effect on the TREK-1 channel. Interestingly, the electrophysiological approach showed that low doses of mini-spadin induced TREK-1 activation which probably induced a brain protection in the acute phase of stroke. This acute protection was confirmed by the reduction number of deaths in mice and the decrease of the infarct volume at 24 hours post-MCAO. These results are in accordance with previous works demonstrating that activation of TREK-1 plays a key role in the mechanisms of protection after stroke (Quast, 1992; Lauritzen et al., 2000; Blondeau et al., 2002a; Blondeau et al., 2002b; Heurteaux et al., 2006a). The protection induced by polyunsaturated fatty acids, which are known to activateTREK-1 disappears in TREK-1 null mice (Heurteaux et al., 2004). TREK-1 is up-regulated after focal ischemia (Wang et al., 2012). Increased TREK-1 expression in ischemic rat brain is expected to prevent homeostatic dysfunctions induced by stroke. TREK-1 is opened by membrane stretch, cell swelling, AA release and intracellular acidosis (Honore, 2007), phenomena that occur during stroke. A decrease of intracellular pH is associated to ischemia (Dirnagl et al., 1999). These toxic stimuli might contribute to the opening of neuronal TREK-1 and provide brain protection. As described for other TREK-1 openers (Quast, 1992; Lauritzen et al., 2000; Blondeau et al., 2002a; Blondeau et al., 2002b; Heurteaux et al., 2006a), TREK-1 activation in the neurons by low doses of mini-spadin would hyperpolarize synaptic terminals, decreasing Ca^{2+} influx and glutamate release and producing a post-synaptic hyperpolarization. These processes would favor the blockade of NMDA receptor associated-channel by Mg^{2+} and counterbalance glutamate-induced depolarization. Astrocytes also play a crucial role in the

pathophysiology of stroke (Nedergaard and Dirnagl, 2005). Astrocytes participate to the regulation of acid-base homeostasis through a variety of exchangers and co-transporters. TREK-1 channels contribute to astrocyte passive conductance (Zhou et al., 2009). TREK-1 is broadly expressed in neurons and astrocytes under physiological conditions, and is up-regulated in these cells after MCAO, which correlates with reactive astrogliosis in the injured region (Wang et al., 2012). In these conditions, TREK-1 may set the negative resting membrane potential of astrocytes to rescue their homeostasis functions (Zhou et al., 2009) leading to brain protection against stroke.

This work also demonstrates for the first time that mini-spadin strongly decreased the depressive-like behavioral alterations induced by MCAO in the chronic phase of stroke. One core features of the chronic depression-like syndrome after stroke is the long-term alterations of the mesolimbic dopaminergic system (Kronenberg et al., 2012). This is in line with the left frontal and basal ganglia lesions observed in stroke patients and linked to the occurrence of major PSD (Morris et al., 1996; Vataja et al., 2004). In the present work, we demonstrated that mini-spadin attenuated the delayed dopaminergic degeneration in *substantia nigra* and prevented the emergence of depressive-like behavior, which occurs during the chronic phase of stroke. In our protocol, we started to administrate higher doses of mini-spadin one week after MCAO to induce an AD effect and to prevent PSD. The higher dose of this peptide (used in this work) has been previously shown to prevent the depressive-like symptoms modeled in AD screening tests like FST or NSF (Heurteaux et al., 2006b; Mazella et al., 2010; Djillani et al., 2017). Consequently, we can expect that the beneficial effects of mini-spadin on PSD are probably due to TREK-1 inhibition during the chronic phase of stroke. In accordance with previous results (Heurteaux et al., 2006b; Mazella et al., 2010; Djillani et al., 2017), the long-term inhibition of TREK-1 by mini-spadin probably increases the firing rate of dorsal raphe nucleus neurons and increase the 5-HT release, which could further contribute to prevent PSD. In further studies, it will be interesting to initiate the peptide treatment after a few weeks of the ischemic event in the aim to see whether mini-spadin given at high dose will reduce PSD. Nevertheless an early AD pharmacotherapy may prevent PSD as reported in a meta-analysis of randomized placebo-controlled trials evaluating the prophylactic effects of ADs in non-depressed stroke patients (Chen et al., 2007). This is in favor to treat patients as early as possible after stroke and to consider ADs along with other vascular preventive strategies in the management of stroke patients.

In human and rodent brains, functional improvement after stroke may be induced through proliferation of neural stem cells induced by stroke, which migrate into the damaged structures (Jin et al., 2001; Jin et al., 2006; Murphy and Corbett, 2009). However, this potential self-repair mechanism only operates acutely after stroke, with the number of generated neurons being small and their existence transitory. Recovery from stroke-induced cognitive deficits is significantly impaired by genetic disruption of neurogenesis, highlighting the importance of neuroprogenitor cells for post-stroke cognitive recovery (Sun et al., 2013). Maximum cell proliferation in the adult brain occurs 1 to 2 weeks after stroke (Jin et al., 2001; Arvidsson et al., 2002), and in neurosphere cultures the recruitment of neuronal stem cells is stimulated during the first week after stroke (Zhang et al., 2004). In our study, we have analyzed neurogenesis at 3 and 10 weeks, but not shortly after MCAO. It is probably the reason why, compared to sham groups, neurogenesis increase after MCAO was not observed. However, interestingly, neurogenesis analyzed in the chronic phase of stroke (10 weeks) showed that mini-spadin as compared to vehicle induced an extensive and long-lasting production of new neurons 10 weeks after MCAO, probably stimulating the self-repair and the neurological recovery of mice after stroke.

In the search of potential mechanisms involved in the beneficial effects of mini-spadin on PSD and neurological recovery after stroke, the stimulation of synaptogenesis, analyzed hence by the expression of PSD-95 and synapsin, two key proteins involved in synaptic network is probably crucial. At 3 weeks post-MCAO, mini-spadin strongly increased PSD-95 and synapsin expression in the ipsilateral cortice (a major site of the remodeling of neural circuits (Carmichael, 2003)). The presence of PSD-95 and synapsin in the non-lesioned (contralateral) cortical region, corresponding to a post-stroke increase in brain activity (Takatsuru et al., 2009), could facilitate the induction of long-lasting changes in the neuronal network of adjacent cortical areas (Carmichael, 2003). These data are in favor of a significant improvement in functional recovery after stroke and a prevention of PSD.

Preliminary results have shown that spadin interacts with the neurotensin receptor 1 (NTR1), well-known to be involved in neuroprotection. Indeed, similarly to neurotensin (NT), spadin at 10^{-6} M binds to NTR1 by displacing 50% of ^{125}I-Spadin in brain homogenates (Mazella, unpublished data). NT and its analogs are potent NTR1 agonists, that induce hypothermia and show marked protective effects against brain injury (Fantegrossi et al., 2005; Orwig et al., 2009; Choi et al., 2012; Wei et al., 2013; Lee et al., 2014; Lee et al., 2016). Thus, mini-spadin like spadin could interact with NTR1 and contribute to induce brain protection.

In the present work, escitalopram was opted as positive AD control because of its clinical use (Montgomery et al., 2001; Burke, 2002). Escitalopram is an efficient AD but displays adverse effects (such as sleepiness, constipation, diarrhea, sexual dysfunction, change in heart rate, sleep disorders) and its efficacy period takes several weeks (2 to 4 weeks). Unlike escitalopram mini-spadin has the advantage to have a rapid onset of action (4 days) and it is devoid of side effects (Djillani et al., 2017). Results obtained in this work clearly show that mini-spadin effects on the stroke outcomes and on PSD were faster (5 weeks instead of 10 weeks in FST) and largely enhanced as compared to those observed with escitalopram.

In conclusion, this is the first study that provides evidence for the potential therapeutic value of mini-spadin as a better alternative to currently used ADs to alleviate neurological and neuropsychiatric disorders following stroke.

5- **Acknowledgments**

The authors are very grateful to Dr Serge Richard for his friendly support, confidence in the spadin's project and fruitful discussions. We thank C. Gandin and C. Widmann for their helpful technical contribution. M.P. was supported by a CIFRE fellowship.

6- **Sources of Funding**

We thank the French Government for the "Investments for the Future" LABEX ICST # ANR-11 LABX 0015. This work was supported by the Centre National de la Recherche Scientifique and the Agence Nationale de la Recherche (ANR-13-SAMA-0001 and -0002 and ANR-13-RPIB-0001 and -0002).

7- Disclosures

The authors are inventors on a filled patent application on " The use of partial sequences of NTSR3 propeptide for the treatment of depression" by CNRS and University of Côte d'Azur. MP was supported by a CIFRE fellowship. The authors declare to have nothing to disclose.

8- References

Angelelli, P., Paolucci, S., Bivona, U., Piccardi, L., Ciurli, P., Cantagallo, A., Antonucci, G., Fasotti, L., Di Santantonio, A., Grasso, M. G., Pizzamiglio, L., 2004. Development of neuropsychiatric symptoms in poststroke patients: a cross-sectional study. Acta Psychiatr Scand 110, 55-63.

Arvidsson, A., Collin, T., Kirik, D., Kokaia, Z., Lindvall, O., 2002. Neuronal replacement from endogenous precursors in the adult brain after stroke. Nat Med 8, 963-970.

Bambico, F. R., Belzung, C., 2013. Novel insights into depression and antidepressants: a synergy between synaptogenesis and neurogenesis? Curr Top Behav Neurosci 15, 243-291.

Blondeau, N., Lauritzen, I., Widmann, C., Lazdunski, M., Heurteaux, C., 2002a. A potent protective role of lysophospholipids against global cerebral ischemia and glutamate excitotoxicity in neuronal cultures. J Cereb Blood Flow Metab 22, 821-834.

Blondeau, N., Widmann, C., Lazdunski, M., Heurteaux, C., 2002b. Polyunsaturated fatty acids induce ischemic and epileptic tolerance. Neuroscience 109, 231-241.

Borsotto, M., Veyssiere, J., Moha Ou Maati, H., Devader, C., Mazella, J., Heurteaux, C., 2015. Targeting two-pore domain K(+) channels TREK-1 and TASK-3 for the treatment of depression: a new therapeutic concept. Br J Pharmacol 172, 771-784.

Bourourou, M., Heurteaux, C., Blondeau, N., 2016. Alpha-linolenic acid given as enteral or parenteral nutritional intervention against sensorimotor and cognitive deficits in a mouse model of ischemic stroke. Neuropharmacology 108, 60-72.

Burke, W. J., 2002. Escitalopram. Expert Opin Investig Drugs 11, 1477-1486.

Carmichael, S. T., 2003. Plasticity of cortical projections after stroke. Neuroscientist 9, 64-75.

Carota, A., Bogousslavsky, J., 2003. Poststroke depression. Adv Neurol 92, 435-445.

Chen, Y., Guo, J. J., Zhan, S., Patel, N. C., 2006. Treatment effects of antidepressants in patients with post-stroke depression: a meta-analysis. Ann Pharmacother 40, 2115-2122.

Chen, Y., Patel, N. C., Guo, J. J., Zhan, S., 2007. Antidepressant prophylaxis for poststroke depression: a meta-analysis. Int Clin Psychopharmacol 22, 159-166.

Choi, K. E., Hall, C. L., Sun, J. M., Wei, L., Mohamad, O., Dix, T. A., Yu, S. P., 2012. A novel stroke therapy of pharmacologically induced hypothermia after focal cerebral ischemia in mice. FASEB J 26, 2799-2810.

Chollet, F., Cramer, S. C., Stinear, C., Kappelle, L. J., Baron, J. C., Weiller, C., Azouvi, P., Hommel, M., Sabatini, U., Moulin, T., Tardy, J., Valenti, M., Montgomery, S., Adams, H., Jr., 2014. Pharmacological therapies in post stroke recovery: recommendations for future clinical trials. J Neurol 261, 1461-1468.

Chollet, F., Tardy, J., Albucher, J. F., Thalamas, C., Berard, E., Lamy, C., Bejot, Y., Deltour, S., Jaillard, A., Niclot, P., Guillon, B., Moulin, T., Marque, P., Pariente, J., Arnaud, C., Loubinoux, I., 2011. Fluoxetine for motor recovery after acute ischaemic stroke (FLAME): a randomised placebo-controlled trial. Lancet Neurol 10, 123-130.

Cole, M. G., Elie, L. M., McCusker, J., Bellavance, F., Mansour, A., 2001. Feasibility and effectiveness of treatments for post-stroke depression in elderly inpatients: systematic review. J Geriatr Psychiatry Neurol 14, 37-41.

Cumming, T. B., Marshall, R. S., Lazar, R. M., 2013. Stroke, cognitive deficits, and rehabilitation: still an incomplete picture. Int J Stroke 8, 38-45.

Curtis, M. J., Bond, R. A., Spina, D., Ahluwalia, A., Alexander, S. P., Giembycz, M. A., Gilchrist, A., Hoyer, D., Insel, P. A., Izzo, A. A., Lawrence, A. J., MacEwan, D. J., Moon, L. D., Wonnacott, S., Weston, A. H., McGrath, J. C., 2015. Experimental design and analysis and their reporting: new guidance for publication in BJP. Br J Pharmacol 172, 3461-3471.

de Bartolomeis, A., Fiore, G., 2004. Postsynaptic density scaffolding proteins at excitatory synapse and disorders of synaptic plasticity: implications for human behavior pathologies. Int Rev Neurobiol 59, 221-254.
Devader, C., Khayachi, A., Veyssiere, J., Moha Ou Maati, H., Roulot, M., Moreno, S., Borsotto, M., Martin, S., Heurteaux, C., Mazella, J., 2015. In vitro and in vivo regulation of synaptogenesis by the novel antidepressant spadin. Br J Pharmacol 172, 2604-2617.
Devader, C., Roulot, M., Moreno, S., Minelli, A., Bortolomasi, M., Congiu, C., Gennarelli, M., Borsotto, M., Heurteaux, C., Mazella, J., 2017. Serum sortilin-derived propeptides concentrations are decreased in major depressive disorder patients. J Affect Disord 208, 443-447.
Dirnagl, U., Iadecola, C., Moskowitz, M. A., 1999. Pathobiology of ischaemic stroke: an integrated view. Trends Neurosci 22, 391-397.
Djillani, A., Pietri, M., Mazella, J., Heurteaux, C., Borsotto, M., 2018. Fighting against depression with TREK-1 blockers: Past and future. A focus on spadin. Pharmacol Ther.
Djillani, A., Pietri, M., Moreno, S., Heurteaux, C., Mazella, J., Borsotto, M., 2017. Shortened Spadin Analogs Display Better TREK-1 Inhibition, In Vivo Stability and Antidepressant Activity. Front Pharmacol 8, 643.
Esparrago Llorca, G., Castilla-Guerra, L., Fernandez Moreno, M. C., Ruiz Doblado, S., Jimenez Hernandez, M. D., 2015. Post-stroke depression: an update. Neurologia 30, 23-31.
Fantegrossi, W. E., Ko, M. C., Woods, J. H., Richelson, E., 2005. Antinociceptive, hypothermic, hypotensive, and reinforcing effects of a novel neurotensin receptor agonist, NT69L, in rhesus monkeys. Pharmacol Biochem Behav 80, 341-349.
Fish, E. W., Faccidomo, S., Gupta, S., Miczek, K. A., 2004. Anxiolytic-like effects of escitalopram, citalopram, and R-citalopram in maternally separated mouse pups. J Pharmacol Exp Ther 308, 474-480.
Francisco, G. S., 1993. An overview of post-stroke depression. N J Med 90, 686-689.
Garthe, A., Kempermann, G., 2013. An old test for new neurons: refining the Morris water maze to study the functional relevance of adult hippocampal neurogenesis. Front Neurosci 7, 63.
Hackett, M. L., Anderson, C. S., House, A., Xia, J., 2008. Interventions for treating depression after stroke. Cochrane Database Syst Rev, CD003437.
Hackett, M. L., Anderson, C. S., House, A. O., 2005. Management of depression after stroke: a systematic review of pharmacological therapies. Stroke 36, 1098-1103.
Heurteaux, C., Gandin, C., Borsotto, M., Widmann, C., Brau, F., Lhuillier, M., Onteniente, B., Lazdunski, M., 2010. Neuroprotective and neuroproliferative activities of NeuroAid (MLC601, MLC901), a Chinese medicine, in vitro and in vivo. Neuropharmacology 58, 987-1001.
Heurteaux, C., Guy, N., Laigle, C., Blondeau, N., Duprat, F., Mazzuca, M., Lang-Lazdunski, L., Widmann, C., Zanzouri, M., Romey, G., Lazdunski, M., 2004. TREK-1, a K(+) channel involved in neuroprotection and general anesthesia. EMBO J 23, 2684-2695.
Heurteaux, C., Laigle, C., Blondeau, N., Jarretou, G., Lazdunski, M., 2006a. Alpha-linolenic acid and riluzole treatment confer cerebral protection and improve survival after focal brain ischemia. Neuroscience 137, 241-251.
Heurteaux, C., Lucas, G., Guy, N., El Yacoubi, M., Thümmler, S., Peng, X., Noble, F., Blondeau, N., Widmann, C., Gobbi, G., Costentin, J., Debonnel, G., Lazdunski, M., 2006b. Deletion of TREK-1, a background potassium channel, results in a depression-resistant phenotype. Nature Neurosci. 9, 1134-1141.
Honore, E., 2007. The neuronal background K2P channels: focus on TREK1. Nat Rev Neurosci. 8, 251-261.

Jin, K., Minami, M., Lan, J. Q., Mao, X. O., Batteur, S., Simon, R. P., Greenberg, D. A., 2001. Neurogenesis in dentate subgranular zone and rostral subventricular zone after focal cerebral ischemia in the rat. Proc Natl Acad Sci U S A 98, 4710-4715.
Jin, K., Wang, X., Xie, L., Mao, X. O., Zhu, W., Wang, Y., Shen, J., Mao, Y., Banwait, S., Greenberg, D. A., 2006. Evidence for stroke-induced neurogenesis in the human brain. Proc Natl Acad Sci U S A 103, 13198-13202.
Johansen, F. F., Hasseldam, H., Nybro Smith, M., Rasmussen, R. S., 2014. Drug-induced hypothermia by 5HT1A agonists provide neuroprotection in experimental stroke: new perspectives for acute patient treatment. J Stroke Cerebrovasc Dis 23, 2879-2887.
Kilkenny, C., Browne, W., Cuthill, I. C., Emerson, M., Altman, D. G., National Centre for the Replacement, R., Reduction of Amimals in, R., 2011. Animal research: reporting in vivo experiments--the ARRIVE guidelines. J Cereb Blood Flow Metab 31, 991-993.
Kronenberg, G., Balkaya, M., Prinz, V., Gertz, K., Ji, S., Kirste, I., Heuser, I., Kampmann, B., Hellmann-Regen, J., Gass, P., Sohr, R., Hellweg, R., Waeber, C., Juckel, G., Hortnagl, H., Stumm, R., Endres, M., 2012. Exofocal dopaminergic degeneration as antidepressant target in mouse model of poststroke depression. Biol Psychiatry 72, 273-281.
Kronenberg, G., Gertz, K., Heinz, A., Endres, M., 2014. Of mice and men: modelling post-stroke depression experimentally. Br J Pharmacol 171, 4673-4689.
Langhorne, P., Coupar, F., Pollock, A., 2009. Motor recovery after stroke: a systematic review. Lancet Neurol 8, 741-754.
Lauritzen, I., Blondeau, N., Heurteaux, C., Widmann, C., Romey, G., Lazdunski, M., 2000. Polyunsaturated fatty acids are potent neuroprotectors. EMBO J 19, 1784-1793.
Lee, J. H., Wei, L., Gu, X., Wei, Z., Dix, T. A., Yu, S. P., 2014. Therapeutic effects of pharmacologically induced hypothermia against traumatic brain injury in mice. J Neurotrauma 31, 1417-1430.
Lee, J. H., Wei, L., Gu, X., Won, S., Wei, Z. Z., Dix, T. A., Yu, S. P., 2016. Improved Therapeutic Benefits by Combining Physical Cooling With Pharmacological Hypothermia After Severe Stroke in Rats. Stroke 47, 1907-1913.
Lorivel, T., Gandin, C., Veyssiere, J., Lazdunski, M., Heurteaux, C., 2015. Positive effects of the traditional Chinese medicine MLC901 in cognitive tasks. J Neurosci Res 93, 1648-1663.
Matsuura, K., Kabuto, H., Makino, H., Ogawa, N., 1997. Pole test is a useful method for evaluating the mouse movement disorder caused by striatal dopamine depletion. J Neurosci Methods 73, 45-48.
Mazella, J., Petrault, O., Lucas, G., Deval, E., Beraud-Dufour, S., Gandin, C., El-Yacoubi, M., Widmann, C., Guyon, A., Chevet, E., Taouji, S., Conductier, G., Corinus, A., Coppola, T., Gobbi, G., Nahon, J. L., Heurteaux, C., Borsotto, M., 2010. Spadin, a sortilin-derived peptide, targeting rodent TREK-1 channels: a new concept in the antidepressant drug design. PLoS Biol 8, e1000355.
Mead, G. E., Hsieh, C. F., Lee, R., Kutlubaev, M., Claxton, A., Hankey, G. J., Hackett, M., 2013. Selective serotonin reuptake inhibitors for stroke recovery: a systematic review and meta-analysis. Stroke 44, 844-850.
Mirza, F. J., Zahid, S., 2018. The Role of Synapsins in Neurological Disorders. Neurosci Bull 34, 349-358.
Moha ou Maati, H., Peyronnet, R., Devader, C., Veyssiere, J., Labbal, F., Gandin, C., Mazella, J., Heurteaux, C., Borsotto, M., 2011. A human TREK-1/HEK cell line: a highly efficient screening tool for drug development in neurological diseases. PLoS One 6, e25602.
Moha Ou Maati, H., Veyssiere, J., Labbal, F., Coppola, T., Gandin, C., Widmann, C., Mazella, J., Heurteaux, C., Borsotto, M., 2012. Spadin as a new antidepressant: absence of TREK-1-related side effects. Neuropharmacology 62, 278-288.

Montgomery, S. A., Loft, H., Sanchez, C., Reines, E. H., Papp, M., 2001. Escitalopram (S-enantiomer of citalopram): clinical efficacy and onset of action predicted from a rat model. Pharmacol Toxicol 88, 282-286.
Morris, P. L., Robinson, R. G., Raphael, B., Hopwood, M. J., 1996. Lesion location and poststroke depression. J Neuropsychiatry Clin Neurosci 8, 399-403.
Munck Petersen, C., Nielsen, M. S., Jacobsen, C., Tauris, J., Jacobsen, L., Gliemann, J., Moestrup, S. K., Madsen, P., 1999. Propeptide cleavage conditions sortilin/neurotensin receptor-3 for ligand binding. Embo J 18, 595-604.
Murphy, T. H., Corbett, D., 2009. Plasticity during stroke recovery: from synapse to behaviour. Nat Rev Neurosci 10, 861-872.
Nedergaard, M., Dirnagl, U., 2005. Role of glial cells in cerebral ischemia. Glia 50, 281-286.
Orwig, K. S., Lassetter, M. R., Hadden, M. K., Dix, T. A., 2009. Comparison of N-terminal modifications on neurotensin(8-13) analogues correlates peptide stability but not binding affinity with in vivo efficacy. J Med Chem 52, 1803-1813.
Peruche, B., Backhauss, C., Prehn, J. H., Krieglstein, J., 1994. Protective effects of 5-HT1A receptor agonists against neuronal damage demonstrated in vivo and in vitro. J Neural Transm Park Dis Dement Sect 8, 73-83.
Pohjasvaara, T., Vataja, R., Leppavuori, A., Kaste, M., Erkinjuntti, T., 2001. Depression is an independent predictor of poor long-term functional outcome post-stroke. Eur J Neurol 8, 315-319.
Porsolt, R. D., 2000. Animal models of depression: utility for transgenic research. Rev Neurosci 11, 53-58.
Quast, U., 1992. Potassium channel openers: pharmacological and clinical aspects. Fundam Clin Pharmacol 6, 279-293.
Quintard, H., Lorivel, T., Gandin, C., Lazdunski, M., Heurteaux, C., 2014. MLC901, a Traditional Chinese Medicine induces neuroprotective and neuroregenerative benefits after traumatic brain injury in rats. Neuroscience 277, 72-86.
Ramos, A. J., Rubio, M. D., Defagot, C., Hischberg, L., Villar, M. J., Brusco, A., 2004. The 5HT1A receptor agonist, 8-OH-DPAT, protects neurons and reduces astroglial reaction after ischemic damage caused by cortical devascularization. Brain Res 1030, 201-220.
Santarelli, L., Saxe, M., Gross, C., Surget, A., Battaglia, F., Dulawa, S., Weisstaub, N., Lee, J., Duman, R., Arancio, O., Belzung, C., Hen, R., 2003. Requirement of hippocampal neurogenesis for the behavioral effects of antidepressants. Science. 301, 805-809.
Sun, C., Sun, H., Wu, S., Lee, C. C., Akamatsu, Y., Wang, R. K., Kernie, S. G., Liu, J., 2013. Conditional ablation of neuroprogenitor cells in adult mice impedes recovery of poststroke cognitive function and reduces synaptic connectivity in the perforant pathway. J Neurosci 33, 17314-17325.
Takatsuru, Y., Fukumoto, D., Yoshitomo, M., Nemoto, T., Tsukada, H., Nabekura, J., 2009. Neuronal circuit remodeling in the contralateral cortical hemisphere during functional recovery from cerebral infarction. J Neurosci 29, 10081-10086.
Vataja, R., Leppavuori, A., Pohjasvaara, T., Mantyla, R., Aronen, H. J., Salonen, O., Kaste, M., Erkinjuntti, T., 2004. Poststroke depression and lesion location revisited. J Neuropsychiatry Clin Neurosci 16, 156-162.
Veyssière, J., Moha-Ou-Maati, H., Mazella, J., Gaudriault, G., Heurteaux, C., Borsotto, M., 2014. Retroinverso analogs of spadin display increased antidepressant effects. Psychopharmacology.
Wang, M., Song, J., Xiao, W., Yang, L., Yuan, J., Wang, W., Yu, Z., Xie, M., 2012. Changes in lipid-sensitive two-pore domain potassium channel TREK-1 expression and its involvement in astrogliosis following cerebral ischemia in rats. J Mol Neurosci 46, 384-392.

Wei, S., Sun, J., Li, J., Wang, L., Hall, C. L., Dix, T. A., Mohamad, O., Wei, L., Yu, S. P., 2013. Acute and delayed protective effects of pharmacologically induced hypothermia in an intracerebral hemorrhage stroke model of mice. Neuroscience 252, 489-500.
Winter, B., Bert, B., Fink, H., Dirnagl, U., Endres, M., 2004. Dysexecutive syndrome after mild cerebral ischemia? Mice learn normally but have deficits in strategy switching. Stroke 35, 191-195.
Zhang, R., Zhang, Z., Zhang, C., Zhang, L., Robin, A., Wang, Y., Lu, M., Chopp, M., 2004. Stroke transiently increases subventricular zone cell division from asymmetric to symmetric and increases neuronal differentiation in the adult rat. J Neurosci 24, 5810-5815.
Zhou, M., Xu, G., Xie, M., Zhang, X., Schools, G. P., Ma, L., Kimelberg, H. K., Chen, H., 2009. TWIK-1 and TREK-1 are potassium channels contributing significantly to astrocyte passive conductance in rat hippocampal slices. J Neurosci 29, 8551-8564.
Zoli, M., Merlo Pich, E., Ferraguti, F., Biagini, G., Fuxe, K., Agnati, L. F., 1993. Indole-pyruvic acid treatment reduces damage in striatum but not in hippocampus after transient forebrain ischemia in the rat. Neurochem Int 23, 139-148.
Zomkowski, A. D., Engel, D., Gabilan, N. H., Rodrigues, A. L., 2010. Involvement of NMDA receptors and L-arginine-nitric oxide-cyclic guanosine monophosphate pathway in the antidepressant-like effects of escitalopram in the forced swimming test. Eur Neuropsychopharmacol 20, 793-801.

9- Figure Legends

Fig. 1. Activity of TREK-1 channel currents by mini-spadin depends on the peptide concentration; **A,** % of TREK-1 activation and TREK-1 inhibition induced, respectively, by low and high doses of mini-spadin in human cell line hTREK-1/HEK using the whole-cell patch-clamp technique (n=7 to 18); **B,** Percentage of activation of TREK-1 currents measured at 0 mV obtained with 10^{-6} M spadin, 10^{-9} M mini-spadin and 10^{-8} M mini-spadin. Whole-cell currents (pA/pF) were measured in hTREK-1/HEK in presence of potassium blockers (K^+ blockers, 10 mM tetraethyl ammonium (TEA), 3 mM 4-aminopyridine (4-AP), 50 nM charybdotoxin, 10 mM glibenclamide, 100 nM apamin). Control value was obtained by using a solution of 0.9% NaCl. Data are reported as Mean ± SEM. **P* < 0.05, ***P* < 0.01 compared to control.

Fig. 2. Effects of mini-spadin compared to spadin and escitalopram on loss of body weight and motor deficits induced by 30 min MCAO; **A,** Evolution of body weight during 7 days recovery after MCAO. Data are reported as Mean ± SEM: saline (n=17), spadin (n=14), mini-spadin (n=15), escitalopram (n=15). $^{***}P < 0.001$ compared to pre-MCAO values, $^{\#}P < 0.05$ compared to Saline group. **B,** Rotarod performance (latency to fall (% of pre-MCAO performance) 3 days following MCAO. Data are reported as Mean ± SEM: saline (n=16), spadin (n=14), mini-spadin (n=15), escitalopram (n=14), $^{\#}P< 0.05$ vs MCAO-saline group, Kruskal-Wallis test); **C-D,** Pole test performance before, 3 and 14 days following MCAO; **C,** Time to rotate (s); **D,** Time to descent (s). Data are reported as Mean ± SEM: saline (n=13), spadin (n=11), mini-spadin (n=14), escitalopram (n=15), $^{***}P<0.001$, versus Pre-MCAO values, $^{\#\#}P<0.01$, $^{\#}P<0.05$ versus MCAO-saline group, one way ANOVA, Dunnett's multiple comparison test.

Fig. 3. Effects of mini-spadin compared to spadin and escitalopram on cognitive deficits induced by 30 min MCAO and evaluated in Morris Water Maze test 3 weeks after MCAO; **A-B,** Evolution of time (s) to reach the hidden platform over the training trials (1 to 4 Days); **C,** Time (s) spent in the NW quadrant (left panel) and latency to first entry in the NW quadrant (right panel) during the probe trial; **D,** Strategies used in the Morris Water Maze test during the probe trial (see supplementary Fig.S5).

Fig. 4. Antidepressant effects of mini-spadin compared to spadin and escitalopram in the Forced Swim Test (FST) and in the Novelty Suppressed Feeding test (NSF) at different times following MCAO; **A,** FST. Immobility time (s) was measured 3, 5, 7 and 10 weeks after MCAO. Data

are reported as Mean ± SEM in the different groups: saline (n=22), spadin (n=27), mini-spadin (n=24), escitalopram (n=22), sham-operated (n=22); **B-D,** NSF. Animals were food deprived for 1 day and then measured for their latency to feed; **B,** Latency to eat (% of sham-operated saline mice) at 3 and 10 weeks post-MCAO showing the strong behavioral effect of MCAO when compared to saline-sham group; **C,** Latency to eat (s) at 10 weeks post-MCAO and **D,** Evolution of the latency to eat (% of MCAO-saline mice) at 3 and 10 weeks post-MCAO, showing the significant antidepressant effect of 3 drugs obtained 10 weeks following MCAO. Data are reported as Mean ± SEM in the different groups: saline (n=14), spadin (n=14), mini-spadin (n=15), escitalopram (n=14) and sham-operated (n=12),$^{*}P<0.05$, $^{**}P<0.01$ *vs* Sham-operated-Saline group; $^{###}P<0.001$, $^{##}P<0.01$ $^{#}P<0.05$ *vs* MCAO-Saline group (one way ANOVA, Dunnett's multiple comparison test for comparing the treatment effect).

Fig .5. Effects of mini-spadin compared to spadin and escitalopram on neurogenesis and synaptogenesis. **A,** (left panel) Representative photomicrographs of BrdU (green), NeuN (red), GFAP (blue) fluorescent labeling in hippocampal dentate gyrus from ischemic saline- or mini-spadin-treated mice 10 weeks and 21 days after BrdU injection, (right panel) Quantitation of BrdU-positive cells per hippocampus 10 weeks after MCAO (4 experimental groups and 2 sham groups). Data are expressed as Mean ± SEM. They were collected from two independent experiments with n = 8 per group, 8 brain slices per mouse ($^{#}P < 0.05$, $^{##}P < 0.01$ *vs* ischemic saline-treated mice, Mann & Whitney U test); **B,** (left panel) Representative images from Western blotting analysis PSD-95, (right panel) optical densitometry quantitation for PSD-95 (95 kDa) and synapsin (75 kDa) in ipsi- and contra-lateral cortical tissues. Tubulin and actin were respectively used as internal controls for the loading of protein levels. Data are representative of 3 separate experiments (n=3 per group). Values (Mean ± SEM) are expressed as percentage of protein control ($^{#}P<0.05$, $^{##}P<0.01$ *vs* vehicle ischemic group, Mann & Whitney U test).

Fig. 6. Effects of mini-spadin compared to spadin and escitalopram on dopaminergic degeneration induced by 30 min MCAO. **A,** Representative photomicrographs of peroxidase immunolabeling of Tyrosine Hydroxylase neurons (TH) 10 weeks after MCAO showing the loss of dopaminergic neurons induced by MCAO in the ipsilateral injured *subtantia nigra* (SN) and the protective effect of mini-spadin (scale bar, 50 μm). Boxed areas in (**A**) are shown in higher magnification in (**B)**; **B**, upper panel, Fluorescent TH (green), NeuN (red) and Hoechst (blue) immunolabeling at high magnification in the ipsilateral injured SN from vehicle- and

mini-spadin-treated mice after 10 weeks of reperfusion (scale bar: 15 μm); **B**, bottom panel, quantitation of mean number of TH positive cells in the ipsilateral injured substantia nigra of mice treated with spadin, mini-spadin or escitalopram (10 sections per mouse). Data are expressed as Mean ± SEM (n=8 to 11 per experimental group) ($^{\#\#}P<0.01$ *vs* vehicle ischemic group, Mann & Whitney U test).

Figures

Figure 1

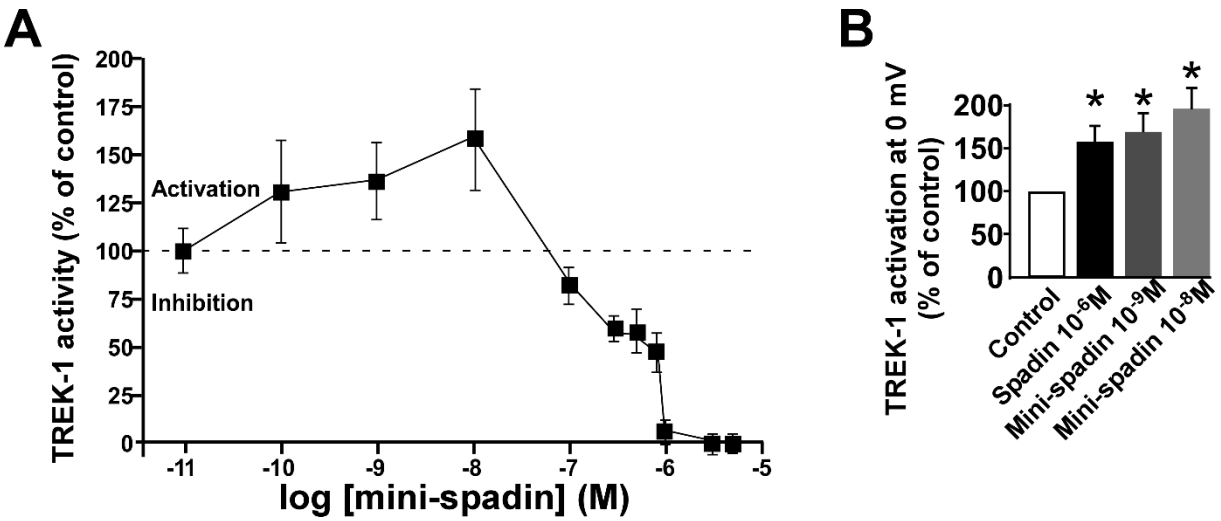

Figure 2

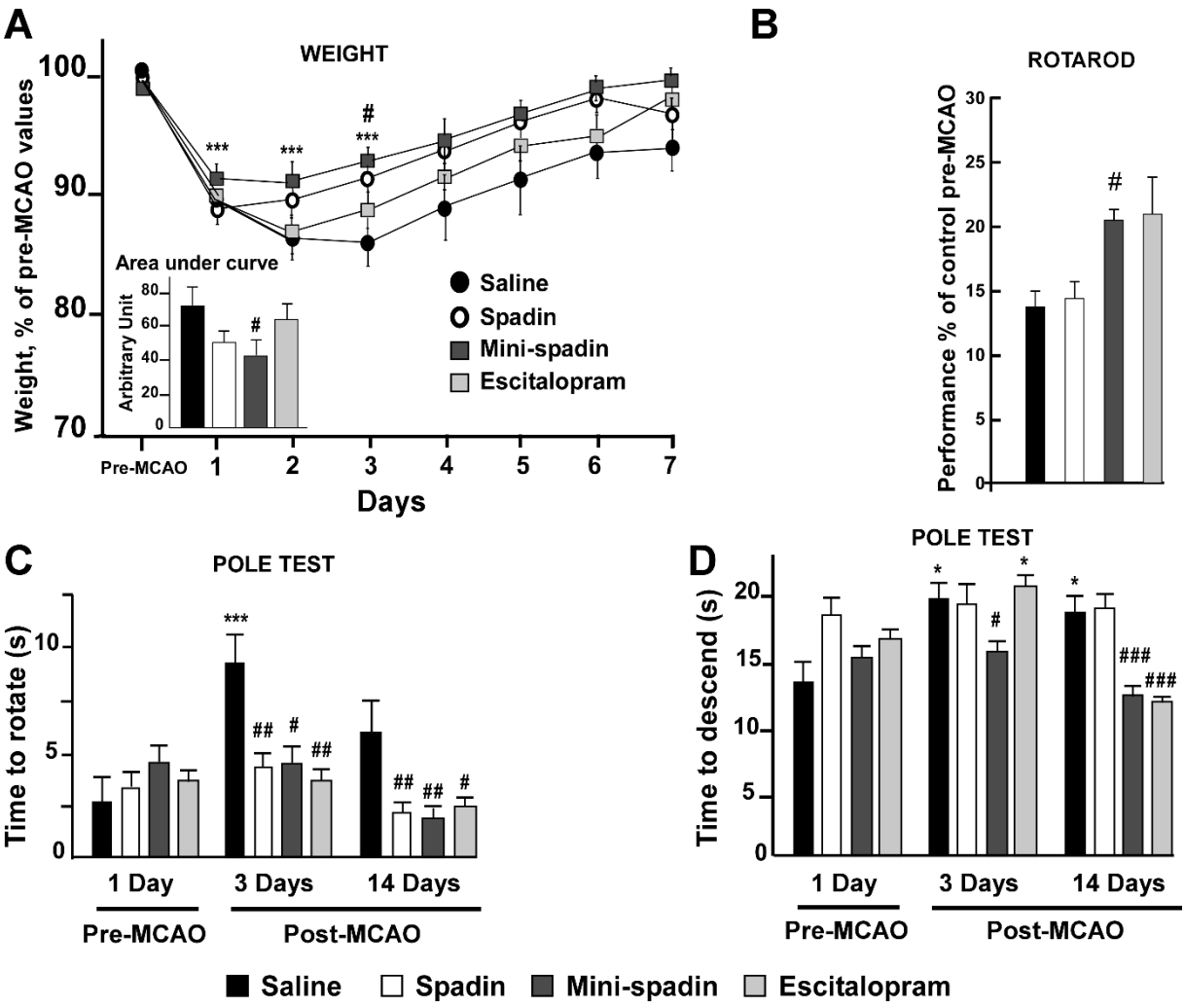
A
WEIGHT
Weight, % of pre-MCAO values
100
90
80
70
***
***
#
***
Area under curve
Arbitrary Unit
80
60
40
20
0
#
Saline
Spadin
Mini-spadin
Escitalopram
Pre-MCAO
1
2
3
4
5
6
7
Days
B
ROTAROD
Performance % of control pre-MCAO
30
25
20
15
10
5
0
#
C
POLE TEST
Time to rotate (s)
10
5
0
***
##
#
##
##
##
#
1 Day
3 Days
14 Days
Pre-MCAO
Post-MCAO
D
POLE TEST
Time to descend (s)
20
15
10
5
0
*
*
#
*
###
###
1 Day
3 Days
14 Days
Pre-MCAO
Post-MCAO
Saline
Spadin
Mini-spadin
Escitalopram

Figure 3

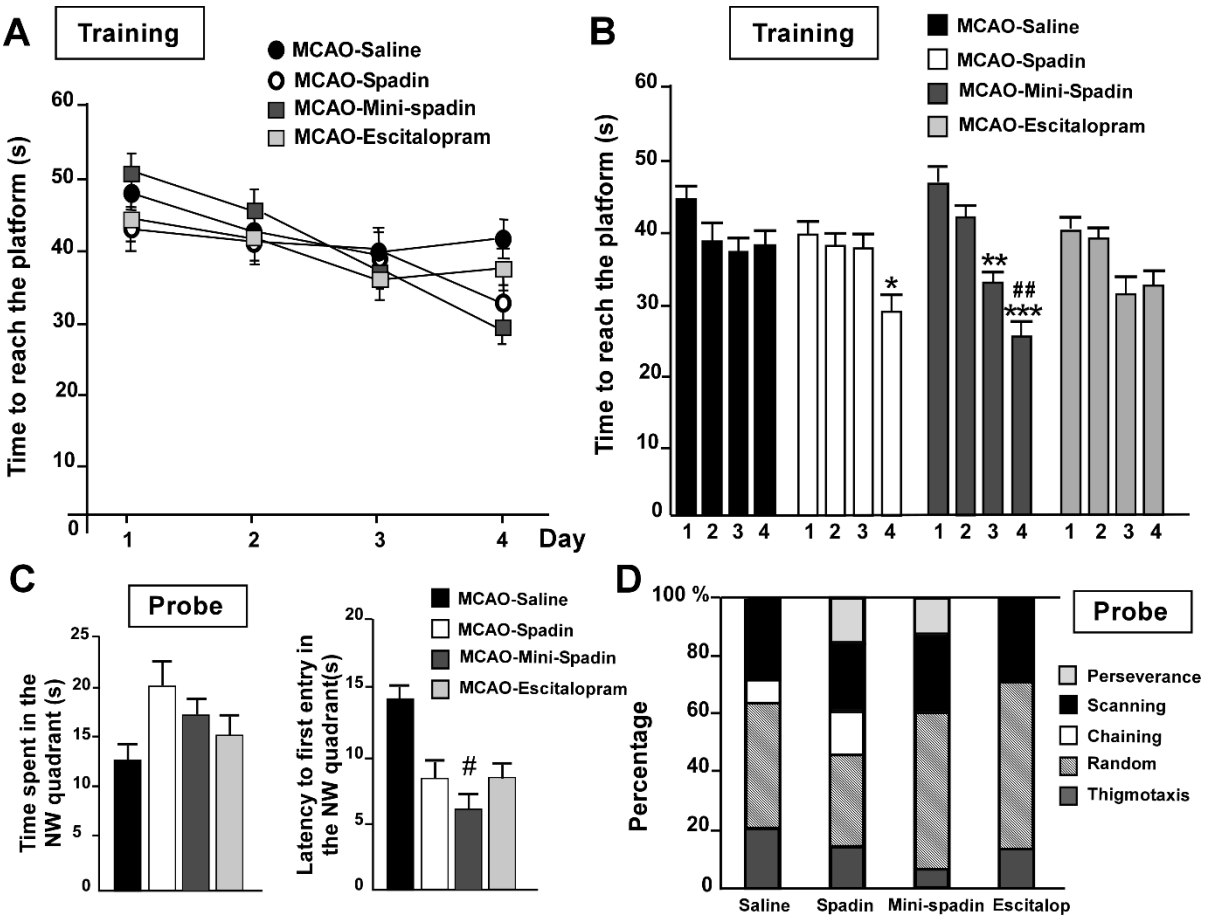
A
Training
MCAO-Saline
MCAO-Spadin
MCAO-Mini-spadin
MCAO-Escitalopram
Time to reach the platform (s)
Day
B
Training
MCAO-Saline
MCAO-Spadin
MCAO-Mini-Spadin
MCAO-Escitalopram
Time to reach the platform (s)
C
Probe
Time spent in the NW quadrant (s)
Latency to first entry in the NW quadrant(s)
D
Probe
Percentage
Perseverance
Scanning
Chaining
Random
Thigmotaxis
Saline
Spadin
Mini-spadin
Escitalop

Figure 4

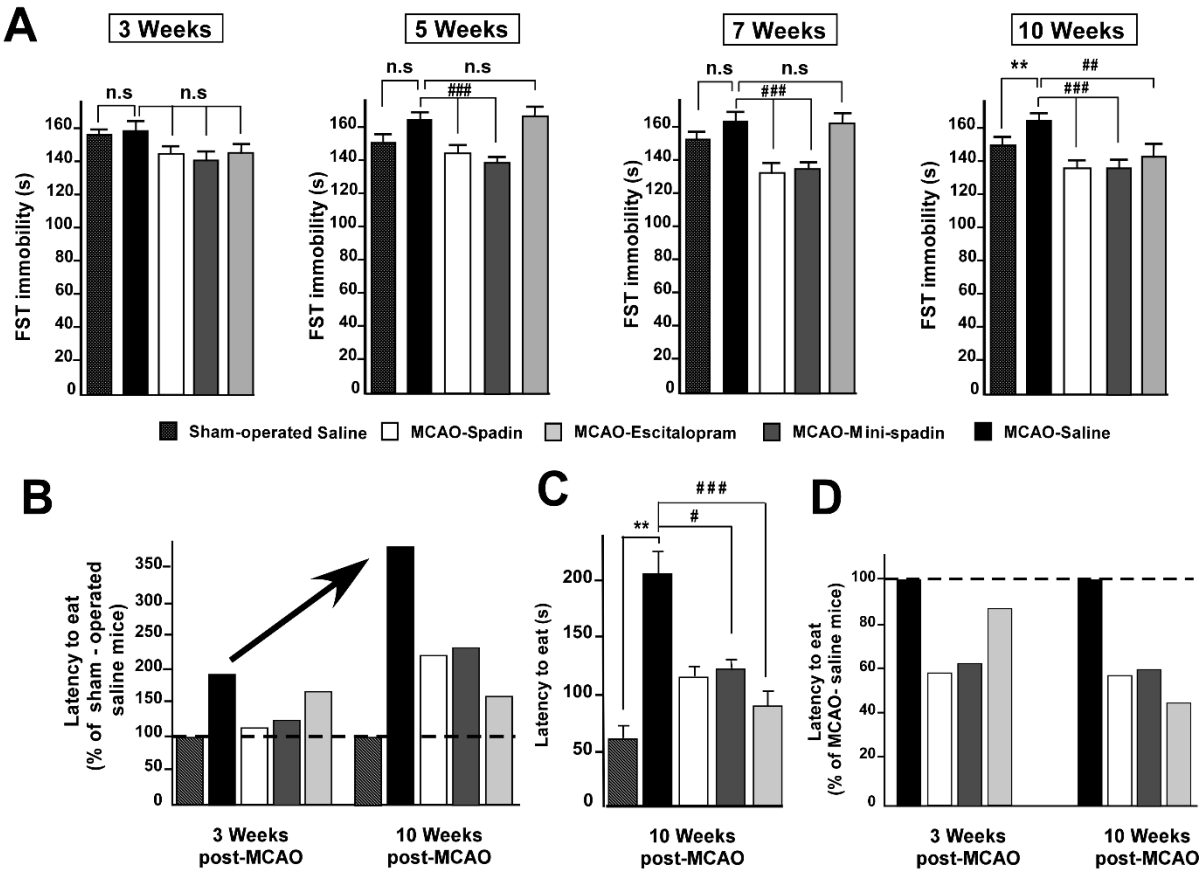
A
3 Weeks
5 Weeks
7 Weeks
10 Weeks
n.s
###
**
##
FST immobility (s)
Sham-operated Saline
MCAO-Spadin
MCAO-Escitalopram
MCAO-Mini-spadin
MCAO-Saline
B
Latency to eat (% of sham - operated saline mice)
3 Weeks post-MCAO
10 Weeks post-MCAO
C
Latency to eat (s)
D
Latency to eat (% of MCAO- saline mice)

Figure 5

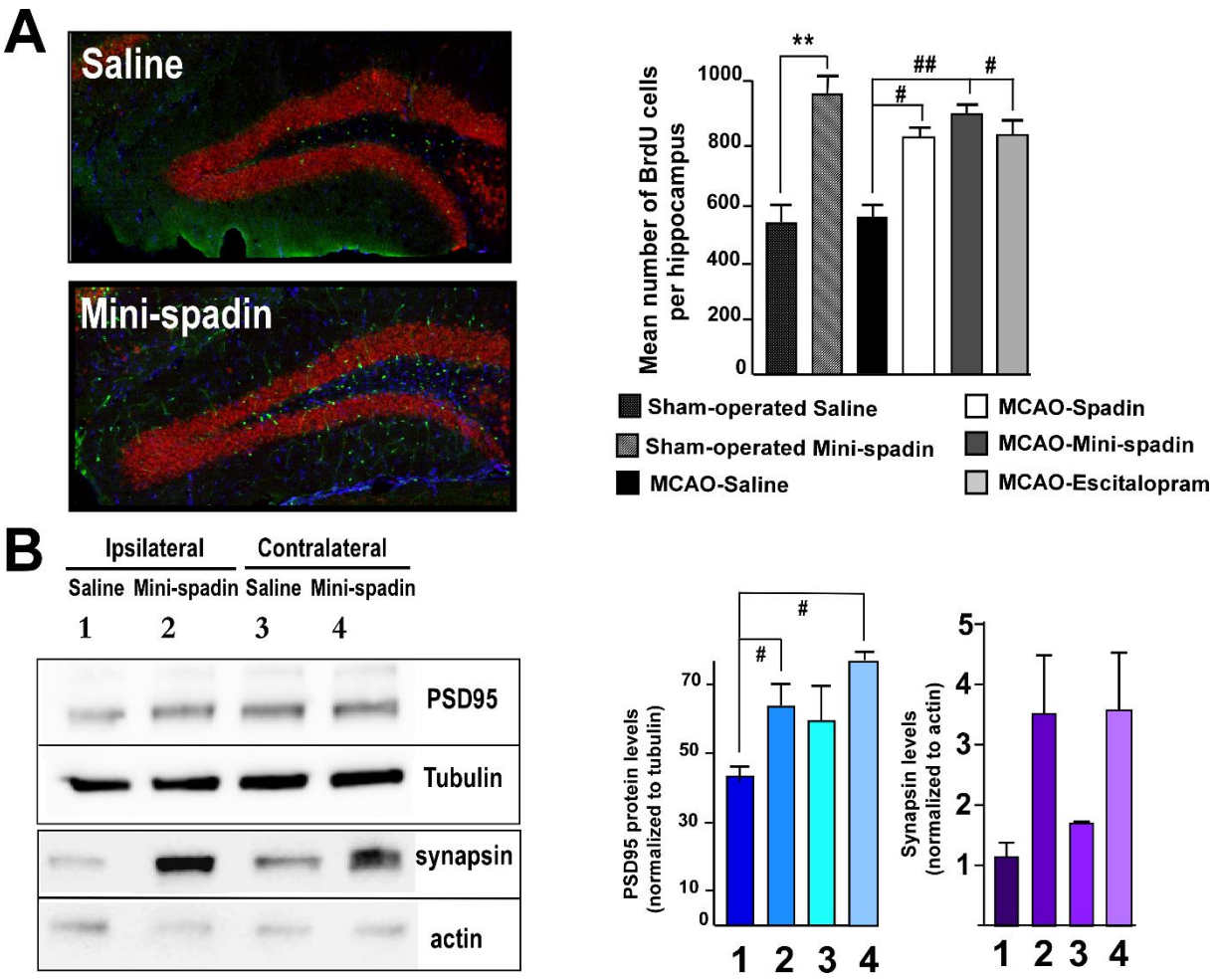
A
Saline
Mini-spadin
Mean number of BrdU cells per hippocampus
1000
800
600
400
200
0
**
##
#
#
Sham-operated Saline
Sham-operated Mini-spadin
MCAO-Saline
MCAO-Spadin
MCAO-Mini-spadin
MCAO-Escitalopram
B
Ipsilateral
Contralateral
Saline Mini-spadin Saline Mini-spadin
1 2 3 4
PSD95
Tubulin
synapsin
actin
PSD95 protein levels (normalized to tubulin)
70
50
30
10
0
#
#
1 2 3 4
Synapsin levels (normalized to actin)
5
4
3
2
1
1 2 3 4

Figure 6

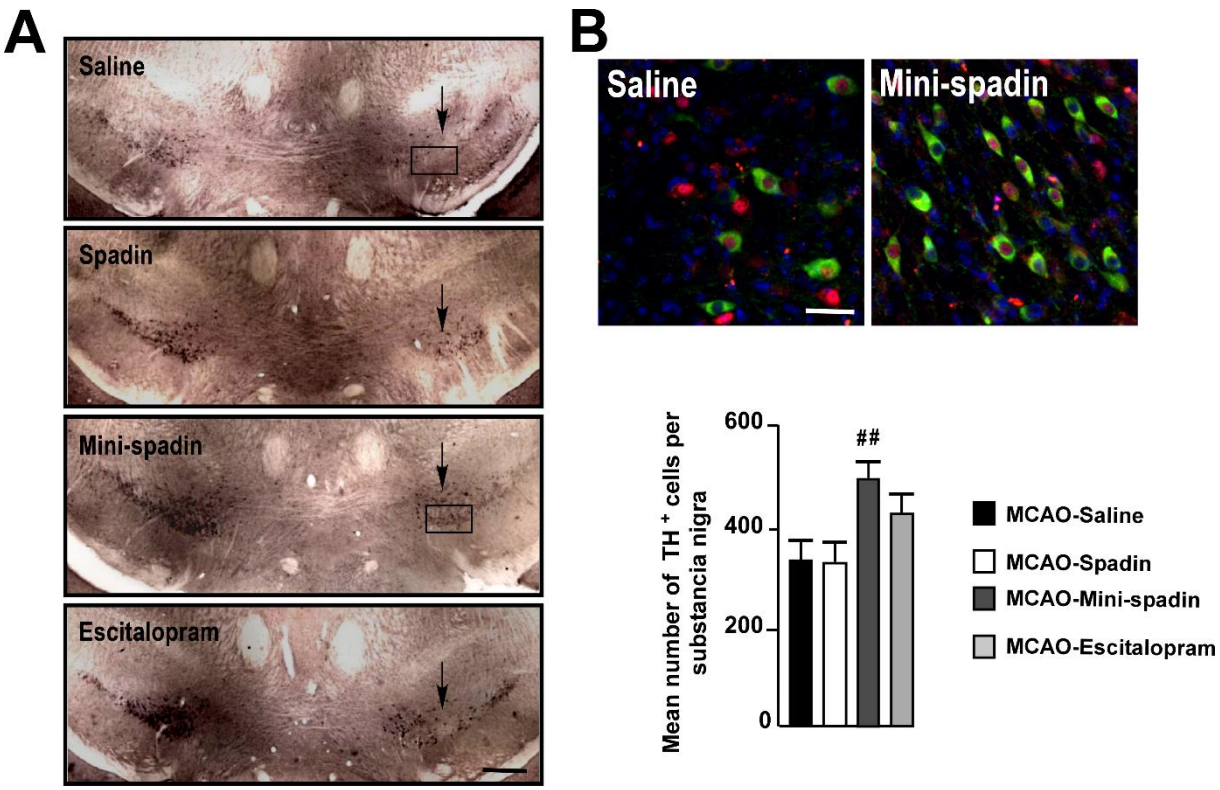

Supplementary Material

Supplemental Methods

Brain perfusion

In immunohistochemistry studies animals were killed by transcardiac perfusion with 0.9% NaCl followed by ice-cold 4% paraformaldehyde in phosphate-buffered saline (0.15M NaCl/0.01M sodium phosphate, pH 7.4). Mice were injected with a bolus of 100 µL of Dolétal. Once asleep they were ventrally incised to access their heart. Around 10 mL of iced NaCl 0.9% were then injected in the left ventricle using an 18G needle while the right atrium was cut open.

Once the organs were bloodless, an iced solution of paraformaldehyde 4% was injected during 10 min. Brain were finally removed and kept in paraformaldehyde 4% for 24 hours before being cut.

Analysis of neurogenesis on brain sections

BrdU treatment consisted of 3 injections (75 mg/kg, i.p. each, 2 hour interval). Brains were removed 24 hours after the last injection. Serial sections of paraformaldehyde-perfused-brains were cut (40 µm) throughout the entire hippocampus on a vibratome (Leica) and kept in a solution of anti-freeze (20% glycérol/30% ethylene glycol) at -20°C. Every sixth section throughout the hippocampus was processed for immunohistochemistry (Heurteaux et al., 2006b). They were incubated 20 minutes in a solution of 0.3% H_2O_2 to neutralize endogenous peroxydases. Then put at 37°C in HCl 2N for 20 minutes to permeabilize the membranes before a bath of 10 minutes in Borate 0.1M to stop the reaction. The slides were then blocked for 2 hours in 2.5% Horse serum buffer and incubated overnight at 4°C with a monoclonal mouse anti-BrdU (1/7000; BD Biosciences, Le Pont de Claix). For BrdU chromogenic immunodetection, sections were then incubated for 1 hour in biotin-conjugated species-specific secondary antibodies (diluted 1/400, Vector Laboratories), followed by a peroxidase-avidin complex solution according to the manufacturer's protocol. The peroxydase activity of immune complexes was visualized with DAB staining using the VectaStain ABC kit (Vector Laboratories). BrdU-labeled cells of the whole granular and subgranular layers of the hippocampus were counted in each mouse brain slice (n=8 mice per group, 8 slices per brain, 2 independent experiments) at 400x under a light microscope by a blind experimenter.

Tyrosine hydroxylase (TH) immunostaining

Serial sections of paraformaldehyde-perfused-brains were cut (40 µm) at the level of midbrain. Immunohistochemistry was processed as described above by using a rabbit polyclonal anti-TH (1/100, Abcam ab51191). Additionally, to specifically identify TH-positive cells colocalized with neuronal cells, double immunofluorescence labeling of TH with NeuN, a specific marker for neurons (Millipore, #MAB377, 1/300) was performed using a mouse monoclonal NeuN antibody. Secondary antibodies were conjugated with Alexa Fluor 488 or 594 (Molecular Probes, 1/1000). Confocal microscopy observations were performed with a Laser Scanning Confocal Microscope (TCS SP, Leica, Rueil Malmaison, France). Immunostained sections were digitized using a X40 objective *via* the Image J computer imaging analysis system. The

number of TH-labeled cells within a total of 10 sections per mouse corresponding to the entire area of the *substantia nigra* (n=8 mice per group, 2 independent experiments) was counted by a blind experimenter. Data are presented as mean number of TH-immunoreactive cells ± SEM (n=8 to 11 mice per experimental group).

Western Blots

Brain tissues (n=3 per group) were collected after MCAO, and the fresh brains were carefully separated into ipsilateral and contralateral hemispheres, and into cortical and subcortical regions, with respect to the infarct location. Samples (n=3 mice per group, 2 independent experiments) were homogenized in four volumes of cold lysis buffer (20 nmol/L Tris pH: 7.5, 137 mmol/L NaCl, 2 mmol/L EDTA, 1% Triton X-100, 10% glycerol, and protease inhibitor cocktail) on ice. The homogenates were centrifuged at 35,000 rpm for 30 min at 4 °C. The supernatant was removed two times and stored at -70°C until further use. Protein concentrations were measured using conventional Bradford's method. Fifty micrograms of proteins from each experimental group were applied to 10% SDS PAGE and electrophoresed for 1 h at 100 mA. Proteins were transferred onto a PVDF membrane in blotting buffer (156 mmol/L Tris, 1 mol/L glycine, PBS) for 90 min at 80 mA and blocked with 5% skim milk (Regilait) in PBS/0.1% Tween20. Membranes were incubated with the rabbit polyclonal antibody directed against PSD-95 or synapsin (dilution 1/1000) overnight at 4°C. Tubulin and actin contents were determined after stripping using an anti-tubulin (1/1000, Clinisciences, Nanterre, France) or anti-actin (1/3000) antibody (Cell Signalleing, Leiden, Netherland). After four washes in 0.1% Tween20/PBS following incubation of primary antibodies, secondary anti-mouse or anti-rabbit HRP-conjugated antibodies (Amersham Biosciences, Orsay, France; 1/10000) were incubated for 1 h at room temperature. Proteins were detected with the ECL plus detection reagents (Amersham Biosciences) using an LAS-3000 imaging system (Fujifilm, Düsseldorf, Germany). Relative intensities of the labeled bands were analyzed by densitometric scanning using ImageJ software (Wayne Rasband, National Institute of Health, Bethesda, MD, USA). Protein activation was normalized using total tubulin or actin as indicated.

Materials

NaCl, KCl, $MgCl_2$, $CaCl_2$, HEPES, Tris, glycine, PBS, Tween/PBS, paraformaldehyde, 4-AP (4-aminopyridine), TEA (tetraethylammonium), Glibenclamide, Apamin, Charybdotoxin,

arachidonic acid and escitalopram were obtained from Sigma-Aldrich (St Quentin Fallavier, France). Spadin and mini-spadin were synthetized by Covalab (Villerbanne, France). BrdU was purchased from Roche Molecular Biochemicals (Mannheim, Germany). The antibodies were obtained from BD Biosciences (Le Pont de Claix, France) for BrdU, Merck Millipore (Molsheim, France) for NeuN, Abcam (Cambridge, UK) for TH, Cell Signalling (Leiden, Netherland) for synapsin, Sigma-Aldrich , Saint-Quentin Fallavier, France) for actin, Clinisciences (Nanterre, France) for PSD-95 and tubulin. Biotin-conjugated secondary antibodies, and peroxidase-avidin complex solution and VectaStain ABC kit were purchased from Vector laboratories (Clinisciences, Nanterre, France). HRP-conjugated antibodies and ECL plus detection reagents were obtained from Amersham Biosciences (Orsay, France).

Supplementary Table

Table I. Percentage of survival of animals: Comparison between mini-spadin 0.3 μg/kg (corresponding to 100 μL of 10^{-7} M per mouse) and mini-spadin 0.03 μg/kg (corresponding to 100 μL of 10^{-8} M per mouse).

		24 h			96 h		
	Total	Alive	Dead	% survival	Alive	Dead	% survival
Saline	26	17	9	65.4	16	10	61.5
Mini-spadin 0.3 μg/kg	19	10	9	52.6	5	14	26.3
Mini-spadin 0.03 μg/kg	20	18	2	90	15	5	75

Supplementary Figures

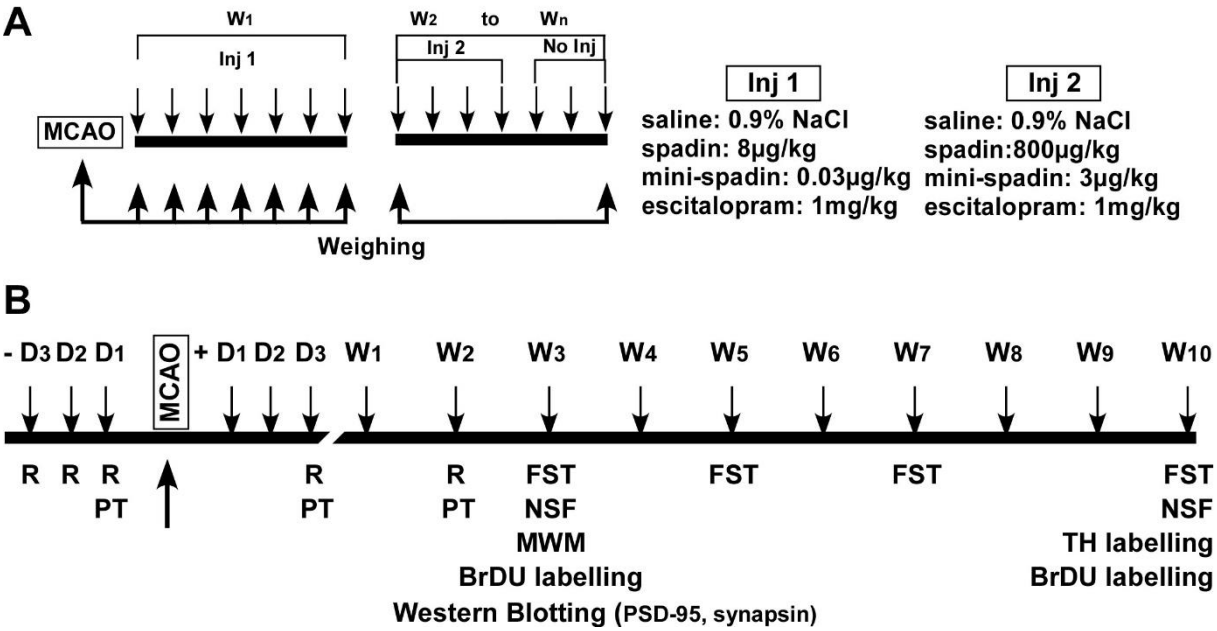

Supplementary Fig.1. Flowchart illustrating the different *in vivo* paradigms. In (**A)** and (**B)** mice were subjected to a left 30 min middle cerebral artery occlusion (MCAO); **A,** Protocol of injection of drugs. A bolus (100 µl/mouse) of spadin (8 µg/kg), mini-spadin (0.03 µg/kg) or escitalopram (1 mg/kg), diluted in NaCl 0.9% (as vehicle) was intraperitoneally injected 30 min after the onset of ischemia and once a day during 7-day reperfusion (Inj 1 during W_1,Week 1). Then, spadin or mini-spadin was injected at the concentration of 800 µg/kg and 3 µg/kg, respectively, once a day during 4 days/week (Inj 2 from D1 to D4) until the sacrifice of animals (from W_2 to Wn). The SSRI Escitalopram (1 mg/kg) was used as control and injected once a day during 4 days/week (Inj 2 from D1 to D4) until the sacrifice of animals. Mice were weighed once a day during the first week following MCAO and then once a week for the next 9 weeks; **B,** Timing of behavioral tests and biochemical experiments (Western blotting, Immunohistochemistry) during the 10 weeks following MCAO. R (Rotarod); FST (Forced Swim Test), PT (Pole Test), MWM (Morris Water Maze test), NSF (Novelty Suppressed Food test).

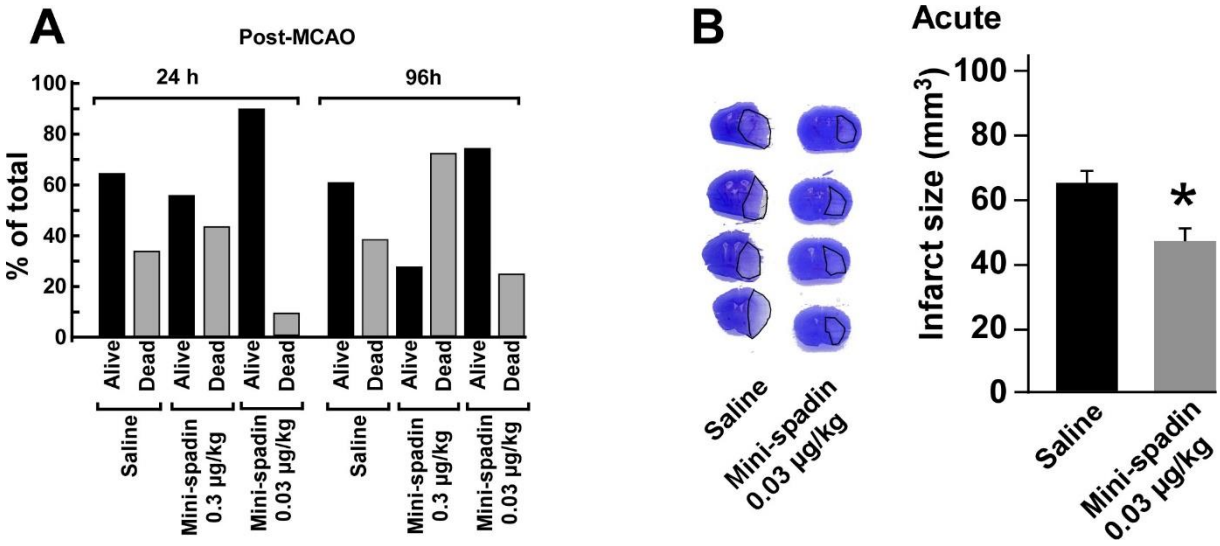

Supplementary Fig. 2. Neuroprotective effects of mini-spadin in vivo in the acute phase of stroke. **A,** Percentage of survival and death of mice 24h and 96h post-MCAO after mini-spadin treatment at 0.3 µg/kg and 0.03 µg/kg; saline (n=26), mini-spadin 0.3 µg/kg (n=19), mini-spadin 0.03 µg/kg (n=20). **B**, Decrease of infarct volume (mm^3) in mice treated with 0.03 µg/kg mini-spadin 24 hours after MCAO (acute phase). Left panel: Representative photographs of infarct area (delimited by black line) in saline (n=13) and mini-spadin (n=18)- treated groups. Right panel: Quantitation of infarct size (mm^3). Data are reported as Mean ± SEM. **P* < 0.05 compared to Saline group.

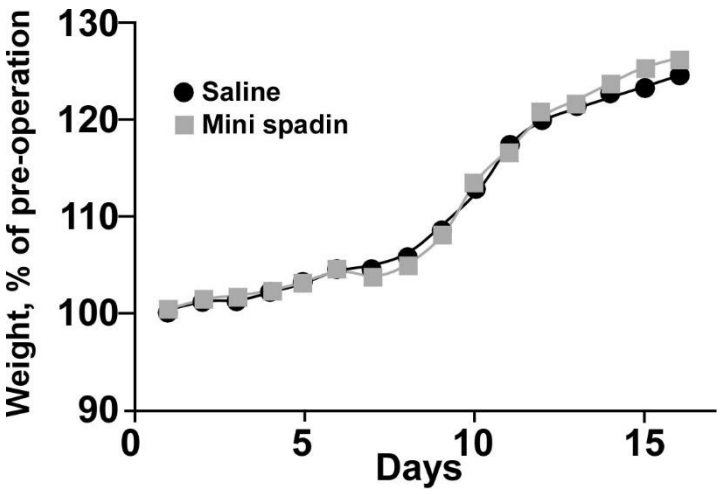

Supplementary Fig. 3. Evolution of body weight (percentage of pre-ischemia values) during 15 days recovery after MCAO in sham groups treated with saline or mini-spadin (n=10 per experimental groups, $P>0.05$, Mann & Whitney U test).

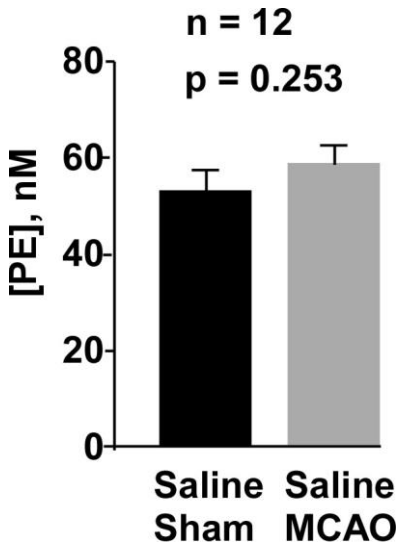

Supplementary Fig. 4. MCAO did not induce significant variation of PE levels (nM) in saline-treated mice. Data are reported as Mean ± SEM in the two groups: MCAO-Saline (n=12), Sham-operated-Saline (n=12), *P*=0.253 (Mann & Whitney U test)

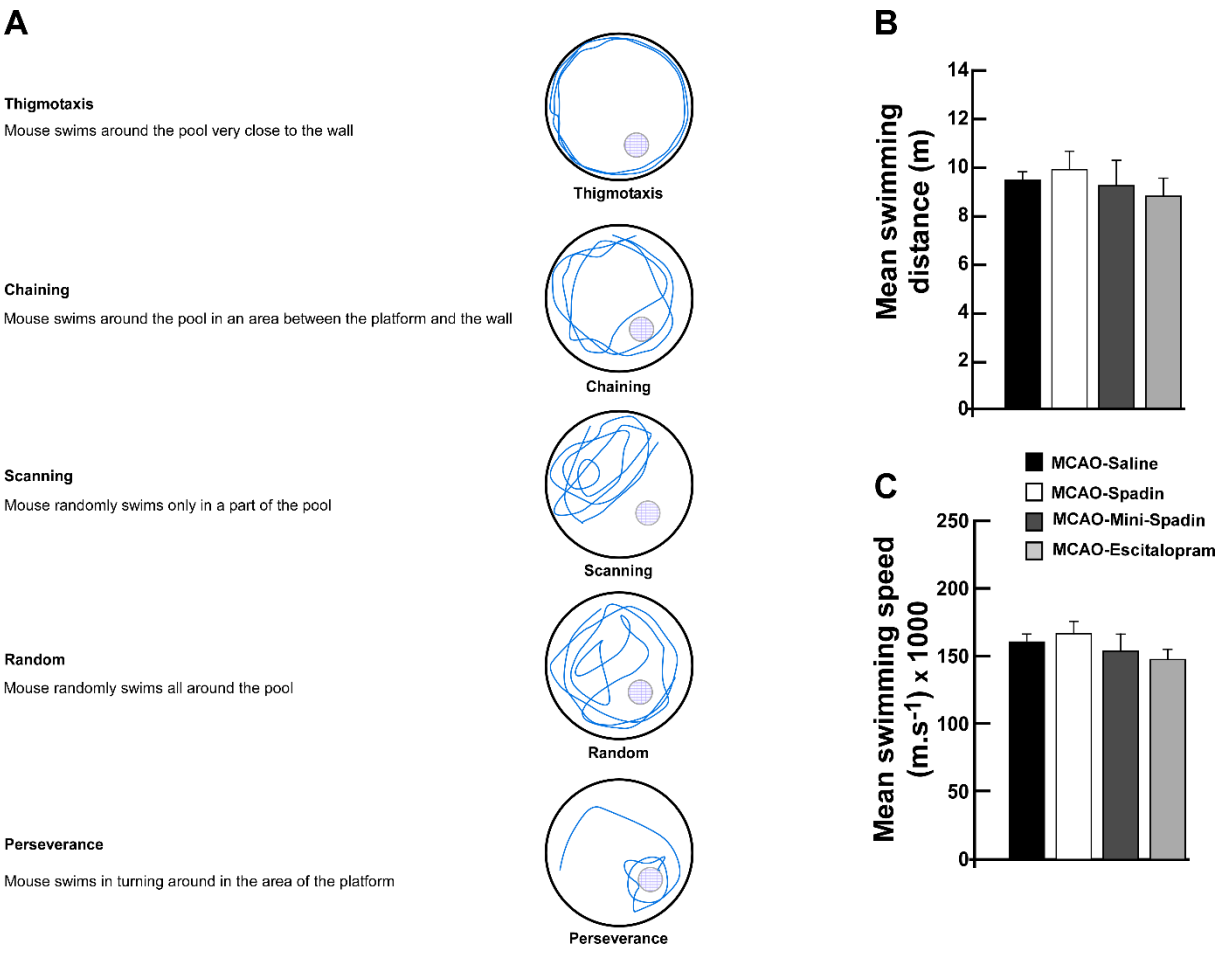

Supplementary Fig. 5. Morris Water Maze Test. **A**, Schematic representation of swimming behaviors. **B-C**, Locomotor activity of different groups. The acquisition procedure did not reveal any significant difference between groups either in swimming distance (**B)** or swimming speed (**C)**, suggesting that the treatments did not affect the locomotor activity. Data are reported as Mean ± SEM: saline (n=16), spadin (n=13), mini-spadin (n=15), escitalopram (n=14), $^{\$\$}P<0.01$ in comparison between MCAO-Mini-spadin group and MCAO-Saline group, $^{\#\#\#}P<0.001$, $^{\#}P<0.05$ versus corresponding Day 1 of training, $^{\#}P<0.05$ versus MCAO saline. (one way ANOVA, Dunnett's multiple comparison test for comparing the treatment effect).

Discussion

La dépression est une pathologie sévère avec un impact social important (Wong and Licinio, 2001). En effet, elle a touché ou touchera près de 20% de la population mondiale. De nos jours, malgré les nombreuses études menées dans ce domaine, cette pathologie n'est ni complètement comprise, ni totalement traitée. Les molécules antidépressives sont variées mais restent inefficaces chez un patient sur trois. De plus, elles ont également de nombreux effets secondaires parfois plus dangereux que la dépression elle-même. La plupart de ces molécules ont été développées dans le but de palier à la diminution de la sérotonine dans la fente synaptique, mais les études les plus récentes se tournent vers d'autres cibles (Schechter et al., 2005). Le canal TREK-1 est l'une d'entre elles (Heurteaux et al., 2006b). D'abord défini comme tel chez la souris, son implication dans le phénomène dépressif a également été confirmée chez l'Homme (Perlis et al., 2008). C'est dans ce contexte, qu'a été identifiée la Spadine.

La Spadine, un puissant inhibiteur spécifique de TREK-1 manifestant de puissantes propriétés antidépressives et une rapidité d'action de 4 jours, délai d'action très court en regard des 3 semaines habituellement nécessaires lors de traitements avec les antidépresseurs classiques. Parmi les nouveautés ces dernières années, du fait de sa rapidité d'action, la Kétamine a fait l'objet de nombreuses études pharmaceutiques. Contrairement à la Spadine elle a certains effets secondaires non négligeables.

Toutes ces caractéristiques ont conduit la Spadine au stade d'études précliniques. Sa stabilité *in vivo* qui était assez faible (6 heures) a poussé le laboratoire vers la recherche d'analogues plus performants. Une première série de ces analogues, basée sur une stratégie RI, a été produite et caractérisée (Veyssiere et al., 2015). Bien qu'ayant donné des résultats encourageants tant au niveau de leurs capacités antidépressives que de leur stabilité, ces analogues se sont avérés dangereux à forte concentration. Ces observations ont été la base de la première partie de ma thèse : la caractérisation d'analogues courts de la Spadine.

Ces analogues ont été créés en réalisant une étude structure-fonction à partir de produits de dégradation du PE (peptide issu de la maturation de la Sortiline) obtenus par une incubation à 37°C dans le sang. En effet, à partir de ces peptides nous avons pu définir un analogue court de 7 aa, appelé PE-22-28 (ou Mini-Spadine). Ce peptide ayant une forte capacité à inhiber le canal potassique TREK-1, a été utilisé comme structure de base pour la conception de 16 nouveaux analogues. Parce que le passage de la barrière hémato-encéphalique est crucial pour une molécule thérapeutique agissant sur des cibles cérébrales et parce qu'il a été démontré que la biotinylation peut augmenter l'absorption des peptides par le cerveau, nous avons synthétisé

certains de ces analogues avec une biotine greffée sur leur extrémité N-terminale (Scherrmann, 2002) (Wu et al., 2002). En utilisant la lignée cellulaire hTREK-1/HEK, lignée qui a été préparée dans notre laboratoire (Moha ou Maati et al., 2011) nous avons déterminé la capacité des différents peptides dérivés du PE 22-28 à inhiber les canaux TREK-1. Ces mesures nous ont permis d'identifier les analogues qui présentent un taux d'inhibition supérieur à 35% de l'activité TREK-1. Seule l'activité antidépressive des analogues a été mesurée par FST. Ensuite, en comparant les mesures électrophysiologiques et les données du FST, nous n'avons retenu que 3 peptides PE 22-28, G/A-PE 22-28 et biotinylated-G/A-PE 22-28 pour les études ultérieures.

Nous avons montré que les analogues de la Spadine bloquent TREK-1 avec une IC_{50} 300 fois plus forte, autrement dit avec une efficacité bien plus importante que la Spadine (Mazella et al., 2010; Moha Ou Maati et al., 2012b). Mais beaucoup plus intéressant, ces peptides sont beaucoup plus stables *in vivo* que la Spadine. En effet, aux doses de 30 et 40 µg/kg, l'efficacité *in vivo* de ces antidépresseurs, mesurée par FST, se maintient environ 24 heures. Il s'agit d'une amélioration importante par rapport à la Spadine, car dans les mêmes conditions, et à la dose de 100 µg/kg, l'effet de la Spadine ne durait que 6 h (Veyssiere et al., 2015).

De plus, les analogues de la Spadine ont conservé leur spécificité pour les canaux TREK-1 (Moha Ou Maati et al., 2012b). Ils sont incapables d'inhiber les canaux TREK-2 et TRAAK, les deux autres membres de la sous-famille des canaux TREK (Kim et al., 2001) (Honore, 2007). Cette spécificité pour le canal TREK-1 pourrait s'expliquer par les différences de séquence entre les trois canaux : TREK-1 et TREK-2 partagent 63 % de leur séquence, et TREK-1 et TRAAK seulement 45 % (Noel et al., 2011). Ils sont également incapables d'inhiber les canaux TRESK (Lafreniere et al., 2010) (Wood, 2010) et TASK-1 (Lauritzen et al., 2003), deux canaux K_{2P} importants dans le cerveau et qui, comme TREK-1, sont modulés par des anesthésiques volatils (Patel and Honore, 2001). Là encore, les différences de séquence pourraient expliquer l'absence d'effets, les homologies entre TREK-1 et les deux canaux étant d'environ 50% (Noel et al., 2011). Mais la propriété la plus remarquable est qu'ils sont sans effet sur les canaux hERG. Ces canaux sont responsables du courant IKr cardiaque, l'un des principaux courants potassiques repolarisants des ventricules cardiaques (Sanguinetti et Jurkiewicz, 1990 ; Cheng et Kodama, 2004). Une inhibition de ce courant étant extrêmement

dangereuse (pouvant aller jusqu'à la mort), toutes les molécules à visée thérapeutique doivent être exemptes d'effets sur ce canal pour pouvoir envisager un traitement en clinique humaine. La Spadine et ses analogues bloquent plus efficacement les canaux TREK-1 lorsqu'ils sont activés par l'acide arachidonique, ce qui indique la nécessité d'une conformation à l'état ouvert du canal pour une inhibition maximale. Nous avons cependant également observé une inhibition, bien que moins efficace, de TREK-1 en condition basale. Cet effet plus faible pourrait être due à la difficulté de la Spadine à accéder à son site de fixation lorsque le canal est dans une conformation fermée.

Nous avons confirmé que les analogues de la Spadine ont également conservé les propriétés AD de la Spadine. En effet, ces derniers se comportent comme des antidépresseurs dans le FST mais également dans le test du LH, deux tests couramment et largement utilisés par les industries pharmaceutiques pour caractériser les nouveaux médicaments contre la dépression. Une propriété très importante, est que ces actions antidépressives des analogues sont conservées quel que soit la voie d'administration du traitement : i.p., i.v. , sc (sous cutanée) ou orale. Nous avons également observé que ces effets antidépresseurs sont toujours présents dans un modèle de dépression induite chimiquement, par un traitement longue durée avec la corticostérone. Ces observations sont autant d'arguments pour la réalité de l'action antidépressive de ces peptides. La rapidité d'action de la Spadine est conservée par les analogues, puisque tout comme la Spadine, ils sont efficaces après un traitement de seulement 4 jours. Cette propriété est un atout majeur pour le « futur médicament » car la majorité des suicides survient dans la première semaine suivant la mise en place d'un traitement avec des antidépresseurs (Moller, 2003).

L'hypothèse monoaminergique de la dépression a été remplacée ou complétée par d'autres hypothèses plus récentes, principalement l'hypothèse neurotrophique et/ou de neurogenèse. Cette hypothèse suggère qu'une diminution des facteurs neurotrophiques, comme le BDNF, ou de la neurogenèse de l'hippocampe adulte sont associés d'une manière ou d'une autre à la dépression (Yohn et al., 2017). Les AD classiques mettent plusieurs semaines à produire une activité antidépressive, un mécanisme que l'on pense médié par la neurogenèse (Santarelli et al., 2003) (Malberg and Schechter, 2005). Par exemple, les traitements chroniques de la maladie d'Alzheimer induisent une neurogenèse dans l'hippocampe (Duman et al., 2001) (Schechter et al., 2005), qui toutefois n'apparaît qu'après 2 à 4 semaines d'administration. La Spadine est capable d'augmenter l'incorporation de BrdU (marqueur des cellules en division) et l'activation

de CREB (facteur de transcription fortement impliqué dans la plasticité neuronale) après seulement 4 jours de traitement (Mazella et al., 2010). Une propriété que ses analogues ont conservée. Les analogues de la Spadine sont également capables d'induire, après un traitement de 4 jours, une augmentation de la neurogenèse dans le gyrus denté. Mais aussi de l'expression de PSD-95, un biomarqueur de la synaptogenèse. Ces résultats indiquent que la plupart des neurones néoformés sont fonctionnels.

Ce délai de 4 jours équivaut au laps de temps nécessaire au développement de la neurogenèse dans l'hippocampe (Devader et al., 2015). L'augmentation rapide de l'expression du BDNF dans l'hippocampe après l'administration *in vivo* de Spadine souligne le fait que la Spadine et les peptides dérivés induisent une expression rapide du BDNF. Cette expression rapide du BDNF se distingue de l'expression lente observée avec les AD classiques. Cette phase rapide a également été décrite pour la Kétamine (Kavalali and Monteggia, 2015). Néanmoins, les voies cellulaires d'activation de la neurogenèse par la Kétamine et la Spadine sont différentes. La Kétamine utilise la voie mTOR (Kavalali and Monteggia, 2015) tandis que la Spadine n'utilise pas cette voie de signalisation mTOR (Devader et al., 2015).

Au moins un tiers des survivants de l'AVC souffre de dépression, appelée dépression post-AVC ou Post Stroke Depression (PSD). Le développement d'une telle dépression survenant à la suite d'un AVC est cliniquement très important parce que la PSD est associée à une mortalité accrue, un ralentissement de la récupération et des déficits fonctionnels d'autant plus sévères que l'état dépressif s'installe. Il existe un certain nombre de facteurs de risque établis pour le développement d'une dépression à la suite d'une ischémie cérébrale. L'incapacité physique, la gravité de l'AVC et la déficience cognitive occupent une place particulièrement importante dans la documentation clinique (pour revue voir (Hackett and Anderson, 2005)).

La plupart des études récentes sur la récupération post-AVC ont souligné l'importance et l'efficacité de l'utilisation des antidépresseurs. Cependant, les effets secondaires (nausées, vertiges, tendance suicidaires, …) de ces molécules sont un frein important dans la population à risque que sont les victimes d'AVC. Ces observations sont à l'origine de la deuxième partie de mon projet de doctorat : étudier les effets des analogues de la Spadine face à l'AVC et à la PSD.

Les mécanismes à l'origine du développement de la PSD sont complexes et mal connus, donc difficiles à modéliser chez les rongeurs. Cependant aujourd'hui, il existe plusieurs modèles reconnus (Kronenberg et al., 2014). Ils permettent de mimer les principales caractéristiques de

l'AVC et ses conséquences délétères observées dans des situations cliniques réelles. La plupart des études précliniques utilisent un modèle de MCAO combiné à un CMS ou à un isolement (Kronenberg et al., 2014). Cependant pour éviter d'induire un biais induit par cet ajout de stress, dans cette étude, nous avons choisi d'utiliser un modèle de MCAO seule. En effet, bien que le CMS induise des comportements dépressifs, les facteurs de stress appliqués tels que l'eau froide et les chocs électriques peuvent également entraîner des dommages neuronaux qui pourraient altérer l'effet de l'AVC lui-même. Dans notre étude nous avons prouvé que ce modèle de MCAO seul était suffisant pour induire une PSD. En effet, 10 semaines après la MCAO le temps d'immobilité dans le test du FST était très largement augmenté chez les animaux opérés. Cette augmentation du temps d'immobilité rend compte de l'établissement de l'état dépressif. Ces 10 semaines correspondent à un délai, chez la souris, comparable à celui observé en clinique humaine où très souvent la dépression apparaît entre deux mois et un an après l'AVC (Francisco, 1993). Ce modèle mime également les séquelles caractéristiques de l'AVC ischémique et de la PSD associée, comme les déficits moteurs et cognitifs, la perte neuronale et la neurogenèse altérée (Kronenberg et al., 2014).

Notre étude démontre pour la première fois que la Mini-Spadine induit une neuroprotection contre l'AVC et la PSD subséquente, par rapport à la Spadine et à l'Escitalopram. Grâce au protocole que j'ai pu développer, nous avons montré que lors de la phase aiguë de la récupération post-AVC (quelques heures à quelques jours), la Mini-Spadine augmentait le taux de survie des souris soumises à la MCAO, prévenait la perte de poids et diminuait le volume de l'infarctus provoqué et que dans la phase chronique (au-delà de 7 jours), la Mini-Spadine augmente la neurogenèse et améliore les déficits moteurs et cognitifs induits par l'ischémie et empêche la dégénérescence dopaminergique retardée de la *substantia nigra* généralement observée à la suite d'une ischémie cérébrale,.

Ces effets bénéfiques résultent probablement de son action biphasique sur le canal TREK-1. En effet, une approche électrophysiologique nous a montré que de faibles doses de Mini-Spadine induisaient une activation TREK-1. Or l'activation des canaux TREK-1 a été mise en évidence dans la protection cérébrale de la phase aiguë d'un AVC ((Blondeau et al., 2002a) (Blondeau et al., 2002b) (Heurteaux et al., 2006a) (Lauritzen et al., 2000) (Quast, 1992)). Cette protection aiguë est validée par la réduction du nombre de décès chez la souris et la diminution du volume de l'infarctus 24 heures après la MCAO. Ces résultats sont tout à fait conformes aux travaux antérieurs démontrant que l'activation de TREK-1 joue un rôle clé dans les mécanismes de neuroprotection après un AVC. Comme dans le cas d'autres ouvreurs TREK-1 (AGPI par

exemple), l'activation des courants TREK-1 dans les neurones par de faibles doses de Mini-Spadine hyperpolarise probablement les membranes plasmiques au niveau des terminaisons synaptiques, réduisant ainsi le flux de Ca^{2+} et le glutamate sécrété, ce qui se traduit par une hyperpolarisation post-synaptique (Blondeau et al., 2002a) (Blondeau et al., 2002b) (Heurteaux et al., 2006a) (Lauritzen et al., 2000) (Quast, 1992). Ces processus favoriseraient le blocage par le Mg^{2+} du canal associé aux récepteurs NMDA et contrebalanceraient la dépolarisation induite par le glutamate. Ainsi, l'activation de TREK-1 par la Mini-Spadine pourrait entraîner les mêmes variations du potentiel de membrane.

A la suite d'un AVC il y a formation d'une cicatrice gliale au niveau de la lésion neuronale. En conditions physiologiques, les astrocytes participent à la régulation de l'homéostasie acido-basique par le biais de divers échangeurs et co-transporteurs. Ces dernières années, les preuves de leur importante implication dans la physiopathologie de l'AVC se sont accumulées (Nedergaard and Dirnagl, 2005). En effet, ils sont activés et leur prolifération est stimulée dans les régions ischémiques. Tout comme dans les neurones, TREK-1 est également largement exprimé dans les astrocytes en conditions physiologiques. Il contribue à leur conductance passive (Zhou et al., 2009). TREK-1 est régulé à la hausse dans ces cellules après la MCAO, ce qui est en corrélation avec l'astrogliose réactive qui se met en place dans la région lésée (Wang et al., 2012). Dans ces conditions, TREK-1 pourrait établir le potentiel négatif de la membrane de repos des astrocytes et ainsi sauver leurs fonctions homéostasiques (Zhou et al., 2009), et donc offrir au cerveau une protection endogène face à l'AVC.

Ce travail a également démontré pour la première fois que la Mini-Spadine diminue fortement les altérations comportementales de type dépressif induites par la MCAO dans la phase chronique de l'AVC, mesurées en FST et NSF. L'une des principales caractéristiques du syndrome de dépression chronique après un AVC est l'altération à long terme du système dopaminergique mésolimbique (Kronenberg et al., 2012). Cela correspond aux lésions des ganglions frontaux et basaux observées chez les patients victimes d'un AVC et liées à l'apparition d'une PSD majeure (Morris et al., 1996) (Vataja et al., 2004). Dans cette étude, nous avons démontré que la Mini-Spadine atténue la dégénérescence dopaminergique de la *substantia nigra,* et prévient l'apparition d'un comportement dépressif qui survient pendant la phase chronique de l'AVC.

La dose plus élevée de Mini-Spadine que nous avons utilisée dans cette étude (Article 2) a été démontrée comme prévenant les symptômes dépressifs grâce à des tests de criblage des

antidépresseurs, tels que FST ou NSF (Article 1) (Heurteaux et al., 2006b) (Mazella et al., 2010). Il s'agit d'un effet lié à l'inhibition de TREK-1. Des données obtenues précédemment (Article 1) (Heurteaux et al., 2006b) (Mazella et al., 2010) suggèrent que l'inhibition chronique de TREK-1 par la Mini-Spadine augmenterait le taux de décharge des neurones du noyau raphé dorsal, et donc, la libération de 5-HT. Cette libération pourrait contribuer à prévenir davantage la PSD. Il faut cependant noter qu'un traitement antidépresseur dans les premiers temps après un AVC peut prévenir la PSD, comme l'indique une méta-analyse d'essais randomisés (Chen et al., 2007). Il serait donc bénéfique d'associer les traitements AD avec les stratégies vasculaires dans la prise en charge des victimes d'AVC dès les premiers jours.

Dans le cerveau des humains ou des rongeurs, la récupération fonctionnelle après un AVC peut être induite par la prolifération des cellules souches neurales elle-même induite par l'AVC (Jin et al., 2001) (Jin et al., 2006) (Murphy and Corbett, 2009). Après l'AVC, les neuroblastes nouvellement formés migrent dans la structure endommagée pour remplacer les neurones morts. Cependant, ce mécanisme potentiel d'autoréparation ne fonctionne que de manière aiguë. En effet, le nombre de neurones générés est faible et leur existence transitoire. La récupération des déficits cognitifs induits par l'AVC est considérablement entravée par la perturbation génétique de la neurogenèse, cela souligne l'importance des cellules neuronales non différenciées dans la récupération cognitive post-AVC (Sun et al., 2013). La prolifération cellulaire maximale dans le cerveau adulte se produit une à deux semaines après l'AVC (Arvidsson et al., 2002) (Jin et al., 2001). De même, dans les cultures de neurosphères, le recrutement des cellules souches neuronales n'est stimulé que pendant la première semaine post-ischémie (Zhang et al., 2004). Dans notre étude, nous avons analysé la neurogenèse à 3 et 10 semaines, mais nous ne l'avons pas mesurée quelques jours seulement après la MCAO. Il s'agit probablement de la raison pour laquelle nous n'avons pas observé ce pic de neurogenèse normalement provoqué par l'AVC. Cependant, comme nous avons analysé la neurogenèse dans la phase chronique de l'AVC, de façon intéressante et par rapport au contrôle, nous avons pu établir que la Mini-Spadine induit une production extensive et durable de nouveaux neurones, jusqu'à 10 semaines après la MCAO, stimulant probablement l'autoréparation et la récupération neurologique.

L'hypothèse marquante de l'implication majeure de la plasticité synaptique dans le développement, et donc le traitement de la PSD nous a également orientés vers l'étude des effets de la Mini-Spadine sur la synaptogenèse. Nous avons constaté une forte augmentation de l'expression de PSD-95 et de la synapsine, deux protéines clés impliquées dans le réseau

synaptique. Trois semaines après la MCAO, le niveau de ces deux marqueurs est beaucoup plus important dans le cortex ipsilatéral (un site majeur du remodelage des circuits neuraux (Carmichael, 2003)). Cette augmentation pourrait être un mécanisme crucial à l'origine des effets bénéfiques de la Mini-Spadine dans les récupérations fonctionnelle et cognitive post-AVC.

D'autres résultats préliminaires ont également montré que la Spadine interagit avec le récepteur 1 de la neurotensine (NTR1), bien connu pour être impliqué dans la neuroprotection. En effet, tout comme la neurotensine (NT), la Spadine à 10^{-6} M se lie à NTR1. La NT et ses analogues qui sont de puissants agonistes du NTR1, provoquent l'hypothermie (neuroprotecteur) et ont des effets protecteurs marqués contre les lésions cérébrales (Choi et al., 2012) (Fantegrossi et al., 2005) (Lee et al., 2014) (Lee et al., 2016) (Orwig et al., 2009) (Wei et al., 2013). Ainsi, la Mini-Spadine comme la Spadine pourrait interagir avec le NTR1 et contribuer à induire la protection cérébrale.

Dans notre étude, l'Escitalopram a été choisi comme témoin positif parce qu'au cours des deux dernières décennies, il a été développé pour une utilisation clinique dans le traitement de la dépression majeure et des troubles anxieux (Burke, 2002) (Montgomery et al., 2001). Les études cliniques ont montré que l'Escitalopram est un AD efficace, mais que, comme la plupart de ses homologues, il a des effets indésirables (somnolence, problèmes digestifs, dysfonction sexuelle, troubles du sommeil ou du rythme cardiaque) et nécessite un laps de temps relativement long (2-4 semaines) avant d'être efficace.

En plus de ses performances plus avantageuses, contrairement à l'Escitalopram, la Mini-Spadine a l'avantage d'avoir un délai d'action rapide (4 jours) et elle est sans effets secondaires (Article 1).

Les résultats obtenus dans ce travail montrent clairement que les effets de la Mini-Spadine sur les séquelles de l'AVC (perte de poids, rotarod et pole test, Piscine de Morris, perte de neurones dopaminergiques) et sur la PSD sont plus rapides (5 semaines au lieu de 10 semaines en FST), mais aussi plus prononcés que ceux obtenus avec l'Escitalopram.

Conclusion et Perspectives

Ce travail de Doctorat s'est orienté autour de deux axes.
L'étude des analogues courts de la Spadine a révélé que ces peptides sont non seulement plus stables *in vivo,* mais aussi plus affins pour TREK-1 et plus efficace face à la dépression. Ces résultats premiers précliniques encourageants ne demandent qu'à être complétés. Il s'agit en effet d'une condition *sine qua none* pour pouvoir espérer amener ces petits peptides aux essais cliniques de phase I et II.
Les résultats que nous avons obtenus montrent que les analogues de la Spadine sont plus efficaces dans l'induction de la neurogenèse hippocampique. Or des travaux précédents avaient montré que la Spadine ne provoquait pas de neurogenèse dans le modèle de dépression induit par la corticostérone. Il sera intéressant de savoir si la Mini-Spadine, qui est plus efficace, peut induire une neurogenèse dans ce modèle.

La dépression est une pathologie complexe et multifactorielle, il est donc difficile d'en modéliser tous les aspects. Toutefois, de nombreux modèles animaux ont été mis au point mais chacun ne mime qu'un symptôme de la dépression, ce peut être le désespoir, l'anhédonie, les troubles de l'appétit ou du sommeil, ...
Ces modèles ont différentes origines : génétique, chimique, chirurgicale, comportementale …
Les souris Rouen (El Yacoubi and Vaugeois, 2007), ou encore les souris C57BL/6NTac (Nestler et al., 2002) (Carlezon et al., 2005) sont des exemples de modèles génétiques. Parmi les modèles chimiquement induits, on peut citer le traitement chronique avec de la corticostérone, qui entraîne le développement d'un état dépressif (le modèle que nous avons utilisé dans nos études) (Zhao et al., 2008). Une bulbectomie permet de créer un modèle chirurgical (Linge et al., 2013). Il est également possible de provoquer un phénotype dépressif en soumettant les animaux à un stress chronique ou traumatisant (succession de situations stressantes dans le modèle du CMS (Chronic Mild Stress) (Willner, 2017), séparation des nouveaux nés et de leur mère (Ognibene et al., 2008)). Nous n'avons utilisé dans cette étude que le modèle d'induction par la corticostérone, il serait donc judicieux de refaire nos tests sur un autre modèle, comme une lignée mutante par exemple.

Mes travaux ont également démontré que les propriétés particulières de la Mini-Spadine sur le canal TREK-1 permettent une amélioration des déficits induits par l'AVC, non seulement durant la phase aiguë, mais également pendant la récupération à long terme.

L'origine de la PSD reste encore floue, et les hypothèses sont nombreuses. Cependant l'implication de la plasticité synaptique dans la récupération post-AVC est indiscutable. Mon travail de thèse s'est majoritairement concentré sur la récupération à long terme après un AVC. Il est cependant nécessaire de s'intéresser également aux effets de notre traitement dans la phase aiguë. Notamment en lien avec la plasticité synaptique, il serait important de mesurer l'effet du traitement sur des marqueurs tels que le BDNF, PSD-95 et la Synapsine dans les quelques heures à quelques jours suivant l'AVC.

Les faibles doses de Mini-Spadine permettent de diminuer la taille des infarctus après 24h. Il serait opportun de regarder si ce traitement à faible dose pendant la première semaine après un AVC peut avoir des effets positifs sur le développement d'une PSD à plus long terme. Parallèlement étudier si le fait d'initier le traitement peptidique à forte dose sans neuroprotection préalable quelques semaines après l'événement ischémique pourrait toujours réduire la PSD.

L'AVC est une pathologie aux multiples processus. Savoir à quel niveau et à quel moment l'activation de TREK-1 aurait les effets les plus bénéfiques. Cela constituerait des informations importantes pour la prise en charge des patients (délai de traitement, …). Il faudrait donc également s'intéresser, par exemple, aux effets du traitement sur l'inflammation (dosage de cytokines), un mécanisme majeur dans l'AVC.

Durant ma thèse, je n'ai traité mes souris que 15 à 30 minutes après l'AVC. Il sera donc important de déterminer la fenêtre thérapeutique de la Mini-Spadine à la suite d'un AVC.

La neurogenèse et la synaptogenèses semblent avoir un rôle crucial aussi bien dans le cas de la dépression que de la PSD. Pour pouvoir confirmer ce fait, il serait également judicieux de reproduire nos études en bloquant la neurogenèse (en utilisant du Témozolomide par exemple, un produit très utilisé dans les études sur la neurogenèse et dont les effets sur la santé de l'animal sont minimes (Castilla-Ortega et al., 2016)).

Qu'il s'agisse de l'axe de la dépression ou celui de l'AVC, l'une des questions majeures à élucider est de caractériser les mécanismes clefs à l'origine des effets de la Spadine et de ses analogues. Pourquoi ont-ils des effets opposés sur TREK-1 selon la concentration utilisée ? Quels sont exactement les mécanismes moléculaires impliqués ? Une autre donnée importante est le fait que lors d'études précédentes, il a été montré que le traitement avec la Spadine ne provoque pas les mêmes effets délétères que ceux observés chez des souris TREK-1$^{-/-}$ (faiblesse face à l'épilepsie, neuroprotection altérée, …). Une de nos hypothèses est que ceci est dû à la présence de TREK-1 sur les neurones GABAergiques (Sandoz et al., 2011). En effet, l'inhibition de TREK-1 par la Spadine sur de tels neurones entraînerait une sécrétion plus

importante de GABA. Laquelle est connue comme ayant un effet neuroprotecteur face aux chocs ischémiques et épileptiques (Ginsberg, 2008). Cependant, nous n'avons aucune certitude à ce sujet, et cette hypothèse reste à être prouvée.

Si les mécanismes moléculaires ne sont pas encore totalement élucidés, ce travail a apporté quelques éléments de réponse. Il reste encore beaucoup de travail pour caractériser plus finement les analogues de la Spadine. Toutefois, nos résultats sont autant d'arguments très positifs, qui s'ajoutent à ceux que l'équipe a déjà obtenus, pour proposer les analogues de la Spadine, très prochainement à des essais cliniques pour confirmer à la fois leurs effets antidépresseurs et neuroprotecteurs.

Bibliographie

Adessi, C., and Soto, C. (2002). Converting a peptide into a drug: strategies to improve stability and bioavailability. *Curr Med Chem* 9(9)**,** 963-978.

Ahmadinejad, F., Geir Moller, S., Hashemzadeh-Chaleshtori, M., Bidkhori, G., and Jami, M.S. (2017). Molecular Mechanisms behind Free Radical Scavengers Function against Oxidative Stress. *Antioxidants (Basel)* 6(3). doi: antiox6030051 [pii]10.3390/antiox6030051.

Alia, C., Spalletti, C., Lai, S., Panarese, A., Lamola, G., Bertolucci, F., et al. (2017). Neuroplastic Changes Following Brain Ischemia and their Contribution to Stroke Recovery: Novel Approaches in Neurorehabilitation. *Front Cell Neurosci* 11**,** 76. doi: 10.3389/fncel.2017.00076.

Alloui, A., Zimmermann, K., Mamet, J., Duprat, F., Noel, J., Chemin, J., et al. (2006). TREK-1, a K+ channel involved in polymodal pain perception. *EMBO J.* 25(11)**,** 2368-2376.

Amantea, D., Nappi, G., Bernardi, G., Bagetta, G., and Corasaniti, M.T. (2009). Post-ischemic brain damage: pathophysiology and role of inflammatory mediators. *FEBS J* 276(1)**,** 13-26. doi: EJB6766 [pii]10.1111/j.1742-4658.2008.06766.x.

Amarenco, P., Bogousslavsky, J., Caplan, L.R., Donnan, G.A., Wolf, M.E., and Hennerici, M.G. (2013). The ASCOD phenotyping of ischemic stroke (Updated ASCO Phenotyping). *Cerebrovasc Dis* 36(1)**,** 1-5. doi: 000352050 [pii]10.1159/000352050.

Angelelli, P., Paolucci, S., Bivona, U., Piccardi, L., Ciurli, P., Cantagallo, A., et al. (2004). Development of neuropsychiatric symptoms in poststroke patients: a cross-sectional study. *Acta Psychiatr Scand* 110(1)**,** 55-63. doi: 10.1111/j.1600-0447.2004.00297.xACP297 [pii].

Arvidsson, A., Collin, T., Kirik, D., Kokaia, Z., and Lindvall, O. (2002). Neuronal replacement from endogenous precursors in the adult brain after stroke. *Nat Med* 8(9)**,** 963-970. doi: 10.1038/nm747nm747 [pii].

Askim, T., Indredavik, B., and Haberg, A. (2010). Internally and externally paced finger movements differ in reorganization after acute ischemic stroke. *Arch Phys Med Rehabil* 91(10)**,** 1529-1536. doi: S0003-9993(10)00602-7 [pii]10.1016/j.apmr.2010.07.217.

Astrup, J., Siesjo, B.K., and Symon, L. (1981). Thresholds in cerebral ischemia - the ischemic penumbra. *Stroke* 12(6)**,** 723-725.

Attwell, D., Mishra, A., Hall, C.N., O'Farrell, F.M., and Dalkara, T. (2016). What is a pericyte? *J Cereb Blood Flow Metab* 36(2)**,** 451-455. doi: 0271678X15610340 [pii]10.1177/0271678X15610340.

Ay, H., Benner, T., Arsava, E.M., Furie, K.L., Singhal, A.B., Jensen, M.B., et al. (2007). A computerized algorithm for etiologic classification of ischemic stroke: the Causative Classification of Stroke System. *Stroke* 38(11)**,** 2979-2984. doi: STROKEAHA.107.490896 [pii]10.1161/STROKEAHA.107.490896.

Ayerbe, L., Ayis, S., Wolfe, C.D., and Rudd, A.G. (2013). Natural history, predictors and outcomes of depression after stroke: systematic review and meta-analysis. *Br J Psychiatry* 202(1)**,** 14-21. doi: S0007125000273133 [pii]10.1192/bjp.bp.111.107664.

Azouvi, P., Bartolomeo, P., Beis, J.M., Perennou, D., Pradat-Diehl, P., and Rousseaux, M. (2006). A battery of tests for the quantitative assessment of unilateral neglect. *Restor Neurol Neurosci* 24(4-6)**,** 273-285.

Badhiwala, J.H., Nassiri, F., Alhazzani, W., Selim, M.H., Farrokhyar, F., Spears, J., et al. (2015). Endovascular Thrombectomy for Acute Ischemic Stroke: A Meta-analysis. *JAMA* 314(17)**,** 1832-1843. doi: 2467553 [pii]10.1001/jama.2015.13767.

Bagriantsev, S.N., Ang, K.H., Gallardo-Godoy, A., Clark, K.A., Arkin, M.R., Renslo, A.R., et al. (2013). A high-throughput functional screen identifies small molecule regulators of temperature- and mechano-sensitive K2P channels. *ACS Chem Biol* 8(8)**,** 1841-1851. doi: 10.1021/cb400289x.

Baharoglu, M.I., Cordonnier, C., Al-Shahi Salman, R., de Gans, K., Koopman, M.M., Brand, A., et al. (2016). Platelet transfusion versus standard care after acute stroke due to spontaneous cerebral haemorrhage associated with antiplatelet therapy (PATCH): a randomised, open-label, phase 3 trial. *Lancet* 387(10038)**,** 2605-2613. doi: S0140-6736(16)30392-0 [pii]10.1016/S0140-6736(16)30392-0.

Bambico, F.R., and Belzung, C. (2013). Novel insights into depression and antidepressants: a synergy between synaptogenesis and neurogenesis? *Curr Top Behav Neurosci* 15**,** 243-291. doi: 10.1007/7854_2012_234.

Bansal, Y., and Kuhad, A. (2016). Mitochondrial Dysfunction in Depression. *Curr Neuropharmacol* 14(6)**,** 610-618. doi: CN-EPUB-74033 [pii].

Barhanin, J., Lesage, F., Guillemare, E., Fink, M., Lazdunski, M., and Romey, G. (1996). K(V)LQT1 and lsK (minK) proteins associate to form the I(Ks) cardiac potassium current. *Nature* 384(6604)**,** 78-80. doi: 10.1038/384078a0.

Barone, F.C., and Feuerstein, G.Z. (1999). Inflammatory mediators and stroke: new opportunities for novel therapeutics. *J Cereb Blood Flow Metab* 19(8)**,** 819-834. doi: 10.1097/00004647-199908000-00001.

Barugh, A.J., Gray, P., Shenkin, S.D., MacLullich, A.M., and Mead, G.E. (2014). Cortisol levels and the severity and outcomes of acute stroke: a systematic review. *J Neurol* 261(3)**,** 533-545. doi: 10.1007/s00415-013-7231-5.

Basic Kes, V., Simundic, A.M., Nikolac, N., Topic, E., and Demarin, V. (2008). Pro-inflammatory and anti-inflammatory cytokines in acute ischemic stroke and their relation to early neurological deficit and stroke outcome. *Clin Biochem* 41(16-17)**,** 1330-1334. doi: S0009-9120(08)00379-2 [pii]10.1016/j.clinbiochem.2008.08.080.

Benakis, C., Garcia-Bonilla, L., Iadecola, C., and Anrather, J. (2014). The role of microglia and myeloid immune cells in acute cerebral ischemia. *Front Cell Neurosci* 8**,** 461. doi: 10.3389/fncel.2014.00461.

Bergendi, L., Benes, L., Durackova, Z., and Ferencik, M. (1999). Chemistry, physiology and pathology of free radicals. *Life Sci* 65(18-19)**,** 1865-1874. doi: S0024-3205(99)00439-7 [pii].

Biernaskie, J., Chernenko, G., and Corbett, D. (2004). Efficacy of rehabilitative experience declines with time after focal ischemic brain injury. *J Neurosci* 24(5)**,** 1245-1254. doi: 10.1523/JNEUROSCI.3834-03.200424/5/1245 [pii].

Bittner, S., Meuth, S.G., Gobel, K., Melzer, N., Herrmann, A.M., Simon, O.J., et al. (2009). TASK1 modulates inflammation and neurodegeneration in autoimmune inflammation of the central nervous system. *Brain* 132(Pt 9)**,** 2501-2516. doi: awp163 [pii]10.1093/brain/awp163.

Blin, S., Ben Soussia, I., Kim, E.J., Brau, F., Kang, D., Lesage, F., et al. (2016). Mixing and matching TREK/TRAAK subunits generate heterodimeric K2P channels with unique properties. *Proc Natl Acad Sci U S A* 113(15)**,** 4200-4205. doi: 1522748113 [pii]10.1073/pnas.1522748113.

Blondeau, N., Lauritzen, I., Widmann, C., Lazdunski, M., and Heurteaux, C. (2002a). A potent protective role of lysophospholipids against global cerebral ischemia and glutamate excitotoxicity in neuronal cultures. *J Cereb Blood Flow Metab* 22(7)**,** 821-834.

Blondeau, N., Widmann, C., Lazdunski, M., and Heurteaux, C. (2002b). Polyunsaturated fatty acids induce ischemic and epileptic tolerance. *Neuroscience* 109(2)**,** 231-241.

Bonita, R., Solomon, N., and Broad, J.B. (1997). Prevalence of stroke and stroke-related disability. Estimates from the Auckland stroke studies. *Stroke* 28(10)**,** 1898-1902.

Bouet, V., Freret, T., Toutain, J., Divoux, D., Boulouard, M., and Schumann-Bard, P. (2007). Sensorimotor and cognitive deficits after transient middle cerebral artery occlusion in

the mouse. *Exp Neurol* 203(2)**,** 555-567. doi: S0014-4886(06)00544-9 [pii]10.1016/j.expneurol.2006.09.006.

Braughler, J.M., and Hall, E.D. (1989). Central nervous system trauma and stroke. I. Biochemical considerations for oxygen radical formation and lipid peroxidation. *Free Radic Biol Med* 6(3)**,** 289-301. doi: 0891-5849(89)90056-7 [pii].

Brohawn, S.G. (2015). How ion channels sense mechanical force: insights from mechanosensitive K2P channels TRAAK, TREK1, and TREK2. *Ann N Y Acad Sci* 1352**,** 20-32. doi: 10.1111/nyas.12874.

Brohawn, S.G., Su, Z., and MacKinnon, R. (2014). Mechanosensitivity is mediated directly by the lipid membrane in TRAAK and TREK1 K+ channels. *Proc Natl Acad Sci U S A* 111(9)**,** 3614-3619. doi: 1320768111 [pii]10.1073/pnas.1320768111.

Brouns, R., and De Deyn, P.P. (2009). The complexity of neurobiological processes in acute ischemic stroke. *Clin Neurol Neurosurg* 111(6)**,** 483-495. doi: S0303-8467(09)00082-1 [pii]10.1016/j.clineuro.2009.04.001.

Brown, A.M. (2004). Drugs, hERG and sudden death. *Cell Calcium* 35(6)**,** 543-547. doi: 10.1016/j.ceca.2004.01.008.

Brunello, A.G., Weissenberger, J., Kappeler, A., Vallan, C., Peters, M., Rose-John, S., et al. (2000). Astrocytic alterations in interleukin-6/Soluble interleukin-6 receptor alpha double-transgenic mice. *Am J Pathol* 157(5)**,** 1485-1493. doi: S0002-9440(10)64787-6 [pii].

Bryer, J.B., Starkstein, S.E., Votypka, V., Parikh, R.M., Price, T.R., and Robinson, R.G. (1992). Reduction of CSF monoamine metabolites in poststroke depression: a preliminary report. *J Neuropsychiatry Clin Neurosci* 4(4)**,** 440-442. doi: 10.1176/jnp.4.4.440.

Buckler, K.J., and Honore, E. (2005). The lipid-activated two-pore domain K+ channel TREK-1 is resistant to hypoxia: implication for ischaemic neuroprotection. *J Physiol* 562(Pt 1)**,** 213-222. doi: jphysiol.2004.077503 [pii]10.1113/jphysiol.2004.077503.

Burke, W.J. (2002). Escitalopram. *Expert Opin Investig Drugs* 11(10)**,** 1477-1486. doi: 10.1517/13543784.11.10.1477.

Busquet, P., Nguyen, N.K., Schmid, E., Tanimoto, N., Seeliger, M.W., Ben-Yosef, T., et al. (2010). CaV1.3 L-type Ca2+ channels modulate depression-like behaviour in mice independent of deaf phenotype. *Int J Neuropsychopharmacol* 13(4)**,** 499-513. doi: S1461145709990368 [pii]10.1017/S1461145709990368.

Carlezon, W.A., Jr., Duman, R.S., and Nestler, E.J. (2005). The many faces of CREB. *Trends Neurosci* 28(8)**,** 436-445. doi: S0166-2236(05)00158-X [pii]10.1016/j.tins.2005.06.005.

Carlo, A.S. (2013). Sortilin, a novel APOE receptor implicated in Alzheimer disease. *Prion* 7(5)**,** 378-382. doi: 26746 [pii]10.4161/pri.26746.

Carmichael, S.T. (2003). Plasticity of cortical projections after stroke. *Neuroscientist* 9(1)**,** 64-75. doi: 10.1177/1073858402239592.

Carmichael, S.T. (2006). Cellular and molecular mechanisms of neural repair after stroke: making waves. *Ann Neurol* 59(5)**,** 735-742. doi: 10.1002/ana.20845.

Carmichael, S.T., Archibeque, I., Luke, L., Nolan, T., Momiy, J., and Li, S. (2005). Growth-associated gene expression after stroke: evidence for a growth-promoting region in peri-infarct cortex. *Exp Neurol* 193(2)**,** 291-311. doi: S0014-4886(05)00010-5 [pii]10.1016/j.expneurol.2005.01.004.

Carson, A.J., MacHale, S., Allen, K., Lawrie, S.M., Dennis, M., House, A., et al. (2000). Depression after stroke and lesion location: a systematic review. *Lancet* 356(9224)**,** 122-126. doi: S0140-6736(00)02448-X [pii]10.1016/S0140-6736(00)02448-X.

Castilla-Ortega, E., Blanco, E., Serrano, A., Ladron de Guevara-Miranda, D., Pedraz, M., Estivill-Torrus, G., et al. (2016). Pharmacological reduction of adult hippocampal

neurogenesis modifies functional brain circuits in mice exposed to a cocaine conditioned place preference paradigm. *Addict Biol* 21(3)**,** 575-588. doi: 10.1111/adb.12248.

Chemin, J., Girard, C., Duprat, F., Lesage, F., Romey, G., and Lazdunski, M. (2003). Mechanisms underlying excitatory effects of group I metabotropic glutamate receptors via inhibition of 2P domain K+ channels. *EMBO J.* 22**,** 5403-5411.

Chemin, J., Patel, A.J., Duprat, F., Lauritzen, I., Lazdunski, M., and Honore, E. (2005). A phospholipid sensor controls mechanogating of the K+ channel TREK-1. *EMBO J* 24(1)**,** 44-53. doi: 10.1038/sj.emboj.7600494.

Chen, C., Wang, L., Rong, X., Wang, W., and Wang, X. (2015a). Effects of fluoxetine on protein expression of potassium ion channels in the brain of chronic mild stress rats. *Acta Pharm Sin B* 5(1)**,** 55-61. doi: 10.1016/j.apsb.2014.12.004S2211-3835(14)00125-7 [pii].

Chen, H.H., Zhang, N., Li, W.Y., Fang, M.R., Zhang, H., Fang, Y.S., et al. (2015b). Overexpression of brain-derived neurotrophic factor in the hippocampus protects against post-stroke depression. *Neural Regen Res* 10(9)**,** 1427-1432. doi: 10.4103/1673-5374.165510NRR-10-1427 [pii].

Chen, L., Sampson, K.J., and Kass, R.S. (2016). Cardiac Delayed Rectifier Potassium Channels in Health and Disease. *Card Electrophysiol Clin* 8(2)**,** 307-322. doi: 10.1016/j.ccep.2016.01.004.

Chen, Y., Guo, J.J., Zhan, S., and Patel, N.C. (2006). Treatment effects of antidepressants in patients with post-stroke depression: a meta-analysis. *Ann Pharmacother* 40(12)**,** 2115-2122. doi: aph.1H389 [pii]10.1345/aph.1H389.

Chen, Y., Patel, N.C., Guo, J.J., and Zhan, S. (2007). Antidepressant prophylaxis for poststroke depression: a meta-analysis. *Int Clin Psychopharmacol* 22(3)**,** 159-166. doi: 10.1097/YIC.0b013e32807fb02800004850-200705000-00006 [pii].

Chen, Y.J., Wallace, B.K., Yuen, N., Jenkins, D.P., Wulff, H., and O'Donnell, M.E. (2015c). Blood-brain barrier KCa3.1 channels: evidence for a role in brain Na uptake and edema in ischemic stroke. *Stroke* 46(1)**,** 237-244. doi: STROKEAHA.114.007445 [pii]10.1161/STROKEAHA.114.007445.

Cheng, J.H., and Kodama, I. (2004). Two components of delayed rectifier K+ current in heart: molecular basis, functional diversity, and contribution to repolarization. *Acta Pharmacol Sin* 25(2)**,** 137-145.

Cheng, S.Y., Zhao, Y.D., Li, J., Chen, X.Y., Wang, R.D., and Zeng, J.W. (2014). Plasma levels of glutamate during stroke is associated with development of post-stroke depression. *Psychoneuroendocrinology* 47**,** 126-135. doi: S0306-4530(14)00178-4 [pii]10.1016/j.psyneuen.2014.05.006.

Choi, D.W. (1985). Glutamate neurotoxicity in cortical cell culture is calcium dependent. *Neurosci Lett* 58(3)**,** 293-297. doi: 0304-3940(85)90069-2 [pii].

Choi, D.W. (1996). Ischemia-induced neuronal apoptosis. *Curr Opin Neurobiol* 6(5)**,** 667-672. doi: S0959-4388(96)80101-2 [pii].

Choi, E.Y., Santoso, S., and Chavakis, T. (2009). Mechanisms of neutrophil transendothelial migration. *Front Biosci (Landmark Ed)* 14**,** 1596-1605. doi: 3327 [pii].

Choi, K.E., Hall, C.L., Sun, J.M., Wei, L., Mohamad, O., Dix, T.A., et al. (2012). A novel stroke therapy of pharmacologically induced hypothermia after focal cerebral ischemia in mice. *FASEB J* 26(7)**,** 2799-2810. doi: 10.1096/fj.11-201822.

Chollet, F., Cramer, S.C., Stinear, C., Kappelle, L.J., Baron, J.C., Weiller, C., et al. (2014). Pharmacological therapies in post stroke recovery: recommendations for future clinical trials. *J Neurol* 261(8)**,** 1461-1468. doi: 10.1007/s00415-013-7172-z.

Chollet, F., Tardy, J., Albucher, J.F., Thalamas, C., Berard, E., Lamy, C., et al. (2011). Fluoxetine for motor recovery after acute ischaemic stroke (FLAME): a randomised placebo-controlled trial. *Lancet Neurol* 10(2)**,** 123-130. doi: 10.1016/S1474-4422(10)70314-8.

Chorev, M., and Goodman, M. (1995). Recent developments in retro peptides and proteins--an ongoing topochemical exploration. *Trends Biotechnol* 13(10)**,** 438-445. doi: S0167-7799(00)88999-4 [pii]10.1016/S0167-7799(00)88999-4.

Chorev, M., Shavitz, R., Goodman, M., Minick, S., and Guillemin, R. (1979). Partially modified retro-inverso-enkephalinamides: topochemical long-acting analogs in vitro and in vivo. *Science* 204(4398)**,** 1210-1212.

Cohen, A., Sagron, R., Somech, E., Segal-Hayoun, Y., and Zilberberg, N. (2009). Pain-associated signals, acidosis and lysophosphatidic acid, modulate the neuronal K(2P)2.1 channel. *Mol Cell Neurosci* 40(3)**,** 382-389. doi: S1044-7431(08)00314-X [pii]10.1016/j.mcn.2008.12.004.

Cole, M.G., Elie, L.M., McCusker, J., Bellavance, F., and Mansour, A. (2001). Feasibility and effectiveness of treatments for post-stroke depression in elderly inpatients: systematic review. *J Geriatr Psychiatry Neurol* 14(1)**,** 37-41. doi: 10.1177/089198870101400109.

Crack, P.J., and Taylor, J.M. (2005). Reactive oxygen species and the modulation of stroke. *Free Radic Biol Med* 38(11)**,** 1433-1444. doi: S0891-5849(05)00037-7 [pii]10.1016/j.freeradbiomed.2005.01.019.

Cramer, S.C. (2000). Stroke recovery: how the computer reprograms itself. Neuronal plasticity: the key to stroke recovery. Kananskis, Alberta, Canada, 19-22 March 2000. *Mol Med Today* 6(8)**,** 301-303. doi: S1357431000017445 [pii].

Cramer, S.C. (2008). Repairing the human brain after stroke: I. Mechanisms of spontaneous recovery. *Ann Neurol* 63(3)**,** 272-287. doi: 10.1002/ana.21393.

Cramer, S.C., and Chopp, M. (2000). Recovery recapitulates ontogeny. *Trends Neurosci* 23(6)**,** 265-271. doi: S0166-2236(00)01562-9 [pii].

Cullen, B., O'Neill, B., Evans, J.J., Coen, R.F., and Lawlor, B.A. (2007). A review of screening tests for cognitive impairment. *J Neurol Neurosurg Psychiatry* 78(8)**,** 790-799. doi: jnnp.2006.095414 [pii]10.1136/jnnp.2006.095414.

Cumming, T.B., Marshall, R.S., and Lazar, R.M. (2013). Stroke, cognitive deficits, and rehabilitation: still an incomplete picture. *Int J Stroke* 8(1)**,** 38-45. doi: 10.1111/j.1747-4949.2012.00972.x.

Dadi, P.K., Vierra, N.C., and Jacobson, D.A. (2014). Pancreatic beta-cell-specific ablation of TASK-1 channels augments glucose-stimulated calcium entry and insulin secretion, improving glucose tolerance. *Endocrinology* 155(10)**,** 3757-3768. doi: 10.1210/en.2013-2051.

Dallerac, G., and Rouach, N. (2016). Astrocytes as new targets to improve cognitive functions. *Prog Neurobiol* 144**,** 48-67. doi: S0301-0082(15)30076-9 [pii]10.1016/j.pneurobio.2016.01.003.

de Bartolomeis, A., and Fiore, G. (2004). Postsynaptic density scaffolding proteins at excitatory synapse and disorders of synaptic plasticity: implications for human behavior pathologies. *Int Rev Neurobiol* 59**,** 221-254. doi: 10.1016/S0074-7742(04)59009-8S0074774204590098 [pii].

De Meyer, S.F., Denorme, F., Langhauser, F., Geuss, E., Fluri, F., and Kleinschnitz, C. (2016). Thromboinflammation in Stroke Brain Damage. *Stroke* 47(4)**,** 1165-1172. doi: STROKEAHA.115.011238 [pii]10.1161/STROKEAHA.115.011238.

De Ryck, A., Brouns, R., Geurden, M., Elseviers, M., De Deyn, P.P., and Engelborghs, S. (2014). Risk factors for poststroke depression: identification of inconsistencies based

on a systematic review. *J Geriatr Psychiatry Neurol* 27(3)**,** 147-158. doi: 0891988714527514 [pii]10.1177/0891988714527514.

Dean, R.T., Fu, S., Stocker, R., and Davies, M.J. (1997). Biochemistry and pathology of radical-mediated protein oxidation. *Biochem J* 324 (Pt 1)**,** 1-18.

Decher, N., Kiper, A.K., and Rinne, S. (2017a). Stretch-activated potassium currents in the heart: Focus on TREK-1 and arrhythmias. *Prog Biophys Mol Biol*. doi: 10.1016/j.pbiomolbio.2017.05.005.

Decher, N., Kiper, A.K., and Rinne, S. (2017b). Stretch-activated potassium currents in the heart: Focus on TREK-1 and arrhythmias. *Prog Biophys Mol Biol* 130(Pt B)**,** 223-232. doi: 10.1016/j.pbiomolbio.2017.05.005.

Dedon, P.C. (2008). The chemical toxicology of 2-deoxyribose oxidation in DNA. *Chem Res Toxicol* 21(1)**,** 206-219. doi: 10.1021/tx700283c.

del Zoppo, G.J., Schmid-Schonbein, G.W., Mori, E., Copeland, B.R., and Chang, C.M. (1991). Polymorphonuclear leukocytes occlude capillaries following middle cerebral artery occlusion and reperfusion in baboons. *Stroke* 22(10)**,** 1276-1283.

Demple, B., and DeMott, M.S. (2002). Dynamics and diversions in base excision DNA repair of oxidized abasic lesions. *Oncogene* 21(58)**,** 8926-8934. doi: 10.1038/sj.onc.1206178.

Denes, A., Thornton, P., Rothwell, N.J., and Allan, S.M. (2010). Inflammation and brain injury: acute cerebral ischaemia, peripheral and central inflammation. *Brain Behav Immun* 24(5)**,** 708-723. doi: S0889-1591(09)00433-4 [pii]10.1016/j.bbi.2009.09.010.

Devader, C., Khayachi, A., Veyssiere, J., Moha Ou Maati, H., Roulot, M., Moreno, S., et al. (2015). In vitro and in vivo regulation of synaptogenesis by the novel antidepressant spadin. *Br J Pharmacol* 172(10)**,** 2604-2617. doi: 10.1111/bph.13083.

DeVane, C.L., and Markowitz, J.S. (2000). Avoiding psychotropic drug interactions in the cardiovascular patient. *Bull Menninger Clin* 64(1)**,** 49-59.

Devilliers, M., Busserolles, J., Lolignier, S., Deval, E., Pereira, V., Alloui, A., et al. (2013). Activation of TREK-1 by morphine results in analgesia without adverse side effects. *Nat Commun* 4**,** 2941. doi: 10.1038/ncomms3941.

Dey, D., Eckle, V.S., Vitko, I., Sullivan, K.A., Lasiecka, Z.M., Winckler, B., et al. (2014). A potassium leak channel silences hyperactive neurons and ameliorates status epilepticus. *Epilepsia* 55(2)**,** 203-213. doi: 10.1111/epi.12472.

Dillon, D.G., Bogdan, R., Fagerness, J., Holmes, A.J., Perlis, R.H., and Pizzagalli, D.A. (2010). Variation in TREK1 gene linked to depression-resistant phenotype is associated with potentiated neural responses to rewards in humans. *Hum Brain Mapp* 31(2)**,** 210-221. doi: 10.1002/hbm.20858.

Dirnagl, U., Iadecola, C., and Moskowitz, M.A. (1999). Pathobiology of ischaemic stroke: an integrated view. *Trends Neurosci* 22(9)**,** 391-397. doi: S0166-2236(99)01401-0 [pii].

Djillani, A., Pietri, M., Mazella, J., Heurteaux, C., and Borsotto, M. (2019). Fighting against depression with TREK-1 blockers: Past and future. A focus on spadin. *Pharmacol Ther* 194**,** 185-198. doi: S0163-7258(18)30178-5 [pii]10.1016/j.pharmthera.2018.10.003.

Djillani, A., Pietri, M., Moreno, S., Heurteaux, C., Mazella, J., and Borsotto, M. (2017). Shortened Spadin Analogs Display Better TREK-1 Inhibition, In Vivo Stability and Antidepressant Activity. *Front Pharmacol* 8**,** 643. doi: 10.3389/fphar.2017.00643.

Dugan, L.L., Sensi, S.L., Canzoniero, L.M., Handran, S.D., Rothman, S.M., Lin, T.S., et al. (1995). Mitochondrial production of reactive oxygen species in cortical neurons following exposure to N-methyl-D-aspartate. *J Neurosci* 15(10)**,** 6377-6388.

Duman, R.S., Nakagawa, S., and Malberg, J. (2001). Regulation of adult neurogenesis by antidepressant treatment. *Neuropsychopharmacology* 25(6)**,** 836-844. doi: S0893133X0100358X [pii]10.1016/S0893-133X(01)00358-X.

Duprat, F., Lesage, F., Patel, A.J., Fink, M., Romey, G., and Lazdunski, M. (2000). The Neuroprotective Agent Riluzole Activates the Two P-Domain K^+ Channels TREK-1 and TRAAK. *Mol. Pharmacol.* 57**,** 906-912.

Egan, M.F., Kojima, M., Callicott, J.H., Goldberg, T.E., Kolachana, B.S., Bertolino, A., et al. (2003). The BDNF val66met polymorphism affects activity-dependent secretion of BDNF and human memory and hippocampal function. *Cell* 112(2)**,** 257-269. doi: S0092867403000357 [pii].

El Yacoubi, M., and Vaugeois, J.M. (2007). Genetic rodent models of depression. *Curr Opin Pharmacol* 7(1)**,** 3-7. doi: S1471-4892(06)00198-6 [pii]10.1016/j.coph.2006.11.002.

Emberson, J., Lees, K.R., Lyden, P., Blackwell, L., Albers, G., Bluhmki, E., et al. (2014). Effect of treatment delay, age, and stroke severity on the effects of intravenous thrombolysis with alteplase for acute ischaemic stroke: a meta-analysis of individual patient data from randomised trials. *Lancet* 384(9958)**,** 1929-1935. doi: S0140-6736(14)60584-5 [pii]10.1016/S0140-6736(14)60584-5.

Endoh, M., Maiese, K., and Wagner, J. (1994). Expression of the inducible form of nitric oxide synthase by reactive astrocytes after transient global ischemia. *Brain Res* 651(1-2)**,** 92-100. doi: 0006-8993(94)90683-1 [pii].

Engel, O., Kolodziej, S., Dirnagl, U., and Prinz, V. (2011). Modeling stroke in mice - middle cerebral artery occlusion with the filament model. *J Vis Exp* (47). doi: 2423 [pii]10.3791/2423.

Esparrago Llorca, G., Castilla-Guerra, L., Fernandez Moreno, M.C., Ruiz Doblado, S., and Jimenez Hernandez, M.D. (2015). Post-stroke depression: an update. *Neurologia* 30(1)**,** 23-31. doi: S0213-4853(12)00203-4 [pii]10.1016/j.nrl.2012.06.008.

Esseltine, J.L., and Scott, J.D. (2013). AKAP signaling complexes: pointing towards the next generation of therapeutic targets? *Trends Pharmacol Sci* 34(12)**,** 648-655. doi: S0165-6147(13)00189-2 [pii]10.1016/j.tips.2013.10.005.

Fang, Y., Huang, X., Wan, Y., Tian, H., Tian, Y., Wang, W., et al. (2017). Deficiency of TREK-1 potassium channel exacerbates secondary injury following spinal cord injury in mice. *J Neurochem* 141(2)**,** 236-246. doi: 10.1111/jnc.13980.

Fantegrossi, W.E., Ko, M.C., Woods, J.H., and Richelson, E. (2005). Antinociceptive, hypothermic, hypotensive, and reinforcing effects of a novel neurotensin receptor agonist, NT69L, in rhesus monkeys. *Pharmacol Biochem Behav* 80(2)**,** 341-349. doi: S0091-3057(04)00394-6 [pii]10.1016/j.pbb.2004.12.005.

Fava, M., and Davidson, K.G. (1996). Definition and epidemiology of treatment-resistant depression. *Psychiatr Clin North Am* 19(2)**,** 179-200. doi: S0193-953X(05)70283-5 [pii].

Fava, M., Johe, K., Ereshefsky, L., Gertsik, L.G., English, B.A., Bilello, J.A., et al. (2016). A Phase 1B, randomized, double blind, placebo controlled, multiple-dose escalation study of NSI-189 phosphate, a neurogenic compound, in depressed patients. *Mol Psychiatry* 21(10)**,** 1372-1380. doi: mp2015178 [pii]10.1038/mp.2015.178.

Feigin, V.L., and Krishnamurthi, R. (2010). Public health strategies could reduce the global stroke epidemic. *Lancet Neurol* 9(9)**,** 847-848. doi: S1474-4422(10)70190-3 [pii]10.1016/S1474-4422(10)70190-3.

Ferguson, J.M. (2001). SSRI Antidepressant Medications: Adverse Effects and Tolerability. *Prim Care Companion J Clin Psychiatry* 3(1)**,** 22-27.

Ferrarese, C., Mascarucci, P., Zoia, C., Cavarretta, R., Frigo, M., Begni, B., et al. (1999). Increased cytokine release from peripheral blood cells after acute stroke. *J Cereb Blood Flow Metab* 19(9)**,** 1004-1009. doi: 10.1097/00004647-199909000-00008.

Ferrari, F., Devecchi, E., Pero, G., Gorini, A., and Villa, R.F. (2016). Bioenergetic characterization of lymphocytes from stroke patients. *Cerebrovasc Dis* 41(S4).

Ferrari, F., and Villa, R.F. (2017). The Neurobiology of Depression: an Integrated Overview from Biological Theories to Clinical Evidence. *Mol Neurobiol* 54(7)**,** 4847-4865. doi: 10.1007/s12035-016-0032-y10.1007/s12035-016-0032-y [pii].

Fink, K., Zhu, J., Namura, S., Shimizu-Sasamata, M., Endres, M., Ma, J., et al. (1998). Prolonged therapeutic window for ischemic brain damage caused by delayed caspase activation. *J Cereb Blood Flow Metab* 18(10)**,** 1071-1076. doi: 10.1097/00004647-199810000-00003.

Fink, M., Duprat, F., Lesage, F., Reyes, R., Romey, G., Heurteaux, C., et al. (1996). Cloning, functional expression and brain localization of a novel unconventional outward rectifier K+ channel. *EMBO J.* 15**,** 6854-6862.

Finlayson, K., Witchel, H.J., McCulloch, J., and Sharkey, J. (2004). Acquired QT interval prolongation and HERG: implications for drug discovery and development. *Eur J Pharmacol* 500(1-3)**,** 129-142. doi: S0014-2999(04)00728-9 [pii]10.1016/j.ejphar.2004.07.019.

Fischer, S., Clauss, M., Wiesnet, M., Renz, D., Schaper, W., and Karliczek, G.F. (1999). Hypoxia induces permeability in brain microvessel endothelial cells via VEGF and NO. *Am J Physiol* 276(4)**,** C812-820. doi: 10.1152/ajpcell.1999.276.4.C812.

Fluri, F., Schuhmann, M.K., and Kleinschnitz, C. (2015). Animal models of ischemic stroke and their application in clinical research. *Drug Des Devel Ther* 9**,** 3445-3454. doi: 10.2147/DDDT.S56071dddt-9-3445 [pii].

Forster, C., Clark, H.B., Ross, M.E., and Iadecola, C. (1999). Inducible nitric oxide synthase expression in human cerebral infarcts. *Acta Neuropathol* 97(3)**,** 215-220.

Francisco, G.S. (1993). An overview of post-stroke depression. *N J Med* 90(9)**,** 686-689.

Franks, N.P., and Honore, E. (2004). The TREK K2P channels and their role in general anaesthesia and neuroprotection. *Trends Pharmacol Sci* 25(11)**,** 601-608. doi: S0165-6147(04)00253-6 [pii]10.1016/j.tips.2004.09.003.

Fu, Z., Gilbert, E.R., and Liu, D. (2013). Regulation of insulin synthesis and secretion and pancreatic Beta-cell dysfunction in diabetes. *Curr Diabetes Rev* 9(1)**,** 25-53.

Fuchs, E., and Cleveland, D.W. (1998). A structural scaffolding of intermediate filaments in health and disease. *Science* 279(5350)**,** 514-519.

Fullerton, A.G., and Agerhom, M. (1984). Side effects of nortripyline treatment for post stroke depression. *Lancet* 323(8375)**,** 519-520. doi: 10.1016/S0140-6736(84)92894-0.

Gallagher, P., Malik, N., Newham, J., Young, A.H., Ferrier, I.N., and Mackin, P. (2015). WITHDRAWN: Antiglucocorticoid treatments for mood disorders. *Cochrane Database Syst Rev* (6)**,** CD005168. doi: 10.1002/14651858.CD005168.pub3.

Garcia-Bonilla, L., and Iadecola, C. (2012). Peroxiredoxin sets the brain on fire after stroke. *Nat Med* 18(6)**,** 858-859. doi: nm.2797 [pii]10.1038/nm.2797.

Gardner, A., and Boles, R.G. (2011). Beyond the serotonin hypothesis: mitochondria, inflammation and neurodegeneration in major depression and affective spectrum disorders. *Prog Neuropsychopharmacol Biol Psychiatry* 35(3)**,** 730-743. doi: S0278-5846(10)00296-4 [pii]10.1016/j.pnpbp.2010.07.030.

Gaudriault, G., Heurteaux, C., Mazella, J., Borsotto, M., MOHA, O.U.M.H., and VEYSSIERE, J. (2015). "Retro-inverso analogs of spadin display increased antidepressant effects". Google Patents).

Gelderblom, M., Leypoldt, F., Steinbach, K., Behrens, D., Choe, C.U., Siler, D.A., et al. (2009). Temporal and spatial dynamics of cerebral immune cell accumulation in stroke. *Stroke* 40(5)**,** 1849-1857. doi: STROKEAHA.108.534503 [pii]10.1161/STROKEAHA.108.534503.

Georgakis, M.K., Gill, D., Rannikmae, K., Traylor, M., Anderson, C.D., Lee, J.M., et al. (2019). Genetically Determined Levels of Circulating Cytokines and Risk of Stroke. *Circulation* 139(2)**,** 256-268. doi: 10.1161/CIRCULATIONAHA.118.035905.

Gidday, J.M., Gasche, Y.G., Copin, J.C., Shah, A.R., Perez, R.S., Shapiro, S.D., et al. (2005). Leukocyte-derived matrix metalloproteinase-9 mediates blood-brain barrier breakdown and is proinflammatory after transient focal cerebral ischemia. *Am J Physiol Heart Circ Physiol* 289(2)**,** H558-568. doi: 01275.2004 [pii]10.1152/ajpheart.01275.2004.

Ginhoux, F., Greter, M., Leboeuf, M., Nandi, S., See, P., Gokhan, S., et al. (2010). Fate mapping analysis reveals that adult microglia derive from primitive macrophages. *Science* 330(6005)**,** 841-845. doi: science.1194637 [pii]10.1126/science.1194637.

Ginsberg, M.D. (2008). Neuroprotection for ischemic stroke: past, present and future. *Neuropharmacology* 55(3)**,** 363-389. doi: S0028-3908(07)00381-4 [pii]10.1016/j.neuropharm.2007.12.007.

Glodzik-Sobanska, L., Slowik, A., McHugh, P., Sobiecka, B., Kozub, J., Rich, K.E., et al. (2006). Single voxel proton magnetic resonance spectroscopy in post-stroke depression. *Psychiatry Res* 148(2-3)**,** 111-120. doi: S0925-4927(06)00128-4 [pii]10.1016/j.pscychresns.2006.08.004.

Go, A.S., Mozaffarian, D., Roger, V.L., Benjamin, E.J., Berry, J.D., Borden, W.B., et al. (2013). Heart disease and stroke statistics--2013 update: a report from the American Heart Association. *Circulation* 127(1)**,** e6-e245. doi: CIR.0b013e31828124ad [pii]10.1161/CIR.0b013e31828124ad.

Goke, R., Fehmann, H.C., Linn, T., Schmidt, H., Krause, M., Eng, J., et al. (1993). Exendin-4 is a high potency agonist and truncated exendin-(9-39)-amide an antagonist at the glucagon-like peptide 1-(7-36)-amide receptor of insulin-secreting beta-cells. *J Biol Chem* 268(26)**,** 19650-19655.

Gomez-Navarro, N., and Miller, E.A. (2016). COP-coated vesicles. *Curr Biol* 26(2)**,** R54-R57. doi: S0960-9822(15)01505-5 [pii]10.1016/j.cub.2015.12.017.

Gonzalez, C., Baez-Nieto, D., Valencia, I., Oyarzun, I., Rojas, P., Naranjo, D., et al. (2012). K(+) channels: function-structural overview. *Compr Physiol* 2(3)**,** 2087-2149. doi: 10.1002/cphy.c110047.

Gouix, E., Buisson, A., Nieoullon, A., Kerkerian-Le Goff, L., Tauskela, J.S., Blondeau, N., et al. (2014). Oxygen glucose deprivation-induced astrocyte dysfunction provokes neuronal death through oxidative stress. *Pharmacol Res* 87**,** 8-17. doi: S1043-6618(14)00094-2 [pii]10.1016/j.phrs.2014.06.002.

Goyal, M., Yu, A.Y., Menon, B.K., Dippel, D.W., Hacke, W., Davis, S.M., et al. (2016). Endovascular Therapy in Acute Ischemic Stroke: Challenges and Transition From Trials to Bedside. *Stroke* 47(2)**,** 548-553. doi: STROKEAHA.115.011426 [pii]10.1161/STROKEAHA.115.011426.

Gregersen, R., Lambertsen, K., and Finsen, B. (2000). Microglia and macrophages are the major source of tumor necrosis factor in permanent middle cerebral artery occlusion in mice. *J Cereb Blood Flow Metab* 20(1)**,** 53-65. doi: 10.1097/00004647-200001000-00009.

Gruss, M., Bushell, T.J., Bright, D.P., Lieb, W.R., Mathie, A., and Franks, N.P. (2004). Two-pore-domain K+ channels are a novel target for the anesthetic gases xenon, nitrous oxide, and cyclopropane. *Mol Pharmacol* 65(2)**,** 443-452. doi: 10.1124/mol.65.2.44365/2/443 [pii].

Hackett, M.L., and Anderson, C.S. (2005). Predictors of depression after stroke: a systematic review of observational studies. *Stroke* 36(10)**,** 2296-2301. doi: 01.STR.0000183622.75135.a4 [pii]10.1161/01.STR.0000183622.75135.a4.

Hackett, M.L., Anderson, C.S., House, A., and Xia, J. (2008). Interventions for treating depression after stroke. *Cochrane Database Syst Rev* (4)**,** CD003437. doi: 10.1002/14651858.CD003437.pub3.

Hackett, M.L., Anderson, C.S., and House, A.O. (2005a). Management of depression after stroke: a systematic review of pharmacological therapies. *Stroke* 36(5)**,** 1098-1103. doi: 01.STR.0000162391.27991.9d [pii]10.1161/01.STR.0000162391.27991.9d.

Hackett, M.L., and Pickles, K. (2014). Part I: frequency of depression after stroke: an updated systematic review and meta-analysis of observational studies. *Int J Stroke* 9(8)**,** 1017-1025. doi: 10.1111/ijs.12357.

Hackett, M.L., Yapa, C., Parag, V., and Anderson, C.S. (2005b). Frequency of depression after stroke: a systematic review of observational studies. *Stroke* 36(6)**,** 1330-1340. doi: 01.STR.0000165928.19135.35 [pii]10.1161/01.STR.0000165928.19135.35.

Hadidi, N., Treat-Jacobson, D.J., and Lindquist, R. (2009). Poststroke depression and functional outcome: a critical review of literature. *Heart Lung* 38(2)**,** 151-162. doi: S0147-9563(08)00097-6 [pii]10.1016/j.hrtlng.2008.05.002.

Han, H.J., Lee, S.W., Kim, G.T., Kim, E.J., Kwon, B., Kang, D., et al. (2016). Enhanced Expression of TREK-1 Is Related with Chronic Constriction Injury of Neuropathic Pain Mouse Model in Dorsal Root Ganglion. *Biomol Ther (Seoul)* 24(3)**,** 252-259. doi: biomolther.2016.038 [pii]10.4062/biomolther.2016.038.

Hanisch, U.K., and Kettenmann, H. (2007). Microglia: active sensor and versatile effector cells in the normal and pathologic brain. *Nat Neurosci* 10(11)**,** 1387-1394. doi: nn1997 [pii]10.1038/nn1997.

Hankey, G.J. (2017). Stroke. *Lancet* 389(10069)**,** 641-654. doi: S0140-6736(16)30962-X [pii]10.1016/S0140-6736(16)30962-X.

Harb, K., Magrinelli, E., Nicolas, C.S., Lukianets, N., Frangeul, L., Pietri, M., et al. (2016). Area-specific development of distinct projection neuron subclasses is regulated by postnatal epigenetic modifications. *Elife* 5**,** e09531. doi: 10.7554/eLife.09531.

Harinath, S., and Sikdar, S.K. (2004). Trichloroethanol enhances the activity of recombinant human TREK-1 and TRAAK channels. *Neuropharmacology* 46(5)**,** 750-760. doi: 10.1016/j.neuropharm.2003.11.023S0028390803004520 [pii].

Harrison, T.C., Silasi, G., Boyd, J.D., and Murphy, T.H. (2013). Displacement of sensory maps and disorganization of motor cortex after targeted stroke in mice. *Stroke* 44(8)**,** 2300-2306. doi: STROKEAHA.113.001272 [pii]10.1161/STROKEAHA.113.001272.

Harter, M., Klesse, C., Bermejo, I., Schneider, F., and Berger, M. (2010). Unipolar depression: diagnostic and therapeutic recommendations from the current S3/National Clinical Practice Guideline. *Dtsch Arztebl Int* 107(40)**,** 700-708. doi: 10.3238/arztebl.2010.0700.

Hatem, S.M., Saussez, G., Della Faille, M., Prist, V., Zhang, X., Dispa, D., et al. (2016). Rehabilitation of Motor Function after Stroke: A Multiple Systematic Review Focused on Techniques to Stimulate Upper Extremity Recovery. *Front Hum Neurosci* 10**,** 442. doi: 10.3389/fnhum.2016.00442.

Hattiangady, B., Rao, M.S., Shetty, G.A., and Shetty, A.K. (2005). Brain-derived neurotrophic factor, phosphorylated cyclic AMP response element binding protein and neuropeptide Y decline as early as middle age in the dentate gyrus and CA1 and CA3 subfields of the hippocampus. *Exp Neurol* 195(2)**,** 353-371. doi: S0014-4886(05)00177-9 [pii]10.1016/j.expneurol.2005.05.014.

Hawkins, B.T., and Davis, T.P. (2005). The blood-brain barrier/neurovascular unit in health and disease. *Pharmacol Rev* 57(2)**,** 173-185. doi: 57/2/173 [pii]10.1124/pr.57.2.4.

Heilman, K.M., Maher, L.M., Greenwald, M.L., and Rothi, L.J. (1997). Conceptual apraxia from lateralized lesions. *Neurology* 49(2)**,** 457-464.

Hemsley, G., and Code, C. (1996). Interactions between recovery in aphasia, emotional and psychosocial factors in subjects with aphasia, their significant others and speech pathologists. *Disabil Rehabil* 18(11)**,** 567-584.

Herson, P.S., and Traystman, R.J. (2014). Animal models of stroke: translational potential at present and in 2050. *Future Neurol* 9(5)**,** 541-551. doi: 10.2217/fnl.14.44.

Hervieu, G.J., Cluderay, J.E., Gray, C.W., Green, P.J., Ranson, J.L., Randall, A.D., et al. (2001). Distribution and expression of TREK-1, a two-pore-domain potassium channel, in the adult rat CNS. *Neuroscience* 103(4)**,** 899-919. doi: S0306452201000306 [pii].

Herx, L.M., and Yong, V.W. (2001). Interleukin-1 beta is required for the early evolution of reactive astrogliosis following CNS lesion. *J Neuropathol Exp Neurol* 60(10)**,** 961-971.

Heurteaux, C., Guy, N., Laigle, C., Blondeau, N., Duprat, F., Mazzuca, M., et al. (2004). TREK-1, a K(+) channel involved in neuroprotection and general anesthesia. *Embo J* 23(13)**,** 2684-2695.

Heurteaux, C., Laigle, C., Blondeau, N., Jarretou, G., and Lazdunski, M. (2006a). Alpha-linolenic acid and riluzole treatment confer cerebral protection and improve survival after focal brain ischemia. *Neuroscience* 137(1)**,** 241-251.

Heurteaux, C., Lucas, G., Guy, N., El Yacoubi, M., Thummler, S., Peng, X.D., et al. (2006b). Deletion of the background potassium channel TREK-1 results in a depression-resistant phenotype. *Nat Neurosci* 9(9)**,** 1134-1141. doi: 10.1038/nn1749.

Hilari, K., Byng, S., Lamping, D.L., and Smith, S.C. (2003). Stroke and Aphasia Quality of Life Scale-39 (SAQOL-39): evaluation of acceptability, reliability, and validity. *Stroke* 34(8)**,** 1944-1950. doi: 10.1161/01.STR.0000081987.46660.ED01.STR.0000081987.46660.ED [pii].

Hirschfeld, R.M. (2000). History and evolution of the monoamine hypothesis of depression. *J Clin Psychiatry* 61 Suppl 6**,** 4-6.

Hivelin, C., Beraud-Dufour, S., Devader, C., Abderrahmani, A., Moreno, S., Moha Ou Maati, H., et al. (2016). Potentiation of Calcium Influx and Insulin Secretion in Pancreatic Beta Cell by the Specific TREK-1 Blocker Spadin. *J Diabetes Res* 2016**,** 3142175. doi: 10.1155/2016/3142175.

Hjort, N., Wu, O., Ashkanian, M., Solling, C., Mouridsen, K., Christensen, S., et al. (2008). MRI detection of early blood-brain barrier disruption: parenchymal enhancement predicts focal hemorrhagic transformation after thrombolysis. *Stroke* 39(3)**,** 1025-1028. doi: STROKEAHA.107.497719 [pii]10.1161/STROKEAHA.107.497719.

Honore, E. (2007). The neuronal background K2P channels: focus on TREK1. *Nat Rev Neurosci.* 8(4)**,** 251-261.

Honore, E., Maingret, F., Lazdunski, M., and Patel, A.J. (2002). An intracellular proton sensor commands lipid- and mechano-gating of the K(+) channel TREK-1. *EMBO J* 21(12)**,** 2968-2976. doi: 10.1093/emboj/cdf288.

Horn, S.D., DeJong, G., Smout, R.J., Gassaway, J., James, R., and Conroy, B. (2005). Stroke rehabilitation patients, practice, and outcomes: is earlier and more aggressive therapy better? *Arch Phys Med Rehabil* 86(12 Suppl 2)**,** S101-S114. doi: S0003-9993(05)01277-3 [pii]10.1016/j.apmr.2005.09.016.

Hosseiny, S., Pietri, M., Petit-Paitel, A., Zarif, H., Heurteaux, C., Chabry, J., et al. (2015). Differential neuronal plasticity in mouse hippocampus associated with various periods of enriched environment during postnatal development. *Brain Struct Funct* 220(6)**,** 3435-3448. doi: 10.1007/s00429-014-0865-y10.1007/s00429-014-0865-y [pii].

Hu, X., Li, P., Guo, Y., Wang, H., Leak, R.K., Chen, S., et al. (2012). Microglia/macrophage polarization dynamics reveal novel mechanism of injury expansion after focal cerebral ischemia. *Stroke* 43(11)**,** 3063-3070. doi: STROKEAHA.112.659656 [pii]10.1161/STROKEAHA.112.659656.

Huang, L., Ma, Q., Li, Y., Li, B., and Zhang, L. (2018). Inhibition of microRNA-210 suppresses pro-inflammatory response and reduces acute brain injury of ischemic stroke in mice. *Exp Neurol* 300**,** 41-50. doi: S0014-4886(17)30284-4 [pii]10.1016/j.expneurol.2017.10.024.

Hubel, D.H., and Wiesel, T.N. (1970). The period of susceptibility to the physiological effects of unilateral eye closure in kittens. *J Physiol* 206(2)**,** 419-436.

Hunter, A.J., Hatcher, J., Virley, D., Nelson, P., Irving, E., Hadingham, S.J., et al. (2000). Functional assessments in mice and rats after focal stroke. *Neuropharmacology* 39(5)**,** 806-816. doi: S0028390899002622 [pii].

Husaini, B., Levine, R., Sharp, L., Cain, V., Novotny, M., Hull, P., et al. (2013). Depression increases stroke hospitalization cost: an analysis of 17,010 stroke patients in 2008 by race and gender. *Stroke Res Treat* 2013**,** 846732. doi: 10.1155/2013/846732.

Iadecola, C. (1997). Bright and dark sides of nitric oxide in ischemic brain injury. *Trends Neurosci* 20(3)**,** 132-139. doi: S0166-2236(96)10074-6 [pii].

Iadecola, C. (2004). Neurovascular regulation in the normal brain and in Alzheimer's disease. *Nat Rev Neurosci* 5(5)**,** 347-360. doi: 10.1038/nrn1387nrn1387 [pii].

Iadecola, C., and Anrather, J. (2011). The immunology of stroke: from mechanisms to translation. *Nat Med* 17(7)**,** 796-808. doi: nm.2399 [pii]10.1038/nm.2399.

Iadecola, C., Forster, C., Nogawa, S., Clark, H.B., and Ross, M.E. (1999). Cyclooxygenase-2 immunoreactivity in the human brain following cerebral ischemia. *Acta Neuropathol* 98(1)**,** 9-14.

Iadecola, C., Niwa, K., Nogawa, S., Zhao, X., Nagayama, M., Araki, E., et al. (2001). Reduced susceptibility to ischemic brain injury and N-methyl-D-aspartate-mediated neurotoxicity in cyclooxygenase-2-deficient mice. *Proc Natl Acad Sci U S A* 98(3)**,** 1294-1299. doi: 10.1073/pnas.98.3.129498/3/1294 [pii].

Iadecola, C., Zhang, F., Casey, R., Nagayama, M., and Ross, M.E. (1997). Delayed reduction of ischemic brain injury and neurological deficits in mice lacking the inducible nitric oxide synthase gene. *J Neurosci* 17(23)**,** 9157-9164.

Jaillard, A., Grand, S., Le Bas, J.F., and Hommel, M. (2010). Predicting cognitive dysfunctioning in nondemented patients early after stroke. *Cerebrovasc Dis* 29(5)**,** 415-423. doi: 000289344 [pii]10.1159/000289344.

Jawaid, A., Krajewska, J., Pawliczak, F., Kandra, V., and Schulz, P.E. (2016). A Macro Role for Microglia in Poststroke Depression. *J Am Geriatr Soc* 64(2)**,** 459-461. doi: 10.1111/jgs.13974.

Ji, X.C., Zhao, W.H., Cao, D.X., Shi, Q.Q., and Wang, X.L. (2011). Novel neuroprotectant chiral 3-n-butylphthalide inhibits tandem-pore-domain potassium channel TREK-1. *Acta Pharmacol Sin* 32(2)**,** 182-187. doi: 10.1038/aps.2010.210.

Jickling, G.C., Liu, D., Stamova, B., Ander, B.P., Zhan, X., Lu, A., et al. (2014). Hemorrhagic transformation after ischemic stroke in animals and humans. *J Cereb Blood Flow Metab* 34(2)**,** 185-199. doi: jcbfm2013203 [pii]10.1038/jcbfm.2013.203.

Jin, K., Minami, M., Lan, J.Q., Mao, X.O., Batteur, S., Simon, R.P., et al. (2001). Neurogenesis in dentate subgranular zone and rostral subventricular zone after focal cerebral ischemia in the rat. *Proc Natl Acad Sci U S A* 98(8)**,** 4710-4715. doi: 10.1073/pnas.08101109898/8/4710 [pii].

Jin, K., Wang, X., Xie, L., Mao, X.O., Zhu, W., Wang, Y., et al. (2006). Evidence for stroke-induced neurogenesis in the human brain. *Proc Natl Acad Sci U S A* 103(35)**,** 13198-13202. doi: 0603512103 [pii]10.1073/pnas.0603512103.

Jorgensen, H.S., Nakayama, H., Raaschou, H.O., and Olsen, T.S. (1995). Recovery of walking function in stroke patients: the Copenhagen Stroke Study. *Arch Phys Med Rehabil* 76(1)**,** 27-32. doi: S0003-9993(95)80038-7 [pii].

Justicia, C., Panes, J., Sole, S., Cervera, A., Deulofeu, R., Chamorro, A., et al. (2003). Neutrophil infiltration increases matrix metalloproteinase-9 in the ischemic brain after occlusion/reperfusion of the middle cerebral artery in rats. *J Cereb Blood Flow Metab* 23(12)**,** 1430-1440. doi: 10.1097/01.WCB.0000090680.07515.C8.

Kang, D., Choe, C., and Kim, D. (2004). Functional expression of TREK-2 in insulin-secreting MIN6 cells. *Biochem Biophys Res Commun* 323(1)**,** 323-331. doi: 10.1016/j.bbrc.2004.08.089.

Karnath, H.O., Rennig, J., Johannsen, L., and Rorden, C. (2011). The anatomy underlying acute versus chronic spatial neglect: a longitudinal study. *Brain* 134(Pt 3)**,** 903-912. doi: awq355 [pii]10.1093/brain/awq355.

Katalinic, N., Lai, R., Somogyi, A., Mitchell, P.B., Glue, P., and Loo, C.K. (2013). Ketamine as a new treatment for depression: a review of its efficacy and adverse effects. *Aust N Z J Psychiatry* 47(8)**,** 710-727. doi: 10.1177/0004867413486842.

Katsura, K., Kristian, T., and Siesjo, B.K. (1994). Energy metabolism, ion homeostasis, and cell damage in the brain. *Biochem Soc Trans* 22(4)**,** 991-996.

Kavalali, E.T., and Monteggia, L.M. (2015). How does ketamine elicit a rapid antidepressant response? *Curr Opin Pharmacol* 20**,** 35-39. doi: 10.1016/j.coph.2014.11.005.

Kawanokuchi, J., Shimizu, K., Nitta, A., Yamada, K., Mizuno, T., Takeuchi, H., et al. (2008). Production and functions of IL-17 in microglia. *J Neuroimmunol* 194(1-2)**,** 54-61. doi: S0165-5728(07)00427-4 [pii]10.1016/j.jneuroim.2007.11.006.

Kelly, M.A., Shuaib, A., and Todd, K.G. (2006). Matrix metalloproteinase activation and blood-brain barrier breakdown following thrombolysis. *Exp Neurol* 200(1)**,** 38-49. doi: S0014-4886(06)00020-3 [pii]10.1016/j.expneurol.2006.01.032.

Kennard, L.E., Chumbley, J.R., Ranatunga, K.M., Armstrong, S.J., Veale, E.L., and Mathie, A. (2005). Inhibition of the human two-pore domain potassium channel, TREK-1, by fluoxetine and its metabolite norfluoxetine. *Br J Pharmacol* 144(6)**,** 821-829. doi: 0706068 [pii]10.1038/sj.bjp.0706068.

Kim, D. (2003). Fatty acid-sensitive two-pore domain K+ channels. *Trends Pharmacol Sci* 24(12)**,** 648-654. doi: 10.1016/j.tips.2003.10.008.

Kim, D., and Clapham, D.E. (1989). Potassium channels in cardiac cells activated by arachidonic acid and phospholipids. *Science* 244(4909)**,** 1174-1176.

Kim, D.M., Wampold, B.E., and Bolt, D.M. (2006). Therapist effects in psychotherapy: A random-effects modeling of the National Institute of Mental Health Treatment of Depression Collaborative Research Program data. *Psychother. Res.* 16(2)**,** 161-172. doi: 10.1080/10503300500264911.

Kim, E., Hwang, E.M., Yarishkin, O., Yoo, J.C., Kim, D., Park, N., et al. (2010). Enhancement of TREK1 channel surface expression by protein-protein interaction with beta-COP. *Biochem Biophys Res Commun* 395(2)**,** 244-250. doi: S0006-291X(10)00646-7 [pii]10.1016/j.bbrc.2010.03.171.

Kim, E.J., Lee, D.K., Hong, S.G., Han, J., and Kang, D. (2017). Activation of TREK-1, but Not TREK-2, Channel by Mood Stabilizers. *Int J Mol Sci* 18(11). doi: 10.3390/ijms18112460.

Kim, Y., Gnatenco, C., Bang, H., and Kim, D. (2001). Localization of TREK-2 K+ channel domains that regulate channel kinetics and sensitivity to pressure, fatty acids and pHi. *Pflugers Arch* 442(6)**,** 952-960.

Kimelberg, H.K. (2005). Astrocytic swelling in cerebral ischemia as a possible cause of injury and target for therapy. *Glia* 50(4)**,** 389-397. doi: 10.1002/glia.20174.

Kindler, C.H., Yost, C.S., and Gray, A.T. (1999). Local anesthetic inhibition of baseline potassium channels with two pore domains in tandem. *Anesthesiology* 90(4)**,** 1092-1102.

Klinedinst, N.J., and Regenold, W.T. (2015). A mitochondrial bioenergetic basis of depression. *J Bioenerg Biomembr* 47(1-2)**,** 155-171. doi: 10.1007/s10863-014-9584-6.

Kouwenhoven, S.E., Kirkevold, M., Engedal, K., and Kim, H.S. (2011). Depression in acute stroke: prevalence, dominant symptoms and associated factors. A systematic literature review. *Disabil Rehabil* 33(7)**,** 539-556. doi: 10.3109/09638288.2010.505997.

Krishnamurthi, R.V., Feigin, V.L., Forouzanfar, M.H., Mensah, G.A., Connor, M., Bennett, D.A., et al. (2013). Global and regional burden of first-ever ischaemic and haemorrhagic stroke during 1990-2010: findings from the Global Burden of Disease Study 2010. *Lancet Glob Health* 1(5)**,** e259-281. doi: S2214-109X(13)70089-5 [pii]10.1016/S2214-109X(13)70089-5.

Krishnan, V., and Nestler, E.J. (2008). The molecular neurobiology of depression. *Nature* 455(7215)**,** 894-902. doi: nature07455 [pii]10.1038/nature07455.

Kronenberg, G., Balkaya, M., Prinz, V., Gertz, K., Ji, S., Kirste, I., et al. (2012). Exofocal dopaminergic degeneration as antidepressant target in mouse model of poststroke depression. *Biol Psychiatry* 72(4)**,** 273-281. doi: S0006-3223(12)00153-9 [pii]10.1016/j.biopsych.2012.02.026.

Kronenberg, G., Gertz, K., Heinz, A., and Endres, M. (2014). Of mice and men: modelling post-stroke depression experimentally. *Br J Pharmacol* 171(20)**,** 4673-4689. doi: 10.1111/bph.12775.

Kumar, A., Aakriti, and Gupta, V. (2016). A review on animal models of stroke: An update. *Brain Res Bull* 122**,** 35-44. doi: S0361-9230(16)30029-6 [pii]10.1016/j.brainresbull.2016.02.016.

Kutlubaev, M.A., and Hackett, M.L. (2014). Part II: predictors of depression after stroke and impact of depression on stroke outcome: an updated systematic review of observational studies. *Int J Stroke* 9(8)**,** 1026-1036. doi: 10.1111/ijs.12356.

Lafreniere, R.G., Cader, M.Z., Poulin, J.F., Andres-Enguix, I., Simoneau, M., Gupta, N., et al. (2010). A dominant-negative mutation in the TRESK potassium channel is linked to familial migraine with aura. *Nat Med* 16(10)**,** 1157-1160. doi: nm.2216 [pii]10.1038/nm.2216.

Lafreniere, R.G., and Rouleau, G.A. (2011). Migraine: Role of the TRESK two-pore potassium channel. *Int J Biochem Cell Biol* 43(11)**,** 1533-1536. doi: 10.1016/j.biocel.2011.08.002.

Lalancette-Hebert, M., Swarup, V., Beaulieu, J.M., Bohacek, I., Abdelhamid, E., Weng, Y.C., et al. (2012). Galectin-3 is required for resident microglia activation and proliferation in response to ischemic injury. *J Neurosci* 32(30)**,** 10383-10395. doi: 32/30/10383 [pii]10.1523/JNEUROSCI.1498-12.2012.

Landis, D.M. (1994). The early reactions of non-neuronal cells to brain injury. *Annu Rev Neurosci* 17**,** 133-151. doi: 10.1146/annurev.ne.17.030194.001025.

Landreneau, M.J., Mullen, M.T., Messe, S.R., Cucchiara, B., Sheth, K.N., McCullough, L.D., et al. (2018). CCL2 and CXCL10 are associated with poor outcome after intracerebral hemorrhage. *Ann Clin Transl Neurol* 5(8)**,** 962-970. doi: 10.1002/acn3.595ACN3595 [pii].

Langhorne, P., Coupar, F., and Pollock, A. (2009). Motor recovery after stroke: a systematic review. *Lancet Neurol* 8(8)**,** 741-754. doi: S1474-4422(09)70150-4 [pii]10.1016/S1474-4422(09)70150-4.

Latour, L.L., Kang, D.W., Ezzeddine, M.A., Chalela, J.A., and Warach, S. (2004). Early blood-brain barrier disruption in human focal brain ischemia. *Ann Neurol* 56(4)**,** 468-477. doi: 10.1002/ana.20199.

Lauritzen, I., Blondeau, N., Heurteaux, C., Widmann, C., Romey, G., and Lazdunski, M. (2000). Polyunsaturated fatty acids are potent neuroprotectors. *Embo J* 19(8)**,** 1784-1793.

Lauritzen, I., Zanzouri, M., Honore, E., Duprat, F., Ehrengruber, M.U., Lazdunski, M., et al. (2003). K+-dependent cerebellar granule neuron apoptosis. Role of task leak K+ channels. *J Biol Chem* 278(34)**,** 32068-32076. doi: 10.1074/jbc.M302631200M302631200 [pii].

Lee, J.H., Wei, L., Gu, X., Wei, Z., Dix, T.A., and Yu, S.P. (2014). Therapeutic effects of pharmacologically induced hypothermia against traumatic brain injury in mice. *J Neurotrauma* 31(16)**,** 1417-1430. doi: 10.1089/neu.2013.3251.

Lee, J.H., Wei, L., Gu, X., Won, S., Wei, Z.Z., Dix, T.A., et al. (2016). Improved Therapeutic Benefits by Combining Physical Cooling With Pharmacological Hypothermia After Severe Stroke in Rats. *Stroke* 47(7)**,** 1907-1913. doi: STROKEAHA.116.013061 [pii]10.1161/STROKEAHA.116.013061.

Lee, J.M., Zipfel, G.J., and Choi, D.W. (1999). The changing landscape of ischaemic brain injury mechanisms. *Nature* 399(6738 Suppl)**,** A7-14.

Leist, M., Single, B., Castoldi, A.F., Kuhnle, S., and Nicotera, P. (1997). Intracellular adenosine triphosphate (ATP) concentration: a switch in the decision between apoptosis and necrosis. *J Exp Med* 185(8)**,** 1481-1486.

Leithner, K., Hirschmugl, B., Li, Y., Tang, B., Papp, R., Nagaraj, C., et al. (2016). TASK-1 Regulates Apoptosis and Proliferation in a Subset of Non-Small Cell Lung Cancers. *PLoS One* 11(6)**,** e0157453. doi: 10.1371/journal.pone.0157453.

Lesage, F., Guillemare, E., Fink, M., Duprat, F., Lazdunski, M., Romey, G., et al. (1996). TWIK-1, a ubiquitous human weakly inward rectifying K+ channel with a novel structure. *EMBO J* 15(5)**,** 1004-1011.

Lesage, F., and Lazdunski, M. (2000). Molecular and functional properties of two pore domain potassium channels. *Am. J. Physiol.* 279**,** 793-801.

Levitz, J., Royal, P., Comoglio, Y., Wdziekonski, B., Schaub, S., Clemens, D.M., et al. (2016). Heterodimerization within the TREK channel subfamily produces a diverse family of highly regulated potassium channels. *Proc Natl Acad Sci U S A* 113(15)**,** 4194-4199. doi: 1522459113 [pii]10.1073/pnas.1522459113.

Li, J., Zhao, Y.D., Zeng, J.W., Chen, X.Y., Wang, R.D., and Cheng, S.Y. (2014a). Serum Brain-derived neurotrophic factor levels in post-stroke depression. *J Affect Disord* 168**,** 373-379. doi: S0165-0327(14)00442-X [pii]10.1016/j.jad.2014.07.011.

Li, M., Lin, Y.P., Chen, J.L., Li, H., Jiang, R.C., and Zhang, J.N. (2015). Role of regulatory T cell in clinical outcome of traumatic brain injury. *Chin Med J (Engl)* 128(8)**,** 1072-1078. doi: ChinMedJ_2015_128_8_1072_155094 [pii]10.4103/0366-6999.155094.

Li, W., Ling, S., Yang, Y., Hu, Z., Davies, H., and Fang, M. (2014b). Systematic hypothesis for post-stroke depression caused inflammation and neurotransmission and resultant on possible treatments. *Neuro Endocrinol Lett* 35(2)**,** 104-109. doi: NEL350214A03 [pii].

Li, Y., and Chopp, M. (1999). Temporal profile of nestin expression after focal cerebral ischemia in adult rat. *Brain Res* 838(1-2)**,** 1-10. doi: S0006-8993(99)01502-4 [pii].

Liebeskind, D.S. (2010). Reperfusion for acute ischemic stroke: arterial revascularization and collateral therapeutics. *Curr Opin Neurol* 23(1)**,** 36-45. doi: 10.1097/WCO.0b013e328334da32.

Liesz, A., Hu, X., Kleinschnitz, C., and Offner, H. (2015). Functional role of regulatory lymphocytes in stroke: facts and controversies. *Stroke* 46(5)**,** 1422-1430. doi: STROKEAHA.114.008608 [pii]10.1161/STROKEAHA.114.008608.

Lin, D.H., Zhang, X.R., Ye, D.Q., Xi, G.J., Hui, J.J., Liu, S.S., et al. (2015). The Role of the Two-Pore Domain Potassium Channel TREK-1 in the Therapeutic Effects of Escitalopram in a Rat Model of Poststroke Depression. *CNS Neurosci Ther* 21(6)**,** 504-512. doi: 10.1111/cns.12384.

Linge, R., Pazos, A., and Diaz, A. (2013). Social isolation differentially affects anxiety and depressive-like responses of bulbectomized mice. *Behav Brain Res* 245**,** 1-6. doi: S0166-4328(13)00068-5 [pii]10.1016/j.bbr.2013.01.041.

Lipsey, J.R., Robinson, R.G., Pearlson, G.D., Rao, K., and Price, T.R. (1984). Nortriptyline treatment of post-stroke depression: a double-blind study. *Lancet* 1(8372)**,** 297-300. doi: S0140-6736(84)90356-8 [pii].

Liu, H.C., Zheng, M.H., Du, Y.L., Wang, L., Kuang, F., Qin, H.Y., et al. (2012). N9 microglial cells polarized by LPS and IL4 show differential responses to secondary environmental stimuli. *Cell Immunol* 278(1-2)**,** 84-90. doi: S0008-8749(12)00113-X [pii]10.1016/j.cellimm.2012.06.001.

Liu, W., and Saint, D.A. (2004). Heterogeneous expression of tandem-pore K+ channel genes in adult and embryonic rat heart quantified by real-time polymerase chain reaction. *Clin Exp Pharmacol Physiol* 31(3)**,** 174-178.

Liu, Z., and Chopp, M. (2016). Astrocytes, therapeutic targets for neuroprotection and neurorestoration in ischemic stroke. *Prog Neurobiol* 144**,** 103-120. doi: S0301-0082(15)30001-0 [pii]10.1016/j.pneurobio.2015.09.008.

Locher, C., Koechlin, H., Zion, S.R., Werner, C., Pine, D.S., Kirsch, I., et al. (2017). Efficacy and Safety of Selective Serotonin Reuptake Inhibitors, Serotonin-Norepinephrine Reuptake Inhibitors, and Placebo for Common Psychiatric Disorders Among Children and Adolescents: A Systematic Review and Meta-analysis. *JAMA Psychiatry* 74(10)**,** 1011-1020. doi: 2652447 [pii]10.1001/jamapsychiatry.2017.2432.

Lolicato, M., Arrigoni, C., Mori, T., Sekioka, Y., Bryant, C., Clark, K.A., et al. (2017). K2P2.1 (TREK-1)-activator complexes reveal a cryptic selectivity filter binding site. *Nature* 547(7663)**,** 364-368. doi: nature22988 [pii]10.1038/nature22988.

Lopes, C.M., Rohacs, T., Czirjak, G., Balla, T., Enyedi, P., and Logothetis, D.E. (2005). PIP2 hydrolysis underlies agonist-induced inhibition and regulates voltage gating of two-pore domain K+ channels. *J Physiol* 564(Pt 1)**,** 117-129. doi: 10.1113/jphysiol.2004.081935.

Lorivel, T., Gandin, C., Veyssiere, J., Lazdunski, M., and Heurteaux, C. (2015). Positive effects of the traditional Chinese medicine MLC901 in cognitive tasks. *J Neurosci Res* 93(11)**,** 1648-1663. doi: 10.1002/jnr.23591.

Luborsky, L., and Singer, B. (1975). Comparative studies of psychotherapies. Is it true that "everywon has one and all must have prizes"? *Arch Gen Psychiatry* 32(8)**,** 995-1008.

Luengo-Fernandez, R., Paul, N.L., Gray, A.M., Pendlebury, S.T., Bull, L.M., Welch, S.J., et al. (2013). Population-based study of disability and institutionalization after transient ischemic attack and stroke: 10-year results of the Oxford Vascular Study. *Stroke* 44(10)**,** 2854-2861. doi: STROKEAHA.113.001584 [pii]10.1161/STROKEAHA.113.001584.

Maes, M., Leonard, B.E., Myint, A.M., Kubera, M., and Verkerk, R. (2011). The new '5-HT' hypothesis of depression: cell-mediated immune activation induces indoleamine 2,3-dioxygenase, which leads to lower plasma tryptophan and an increased synthesis of detrimental tryptophan catabolites (TRYCATs), both of which contribute to the onset of depression. *Prog Neuropsychopharmacol Biol Psychiatry* 35(3)**,** 702-721. doi: S0278-5846(10)00511-7 [pii]10.1016/j.pnpbp.2010.12.017.

Maingret, F., Lauritzen, I., Patel, A.J., Heurteaux, C., Reyes, R., Lesage, F., et al. (2000). TREK-1 is a heat-activated background K($^{+}$) channel. *EMBO J* 19(11)**,** 2483-2491.

Maingret, F., Patel, A.J., Lesage, F., Lazdunski, M., and Honore, E. (1999). Mechano- or acid stimulation, two interactive modes of activation of the TREK-1 potassium channel. *J Biol Chem* 274(38)**,** 26691-26696.

Malberg, J.E., and Schechter, L.E. (2005). Increasing hippocampal neurogenesis: a novel mechanism for antidepressant drugs. *Curr Pharm Des* 11(2)**,** 145-155.

Marsden, V.S., and Strasser, A. (2003). Control of apoptosis in the immune system: Bcl-2, BH3-only proteins and more. *Annu Rev Immunol* 21**,** 71-105. doi: 10.1146/annurev.immunol.21.120601.141029120601.141029 [pii].

Marsh, B., Acosta, C., Djouhri, L., and Lawson, S.N. (2012). Leak K(+) channel mRNAs in dorsal root ganglia: relation to inflammation and spontaneous pain behaviour. *Mol Cell Neurosci* 49(3)**,** 375-386. doi: 10.1016/j.mcn.2012.01.002.

Martin, D.J., Garske, J.P., and Davis, M.K. (2000). Relation of the therapeutic alliance with outcome and other variables: a meta-analytic review. *J Consult Clin Psychol* 68(3)**,** 438-450.

Martinowich, K., Manji, H., and Lu, B. (2007). New insights into BDNF function in depression and anxiety. *Nat Neurosci* 10(9)**,** 1089-1093. doi: nn1971 [pii]10.1038/nn1971.

Masi, G., and Brovedani, P. (2011). The hippocampus, neurotrophic factors and depression: possible implications for the pharmacotherapy of depression. *CNS Drugs* 25(11)**,** 913-931. doi: 2 [pii]10.2165/11595900-000000000-00000.

Massey, J.M., Hubscher, C.H., Wagoner, M.R., Decker, J.A., Amps, J., Silver, J., et al. (2006). Chondroitinase ABC digestion of the perineuronal net promotes functional collateral sprouting in the cuneate nucleus after cervical spinal cord injury. *J Neurosci* 26(16)**,** 4406-4414. doi: 26/16/4406 [pii]10.1523/JNEUROSCI.5467-05.2006.

Mataga, N., Nagai, N., and Hensch, T.K. (2002). Permissive proteolytic activity for visual cortical plasticity. *Proc Natl Acad Sci U S A* 99(11)**,** 7717-7721. doi: 10.1073/pnas.102088899.

Mathie, A., and Veale, E.L. (2007). Therapeutic potential of neuronal two-pore domain potassium-channel modulators. *Curr Opin Investig Drugs* 8(7)**,** 555-562.

Matsui, T., Mori, T., Tateishi, N., Kagamiishi, Y., Satoh, S., Katsube, N., et al. (2002). Astrocytic activation and delayed infarct expansion after permanent focal ischemia in rats. Part I: enhanced astrocytic synthesis of s-100beta in the periinfarct area precedes delayed infarct expansion. *J Cereb Blood Flow Metab* 22(6)**,** 711-722. doi: 10.1097/00004647-200206000-00010.

Matsuura, K., Kabuto, H., Makino, H., and Ogawa, N. (1997). Pole test is a useful method for evaluating the mouse movement disorder caused by striatal dopamine depletion. *J Neurosci Methods* 73(1)**,** 45-48. doi: S0165-0270(96)02211-X [pii].

Mayberg, H.S., Robinson, R.G., Wong, D.F., Parikh, R., Bolduc, P., Starkstein, S.E., et al. (1988). PET imaging of cortical S2 serotonin receptors after stroke: lateralized changes and relationship to depression. *Am J Psychiatry* 145(8)**,** 937-943. doi: 10.1176/ajp.145.8.937.

Mazella, J., Petrault, O., Borsotto, M., Heurteaux, C., and Widmann, C. (2012). "Peptide derived from neurotensin receptor 3 and use thereof in the treatment of psychiatric diseases". Google Patents).

Mazella, J., Petrault, O., Lucas, G., Deval, E., Beraud-Dufour, S., Gandin, C., et al. (2010). Spadin, a sortilin-derived peptide, targeting rodent TREK-1 channels: a new concept in the antidepressant drug design. *PLoS Biol* 8(4)**,** e1000355. doi: 10.1371/journal.pbio.1000355.

Mazella, J., Zsurger, N., Navarro, V., Chabry, J., Kaghad, M., Caput, D., et al. (1998). The 100-kDa neurotensin receptor is gp95/sortilin, a non-G-protein-coupled receptor. *J Biol Chem* 273(41)**,** 26273-26276.

McClenaghan, C., Schewe, M., Aryal, P., Carpenter, E.P., Baukrowitz, T., and Tucker, S.J. (2016). Polymodal activation of the TREK-2 K2P channel produces structurally distinct open states. *J Gen Physiol* 147(6)**,** 497-505. doi: 10.1085/jgp.201611601.

McColl, B.W., Rothwell, N.J., and Allan, S.M. (2008). Systemic inflammation alters the kinetics of cerebrovascular tight junction disruption after experimental stroke in mice.

J Neurosci 28(38)**,** 9451-9462. doi: 28/38/9451 [pii]10.1523/JNEUROSCI.2674-08.2008.

McCoy, M.K., and Tansey, M.G. (2008). TNF signaling inhibition in the CNS: implications for normal brain function and neurodegenerative disease. *J Neuroinflammation* 5**,** 45. doi: 1742-2094-5-45 [pii]10.1186/1742-2094-5-45.

McHenry, L. (2006). Ethical issues in psychopharmacology. *J Med Ethics* 32(7)**,** 405-410. doi: 32/7/405 [pii]10.1136/jme.2005.013185.

McTaggart, J.S., Clark, R.H., and Ashcroft, F.M. (2010). The role of the KATP channel in glucose homeostasis in health and disease: more than meets the islet. *J Physiol* 588(Pt 17)**,** 3201-3209. doi: 10.1113/jphysiol.2010.191767.

Medhurst, A.D., Rennie, G., Chapman, C.G., Meadows, H., Duckworth, M.D., Kelsell, R.E., et al. (2001). Distribution analysis of human two pore domain potassium channels in tissues of the central nervous system and periphery. *Brain Res Mol Brain Res* 86(1-2)**,** 101-114. doi: S0169328X00002631 [pii].

Mirza, F.J., and Zahid, S. (2018). The Role of Synapsins in Neurological Disorders. *Neurosci Bull* 34(2)**,** 349-358. doi: 10.1007/s12264-017-0201-710.1007/s12264-017-0201-7 [pii].

Mitchell, A.J., Sheth, B., Gill, J., Yadegarfar, M., Stubbs, B., and Meader, N. (2017). Prevalence and predictors of post-stroke mood disorders: A meta-analysis and meta-regression of depression, anxiety and adjustment disorder. *Gen Hosp Psychiatry* 47**,** 48-60. doi: S0163-8343(17)30143-3 [pii]10.1016/j.genhosppsych.2017.04.001.

Mitsios, N., Gaffney, J., Krupinski, J., Mathias, R., Wang, Q., Hayward, S., et al. (2007). Expression of signaling molecules associated with apoptosis in human ischemic stroke tissue. *Cell Biochem Biophys* 47(1)**,** 73-86. doi: CBB:47:1:73 [pii].

Moha Ou Maati, H., Borsotto, M., Chatelain, F., Widmann, C., Lazdunski, M., and Heurteaux, C. (2012a). Activation of ATP-sensitive potassium channels as an element of the neuroprotective effects of the Traditional Chinese Medicine MLC901 against oxygen glucose deprivation. *Neuropharmacology* 63(4)**,** 692-700. doi: S0028-3908(12)00233-X [pii]10.1016/j.neuropharm.2012.05.035.

Moha Ou Maati, H., Bourcier-Lucas, C., Veyssiere, J., Kanzari, A., Heurteaux, C., Borsotto, M., et al. (2014). The peptidic antidepressant spadin interacts with prefrontal 5-HT and mGluR receptors in the control of serotonergic function. *Brain Struct Funct*. doi: 10.1007/s00429-014-0890-x.

Moha ou Maati, H., Peyronnet, R., Devader, C., Veyssiere, J., Labbal, F., Gandin, C., et al. (2011). A human TREK-1/HEK cell line: a highly efficient screening tool for drug development in neurological diseases. *PLoS One* 6(10)**,** e25602. doi: 10.1371/journal.pone.0025602PONE-D-11-15481 [pii].

Moha Ou Maati, H., Veyssiere, J., Labbal, F., Coppola, T., Gandin, C., Widmann, C., et al. (2012b). Spadin as a new antidepressant: absence of TREK-1-related side effects. *Neuropharmacology* 62(1)**,** 278-288. doi: S0028-3908(11)00295-4 [pii]10.1016/j.neuropharm.2011.07.019.

Molendijk, M.L., Spinhoven, P., Polak, M., Bus, B.A., Penninx, B.W., and Elzinga, B.M. (2014). Serum BDNF concentrations as peripheral manifestations of depression: evidence from a systematic review and meta-analyses on 179 associations (N=9484). *Mol Psychiatry* 19(7)**,** 791-800. doi: mp2013105 [pii]10.1038/mp.2013.105.

Moller, H.J. (2003). Suicide, suicidality and suicide prevention in affective disorders. *Acta Psychiatr Scand Suppl* (418)**,** 73-80. doi: 185 [pii].

Moller, M., Andersen, G., and Gjedde, A. (2007). Serotonin 5HT1A receptor availability and pathological crying after stroke. *Acta Neurol Scand* 116(2)**,** 83-90. doi: ANE869 [pii]10.1111/j.1600-0404.2007.00869.x.

Montaner, J., Alvarez-Sabin, J., Molina, C., Angles, A., Abilleira, S., Arenillas, J., et al. (2001). Matrix metalloproteinase expression after human cardioembolic stroke: temporal profile and relation to neurological impairment. *Stroke* 32(8)**,** 1759-1766.

Montgomery, S.A., Loft, H., Sanchez, C., Reines, E.H., and Papp, M. (2001). Escitalopram (S-enantiomer of citalopram): clinical efficacy and onset of action predicted from a rat model. *Pharmacol Toxicol* 88(5)**,** 282-286.

Moreno, S., Devader, C.M., Pietri, M., Borsotto, M., Heurteaux, C., and Mazella, J. (2018). Altered Trek-1 Function in Sortilin Deficient Mice Results in Decreased Depressive-Like Behavior. *Front Pharmacol* 9**,** 863. doi: 10.3389/fphar.2018.00863.

Morris, P.L., Robinson, R.G., Raphael, B., and Hopwood, M.J. (1996). Lesion location and poststroke depression. *J Neuropsychiatry Clin Neurosci* 8(4)**,** 399-403. doi: 10.1176/jnp.8.4.399.

Morris, R. (1984). Developments of a water-maze procedure for studying spatial learning in the rat. *J Neurosci Methods* 11(1)**,** 47-60. doi: 0165-0270(84)90007-4 [pii].

Moskowitz, M.A., Lo, E.H., and Iadecola, C. (2010). The science of stroke: mechanisms in search of treatments. *Neuron* 67(2)**,** 181-198. doi: S0896-6273(10)00540-4 [pii]10.1016/j.neuron.2010.07.002.

Mould, W.A., Carhuapoma, J.R., Muschelli, J., Lane, K., Morgan, T.C., McBee, N.A., et al. (2013). Minimally invasive surgery plus recombinant tissue-type plasminogen activator for intracerebral hemorrhage evacuation decreases perihematomal edema. *Stroke* 44(3)**,** 627-634. doi: STROKEAHA.111.000411 [pii]10.1161/STROKEAHA.111.000411.

Mun-Bryce, S., and Rosenberg, G.A. (1998). Matrix metalloproteinases in cerebrovascular disease. *J Cereb Blood Flow Metab* 18(11)**,** 1163-1172. doi: 10.1097/00004647-199811000-00001.

Munck Petersen, C., Nielsen, M.S., Jacobsen, C., Tauris, J., Jacobsen, L., Gliemann, J., et al. (1999). Propeptide cleavage conditions sortilin/neurotensin receptor-3 for ligand binding. *Embo J* 18(3)**,** 595-604.

Murbartian, J., Lei, Q., Sando, J.J., and Bayliss, D.A. (2005). Sequential phosphorylation mediates receptor- and kinase-induced inhibition of TREK-1 background potassium channels. *J Biol Chem* 280(34)**,** 30175-30184. doi: 10.1074/jbc.M503862200.

Murphy, T.H., and Corbett, D. (2009). Plasticity during stroke recovery: from synapse to behaviour. *Nat Rev Neurosci* 10(12)**,** 861-872. doi: nrn2735 [pii]10.1038/nrn2735.

Naarding, P., and Beekman, A.T. (2011). Vascular depression: where do we go from here? *Expert Rev Neurother* 11(1)**,** 77-83. doi: 10.1586/ern.10.92.

Namura, S., Zhu, J., Fink, K., Endres, M., Srinivasan, A., Tomaselli, K.J., et al. (1998). Activation and cleavage of caspase-3 in apoptosis induced by experimental cerebral ischemia. *J Neurosci* 18(10)**,** 3659-3668.

Narushima, K., Kosier, J.T., and Robinson, R.G. (2003). A reappraisal of poststroke depression, intra- and inter-hemispheric lesion location using meta-analysis. *J Neuropsychiatry Clin Neurosci* 15(4)**,** 422-430. doi: 10.1176/jnp.15.4.422.

Nasr, N., Faucherre, A., Borsotto, M., Heurteaux, C., Mazella, J., Jopling, C., et al. (2018). Identification and characterization of two zebrafish Twik related potassium channels, Kcnk2a and Kcnk2b. *Scientific Reports* 8(1)**,** 15311. doi: 10.1038/s41598-018-33664-9.

Nedergaard, M., and Dirnagl, U. (2005). Role of glial cells in cerebral ischemia. *Glia* 50(4)**,** 281-286. doi: 10.1002/glia.20205.

Nestler, E.J., Barrot, M., DiLeone, R.J., Eisch, A.J., Gold, S.J., and Monteggia, L.M. (2002). Neurobiology of depression. *Neuron* 34(1)**,** 13-25. doi: S0896627302006530 [pii].

Nicolas, S., Veyssiere, J., Gandin, C., Zsurger, N., Pietri, M., Heurteaux, C., et al. (2015). Neurogenesis-independent antidepressant-like effects of enriched environment is

dependent on adiponectin. *Psychoneuroendocrinology* 57**,** 72-83. doi: S0306-4530(15)00121-3 [pii]10.1016/j.psyneuen.2015.03.017.

Nielsen, M.S., Jacobsen, C., Olivecrona, G., Gliemann, J., and Petersen, C.M. (1999). Sortilin/neurotensin receptor-3 binds and mediates degradation of lipoprotein lipase. *J Biol Chem* 274(13)**,** 8832-8836.

Noel, J., Sandoz, G., and Lesage, F. (2011). Molecular regulations governing TREK and TRAAK channel functions. *Channels (Austin)* 5(5)**,** 402-409. doi: 10.4161/chan.5.5.16469.

Noel, J., Zimmermann, K., Busserolles, J., Deval, E., Alloui, A., Diochot, S., et al. (2009). The mechano-activated K+ channels TRAAK and TREK-1 control both warm and cold perception. *EMBO J* 28(9)**,** 1308-1318. doi: emboj200957 [pii]10.1038/emboj.2009.57.

Nykjaer, A., Lee, R., Teng, K.K., Jansen, P., Madsen, P., Nielsen, M.S., et al. (2004). Sortilin is essential for proNGF-induced neuronal cell death. *Nature* 427(6977)**,** 843-848.

O'Donnell, M.E. (2014). Blood-brain barrier Na transporters in ischemic stroke. *Adv Pharmacol* 71**,** 113-146. doi: S1054-3589(14)00012-X [pii]10.1016/bs.apha.2014.06.011.

O'Keefe, L.M., Doran, S.J., Mwilambwe-Tshilobo, L., Conti, L.H., Venna, V.R., and McCullough, L.D. (2014). Social isolation after stroke leads to depressive-like behavior and decreased BDNF levels in mice. *Behav Brain Res* 260**,** 162-170. doi: S0166-4328(13)00672-4 [pii]10.1016/j.bbr.2013.10.047.

Offner, H., and Hurn, P.D. (2012). A novel hypothesis: regulatory B lymphocytes shape outcome from experimental stroke. *Transl Stroke Res* 3(3)**,** 324-330. doi: 10.1007/s12975-012-0187-4.

Ognibene, E., Adriani, W., Caprioli, A., Ghirardi, O., Ali, S.F., Aloe, L., et al. (2008). The effect of early maternal separation on brain derived neurotrophic factor and monoamine levels in adult heterozygous reeler mice. *Prog Neuropsychopharmacol Biol Psychiatry* 32(5)**,** 1269-1276. doi: S0278-5846(08)00102-4 [pii]10.1016/j.pnpbp.2008.03.023.

Olney, J.W., Price, M.T., Samson, L., and Labruyere, J. (1986). The role of specific ions in glutamate neurotoxicity. *Neurosci Lett* 65(1)**,** 65-71. doi: 0304-3940(86)90121-7 [pii].

Orwig, K.S., Lassetter, M.R., Hadden, M.K., and Dix, T.A. (2009). Comparison of N-terminal modifications on neurotensin(8-13) analogues correlates peptide stability but not binding affinity with in vivo efficacy. *J Med Chem* 52(7)**,** 1803-1813. doi: 10.1021/jm801072v.

Otte, C., Gold, S.M., Penninx, B.W., Pariante, C.M., Etkin, A., Fava, M., et al. (2016). Major depressive disorder. *Nat Rev Dis Primers* 2**,** 16065. doi: 10.1038/nrdp.2016.65.

Palucha-Poniewiera, A. (2018). The role of glutamatergic modulation in the mechanism of action of ketamine, a prototype rapid-acting antidepressant drug. *Pharmacol Rep* 70(5)**,** 837-846. doi: S1734-1140(17)30744-2 [pii]10.1016/j.pharep.2018.02.011.

Pan, L., Yang, F., Lu, C., Jia, C., Wang, Q., and Zeng, K. (2017). Effects of sevoflurane on rats with ischemic brain injury and the role of the TREK-1 channel. *Exp Ther Med* 14(4)**,** 2937-2942. doi: 10.3892/etm.2017.4906ETM-0-0-4906 [pii].

Paolucci, S. (2008). Epidemiology and treatment of post-stroke depression. *Neuropsychiatr Dis Treat* 4(1)**,** 145-154.

Pardridge, W.M. (2005). Molecular biology of the blood-brain barrier. *Mol Biotechnol* 30(1)**,** 57-70. doi: MB:30:1:057 [pii]10.1385/MB:30:1:057.

Patel, A.J., and Honore, E. (2001). Properties and modulation of mammalian 2P domain K^+ channels. *Trends Neurosci* 24(6)**,** 339-346.

Patel, A.J., Honore, E., Lesage, F., Fink, M., Romey, G., and Lazdunski, M. (1999). Inhalational anesthetics activate two-pore-domain background K+ channels. *Nat Neurosci* 2(5)**,** 422-426. doi: 10.1038/8084.

Patel, A.J., Honore, E., Maingret, F., Lesage, F., Fink, M., Duprat, F., et al. (1998a). A mammalian two pore domain mechano-gated S-like K+ channel. *EMBO J* 17(15)**,** 4283-4290. doi: 10.1093/emboj/17.15.4283.

Patel, A.J., Honore, E., Maingret, F., Lesage, F., Fink, M., Duprat, F., et al. (1998b). A mammalian two pore domain mechano-gated S-like K+ channel. *EMBO J.* 17**,** 4283-4290.

Patel, A.R., Ritzel, R., McCullough, L.D., and Liu, F. (2013). Microglia and ischemic stroke: a double-edged sword. *Int J Physiol Pathophysiol Pharmacol* 5(2)**,** 73-90.

Pedersen, P.M., Jorgensen, H.S., Nakayama, H., Raaschou, H.O., and Olsen, T.S. (1995). Aphasia in acute stroke: incidence, determinants, and recovery. *Ann Neurol* 38(4)**,** 659-666. doi: 10.1002/ana.410380416.

Penninx, B.W., Milaneschi, Y., Lamers, F., and Vogelzangs, N. (2013). Understanding the somatic consequences of depression: biological mechanisms and the role of depression symptom profile. *BMC Med* 11**,** 129. doi: 1741-7015-11-129 [pii]10.1186/1741-7015-11-129.

Perlis, R.H., Moorjani, P., Fagerness, J., Purcell, S., Trivedi, M.H., Fava, M., et al. (2008). Pharmacogenetic Analysis of Genes Implicated in Rodent Models of Antidepressant Response: Association of TREK1 and Treatment Resistance in the STAR(*)D Study. *Neuropsychopharmacology*. doi: npp20086 [pii]10.1038/npp.2008.6.

Petersen, C.M., Nielsen, M.S., Nykjaer, A., Jacobsen, L., Tommerup, N., Rasmussen, H.H., et al. (1997). Molecular identification of a novel candidate sorting receptor purified from human brain by receptor-associated protein affinity chromatography. *J Biol Chem* 272(6)**,** 3599-3605.

Petr, G.T., Sun, Y., Frederick, N.M., Zhou, Y., Dhamne, S.C., Hameed, M.Q., et al. (2015). Conditional deletion of the glutamate transporter GLT-1 reveals that astrocytic GLT-1 protects against fatal epilepsy while neuronal GLT-1 contributes significantly to glutamate uptake into synaptosomes. *J Neurosci* 35(13)**,** 5187-5201. doi: 35/13/5187 [pii]10.1523/JNEUROSCI.4255-14.2015.

Pham, T.H., and Gardier, A.M. (2019). Fast-acting antidepressant activity of ketamine: highlights on brain serotonin, glutamate, and GABA neurotransmission in preclinical studies. *Pharmacol Ther*. doi: S0163-7258(19)30040-3 [pii]10.1016/j.pharmthera.2019.02.017.

Pietra Pedroso, V.S., Rachid, M.A., and Teixeira, A.L. (2016). Biomarkers in Post-stroke Depression. *Curr Neurovasc Res* 13(2)**,** 163-173. doi: CNR-EPUB-73836 [pii].

Pietri, M., Djillani, A., Mazella, J., Borsotto, M., and Heurteaux, C. (2019). First evidence of protective effects on stroke recovery and post-stroke depression induced by sortilin-derived peptides. *Neuropharmacology*.

Pizzorusso, T., Medini, P., Landi, S., Baldini, S., Berardi, N., and Maffei, L. (2006). Structural and functional recovery from early monocular deprivation in adult rats. *Proc Natl Acad Sci U S A* 103(22)**,** 8517-8522. doi: 0602657103 [pii]10.1073/pnas.0602657103.

Pohjasvaara, T., Vataja, R., Leppavuori, A., Kaste, M., and Erkinjuntti, T. (2001). Depression is an independent predictor of poor long-term functional outcome post-stroke. *Eur J Neurol* 8(4)**,** 315-319. doi: ene182 [pii].

Porsolt, R.D., Le Pichon, M., and Jalfre, M. (1977). Depression: a new animal model sensitive to antidepressant treatments. *Nature* 266(5604)**,** 730-732.

Poulin, H., Bruhova, I., Timour, Q., Theriault, O., Beaulieu, J.M., Frassati, D., et al. (2014). Fluoxetine blocks Nav1.5 channels via a mechanism similar to that of class 1 antiarrhythmics. *Mol Pharmacol* 86(4)**,** 378-389. doi: mol.114.093104 [pii]10.1124/mol.114.093104.

Poupon, L., Lamoine, S., Pereira, V., Barriere, D.A., Lolignier, S., Giraudet, F., et al. (2018). Targeting the TREK-1 potassium channel via riluzole to eliminate the neuropathic and depressive-like effects of oxaliplatin. *Neuropharmacology* 140**,** 43-61. doi: S0028-3908(18)30404-0 [pii]10.1016/j.neuropharm.2018.07.026.

Provinciali, L., and Coccia, M. (2002). Post-stroke and vascular depression: a critical review. *Neurol Sci* 22(6)**,** 417-428. doi: 10.1007/s100720200000.

Qi, Z., Liang, J., Pan, R., Dong, W., Shen, J., Yang, Y., et al. (2016). Zinc contributes to acute cerebral ischemia-induced blood-brain barrier disruption. *Neurobiol Dis* 95**,** 12-21. doi: S0969-9961(16)30161-9 [pii]10.1016/j.nbd.2016.07.003.

Quast, U. (1992). Potassium channel openers: pharmacological and clinical aspects. *Fundam Clin Pharmacol* 6(7)**,** 279-293.

Rabchevsky, A.G., Weinitz, J.M., Coulpier, M., Fages, C., Tinel, M., and Junier, M.P. (1998). A role for transforming growth factor alpha as an inducer of astrogliosis. *J Neurosci* 18(24)**,** 10541-10552.

Radak, Z., Zhao, Z., Goto, S., and Koltai, E. (2011). Age-associated neurodegeneration and oxidative damage to lipids, proteins and DNA. *Mol Aspects Med* 32(4-6)**,** 305-315. doi: S0098-2997(11)00054-9 [pii]10.1016/j.mam.2011.10.010.

Rannikmae, K., Woodfield, R., Anderson, C.S., Charidimou, A., Chiewvit, P., Greenberg, S.M., et al. (2016). Reliability of intracerebral hemorrhage classification systems: A systematic review. *Int J Stroke* 11(6)**,** 626-636. doi: 1747493016641962 [pii]10.1177/1747493016641962.

Ransohoff, R.M., and Brown, M.A. (2012). Innate immunity in the central nervous system. *J Clin Invest* 122(4)**,** 1164-1171. doi: 58644 [pii]10.1172/JCI58644.

Ratti, E., Bettica, P., Alexander, R., Archer, G., Carpenter, D., Evoniuk, G., et al. (2013). Full central neurokinin-1 receptor blockade is required for efficacy in depression: evidence from orvepitant clinical studies. *J Psychopharmacol* 27(5)**,** 424-434. doi: 0269881113480990 [pii]10.1177/0269881113480990.

Razmara, A., Valle, N., Markovic, D., Sanossian, N., Ovbiagele, B., Dutta, T., et al. (2017). Depression Is Associated with a Higher Risk of Death among Stroke Survivors. *J Stroke Cerebrovasc Dis* 26(12)**,** 2870-2879. doi: S1052-3057(17)30363-4 [pii]10.1016/j.jstrokecerebrovasdis.2017.07.006.

Rennolds, J., Tower, C., Musgrove, L., Fan, L., Maloney, K., Clancy, J.P., et al. (2008). Cystic fibrosis transmembrane conductance regulator trafficking is mediated by the COPI coat in epithelial cells. *J Biol Chem* 283(2)**,** 833-839. doi: M706504200 [pii]10.1074/jbc.M706504200.

Renshaw, P.F., Parow, A.M., Hirashima, F., Ke, Y., Moore, C.M., Frederick Bde, B., et al. (2001). Multinuclear magnetic resonance spectroscopy studies of brain purines in major depression. *Am J Psychiatry* 158(12)**,** 2048-2055. doi: 10.1176/appi.ajp.158.12.2048.

Rezin, G.T., Amboni, G., Zugno, A.I., Quevedo, J., and Streck, E.L. (2009). Mitochondrial dysfunction and psychiatric disorders. *Neurochem Res* 34(6)**,** 1021-1029. doi: 10.1007/s11064-008-9865-8.

Ridet, J.L., Malhotra, S.K., Privat, A., and Gage, F.H. (1997). Reactive astrocytes: cellular and molecular cues to biological function. *Trends Neurosci* 20(12)**,** 570-577. doi: S0166-2236(97)01139-9 [pii].

Ridnour, L.A., Thomas, D.D., Mancardi, D., Espey, M.G., Miranda, K.M., Paolocci, N., et al. (2004). The chemistry of nitrosative stress induced by nitric oxide and reactive nitrogen oxide species. Putting perspective on stressful biological situations. *Biol Chem* 385(1)**,** 1-10. doi: 10.1515/BC.2004.001.

Ringman, J.M., Saver, J.L., Woolson, R.F., Clarke, W.R., and Adams, H.P. (2004). Frequency, risk factors, anatomy, and course of unilateral neglect in an acute stroke cohort. *Neurology* 63(3)**,** 468-474. doi: 63/3/468 [pii].

Robinson, R.G. (2003). Poststroke depression: prevalence, diagnosis, treatment, and disease progression. *Biol Psychiatry* 54(3)**,** 376-387. doi: S0006322303004232 [pii].

Robinson, R.G., Kubos, K.L., Starr, L.B., Rao, K., and Price, T.R. (1984). Mood disorders in stroke patients. Importance of location of lesion. *Brain* 107 (Pt 1)**,** 81-93.

Robinson, R.G., Schultz, S.K., Castillo, C., Kopel, T., Kosier, J.T., Newman, R.M., et al. (2000). Nortriptyline versus fluoxetine in the treatment of depression and in short-term recovery after stroke: a placebo-controlled, double-blind study. *Am J Psychiatry* 157(3)**,** 351-359. doi: 10.1176/appi.ajp.157.3.351.

Robinson, R.G., Spalletta, G., Jorge, R.E., Bassi, A., Colivicchi, F., Ripa, A., et al. (2008). Decreased heart rate variability is associated with poststroke depression. *Am J Geriatr Psychiatry* 16(11)**,** 867-873. doi: 16/11/867 [pii]10.1097/JGP.0b013e318180057d.

Rodriguez-Arellano, J.J., Parpura, V., Zorec, R., and Verkhratsky, A. (2016). Astrocytes in physiological aging and Alzheimer's disease. *Neuroscience* 323**,** 170-182. doi: S0306-4522(15)00031-7 [pii]10.1016/j.neuroscience.2015.01.007.

Rosell, A., Ortega-Aznar, A., Alvarez-Sabin, J., Fernandez-Cadenas, I., Ribo, M., Molina, C.A., et al. (2006). Increased brain expression of matrix metalloproteinase-9 after ischemic and hemorrhagic human stroke. *Stroke* 37(6)**,** 1399-1406. doi: 01.STR.0000223001.06264.af [pii]10.1161/01.STR.0000223001.06264.af.

Rossi, D.J., Oshima, T., and Attwell, D. (2000). Glutamate release in severe brain ischaemia is mainly by reversed uptake. *Nature* 403(6767)**,** 316-321. doi: 10.1038/35002090.

Rush, A.J., Trivedi, M.H., Wisniewski, S.R., Nierenberg, A.A., Stewart, J.W., Warden, D., et al. (2006). Acute and longer-term outcomes in depressed outpatients requiring one or several treatment steps: a STAR*D report. *Am J Psychiatry* 163(11)**,** 1905-1917. doi: 10.1176/ajp.2006.163.11.1905.

Saeed, S.A., Shad, K.F., Saleem, T., Javed, F., and Khan, M.U. (2007). Some new prospects in the understanding of the molecular basis of the pathogenesis of stroke. *Exp Brain Res* 182(1)**,** 1-10. doi: 10.1007/s00221-007-1050-9.

Sairanen, T., Karjalainen-Lindsberg, M.L., Paetau, A., Ijas, P., and Lindsberg, P.J. (2006). Apoptosis dominant in the periinfarct area of human ischaemic stroke--a possible target of antiapoptotic treatments. *Brain* 129(Pt 1)**,** 189-199. doi: awh645 [pii]10.1093/brain/awh645.

Salter, K., Jutai, J., Hartley, M., Foley, N., Bhogal, S., Bayona, N., et al. (2006). Impact of early vs delayed admission to rehabilitation on functional outcomes in persons with stroke. *J Rehabil Med* 38(2)**,** 113-117. doi: H578581411111731 [pii]10.1080/16501970500314350.

Sanacora, G., Treccani, G., and Popoli, M. (2012). Towards a glutamate hypothesis of depression: an emerging frontier of neuropsychopharmacology for mood disorders. *Neuropharmacology* 62(1)**,** 63-77. doi: S0028-3908(11)00324-8 [pii]10.1016/j.neuropharm.2011.07.036.

Sanacora, G., Zarate, C.A., Krystal, J.H., and Manji, H.K. (2008). Targeting the glutamatergic system to develop novel, improved therapeutics for mood disorders. *Nat Rev Drug Discov* 7(5)**,** 426-437. doi: nrd2462 [pii]10.1038/nrd2462.

Sandoz, G., Bell, S.C., and Isacoff, E.Y. (2011). Optical probing of a dynamic membrane interaction that regulates the TREK1 channel. *Proc Natl Acad Sci U S A* 108(6)**,** 2605-2610. doi: 1015788108 [pii]10.1073/pnas.1015788108.

Sandoz, G., Tardy, M.P., Thummler, S., Feliciangeli, S., Lazdunski, M., and Lesage, F. (2008). Mtap2 is a constituent of the protein network that regulates twik-related K+ channel

expression and trafficking. *J Neurosci* 28(34)**,** 8545-8552. doi: 28/34/8545 [pii]10.1523/JNEUROSCI.1962-08.2008.

Sandoz, G., Thummler, S., Duprat, F., Feliciangeli, S., Vinh, J., Escoubas, P., et al. (2006). AKAP150, a switch to convert mechano-, pH- and arachidonic acid-sensitive TREK K(+) channels into open leak channels. *EMBO J* 25(24)**,** 5864-5872. doi: 7601437 [pii]10.1038/sj.emboj.7601437.

Sanguinetti, M.C., Curran, M.E., Zou, A., Shen, J., Spector, P.S., Atkinson, D.L., et al. (1996). Coassembly of K(V)LQT1 and minK (IsK) proteins to form cardiac I(Ks) potassium channel. *Nature* 384(6604)**,** 80-83. doi: 10.1038/384080a0.

Sanguinetti, M.C., and Jurkiewicz, N.K. (1990). Two components of cardiac delayed rectifier K+ current. Differential sensitivity to block by class III antiarrhythmic agents. *J Gen Physiol* 96(1)**,** 195-215.

Santarelli, L., Saxe, M., Gross, C., Surget, A., Battaglia, F., Dulawa, S., et al. (2003). Requirement of hippocampal neurogenesis for the behavioral effects of antidepressants. *Science.* 301(5634)**,** 805-809.

Santos, M., Kovari, E., Gold, G., Bozikas, V.P., Hof, P.R., Bouras, C., et al. (2009). The neuroanatomical model of post-stroke depression: towards a change of focus? *J Neurol Sci* 283(1-2)**,** 158-162. doi: S0022-510X(09)00430-4 [pii]10.1016/j.jns.2009.02.334.

Sauter, D.R., Sorensen, C.E., Rapedius, M., Bruggemann, A., and Novak, I. (2016). pH-sensitive K(+) channel TREK-1 is a novel target in pancreatic cancer. *Biochim Biophys Acta* 1862(10)**,** 1994-2003. doi: S0925-4439(16)30177-6 [pii]10.1016/j.bbadis.2016.07.009.

Schechter, L.E., Ring, R.H., Beyer, C.E., Hughes, Z.A., Khawaja, X., Malberg, J.E., et al. (2005). Innovative approaches for the development of antidepressant drugs: current and future strategies. *NeuroRx* 2(4)**,** 590-611.

Scherrmann, J.M. (2002). Drug delivery to brain via the blood-brain barrier. *Vascul Pharmacol* 38(6)**,** 349-354. doi: S1537189102002021 [pii].

Schnoor, M., and Parkos, C.A. (2008). Disassembly of endothelial and epithelial junctions during leukocyte transmigration. *Front Biosci* 13**,** 6638-6652. doi: 3178 [pii].

Selman, W.R., Crumrine, R.C., Ricci, A.J., LaManna, J.C., Ratcheson, R.A., and Lust, W.D. (1990). Impairment of metabolic recovery with increasing periods of middle cerebral artery occlusion in rats. *Stroke* 21(3)**,** 467-471.

Serlin, Y., Shelef, I., Knyazer, B., and Friedman, A. (2015). Anatomy and physiology of the blood-brain barrier. *Semin Cell Dev Biol* 38**,** 2-6. doi: S1084-9521(15)00004-X [pii]10.1016/j.semcdb.2015.01.002.

Sharif, Y., Jumah, F., Coplan, L., Krosser, A., Sharif, K., and Tubbs, R.S. (2018). Blood brain barrier: A review of its anatomy and physiology in health and disease. *Clin Anat* 31(6)**,** 812-823. doi: 10.1002/ca.23083.

Shi, D.N., Yuan, Y.T., Ye, D., Kang, L.M., Wen, J., and Chen, H.P. (2018a). MiR-183-5p Alleviates Chronic Constriction Injury-Induced Neuropathic Pain Through Inhibition of TREK-1. *Neurochem Res*. doi: 10.1007/s11064-018-2529-4.

Shi, D.N., Yuan, Y.T., Ye, D., Kang, L.M., Wen, J., and Chen, H.P. (2018b). MiR-183-5p Alleviates Chronic Constriction Injury-Induced Neuropathic Pain Through Inhibition of TREK-1. *Neurochem Res* 43(6)**,** 1143-1149. doi: 10.1007/s11064-018-2529-410.1007/s11064-018-2529-4 [pii].

Shi, Y., Yang, D., Zeng, Y., and Wu, W. (2017). Risk Factors for Post-stroke Depression: A Meta-analysis. *Front Aging Neurosci* 9**,** 218. doi: 10.3389/fnagi.2017.00218.

Shin, W.H., Lee, D.Y., Park, K.W., Kim, S.U., Yang, M.S., Joe, E.H., et al. (2004). Microglia expressing interleukin-13 undergo cell death and contribute to neuronal survival in vivo. *Glia* 46(2)**,** 142-152. doi: 10.1002/glia.10357.

Sibolt, G., Curtze, S., Melkas, S., Pohjasvaara, T., Kaste, M., Karhunen, P.J., et al. (2013). Post-stroke depression and depression-executive dysfunction syndrome are associated with recurrence of ischaemic stroke. *Cerebrovasc Dis* 36(5-6)**,** 336-343. doi: 000355145 [pii]10.1159/000355145.

Siebert, J.R., Conta Steencken, A., and Osterhout, D.J. (2014). Chondroitin sulfate proteoglycans in the nervous system: inhibitors to repair. *Biomed Res Int* 2014**,** 845323. doi: 10.1155/2014/845323.

Silver, J., and Miller, J.H. (2004). Regeneration beyond the glial scar. *Nat Rev Neurosci* 5(2)**,** 146-156. doi: 10.1038/nrn1326nrn1326 [pii].

Smith, J.A., Park, S., Krause, J.S., and Banik, N.L. (2013). Oxidative stress, DNA damage, and the telomeric complex as therapeutic targets in acute neurodegeneration. *Neurochem Int* 62(5)**,** 764-775. doi: S0197-0186(13)00058-2 [pii]10.1016/j.neuint.2013.02.013.

Sofroniew, M.V. (2009). Molecular dissection of reactive astrogliosis and glial scar formation. *Trends Neurosci* 32(12)**,** 638-647. doi: S0166-2236(09)00153-2 [pii]10.1016/j.tins.2009.08.002.

Spalletta, G., Bossu, P., Ciaramella, A., Bria, P., Caltagirone, C., and Robinson, R.G. (2006). The etiology of poststroke depression: a review of the literature and a new hypothesis involving inflammatory cytokines. *Mol Psychiatry* 11(11)**,** 984-991. doi: 4001879 [pii]10.1038/sj.mp.4001879.

Spalletta, G., Cravello, L., Imperiale, F., Salani, F., Bossu, P., Picchetto, L., et al. (2013). Neuropsychiatric symptoms and interleukin-6 serum levels in acute stroke. *J Neuropsychiatry Clin Neurosci* 25(4)**,** 255-263. doi: 1770338 [pii]10.1176/appi.neuropsych.12120399.

Starkstein, S.E., Mizrahi, R., and Power, B.D. (2008). Antidepressant therapy in post-stroke depression. *Expert Opin Pharmacother* 9(8)**,** 1291-1298. doi: 10.1517/14656566.9.8.129110.1517/14656566.9.8.1291 [pii].

Starossom, S.C., Mascanfroni, I.D., Imitola, J., Cao, L., Raddassi, K., Hernandez, S.F., et al. (2012). Galectin-1 deactivates classically activated microglia and protects from inflammation-induced neurodegeneration. *Immunity* 37(2)**,** 249-263. doi: S1074-7613(12)00323-8 [pii]10.1016/j.immuni.2012.05.023.

Steiner, T., Poli, S., Griebe, M., Husing, J., Hajda, J., Freiberger, A., et al. (2016). Fresh frozen plasma versus prothrombin complex concentrate in patients with intracranial haemorrhage related to vitamin K antagonists (INCH): a randomised trial. *Lancet Neurol* 15(6)**,** 566-573. doi: S1474-4422(16)00110-1 [pii]10.1016/S1474-4422(16)00110-1.

Strasser, A. (2005). The role of BH3-only proteins in the immune system. *Nat Rev Immunol* 5(3)**,** 189-200. doi: nri1568 [pii]10.1038/nri1568.

Sun, C., Sun, H., Wu, S., Lee, C.C., Akamatsu, Y., Wang, R.K., et al. (2013). Conditional ablation of neuroprogenitor cells in adult mice impedes recovery of poststroke cognitive function and reduces synaptic connectivity in the perforant pathway. *J Neurosci* 33(44)**,** 17314-17325. doi: 33/44/17314 [pii]10.1523/JNEUROSCI.2129-13.2013.

Sykova, E. (2001). Glial diffusion barriers during aging and pathological states. *Prog Brain Res* 132**,** 339-363. doi: S0079-6123(01)32087-3 [pii]10.1016/S0079-6123(01)32087-3.

Szalay, G., Martinecz, B., Lenart, N., Kornyei, Z., Orsolits, B., Judak, L., et al. (2016). Microglia protect against brain injury and their selective elimination dysregulates neuronal network activity after stroke. *Nat Commun* 7**,** 11499. doi: ncomms11499 [pii]10.1038/ncomms11499.

Szczudlik, A., Dziedzic, T., Bartus, S., Slowik, A., and Kieltyka, A. (2004). Serum interleukin-6 predicts cortisol release in acute stroke patients. *J Endocrinol Invest* 27(1)**,** 37-41. doi: 5428 [pii]10.1007/BF03350908.

Talley, E.M., Solorzano, G., Lei, Q., Kim, D., and Bayliss, D.A. (2001). Cns distribution of members of the two-pore-domain (KCNK) potassium channel family. *J Neurosci* 21(19)**,** 7491-7505. doi: 21/19/7491 [pii].

Tatemichi, T.K., Desmond, D.W., Stern, Y., Paik, M., Sano, M., and Bagiella, E. (1994). Cognitive impairment after stroke: frequency, patterns, and relationship to functional abilities. *J Neurol Neurosurg Psychiatry* 57(2)**,** 202-207.

Taylor, R.A., and Sansing, L.H. (2013). Microglial responses after ischemic stroke and intracerebral hemorrhage. *Clin Dev Immunol* 2013**,** 746068. doi: 10.1155/2013/746068.

Taylor, W.D., Aizenstein, H.J., and Alexopoulos, G.S. (2013). The vascular depression hypothesis: mechanisms linking vascular disease with depression. *Mol Psychiatry* 18(9)**,** 963-974. doi: mp201320 [pii]10.1038/mp.2013.20.

Teitelbaum, P., Cheng, M.F., and Rozin, P. (1969). Development of feeding parallels its recovery after hypothalamic damage. *J Comp Physiol Psychol* 67(4)**,** 430-441.

Terrenoire, C., Lauritzen, I., Lesage, F., Romey, G., and Lazdunski, M. (2001). A TREK-1-like potassium channel in atrial cells inhibited by beta-adrenergic stimulation and activated by volatile anesthetics. *Circ Res* 89(4)**,** 336-342.

Terroni, L., Amaro, E., Iosifescu, D.V., Tinone, G., Sato, J.R., Leite, C.C., et al. (2011). Stroke lesion in cortical neural circuits and post-stroke incidence of major depressive episode: a 4-month prospective study. *World J Biol Psychiatry* 12(7)**,** 539-548. doi: 10.3109/15622975.2011.562242.

Tertyshnikova, S., Knox, R.J., Plym, M.J., Thalody, G., Griffin, C., Neelands, T., et al. (2005). BL-1249 [(5,6,7,8-tetrahydro-naphthalen-1-yl)-[2-(1H-tetrazol-5-yl)-phenyl]-amine]: a putative potassium channel opener with bladder-relaxant properties. *J Pharmacol Exp Ther* 313(1)**,** 250-259. doi: jpet.104.078592 [pii]10.1124/jpet.104.078592.

Thomas, S.A., and Lincoln, N.B. (2008). Predictors of emotional distress after stroke. *Stroke* 39(4)**,** 1240-1245. doi: STROKEAHA.107.498279 [pii]10.1161/STROKEAHA.107.498279.

Thornberry, N.A., and Lazebnik, Y. (1998). Caspases: enemies within. *Science* 281(5381)**,** 1312-1316.

Thummler, S., Duprat, F., and Lazdunski, M. (2007). Antipsychotics inhibit TREK but not TRAAK channels. *Biochem Biophys Res Commun* 354(1)**,** 284-289. doi: 10.1016/j.bbrc.2006.12.199.

Tong, L., Cai, M., Huang, Y., Zhang, H., Su, B., Li, Z., et al. (2014). Activation of K(2)P channel-TREK1 mediates the neuroprotection induced by sevoflurane preconditioning. *Br J Anaesth* 113(1)**,** 157-167. doi: S0007-0912(17)31556-8 [pii]10.1093/bja/aet338.

Truelsen, T., Piechowski-Jozwiak, B., Bonita, R., Mathers, C., Bogousslavsky, J., and Boysen, G. (2006). Stroke incidence and prevalence in Europe: a review of available data. *Eur J Neurol* 13(6)**,** 581-598. doi: ENE1138 [pii]10.1111/j.1468-1331.2006.01138.x.

Tsivgoulis, G., Katsanos, A.H., Butcher, K.S., Boviatsis, E., Triantafyllou, N., Rizos, I., et al. (2014). Intensive blood pressure reduction in acute intracerebral hemorrhage: a meta-analysis. *Neurology* 83(17)**,** 1523-1529. doi: WNL.0000000000000917 [pii]10.1212/WNL.0000000000000917.

Tulleuda, A., Cokic, B., Callejo, G., Saiani, B., Serra, J., and Gasull, X. (2011). TRESK channel contribution to nociceptive sensory neurons excitability: modulation by nerve injury. *Mol Pain* 7**,** 30. doi: 10.1186/1744-8069-7-30.

Vataja, R., Leppavuori, A., Pohjasvaara, T., Mantyla, R., Aronen, H.J., Salonen, O., et al. (2004). Poststroke depression and lesion location revisited. *J Neuropsychiatry Clin Neurosci* 16(2)**,** 156-162. doi: 10.1176/jnp.16.2.15616/2/156 [pii].

Veale, E.L., Al-Moubarak, E., Bajaria, N., Omoto, K., Cao, L., Tucker, S.J., et al. (2014). Influence of the N terminus on the biophysical properties and pharmacology of TREK1

potassium channels. *Mol Pharmacol* 85(5)**,** 671-681. doi: mol.113.091199 [pii]10.1124/mol.113.091199.

Veyssiere, J., Moha Ou Maati, H., Mazella, J., Gaudriault, G., Moreno, S., Heurteaux, C., et al. (2015). Retroinverso analogs of spadin display increased antidepressant effects. *Psychopharmacology (Berl)* 232(3)**,** 561-574. doi: 10.1007/s00213-014-3683-2.

Vierra, N.C., Dadi, P.K., Jeong, I., Dickerson, M., Powell, D.R., and Jacobson, D.A. (2015). Type 2 Diabetes-Associated K+ Channel TALK-1 Modulates beta-Cell Electrical Excitability, Second-Phase Insulin Secretion, and Glucose Homeostasis. *Diabetes* 64(11)**,** 3818-3828. doi: 10.2337/db15-0280.

Voloshyna, I., Besana, A., Castillo, M., Matos, T., Weinstein, I.B., Mansukhani, M., et al. (2008). TREK-1 is a novel molecular target in prostate cancer. *Cancer Res* 68(4)**,** 1197-1203. doi: 10.1158/0008-5472.CAN-07-5163.

Vorhees, C.V., and Williams, M.T. (2006). Morris water maze: procedures for assessing spatial and related forms of learning and memory. *Nat Protoc* 1(2)**,** 848-858. doi: nprot.2006.116 [pii]10.1038/nprot.2006.116.

Walter, S., Kostopoulos, P., Haass, A., Keller, I., Lesmeister, M., Schlechtriemen, T., et al. (2012). Diagnosis and treatment of patients with stroke in a mobile stroke unit versus in hospital: a randomised controlled trial. *Lancet Neurol* 11(5)**,** 397-404. doi: S1474-4422(12)70057-1 [pii]10.1016/S1474-4422(12)70057-1.

Walter, S., Kostpopoulos, P., Haass, A., Helwig, S., Keller, I., Licina, T., et al. (2010). Bringing the hospital to the patient: first treatment of stroke patients at the emergency site. *PLoS One* 5(10)**,** e13758. doi: 10.1371/journal.pone.0013758.

Wang, C.K., Northfield, S.E., Colless, B., Chaousis, S., Hamernig, I., Lohman, R.J., et al. (2014). Rational design and synthesis of an orally bioavailable peptide guided by NMR amide temperature coefficients. *Proc Natl Acad Sci U S A* 111(49)**,** 17504-17509. doi: 10.1073/pnas.1417611111.

Wang, M., Song, J., Xiao, W., Yang, L., Yuan, J., Wang, W., et al. (2012). Changes in lipid-sensitive two-pore domain potassium channel TREK-1 expression and its involvement in astrogliosis following cerebral ischemia in rats. *J Mol Neurosci* 46(2)**,** 384-392. doi: 10.1007/s12031-011-9598-z.

Wang, Q., and Doerschuk, C.M. (2002). The signaling pathways induced by neutrophil-endothelial cell adhesion. *Antioxid Redox Signal* 4(1)**,** 39-47. doi: 10.1089/152308602753625843.

Wang, S.H., Zhang, Z.J., Guo, Y.J., Teng, G.J., and Chen, B.A. (2008). Hippocampal neurogenesis and behavioural studies on adult ischemic rat response to chronic mild stress. *Behav Brain Res* 189(1)**,** 9-16. doi: S0166-4328(07)00632-8 [pii]10.1016/j.bbr.2007.11.028.

Wang, W., Liu, D., Xiao, Q., Cai, J., Feng, N., Xu, S., et al. (2018). Lig4-4 selectively inhibits TREK-1 and plays potent neuroprotective roles in vitro and in rat MCAO model. *Neurosci Lett* 671**,** 93-98. doi: 10.1016/j.neulet.2018.02.015.

Wei, N., Yong, W., Li, X., Zhou, Y., Deng, M., Zhu, H., et al. (2015). Post-stroke depression and lesion location: a systematic review. *J Neurol* 262(1)**,** 81-90. doi: 10.1007/s00415-014-7534-1.

Wei, S., Sun, J., Li, J., Wang, L., Hall, C.L., Dix, T.A., et al. (2013). Acute and delayed protective effects of pharmacologically induced hypothermia in an intracerebral hemorrhage stroke model of mice. *Neuroscience* 252**,** 489-500. doi: S0306-4522(13)00646-5 [pii]10.1016/j.neuroscience.2013.07.052.

Weinstein, P.R., Anderson, G.G., and Telles, D.A. (1986). Neurological deficit and cerebral infarction after temporary middle cerebral artery occlusion in unanesthetized cats. *Stroke* 17(2)**,** 318-324.

Werheid, K. (2015). A Two-Phase Pathogenetic Model of Depression after Stroke. *Gerontology* 62(1)**,** 33-39. doi: 000381876 [pii]10.1159/000381876.

Wiart, L., Petit, H., Joseph, P.A., Mazaux, J.M., and Barat, M. (2000). Fluoxetine in early poststroke depression: a double-blind placebo-controlled study. *Stroke* 31(8)**,** 1829-1832.

Willner, P. (2017). The chronic mild stress (CMS) model of depression: History, evaluation and usage. *Neurobiol Stress* 6**,** 78-93. doi: 10.1016/j.ynstr.2016.08.002S2352-2895(16)30017-0 [pii].

Winter, B., Bert, B., Fink, H., Dirnagl, U., and Endres, M. (2004). Dysexecutive syndrome after mild cerebral ischemia? Mice learn normally but have deficits in strategy switching. *Stroke* 35(1)**,** 191-195. doi: 10.1161/01.STR.0000107188.29688.2C01.STR.0000107188.29688.2C [pii].

Wong, D.T., Perry, K.W., and Bymaster, F.P. (2005). Case history: the discovery of fluoxetine hydrochloride (Prozac). *Nat Rev Drug Discov* 4(9)**,** 764-774. doi: nrd1821 [pii]10.1038/nrd1821.

Wong, M.L., and Licinio, J. (2001). Research and treatment approaches to depression. *Nat Rev Neurosci* 2(5)**,** 343-351. doi: 10.1038/3507256635072566 [pii].

Wood, H. (2010). Migraine: Familial migraine with aura is associated with a mutation in the TRESK potassium channel. *Nat Rev Neurol* 6(12)**,** 643. doi: 10.1038/nrneurol.2010.166.

Wu, D., Song, B.W., Vinters, H.V., and Pardridge, W.M. (2002). Pharmacokinetics and brain uptake of biotinylated basic fibroblast growth factor conjugated to a blood-brain barrier drug delivery system. *J Drug Target* 10(3)**,** 239-245. doi: 10.1080/10611860290022679.

Wu, X., Liu, Y., Chen, X., Sun, Q., Tang, R., Wang, W., et al. (2013). Involvement of TREK-1 activity in astrocyte function and neuroprotection under simulated ischemia conditions. *J Mol Neurosci* 49(3)**,** 499-506. doi: 10.1007/s12031-012-9875-5.

Xian Tao, L., Dyachenko, V., Zuzarte, M., Putzke, C., Preisig-Muller, R., Isenberg, G., et al. (2006). The stretch-activated potassium channel TREK-1 in rat cardiac ventricular muscle. *Cardiovasc Res* 69(1)**,** 86-97. doi: S0008-6363(05)00424-4 [pii]10.1016/j.cardiores.2005.08.018.

Xie, X., Ma, L., Xi, K., Zhang, W., and Fan, D. (2017). MicroRNA-183 Suppresses Neuropathic Pain and Expression of AMPA Receptors by Targeting mTOR/VEGF Signaling Pathway. *Cell Physiol Biochem* 41(1)**,** 181-192. doi: 000455987 [pii]10.1159/000455987.

Xu, X.M., Zou, D.Z., Shen, L.Y., Liu, Y., Zhou, X.Y., Pu, J.C., et al. (2016). Efficacy and feasibility of antidepressant treatment in patients with post-stroke depression. *Medicine (Baltimore)* 95(45)**,** e5349. doi: 10.1097/MD.0000000000005534900005792-201611080-00020 [pii].

Yang, L., Zhang, Z., Sun, D., Xu, Z., Yuan, Y., Zhang, X., et al. (2011). Low serum BDNF may indicate the development of PSD in patients with acute ischemic stroke. *Int J Geriatr Psychiatry* 26(5)**,** 495-502. doi: 10.1002/gps.2552.

Yang, X., Chu, H., Tang, Y., and Dong, Q. (2016). The role of connexin43 in hemorrhagic transformation after thrombolysis in vivo and in vitro. *Neuroscience* 329**,** 54-65. doi: S0306-4522(16)30125-7 [pii]10.1016/j.neuroscience.2016.04.040.

Ye, D., Li, Y., Zhang, X., Guo, F., Geng, L., Zhang, Q., et al. (2015). TREK1 channel blockade induces an antidepressant-like response synergizing with 5-HT1A receptor signaling. *Eur Neuropsychopharmacol* 25(12)**,** 2426-2436. doi: 10.1016/j.euroneuro.2015.09.007.

Yemisci, M., Gursoy-Ozdemir, Y., Vural, A., Can, A., Topalkara, K., and Dalkara, T. (2009). Pericyte contraction induced by oxidative-nitrative stress impairs capillary reflow

despite successful opening of an occluded cerebral artery. *Nat Med* 15(9)**,** 1031-1037. doi: nm.2022 [pii]10.1038/nm.2022.

Yohn, C.N., Gergues, M.M., and Samuels, B.A. (2017). The role of 5-HT receptors in depression. *Mol Brain* 10(1)**,** 28. doi: 10.1186/s13041-017-0306-y.

Yoon, T.H., Han, S.J., Yoon, T.S., Kim, J.S., and Yi, T.I. (2015). Therapeutic effect of repetitive magnetic stimulation combined with speech and language therapy in post-stroke non-fluent aphasia. *NeuroRehabilitation* 36(1)**,** 107-114. doi: T422863512287MJ3 [pii]10.3233/NRE-141198.

Yu, S.P., Yeh, C.H., Sensi, S.L., Gwag, B.J., Canzoniero, L.M., Farhangrazi, Z.S., et al. (1997). Mediation of neuronal apoptosis by enhancement of outward potassium current. *Science* 278(5335)**,** 114-117.

Yuan, Z.H., Jiang, J.K., Huang, W.D., Pan, J., Zhu, J.Y., and Wang, J.Z. (2010). A meta-analysis of the efficacy and safety of recombinant activated factor VII for patients with acute intracerebral hemorrhage without hemophilia. *J Clin Neurosci* 17(6)**,** 685-693. doi: S0967-5868(10)00050-0 [pii]10.1016/j.jocn.2009.11.020.

Zhang, R., Zhang, Z., Zhang, C., Zhang, L., Robin, A., Wang, Y., et al. (2004). Stroke transiently increases subventricular zone cell division from asymmetric to symmetric and increases neuronal differentiation in the adult rat. *J Neurosci* 24(25)**,** 5810-5815. doi: 10.1523/JNEUROSCI.1109-04.200424/25/5810 [pii].

Zhang, Z.H., Wu, L.N., Song, J.G., and Li, W.Q. (2012). Correlations between cognitive impairment and brainderived neurotrophic factor expression in the hippocampus of post-stroke depression rats. *Mol Med Rep* 6(4)**,** 889-893. doi: 10.3892/mmr.2012.1009.

Zhao, Y., Ma, R., Shen, J., Su, H., Xing, D., and Du, L. (2008). A mouse model of depression induced by repeated corticosterone injections. *Eur J Pharmacol* 581(1-2)**,** 113-120. doi: S0014-2999(07)01322-2 [pii]10.1016/j.ejphar.2007.12.005.

Zhou, M., Xu, G., Xie, M., Zhang, X., Schools, G.P., Ma, L., et al. (2009). TWIK-1 and TREK-1 are potassium channels contributing significantly to astrocyte passive conductance in rat hippocampal slices. *J Neurosci* 29(26)**,** 8551-8564. doi: 29/26/8551 [pii]10.1523/JNEUROSCI.5784-08.2009.

Zhou, X., Spittau, B., and Krieglstein, K. (2012). TGFbeta signalling plays an important role in IL4-induced alternative activation of microglia. *J Neuroinflammation* 9**,** 210. doi: 1742-2094-9-210 [pii]10.1186/1742-2094-9-210.

Ziai, W.C., Tuhrim, S., Lane, K., McBee, N., Lees, K., Dawson, J., et al. (2014). A multicenter, randomized, double-blinded, placebo-controlled phase III study of Clot Lysis Evaluation of Accelerated Resolution of Intraventricular Hemorrhage (CLEAR III). *Int J Stroke* 9(4)**,** 536-542. doi: 10.1111/ijs.12097.

Zong, W.X., and Thompson, C.B. (2006). Necrotic death as a cell fate. *Genes Dev* 20(1)**,** 1-15. doi: 20/1/1 [pii]10.1101/gad.1376506.

Bibliographie personnelle

Article 1

Djillani, A., et al., *Shortened Spadin Analogs Display Better TREK-1 Inhibition, In Vivo Stability and Antidepressant Activity.* Front Pharmacol, 2017. **8**: p. 643.

Article 2

Pietri, M., et al., *First evidence of protective effects on stroke recovery and post-stroke depression induced by sortilin-derived peptides.* Neuropharmacology, 2019.

Article 3

Djillani, A., et al., *Fighting against depression with TREK-1 blockers: Past and future. A focus on spadin.* Pharmacol Ther, 2019. **194**: p. 185-198.

Article 4

Moreno, S., et al., *Altered Trek-1 Function in Sortilin Deficient Mice Results in Decreased Depressive-Like Behavior*. Front Pharmacol, 2018. **9**: p. 863.

Article 5

Hosseiny, S., et al., *Differential neuronal plasticity in mouse hippocampus associated with various periods of enriched environment during postnatal development.* Brain Struct Funct, 2015. **220**(6): p. 3435-48.

Article 6

Nicolas, S., et al., *Neurogenesis-independent antidepressant-like effects of enriched environment is dependent on adiponectin.* Psychoneuroendocrinology, 2015. **57**: p. 72-83.

Article 7

Harb, K., et al., *Area-specific development of distinct projection neuron subclasses is regulated by postnatal epigenetic modifications.* Elife, 2016. **5**: p. e09531.

Annexes

A- Article 3 : "Fighting against depression with TREK-1 blockers: Past and future. A focus on spadin"

Les résultats obtenus lors de mon doctorat ont également été valorisés dans une revue parue dans Pharmacology & Therapeutics en 2019 (if : 10.5).

Cette revue rappelle les propriétés de la Spadine et résume les différentes stratégies utilisées dans le but d'améliorer sa stabilité *in vivo*. Elle présente le développement de la Spadine et de ses analogues depuis l'hypothèse de ses propriétés antidépressives, jusqu'au développement des analogues courts qui sont, aujourd'hui, les peptides présentant le plus d'intérêts pharmacologiques et pharmaceutiques quant à leur développement comme médicaments antidépresseurs.

Cette revue aborde également les propriétés d'autres inhibiteurs de TREK-1, tels que la Fluoxétine, qui est un des antidépresseurs les plus couramment utilisés en clinique.

Pour finir, elle insiste sur le fait que, pour l'instant, la plupart des études ont été effectuées sur des modèles animaux. Toutefois, elle met également en avant des études réalisées au laboratoire en collaboration avec une équipe italienne qui démontrent en utilisant une méthode de dosage spécifique que le taux circulant d'activité spadine, mesurée par les taux de PE, sont plus faibles chez les patients dépressifs que chez les contrôles. De façon intéressante, les traitements pharmacologiques avec des antidépresseurs restaurent un niveau normal de PE. La quantification longitudinale de la concentration sérique de PE pourrait ainsi assister les psychiatres dans le diagnostic et la définition de l'efficacité de la réponse aux traitements et donc, le cas échéant, de modifier la stratégie thérapeutique.

Toutefois, des cohortes plus importantes devront être utilisées pour pouvoir définir avec certitude la Spadine comme un marqueur de dépression.

Pharmacology & Therapeutics 194 (2019) 185–198

Contents lists available at ScienceDirect

Pharmacology & Therapeutics

journal homepage: www.elsevier.com/locate/pharmthera

Fighting against depression with TREK-1 blockers: Past and future. A focus on spadin

Alaeddine Djillani [a,b], Mariel Pietri [a,b], Jean Mazella [a,b], Catherine Heurteaux [a,b], Marc Borsotto [a,b,*]

[a] Centre National de la Recherche Scientifique, Institut de Pharmacologie Moléculaire et Cellulaire, UMR7275, Université Côte d'Azur, Valbonne, France
[b] Université Côte d'Azur, CNRS, IPMC, France

ARTICLE INFO

Available online 3 October 2018

Keywords:
TREK-1
Depression
Blockers
Spadin
Peptide
Analogs

ABSTRACT

Depression is a devastating mood disorder and a leading cause of disability worldwide. Depression affects approximately one in five individuals in the world and represents heavy economic and social burdens. The neurobiological mechanisms of depression are not fully understood, but evidence highlights the role of monoamine neurotransmitter balance. Several antidepressants (ADs) are marketed to treat depression and related mood disorders. However, despite their efficacy, they remain nonspecific and unsafe because they trigger serious adverse effects. Therefore, developing new molecules for new targets in depression has become a real necessity. Eight years ago, spadin was described as a natural peptide with AD properties. This 17-amino acid peptide blocks TREK-1 channels, an original target in depression. Compared to the classical AD drugs such as fluoxetine, which requires 3–4 weeks for the AD effect to manifest, spadin acts rapidly within only 4 days of treatment. The AD properties are associated with increased neurogenesis and synaptogenesis in the brain. Despite the advantages of this fast-acting AD, the *in vivo* stability is weak and does not last for >7 h. The present review summarizes different strategies such as retro-inverso strategy, cyclization, and shortening the spadin sequence that has led to the development and optimization of spadin as an AD. Shortened spadin analogs present increased inhibition potency for TREK-1, an improved AD activity, and prolonged *in vivo* bioavailability. Finally, we also discuss about other inhibitors of TREK-1 channels with a proven efficacy in treating depression in the clinic, such as fluoxetine.

Contents

Abbreviations: 5-HT, serotonin; AA, arachidonic acid; AD, antidepressant; AKAP, A-kinase-anchoring protein; BBB, blood–brain barrier; BDNF, Brain-derived neurotrophic factor; BrdU, 5-Bromo-2′-Deoxyuridine; CNS, central nervous system; CREB, cAMP response element-binding protein; CSMT, conditioned suppression of motility test; DA, dopamine; DAT, dopamine transporter; DRN, dorsal raphe nucleus; FST, forced swim test; GABA, γ-Aminobutyric acid; GLP-1, glucagon-like peptide-1; IC_{50}, half-maximal inhibitory concentration; i.c.v., intracerebroventricular route; i.p., intraperitoneal route; i.v., intravenous route; K_{2P}, two-pore domain K^+ channel; K_{ATP}, ATP-sensitive potassium channels; LHT, learned helplessness test; MAO, monoamine oxidase; MDD, major depression disorder; mGluR, metabotropic glutamate receptor; MMP, matrix metalloproteinase; Mtap2, microtubule-associated protein; NA, norepinephrine; NAT, norepinephrine transporter; NBP, 3-*n*-Butylphthalide; NSF, novelty-suppressed feeding test; NT, neurotensin; NTSR-3, neurotensin receptor-3; PE, propeptide; PKA, protein kinase A; ProNGF, precursor of the nerve growth factor; PSD-95, postsynaptic density protein-95; PTZ, pentylenetetrazol; RI, retro-inverso; SERT, serotonin transporter; SNRI, serotonin–norepinephrine reuptake inhibitor; Spadin, sortilin-derived peptide with antidepressant activity; SSRI, selective serotonin reuptake inhibitor; TdP, Torsades de pointes; TRAAK, TWIK-related arachidonic acid-activated K^+ channel; TREK-1, TWIK-related K^+ channel-1; TWIK-1, Tandem of P domains in weak inward rectifying K^+ channel-1; TST, tail suspension test.

* Corresponding author at: IPMC, UMR7275, 660 route des Lucioles, Sophia Antipolis, 06560 Valbonne, France.
E-mail address: borsotto@ipmc.cnrs.fr (M. Borsotto).

https://doi.org/10.1016/j.pharmthera.2018.10.003

1. Introduction

Depression is a devastating mental disorder that affects one in five individuals and is considered as a leading cause of disability worldwide (Nestler et al., 2002; Otte et al., 2016). Thus, the economic burden is huge for governments and particularly for patients suffering from depression (Kessler, 2012). Depression is a product of several and complex molecular and cellular mechanisms that are difficult to identify. One of the main common hypotheses that attempt to explain the neurobiology of depression is the imbalance in monoamine levels in the brain known as the "monoaminergic theory of depression" (Delgado, 2000). Presently, the majority of antidepressant (AD) drugs aim to restore the physiological amount of three central monoamines (serotonin (5-HT), norepinephrine (NA), and dopamine (DA)) in the synaptic cleft. Indeed, this is achievable by blocking the serotonin transporter (SERT), norepinephrine transporter (NAT), and dopamine transporter (DAT) responsible for the reuptake of 5-HT, NA, and DA, respectively, in the brain (Tatsumi, Groshan, Blakely, & Richelson, 1997). Inhibiting 5-HT and NA degradation through monoamine oxidase (MAO) enzyme increases the synaptic concentrations of monoamines (Brandon, 1982). However, with their proven efficacy, these AD drugs present a delay of action that remains very long (Cipriani et al., 2018; Stassen, Angst, & Delini-Stula, 1997). The late onset of action of current AD drugs takes several weeks to manifest. Given the complexity of the physiopathology of depression, many mechanisms and factors could be responsible for monoaminergic transmission, stress, inflammation, neurogenesis, and neuroplasticity (Dean & Keshavan, 2017). Moreover, AD drugs are frequently associated with various adverse effects such as fatigue, anxiety, sexual dysfunction, headache, and nausea. Often, these adverse effects lead patients to discontinue their AD treatment and in some cases can worsen or even cause increased suicide risk (Bull et al., 2002; Nischal, Tripathi, Nischal, & Trivedi, 2012; Sharma, Guski, Freund, & Gotzsche, 2016; Sicouri & Antzelevitch, 2008). This increased risk could be attributed to either the drug itself, a delayed onset of action, a wrong dosage, or a discontinuity in the treatment (Fergusson et al., 2005; Otte et al., 2016). To date, the main goals of the new AD strategy in drug design and development are to shorten the latency time for AD activity to manifest and substantially reduce adverse effects (Ramaker & Dulawa, 2017). The most common AD drugs in use currently as a first-line treatment are the selective serotonin reuptake inhibitors (SSRIs) and the serotonin–norepinephrine reuptake inhibitors (SNRIs). Their safety is seriously questioned in a series of studies (Cascade, Kalali, & Kennedy, 2009; Ferguson, 2001; Masand & Gupta, 2002; Montgomery, 2008; Read & Williams, 2018). As a result, the biggest challenge currently is to prescribe efficient AD drugs but with an acceptable tolerance in depressive patients. Newer AD classes have been discovered, such as multimodal AD drugs (Richelson, 2013). In addition to SERT inhibition, these drugs also antagonize $5HT_3$ and $5HT_7$ receptors and behave as partial agonists of $5HT_{1B}$ and full agonists of $5HT_{1A}$ receptors (Katona & Katona, 2014). Recently, the fast-acting AD drug ketamine has been identified and might represent a new generation of AD drugs able to counteract depression with a fast onset of action (Caraci, Leggio, Salomone, & Drago, 2017; Kavalali & Monteggia, 2015). However, despite the advanced level of clinical development accomplished by ketamine, this drug licensed as an anesthetic and painkiller has to be handled with extreme caution. A long list of serious adverse effects caused by ketamine was reported in many studies as described in the review of Short et al. (Short, Fong, Galvez, Shelker, & Loo, 2017). More recently, a study has identified ELK-1 transcription factor, which is an ERK downstream module as a potential target for treating depression. ELK-1 is upregulated in depressive patients. In mice, selective inhibition of ELK-1 phosphorylation using a 31-amino acid peptide, called TDE, produces AD-like behavior in different tests (Apazoglou et al., 2018). To improve AD efficacy, or suppress unwanted adverse effects, new strategies should be considered involving endogenous molecules. This includes essentially peptides that are naturally synthesized in the human body to exert specific actions. Indeed, peptides are involved in numerous biological functions in the cell, mainly as signaling molecules and also as ligands for several types of receptors. Considering their attractive pharmacological properties, peptides constitute an excellent starting point for designing novel therapeutic molecules. Their specificity results in excellent efficacy, safety, and tolerability in humans (Fosgerau & Hoffmann, 2015).

Growing evidence places therapeutic peptides as a very promising market, and the number of candidate peptides has shown an important increase in clinical trials (Uhlig et al., 2014). To date, approximately 100 therapeutic peptides are marketed in the United States, Europe, and Japan (Kaspar & Reichert, 2013). In a pharmaceutical industry that lacks efficient innovations, peptides constitute a potential alternative in the treatment of numerous diseases and disorders. Furthermore, new targets in depression need to be discovered and validated for innovative molecules. The goals are to improve AD therapy, eliminate adverse effects, and treat patients who are resistant to classical AD drugs. Ion channels represent almost 20% of all the human protein targets (Santos et al., 2017). Until 2015, 177 small molecules and biologic effectors of ion channels had been approved as treatments for several pathologies (Santos et al., 2017). In the present review, we discuss the spadin (or its analogs)–TREK-1 channel interaction that leads to channel blocking, one of the most promising drug–target interactions in term of CNS disorder treatments, mainly in the depression process.

2. TREK-1 in depression

2.1. TREK-1 channel

The TWIK-related K^+ channel-1 (TREK-1) is a member of the two-pore domain K^+ channel family (K_{2P}) (Honore, 2007; Lesage & Lazdunski, 1998). As with other K_{2P} channels, TREK-1 channels are responsible for maintaining the neuronal resting membrane potential and controlling action potential duration and also participate in neurotransmitter release (Honore, 2007). TREK-1, TREK-2, and TRAAK are part of lipid and mechanosensitive K_{2P} channel subfamily. TREK-1 and TREK-2 share >78% of homology (Lesage & Lazdunski, 2000). In the cell, TREK-1 is regulated by a variety of physical and chemical stimuli (Honore, 2007). Activation of TREK-1 channels can be mediated by membrane stretch (Maingret, Patel, Lesage, Lazdunski, & Honore, 1999; Patel et al., 1998), internal acidosis (Honore, Maingret, Lazdunski, & Patel, 2002; Maingret et al., 1999), heat (Maingret et al., 2000), lipids (Kim, 2003; Patel & Honore, 2001), and polyunsaturated fatty acids such as arachidonic acid (AA) (Patel et al., 1998). Pharmacological opening of the channel is mediated by volatile general anesthetics (Patel et al., 1999) and analgesics such as morphine through the activation of μ-opioid receptors (Devilliers et al., 2013). TREK-1 is downregulated upon stimulation of Gs- and Gq-coupled receptors. In fact, stimulation of $5\text{-}HT_4$ receptors by 5-HT (Fink et al., 1996; Patel et al., 1998) or the metabotropic glutamate receptors mGluR1 and mGluR5 by glutamate inhibits the TREK-1 channel (Chemin et al., 2003; Lopes et al., 2005). TREK-1 is also inhibited by SSRIs such as fluoxetine (Heurteaux et al., 2006b; Kennard et al., 2005) and the endogenous peptide spadin; this is described in detail in this review (Mazella et al., 2010).

2.2. Screening of TREK-1 modulators in vitro

Since its discovery, TREK-1 was shown to play a major role in several physiopathological processes (Honore, 2007). Its widespread presence in a multitude of functions varying from neurologic brain disorders to arrhythmia in the heart confirms the highly attractive target that TREK-1 represents currently. Through the generation of TREK-1 knockout ($kcnk2^{-/-}$) mice, it was clearly demonstrated that TREK-1 channels are involved in several pathologies. TREK-1 activation is known to have neuroprotective properties against ischemia or epilepsy (Blondeau

et al., 2007; Heurteaux et al., 2004; Lauritzen et al., 2000). More interestingly, *kcnk2*$^{-/-}$ mice demonstrated that TREK-1 channels are involved in the depression process. Deletion of TREK-1 channels resulted in a depression-resistant phenotype. This particular phenotype was identified by different animal assays for depressive-like behaviors (such as FST, TST, CMST, NSF, or LHT), *i.e.*, an increase in 5-HT neurotransmission and a reduction in elevated corticosterone levels under stress (Heurteaux, Lucas, et al., 2006b). Together, these data indicate that TREK-1 modulators are of great pharmacological interest. With the aim to efficiently and easily screen TREK-1 modulators, a HEK293 cell line that stably expresses the human TREK-1 channel was generated and named as the hTREK-1/HEK cell line (Moha ou Maati et al., 2011). Thus, screening TREK-1 activators for characterizing new neuroprotective molecules could be made easier using the hTREK-1/HEK cell line. The hTREK-1/HEK cell line was validated as an efficient pharmacological tool for screening TREK-1 effectors because it responded to various chemical and physical stimuli that modulate TREK-1 activity. In addition, TREK-1 was associated with pain perception (Alloui et al., 2006). Consequently, activators of TREK-1 channels displaying *in vivo* analgesic activity were also screened using the hTREK-1/HEK cell line (Vivier et al., 2017). Another stable TREK-1 transfected HEK cell line was used to study the role of TREK-1 channels in maintaining uterine quiescence during pregnancy (Heyman et al., 2013). Recently, a CHO cell line stably expressing hTREK-1, named as CHO/hTREK-1 cells, was generated to study the effect of overexpression of TREK-1 on cell proliferation (Zhang, Yin, Wang, Li, & Wang, 2016). The design of the hTREK-1/HEK cell line was also of great importance for research and screening of new and specific TREK-1 inhibitors with AD properties (Borsotto et al., 2015; Djillani et al., 2017; Moha Ou Maati et al., 2012; Veyssiere et al., 2015).

2.3. Small molecule inhibitors of TREK-1

2.3.1. Selective serotonin reuptake inhibitors

The monoaminergic hypothesis of depression has driven a number of research laboratories to search for new molecules that block 5-HT reuptake. Fluoxetine was approved as an AD in 1986, and clinical trials showed a clear improvement in adverse effects previously observed with tricyclics (Perez-Caballero, Torres-Sanchez, Bravo, Mico, & Berrocoso, 2014). The AD activity was attributed to the high-affinity blockade of SERT, thereby leading to an increase in the amount of 5-HT in the synapses (Wong, Horng, Bymaster, Hauser, & Molloy, 1974).

At clinical concentrations, TREK-1 channels were significantly blocked by fluoxetine and its active metabolite norfluoxetine in a concentration-dependent manner, and the IC_{50}s were 19 μM and 9 μM, respectively (Heurteaux, Lucas, et al., 2006b; Kennard et al., 2005) (Table 1). TREK-1 inhibition seems to be state dependent because norfluoxetine binds to the fenestration in TREK-1 that is only available in the down state (when the lower sections of M2, M3, and M4 transmembrane domains project into the cytoplasm) corresponding to the channel lower activity (Dong et al., 2015). However, when TREK-1 is activated by stretch or AA, the channel conformation changes to the up state (when lower sections of M2, M3, and M4 transmembrane domains project into the membrane), which suppresses the fenestration and does not allow norfluoxetine to bind (Dong et al., 2015; Kennard et al., 2005). In a recent study, other SSRIs have been shown to be potent blockers of TREK-1 and TREK-2 channels in HEK-293 cells and HT-22 neuronal cells. In addition to fluoxetine, TREK-1 inhibition was also observed with paroxetine and citalopram, two other commonly prescribed AD drugs (Kim, Lee, Hong, Han, & Kang, 2017) (Table 1).

2.3.2. Other inhibitors of TREK-1 channels

Few molecules were identified in the literature as potent TREK-1 channel blockers (Table 1). SID1900, a small molecule screened from a large library of 487 compounds, has been shown to block TREK-1 channels in a manner similar to that of spadin and to induce an AD-like behavior in a rat model of chronic unpredictable mild stress (Ye et al., 2015). SID1900 inhibits TREK-1 with an IC_{50} of 29.72 μM, which largely exceeds that obtained with spadin (peptide #1 Table 2) (IC_{50} = 40 nM) (Djillani et al., 2017). Furthermore, antipsychotic drugs have been shown to be modulators of TREK-1 channels (Thummler, Duprat, & Lazdunski, 2007). Typical and atypical antipsychotics such as fluphenazine, chlorpromazine, haloperidol, loxapine, and clozapine inhibit TREK-1 and TREK-2 channels in a dose-dependent manner without affecting TRAAK channels (Kim et al., 2017; Thummler et al., 2007) (Table 1). In contrast to antipsychotic drugs, mood stabilizers such as lithium chloride, valproate, gabapentin, and carbamazepine activate TREK-1 channels but have no effect on TREK-2 channels (Kim et al., 2017). Dihydropyridine Ca^{2+} channel antagonists such as amlodipine and niguldipine are nonspecific blockers of TREK-1 channels (Table 1). They inhibit TREK-1 channels with an IC_{50} of 0.43 and 0.75 μM, respectively (Liu, Enyeart, & Enyeart, 2007). *In vitro*, they potently block calcium-induced vascular smooth muscle contractions with IC_{50} of 1.9 and 4.1 nM for amlodipine and nifedipine, respectively (Burges et al., 1987). In addition, L-methionine was reported to decrease the probability of TREK-1 opening in a cell-attached patch-clamp configuration (Baker et al., 2008; Lei et al., 2014) (Table 1). This amino acid was used as a tool to investigate the role of TREK-1 in uterine contraction (Yin et al., 2018) and in controlling bladder smooth muscle cell excitability following contraction (Baker et al., 2008). However, L-methionine inhibition on TREK-1 has been shown to have contrast in another study where no TREK-1 inhibitory effect was observed in rat colon smooth muscle cells after activation with AA (Gil et al., 2012). The neuroprotective compound 3-*n*-Butylphthalide (NBP) and its racemic form *dl*-NBP were reported to block TREK-1 (Ji, Zhao, Cao, Shi, & Wang, 2011). Recently, another NBP analog, named as lig4-4, was described as a specific blocker of TREK-1 (Wang et al., 2018). The authors presumed that the neuroprotective effects of lig4-4 observed in ischemic stroke might be related to TREK-1 inhibition (Wang et al., 2018). This hypothesis shows total contradiction to data published >10 years ago that showed that the opening of TREK-1 is neuroprotective (Heurteaux, Laigle, Blondeau, Jarretou, & Lazdunski, 2006a). However, neither NBP nor lig4-4 can be considered as specific blockers for TREK-1 because lig4-4 also inhibits hERG, K_v1.5, K_v2.1, K_v3.1, and neuronal Na^+ and Ca^{2+} channels (Wang et al., 2018).

2.4. Birth of an idea…

Approximately 10 years ago, TREK-1 was described as a new target in depression (Heurteaux, Lucas, et al., 2006b). This K_{2P} mechanosensitive channel is mainly expressed in the prefrontal cortex and the hippocampus (Heurteaux, Lucas, et al., 2006b; Medhurst et al., 2001). These regions are known to mediate cognitive aspects of depression, such as memory impairment, feeling of worthlessness, guilt, and suicidality (Nestler et al., 2002; Otte et al., 2016). TREK-1 is also expressed in the amygdala, hypothalamus, and in the striatum, particularly in the nucleus accumbens to mediate memory of emotional events. Finally, TREK-1 is abundant in GABA (γ-aminobutyric acid)-containing neurons of the caudate nucleus and putamen (Hervieu et al., 2001) and in hippocampal glutamatergic neurons (Medhurst et al., 2001). Investigation of the role of TREK-1 channel in the physiopathology of depression by using the knockout of *Kcnk2* (the gene coding for TREK-1 channel) in mice demonstrated a depression-resistant phenotype (Heurteaux, Lucas, et al., 2006b) in five assays for depression-like behaviors (Cryan & Holmes, 2005): Tail Suspension Test (TST), Forced Swim Test (FST), Conditioned Suppression of Motility Test (CSMT), Learned Helplessness Test (LHT), and Novelty-Suppressed Feeding Test (NSF). In TREK-1-deficient mice, neurogenesis induced by the well-known SSRI fluoxetine was significantly increased compared to the wild-type mice (Heurteaux, Lucas, et al., 2006b). However, the proliferation of newborn cells manifested only after 21 days of treatment.

Table 1
Molecules described as TREK-1 blockers.

TREK-1 blockers		Cell types	IC_{50}	Specificity	Antidepressant activity	Onset of action	Reference
SSRIs	Fluoxetine	HEK 293	19 μM 37.9 ± 7.7 μM	Blocks TREK-2 (IC_{50} = 28.7 ± 7.6 μM), SERT and TASK-3	FST (acute and chronic – 14-21 days) No effect after 3 day subchronic treatment	Slow 2–4 weeks	(Detke, Rickels, & Lucki, 1995; Kennard et al., 2005; Kim et al., 2017; Wong et al., 1974)
	Norfluoxetine	HEK 293	9 μM	Blocks TREK-2 (IC_{50} = 4.9 ± 0.5 μM)	nd	nd	(Kim et al., 2017; Kobayashi, Washiyama, & Ikeda, 2006; Lee, Chai, Hahn, & Choi, 2018; McClenaghan et al., 2016; Thummler et al., 2007)
	Paroxetine	COS-7	20 μM tested	Blocks TREK-2 (at 20 μM tested), SERT, GIRK and Kv3.1	FST (acute)	Slow 2–4 weeks	
	Citalopram	HEK 293	100 μM tested	Blocks TREK-2 (at 100 μM tested), SERT, Kv1.5 (IC_{50} = 2.8 ± 1.1 μM) and L-type Ca^{2+} channels (IC_{50} = 60.3 ± 8.5 μM)	nd	Slow 2–4 weeks	(Hamplova-Peichlova et al., 2002; Kim et al., 2017; Lee, Hahn, & Choi, 2010)
Spadin and analogs	Spadin (PE 12–28)	**Cos-7, HEK293**	**40 nM**	Specific to TREK-1 No effect on TREK-2, TRAAK, TRESK, TASK-1, and hERG channels	FST (acute and subchronic), TST, LHT, and NSF (subchronic)	**Fast only after 4 days**	(Mazella et al., 2010; Moha Ou Maati et al., 2012) (Djillani et al., 2017)
	PE 22–28	**HEK 293**	**0.12 nM**				
	G/A-PE 22–28	**HEK 293**	**0.10 nM**				
	Biotin-G/A-PE 22–28	**HEK 293**	**1.2 nM**				
Antipsychotics	Fluphenazine	Cos-7	4.7 μM	Block TREK-2 (at 10 μM tested), no effect on TRAAK at 10 μM	nd	nd	(Thummler et al., 2007)
	Chlorpromazine	Cos-7	2.7 μM				
	Haloperidol	Cos-7	5.5 μM				
	Flupenthixol	Cos-7	2.0 μM				
	Loxapine	Cos-7	19.7 μM				
	Pimozide	Cos-7	1.8 μM				
	Clozapine	Cos-7	10 μM tested				
Dihydropyridine Ca^{2+} channel antagonists	Amlodipine	AZF cells (adrenal gland)	0.43 μM	Block L-type Ca^{2+} channels	nd	nd	(Liu et al., 2007)
	Niguldipine	AZF cells (adrenal gland)	0.75 μM		nd	nd	
Other TREK-1 blockers	SID1900	HEK 293	29.72 μM	nd	Rat model of CUMS, 14 day and 21 day FST, Sucrose preference (14 d and 28 d)	2 weeks	(Ye et al., 2015)
	L-methionine	Bladder smooth muscle cells	1 mM (controversial)	nd	nd	nd	(Lei et al., 2014)
	l-NBP, *d*-NBP, *ld*-NBP	CHO	0.06 ± 0.03 μM	nd	nd	nd	(Ji et al., 2011)
	lig4–4	CHO	2.06 μM	Blocks K_v2.1, K_v1.5, K_v3.1, hERG and neuronal Na^+ and Ca^{2+} channels (IC_{50} = 30 μM)	nd	nd	(Wang et al., 2018)

On the other hand, deletion of the *Kcnk2* gene enhanced the firing of 5-HT neurons in the dorsal raphe nucleus (Heurteaux, Lucas, et al., 2006b). Knowing the importance of 5-HT in the neurobiology of depression "Monoaminergic Theory of Depression" (Duman, Heninger, & Nestler, 1997) and because TREK-1 is inhibited by SSRIs such as fluoxetine, this K_{2P} channel has been considered as a serious candidate to play a key role in the physiopathology of depression (Heurteaux, Lucas, et al., 2006b).

In humans, Star*D study has identified an association between the existence of four genetic variants (single nucleotide polymorphisms [SNPs]) in the TREK-1 locus and resistance to multiple AD classes (Perlis et al., 2008). Another study showed that an SNP at the 3′-untranslated region on exon 7 of the kcnk2 gene could be associated with both depression incidence and poor treatment efficacy (Liou et al., 2009). Although no brain imaging studies in depressive patients have been published yet, a study suggested that some TREK-1 genotypes in humans can be associated with a depression-resistant phenotype (Dillon et al., 2010). Taken together, these studies in humans strengthen the idea that TREK-1 represents a crucial target in the field of depression and the search for selective blockers of TREK-1 might potentially lead to a new generation of AD drugs.

2.5. SORTing TREK-1...

Within the neuron, the TREK-1 channel forms a complex made of the A-kinase-anchoring protein AKAP150 (Sandoz et al., 2006) and the microtubule-associated protein Mtap2 (Sandoz et al., 2008). Both proteins regulate the sorting of TREK-1 to the plasma membrane. However, these partner proteins are not unique. In 2010, another crucial interacting protein, named as sortilin, was discovered. Sortilin regulates, transports, and targets the TREK-1 channel to the plasma membrane where it exerts its role as a background potassium channel (Mazella et al., 2010). Two decades ago, sortilin, a 95 kDa protein, was identified as a sorting molecule in the human brain (Petersen et al., 1997). It was also described shortly later in another study as the neurotensin receptor-3 (NTSR-3) (Mazella et al., 1998). Sortilin/NTSR-3 binds a number of ligands such as neurotensin (NT), precursor of the nerve growth factor (proNGF) (Nykjaer et al., 2004), lipoprotein lipase (Nielsen, Jacobsen, Olivecrona, Gliemann, & Petersen, 1999), and propeptide (PE) (Munck Petersen et al., 1999). In the Golgi network, the post-translational cleavage of prosortilin (precursor of sortilin) by the protein convertase furin results in mature sortilin and the release

Table 2
Summary of effects of spadin analogs on TREK-1 inhibition and FST immobility time.

Peptide number	Peptide names	Modifications	% of TREK-1 inhibition	Significance	FST in acute (s)	Significance
1	**PE 12-28 (Spadin)**	**No modification**	**87.08 ± 7.32**	***	**107.40 ± 5.05**	***
2	Ac-PE 12-28	*N*-acetylation	83.46 ± 8.33	***	nd	nd
3	Ac-RI-PE 12-28	retro-inverso of spadin	94.43 ± 10.87	***	135.10 ± 8.11	**
4	Ac-PE-22-28	*N*-acetylation	19.29 ± 25.7	ns	nd	nd
5	Ac-PE-21-28	*N*-acetylation	26.89 ± 14.9	ns	nd	nd
6	Ac-RI-PE-21-28	*N*-acetylation + retro-inverso	31.19 ± 17.8	ns	nd	nd
7	Ac-PE 1-28	*N*-acetylation	10.43 ± 28.5	ns	nd	nd
8	Ac-RI-PE 1-28	*N*-acetylation + retro-inverso	108.59 ± 10	***	83.60 ± 9.01	***
9	Ac-PE 6-28	*N*-acetylation	71.85 ± 28.12	**	nd	nd
10	Ac-RI-PE 6-28	*N*-acetylation + retro-inverso	56.47 ± 24.13	*	nd	nd
11	Ac-PE 1-44	*N*-acetylation	26.97 ± 6.25	ns	nd	nd
12	Ac-RI-PE 1-44	*N*-acetylation + retro-inverso	37.73 ± 8.77	ns	nd	nd
13	G/A-PE 12-28	aa substitution	83.5 ± 9.76	***	120.4 ± 9.7	**
14	RI-G/A-PE 12-28	retro-inverso +aa substitution	72.15 ± 11.75	***	127.7 ± 8.32	**
15	c(RI-PE 12-28)	cyclization	67.24 ± 3.41	***	157 ± 8.09	ns
16	$c(RI\text{-}PE\ 12\text{-}28)_2$	cyclization	91.25 ± 8.14	***	146.7 ± 12.99	ns
17	PE 12-27	No modification	28.39 ± 9.916	**	100.2 ± 5.0	***
18	PE 14-25	No modification	0	ns	112.2 ± 7.1	**
19	PE 22-27	No modification	25.7 ± 20.01	ns	168.2 ± 4.2	ns
20	PE 22-25	No modification	36.02 ± 17.47	*	100.2 ± 5.0	***
21	**PE 22-28**	**No modification**	**55.46 ± 4.555**	***	**91.8 ± 6.1**	***
22	Biotin-PE 22-28	N-biotinylation	53.03 ± 6.416	***	112.1 ± 4.3	***
23	Dansyl-PE 22-28	N-dansylation	48.78 ± 14.52	**	104.6 ± 11.8	***
24	PE 22-28-O-Methyl	C-methoxylation	42.98 ± 13.47	**	137.1 ± 8.1	*
25	PE 22-28-O-Ethyl	C-ethoxylation	41.39 ± 11.52	**	113.2 ± 8.5	***
26	Formyl-PE 22-28	N-formylation	32.45 ± 12.22	*	nd	nd
27	**G/A-PE 22-28**	**aa substitution**	**50.61 ± 7.935**	***	**110.2 ± 3.6**	***
28	**Biotin-G/A-PE 22-28**	**aa substitution + N-biotinylation**	**46.11 ± 7.743**	***	**140.7 ± 7.1**	*
29	PI-PE 22-28	No modification	46.19 ± 7.565	***	119.7 ± 11.8	**
30	Biotin-PI-PE 22-28	N-biotinylation	49.11 ± 7.454	***	124.1 ± 11.7	**
31	Palmitoyl-PE 22-28	N-palmitoylation	26.69 ± 16.45	ns	nd	nd
32	FITC-PE 22-28	N-FITC group	22.1 ± 12.63	ns	nd	nd
33	Acetyl-PE 22-28	*N*-acetylation	20.49 ± 8.777	*	nd	nd
34	Myristoyl-PE 22-28	N-myristoylation	18.04 ± 17.77	ns	nd	nd
35	LC biotin-PE 22-28	N-long chain biotinylation	15.86 ± 11.21	ns	nd	nd
36	5'FAM-PE 22-28	N-5'FAM group	6.633 ± 7.065	ns	nd	nd
37	FMoc-PE 22-28	N-Fmoc group	5.826 ± 10.91	ns	nd	nd
38	Stearic acid-PE 22-28	N-stearic acid group	5.412 ± 5.496	ns	nd	nd

of a 44-amino acid peptide named as PE (Fig. 1) (Munck Petersen et al., 1999).

Sortilin/NTSR-3 co-localizes with TREK-1 in numerous brain areas involved in mood, such as the prefrontal cortex, hippocampus, striatum, amygdala, and hypothalamus (Mazella et al., 2010). In addition, physical interaction between TREK-1 and sortilin/NTSR-3 was characterized by pull down experiments. It has been showed that TREK-1 expression at the plasma membrane is greatly enhanced in the presence of sortilin/NTSR-3 (Mazella et al., 2010). Although present in low amounts at the plasma membrane in the absence of sortilin, TREK-1 channels can be modulated by the different effectors described above.

Furthermore, an interesting observation from our team showed that sortilin/NTSR-3-deficient mice represent a depression-resistant phenotype similar to the behavior of *kcnk2*$^{-/-}$ mice (Moreno et al., 2018). Arguments cited above support the involvement of both TREK-1 and sortilin/NTSR-3 in the physiopathology of depression.

3. Discovery of SPADIN

3.1. Sortilin-derived peptide with antidepressant properties

PE is a 44-amino acid peptide that binds with high affinity (Kd ~20–30 nM) to the mature sortilin/NTSR-3 (Munck Petersen et al., 1999). The peptide sequence required for the binding of PE to sortilin/NTSR-3 was identified as Gln^{1}-Arg^{28} (Fig. 1). Moreover, the PE fragment corresponding to Gln^{1}-Arg^{16} had lower affinity in binding the mature sortilin (Westergaard et al., 2004). In this study, a 17-amino acid-containing peptide was designed and named as spadin, acronym generated from Sortilin-derived Peptide with Antidepressant properties. Spadin contains the main fragment of PE, Trp^{17}-Arg^{28}, capable of binding to sortilin/NTSR-3 and stabilized by the sequence Ala^{12}-Pro^{13}-Leu^{14}-Pro^{15}-Arg^{16} added upstream to finally generate a 17-amino acid peptide corresponding to the sequence Ala^{12}-Arg^{28} or PE 12-28 (Fig. 1, Table 2, **peptide #1**) (Mazella et al., 2010).

PE has been shown to antagonize the effects of NT on cell migration of the human microglia cell line C13NJ that expresses the NTSR-3 subtype, exclusively (Martin, Vincent, & Mazella, 2003). Similarly to PE, spadin (PE 12-28) is able to bind with an identical affinity (Kd = 8 nM) to sortilin/NTSR-3 (Mazella et al., 2010). The similarity between PE and spadin to bind to sortilin/NTSR-3 is extended to their functional properties. For example, spadin totally blocks cell migration by displacing NT from the binding site of sortilin/NTSR3 (Mazella et al., 2010).

Given the role of TREK-1 channels in depression (Heurteaux, Lucas, et al., 2006b), the question that arose was to determine whether PE or spadin could regulate TREK-1 channels and consequently generate a depression-resistant phenotype in mice. To answer this question, spadin was tested on TREK-1-expressing COS-7 cells in electrophysiological experiments. In the patch-clamp technique using whole-cell configuration, TREK-1 was first activated by 10 μM of AA, and then, when spadin was applied extracellularly, TREK-1 was potently blocked by spadin with an IC_{50} of 70.7 nM (Tables 1 and 2) (Mazella et al., 2010). TREK-1 blockade was confirmed on other type of cell lines such as the hTREK-1/HEK (IC_{50} = 40 nM) or the pancreatic β-TC3 cells (Djillani et al., 2017; Mazella et al., 2010). The direct blocking of TREK-1 channel activity was demonstrated on the h-TREK-1/HEK cell line by using excised patches in an inside-out configuration (Gil et al., 2012). On brain slices, endogenous TREK-1 currents recorded in the hippocampal CA3

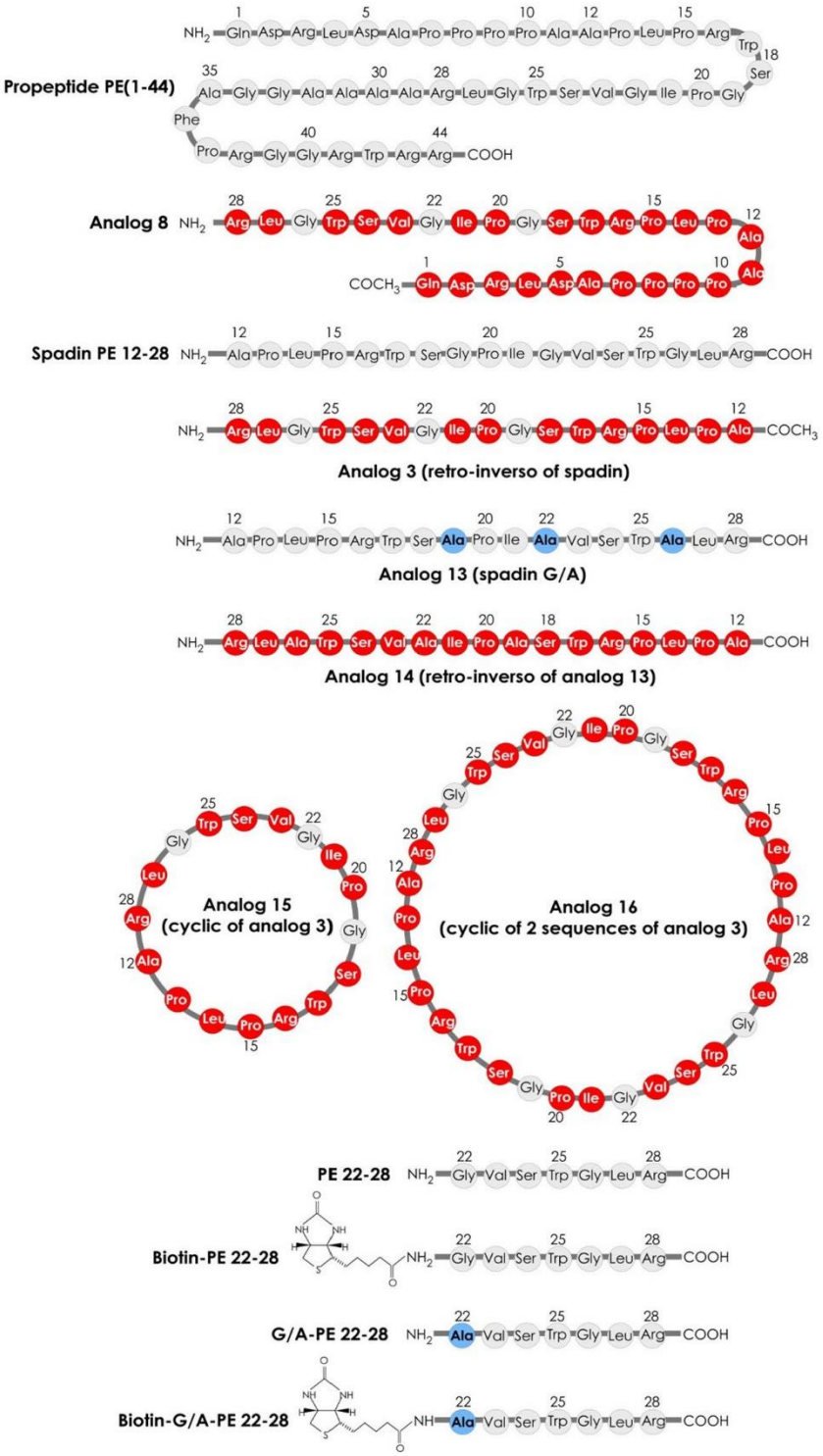

Fig. 1. Spadin analog sequences. Peptide sequences designed from the parent molecule spadin using the RI strategy, peptide cyclization and shortening sequence. The peptidic sequences are shown as three-letter nomenclature and numbered according to the sequence of PE (1–44). Amino-acids in L-configuration are shown in grey circles while amino-acids in D-configuration (inverso aa) are represented as red circles. Replacement of glycine residue by an alanine is shown by blue circles.

pyramidal cells were also activated by AA and strongly blocked by spadin (Mazella et al., 2010). More interestingly, on hippocampal brain slices, the spadin effect totally disappeared in TREK-1-deficient mice, which confirms TREK-1 as a target for spadin (Mazella et al., 2010).

TREK-1 is known to be highly expressed in the dorsal raphe nucleus (DRN) (Medhurst et al., 2001) and *kcnk2*$^{-/-}$ mice showed an enhanced serotonergic neurotransmission (Heurteaux, Lucas, et al., 2006b). To address the question whether pharmacological blockade of TREK-1 by spadin affects 5-HT neurotransmission, mice were given a 10 μM dose of spadin as an i.p injection and the unitary extracellular activity of serotonergic neurons was recorded in anesthetized animals. Data showed that spadin potentiates 5-HT neurotransmission firing *in vivo* (Mazella et al., 2010), similar to the activity of the 5-HT neurons in *kcnk2*$^{-/-}$

mice (Heurteaux, Lucas, et al., 2006b). To investigate further, we addressed the question whether blocking TREK-1 and increasing 5-HT firing in the DRN by spadin could have an impact on mouse behavior. Spadin was administered to mice in acute and subchronic treatments and AD activity was assessed using several mouse models of depression. Spadin displays AD properties in mice in depression-like behavior tests (FST, TST, CSMT, LHT, and NSF). Moreover, spadin treatments generate two canonical effects of AD drugs: the increase in 5-HT neurotransmission and the induction of neurogenesis (Mazella et al., 2010). These results confirmed the previous data obtained with *Kcnk2*$^{-/-}$ mice, whose main phenotype is resistance to depression (Heurteaux, Lucas, et al., 2006b). In addition, subchronic treatment with spadin results in increasing CREB activation and hippocampal neurogenesis. This effect is outstanding, as it occurs only after a 4 day treatment in contrast to SSRIs that need 3–4 weeks of treatment to increase hippocampal neurogenesis (Mazella et al., 2010).

Moreover, *in vitro* (in cortical neurons) and *in vivo* (in the hippocampus), studies showed that spadin increases both mRNA and protein expression of markers of synaptogenesis, such as the post-synaptic density protein-95 (PSD-95) or synapsin (Devader et al., 2015). These data indicated that spadin increases the number of functional neurons. This observation was supported by the fact that spadin treatment significantly increases the number of mature spines on axons (Devader et al., 2015).

Taken together, these data confirmed that the newly generated neurons by spadin are indeed functional and able to interact within the neuronal complex network.

3.2. Spadin is a specific and safe blocker of TREK-1

Despite the high homology in structure, function, and regulation between TREK-1, TREK-2, and TRAAK channels (Lesage & Lazdunski, 2000), spadin specifically blocks TREK-1, as no effect is observed on the other stretch-activated K_{2P} channels such as TREK-2 and TRAAK. TASK-1 and TRESK, two other members of the K_{2P} channel family, are also insensitive to spadin (Table 1) (Moha Ou Maati et al., 2012). As TASK-1 is involved in inflammation (Bittner et al., 2009) and apoptosis (Lauritzen et al., 2003; Leithner et al., 2016) and TRESK in migraine (Lafreniere & Rouleau, 2011) and pain (Marsh, Acosta, Djouhri, & Lawson, 2012; Tulleuda et al., 2011), the absence of spadin effect on these channels might be beneficial.

TREK-1 was also shown to play an important role in pain perception (Alloui et al., 2006). *Kcnk2*$^{-/-}$ mice are more sensitive to thermal pain (Alloui et al., 2006). Here again, spadin is unable to modify pain perception in tail flick and hot plate tests (Moha Ou Maati et al., 2012).

Undoubtedly, TREK-1 plays a crucial role in the regulation of neuronal excitability (Heurteaux et al., 2004). TREK-1-mediated neuroprotection against epilepsy and cerebrovascular diseases is not affected by spadin treatment. Spadin does not increase pentylenetetrazol (PTZ) or kainate-induced seizures (Moha Ou Maati et al., 2012). Furthermore, a 3-week spadin treatment does not increase the infarct size after focal ischemia (Moha Ou Maati et al., 2012).

Finally, at the cardiovascular level, long-term treatment by spadin has no effect on systolic blood pressure and heart pulses (Moha Ou Maati et al., 2012).

One of the major challenges in the development of safe drugs is the early detection of prolongation of the QT interval, which causes Torsades de pointes (TdP). Long QT-inducing drugs block two types of potassium currents: the rapid (I_{Kr}) and the slow (I_{Ks}) potassium currents (Cheng & Kodama, 2004; Sanguinetti & Jurkiewicz, 1990). I_{Kr} current is carried by the hERG channel. However, I_{Ks} activity requires the association of KCNQ1 with KCNE1 (Barhanin et al., 1996; Sanguinetti et al., 1996). As I_{Kr} and I_{Ks} are essential components for normal cardiac function, drug-acquired QT interval prolongation due to hERG inhibition causes an increase in sudden death (Brown, 2004). Consequently, several cardiovascular and non-cardiovascular drugs have been withdrawn from the market (Finlayson, Witchel, McCulloch, & Sharkey, 2004). Presently, all drug candidates should be tested *in vitro* to check whether or not they inhibit hERG channels (Chen, Sampson, & Kass, 2016). With the aim to develop spadin as an approved drug in the treatment of depression, this peptide was tested for a possible hERG channel inhibition. Spadin does not affect hERG channel biophysical properties, as the use of 10 μM or higher concentrations of spadin do not show any modifications of I_{Kr} or I_{Ks} (Djillani et al., 2017; Moha Ou Maati et al., 2012). Taken together, these observations confirm spadin as a safe molecule for further use in clinic. The potent AD properties of spadin have given rise to the patent published under the no. US8252748B2 (Mazella, Petrault, Borsotto, Heurteaux, & Widmann, 2012).

3.3. Increasing spadin efficacy and in vivo bioavailability

In FST, spadin AD activity lasts for 7 h after a single i.p injection (Veyssiere et al., 2015). To improve *in vivo* stability of spadin and prolong AD activity beyond 7 h after an acute treatment, different strategies have been thoroughly considered, such as the retro-inverso (RI) strategy, peptide cyclization, amino acid replacement, protection of C– and N-terminal ends of the peptides, and finally shortening of the spadin sequence. The RI strategy consists of changing the amino acid configuration from L to D. At the same time, the amino acid sequences are inverted. RI technology was shown in many studies to increase the resistance of peptides to proteolysis and thus improve their bioavailability in the blood (Chorev & Goodman, 1995; Chorev, Shavitz, Goodman, Minick, & Guillemin, 1979). Eleven spadin analogs including RI spadin analogs were synthesized and screened on the hTREK-1/HEK cell line by the patch-clamp technique (Table 2, **peptides #2 to #12)** Two RI analogs were identified: analog 3 (Ac-RI-PE 12-28, peptide # 3) and 8 (Ac-RI-PE 1-28, peptide # 8) (Fig. 1, Table 2). They display a better inhibition potency for TREK-1 channel activity, IC_{50} were 11.5 ± 0.59 nM and 9.95 ± 0.85 nM for analog 3 and analog 8, respectively, compared to 56.39 ± 0.01 nM for spadin (Veyssiere et al., 2015).

The analogs 3 and 8 share the same AD properties with spadin after acute or subchronic treatments. Similar to spadin, analogs 3 and 8 significantly reduce the immobility time in the FST (Veyssiere et al., 2015). Moreover, in the NSF, the two RI analogs shorten the latency time for eating in mice. More interestingly, these analogs induce hippocampal neurogenesis.

One of the challenges in terms of development is to improve the *in vivo* stability of spadin. RI analogs prolong the AD activity by three times compared to spadin (Veyssiere et al., 2015). Specifically, analog 3 does not produce any adverse effects on pain, epilepsy, or arrhythmia. RI analogs including analog 3 and analog 8 were patented for the treatment of depression under the number WO2015110915A2 (Gaudriault et al., 2015).

Other analogs were designed by the RI strategy, such as analog 13 (G/A-PE 12-28, Table 2 peptide #13), analog 14 (RI-G/A-PE 12-28, Table 2 peptide #14), analog 15 (c(RI-PE 12-28), Table 2 peptide #15), and analog 16 (a tandem of c(RI-PE 12-28), Table 2 peptide #16). The peptide sequences are depicted in Fig. 1.

Analog 13 contains the same sequence as spadin, but the three glycine residues were replaced by three alanine residues. Analog 14 is the RI of analog 13. Both analogs 13 and 14 are able to strongly inhibit TREK-1 channels (83.50% ± 9.76%, $n = 8$, $p = 0.94$), (72.15% ± 11.75%, $n = 9$, $p = 0.36$), respectively, compared to spadin (87.08% ± 7.32%, n = 8) (Fig. 2 **a, b**). More interestingly, both analogs conserve their AD activity in FST when injected intravenously (i.v.). The immobility time is significantly decreased (120.4 ± 9.7 s, $n = 10$, $p = 0.0049$ and 127.7 ± 8.32 s, n = 10, $p = 0.0105$, respectively) for analogs 13 and 14 compared to saline (160.6 ± 7.97 s, n = 10) (Fig. 3a).

Peptide cyclization is one of the common strategies used to increase peptide stability and efficacy (Adessi & Soto, 2002). It has been shown that cyclization could increase peptide resistance against proteolytic degradation that subsequently enhances the peptide bioavailability

(Wang et al., 2014). Therefore, the strategy consisted of cyclizing analog 3 alone (analog 15, Table 2 peptide #15) or in tandem (analog 16, Table 2 peptide #16) sequence (Fig. 1) to study the impact of the cyclization on peptides crossing the blood–brain barrier (BBB). Using the whole-cell configuration of the patch-clamp technique, both analogs 15 and 16 inhibit TREK-1 current with different potencies (67.24% ± 3.41%, n = 9, $p = 0.046$ and 91.25% ± 8.14%, n = 10, $p = 0.67$), respectively (Fig. 2). However, in the FST, when both analogs are administered through the i.v. route, neither analog 15 nor analog 16 is able to produce a significant decrease in immobility time (157 ± 8.09 s, n = 10, $p = 0.755$ and 146.7 ± 12.99 s, n = 10, $p = 0.374$, respectively) compared to saline (160.6 ± 7.97 s, n = 10) (Fig. 3a). It appears that the lack of activity of analog 15 is due to its inability to cross the BBB, as it displays AD activity only when injected directly in the brain by an intracerebroventricular route (i.c.v.) (Fig. 3b).

3.4. Shortened spadin analogs with antidepressant activity

Spadin blood degradation products revealed by high-pressure liquid chromatography (HPLC) consist of at least two short peptides PE 12–27 (Table 2, peptide #17) and PE 14–25 (Table 2, peptide #18) (Djillani et al., 2017). On the basis of this analysis, several short analogs were designed and screened on the hTREK-1/HEK cell line. PE 22–28 (Table 2, peptide #21) is the shortest, most efficient sequence capable of blocking the TREK-1 channel with higher potency ($IC_{50} = 0.12$ nM *versus* $IC_{50} =$ 40 nM for spadin (PE 12–28)) (Fig. 1). Then, PE 22–28 (peptide #21) was used as the core peptide to design other analogs with different N- and C-terminal end modifications. These PE 22–28 analogs abolish or maintain TREK-1 inhibition on the basis of the nature of the chemical group attached to C or N-terminus (Table 2) (Djillani et al., 2017).

With PE 22–28, two other analogs were retained for further studies, as they inhibit the TREK-1 channel with a higher potency. They correspond to the PE 22–28, where Gly^{22} is replaced by an Ala^{22} (G/A-PE 22–28, Table 2 peptide #27) and its biotinylated derivative (biotin-G/A-PE 22–28, Table 2 peptide #28) (Fig. 1). Their TREK-1-inhibiting potencies are $IC_{50} = 0.10$ nM and $IC_{50} = 1.2$ nM for G/A-PE 22–28 and biotin-G/A-PE 22–28, respectively (Djillani et al., 2017). This represents, respectively, a 400- and 33-fold increase in TREK-1 inhibition potency in comparison to spadin.

Current blockade is specific to TREK-1, as TREK-2, TRAAK, TRESK, and TASK-1 channels are not inhibited by these shortened peptides. How about their ability to counteract depression behavior? Does shortening spadin sequence and replacing Gly^{22} by Ala^{22} have any consequences on mice behavior? To answer these questions, a series of behavioral studies on mice treated with short spadin analogs were performed (Djillani et al., 2017).

These candidate peptides display AD properties after acute and 4 day subchronic treatments in FST, NSF, and LHT. More interestingly, similar to spadin, they produce an AD-like behavior regardless of the route of administration. They efficiently reduce the immobility time in the FST after i.p, i.v., and gavage administration (Djillani et al., 2017).

Similar to spadin, hippocampal neurogenesis is increased as revealed by BrdU (5-Bromo-2′-Deoxyuridine) labeling with a prominent effect of G/A-PE 22–28 (Table 2, peptide #27). At the same time, neurogenesis induced by spadin short analogs is consistent with the increase in PSD-95 expression, a marker of synaptogenesis (Djillani et al., 2017).

One of the most important effects observed with short spadin analogs is the improvement in terms of *in vivo* stability compared to spadin. Indeed, G/A-PE 22–28 (21*h*) and biotin-G/A-PE 22–28 (23*h*) prolong significantly the action duration of spadin (only 7 h) as revealed by FST (Djillani et al., 2017). This is extremely promising and interesting, as the ultimate goal in the near future is to test them in clinical trials and eventually commercialize these long-lasting peptides as ADs of a new generation (Fig. 4).

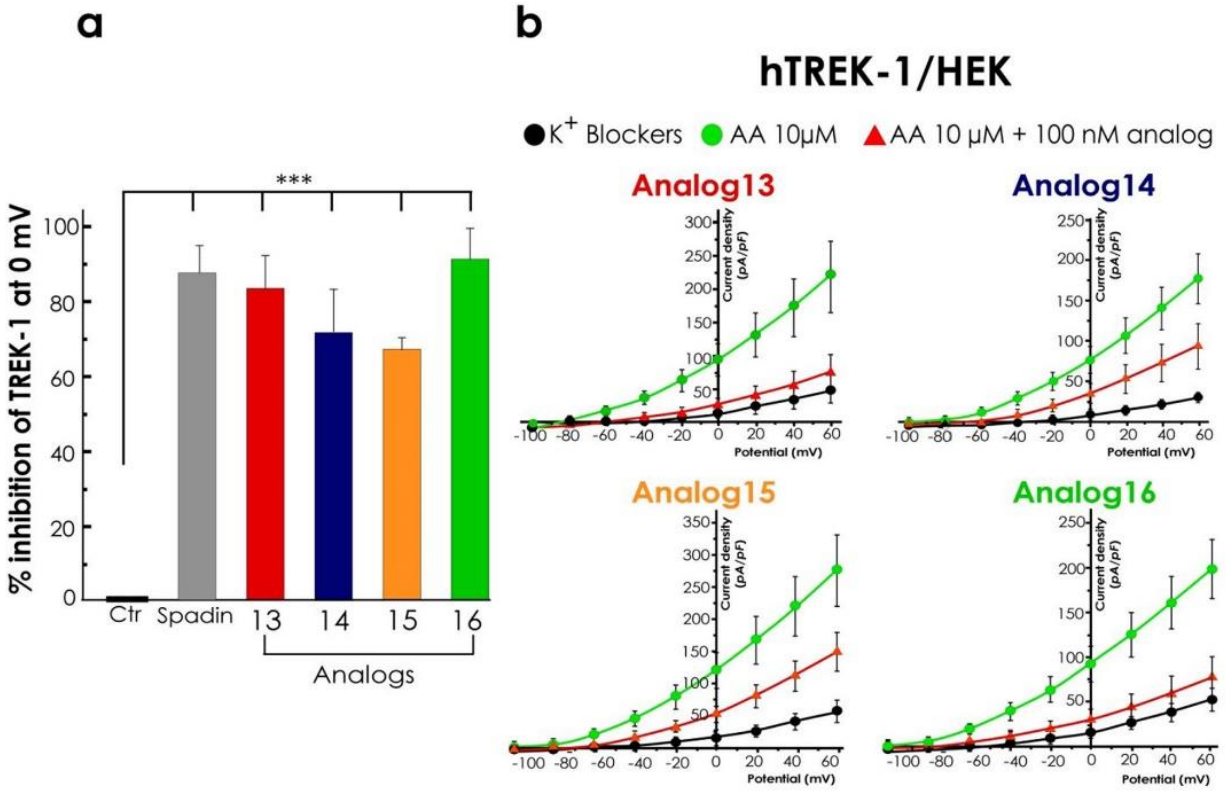

Fig. 2. Spadin analogs display strong TREK-1 inhibition. Spadin analogs named analog 13, analog 14, analog 15 and analog 16 were screened on the hTREK-1/HEK cell line for their ability to block TREK-1 channels. **a.** Following activation by 10 µM AA, TREK-1 inhibition by 100 nM spadin analogs was measured at 0 mV using the whole-cell configuration of the patch-clamp technique in voltage-clamp mode. **b.** I/V curves obtained with spadin analogs and generated by a ramp protocol from −100 mV to +60 mV with a holding potential at −80 mV. *, $p < 0.01$, ***, $p < 0.001$.

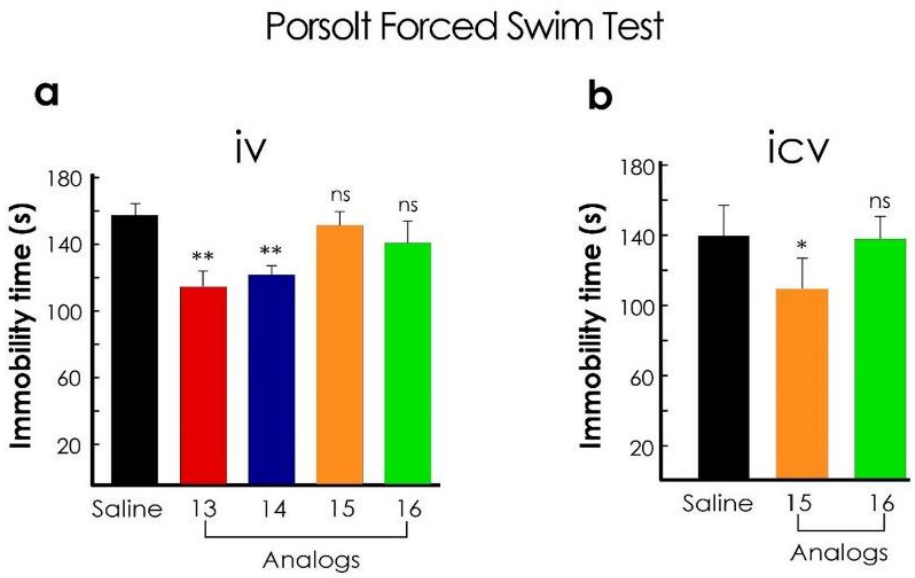

Fig. 3. Antidepressant activity of spadin analogs in the Forced Swim Test. a. In the FST, when administered intravenously, analog 13 and analog 14 significantly decreased the immobility time in mice compared to saline injected mice (control). However, analog 15 and analog 16 were unable to display AD-like behavior when i.v injected. **b.** Intracerebroventricular route (i.c.v) demonstrated that analog 15 did not cross the BBB while analog 16 remains inefficient in reducing the immobility time in mice. *, $p < 0.05$; **, $p < 0.01$; ns, not significant. *Methods*. 30 min before the test, animals were injected with the different spadin's analogs by using either the intraveinous route (iv) or the intracerebroventricular route (icv). Mice were individually placed for 6 min in a non-escapable cylinder (30 cm height and 15 cm diameter) half-filled with water at 22 °C ± 1 °C. The immobility time was manually measured only during the last 4 min. A mouse was considered immobile when it remained immobile with only slight movements in order to keep its head above water (Porsolt, Le Pichon, & Jalfre, 1977). Statistical comparisons were performed using ANOVA one-way.

However, for the clinical development of any molecule, whether a small drug or a therapeutic peptide, it should be screened to detect any change in the QT interval. PE 22–28 and analogs do not modify hERG channel activity, which render them more specific and safer for a possible further pharmaceutical development (Djillani et al., 2017).

3.5. Spadin and analogs as biomarkers of major depressive disorder

To clinically predict patients with major depressive disorder (MDD) who respond to classical AD treatment and routinely monitor AD activity, there is a pressing need to validate biomarkers for MDD. This will allow an inexpensive diagnosis and predictive test for an MDD response to facilitate patient follow-up (Woods, Iosifescu, & Darie, 2014). Thus far, there has been no validated biomarker for MDD, and clinical diagnosis is only symptomatic. Recently, various candidates as biomarkers for MDD were described in the literature, such as inflammatory mediators, growth factors, neurotransmitters, neurotrophic factors, and metabolic biomarkers (Gururajan, Clarke, Dinan, & Cryan, 2016; Strawbridge, Young, & Cleare, 2017). Many preclinical studies have pointed out the crucial role of BDNF in the physiopathology of MDD, as BDNF serum levels are lower in patients with MDD than in healthy volunteers or MDD-medicated patients (Aydemir et al., 2006; Aydemir, Deveci, Taskin, Taneli, & Esen-Danaci, 2007; Gervasoni et al., 2005; Gonul et al., 2005; Huang, Lee, & Liu, 2008; Karege et al., 2005; Monteleone, Serritella, Martiadis, & Maj, 2008; Piccinni et al., 2008; Shimizu et al., 2003; Yoshimura et al., 2007).

It was already demonstrated that sortilin is an important regulator of BDNF sorting and trafficking to the secretory pathways (Chen et al., 2005). A clinical study confirmed the correlation between circulating levels of sortilin, BDNF, and MDD (Buttenschon et al., 2015). A recent study was conducted with a cohort of 37 patients suffering from MDD and treated with an AD drug for 12 weeks. They were compared to 49 healthy volunteers (Devader et al., 2017). Using the dosing alpha-screen method validated for PE detection in the serum (Mazella et al., 2010), the concentrations of PE, spadin (PE 12–28, Table 2 peptide #1), PE 12–27 (Table 2 peptide #17), and PE 14–25 (Table 2 peptide #18) were measured with the aim to find a correlation between the serum levels of PE peptides in healthy and patients with MDD whether or not treated with AD drugs. Serum concentrations of the PE peptides are significantly decreased in patients with MDD. Interestingly, PE peptide levels are partially but significantly restored after a 12 week treatment with an AD drug, thus indicating a correlation between the serum levels of PE-like activity and the mood of patients.

Recently, Buttenschon et al. conducted a new study, and they concluded that sortilin could not serve as a biomarker to follow AD treatment in patients with MDD (Buttenschon, Nielsen, Glerup, & Mors, 2017). At this stage, it is important to underline that the release of soluble sortilin (as measured in the Buttenschon's work) depends on matrix metalloproteinases (MMPs) (Navarro, Vincent, & Mazella, 2002), whereas PE release depends on the intracellular maturation of sortilin by furin (Devader et al., 2017). To validate whether or not PE and sortilin could be used as biomarkers in MDD, further complete clinical studies, which include larger cohorts of patients with MDD whether or not treated with AD drugs, need to be performed in the future. Moreover, advances in developing specific antibodies able to recognize the short peptide sequences with higher sensitivity could guide research toward new biomarkers of MDD.

4. Conclusions and perspectives

The main advantages that peptides present compared to xenobiotics are their high specificity and low toxicity owing to their high binding affinity to their specific targets. Two categories of currently available drugs exist, small molecules <500 Da active *per os*, and large molecules >5000 Da that are inefficient orally and need to be administered in the parenteral form as injections (Craik, Fairlie, Liras, & Price, 2013). If small molecules are orally bioavailable, they could be designed with a lesser cost. However, owing to their size, they could lack specificity and potentially could lead to off-target adverse effects. Large biologic drugs show high affinity for their targets but need to be injected into patients (Craik et al., 2013). Spadin and its analogs belong to a class of molecules that range between small molecules and large polypeptides that represent a nonnegligible advantage for both drug administration and specificity for targets. Advantages of spadin and its analogs as promising AD drugs are summarized in Box 1. In addition to the central effect of spadin on depression through targeting TREK-1 channels in the brain,

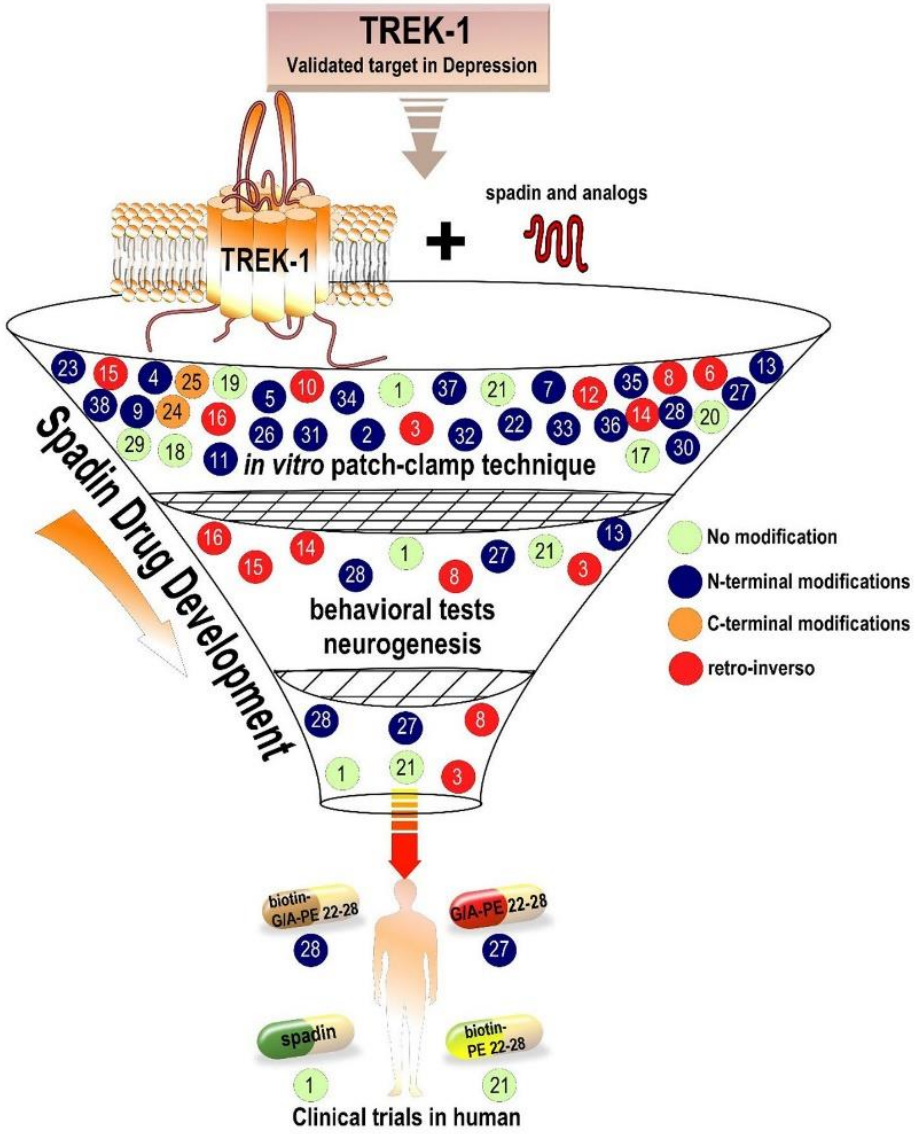

Fig. 4. Schematic representation of spadin development as new concept in AD drug discovery. Since the validation of TREK-1 channel as a novel target for AD drugs, spadin was discovered to be a specific blocker of TREK-1 with high affinity. Different optimization processes were conducted in order to improve the affinity, efficacy and *in vivo* stability while maintaining the AD properties. The strategies used led to the identification as AD drug promising candidates: G/A-PE 22–28, biotin-G/A-PE 22–28 in addition to spadin. The final goal is to complete preclinical development before launching clinical trials in human and finally develop spadin and/or its analogs as AD drugs. The number in circle corresponds to the analog number indicated in Table 2.

spadin diffuses in the blood circulation and reaches a number of organs including the pancreas and prostate. Indeed, as described above, in the pancreatic β-cells, spadin plays a crucial role as an insulin-releasing peptide upon hyperglycemia (Hivelin et al., 2016).

>60 peptides have been approved by the US *Food and Drug Administration* (FDA), and this is expected to greatly increase in the near future, as >140 molecules are currently being processed and tested in clinical trials. In addition, at least 500 peptides are under investigation in preclinical studies (Fosgerau & Hoffmann, 2015; Kaspar & Reichert, 2013) and are quite ready to be tested in humans.

Spadin and its analogs undoubtedly constitute important candidate peptides intended to treat depression in clinic. As natural peptides, they irrefutably represent a huge advantage compared to small classical ADs, as the risk–benefit ratio will be sharply improved. The next step consists of validating their efficacy and tolerability processes in healthy volunteers during clinical trials. Many peptides have been designed for various pathologies such as cancer, diabetes, and infectious diseases. However, only few peptides are used in the treatment of neurological disorders; this is mainly due to their weak BBB crossing and their rapid degradation *in vivo* (McGowan, Bidwell 3rd, & Vig, 2015). These observations are not applicable to spadin because the effects of peripheral i.p. injections of spadin and its analogs (at doses as low as 100 μg/kg) can be measured in the brain (Mazella et al., 2010). Additionally, the *in vivo* stability of spadin ranges between 7 and 23 h, a duration that is compatible with the use in human clinic. As the validation of TREK-1 as a potential target in the treatment of depression, TREK-1 druggability was made possible after the discovery of spadin and its analogs (Fig. 4). Thereafter, spadin efficacy was gradually optimized through different strategies such as RI strategy, cyclization, sequence shortening, and modifications of N- and C-terminal ends. Ultimately, efficiency, inhibition potency, and *in vivo* stability of these analogs are significantly improved compared to spadin. Moreover, AD activity is maintained despite shortening and modifying the peptide sequence. Interestingly, the AD phenotype is associated with an enhancement of both *in vivo* hippocampal neurogenesis and cortical synaptogenesis. It will be challenging to overcome obstacles and therefore lead spadin analogs to the finish line, *i.e.*, marketing spadin analogs as novel AD drugs with an original mechanism of action. However, all these observations give

Box 1
Potential advantages of spadin and its analogs as antidepressant molecules

Fast acting
Psychiatrists, physicians, and patients want drugs that act more rapidly than those that are prescribed presently. Current marketed AD drugs often take several weeks to be efficient. Spadin or its analogs only need 4 days to exert their AD effects (Mazella et al., 2010). Additionally, spadin and its analogs are effective regardless of the route they are administered: intravenous, intraperitoneal, intracerebroventricular, subcutaneous, or *per os*.

Specificity
Spadin and its analogs are highly specific for TREK-1 channels. They do not modify the activity of other K_{2P} channels such as TREK-2, TRAAK, TRESK, and TASK 1 channels (Djillani et al., 2017; Moha Ou Maati et al., 2012). This is particularly remarkable because TREK-2 and TRAAK belong to the same subfamily and share almost 80% homologies with TREK-1 (Noel, Sandoz, & Lesage, 2011).

Cardiac safety
In rodent, spadin and its analogs do not affect hERG or KCNQ1/KCNE1 channels and do not modify heart rates. These data indicate that spadin and its analogs have no deleterious effects at the cardiac level (Djillani et al., 2017; Moha Ou Maati et al., 2012).

No side effects on TREK-1-controlled functions
In addition to the absence of effects on the heart, preclinical studies have shown that spadin and its analogs have no deleterious side effects on pathologies that are under the control of TREK-1 channels, such as pain, epilepsy, or ischemia (Moha Ou Maati et al., 2012).

High efficiency
The development of spadin analogs has increased the AD potency of the original peptide. Analogs of concentration 3 μg/kg are adequate to produce an AD effect same as that obtained with a concentration of 100 μg/kg (Djillani et al., 2017).

Natural peptides
In addition to the fact that they are natural peptides, we can reasonably expect a high level of specificity and safety for these peptides. Converse to the majority of actual ADs that provoke withdrawal behavior, the probability to observe such a phenomenon with a natural peptide is low.

Duration effects
The relatively short time (7 h) of *in vivo* effects of spadin could have been a problem, but it was solved with the development of spadin analogs. Therefore, the *in vivo* stability has become very close to 24 h (Djillani et al., 2017). This sustained effect is important for use in clinics.

Biomarker
Spadin-like activity in the serum, mainly corresponding to PE and its degradation products, is significantly decreased in patients suffering from MDD in comparison to healthy controls (Devader et al., 2017).

Comparison with other putative drugs
Other TREK-1 blockers such as SID1900 or lig4–4 have been recently identified. Although these molecules were described to be specific blockers of TREK-1 channels, they probably affect other types of ion channels as indicated in Table 1. Furthermore, they show very low affinities for TREK-1 channels (Wang et al., 2018; Ye et al., 2015) in comparison to spadin or its analogs (several μM *vs.* nM) (Djillani et al., 2017). Many other molecules are able to block TREK-1 channels, but none of them is specific for TREK-1. Nevertheless, these molecules were not extensively studied in the field of depression, and their properties are detailed in the paragraph 2.3.2 of this review.
Some microRNAs were also supposed to be involved in the depression process, but it is very soon to really define a therapeutic strategy using microRNAs (Yuan, Mischoulon, Fava, & Otto, 2017).
Recently, ketamine was also described (Ramaker & Dulawa, 2017) as a fast-acting molecule, but ketamine needs to be frequently administered (sometimes in hours) to obtain a sustained effect (Schwartz, Murrough, & Iosifescu, 2016). This point is an important drawback in the use of ketamine. Additionally, ketamine displays numerous adverse effects (Li & Vlisides, 2016).

rise to a very positive signal for the use of spadin and/or its derivatives as new ADs. Nevertheless, we have to keep in mind that all these preclinical studies were performed on animal models described to mimic a part of a clinical symptom of depression. Definitive answers can be obtained from clinical trials.

To our knowledge, spadin and its analogs are the first therapeutic peptides with a high potential to successfully go through clinical trials and thus be marketed for the treatment of mood disorders.

Conflict of interest statement

The authors declare that they are no conflicts of interest.

Funding sources

This work was supported by the Centre National de la Recherche Scientifique and the Agence Nationale de la Recherche (ANR-13-SAMA-0001 and 0002 and ANR-13-RPIB-0001 and 0002). We also thank the French Government for the "Investments for the Future" LabEx ICST #ANR-11 LabEx 0015 and the Fondation de l'Avenir No. AP-RMA-2015-021. M. Pietri was supported by a CIFRE fellowship.

Methods. hTREK-1/HEK cells were seeded at a density of 20,000 cells/35 mm dish. Electrophysiological recordings were performed 24–48 h after plating using the whole-cell configuration of patch-clamp technique. In order to measure TREK-1 current (I_{TREK-1}), a cocktail of potassium channel blockers was added to the bath solution. This cocktail contained: 3 mM 4-AP (4-aminopyridine), 10 mM TEA (tetraethylammonium), 10 μM Glibenclamide, 100 nM Apamin and 50 nM Charybdotoxin (for more experimental details see (Djillani et al., 2017)). Whole-cell I_{TREK-1} currents were generated by running a pulse or ramp protocol every 5 s from −100 to +60 mV with a holding potential maintained at −80 mV. The inhibitory effect on TREK-1 channels of 100 nM of spadin analogs were compared with the inhibitory effect of spadin, on cells pre- activated with 10 μM of arachidonic acid (AA). Patch-clamp recording data were analyzed using Clampfit (Molecular Devices, USA). I = f(V) curves were obtained from −100 to +60 mV ramp. Data were presented as mean ± SEM from at least 3 independent experiments. In GraphPad Prism (GraphPad software, La Jolla, USA), statistical comparisons were performed using Student's *t*-test or ANOVA one-way. A result is considered as statistically significant when $p < 0.05$.

Acknowledgments

We thank 3P3D startup, and particularly its director Dr. Serge Richard for his friendly support, confidence in the spadin project, and fruitful discussions. We thank Franck Aguila for artwork contribution. We particularly thank Dr. A. Patel and S. Morgan for careful reading of the manuscript.

Authorship contributions

AD wrote the manuscript. CH, JM, and MB corrected and improved the manuscript. AD conducted patch-clamp experiments, and MP and MB performed behavioral tests. CH, JM, and MB contributed to reagents/materials/analysis tools.

References

Adessi, C., & Soto, C. (2002). Converting a peptide into a drug: Strategies to improve stability and bioavailability. *Current Medicinal Chemistry 9*, 963–978.

Alloui, A., Zimmermann, K., Mamet, J., Duprat, F., Noel, J., Chemin, J., ... Lazdunski, M. (2006). TREK-1, a K+ channel involved in polymodal pain perception. *The EMBO Journal 25*, 2368–2376.

Apazoglou, K., Farley, S., Gorgievski, V., Belzeaux, R., Lopez, J. P., Grenier, J., ... Tzavara, E. T. (2018). Antidepressive effects of targeting ELK-1 signal transduction. *Nature Medicine 24*, 591–597.

Aydemir, C., Yalcin, E. S., Aksaray, S., Kisa, C., Yildirim, S. G., Uzbay, T., & Goka, E. (2006). Brain-derived neurotrophic factor (BDNF) changes in the serum of depressed women. *Progress in Neuro-Psychopharmacology & Biological Psychiatry 30*, 1256–1260.

Aydemir, O., Deveci, A., Taskin, O. E., Taneli, F., & Esen-Danaci, A. (2007). Serum brain-derived neurotrophic factor level in dysthymia: A comparative study with major depressive disorder. *Progress in Neuro-Psychopharmacology & Biological Psychiatry 31*, 1023–1026.

Baker, S. A., Hennig, G. W., Han, J., Britton, F. C., Smith, T. K., & Koh, S. D. (2008). Methionine and its derivatives increase bladder excitability by inhibiting stretch-dependent K(+) channels. *British Journal of Pharmacology 153*, 1259–1271.

Barhanin, J., Lesage, F., Guillemare, E., Fink, M., Lazdunski, M., & Romey, G. (1996). K(V)LQT1 and lsK (minK) proteins associate to form the I(Ks) cardiac potassium current. *Nature 384*, 78–80.

Bittner, S., Meuth, S. G., Gobel, K., Melzer, N., Herrmann, A. M., Simon, O. J., ... Wiendl, H. (2009). TASK1 modulates inflammation and neurodegeneration in autoimmune inflammation of the central nervous system. *Brain 132*, 2501–2516.

Blondeau, N., Petrault, O., Manta, S., Giordanengo, V., Gounon, P., Bordet, R., ... Heurteaux, C. (2007). Polyunsaturated fatty acids are cerebral vasodilators via the TREK-1 potassium channel. *Circulation Research 101*, 176–184.

Borsotto, M., Veyssiere, J., Moha Ou Maati, H., Devader, C., Mazella, J., & Heurteaux, C. (2015). Targeting two-pore domain K(+) channels TREK-1 and TASK-3 for the treatment of depression: A new therapeutic concept. *British Journal of Pharmacology 172*, 771–784.

Brandon, S. (1982). Monoamine oxidase inhibitors in depression. *British Medical Journal (Clinical Research Ed.) 285*, 1594–1595.

Brown, A. M. (2004). Drugs, hERG and sudden death. *Cell Calcium 35*, 543–547.

Bull, S. A., Hunkeler, E. M., Lee, J. Y., Rowland, C. R., Williamson, T. E., Schwab, J. R., & Hurt, S. W. (2002). Discontinuing or switching selective serotonin-reuptake inhibitors. *The Annals of Pharmacotherapy 36*, 578–584.

Burges, R. A., Gardiner, D. G., Gwilt, M., Higgins, A. J., Blackburn, K. J., Campbell, S. F., ... Stubbs, J. K. (1987). Calcium channel blocking properties of amlodipine in vascular smooth muscle and cardiac muscle in vitro: Evidence for voltage modulation of vascular dihydropyridine receptors. *Journal of Cardiovascular Pharmacology 9*, 110–119.

Buttenschon, H. N., Demontis, D., Kaas, M., Elfving, B., Molgaard, S., Gustafsen, C., ... Glerup, S. (2015). Increased serum levels of sortilin are associated with depression and correlated with BDNF and VEGF. *Translational Psychiatry 5*, e677.

Buttenschon, H. N., Nielsen, M., Glerup, S., & Mors, O. (2017). Investigation of serum levels of sortilin in response to antidepressant treatment. *Acta Neuropsychiatrica*, 1–6.

Caraci, F., Leggio, G. M., Salomone, S., & Drago, F. (2017). New drugs in psychiatry: Focus on new pharmacological targets. *F1000Research 6*, 397.

Cascade, E., Kalali, A. H., & Kennedy, S. H. (2009). Real-world data on SSRI antidepressant side effects. *Psychiatry (Edgmont) 6*, 16–18.

Chemin, J., Girard, C., Duprat, F., Lesage, F., Romey, G., & Lazdunski, M. (2003). Mechanisms underlying excitatory effects of group I metabotropic glutamate receptors via inhibition of 2P domain K+ channels. *The EMBO Journal 22*, 5403–5411.

Chen, L., Sampson, K. J., & Kass, R. S. (2016). Cardiac delayed rectifier potassium channels in health and disease. *Cardiac Electrophysiology Clinics 8*, 307–322.

Chen, Z. Y., Ieraci, A., Teng, H., Dall, H., Meng, C. X., Herrera, D. G., ... Lee, F. S. (2005). Sortilin controls intracellular sorting of brain-derived neurotrophic factor to the regulated secretory pathway. *The Journal of Neuroscience 25*, 6156–6166.

Cheng, J. H., & Kodama, I. (2004). Two components of delayed rectifier K+ current in heart: Molecular basis, functional diversity, and contribution to repolarization. *Acta Pharmacologica Sinica 25*, 137–145.

Chorev, M., & Goodman, M. (1995). Recent developments in retro peptides and proteins–an ongoing topochemical exploration. *Trends in Biotechnology 13*, 438–445.

Chorev, M., Shavitz, R., Goodman, M., Minick, S., & Guillemin, R. (1979). Partially modified retro-inverso-enkephalinamides: Topochemical long-acting analogs in vitro and in vivo. *Science 204*, 1210–1212.

Cipriani, A., Furukawa, T. A., Salanti, G., Chaimani, A., Atkinson, L. Z., Ogawa, Y., ... Geddes, J. R. (2018). Comparative efficacy and acceptability of 21 antidepressant drugs for the acute treatment of adults with major depressive disorder: A systematic review and network meta-analysis. *Lancet 391*, 1357–1366.

Craik, D. J., Fairlie, D. P., Liras, S., & Price, D. (2013). The future of peptide-based drugs. *Chemical Biology & Drug Design 81*, 136–147.

Cryan, J. F., & Holmes, A. (2005). The ascent of mouse: Advances in modelling human depression and anxiety. *Nature Reviews. Drug Discovery 4*, 775–790.

Dean, J., & Keshavan, M. (2017). The neurobiology of depression: An integrated view. *Asian Journal of Psychiatry 27*, 101–111.

Delgado, P. L. (2000). Depression: The case for a monoamine deficiency. *The Journal of Clinical Psychiatry 61* (Suppl. 6), 7–11.

Detke, M. J., Rickels, M., & Lucki, I. (1995). Active behaviors in the rat forced swimming test differentially produced by serotonergic and noradrenergic antidepressants. *Psychopharmacology 121*, 66–72.

Devader, C., Khayachi, A., Veyssiere, J., Moha Ou Maati, H., Roulot, M., Moreno, S., ... Mazella, J. (2015). In vitro and in vivo regulation of synaptogenesis by the novel antidepressant spadin. *British Journal of Pharmacology 172*, 2604–2617.

Devader, C., Roulot, M., Moreno, S., Minelli, A., Bortolomasi, M., Congiu, C., ... Mazella, J. (2017). Serum sortilin-derived propeptides concentrations are decreased in major depressive disorder patients. *Journal of Affective Disorders 208*, 443–447.

Devilliers, M., Busserolles, J., Lolignier, S., Deval, E., Pereira, V., Alloui, A., ... Eschalier, A. (2013). Activation of TREK-1 by morphine results in analgesia without adverse side effects. *Nature Communications 4*, 2941.

Dillon, D. G., Bogdan, R., Fagerness, J., Holmes, A. J., Perlis, R. H., & Pizzagalli, D. A. (2010). Variation in TREK1 gene linked to depression-resistant phenotype is associated with potentiated neural responses to rewards in humans. *Human Brain Mapping 31*, 210–221.

Djillani, A., Pietri, M., Moreno, S., Heurteaux, C., Mazella, J., & Borsotto, M. (2017). Shortened spadin analogs display better TREK-1 inhibition, in vivo stability and antidepressant activity. *Frontiers in Pharmacology 8*, 643.

Dong, Y. Y., Pike, A. C., Mackenzie, A., McClenaghan, C., Aryal, P., Dong, L., ... Carpenter, E. P. (2015). K2P channel gating mechanisms revealed by structures of TREK-2 and a complex with Prozac. *Science 347*, 1256–1259.

Duman, R. S., Heninger, G. R., & Nestler, E. J. (1997). A molecular and cellular theory of depression. *Archives of General Psychiatry 54*, 597–606.

Ferguson, J. M. (2001). SSRI antidepressant medications: Adverse effects and tolerability. *Primary Care Companion to The Journal of Clinical Psychiatry 3*, 22–27.

Fergusson, D., Doucette, S., Glass, K. C., Shapiro, S., Healy, D., Hebert, P., & Hutton, B. (2005). Association between suicide attempts and selective serotonin reuptake inhibitors: Systematic review of randomised controlled trials. *BMJ 330*, 396.

Fink, M., Duprat, F., Lesage, F., Reyes, R., Romey, G., Heurteaux, C., & Lazdunski, M. (1996). Cloning, functional expression and brain localization of a novel unconventional outward rectifier K+ channel. *The EMBO Journal 15*, 6854–6862.

Finlayson, K., Witchel, H. J., McCulloch, J., & Sharkey, J. (2004). Acquired QT interval prolongation and HERG: Implications for drug discovery and development. *European Journal of Pharmacology 500*, 129–142.

Fosgerau, K., & Hoffmann, T. (2015). Peptide therapeutics: Current status and future directions. *Drug Discovery Today 20*, 122–128.

Gaudriault, G., Heurteaux, C., Mazella, J., Borsotto, M., Moha, O. U. M. H., & Veyssiere, J. (2015). Retro-inverso analogs of spadin display increased antidepressant effects. *Google Patents*.

Gervasoni, N., Aubry, J. M., Bondolfi, G., Osiek, C., Schwald, M., Bertschy, G., & Karege, F. (2005). Partial normalization of serum brain-derived neurotrophic factor in remitted patients after a major depressive episode. *Neuropsychobiology 51*, 234–238.

Gil, V., Gallego, D., Moha Ou Maati, H., Peyronnet, R., Martinez-Cutillas, M., Heurteaux, C., ... Jimenez, M. (2012). Relative contribution of SKCa and TREK1 channels in purinergic and nitrergic neuromuscular transmission in the rat colon. *American Journal of Physiology. Gastrointestinal and Liver Physiology 303*, G412–G423.

Gonul, A. S., Akdeniz, F., Taneli, F., Donat, O., Eker, C., & Vahip, S. (2005). Effect of treatment on serum brain-derived neurotrophic factor levels in depressed patients. *European Archives of Psychiatry and Clinical Neuroscience 255*, 381–386.

Gururajan, A., Clarke, G., Dinan, T. G., & Cryan, J. F. (2016). Molecular biomarkers of depression. *Neuroscience and Biobehavioral Reviews 64*, 101–133.

Hamplova-Peichlova, J., Krusek, J., Paclt, I., Slavicek, J., Lisa, V., & Vyskocil, F. (2002). Citalopram inhibits L-type calcium channel current in rat cardiomyocytes in culture. *Physiological Research 51*, 317–321.

Hervieu, G. J., Cluderay, J. E., Gray, C. W., Green, P. J., Ranson, J. L., Randall, A. D., & Meadows, H. J. (2001). Distribution and expression of TREK-1, a two-pore-domain potassium channel, in the adult rat CNS. *Neuroscience 103*, 899–919.

Heurteaux, C., Guy, N., Laigle, C., Blondeau, N., Duprat, F., Mazzuca, M., ... Lazdunski, M. (2004). TREK-1, a K(+) channel involved in neuroprotection and general anesthesia. *The EMBO Journal 23*, 2684–2695.

Heurteaux, C., Laigle, C., Blondeau, N., Jarretou, G., & Lazdunski, M. (2006a). Alpha-linolenic acid and riluzole treatment confer cerebral protection and improve survival after focal brain ischemia. *Neuroscience 137*, 241–251.

Heurteaux, C., Lucas, G., Guy, N., El Yacoubi, M., Thummler, S., Peng, X. D., ... Lazdunski, M. (2006b). Deletion of the background potassium channel TREK-1 results in a depression-resistant phenotype. *Nature Neuroscience 9*, 1134–1141.

Heyman, N. S., Cowles, C. L., Barnett, S. D., Wu, Y. Y., Cullison, C., Singer, C. A., ... Buxton, I. L. (2013). TREK-1 currents in smooth muscle cells from pregnant human myometrium. *American Journal of Physiology. Cell Physiology 305*, C632–C642.

Hivelin, C., Beraud-Dufour, S., Devader, C., Abderrahmani, A., Moreno, S., Moha Ou Maati, H., ... Coppola, T. (2016). Potentiation of calcium influx and insulin secretion in pancreatic beta cell by the specific TREK-1 blocker spadin. *Journal of Diabetes Research 2016*, 3142175.

Honore, E. (2007). The neuronal background K2P channels: Focus on TREK1. *Nature Reviews. Neuroscience 8*, 251–261.

Honore, E., Maingret, F., Lazdunski, M., & Patel, A. J. (2002). An intracellular proton sensor commands lipid- and mechano-gating of the K(+) channel TREK-1. *The EMBO Journal 21*, 2968–2976.

Huang, T. L., Lee, C. T., & Liu, Y. L. (2008). Serum brain-derived neurotrophic factor levels in patients with major depression: Effects of antidepressants. *Journal of Psychiatric Research 42*, 521–525.

Ji, X. C., Zhao, W. H., Cao, D. X., Shi, Q. Q., & Wang, X. L. (2011). Novel neuroprotectant chiral 3-n-butylphthalide inhibits tandem-pore-domain potassium channel TREK-1. *Acta Pharmacologica Sinica 32*, 182–187.

Karege, F., Bondolfi, G., Gervasoni, N., Schwald, M., Aubry, J. M., & Bertschy, G. (2005). Low brain-derived neurotrophic factor (BDNF) levels in serum of depressed patients probably results from lowered platelet BDNF release unrelated to platelet reactivity. *Biological Psychiatry 57*, 1068–1072.

Kaspar, A. A., & Reichert, J. M. (2013). Future directions for peptide therapeutics development. *Drug Discovery Today 18*, 807–817.

Katona, C. L., & Katona, C. P. (2014). New generation multi-modal antidepressants: Focus on vortioxetine for major depressive disorder. *Neuropsychiatric Disease and Treatment 10*, 349–354.

Kavalali, E. T., & Monteggia, L. M. (2015). How does ketamine elicit a rapid antidepressant response? *Current Opinion in Pharmacology 20*, 35–39.

Kennard, L. E., Chumbley, J. R., Ranatunga, K. M., Armstrong, S. J., Veale, E. L., & Mathie, A. (2005). Inhibition of the human two-pore domain potassium channel, TREK-1, by fluoxetine and its metabolite norfluoxetine. *British Journal of Pharmacology 144*, 821–829.

Kessler, R. C. (2012). The costs of depression. *The Psychiatric Clinics of North America 35*, 1–14.

Kim, D. (2003). Fatty acid-sensitive two-pore domain K+ channels. *Trends in Pharmacological Sciences 24*, 648–654.

Kim, E. J., Lee, D. K., Hong, S. G., Han, J., & Kang, D. (2017). Activation of TREK-1, but not TREK-2, channel by mood stabilizers. *International Journal of Molecular Sciences 18*.

Kobayashi, T., Washiyama, K., & Ikeda, K. (2006). Inhibition of G protein-activated inwardly rectifying K+ channels by the antidepressant paroxetine. *Journal of Pharmacological Sciences 102*, 278–287.

Lafreniere, R. G., & Rouleau, G. A. (2011). Migraine: Role of the TRESK two-pore potassium channel. *The International Journal of Biochemistry & Cell Biology 43*, 1533–1536.

Lauritzen, I., Blondeau, N., Heurteaux, C., Widmann, C., Romey, G., & Lazdunski, M. (2000). Polyunsaturated fatty acids are potent neuroprotectors. *The EMBO Journal 19*, 1784–1793.

Lauritzen, I., Zanzouri, M., Honore, E., Duprat, F., Ehrengruber, M. U., Lazdunski, M., & Patel, A. J. (2003). K+−dependent cerebellar granule neuron apoptosis. Role of task leak K+ channels. *The Journal of Biological Chemistry 278*, 32068–32076.

Lee, H. M., Chai, O. H., Hahn, S. J., & Choi, B. H. (2018). Antidepressant drug paroxetine blocks the open pore of Kv3.1 potassium channel. *The Korean Journal of Physiology & Pharmacology 22*, 71–80.

Lee, H. M., Hahn, S. J., & Choi, B. H. (2010). Open channel block of Kv1.5 currents by citalopram. *Acta Pharmacologica Sinica 31*, 429–435.

Lei, Q., Pan, X. Q., Chang, S., Malkowicz, S. B., Guzzo, T. J., & Malykhina, A. P. (2014). Response of the human detrusor to stretch is regulated by TREK-1, a two-pore-domain (K2P) mechano-gated potassium channel. *The Journal of Physiology 592*, 3013–3030.

Leithner, K., Hirschmugl, B., Li, Y., Tang, B., Papp, R., Nagaraj, C., ... Hrzenjak, A. (2016). TASK-1 regulates apoptosis and proliferation in a subset of non-small cell lung cancers. *PLoS One 11*, e0157453.

Lesage, F., & Lazdunski, M. (1998). Mapping of human potassium channel genes TREK-1 (KCNK2) and TASK (KCNK3) to chromosomes 1q41 and 2p23. *Genomics 51*, 478–479.

Lesage, F., & Lazdunski, M. (2000). Molecular and functional properties of two pore domain potassium channels. *The American Journal of Physiology 279*, 793–801.

Li, L., & Vlisides, P. E. (2016). Ketamine: 50 years of modulating the mind. *Frontiers in Human Neuroscience 10*, 612.

Liou, Y. J., Chen, T. J., Tsai, S. J., Yu, Y. W., Cheng, C. Y., & Hong, C. J. (2009). Support for the involvement of the KCNK2 gene in major depressive disorder and response to antidepressant treatment. *Pharmacogenetics and Genomics 19*, 735–741.

Liu, H., Enyeart, J. A., & Enyeart, J. J. (2007). Potent inhibition of native TREK-1 K+ channels by selected dihydropyridine Ca2+ channel antagonists. *The Journal of Pharmacology and Experimental Therapeutics 323*, 39–48.

Lopes, C. M., Rohacs, T., Czirjak, G., Balla, T., Enyedi, P., & Logothetis, D. E. (2005). PIP2 hydrolysis underlies agonist-induced inhibition and regulates voltage gating of two-pore domain K+ channels. *The Journal of Physiology 564*, 117–129.

Maingret, F., Lauritzen, I., Patel, A. J., Heurteaux, C., Reyes, R., Lesage, F., ... Honore, E. (2000). TREK-1 is a heat-activated background K(+) channel. *The EMBO Journal 19*, 2483–2491.

Maingret, F., Patel, A. J., Lesage, F., Lazdunski, M., & Honore, E. (1999). Mechano- or acid stimulation, two interactive modes of activation of the TREK-1 potassium channel. *The Journal of Biological Chemistry 274*, 26691–26696.

Marsh, B., Acosta, C., Djouhri, L., & Lawson, S. N. (2012). Leak K(+) channel mRNAs in dorsal root ganglia: Relation to inflammation and spontaneous pain behaviour. *Molecular and Cellular Neurosciences 49*, 375–386.

Martin, S., Vincent, J. P., & Mazella, J. (2003). Involvement of the neurotensin receptor-3 in the neurotensin-induced migration of human microglia. *The Journal of Neuroscience 23*, 1198–1205.

Masand, P. S., & Gupta, S. (2002). Long-term side effects of newer-generation antidepressants: SSRIS, venlafaxine, nefazodone, bupropion, and mirtazapine. *Annals of Clinical Psychiatry 14*, 175–182.

Mazella, J., Petrault, O., Borsotto, M., Heurteaux, C., & Widmann, C. (2012). Peptide derived from neurotensin receptor 3 and use thereof in the treatment of psychiatric diseases. *Google Patents*.

Mazella, J., Petrault, O., Lucas, G., Deval, E., Beraud-Dufour, S., Gandin, C., ... Borsotto, M. (2010). Spadin, a sortilin-derived peptide, targeting rodent TREK-1 channels: A new concept in the antidepressant drug design. *PLoS Biology 8*, e1000355.

Mazella, J., Zsurger, N., Navarro, V., Chabry, J., Kaghad, M., Caput, D., ... Vincent, J. P. (1998). The 100-kDa neurotensin receptor is gp95/sortilin, a non-G-protein-coupled receptor. *The Journal of Biological Chemistry 273*, 26273–26276.

McClenaghan, C., Schewe, M., Aryal, P., Carpenter, E. P., Baukrowitz, T., & Tucker, S. J. (2016). Polymodal activation of the TREK-2 K2P channel produces structurally distinct open states. *The Journal of General Physiology 147*, 497–505.

McGowan, J. W., Bidwell, G. L., 3rd, & Vig, P. J. (2015). Challenges and new strategies for therapeutic peptide delivery to the CNS. *Therapeutic Delivery 6*, 841–853.

Medhurst, A. D., Rennie, G., Chapman, C. G., Meadows, H., Duckworth, M. D., Kelsell, R. E., ... Pangalos, M. N. (2001). Distribution analysis of human two pore domain potassium channels in tissues of the central nervous system and periphery. *Brain Research. Molecular Brain Research 86*, 101–114.

Moha ou Maati, H., Peyronnet, R., Devader, C., Veyssiere, J., Labbal, F., Gandin, C., ... Borsotto, M. (2011). A human TREK-1/HEK cell line: A highly efficient screening tool for drug development in neurological diseases. *PLoS One 6*, e25602.

Moha Ou Maati, H., Veyssiere, J., Labbal, F., Coppola, T., Gandin, C., Widmann, C., ... Borsotto, M. (2012). Spadin as a new antidepressant: Absence of TREK-1-related side effects. *Neuropharmacology 62*, 278–288.

Monteleone, P., Serritella, C., Martiadis, V., & Maj, M. (2008). Decreased levels of serum brain-derived neurotrophic factor in both depressed and euthymic patients with unipolar depression and in euthymic patients with bipolar I and II disorders. *Bipolar Disorders 10*, 95–100.

Montgomery, S. A. (2008). Tolerability of serotonin norepinephrine reuptake inhibitor antidepressants. *CNS Spectrums 13*, 27–33.

Moreno, S., Devader, C. M., Pietri, M., Borsotto, M., Heurteaux, C., & Mazella, J. (2018). Altered Trek-1 function in Sortilin deficient mice results in decreased depressive-like behavior. *Frontiers in Pharmacology 9*, 863.

Munck Petersen, C., Nielsen, M. S., Jacobsen, C., Tauris, J., Jacobsen, L., Gliemann, J., ... Madsen, P. (1999). Propeptide cleavage conditions sortilin/neurotensin receptor-3 for ligand binding. *The EMBO Journal 18*, 595–604.

Navarro, V., Vincent, J. P., & Mazella, J. (2002). Shedding of the luminal domain of the neurotensin receptor-3/sortilin in the HT29 cell line. *Biochemical and Biophysical Research Communications 298*, 760–764.

Nestler, E. J., Barrot, M., Dileone, R. J., Eisch, A. J., Gold, S. J., & Monteggia, L. M. (2002). Neurobiology of depression. *Neuron 34*, 13–25.

Nielsen, M. S., Jacobsen, C., Olivecrona, G., Gliemann, J., & Petersen, C. M. (1999). Sortilin/neurotensin receptor-3 binds and mediates degradation of lipoprotein lipase. *The Journal of Biological Chemistry 274*, 8832–8836.

Nischal, A., Tripathi, A., Nischal, A., & Trivedi, J. K. (2012). Suicide and antidepressants: What current evidence indicates. *Mens Sana Monographs 10*, 33–44.

Noel, J., Sandoz, G., & Lesage, F. (2011). Molecular regulations governing TREK and TRAAK channel functions. *Channels (Austin, Tex.) 5*, 402–409.

Nykjaer, A., Lee, R., Teng, K. K., Jansen, P., Madsen, P., Nielsen, M. S., ... Petersen, C. M. (2004). Sortilin is essential for proNGF-induced neuronal cell death. *Nature 427*, 843–848.

Otte, C., Gold, S. M., Penninx, B. W., Pariante, C. M., Etkin, A., Fava, M., ... Schatzberg, A. F. (2016). Major depressive disorder. *Nature Reviews Disease Primers 2*, 16065.

Patel, A. J., & Honore, E. (2001). Properties and modulation of mammalian 2P domain K^+ channels. *Trends in Neurosciences 24*, 339–346.

Patel, A. J., Honore, E., Lesage, F., Fink, M., Romey, G., & Lazdunski, M. (1999). Inhalational anesthetics activate two-pore-domain background K+ channels. *Nature Neuroscience 2*, 422–426.

Patel, A. J., Honore, E., Maingret, F., Lesage, F., Fink, M., Duprat, F., & Lazdunski, M. (1998). A mammalian two pore domain mechano-gated S-like K+ channel. *The EMBO Journal 17*, 4283–4290.

Perez-Caballero, L., Torres-Sanchez, S., Bravo, L., Mico, J. A., & Berrocoso, E. (2014). Fluoxetine: A case history of its discovery and preclinical development. *Expert Opinion on Drug Discovery 9*, 567–578.

Perlis, R. H., Moorjani, P., Fagerness, J., Purcell, S., Trivedi, M. H., Fava, M., ... Smoller, J. W. (2008). Pharmacogenetic analysis of genes implicated in rodent models of antidepressant response: Association of TREK1 and treatment resistance in the STAR(*)D study. *Neuropsychopharmacology 33*(12), 2810–2819.

Petersen, C. M., Nielsen, M. S., Nykjaer, A., Jacobsen, L., Tommerup, N., Rasmussen, H. H., ... Moestrup, S. K. (1997). Molecular identification of a novel candidate sorting receptor purified from human brain by receptor-associated protein affinity chromatography. *The Journal of Biological Chemistry 272*, 3599–3605.

Piccinni, A., Marazziti, D., Catena, M., Domenici, L., Del Debbio, A., Bianchi, C., ... Dell'Osso, L. (2008). Plasma and serum brain-derived neurotrophic factor (BDNF) in depressed patients during 1 year of antidepressant treatments. *Journal of Affective Disorders 105*, 279–283.

Porsolt, R. D., Le Pichon, M., & Jalfre, M. (1977). Depression: A new animal model sensitive to antidepressant treatments. *Nature 266*, 730–732.

Ramaker, M. J., & Dulawa, S. C. (2017). Identifying fast-onset antidepressants using rodent models. *Molecular Psychiatry 22*, 656–665.

Read, J., & Williams, J. (2018). Adverse effects of antidepressants reported by 1,431 people from 38 countries: Emotional blunting, suicidality, and withdrawal effects. *Current Drug Safety 13*(3), 176–186.

Richelson, E. (2013). Multi-modality: A new approach for the treatment of major depressive disorder. *The International Journal of Neuropsychopharmacology 16*, 1433–1442.

Sandoz, G., Tardy, M. P., Thummler, S., Feliciangeli, S., Lazdunski, M., & Lesage, F. (2008). Mtap2 is a constituent of the protein network that regulates twik-related K+ channel expression and trafficking. *The Journal of Neuroscience 28*, 8545–8552.

Sandoz, G., Thummler, S., Duprat, F., Feliciangeli, S., Vinh, J., Escoubas, P., ... Lesage, F. (2006). AKAP150, a switch to convert mechano-, pH- and arachidonic acid-sensitive TREK K(+) channels into open leak channels. *The EMBO Journal 25*, 5864–5872.

Sanguinetti, M. C., Curran, M. E., Zou, A., Shen, J., Spector, P. S., Atkinson, D. L., & Keating, M. T. (1996). Coassembly of K(V)LQT1 and minK (IsK) proteins to form cardiac I(Ks) potassium channel. *Nature 384*, 80–83.

Sanguinetti, M. C., & Jurkiewicz, N. K. (1990). Two components of cardiac delayed rectifier K+ current. Differential sensitivity to block by class III antiarrhythmic agents. *The Journal of General Physiology 96*, 195–215.

Santos, R., Ursu, O., Gaulton, A., Bento, A. P., Donadi, R. S., Bologa, C. G., ... Overington, J. P. (2017). A comprehensive map of molecular drug targets. *Nature Reviews. Drug Discovery 16*, 19–34.

Schwartz, J., Murrough, J. W., & Iosifescu, D. V. (2016). Ketamine for treatment-resistant depression: Recent developments and clinical applications. *Evidence-Based Mental Health 19*, 35–38.

Sharma, T., Guski, L. S., Freund, N., & Gotzsche, P. C. (2016). Suicidality and aggression during antidepressant treatment: Systematic review and meta-analyses based on clinical study reports. *BMJ 352*, i65.

Shimizu, E., Hashimoto, K., Okamura, N., Koike, K., Komatsu, N., Kumakiri, C., ... Iyo, M. (2003). Alterations of serum levels of brain-derived neurotrophic factor (BDNF) in depressed patients with or without antidepressants. *Biological Psychiatry 54*, 70–75.

Short, B., Fong, J., Galvez, V., Shelker, W., & Loo, C. K. (2017). Side-effects associated with ketamine use in depression: A systematic review. *Lancet Psychiatry 5*(1), 65–78.

Sicouri, S., & Antzelevitch, C. (2008). Sudden cardiac death secondary to antidepressant and antipsychotic drugs. *Expert Opinion on Drug Safety 7*, 181–194.

Stassen, H. H., Angst, J., & Delini-Stula, A. (1997). Delayed onset of action of antidepressant drugs? Survey of recent results. *European Psychiatry 12*, 166–176.

Strawbridge, R., Young, A. H., & Cleare, A. J. (2017). Biomarkers for depression: Recent insights, current challenges and future prospects. *Neuropsychiatric Disease and Treatment 13*, 1245–1262.

Tatsumi, M., Groshan, K., Blakely, R. D., & Richelson, E. (1997). Pharmacological profile of antidepressants and related compounds at human monoamine transporters. *European Journal of Pharmacology 340*, 249–258.

Thummler, S., Duprat, F., & Lazdunski, M. (2007). Antipsychotics inhibit TREK but not TRAAK channels. *Biochemical and Biophysical Research Communications 354*, 284–289.

Tulleuda, A., Cokic, B., Callejo, G., Saiani, B., Serra, J., & Gasull, X. (2011). TRESK channel contribution to nociceptive sensory neurons excitability: Modulation by nerve injury. *Molecular Pain 7*, 30.

Uhlig, T., Kyprianou, T., Martinelli, F. G., Oppici, C. A., Heiligers, D., Hills, D., ... Verhaert, P. (2014). The emergence of peptides in the pharmaceutical business: From exploration to exploitation. *EuPA Open Proteomics 4*, 58–69.

Veyssiere, J., Moha Ou Maati, H., Mazella, J., Gaudriault, G., Moreno, S., Heurteaux, C., & Borsotto, M. (2015). Retroinverso analogs of spadin display increased antidepressant effects. *Psychopharmacology 232*, 561–574.

Vivier, D., Soussia, I. B., Rodrigues, N., Lolignier, S., Devilliers, M., Chatelain, F. C., ... Ducki, S. (2017). Development of the first two-pore domain potassium channel TWIK-related K+ channel 1-selective agonist possessing in vivo antinociceptive activity. *Journal of Medicinal Chemistry 60*, 1076–1088.

Wang, C. K., Northfield, S. E., Colless, B., Chaousis, S., Hamernig, I., Lohman, R. J., ... Craik, D. J. (2014). Rational design and synthesis of an orally bioavailable peptide guided by NMR amide temperature coefficients. *Proceedings of the National Academy of Sciences of the United States of America 111*, 17504–17509.

Wang, W., Liu, D., Xiao, Q., Cai, J., Feng, N., Xu, S., ... Wang, X. (2018). Lig4-4 selectively inhibits TREK-1 and plays potent neuroprotective roles in vitro and in rat MCAO model. *Neuroscience Letters 671*, 93–98.

Westergaard, U. B., Sorensen, E. S., Hermey, G., Nielsen, M. S., Nykjaer, A., Kirkegaard, K., ... Petersen, C. M. (2004). Functional organization of the sortilin Vps10p domain. *The Journal of Biological Chemistry 279*, 50221–50229.

Wong, D. T., Horng, J. S., Bymaster, F. P., Hauser, K. L., & Molloy, B. B. (1974). A selective inhibitor of serotonin uptake: Lilly 110140, 3-(p-trifluoromethylphenoxy)-N-methyl-3-phenylpropylamine. *Life Sciences 15*, 471–479.

Woods, A. G., Iosifescu, D. V., & Darie, C. C. (2014). Biomarkers in major depressive disorder: The role of mass spectrometry. *Advances in Experimental Medicine and Biology 806*, 545–560.

Ye, D., Li, Y., Zhang, X., Guo, F., Geng, L., Zhang, Q., & Zhang, Z. (2015). TREK1 channel blockade induces an antidepressant-like response synergizing with 5-HT1A receptor signaling. *European Neuropsychopharmacology 25*, 2426–2436.

Yin, Z., Li, Y., He, W., Li, D., Li, H., Yang, Y., ... Khalil, R. A. (2018). Progesterone inhibits contraction and increases TREK-1 potassium channel expression in late pregnant rat uterus. *Oncotarget 9*, 651–661.

Yoshimura, R., Mitoma, M., Sugita, A., Hori, H., Okamoto, T., Umene, W., ... Nakamura, J. (2007). Effects of paroxetine or milnacipran on serum brain-derived neurotrophic factor in depressed patients. *Progress in Neuro-Psychopharmacology & Biological Psychiatry 31*, 1034–1037.

Yuan, H., Mischoulon, D., Fava, M., & Otto, M. W. (2017). Circulating microRNAs as biomarkers for depression: Many candidates, few finalists. *Journal of Affective Disorders 233*, 68–78.

Zhang, M., Yin, H. J., Wang, W. P., Li, J., & Wang, X. L. (2016). Over-expressed human TREK-1 inhibits CHO cell proliferation via inhibiting PKA and p38 MAPK pathways and subsequently inducing G1 arrest. *Acta Pharmacologica Sinica 37*, 1190–1198.

B- Article 4 : "Altered Trek-1 Function in Sortilin Deficient Mice Results in Decreased Depressive-Like Behavior"

Parallèlement à mon projet qui portait principalement sur TREK-1, la Spadine et ses dérivés, j'ai également participé à une étude sur le rôle de la Sortiline dans la pathologie de la dépression. De façon évidente le laboratoire s'est intéressé à la protéine partenaire de TREK-1, la Sortiline. En effet, le phénotype de résistance à la dépression que manifestent les souris TREK-$1^{-/-}$ a orienté une étude sur le comportement des souris Sort$1^{-/-}$ (KO pour le gène de la Sortiline). Pour caractériser les conséquences de la suppression de la Sortiline, à l'exemple de ce qui avait été réalisé pour caractériser les KO TREK-1, le laboratoire a combiné des approches comportementales, électrophysiologiques et biochimiques aussi bien *in vivo* qu'*in vitro*.

Ces études ont révélé que les souris Sort$1^{-/-}$ manifestent un comportement anxieux dont le développement n'est pas lié au taux de corticostérone, une résistance à la dépression dans plusieurs tests comportementaux. Ces KO présentent une activité accrue des neurones des noyaux du raphé dorsal, structure fortement impliquée dans le processus de la dépression. Toutes ces propriétés ont été associées à une activité de TREK-1 insuffisante, qui est la conséquence directe de la diminution de l'expression de ce canal à la surface cellulaire. Une augmentation de l'expression du BDNF due à l'activation de la voie constitutive dépendante de la furine, ainsi qu'une augmentation de l'activation de TrkB par le BDNF ont également pu être observées chez ces KO. Ces deux caractéristiques sont en accord avec le phénotype de résistance face à la dépression.

Les résultats obtenus lors de cette étude démontrent que l'expression fonctionnelle de TREK-1 est altérée en l'absence de Sortiline. Ces résultats sont une confirmation essentielle de l'implication de TREK-1 dans la régulation de l'humeur, et sa définition comme cible importante dans le traitement de la dépression.

frontiers in Pharmacology

ORIGINAL RESEARCH
published: 06 August 2018
doi: 10.3389/fphar.2018.00863

Altered Trek-1 Function in Sortilin Deficient Mice Results in Decreased Depressive-Like Behavior

Sébastien Moreno, Christelle M. Devader, Mariel Pietri, Marc Borsotto, Catherine Heurteaux and Jean Mazella**

Centre National de la Recherche Scientifique, Institut de Pharmacologie Moléculaire et Cellulaire, UMR 7275, Université Côte d'Azur, Valbonne, France

The background potassium channel TREK-1 has been shown to be a potent target for depression treatment. Indeed, deletion of this channel in mice resulted in a depression resistant phenotype. The association of TREK-1 with the sorting protein sortilin prompted us to investigate the behavior of mice deleted from the gene encoding sortilin (*Sort1*$^{-/-}$). To characterize the consequences of sortilin deletion on TREK-1 activity, we combined behavioral, electrophysiological and biochemical approaches performed *in vivo* and *in vitro*. Analyses of *Sort1*$^{-/-}$ mice revealed that they display: (1) a corticosterone-independent anxiety-like behavior, (2) a resistance to depression as demonstrated by several behavioral tests, and (3) an increased activity of dorsal raphe nucleus neurons. All these properties were associated with TREK-1 action deficiency consequently to a decrease of its cell surface expression and to the modification of its electrophysiological activity. An increase of BDNF expression through activation of the furin-dependent constitutive pathway as well as an increase of the activated BDNF receptor TrkB were in agreement with the decrease of depressive-like behavior of *Sort1*$^{-/-}$ mice. Our results demonstrate that the TREK-1 expression and function are altered in the absence of sortilin confirming the importance of this channel in the regulation on the mood as a crucial target to treat depression.

Keywords: depression, sortilin, TREK-1, behavior, electrophysiology

OPEN ACCESS

Edited by:
Pascal Bonaventure, Janssen Research and Development, United States

Reviewed by:
Michel Hamon, Université Pierre et Marie Curie, France
Chunsheng Ruan, Columbia University, United States

****Correspondence:***
Sébastien Moreno
smoreno@ipmc.cnrs.fr
Jean Mazella
mazella@ipmc.cnrs.fr

Specialty section:
This article was submitted to Neuropharmacology, a section of the journal Frontiers in Pharmacology

Received: *07 May 2018*
Accepted: *17 July 2018*
Published: *06 August 2018*

Citation:
Moreno S, Devader CM, Pietri M, Borsotto M, Heurteaux C and Mazella J (2018) Altered Trek-1 Function in Sortilin Deficient Mice Results in Decreased Depressive-Like Behavior. Front. Pharmacol. 9:863. doi: 10.3389/fphar.2018.00863

INTRODUCTION

The origins of mood disorders result from a complex cross-talk between multiple genes in relation with environmental and developmental epigenetic components. Our understanding of the biological mechanisms of such diseases is therefore limited. We only accumulate informations about the roles of some crucial central and peripheral mediators such as corticosterone, 5-HT and BDNF. Briefly, depressive patients show an increase of circulating corticosterone, a modification of 5-HT content and a marked decrease of both cerebral and peripheral circulating BDNF levels. These mediators belong to the epigenetics and gene expression marker family of major depressive disorder and AD response (for review see Fabbri et al., 2017). At the level of animal models, transgenic mice allowed to identify some new targets.

Abbreviations: 5-HT, serotonin; AD, antidepressant; BDNF, brain derived neurotrophic factor; BrdU, 5-bromo-2′-deoxyuridine; DCX, doublecortin; DRN, dorsal raphe nucleus; FST, forced swimming test; H/LDM, high and low density microsomes; NSF, novelty suppressed feeding; NT, neurotensin; NTSR2, neurotensin receptor-2; NTSR3, neurotensin receptor-3; p75NTR, neurotrophin receptor of 75 kDa; PM, plasma membrane; TGN38, trans-golgi network protein of 38 kDa; TrkB, tropomyosin receptor kinase B; TST, tail suspension test; WT, wild type.

Phenotyping mice in which a gene has been deleted may appear relatively easy in terms of preliminary observations for detecting a major health problem or a motor defect. A series of physical parameters including body weight and temperature, home cage locomotion, grooming, nesting and sleeping, neurological reflexes can be tested before starting behavioral tasks related to anxiety and mood disorders (Crawley, 1999). In the field of depression and anxiety-related disorders, the background potassium channel TREK-1 (Twik related potassium channel 1) has been one of the first targets for which deletion of its gene (*Kcnk2*$^{-/-}$) in mice resulted in a depression-resistant phenotype highlighted by behavioral tests (Heurteaux et al., 2006). Interestingly, in several behavior tests, *Kcnk2*$^{-/-}$ mice behave, similarly, to naive mice treated with ADs like fluoxetine. In addition, an increase in firing rate of serotoninergic neurons from the DRN is observed, increasing the 5-HT transmission being one of the main characteristics of AD action (Heurteaux et al., 2006). Taken together, results obtained from *Kcnk2*$^{-/-}$ mice led to the hypothesis that the search of selective blockers of the TREK-1 channel could lead to a new type of AD. More recently, the discovery of spadin, which is a sortilin-derived peptide acting as a potent AD and specifically targeting TREK-1 channels, supported this hypothesis (Mazella et al., 2010). Interestingly, in addition to the AD properties of spadin, we have demonstrated the existence of a protein complex between the TREK-1 channel and sortilin. The expression of the TREK-1 channel at the PM of COS-7 cells is increased when the channel is co-expressed with sortilin. Consequently, because sortilin is a crucial partner in the sorting of several factors and enzymes (Lefrancois et al., 2003; Kandror and Pilch, 2011), we analyzed in details the depression-related phenotype of mice in which the gene encoding sortilin (*Sort1*) has been inactivated, with a focus on the expression of its partner TREK-1 and the subsequent consequences on the TREK-1 function.

To date, inactivation of *Sort1* gene demonstrated that sortilin is involved in the proNGF (precursor of nerve growth factor)-induced neuronal cell death when associated with p75NTR (p75 neurotrophin receptor) (Nykjaer et al., 2004) as well as in the binding and internalization of the fronto-demential protein progranulin (Hu et al., 2010). More recently a controversial role of sortilin in the regulation of cholesterol metabolism has been described (Kjolby et al., 2010; Musunuru et al., 2010), and largely commented in the literature (Dube et al., 2011; Tall and Ai, 2011). Sortilin [also called NTSR3] belongs to the neurotensinergic system (Mazella et al., 1998). A recent study showed that the lack of sortilin expression leads to the increase in brain of both NT and NTSR2 receptors. These *Sort1*$^{-/-}$ mice are less sensitive to thermal and chemical nociception (Devader et al., 2016).

Sortilin is subjected to membrane protease-induced shedding leading to the release of a soluble form (Navarro et al., 2002). Interestingly, increased serum concentrations of soluble sortilin have been detected in patients suffering from major depression when compared to control healthy subjects (Buttenschon et al., 2015). The higher level of soluble sortilin in depressive patients is correlated with an increase of BDNF and VEGF levels, indicating that the circulating soluble sortilin could be a new candidate as a biomarker of depression state. However, a more recent study investigating the serum level of sortilin in response to AD treatment revealed that the depression score and response to treatment were not predicted by sortilin level (Buttenschon et al., 2017), then invalidating the former hypothesis.

Because sortilin and TREK-1 have been shown to be associated at the cellular and molecular levels (Mazella et al., 2010) and because sortilin plays an important role in the sorting of numerous proteins we hypothesized that the absence of sortilin could result in modifications of TREK-1 expression, its cellular location and its functions. On another hand, since TREK-1 was described to be a potent target in depression (Heurteaux et al., 2006), the aim of the present work was to analyze using electrophysiological, biochemical, and behavioral approaches, the phenotype of *Sort1*$^{-/-}$ mice regarding antidepressive-like behavior.

MATERIALS AND METHODS

Animals

The NTSR3/sortilin homozygous KO mice (*Sort1*$^{-/-}$) were generated by the Morales's laboratory by incorporation of a GFP cassette after exon 1 (Zeng et al., 2009) and controls were C57Bl/6J male mice from Janvier Labs (Saint-Berthevin, France). Both strains were of the same C57Bl/6J genetic background. *Sort1*$^{-/-}$ mice were used after more than 10 generations and then considered with a stable genetic background. The local Ethics Committee (CIEPAL) (protocol number 00893.02) approved experimental procedures and animal cares are in accordance with the policies on the care and use of laboratory animals of European Community legislation 2010/63/EU. Animal studies were conducted in compliance with the ARRIVE guidelines (Kilkenny et al., 2011; McGrath and Lilley, 2015). Adult male (8–10 weeks old) mice were housed under controlled laboratory conditions according to the FELASA guidelines and recommendations; 6 mice/cage with a 12 h dark–light cycle, a temperature of 21 ± 2°C, and a 40–60% humidity. They have free access to standard rodent diet and tap water.

Sources of Reagents and Equipment

The ELISA kit to measure corticosterone was from Enzo Life Science. Rabbit polyclonal antibodies anti-TREK-1 and anti-proBDNF were from Alomone Labs (Israel). Rabbit polyclonal antibodies anti-furin and anti-NaKATPase, the mouse monoclonal anti-beta-actin and goat anti-TGN38 and anti-DCX antibodies were from SantaCruz Technologies (United States). Rabbit polyclonal antibodies anti-TrkB and anti-phospho-(Tyr 705)-TrkB were from Signalway Antibody (United States). Rabbit polyclonal antibodies against BDNF and plasminogen were from GeneTex (United States). Mouse monoclonal anti-BrdU antibody was from Becton Dickinson (United States). Anti-rabbit, anti-mouse, and anti-goat secondary antibodies were from Cell Signaling Technologies. HRP substrate (Immobilon Forte, Millipore), Nitrocellulose (BioTrace NT, Life Sciences), SDS-PAGE gels and Mini Protean apparatus were from Biorad. BrdU was from Interchim (France). Neurobasal medium, B-27 and Penicillin-Streptomycin were from Thermo Fisher

Scientific. Poly-D-Lysine was from Sigma-Aldrich. Patch clamp was performed on a pClamp 8.2 apparatus (Molecular Devices)

Primary Culture of Cortical Neurons

Primary cortical neurons were isolated from 14-day-old mouse embryo cortice (E14) from *Sort1*$^{-/-}$ and control females. Cells were mechanically dissociated and seeded in 35 mm diameter dishes previously treated with Poly-D-Lysine and maintained in culture in a Neurobasal/B27 medium for 10–14 days.

Data and Statistical Analysis

Group Sizes

The group sizes provided for the following experiments were variable due to the difficulties to regularly obtains the same number of adult males (8–10 weeks old) house breeded animals (i.e., *Sort1*$^{-/-}$ mice). For each kind of experiment, we adapted the number of WT mice to the number of available *Sort1*$^{-/-}$ mice.

Each animal was used once and the total of 218 male WT and *Sort1*$^{-/-}$ mice were used for these studies. Behavioral experiments were performed with naïve mice for all used tests. Mice were isolated 30 min in neutral room before tests. The experimenter was blind to randomized experimental groups. Randomization was performed using the TST software (Bioseb, France).

Behavioral tests used in this work have been validated for mouse behavioral phenotypes related to neuropsychiatric disorders, such as depression or anxiety (for review, see Samsom and Wong, 2015). Group sizes for behavioral, biochemical, and electrophysiological experiments were equal with the exception for firing rate recordings for which measurements were recorded from 36 5-HT neurons for WT and 26 neurons for *Sort1*$^{-/-}$ mice. These *in vivo* experiments were performed on five animals for each group and the number of recorded neurons from each animal varied depending on the position of electrodes.

For Western blot analyses, results were normalized using either an intracellular protein (actin) or a protein specific for a given intracellular compartment for sub-cellular fractionation experiments.

All data (displayed as mean ± SEM) were analyzed using Prism 6-2 Software (GraphPad, San Diego, CA, United States). For the comparison of two groups, Mann–Whitney test was used except for measurement of the DRN firing rates for which Student's *t*-test was used. All remaining data were compared using a two-way ANOVA with a Tukey's multiple comparison test. The level of significance was set at $p < 0.05$. The data and statistical analysis comply with the recommendations on experimental design and analysis in pharmacology (Curtis et al., 2015).

Behavioral Tests

Forced Swimming Test (FST)

Forced swimming test was performed according to the procedure initially described (Porsolt et al., 1977). In order to validate the test and to analyze whether the effects observed can be additive, in some cases, spadin (i.p. 100 µl of 10^{-6} M) or saline were injected 30 min before the test. Each animal was placed in a cylinder (height 30 cm, diameter 15 cm) filled with 15 cm water at 22 ± 1°C with no escape possibility during 6 min. The period of immobility was measured only during the last 4 min of the trial. We considered an immobile mouse when it only remained floating with slight movements to maintain head above surface.

Novelty Suppressed Feeding (NSF)

Mice were deprived from food for 24 h. On test day, mice were placed in a highly brightly lit box (45 cm × 45 cm × 20 cm), with floor covered with wood chip bedding, during 10 min. At the center of the box, a food pellet was placed on a white platform. The latency for the animal to eat the pellet was measured as previously described (Santarelli et al., 2003).

Tail Suspension Test (TST)

Mice were suspended by the tail by using a piece of adhesive tape. After "agitation" or "escape-like" behavior, mice adopted an immobile posture, suggested to mirror a state of depression. We recorded the immobility time during a 6 min test session according to Cryan et al. (2005).

Marble Burying

Burying object relates to a natural defense mechanism that occurs in mice under stress condition or anxiety state. Marble burying is able to detect anxiety and obsessive compulsive disorders-related phenotypes (Deacon, 2006). In response to novel bedding/environment mice exhibit digging behavior. Mice were placed during 30 min in a cage filled with approximately 5 cm deep with wood chip bedding and a regular pattern of 13 glass marbles disposed on the surface, evenly spaced, each about 4 cm apart. At the end of the time, buried marbles were counted (2/3 minimum of depth). Seventy-five percent of buried marbles was a typical score for naïve C57BL/6.

Elevated Plus Maze

Elevated Plus Maze allows to define an anxiety response in rodents (Gross et al., 2002). The apparatus consisted of central platform (5 cm × 5 cm), two open arms and two closed arms across from each other and perpendicular, with the same size (45 cm × 5 cm) and 15 cm wall height for the closer arms. The apparatus was placed at 45 cm height above the floor. Mice were placed in the central platform facing one open arm and were allowed to freely move during 10 min. During this period, number of entries and time spent in both arms were measured. To define an anxiety response, the time and number of entries in open arms were evaluated in relation to whole time spent or the total entries.

Light Dark

Mice were placed in a box divided into two compartments by a black partition with a small opening that allows mouse to move from one compartment to the other (Welch et al., 2007). One compartment, corresponding to one-third of the surface area, was made of white plastic and was brightly illuminated. The adjoining smaller compartment was black and dark. Mice were placed in the white compartment and allowed to move freely between the two chambers for 5 min. Time spent in the white chamber, and

latency to the first transition were recorded. Mice tended to avoid the white compartment. The measures of exploration in this area were used as experimental indices of anxiety.

Measurement of Serum Corticosterone Levels

Corticosterone concentration present in the serum from WT and *Sort1*$^{-/-}$ mice was determined by blood punctures made between 9 and 10 a.m. using the ELISA kit from Enzo Life Science (Cat. No. ADI-900-097) according to the manufacturer recommendations. The sensitivity of the detection was between 32 and 20,000 pg/ml and was species independent.

Whole Cell Patch Clamp Recordings and Membrane Potential Measurements

Electrophysiological experiments were performed on primary cortical neurons seeded at a density of 100,000 cells/35 mm dish after 10 days of culture. Membrane potential was recorded in whole cell configuration (Hamill et al., 1981) in current clamp mode (no current is injected, I = 0). Each membrane potential was evaluated by using a RK 400 patch clamp amplifier (Axon Instruments, United States), low-pass filtered at 3 kHz and digitized at 10 kHz using a 12-bit analog-to-digital converter Digidata (1322 series, Axon Instruments, United States). Patch clamp pipettes were pulled using vertical puller (PC-10, Narishige) from borosilicate glass capillaries and had a resistance of 10 MΩ. The bath solution contained (in mM) 150 NaCl, 5 KCl, 3 $MgCl_2$, 1 $CaCl_2$, and 10 HEPES adjusted to pH 7.4 with NaOH. The pipette solution contained (in mM) 155 KCl, 3 $MgCl_2$, 5 EGTA, and 10 HEPES adjusted to pH 7.2 with KOH. All experiments were performed at room temperature (21–22°C). Data acquisition was carried out using a microcomputer (Dell Pentium) with commercial software and hardware (pClamp 8.2). All values of membrane potentials are expressed in mV as mean ± standard error of the mean (SEM).

Sub-cellular Fractionation

In order to quantify the amount of TREK-1 expressed at the PM and intracellularly, we performed sub-cellular fractionation from brain homogenates. PMs were prepared from brain homogenates of WT or *Sort1*$^{-/-}$ mice according to the protocol previously described (Clancy and Czech, 1990). Briefly, brain from WT or *Sort1*$^{-/-}$ mice were collected in Solution A (250 mM sucrose, 20 mM HEPES, 1 mM EDTA and 1 mM PMSF at pH 7.4), homogenized with a Teflon pestle, and centrifuged at 16,000 × *g* for 20 min to yield Pellet 1 and Supernatant 1. Pellet 1 was resuspended in Solution B (20 mM HEPES and 1 mM EDTA at pH 7.4) using a Dounce homogenizer, loaded on a sucrose solution (1.12 M Sucrose in Buffer B), and centrifuged at 100,000 × *g* for 60 min to yield Pellet 2 and Supernatant 2. Pellet 2 representing the nuclear/mitochondrial fraction was discarded. Supernatant 2 was collected at the interface between the sucrose solution and Buffer B and was resuspended in Buffer B and centrifuged at 30,000 × *g* for 30 min to yield Pellet 3; pellet 3 was resuspended in Buffer B and represented the PM fraction. Meanwhile, Supernatant 1 was centrifuged at 30,000 × *g* for 30 min to produce Pellet 4 and Supernatant 3. Pellet 4 was resuspended in Buffer B and represented the HDM fraction. Supernatant 3 was centrifuged at 200,000 × *g* for 90 min to yield Pellet 5 resuspended in Buffer B and represented the LDM fraction. HDM and LDM were pooled for Western blot analyses 30 μg of crude homogenates, purified PMs and H/LDM were submitted to Western blot analysis using the rabbit polyclonal antibody against Anti-K2P2.1 (TREK-1) (1:500) (Alomone Labs, Israel). Proteins detected with this antibody were normalized using antibodies specific for each intracellular compartment (NaKATPase for PMs, TGN38 for H/LDM and beta-actin for total extracts) from SantaCruz Technologies (United States).

Western Blot

Mouse brains were dissected on ice and then homogenized in a solubilization buffer containing 20 mM HEPES (pH:7.4), 1 mM EDTA, 1 mM PMSF, 250 mM sucrose, and protease inhibitor cocktail using a polytron at the lowest speed. The homogenates were centrifuged 20 min at 100,000 × *g* at 4°C. Supernatants were resupended in 20 mM HEPES (pH: 7.4), 1 mM EDTA and stored at −20°C until further use. Solubilized proteins were loaded at 50 μg in SDS buffer, separated on 10% SDS PAGE gels and then transferred to a nitrocellulose membrane.

Membranes were incubated with rabbit polyclonal Anti-BDNF (1:1000) (GeneTex, United States), Anti-Phospho(Tyr705)TrkB (1:500), Anti-TrkB (1:1000) (Signalway Antibody, United States), Anti-K2P2.1 (TREK-1) (1:500) and anti-ProBDNF (1:400) (Alomone Labs, Israel), Anti-Furin (1:1000) (SantaCruz Technologies, United States), Anti-Phospho(Ser133) CREB (1:500) and mouse monoclonal Anti-CREB (1:1000) (CST, United States), mouse monoclonal Anti-beta-Actin (1:5000) (SantaCruz Technologies, United States) over night at 4°C. Afterwards, membranes were incubed 30 min with secondary antibody (related to species of first antibody) coupled HRP. Protein bands were revealed, images were acquired with FX Fusion (Vilber) and analyzed with ImageJ (US NIH, Bethesda, MD, United States) (Schneider et al., 2012).

Measurement of Hippocampal Neurogenesis

Mice were treated either with saline or with spadin (i.p. 100 μl of 10^{-6} M) once daily for 4 days and the fourth day BrdU was also injected (120 mg per kg of body weight in a 300 μl bolus). Twenty-four hours after the BrdU injection, mice were euthanized and transcardially perfused with 4% cold paraformaldehyde. Serial brain sections were cut (40 μm) throughout the entire hippocampus on a vibratome (Leica). Every sixth sections, slices were processed for BrdU and DCX immunohistochemistry, as previously described (Heurteaux et al., 2006). For each immunodetection, slices were first incubated overnight at 4°C with a mouse monoclonal anti-BrdU antibody (1:200; Becton Dickinson). For chromogenic immunodetection, sections were then incubated for 1 h in biotin-conjugated species-specific secondary antibodies (1:100; Vector

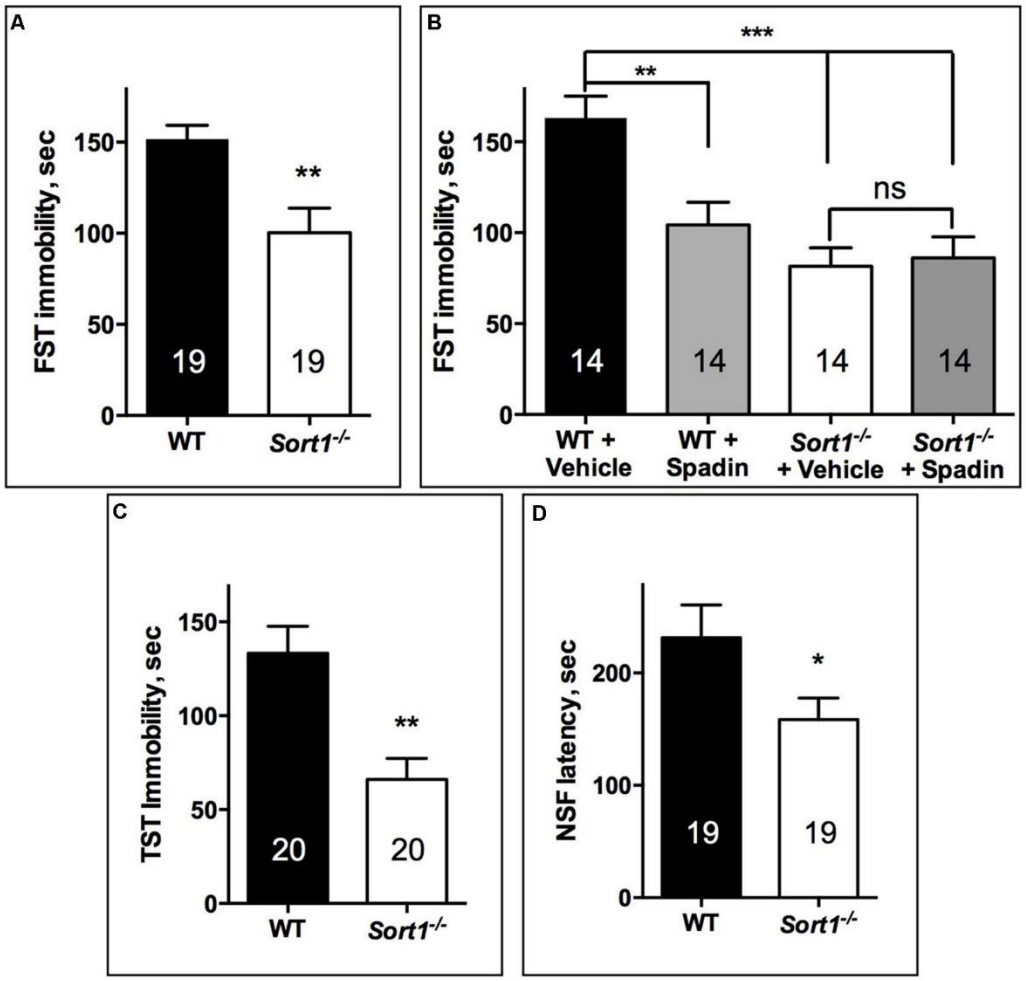

FIGURE 1 | Antidepressant-like behavior in *Sort1*$^{-/-}$ mice. **(A)** FST, *Sort1*$^{-/-}$ mice had a shorter immobility time than WT mice. **(B)** WT spadin-treated mice had also a shorter immobility time than vehicle-treated mice. Spadin had no effect on *Sort1*$^{-/-}$ mice. **(C)** TST, *Sort1*$^{-/-}$ mice had a significant reduced immobility time than WT mice. **(D)** NSF, the latency time for *Sort1*$^{-/-}$ mice was shorter than that measured for WT mice. Values are expressed as mean ± SEM. $^{*}p < 0.05$, $^{**}p < 0.01$, $^{***}p < 0.001$.

Laboratories) followed by a peroxidase-avidin complex solution according to the manufacturer's protocol. The peroxidase activity of immune complexes was visualized with DAB staining using the VectaStain ABC kit (Vector Laboratories). For fluorescent double labeling, that were performed to determine the cell phenotype, sections were incubated overnight at 4°C with a mouse monoclonal anti-BrdU antibody (1:200; Becton Dickinson), and a goat anti-DCX (1:200, Santa Cruz Laboratories). Antibodies were revealed with anti-mouse Alexa 488 and anti-goat Alexa 594 coupled antibodies (1:400; Molecular Probes). All BrdU-labeled cells in the granular cell layer and subgranular zone (SGZ) were counted in each section (n = 10 and 5 mice per group) at 400× magnification under a light microscope (Olympus) by an experimenter blinded to the study code. The total number of BrdU-positive cells per section was multiplied by 6 to obtain the total number of cells per dentate gyrus. The counting of BrdU/DCX labeled cells was performed using a Laser Scanning Confocal Microscope (TCS SP, Leica) equipped with a DMIRBE inverted microscope.

Extracellular Unitary Recordings of DRN 5-HT Neurons

Single-barreled glass micropipettes (recording electrodes) were filled with a 2 M NaCl solution saturated with Fast Green FCF, resulting in an impedance of 2–5 MΩ. Mice were anesthetized with chloral hydrate (400 mg/kg, using a 2% solution), and placed in a stereotaxic frame equipped with the Stoelting mouse adapter. Electrodes were positioned 0.5–1 mm posterior to the interaural line on the midline, and were then lowered into the DRN at a depth of 2.5 mm from the brain surface. 5-HT neurons were then encountered over a maximal distance of 1 mm. They were identified using the following criteria: a slow (0.5–2.5 Hz) and regular firing rate and long-duration (0.8–1.2 ms) action potentials (Heurteaux et al., 2006). Spikes were computed by

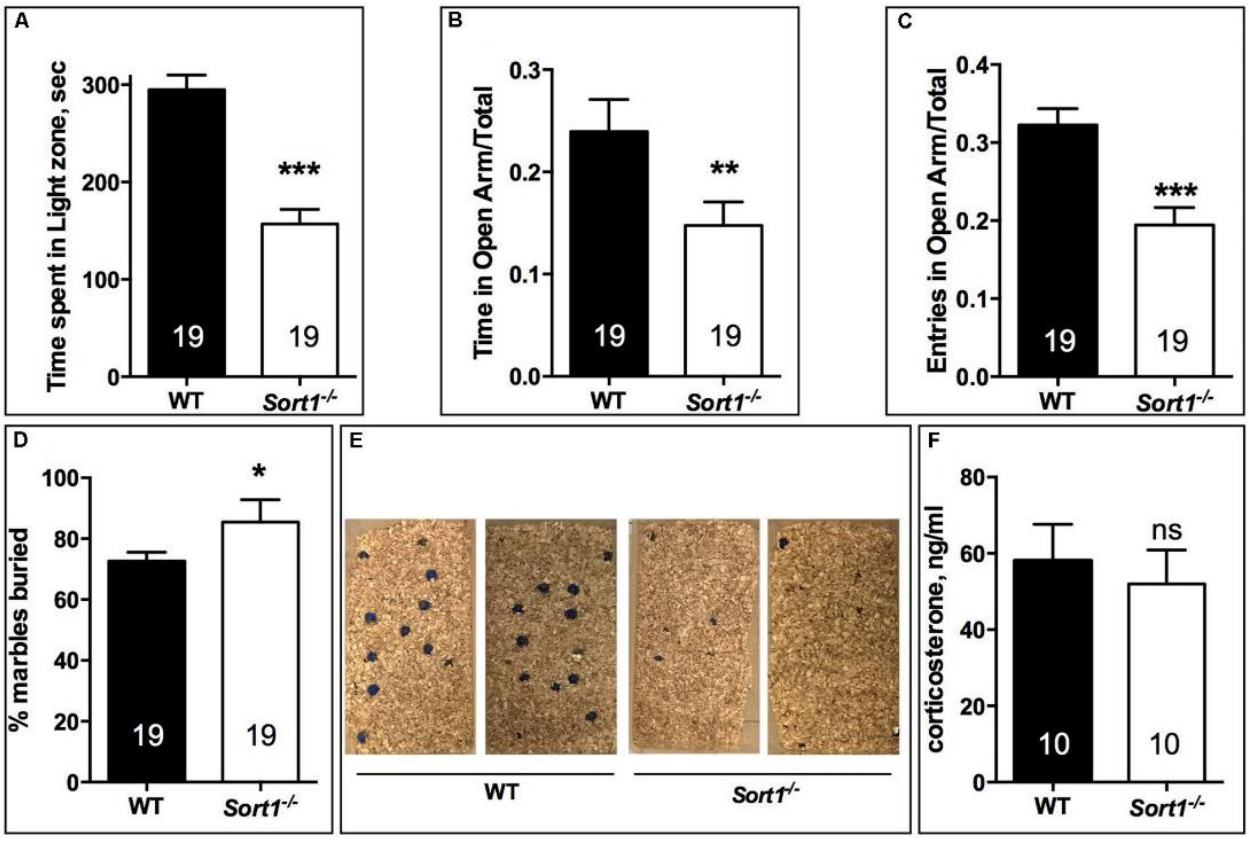

FIGURE 2 | Anxiety-like behavior in *Sort1*$^{-/-}$ mice. **(A)** Light-dark test, the time spent in the light zone was shorter for *Sort1*$^{-/-}$ mice compared to WT mice. **(B,C)** Elevated-plus Maze test, the ratio of the time spent in the open arm was reduced in *Sort1*$^{-/-}$ mice compared to WT mice. The ratio in the number of entries was also reduced in *Sort1*$^{-/-}$ mice. **(D,E)** Glass marbles burying test, the percent of marbles buried by WT mice was significantly increased by *Sort1*$^{-/-}$ mice as shown in **E**. **(F)** Serum corticosterone level in WT and *Sort1*$^{-/-}$ mice remained unchanged. Values are expressed as mean ± SEM. $^{*}p < 0.05$, $^{**}p < 0.01$, $^{***}p < 0.001$, ns, non-significant.

using the Spike 2 software. Firing rates were calculated as the mean number of events occurring within a 10 s period. For each neuron, discharges were monitored during 60 s. Three to four successive descents were performed along the DRN, for a total of 4–8 cells recorded per animal. Recordings were performed for a maximal duration of 4 h post-injection.

RESULTS

Sort1$^{-/-}$ Mice Behavior in Depression and Anxiety Tests

In the aim to confirm the role of sortilin on the TREK-1 functions in depression, we first investigated the behavior of *Sort1*$^{-/-}$ mice in a series of behavioral tests related to depression and anxiety.

Depression Tests

The FST performed directly on both WT and *Sort1*$^{-/-}$ mouse groups indicated that *Sort1*$^{-/-}$ mice presented a significant lower immobility time (100.3 ± 13.5 s) than WT mice (151.4 ± 7.8 s, $p = 0.0041$) (**Figure 1A**). FST was validated on WT mice by the use of a novel potential AD spadin validated at least in rodents (Mazella et al., 2010) (10 μg/kg) which after i.p. injection decreased the immobility time from 162.9 ± 12 s for vehicle injected to 104.4 ± 12.5 s ($p = 0.0045$) (**Figure 1B**). We also confirmed the effect of genotype since vehicle injected *Sort1*$^{-/-}$ mice presented a significant lower immobility time (81.6 ± 10.1 s) than WT vehicle injected (162.9 ± 12 s, $p < 0.001$) [two-way ANOVA, $F(3,39) = 10.69$, $p < 0.001$] (**Figure 1B**). Interestingly, injection of spadin had no effect on *Sort1*$^{-/-}$ mice (86.1 ± 11.6 s, $p = 0.992$) (**Figure 1B**). This result prompted us to perform two other tests, the TST and the NSF test. The TST confirmed that *Sort1*$^{-/-}$ mice had an immobility time (65.9 ± 11.2 s) significantly reduced when compared to WT mice (133.2 ± 14.4 s, $p = 0.0013$) (**Figure 1C**). Finally, in the NSF test, the latency time measured for WT mice (231.4 ± 29.2 s) was also significantly decreased in *Sort1*$^{-/-}$ mice (158.5 ± 19.1 s, $p = 0.043$) (**Figure 1D**).

Anxiety Tests

In the light dark test, the time spent in the light zone for WT mice was 294.9 ± 14.9 s, time significantly higher than that of *Sort1*$^{-/-}$ mice (156.9 ± 15.1 s, $p < 0.001$) (**Figure 2A**). Therefore, we tested the two groups in the elevated-plus maze test by measuring the

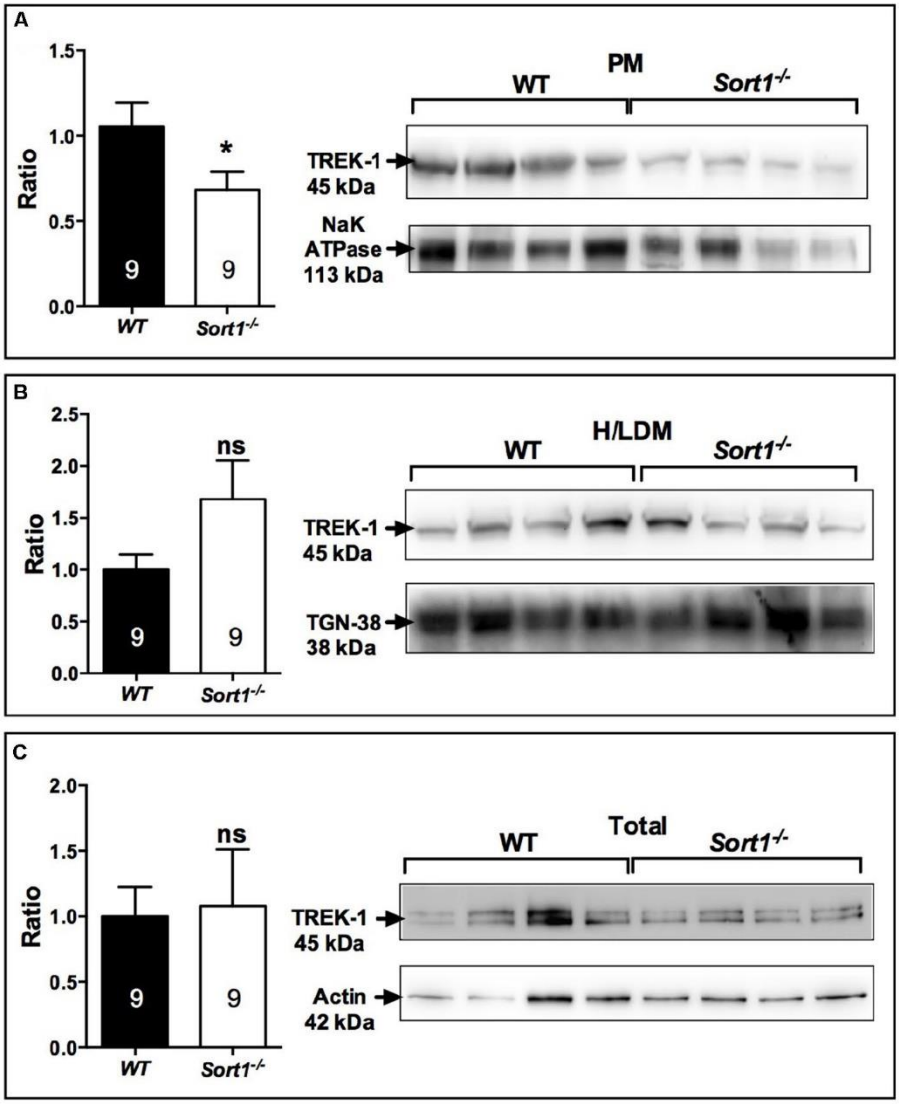

FIGURE 3 | Sub-cellular location of the TREK-1 channel protein in the brain of *Sort1*$^{-/-}$ and WT mice. **(A)** The TREK-1 expression was decreased by 36% (histogram, Left) in the plasma membrane (PM) prepared from *Sort1*$^{-/-}$ mouse brain when compared to PM prepared from WT mouse brain as visualized by Western blots (Right). **(B)** The expression of TREK-1 channels remained unchanged in high and low density vesicles (H/LDM) prepared from brains of *Sort1*$^{-/-}$ and WT mice, as well as in total brain extracts **(C)**. The sub-cellular compartments were identified by specific markers: NaKATPase for plasma membranes **(A)**, TGN38 for H/LDM **(B),** and actin for total brain extracts **(C)**. $^{*}p < 0.05$, ns, non-significant.

ratio of the time and the number of entries in the open arm. The time ratio in the open arm of WT mice (0.239 ± 0.031) was significantly reduced in *Sort1*$^{-/-}$ mice (0.148 ± 0.023, $p = 0.0082$) (**Figure 2B**). In the same way the number of entries ratio of WT mice (0.322 ± 0.021) was decreased in *Sort1*$^{-/-}$ mice (0.194 ± 0.022, $p = 0.0003$) (**Figure 2C**). Finally, we tested the ability of WT and *Sort1*$^{-/-}$ mice to bury glass marbles, a test able to detect anxiety and obsessive compulsive disorders related phenotypes (Deacon, 2006). **Figures 2D,E** showed that WT mice were able to bury 72.7 ± 2.9% of marbles whereas *Sort1*$^{-/-}$ mice buried 85.5 ± 7.3% ($p = 0.0131$) of marbles suggesting again an anxiety-like behavior of *Sort1*$^{-/-}$ mice as previously observed (Ruan et al., 2016). The serum concentration of corticosterone in basal conditions remained unchanged between WT and *Sort1*$^{-/-}$ mice (**Figure 2F**, $p = 0.642$) indicating that the anxiety-like behavior of *Sort1*$^{-/-}$ mice was not the consequence of the hormone increase.

Depression Resistant Phenotype of *Sort1*$^{-/-}$ Mice and Modification of TREK-1 Membrane Expression and Function

The decrease of depressive-like behavior of *Sort1*$^{-/-}$ mice may suggest some dysfunctions of the TREK-1 channel for which its blockade or its deletion results in a depression-resistant

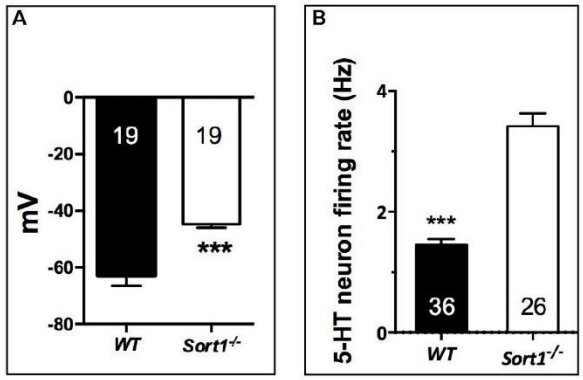

FIGURE 4 | Neuronal activity in *Sort1*$^{-/-}$ mice. **(A)** Membrane potential mean values obtained on primary cortical neurons prepared from *Sort1*$^{-/-}$ and WT mice showed an important depolarization in *Sort1*$^{-/-}$ neurons when compared with WT neurons (ΔmV = 18.21 mV). **(B)** Dorsal Raphe Nucleus 5-HT neuronal firing activity recorded from WT and *Sort1*$^{-/-}$ mice. ***$p < 0.001$.

phenotype. We first investigated the subcellular location of TREK-1 performed on sub-cellular fractionation from WT and *Sort1*$^{-/-}$ mouse brains. Surprisingly, the amount of TREK-1 channels present at the PM was significantly decreased by 36% in *Sort1*$^{-/-}$ mice ($p = 0.0376$) when compared to WT mice (**Figure 3A**). The loss of TREK-1 at the PM appeared to be compensated by an increase of the protein at the level of high and low density vesicles (H/LDM) although not significant (**Figure 3B**, $p = 0.159$). The total amount of TREK-1 was not modified between WT and *Sort1*$^{-/-}$ mice (**Figure 3C**, $p = 0.776$). The loss of the TREK-1 channels at the cell surface without modification of total TREK-1 expression is in agreement with the role of sortilin in the channel cell sorting as already observed (Mazella et al., 2010).

To determine the consequence of the TREK-1 expression loss at the PM, we performed electrophysiological experiments on neurons prepared from WT and *Sort1*$^{-/-}$ mice. The membrane potential measured on neurons from *Sort1*$^{-/-}$ mice was 44.7 ± 1.3 mV consisting to a significant increase of membrane potential of 18.21 mV ($p = 0.0003$) when compared to neurons from WT mice (62.9 ± 3.6 mV) (**Figure 4A**). This result indicated that the decrease of TREK-1 channels at the cell surface of *Sort1*$^{-/-}$ neurons leads to an increase of membrane potential very similar to that obtained with the channel blocker spadin on WT neurons (Devader et al., 2015).

Previous studies have shown that the blockade (Mazella et al., 2010) or the TREK-1 deletion (Heurteaux et al., 2006) enhances the midbrain 5-HT neuron firing rate, a key parameter predictive of AD efficacy. Therefore, we performed unitary extracellular recordings of 5-HT neurons in the DRN in anesthetized animals. The basal firing activities were recorded in both WT and *Sort1*$^{-/-}$ mice by successive tracks along the DRN. 5-HT neurons found in WT mice discharged within a normal frequency range (1.5–2 Hz) with a twofold lower average than in *Sort1*$^{-/-}$ mice (1.46 ± 0.09 Hz versus 3.42 ± 0.21 Hz, $p < 0.001$, $t = 9.21$, $df = 60$) (**Figure 4B**).

It is established that chronic AD treatments, including fluoxetine but also the fast-acting AD spadin induce neurogenesis in the hippocampus of rodents visualized by an increase of progenitor cells that incorporate BrdU. WT mice treated with spadin (100 μg per kg body weight, ip) for 4 days showed a significant increase in the number of hippocampal BrdU-positive cells compared with WT mice treated with vehicle [1919 ± 134 cells/hippocampus vs. 1218 ± 105 cells/hippocampus, respectively, two-way ANOVA, $F(3,12) = 31.36$, $p < 0.001$] (**Figure 5C**). In *Sort1*$^{-/-}$ mice, although the number of BrdU-positive cells was slightly lower in basal conditions ($p = 0.113$), spadin remained efficient with a lower but significant increase of hippocampal newborn cells from 927 ± 83 in WT to 1306 ± 37 in *Sort1*$^{-/-}$ hippocampus, respectively ($p = 0.0331$) (**Figure 5**).

Constitutive Activation of BDNF Content in *Sort1*$^{-/-}$ Mice

Brain derived neurotrophic factor displays a potential role as a marker of treatment response in patients with major depressive disorder although its effects on mood variations remain unclear. The release of BDNF from the neuronal regulatory pathway has been shown to be dependent on the presence of sortilin (Chen et al., 2005). For these reasons and because *Sort1*$^{-/-}$ mice displayed a depressive resistant phenotype, we evaluated the expression profiles of BDNF and its precursor proBDNF in the brain of WT and *Sort1*$^{-/-}$ mice. Western blot analyses of BDNF content from WT or *Sort1*$^{-/-}$ mouse brains clearly demonstrated that the neurotrophin amount was strongly increased in *Sort1*$^{-/-}$ mice versus WT ($p = 0.0005$) (**Figure 6A**). By contrast, no change in amount of proBDNF was observed (**Figure 6B**, $p = 0.441$). The BDNF increase prompted us to examine the expression of the active phosphorylated form of the BDNF receptor TrkB. The p-TrkB expression was significantly enhanced in *Sort1*$^{-/-}$ ($p = 0.0023$) mice when compared with WT mouse brain (**Figure 6C**).

To determine which of BDNF secretion pathway was affected in *Sort1*$^{-/-}$ mice we examined both the expression of furin, responsible for the intracellular maturation of proBDNF to the constitutive secretion pathway, and the expression of the complex plasmin/tPA, responsible for the extracellular maturation of the regulated proBDNF secretion (Lu et al., 2005). Interestingly, in *Sort1*$^{-/-}$ mice, the brain expression of furin was strongly enhanced ($p = 0.0014$) (**Figure 7A**) whereas the expression of tPA, the plasmin activator, was significantly decreased in *Sort1*$^{-/-}$ mice ($p = 0.0385$) (**Figure 7B**). Plasmin expression was not modified ($p = 0.56$) (**Figure 7C**).

The increase in the expression of BDNF and its activated receptor TrkB observed in *Sort1*$^{-/-}$ mice could suggest a constitutive activity of the BDNF signaling system.

DISCUSSION

The present work shows for the first time that the cellular localization and function of the TREK-1 channel were altered in mice lacking sortilin. The TREK-1 expression decrease

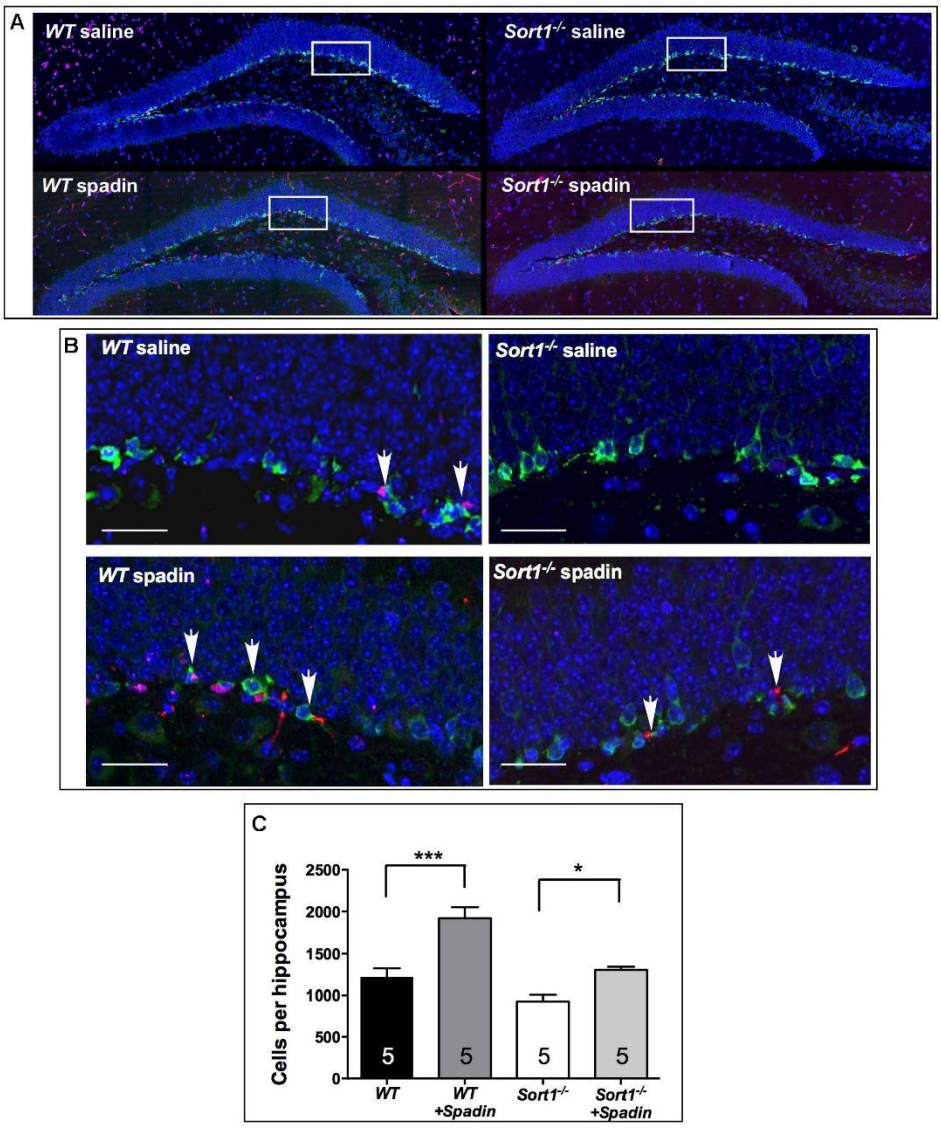

FIGURE 5 | Neurogenesis in *Sort1*$^{-/-}$ mice. **(A)** BrdU staining of dentate gyrus slices from WT and *Sort1*$^{-/-}$ mice treated with saline or spadin for 4 days. **(B)** Double labeling of BrdU-labeled neurons with DCX (neuronal precursor marker), showing a colocalization in magnificated regions, bar: 50 μm. **(C)** 4 Days spadin treatment increased the number of BrdU cells in hippocampus from WT and *Sort1*$^{-/-}$ mice ($n = 5$ per genotype), expressed as mean ± SEM. ***$p < 0.001$ versus vehicle injected WT mice and *$p < 0.05$ versus vehicle-injected *Sort1*$^{-/-}$ mice (vehicle-or-spadin-injected, Tukey's multiple comparison test).

within the brain PM of *Sort1*$^{-/-}$ mice compared to WT mice (**Figures 3A–C**) highly suggests a crucial role of sortilin in the correct sorting of the TREK-1 channel. Further quantification of immunocytochemical labeling of TREK-1 could improve demonstration of its decreased PM expression but specific TREK-1 antibodies are not yet available for such studies. The involvement of sortilin in the TREK-1 trafficking has previously been documented in a heterologous expression system by cotransfection of the two proteins (Mazella et al., 2010). TREK-1 is not the only membrane protein that is regulated by an interaction with sortilin. In particular, sortilin displays important action in the function of several receptors including the proNGF receptor p75NTR (Nykjaer et al., 2004), the BDNF receptor TrkB (Yang et al., 2011), the neurotensin receptor NTSR1 (Martin et al., 2002), and NTSR2 (Beraud-Dufour et al., 2009). In the present work, the absence of sortilin allowed us to definitively determine that either the TREK-1 dysfunction by alteration of its sorting or its inhibition by spadin leads to a common result: the resistance to depression behavior. This phenotype is confirmed in the three different behavioral tests performed in *Sort1*$^{-/-}$ mice (**Figure 1**). Taken together, these results indicated that *Sort1*$^{-/-}$ mice appear to display a depression-resistant behavior resembling that of *kcnk2*$^{-/-}$ mice (Heurteaux et al., 2006). Indeed, this phenotype was comparable to that of *Kcnk2*$^{-/-}$ mice (lacking TREK-1) which behaved as wild-type mice treated with classical ADs. However and paradoxically, *Sort1*$^{-/-}$ mice

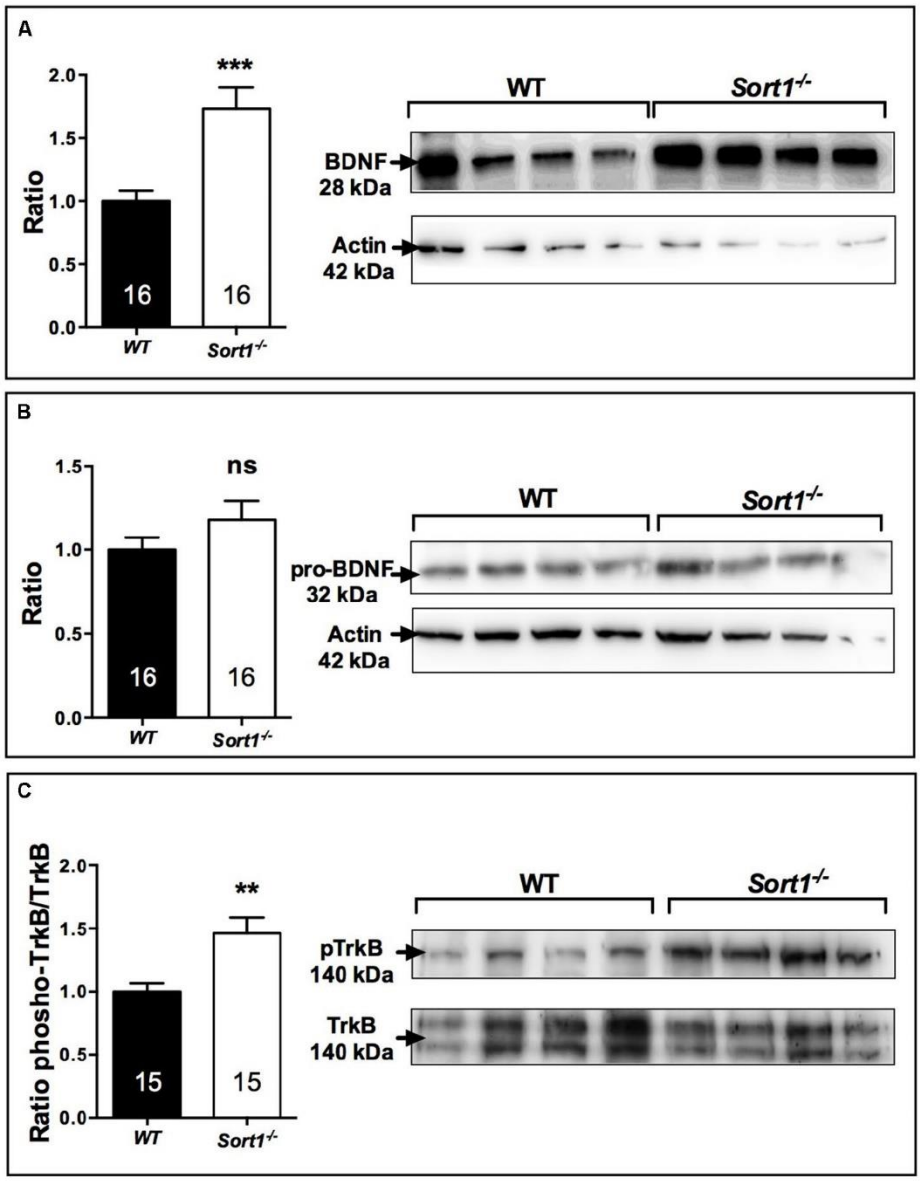

FIGURE 6 | Effect of deletion of *Sort1*$^{-/-}$ gene on BDNF system. Western blot analyses and their corresponding histogram quantification of the expression of proteins involved in the BDNF system in brain extracts from WT and *Sort1*$^{-/-}$ mice. **(A)** BDNF, **(B)** proBDNF, and **(C)** phospho-TrkB. $^{**}p < 0.01$, $^{***}p < 0.001$, ns, non-significant.

displayed an anxiety-like behavior in several anxiety-related tests including the light dark and the marbles burying tests (**Figure 2**). This latter observation that appears not to be associated with an elevated level of serum corticosterone, is in agreement with a recent study relating that *Sort1*$^{-/-}$ mice displayed elevated anxiety-like behavior and that chronically stressed wild-type mice showed an increase in the sortilin expression in neocortex and hippocampus leading to an increased depression-like behavior (Ruan et al., 2016). Since the increase of sortilin expression is associated with depression, our results describing a resistance to depression in *Sort1*$^{-/-}$ mice could be the consequence of the absence of sortilin.

The neuronal consequences resulting from the decreased cell surface TREK-1 expression led to several observations: (i) the membrane potential measured on *Sort1*$^{-/-}$ neurons was strongly increased when compared to WT neurons (**Figure 4A**), and (ii) the firing rate activity of neurons from the DRN was twofold increased indicating an accelerated efficacy of the DRN neurotransmission which could be attributed to 5-HT neurotransmission (**Figure 4B**) although further additional pharmacological and microdialysis approaches have to be performed to definitively identify 5-HT neurotransmission. Both observations were very similar to those obtained with the blocking of TREK-1 activity

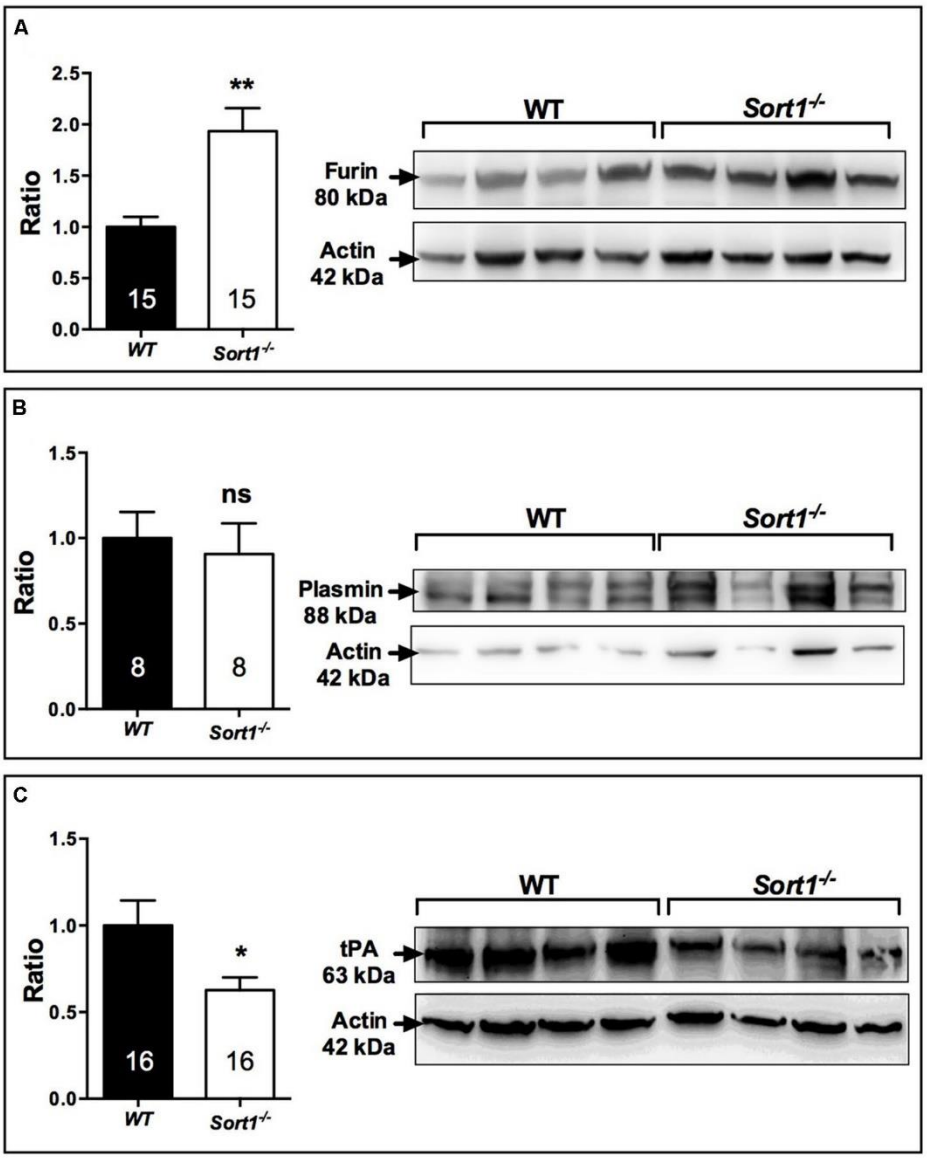

FIGURE 7 | Effect of deletion of *Sort1*$^{-/-}$ gene on BDNF releasing pathways. Western blot analyses and their corresponding histogram quantification of the expression of proteins involved in the BDNF releasing pathways in brain extracts from WT and *Sort1*$^{-/-}$ mice. **(A)** Furin, **(B)** Plasmin, and **(C)** tPA. Histograms represented ratio of mean ± SEM of protein quantification from indicated number of brain samples. Mann–Whitney test, $^{*}p < 0.05$; $^{**}p < 0.01$, ns, non-significant.

by spadin (Mazella et al., 2010; Devader et al., 2015) and by fluoxetine or when kcnk2 gene was deleted in TREK-1 null mice (Heurteaux et al., 2006). These properties are in good agreement with the observation that pharmacological and electroconvulsive AD treatments enhance activation of hippocampal post-synaptic 5-HT_{1A} receptors (Haddjeri et al., 1998).

While the number of hippocampal progenitor cells remained unchanged between *Sort1*$^{-/-}$ and WT mice, surprisingly, both strains responded, similarly, to a 4 days spadin treatment with a significant increase in the number of BrdU-positive cells. This result suggests that (1) despite the lower level of TREK-1 membrane expression measured in *Sort1*$^{-/-}$ mice, the remaining functional channels are sufficient to trigger neurogenesis under spadin exposure (note that the response to spadin was quite lower in *Sort1*$^{-/-}$ mice) or (2) TREK-1 is not the only membrane protein responsible for the response to the peptide. In neurogenesis experiments *Sort1*$^{-/-}$ mice were still able to respond to spadin (**Figure 5C**). Similar observations were obtained from *kcnk2*$^{-/-}$ mice in which basal hippocampal neurogenesis was identical to that measured from WT mice but *kcnk2*$^{-/-}$ mice remained able to respond to fluoxetine (Heurteaux et al., 2006). In *Sort1*$^{-/-}$ mice, spadin was unable to display a significant behavioral effect in FST but was able to increase neurogenesis. This can be explained by methodological differences between the two types of experiments, for FST,

spadin was injected 30 min before the test whereas neurogenesis quantification was performed after a spadin treatment for 4 days. This could correspond to the difference of effects between an acute effect (FST) and a semi-chronic effect (neurogenesis) for spadin. The other possible interpretation could be that the signaling pathways involved in neurogenesis are partly distinct in *Sort1*$^{-/-}$ and *kcnk2*$^{-/-}$ mice.

Finally, we observed that the level of brain BDNF, as well as its activated receptor TrkB, was significantly increased in *Sort1*$^{-/-}$ mice, whereas the level of its precursor form proBDNF remained unchanged (**Figures 6A–C**). This finding can be explained by the brain over-expression in *Sort1*$^{-/-}$ mice of the convertase furin involved in the regulated pathway of BDNF secretion (**Figure 6A**). Concomitantly, the plasmin and tPA expression involved in the constitutive secretion pathway, appeared slightly decreased (**Figures 6B,C**). The increase in both BDNF secretion and expression has been already observed in *Sort1*$^{-/-}$ neurons (Chen et al., 2005) that have been prepared slightly differently than those used in this study (Devader et al., 2016). The elevated levels of BDNF and of its activated receptor TrkB in the *Sort1*$^{-/-}$ brains could be responsible for the antidepressive-like behavior although we cannot compare data from neurogenesis measured in the hippocampus with the level of BDNF measured from the whole brain.

The limitations of this study concern first the fact that only male were used in this work. Further experiments with females as well as more detailed characterization of signaling pathways involved in the observed effects will be necessary.

CONCLUSION

In conclusion, data presented in this work could explain the molecular and physiological mechanisms that are responsible for the decrease of depressive-like behavior observed when the expression of TREK-1 was decreased or totally absent.

AUTHOR CONTRIBUTIONS

SM, CD, MP, and JM performed the experiments. MB, CH, and JM conceived and designed the experiments, contributed reagents, materials, and analysis tools, and wrote the paper.

FUNDING

This work was supported by the Centre National de la Recherche Scientifique and the Agence Nationale de la Recherche (ANR-13-SAMA-0001 and -0002 and ANR-13-RPIB-0001 and -0002). We also thank the French Government for the "Investments for the Future" LABEX ICST # ANR-11 LABX 0015. This work constitutes a chapter in the thesis of SM (Moreno, 2017).

ACKNOWLEDGMENTS

We thank Carlos Morales (McGill University, Montreal, QC, Canada) for providing *Sort1*$^{-/-}$ mice. We also thank E-Phy-Science for the 5-HT firing rate experiments.

REFERENCES

Beraud-Dufour, S., Coppola, T., Massa, F., and Mazella, J. (2009). Neurotensin receptor-2 and -3 are crucial for the anti-apoptotic effect of neurotensin on pancreatic beta-TC3 cells. *Int. J. Biochem. Cell Biol.* 41, 2398–2402. doi: 10.1016/j.biocel.2009.04.002

Buttenschon, H. N., Demontis, D., Kaas, M., Elfving, B., Molgaard, S., Gustafsen, C., et al. (2015). Increased serum levels of sortilin are associated with depression and correlated with BDNF and VEGF. *Transl. Psychiatry* 5:e677. doi: 10.1038/tp.2015.167

Buttenschon, H. N., Nielsen, M., Glerup, S., and Mors, O. (2017). Investigation of serum levels of sortilin in response to antidepressant treatment. *Acta Neuropsychiatr.* 30, 111–116. doi: 10.1017/neu.2017.13

Chen, Z. Y., Ieraci, A., Teng, H., Dall, H., Meng, C. X., Herrera, D. G., et al. (2005). Sortilin controls intracellular sorting of brain-derived neurotrophic factor to the regulated secretory pathway. *J. Neurosci.* 25, 6156–6166. doi: 10.1523/JNEUROSCI.1017-05.2005

Clancy, B. M., and Czech, M. P. (1990). Hexose transport stimulation and membrane redistribution of glucose transporter isoforms in response to cholera toxin, dibutyryl cyclic AMP, and insulin in 3T3-L1 adipocytes. *J. Biol. Chem.* 265, 12434–12443.

Crawley, J. N. (1999). Behavioral phenotyping of transgenic and knockout mice: experimental design and evaluation of general health, sensory functions, motor abilities, and specific behavioral tests. *Brain Res.* 835, 18–26. doi: 10.1016/S0006-8993(98)01258-X

Cryan, J. F., Mombereau, C., and Vassout, A. (2005). The tail suspension test as a model for assessing antidepressant activity: review of pharmacological and genetic studies in mice. *Neurosci. Biobehav. Rev.* 29, 571–625. doi: 10.1016/j.neubiorev.2005.03.009

Curtis, M. J., Bond, R. A., Spina, D., Ahluwalia, A., Alexander, S. P., Giembycz, M. A., et al. (2015). Experimental design and analysis and their reporting: new guidance for publication in BJP. *Br. J. Pharmacol.* 172, 3461–3471. doi: 10.1111/bph.12856

Deacon, R. M. (2006). Digging and marble burying in mice: simple methods for in vivo identification of biological impacts. *Nat. Protoc.* 1, 122–124. doi: 10.1038/nprot.2006.20

Devader, C., Khayachi, A., Veyssiere, J., Moha Ou Maati, H., Roulot, M., Moreno, S., et al. (2015). In vitro and in vivo regulation of synaptogenesis by the novel antidepressant spadin. *Br. J. Pharmacol.* 172, 2604–2617. doi: 10.1111/bph.13083

Devader, C., Moreno, S., Roulot, M., Deval, E., Dix, T., Morales, C. R., et al. (2016). Increased brain neurotensin and NTSR2 lead to weak nociception in NTSR3/Sortilin knockout mice. *Front. Neurosci.* 10:542. doi: 10.3389/fnins.2016.00542

Dube, J. B., Johansen, C. T., and Hegele, R. A. (2011). Sortilin: an unusual suspect in cholesterol metabolism: from GWAS identification to in vivo biochemical analyses, sortilin has been identified as a novel mediator of human lipoprotein metabolism. *Bioessays* 33, 430–437. doi: 10.1002/bies.201100003

Fabbri, C., Hosak, L., Mossner, R., Giegling, I., Mandelli, L., Bellivier, F., et al. (2017). Consensus paper of the WFSBP task force on genetics: genetics, epigenetics and gene expression markers of major depressive disorder and antidepressant response. *World J. Biol. Psychiatry* 18, 5–28. doi: 10.1080/15622975.2016.1208843

Gross, C., Zhuang, X., Stark, K., Ramboz, S., Oosting, R., Kirby, L., et al. (2002). Serotonin1A receptor acts during development to establish normal anxiety-like behaviour in the adult. *Nature* 416, 396–400. doi: 10.1038/416396a

Haddjeri, N., Blier, P., and de Montigny, C. (1998). Long-term antidepressant treatments result in a tonic activation of forebrain 5-HT1A receptors.

J. Neurosci. 18, 10150–10156. doi: 10.1523/JNEUROSCI.18-23-10150.1998

Hamill, O. P., Marty, A., Neher, E., Sakmann, B., and Sigworth, F. J. (1981). Improved patch-clamp techniques for high-resolution current recording from cells and cell-free membrane patches. *Pflugers Arch.* 391, 85–100. doi: 10.1007/BF00656997

Heurteaux, C., Lucas, G., Guy, N., El Yacoubi, M., Thummler, S., Peng, X. D., et al. (2006). Deletion of the background potassium channel TREK-1 results in a depression-resistant phenotype. *Nat. Neurosci.* 9, 1134–1141. doi: 10.1038/nn1749

Hu, F., Padukkavidana, T., Vaegter, C. B., Brady, O. A., Zheng, Y., Mackenzie, I. R., et al. (2010). Sortilin-mediated endocytosis determines levels of the frontotemporal dementia protein, progranulin. *Neuron* 68, 654–667. doi: 10.1016/j.neuron.2010.09.034

Kandror, K. V., and Pilch, P. F. (2011). The sugar is sIRVed: sorting Glut4 and its fellow travelers. *Traffic* 12, 665–671. doi: 10.1111/j.1600-0854.2011.01175.x

Kilkenny, C., Browne, W., Cuthill, I. C., Emerson, M., Altman, D. G., and National Centre for the Replacement Refinement and Reduction of Amimals in Research (2011). Animal research: reporting in vivo experiments–the ARRIVE guidelines. *J. Cereb. Blood Flow Metab.* 31, 991–993. doi: 10.1038/jcbfm.2010.220

Kjolby, M., Andersen, O. M., Breiderhoff, T., Fjorback, A. W., Pedersen, K. M., Madsen, P., et al. (2010). Sort1, encoded by the cardiovascular risk locus 1p13.3, is a regulator of hepatic lipoprotein export. *Cell Metab.* 12, 213–223. doi: 10.1016/j.cmet.2010.08.006

Lefrancois, S., Zeng, J., Hassan, A. J., Canuel, M., and Morales, C. R. (2003). The lysosomal trafficking of sphingolipid activator proteins (SAPs) is mediated by sortilin. *EMBO J.* 22, 6430–6437. doi: 10.1093/emboj/cdg629

Lu, B., Pang, P. T., and Woo, N. H. (2005). The yin and yang of neurotrophin action. *Nat. Rev. Neurosci.* 6, 603–614. doi: 10.1038/nrn1726

Martin, S., Navarro, V., Vincent, J. P., and Mazella, J. (2002). Neurotensin receptor-1 and -3 complex modulates the cellular signaling of neurotensin in the HT29 cell line. *Gastroenterology* 123, 1135–1143. doi: 10.1053/gast.2002.36000

Moreno, S. (2017). *Neurotensin Receptor 3/Sortilin in Depressive State Regulation.* Ph.D. thesis. Available at: https://www.theses.fr/2017AZUR4136

Mazella, J., Petrault, O., Lucas, G., Deval, E., Beraud-Dufour, S., Gandin, C., et al. (2010). Spadin, a sortilin-derived peptide, targeting rodent TREK-1 channels: a new concept in the antidepressant drug design. *PLoS Biol.* 8:e1000355. doi: 10.1371/journal.pbio.1000355

Mazella, J., Zsurger, N., Navarro, V., Chabry, J., Kaghad, M., Caput, D., et al. (1998). The 100-kDa neurotensin receptor is gp95/sortilin, a non-G-protein-coupled receptor. *J. Biol. Chem.* 273, 26273–26276. doi: 10.1074/jbc.273.41.26273

McGrath, J. C., and Lilley, E. (2015). Implementing guidelines on reporting research using animals (ARRIVE etc.): new requirements for publication in BJP. *Br. J. Pharmacol.* 172, 3189–3193. doi: 10.1111/bph.12955

Musunuru, K., Strong, A., Frank-Kamenetsky, M., Lee, N. E., Ahfeldt, T., Sachs, K. V., et al. (2010). From noncoding variant to phenotype via SORT1 at the 1p13 cholesterol locus. *Nature* 466, 714–719. doi: 10.1038/nature09266

Navarro, V., Vincent, J. P., and Mazella, J. (2002). Shedding of the luminal domain of the neurotensin receptor-3/sortilin in the HT29 cell line. *Biochem. Biophys. Res. Commun.* 298, 760–764. doi: 10.1016/S0006-291X(02)02564-0

Nykjaer, A., Lee, R., Teng, K. K., Jansen, P., Madsen, P., Nielsen, M. S., et al. (2004). Sortilin is essential for proNGF-induced neuronal cell death. *Nature* 427, 843–848. doi: 10.1038/nature02319

Porsolt, R. D., Le Pichon, M., and Jalfre, M. (1977). Depression: a new animal model sensitive to antidepressant treatments. *Nature* 266, 730–732. doi: 10.1038/266730a0

Ruan, C. S., Yang, C. R., Li, J. Y., Luo, H. Y., Bobrovskaya, L., and Zhou, X. F. (2016). Mice with Sort1 deficiency display normal cognition but elevated anxiety-like behavior. *Exp. Neurol.* 281, 99–108. doi: 10.1016/j.expneurol.2016.04.015

Samsom, J. N., and Wong, A. H. (2015). Schizophrenia and Depression Co-Morbidity: what We have Learned from Animal Models. *Front. Psychiatry* 6:13. doi: 10.3389/fpsyt.2015.00013

Santarelli, L., Saxe, M., Gross, C., Surget, A., Battaglia, F., Dulawa, S., et al. (2003). Requirement of hippocampal neurogenesis for the behavioral effects of antidepressants. *Science* 301, 805–809. doi: 10.1126/science.1083328

Schneider, C. A., Rasband, W. S., and Eliceiri, K. W. (2012). NIH Image to ImageJ: 25 years of image analysis. *Nat. Methods* 9, 671–675. doi: 10.1038/nmeth.2089

Tall, A. R., and Ai, D. (2011). Sorting out sortilin. *Circ. Res.* 108, 158–160. doi: 10.1161/RES.0b013e31820d7daa

Welch, J. M., Lu, J., Rodriguiz, R. M., Trotta, N. C., Peca, J., Ding, J. D., et al. (2007). Cortico-striatal synaptic defects and OCD-like behaviours in Sapap3-mutant mice. *Nature* 448, 894–900. doi: 10.1038/nature06104

Yang, M., Lim, Y., Li, X., Zhong, J. H., and Zhou, X. F. (2011). Precursor of brain-derived neurotrophic factor (proBDNF) forms a complex with Huntingtin-associated protein-1 (HAP1) and sortilin that modulates proBDNF trafficking, degradation, and processing. *J. Biol. Chem.* 286, 16272–16284. doi: 10.1074/jbc.M110.195347

Zeng, J., Racicott, J., and Morales, C. R. (2009). The inactivation of the sortilin gene leads to a partial disruption of prosaposin trafficking to the lysosomes. *Exp. Cell Res.* 315, 3112–3124. doi: 10.1016/j.yexcr.2009.08.016

Conflict of Interest Statement: The authors declare that the research was conducted in the absence of any commercial or financial relationships that could be construed as a potential conflict of interest.

C- Articles 5 et 6 : “Differential neuronal plasticity in mouse hippocampus associated with various periods of enriched environment during postnatal development” & “Neurogenesis-independent antidepressant-like effects of enriched environment is dependent on adiponectin”

Comme nous l’avons mentionné plus haut, les traitements face à la dépression sont encore trop peu efficaces et souvent mal supportés. Si la plupart des recherches sont aujourd’hui menées dans le but de trouver de nouvelles molécules plus efficaces et moins dangereuses, d’autres se sont axées sur la thérapie comportementale. En effet, l’entourage du patient dépressif est également essentiel pour accroître ses chances de récupérer. Afin de modéliser cette thérapie comportementale chez l’animal, un modèle d'environnement enrichi (EE) a été mis au point. Ce dernier se caractérise par de plus importantes possibilités d'exploration, d'activité cognitive, d'interaction sociale et d'exercice physique. Des stimuli qui, dans le cerveau des rongeurs, provoquent des changements profonds aux niveaux moléculaire, anatomique et comportemental. Par exemple, il a été démontré que l'EE régule positivement le remodelage des circuits neuronaux et la consolidation de la mémoire, ou encore augmente la neurogenèse. Cependant, les mécanismes fins par lesquels l'environnement façonne le cerveau à différents stades du développement postnatal et la durée nécessaire pour induire de tels changements sont encore soumis à controverse. Dans nos études, les conditions EE consistaient à utiliser des groupes de souris plus importants, hébergés dans de grandes cages contenant de nombreux équipements favorisant l'activité physique notamment des jouets et du matériel de nidification. Dans le premier projet, les souris sevrées (4 semaines) ont été placées en EE pendant 4, 6 ou 8 semaines et leurs caractéristiques ont été comparées à des souris témoins élevées dans un environnement standard. Pour étudier les effets différentiels de l'EE sur les cerveaux immatures et matures, nous avons également stabulé de jeunes souris adultes (8 semaines) pendant 4 semaines en EE. Nous avons étudié l'influence de l'apparition et de la durée de la stabulationen EE sur la structure et la fonction des neurones de l'hippocampe. Nous avons ainsi observé que L'EE améliore la neurogenèse chez les jeunes souris, mais pas chez les souris adultes et augmente le nombre de contacts synaptiques. L’EE affecte également la potentialisation à long terme (LTP) et l'activité spontanée et miniature des synapses glutamatergiques.

Cette étude fournit donc une vue intégrative du rôle de l'EE pendant le développement postnatal dans divers mécanismes de plasticité de l'hippocampe, notamment la neurogenèse, la morphologie synaptique et les paramètres électrophysiologiques de la connectivité synaptique. Dans le second projet (article 6) nous avons montré que l'EE réduit efficacement l'anxiété et les comportements dépressifs dans un modèle murin de dépression induite par un traitement chronique avec la corticostérone. Les mécanismes qui sous-tendent les effets bénéfiques liés à l'EE demeurent largement inexplorés, cependant nos résultats indiquent que l'adiponectine, une protéine sécrétée par les adipocytes, est l'un des principaux facteurs impliqués. En effet, les souris déficientes en adiponectine (adipo$^{-/-}$) ne bénéficient pas de la totalité des effets anxiolytiques et antidépresseurs de l'EE, comme en témoignent leurs réponses différentielles dans une série de tests comportementaux. Nous avons également constaté qu'à l'inverse, une seule injection intraveineuse d'adiponectine restaure la sensibilité des souris adipo$^{-/-}$ face aux bénéfices comportementaux induits par l'EE. En revanche, l'absence d'adiponectine n'empêche pas la neurogenèse hippocampique induite par l'EE. Ce qui signifie que les propriétés antidépressives de l'adiponectine sont probablement liées à des changements dans la signalisation de l'hypothalamus plutôt qu'à des mécanismes de neurogenèse de l'hippocampe. De plus, l'EE ne modifie pas les taux plasmatiques d'adiponectine. En revanche, il peut favoriser le passage de l'adiponectine du sang vers le liquide céphalorachidien.

Ces résultats permettent de mieux comprendre les effets anxiolytiques et antidépresseurs de l'EE et mettent en évidence l'adiponectine comme médiateur essentiel.

Brain Struct Funct (2015) 220:3435–3448
DOI 10.1007/s00429-014-0865-y

ORIGINAL ARTICLE

Differential neuronal plasticity in mouse hippocampus associated with various periods of enriched environment during postnatal development

Salma Hosseiny · Mariel Pietri · Agnès Petit-Paitel · Hadi Zarif · Catherine Heurteaux · Joëlle Chabry · Alice Guyon

Received: 5 March 2014 / Accepted: 29 July 2014 / Published online: 6 August 2014

Abstract Enriched environment (EE) is characterized by improved conditions for enhanced exploration, cognitive activity, social interaction and physical exercise. It has been shown that EE positively regulates the remodeling of neural circuits, memory consolidation, long-term changes in synaptic strength and neurogenesis. However, the fine mechanisms by which environment shapes the brain at different postnatal developmental stages and the duration required to induce such changes are still a matter of debate. In EE, large groups of mice were housed in bigger cages and were given toys, nesting materials and other equipment that promote physical activity to provide a stimulating environment. Weaned mice were housed in EE for 4, 6 or 8 weeks and compared with matched control mice that were raised in a standard environment. To investigate the differential effects of EE on immature and mature brains, we also housed young adult mice (8 weeks old) for 4 weeks in EE. We studied the influence of onset and duration of EE housing on the structure and function of hippocampal neurons. We found that: (1) EE enhances neurogenesis in juvenile, but not young adult mice; (2) EE increases the number of synaptic contacts at every stage; (3) long-term potentiation (LTP) and spontaneous and miniature activity at the glutamatergic synapses are affected differently by EE depending on its onset and duration. Our study provides an integrative view of the role of EE during postnatal development in various mechanisms of plasticity in the hippocampus including neurogenesis, synaptic morphology and electrophysiological parameters of synaptic connectivity. This work provides an explanation for discrepancies found in the literature about the effects of EE on LTP and emphasizes the importance of environment on hippocampal plasticity.

Keywords Enriched environment · Hippocampus neurogenesis and synaptogenesis · Long-term potentiation · Excitatory postsynaptic currents · Postnatal development

This article is dedicated to the memory of our friend and colleague Nicole Zsürger.

Electronic supplementary material The online version of this article (doi:10.1007/s00429-014-0865-y) contains supplementary material, which is available to authorized users.

S. Hosseiny · M. Pietri · A. Petit-Paitel · H. Zarif · C. Heurteaux · J. Chabry · A. Guyon
Université de Nice Sophia Antipolis, 06103 Nice, France

S. Hosseiny · M. Pietri · A. Petit-Paitel · H. Zarif · C. Heurteaux · J. Chabry · A. Guyon (✉)
Centre National de La Recherche Scientifique (CNRS), Institut de Pharmacologie Moléculaire et Cellulaire, UMR 7275, 660 Route Des Lucioles, 06560 Valbonne, France
e-mail: alice.guyon@ipmc.cnrs.fr

Introduction

The capacity of the brain to respond to environmental input, specifically "enrichment," has become an accepted fact in neuroscience since the 1970s. Environmental enrichment (EE) was introduced as an experimental protocol to investigate the influence of environment on brain and behavior in rodents in 1996 (Bennett et al. 1996) when it was shown that the morphology, chemistry and physiology of the brain can be remarkably altered by modifying the quality and diversity of environmental stimulation. Since then, many studies have shown that EE elicits changes in the brain ranging from the molecular to anatomical and functional levels (Sale et al. 2009).

EE is composed of a combination of complex inanimate and social stimulations. Enriched animals are reared in

large groups and maintained in large environments where a variety of objects (for example, toys, tunnels, nesting material and stairs) are present and frequently changed. An essential component of a typical EE setting is the opportunity to reach high levels of voluntary physical activity on running wheels. Therefore, living in an EE provides animals with improved conditions for enhanced exploration, cognitive activity, social interaction and physical exercise (Sale et al. 2009). Exposure to EE has remarkably beneficial effects in animal models of nervous system disorders, including neurodegenerative diseases, brain injury and targeted mutations that compromise synaptic plasticity and learning (Young et al. 1999; Ilin and Richter-Levin 2009; Nithianantharajah and Hannan 2006; Baroncelli et al. 2010). EE also has been shown to have powerful beneficial effects on a variety of physiological processes. For example, EE enhances learning and memory and reduces the cognitive decline typically associated with aging (Sale et al. 2009).

EE has multiple effects on the hippocampus, a highly adaptive brain structure that plays a major role in learning and constantly reorganizes in response to changing inputs. Indeed, in the dentate gyrus of the hippocampus, exposure to EE increases neurogenesis and reduces apoptotic cell death (Nithianantharajah and Hannan 2006; Kempermann et al. 1997, 2002). EE also enhances hippocampal synaptogenesis, increases the number of dendritic spines and increases the size of synapses in some neuronal populations (Moser et al. 1994; Rampon et al. 2000). EE also modifies hippocampal synaptic plasticity, particularly long-term potentiation and depression (LTP/LTD), two forms of synaptic plasticity characterized by an increase or decrease in synaptic strength driven by neuronal activity that lasts from hours to days. LTP/LTD is widely considered to be one of the major cellular mechanisms that underlie learning and memory (Kandel et al. 2014). Studies on LTP are often carried out in vitro, in slices of the hippocampus, where it is possible to trigger artificial LTP by stimulating an identified group of fibers such as the Schaffer collaterals (which contain only glutamatergic fibers connecting CA3 to CA1 pyramidal neurons) with experimental protocols that induce a depolarization of the postsynaptic neurons (Bliss and Collingridge 1993). The response of the postsynaptic target (recorded either in a single neuron or in field potentials corresponding to an ensemble of neurons) is usually increased following this type of stimulation, a potentiation that can last for hours.

The effects of EE on LTP remain controversial likely due to the wide variety of experimental conditions that have been used in each study (Redolat and Mesa-Gresa 2012). Indeed, EE has been shown to either enhance (Tang and Zou 2002; Artola et al. 2006; Malik and Chattarji 2012), impair or have no effect on LTP at the CA3–CA1 synapse (Foster and Dumas 2001; Eckert et al. 2010; Bouet et al. 2011; Waters et al. 1997). Because LTP induction and expression is age dependent (Foster 2002; Bouet et al. 2011; Leger et al. 2012), we hypothesized that EE might have different consequences on plasticity of these synapses depending on the duration of enrichment and the postnatal developmental stage of the mice. We thus performed an accurate kinetic analysis of the features of hippocampal neurons in standard enrichment (SE)- and EE-reared mice after different periods of housing (i.e., 4, 6, 8 weeks in SE or EE housing conditions).

In this study, we show that the consequences of EE on neurogenesis, neuronal morphology, functional contacts and neuronal plasticity in the hippocampus vary depending on the duration of EE and the age of initial exposure to EE (juvenile or young adult). EE enhances neurogenesis in the hippocampus in juvenile, but not young adult mice, increases the number of synaptic contacts at every stage and modifies synaptic strength differently depending on EE onset and duration. Therefore, although the hippocampus can be shaped by the environment at any age, the mechanisms by which these plasticity processes occur are different in juvenile and young adult mice.

Materials and methods

EE breeding conditions

We set up an EE paradigm in which C57Bl6/J female mice were exposed to EE starting 4 (i.e., at weaning) or 8 weeks after birth for 4, 6 and 8 weeks' period (Fig. 1). Female mice are preferred because males show territorial behavior (appropriation of the running wheels for example), aggression, and fighting due to social hierarchies which result in increased variability of the results. Since the estrus cycle can influence hippocampal physiology, we performed vaginal smears and checked the level of the cycle for each mouse (pre-estrus, estrus, metestrus, diestrus). 12 age- and sex-matched mice were housed in large-sized cages (9,120 cm^2; $L \times l \times h$: 120 × 76 × 21 cm) with nesting material, houses, running wheels, hammocks, scales, plastic toys and tunnels (Fig. 1). Objects were changed twice a week. Control mice (SE) were housed in medium-sized cages (666 cm^2; $L \times l \times h$: 36 × 18.5 × 14 cm) with 5 mice/cage without objects. All mice had access to tap water and standard laboratory chow (diet SAFE A04, 2,900 kcal/kg) ad libitum and were housed on a 12 h light/12 h dark cycle at 22–23 °C with 40–60 % humidity. The animals analyzed for each experiment raised either in SE or EE came from the same cage. Experiments were reproduced several times over a year and data from one experiment to another were not significantly different for a considered

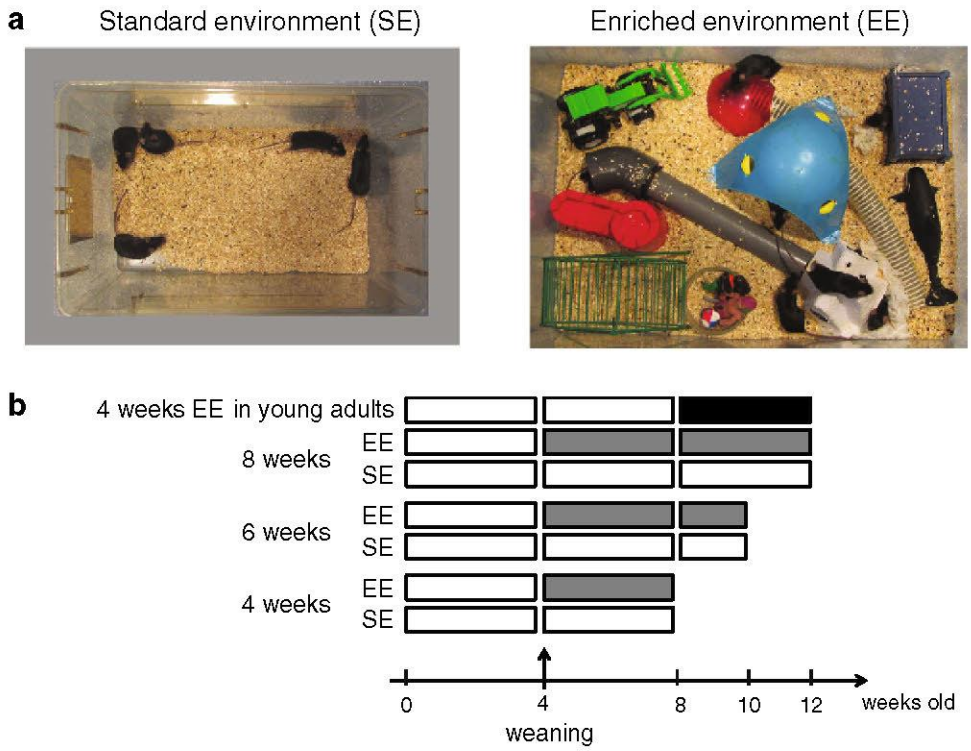

Fig. 1 Enriched environment protocol. **a** Twelve mice raised in an enriched environment (*right*) were placed in large cages (9,120 cm^2; $L \times l \times h$: 120 × 76 × 21 cm) equipped with nesting material, houses, running wheels, hammocks, scales, plastic toys and tunnels. Objects were changed twice a week. In contrast, standard environment consisted of middle-sized cages (666 cm^2; $L \times l \times h$: 36 × 18.5 × 14 cm) with five mice/cage without objects. **b** Different housing durations in SE/EE were used for different ages of the animals. *White rectangles* standard environment, *gray bars* EE in juvenile mice, *black rectangle* EE in young adults

group, thus they were pooled. The authors certify that all animal studies were carried out in accordance with French standard ethical guidelines for laboratory animals (Agreement No. 75–178, 05/16/2000) and the European Communities Council Directive of 24 November 1986 (86/609/EEC). The authors also certify that formal approval to conduct the experiments described has been obtained from the animal subjects review board of their institution and can be provided upon request. The authors further attest that all efforts were made to minimize the number of animals used and their suffering.

Morphological analysis

Hippocampal neurogenesis

We measured hippocampal neurogenesis in EE and control SE mice using intraperitoneal injections of bromodeoxyuridine (BrdU) (50 mg/kg, once a day for 5 consecutive days) followed by immunohistochemistry quantification of BrdU-stained cells in the hippocampus, according to (Heurteaux et al. 2006). Briefly, mice were euthanized with pentobarbital 21 days after the last injection, perfused with HBSS and fixed by 3.2 % PFA through intracardiac perfusion. The brain was rapidly removed and fixed in 3.2 % paraformaldehyde (PFA) for 48 h. 40-μm-thick serial sections of PFA-fixed brains were cut throughout the hippocampus (from bregma 3.3 to 5.3) on a vibratome (Microm). One slice of every five was collected for a total number of eight to proceed to immunohistochemistry staining using a monoclonal mouse anti-BrdU (1/200; BD Biosciences). For BrdU chromogenic immunodetection, sections were incubated for 1 h in biotin-conjugated species-specific secondary antibodies (1/100, Vector Laboratories), followed by a peroxidase–avidin complex solution according to the manufacturer's protocol. The peroxidase activity of immune complexes was visualized with 3,3′-diaminobenzidine (DAB) staining using VectaStain ABC kit (Vector Laboratories). BrdU-labeled cells of granular and subgranular layers were counted in each section at 400× under a light microscope. All BrdU cells in the granular cell layer and subgranular zone were counted in each section ($N = 8$ and 4 mice per group) at 400 and 1,000× under a light microscope (Olympus) by an experimenter blinded to the study code. The total number of BrdU+ cells counted per eight slices was multiplied by 5 to obtain the total number of BrdU+ cells per dentate gyrus.

Morphology of neurons and dendritic spines

Mice were deeply anesthetized with halothane and perfused with 3.2 % paraformaldehyde (PFA). Brain serial sections were cut (200 μm) throughout the entire hippocampus on a vibratome (Microm). The slices were then stored in 0.1 % (wt/vol) NaN_3 in PBS at 4 °C until microinjections of fluorescent dye (Alexa fluor 568) by iontophoresis coupled with

pressure ejection using micropipettes with high tip resistance (15–20 MΩ). The slices were then mounted using Vecta-Shield mounting medium and stored until imaging. High-resolution stacks of images from segments of dendrites of a length of 40 µm were obtained through a 63X/1.4 NA objective of an LSM780 laser-scanning confocal microscope (Carl Zeiss, Le Pecq, France). Detailed morphometric analysis of spines was performed using first ImageJ (Rasband, W.S., ImageJ, US National Institutes of Health, Bethesda, Maryland, USA, http://imagej.nih.gov/ij/, 1997–2012) software to get binary projection images from the stacks recorded. Then, these images were analyzed with NeuronStudio software and spines were classified into thin, mushroom and stubby according to Peters and Kaiserman-Abramof (1970) using the following parameters: the maximum and minimum spine heights were set at <3.5 and 0.5 µm, respectively. Minimum stubby spine was set at >22 voxels. In each group, we used 23 to 46 segments of dendrites from 8 to 15 neurons, 3 to 7 slices and 3 to 7 mice.

Electrophysiology

Acute brain slices

At the end of the housing period, mice were deeply anesthetized with halothane, then decapitated and brains were immediately placed in ice-cold gassed medium (95 % O2/5 % CO2) containing (in mM): 125 NaCl, 2.5 KCl, 1 MgCl2, 0.4 CaCl2, 1.25 NaH2PO4, 26 NaHCO3 and 25 glucose. Coronal slices of hippocampus (350 µM thick) were cut with an HM650V vibratome (Microm, Walldorf, Germany) and placed in a holding chamber at 34 °C for 1 h. Slices were then transferred into a phosphate bicarbonate buffer saline (PBBS) composed of (in mM) of 125 NaCl, 2.5 KCl, 1 $MgCl_2$, 2 CaCl2, 1.25 NaH2P04, 26 NaHC03 and 25 glucose, pH 7.4, when bubbled with 95 % O2/5 % CO2.

LTP protocol

Hippocampal slices were placed under a Nomarski microscope (Zeiss, Germany) equipped with infrared video camera (Axiocam, Zeiss) in a recording chamber superfused at a flow rate of 1/ml/min with oxygenated PBBS. Pictures were taken using a digital camera (Axiocam, Zeiss) connected to image-acquisition software (Axiovision, Zeiss). Recordings were made at room temperature (20–25 °C) using an Axopatch 200B (Axon Instruments, Foster City, CA, USA). At the beginning of each recording, a tungsten bipolar stimulating electrode was positioned to the stratum radiatum for stimulation of the Schaffer collateral projections to CA1, using a stimulator (WPI, New Heaven, Connecticut USA).

Field potentials in the dendritic tree of CA1 neurons were recorded with pipettes (made from borosilicate glass capillary (Hilgenberg, Masfeld, Germany) with resistance of 3–6 MΩ when filled with extracellular solution). The intensity of stimulation was adjusted in each experiment to evoke about 50 % of the maximal field potential amplitude without appreciable population spike contamination. Low-frequency stimulation (0.1 HZ) was applied to the Schaffer collaterals to establish a stable baseline (for 20–30 min) of the excitatory postsynaptic potential (EPSP) slope, after which LTP was induced by high-frequency stimulation (HFS; 100 Hz/1 s), followed by the initial low-frequency stimulation. To analyze the time course of the EPSP slope, the recorded fEPSP were routinely averaged over 1 min ($N = 6$). Successful induction of LTP was obtained when the postHFS EPSP exceeded that seen before HFS and was maintained for at least 40–60 min. Five to six mice per group were used.

Patch-clamp technique

CA1 pyramidal neurons were patch clamped in the whole-cell configuration. This technique allows for recording currents from the whole surface of a single neuron in the living slice while it is still connected with the rest of the neuronal network. Using pipettes (2–8 MΩ) filled with a cesium chloride (CsCl) solution supplemented with *N*-(2,6-dimethylphenylcarbamoylmethy-l)triethylammonium bromide (QX314, a sodium channel blocker to block action potentials) we recorded the glutamatergic excitatory postsynaptic currents (EPSCs) which were pharmacologically isolated using the $GABA_A$ receptor antagonist bicuculline (10 µM) in the bath solution. We recorded both spontaneous (without the sodium channel inhibitor tetrodotoxin TTX) and miniature (in the presence of 2 µM TTX) EPSCs. Three minute recordings were used to determine the properties of the spontaneous events. 4–16 neurons were recorded in two to three mice in each group.

Drugs

APV [(2*R*)-amino-5-phosphonovaleric acid, a *N*-methyl-D-aspartate (NMDA) receptor antagonist] and 6-cyano-7-nitroquinoxaline-2,3-dione (CNQX), a α-amino-3-hydroxy-5-methyl-4-isoxazolepropionic acid receptor (AMPA)/kainate receptor antagonist, QX314, TTX and bicuculline were from Sigma Aldrich, France.

Data analysis

Voltage clamp data were digitized at 0.5 kHz using a Digidata interface coupled to a microcomputer running p-Clamp 9 (Axon Instruments). Currents were digitally

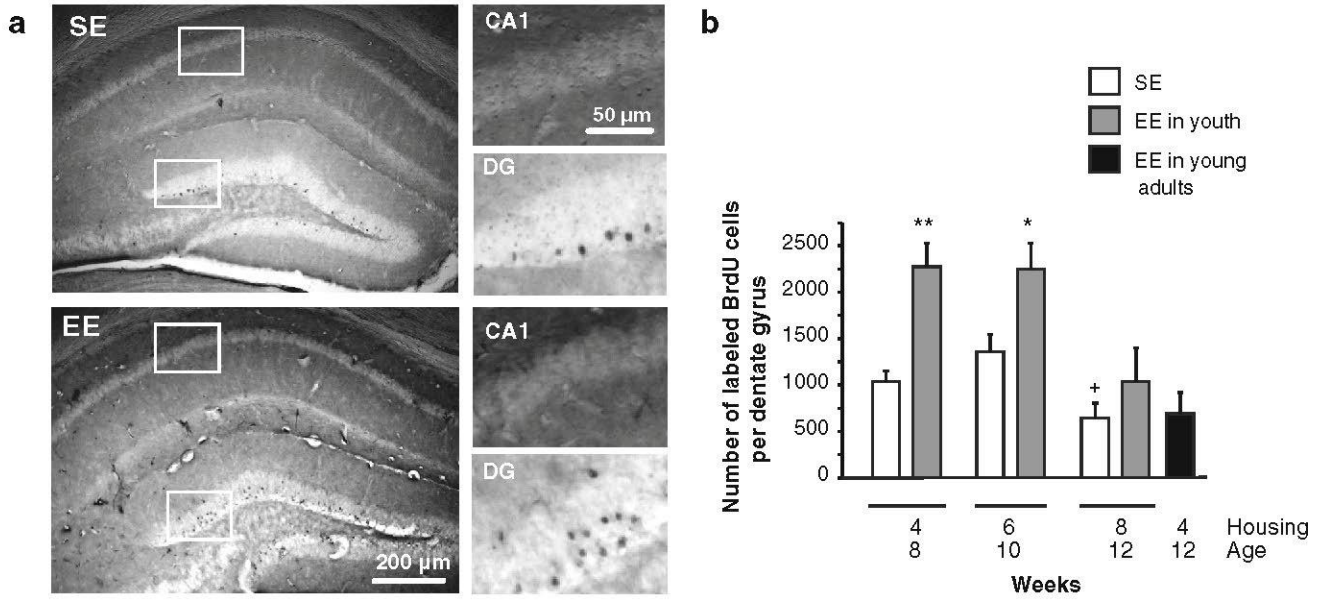

Fig. 2 Neurogenesis in the dentate gyrus (DG) of the hippocampus is increased by EE in juvenile, but not in young adult mice. **a** Examples of representative photomicrographs used for BrdU-labeled nuclei quantification per hippocampal slice from brains obtained from 4 weeks' SE and EE mice. Notice the numerous stained nuclei in the dentate gyrus of mouse raised in EE compared to the mouse raised in SE (see *insets* at higher magnification on the *right*), and the absence of labeled nuclei in the CA1 region of the hippocampus. **b** *Histograms* presenting the mean number of BrdU-positive nuclei (±SEM) counted at the indicated ages and periods of housing in SE or EE. $^{*}p < 0.05$, $^{**}p < 0.01$, comparison of EE vs. matched SE group; $^{+}p < 0.05$, comparison of SE group at 10 weeks vs. 12 weeks. $N = 4$ mice in each group

filtered at 1–3 kHz. Average data are expressed as mean ± SEM, and N = number of neurons that were recorded. Statistical significance between groups was calculated using the Student's t test, ANOVA followed by the Fisher test, or the Kruskal–Wallis followed by the Mann–Whitney test and were considered significant at $^{*}p < 0.05$, $^{**}p < 0.01$ or $p < 0.02$ as mentioned, and $^{***}p < 0.001$ using a statistical software package (SigmaStat 2.03, Jandel Sci). Cumulative histograms were compared by Kolmogorov–Smirnov analysis using Clampfit (Axon Instruments), with an equal number of events for each group.

Results

EE promotes hippocampal neurogenesis in juvenile, but not in young adult mice

Figure 1 illustrates the various protocols used depending on the age and the duration of exposure of mice to SE or EE. We first investigated the effect of EE on neurogenesis in the dentate gyrus of mice using intraperitoneal injections of BrdU at different ages and housing periods of SE and EE. Dentate gyrus granule cells are generated throughout the entire life span and migrate into the molecular and granule cell layers. To investigate the effects on the induction of newborn neurons by EE compared to SE, we measured in both conditions the number of newborn cells that survived 21 days after injection of BrdU, reflecting newly born neurons and neurons undergoing maturation (Fig. 2a).

Our EE housing protocol for 4 and 6 weeks after weaning resulted in a significant increase of neurogenesis in the dentate gyrus (Fig. 2b, gray vs. white bars) (respectively $p < 0.02$ and $p < 0.05$). However, the effect of EE on neurogenesis compared to control groups was not significant when BrdU was injected later in development (group 8 weeks of EE after weaning or 4 weeks of EE in young adults, black bar). In the SE group (white bars), the number of BrdU-positive cells in the dentate gyrus was significantly lower at 12 weeks compared to 10 weeks (Fig. 2b, $p < 0.05$) consistent with the exponential decrease in the rate of neurogenesis measured across the life span (Bizon and Gallagher 2003; Lazic 2012).

To test whether EE housing conditions result in alterations of hippocampal synaptic plasticity, we analyzed the morphology and density of spines on hippocampal neurons in mice raised in various housing conditions.

EE increases spine density relative to SE

By comparing confocal imaging of all Cornus Amonis 1 (CA1) neurons from different groups, we quantified precisely the number of spines in the secondary basilar

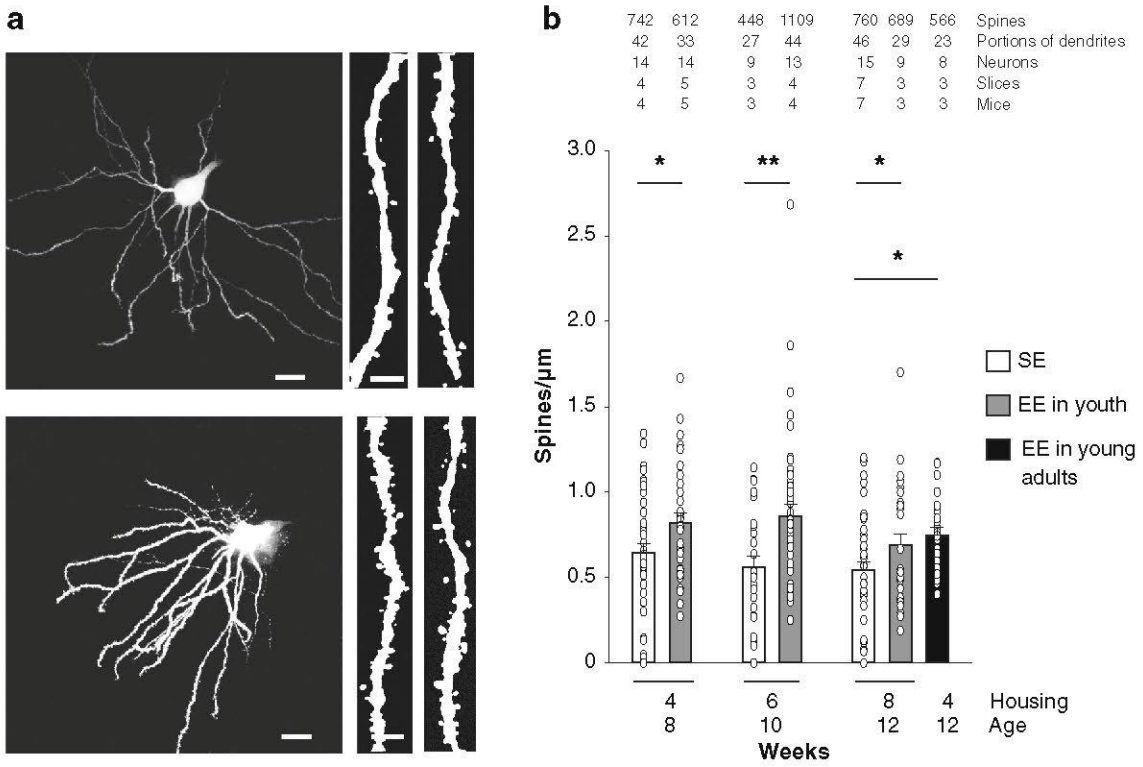

Fig. 3 Prolonged exposure to an enriched environment modifies dendritic spine density. **a** Confocal imaging of CA1 pyramidal neurons (*left panels*) and two examples of their spiny second basilar dendrites (*right pannels*) for a mouse housed in SE (*top*) and for a mouse housed in EE (*bottom*). Note the numerous branchings and spines for the EE mouse compared to the SE mouse. **b** Number of spines/µm at 4–6 and 8 weeks of different housing conditions, SE is shown in *white* and EE in *gray*. $*p < 0.05$, and $**p < 0.01$, Mann–Whitney test, EE vs. SE at the same age

dendrites (that mainly receive glutamatergic inputs from the Schaffer collaterals (Spruston 2008) and their shape as a function of the housing period in either SE or EE conditions (i.e., 4, 6, 8 weeks in juvenile and 4 weeks in young adult mice; Fig. 3a).

EE increased the density of spines in all groups, including 4 weeks in young adults (black bars). As illustrated in Fig. 3b, there was a tendency for a decrease in spine density with age in the SE group, although this variation was not significant (white bars).

Using NeuroStudio software, we analyzed the shapes of the spines in the different experimental groups (Fig. 4). Three types of spines were considered (thin, mushroom and stubby; Fig. 4a). No significant difference between the distribution of these three types of spines was observed in SE across age (~25 % thin, ~25 % mushroom and ~50 % stubby) and EE housing did not induce major changes in the distribution of spine shapes (Fig. 4b). However, EE induced subtle changes in some spine morphological parameters: a slight increase in spine head diameter coupled to a decrease in spine neck diameter at 4 weeks of EE (Fig. 4c, d), a slight decrease in spine head diameter and a decrease in mean spine length at 6 weeks of EE in juvenile mice (Fig. 4c–e). These effects were transient since no difference in spine shape was observed after 8 weeks of EE in juvenile mice. Moreover, an increase in neck diameter coupled to a decrease in spine length was observed after 4 weeks of EE in young adults (Fig. 4d, e).

EE modifies LTP

Morphological features such as size, shape and density of dendritic spines have been shown to reflect important synaptic function. To confirm the effects of EE on synaptic plasticity, we used a standard LTP protocol (Fig. 5a) to evaluate synaptic plasticity in mice raised in different housing conditions.

Surprisingly, LTP at the CA3–CA1 synapses was reduced in EE mice after 4 weeks of enrichment in juvenile mice compared to mice of the same age housed in SE (Fig. 5b, e). The lower level of LTP in 4 weeks of EE mice at youth compared to matched SE mice was correlated with a tendency for an increase in the size of fEPSPs before the conditioning protocol (baseline fEPSCs, $p < 0.06$) (Fig. 5f). This suggests that synaptic

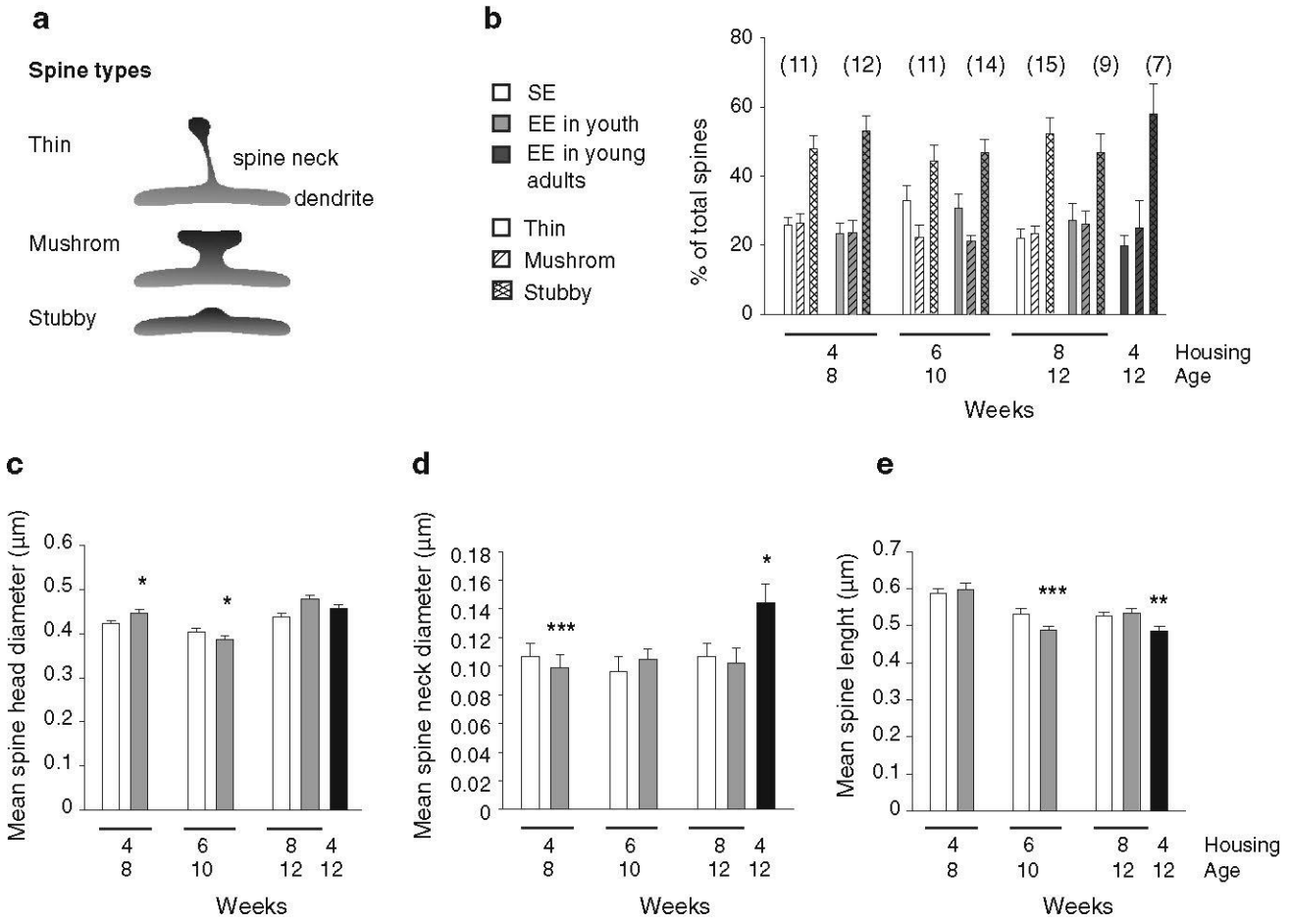

Fig. 4 Prolonged exposure to an enriched environment modifies dendritic spine morphology. **a** Schema of the spine types. **b** Repartition of different dendritic spine types in the hippocampus of mice housed 4–6 and 8 weeks in SE or EE (number of neurons in parenthesis). **c** Mean spine head diameter (±SEM) for mice raised in diverse conditions. **d** Mean spine neck diameter (±SEM) for mice raised in diverse conditions. **e** Mean spine length (±SEM) for mice raised in diverse conditions. $*p < 0.05$, $**p < 0.01$, $***p < 0.001$, Mann–Whitney test, EE vs. SE at the same age

strength could have already been enhanced in the EE group making them less prone to potentiation. EE did not affect the paired-pulse facilitation ratio (determined in patch clamp in the whole-cell mode; Fig. 5g) indicating that an effect of EE on the presynaptic side of the synapse is unlikely. In contrast to 4 weeks in EE, there was no difference observed in the induction of LTP after 6 weeks in EE compared to 6 weeks in SE (Fig. 5c, e). However, 8 weeks in EE led to a significant increase in LTP compared to SE-housed mice of the same age (Fig. 5d, e). Similar to the effect observed at 4 weeks, EE did not affect the paired-pulse facilitation ratio (as determined with extracellular recordings Fig. 5h).

Between postnatal ages 4 to 8 weeks, the mouse brain is still developing and it is likely that EE acts at the synaptic level in a way that competes with the LTP protocol we used. To test this hypothesis, we transferred mice to EE for 4 weeks only in young adults (i.e., 8 weeks postnatal), instead of housing them in EE immediately after weaning. Whereas 4 weeks of EE in juvenile mice decreased LTP, LTP was found to be significantly increased by 4 weeks of EE in young adult mice compared to matched SE mice (Fig. 5e, black bar) indicating that a 4-week EE period in young adults is sufficient to change neuronal features in the form of increased LTP. Consistent with all other previous measurements, EE did not affect the paired-pulse facilitation ratio in this condition (Fig. 5h). Therefore, 4 weeks of enrichment in young adults leads to a larger susceptibility of synapses to respond to a pertinent signal by LTP and thus to an increase in the signal to noise ratio.

Overall, our results revealed that EE acts differently in neuronal plasticity at different points during postnatal development of the mouse brain.

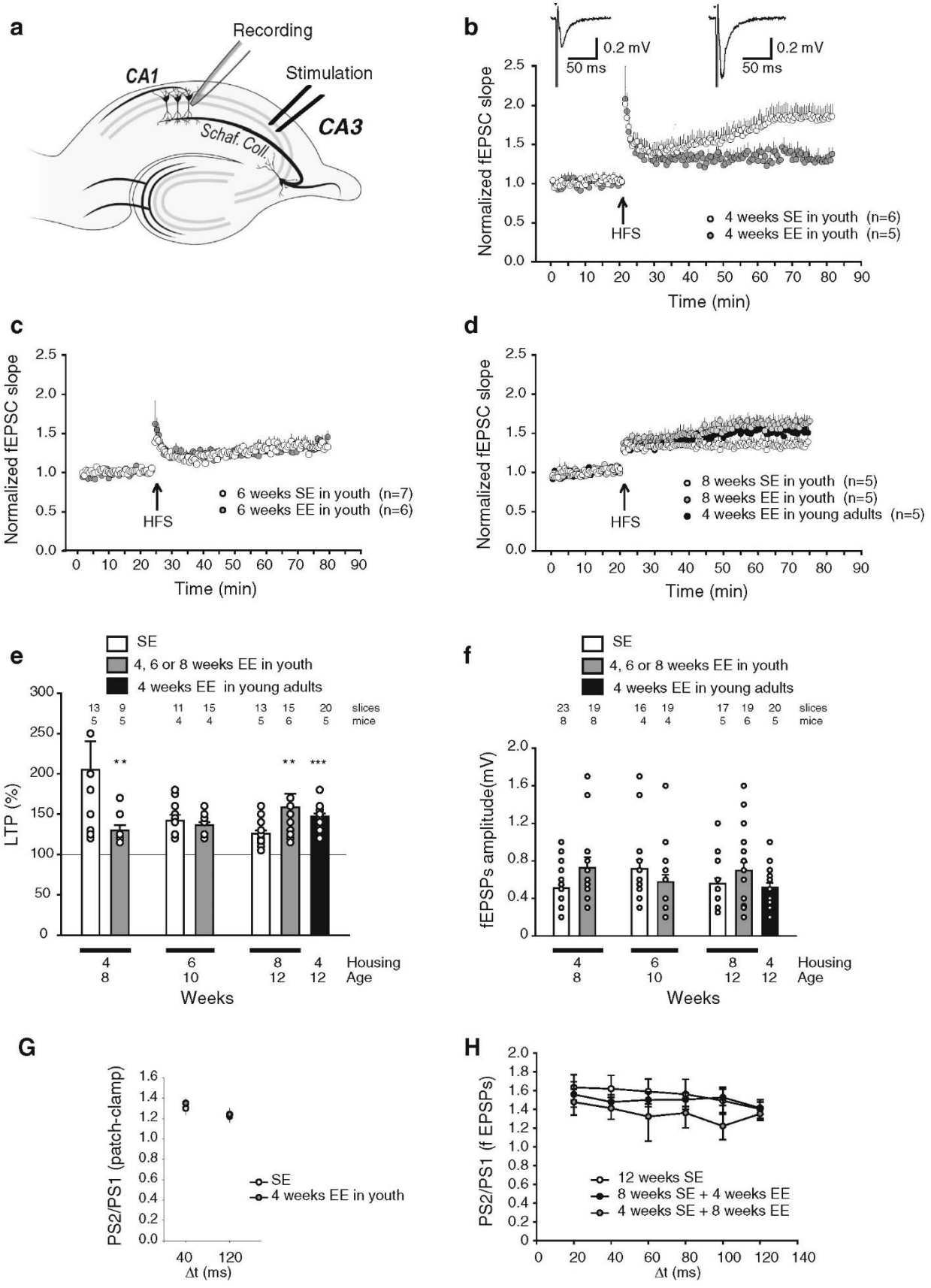
a
Recording
CA1
Stimulation
CA3
Schaf. Coll.
b
0.2 mV
50 ms
0.2 mV
50 ms
Normalized fEPSC slope
HFS
4 weeks SE in youth (n=6)
4 weeks EE in youth (n=5)
Time (min)
c
Normalized fEPSC slope
HFS
6 weeks SE in youth (n=7)
6 weeks EE in youth (n=6)
Time (min)
d
Normalized fEPSC slope
HFS
8 weeks SE in youth (n=5)
8 weeks EE in youth (n=5)
4 weeks EE in young adults (n=5)
Time (min)
e
SE
4, 6 or 8 weeks EE in youth
4 weeks EE in young adults
slices
mice
LTP (%)
Housing
Age
Weeks
f
SE
4, 6 or 8 weeks EE in youth
4 weeks EE in young adults
slices
mice
fEPSPs amplitude(mV)
Housing
Age
Weeks
G
PS2/PS1 (patch-clamp)
SE
4 weeks EE in youth
Δt (ms)
H
PS2/PS1 (f EPSPs)
12 weeks SE
8 weeks SE + 4 weeks EE
4 weeks SE + 8 weeks EE
Δt (ms)

◀**Fig. 5** LTP is differently modulated depending on the duration of enriched environment and the age of the mouse: **a** LTP experimental protocol: a bipolar electrode was located on the surface of the transversal hippocampal slice (350 μm thick) in a region where Schaffer collaterals containing the axons of CA3 pyramidal neurons were stimulated. Recording pipette was located in the CA1 region, at about 200 μm distance from the stimulating electrode. **b** Field excitatory postsynaptic potentials (fEPSPs) recorded in the CA1 region of the hippocampus in response to a stimulation of Schaffer collaterals every 30 s. Stimulating intensity was chosen to trigger a fEPSP of 50 % of the maximum response. After a stable baseline of 20 min, the high-frequency stimulation (HFS) protocol was applied (100 Hz during 1 s). The 30 s stimulation with the same intensity restarted and a potentiation of the response to the stimulation was observed as expected, to 125–300 % of the initial response. Examples of fEPSPs recorded before and 40 min after the HFS are presented in inset. *Curves* show the time course of the slope amplitude of the EPSCs for an average of slices of each group of mice, a group that was raised 8 weeks in SE and a group raised 4 weeks in EE since 4 weeks of age (*n* in *parenthesis*). LTP was established in both groups after the HFS, but its magnitude was less pronounced in the group of mice that was raised in 4 weeks of EE. **c** Time course of the slope amplitude of the EPSCs for an average of slices from a group of mice raised 10 weeks in SE and a group raised 6 weeks in EE since 4 weeks of age (*n* in *parenthesis*). **d** Time course of the slope amplitude of the EPSCs for an average of slices from a group of mice raised 12 weeks in SE and a group raised 8 weeks in EE since 4 weeks of age (*n* in *parenthesis*). **e** *Histograms* showing the mean amplitude of LTP (±SEM) measured 40 min after HFS according to the different housing conditions of mice after weaning: SE or EE for 4, 6 or 8 weeks, or 8 weeks SE plus 4 weeks of EE (*black*). $^{**}p < 0.02$, $^{***}p < 0.001$, Mann–Whitney test, EE vs. SE at the same age. **f** Mean amplitude (±SEM) of the field EPSP measured in different groups. **g** Paired-pulse protocol in patch clamp: PS2/PS1 showing no change in the paired-pulse EPSP ratio between the CA1 neurons from 4 weeks of EE mice in youth and matched SE mice ($N = 4$–5 neurons tested in 4–5 slices and 2–3 mice each). **h** Paired-pulse protocol in field potentials: PS2/PS1 indicating no difference between different groups (8 weeks of EE after 4 weeks SE in *gray*, 4 weeks of EE after 8 weeks SE in *black* and 8 weeks SE in *white*). ($N = 5$–7 slices in 3–5 mice for each group)

EE modifies spontaneous glutamatergic and miniature synaptic activity

The observed increase in spine density combined with the observed increase in dendritic length and branching should lead to a large increase in the total number of synaptic contacts reaching CA1 neurons in mice raised in EE compared to SE. EPSCs reflect the synaptic release of glutamate on CA1 neurons. An increase in the number of functional boutons should result in an enhancement of spontaneous EPSC frequency.

To determine if the observed spine morphological changes are correlated to physiological changes and also to understand the basis of the observed changes in LTP, we investigated whether EE modifies the number and/or strength of functional synaptic contacts. We used patch-clamp recordings in the whole-cell configuration and recorded the spontaneous excitatory postsynaptic currents,

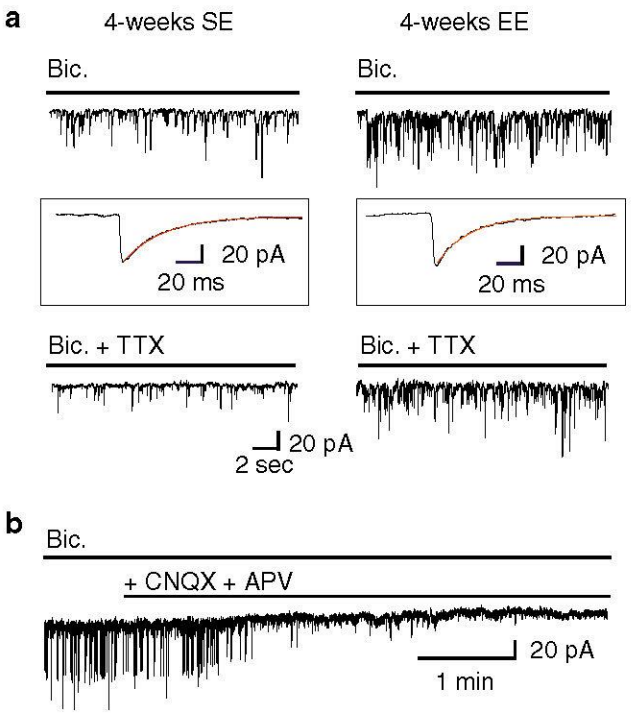

Fig. 6 Examples of recordings of spontaneous and miniature EPSCs recorded in pyramidal CA1 neurons in whole cell. **a** Spontaneous (*top*, recorded in the presence of 10 μM bicuculline) and miniatures (*bottom*, recorded in the presence of both bicuculline, 10 μM and tetrodotoxin, 2 μM) EPSCs events in 4 weeks of EE and SE groups in youth. *Insets* show examples of the kinetics of spontaneous events in an expanded scale, with their decays fitted to an exponential curve. **b** Representative trace showing that spontaneous activity recorded in bicuculline was fully blocked by the application of 10 μM CNQX and 50 μM DL-APV (in a mouse raised 8 weeks in SE)

which are due to the synaptic release of glutamate on CA1 neurons (sEPSCs were recorded after adding the $GABA_A$ receptor blocker bicuculline, and mEPSCs were recorded after adding TTX to block action potentials). An example recording is shown in Fig. 6a for mice with 4 weeks of EE/SE at youth. We chose to record EPSPs for two reasons. First, in the region of the dendritic tree where the spine density was measured, it is known that the inputs are mainly glutamatergic. Second, in the LTP protocol used, the Schaffer collaterals stimulated are glutamatergic fibers. sEPSCs and mESPCs were blocked by the combined application of APV and CNQX, confirming their glutamatergic origin (Fig. 6b).

There was no significant difference in the average event amplitude of the spontaneous or miniature EPSCs between SE and EE conditions at 4, 6 or 8 weeks (Fig. 7a, b), suggesting that the average strength of active synapses was not affected by EE. In addition, regardless of age and housing condition, there was no major difference between spontaneous and miniature EPSC amplitude in juvenile animals. This suggests that with or without action

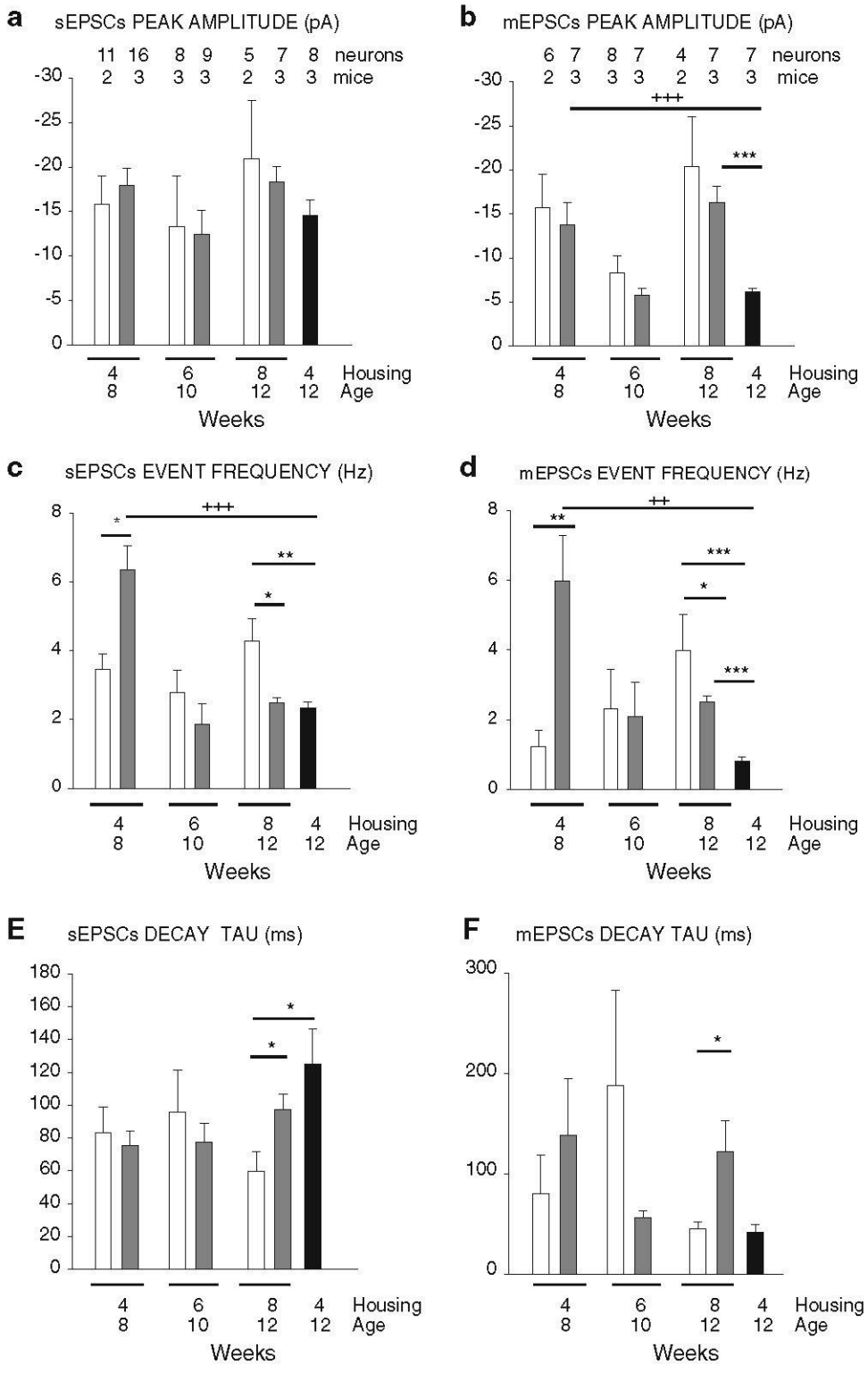

Fig. 7 Spontaneous (*left*) and miniature (*right*) EPSC properties are modified by enriched environment in a time- and age-dependent manner. *Histograms* show, in different housing conditions, mice after weaning or young adults. **a**, **b** the sEPSCs (**a**) and mEPSCs (**b**) peak amplitude (±SEM); **c**, **d** the sEPSCs (**c**) and mEPSCs (**d**) event frequency (±SEM); **e**, **f** the sEPSCs (**e**) and mEPSCs (**f**) time constant of decay of the exponential fitted to the decay of the events, tau decay (±SEM). SE in *white* and EE in *gray*, *black bar* represents 8 weeks of SE plus 4 weeks of EE. $^{*}p < 0.05$, $^{***}p < 0.001$, *t* test against SE, $^{++}p < 0.02$, $^{+++}p < 0.001$ Mann–Whitney test comparing 4 weeks in EE of juvenile or young adult mice

potentials, neurotransmitter release leads to a similar response or that there was no spontaneous action potentials generated in the slice. Similar results were obtained when comparing the cumulative histograms of sEPSCs and mEPSCs amplitude (Suppl 1 and 2).

By contrast, the event frequency of both sEPSCs and mEPSCs were significantly increased at 4 weeks of EE compared to SE (Fig. 7c, d; Suppl 1, 2), which is in agreement with the increased spine density measured at this stage (Fig. 3). This suggests that most glutamatergic

contacts observed at 4 weeks of EE housing condition were probably functional. Since most synaptic contacts were already strongly connected, this could explain why the experimentally inducible LTP was low. There was no difference in the kinetics of the events between these conditions (Fig. 7e, f; Suppl 1, 2).

Unlike mice raised in EE for 4 weeks, after raising mice for 6 weeks in EE, we found no significant difference in the average EPSC event frequency compared to the matched SE group (Fig. 7c, d), although the histograms in cumulative inter-event interval suggested a decrease in frequency (Suppl 1, 2). The time constant of decay of the sEPSCs were not modified by EE (Fig. 7e; Suppl 1), although the kinetics of decay of the mEPSCs appeared slightly faster in EE conditions (Fig. 7f; Suppl 2, $p < 0.07$).

After 8 weeks in EE conditions, the average spontaneous and miniature event frequencies were significantly decreased compared to SE (in spite of the continuous increase of spine density) (Fig. 7c, d), which was confirmed by the cumulative histograms (Suppl 1, 2). We also observed at this stage a slowing of the sEPSCs and mEPSCs (significant increase in the average time constant of decay of the mEPSCs and sEPSCs), which was confirmed in the cumulative histogram, Fig. 7, $p < 0.05$, Suppl 1 and 2.

After 4 weeks of EE in young adults, the picture was radically different compared to 4 weeks of EE in juvenile mice, but was relatively comparable to mice enriched for 8 weeks in youth. The average amplitude of the sEPSCs was similar to that of matched control (Fig. 7a; Suppl 1). Interestingly, there was an increased ratio between sEPSC/mEPSC amplitude, which has been described to reflect increased connectivity and redundancy of afferent synaptic inputs (Hsia et al. 1998), but this was due to a decrease in the mean mEPSC amplitude (Fig. 7b; Suppl 2). The frequency of mEPSCs in young adult mice with 4 weeks of EE was also significantly decreased compared to matched control mice (Fig. 7d; Suppl 2), confirming a decrease in miniature synaptic release sites.

Discussion

The present study provides an integrative view of the role of EE during postnatal development on various mechanisms of plasticity in the hippocampus including neurogenesis as well as morphological and physiological parameters of synaptic connections. We have shown that these effects depend mainly on the age and the duration of an animal's exposure to EE. In addition to giving additional clues on the mechanisms by which EE alters plasticity in the hippocampus, our results provide an explanation for the discrepancies and variability seen in the literature about the effects of EE on LTP (Tang and Zou 2002; Artola et al. 2006; Malik and Chattarji 2012; Foster and Dumas 2001; Eckert et al. 2010; Bouet et al. 2011; Waters et al. 1997).

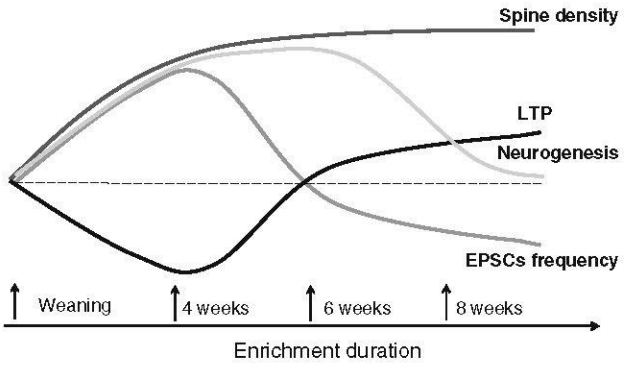

Fig. 8 Scheme representing the various effects of different periods of EE at youth on neurogenesis, spine density, LTP and EPSC frequency. The effects of EE are schematized relative to a baseline (*dashed line*) which represents the SE group levels

When started immediately after weaning, EE (4–6 weeks) increased neurogenesis in juvenile animals (up to 10 weeks old) (Fig. 8). Interestingly, when BrdU was injected later in development, there was not a significant effect of EE on the number of BrdU-labeled cells measured 21 days after injection, contrary to what has been observed in other studies with slightly different protocols and measurements taken later in development (Kempermann et al. 2002). This suggests that the plasticity induced by our EE protocol in young adults does not induce neurogenesis, but rather synaptogenesis as proposed by (Bizon and Gallagher 2003). Indeed, whatever the duration of the housing and the initial age, more dendritic branching was observed in the EE groups compared to the SE groups (an example is shown in Fig. 3a), as previously reported (Nithianantharajah and Hannan 2006; Sale et al. 2009). We also quantified spine density and morphology at the level of the secondary basilar dendrites of CA1 neurons, which receive mainly glutamatergic inputs from CA3 Schaffer collaterals, and correlated these data to electrophysiological data obtained at the same time points (fEPSP, LTP and EPSCs). The lower density of spines that we found (around 1 spine/μm) compared to the average of 2 spines/μm measured using serial electron microscopy followed by 3-D reconstruction (Harris and Stevens 1989) can easily be explained by a difference in the method used, since we used projection images where spines above and below the dendrites were not taken into consideration.

Our study suggests that in juvenile mice, 4 weeks of enrichment induces a strengthening of the glutamatergic synapses between CA3 and CA1 that make them less prone to LTP, as if there was a competition between the

mechanisms of LTP and the changes induced by EE during postnatal development. Therefore, results obtained using experimental LTP procedures should be interpreted with caution, since they do not simply correlate with learning, but rather reveal the aptitude of a given pathway to be reinforced, depending on its initial synaptic strength. EE at early stages may accelerate the maturation of the hippocampus as has been described in the visual system (Cancedda et al. 2004). Such increase in synaptic strength between CA3 and CA1 neurons following EE has already been described (Ashby et al. 2006; Foster and Dumas 2001) and could be due to a larger number of active synapses, changes in the morphology of the synapse, increased density of receptors present at the postsynaptic site at each synapse and/or increased neurotransmitter released in the synaptic cleft. Indeed, we observed an increase in spine density (Fig. 3b) and changes in spine morphology (increase in head spine diameter and decrease in neck diameter, Fig. 4c–e) at basilar dendrites of CA1 neurons, which receive Schaffer collateral. An increase in the surface of the synapse has been described to be associated with reinforcement of the synapse (Kasai et al. 2010; Tada and Sheng 2006), and lateral diffusion of AMPA receptors is dependent on spine morphology and is restricted at the spine neck (Ashby et al. 2006; Jaskolski et al. 2009). Thus, these morphological changes could explain the basal increase in synaptic strength that is accompanied by a decline in the ability to induce LTP following tetanic stimulation. The synapses reinforced by EE appear to stabilize better as the density of spines is elevated soon after 4 weeks of EE, leading to larger synaptic networks.

As illustrated in Fig. 8, after 6 weeks in EE, the number of spines was still increased in mice compared to matched controls raised in SE (Fig. 3b). However, surprisingly, the frequency of spontaneous excitatory synaptic events recorded on the whole CA1 neuron started to decrease compared to 4 weeks of EE. Overall, no difference was observed in the amplitude of LTP (Fig. 5). Similarly, after 8 weeks of housing conditions at youth, EE still induced an increase in spine density compared to SE (Fig. 3b), again with a surprising decrease in sEPSC and mEPSC frequency. No apparent morphological changes in spine morphology were observed compared to SE mice of the same age (Fig. 4b–e), but there was a significant increase in LTP (Fig. 5e, white vs. gray bars). After 4 weeks of EE in young adult mice, the spine density was also significantly increased (Fig. 3b), as in juvenile mice exposed 4 weeks to EE, while there was a decreased frequency of the miniature and spontaneous glutamatergic events contrary to the increased EPSC frequency observed in juvenile mice suggesting that most formed synaptic contacts rapidly became silent.

This discrepancy between the anatomical data (number of spines) and the functional data (frequency of EPSCs) could be due to a homeostatic process of synaptic scaling (Siddoway et al. 2013). The lack of variation in the paired-pulse ratio (Fig. 5g, h) suggests postsynaptic rather than presynaptic changes. Indeed, after 6 weeks of EE, we observed a decrease in spine head diameter and spine length (Fig. 4c–e) that could be the result of a retraction of the spines. There were also slower kinetics of the sEPSCs and mEPSCs in the 8 weeks' EE group (Fig. 7e, f) that could be the result of a modification in the subunit composition and/or different repartition of AMPA receptors at the synapse. New connections by non-glutamatergic inputs (for example, gamma aminobutyric acid, GABA, inputs that have been shown to be essential for plasticity in other systems) (Sale et al. 2010) are also possible, although the majority of GABAergic and peptidergic inputs connect the soma and the basal part of the spines (Harris and Stevens 1989). The formed glutamatergic synapses remain active upon stimulation, as measured by their similar fEPSPs amplitude (Fig. 5f) and their higher ability to be potentiated after 8 weeks in EE compared to the matched SE mice (Fig. 5e). EE thus increases the signal to noise ratio of the synaptic connections between CA3 and CA1 pyramidal neurons and allows a greater ability of pertinent synaptic network to be stabilized. Overall, mice raised for 8 weeks in EE at youth develop neural networks that, as a consequence of their enhanced exploration and stimulation, are primed to be modified in their hippocampus, and thus these mice should be able to learn better than their matched controls raised in SE.

After 4 weeks of EE in young adult mice, the amplitude of mEPSCs was decreased without a change in kinetics or amplitude of sEPSCS compared to SE mice of the same age. This suggests that changes in the shape of the synapse and/or the repartition of the AMPA receptors at the synapse occurred. Moreover, the sEPSCs were significantly slower than the mEPSCs, suggesting that glutamate synaptic release induced by action potentials possibly reached receptors which were in the periphery of the synaptic boutons that were not reached by the glutamate release by a single vesicle. Indeed, after 4 weeks of EE in young adult mice, we observed some modifications in the spine shape at the basal dendrites of CA1 neurons (decrease in spine length and increase in spine neck diameter, Fig. 4d, e), which suggests that a retraction of the spines occurred. Interestingly, the synapses formed after 4 weeks of EE in young adult mice appear more susceptible to LTP induction (Fig. 5e), possibly through a re-localization of the AMPA receptors at the synapse following a tetanic stimulation (Ashby et al. 2006; Henley and Wilkinson 2013).

In juvenile animals, 4 weeks of EE exposure induces a transient increase in the number of active synapses which

could correspond to a high level of learning processes triggered by novel experiences in these mice. However, it appears that prolonged exposure to enrichment leads to a progressive silencing of synapses, which could correspond to some kind of habituation to EE. However, these mice apparently keep more connections and neural networks which should be ready to operate if they are triggered in new learning tasks.

Interestingly, the effects of EE were different in juvenile and young adult mice. In juvenile animals, 4 weeks of EE induced a transient increase in the number of active synapses coupled to a decrease of the ability of Shaffer collateral stimulation to induce LTP, whereas in young adult animals it induced a moderate increase in the number of synapses (as if the morphological plasticity was reduced compared to juvenile mice), coupled to large silencing of the synapses and a larger susceptibility to LTP, as if the stimulation of synapses already formed was leading to their downregulation.

During the life span, the effect of EE will have different consequences on the organization of the brain. During adolescence, the brain undergoes massive synaptic remodeling, including reduction in dendritic arborization, axon myelination and pruning of synapses (Sisk and Zehr 2005). Perturbations in 4–6 weeks postnatal mice are crucial in determining hippocampal function in adulthood (Guo et al. 2013), highlighting the importance of critical periods during brain development.

By comparing electrophysiological activity of the synapses to their morphology, our results stress a distinction between anatomical spines and functional synaptic structures, as previously suggested by (Zito et al. 2009; Bednarek and Caroni 2011). Our findings show that extra spines can be maintained following enrichment periods even when these fail to establish functional synapses. These silent structures could constitute a pool of synapses ready to be activated upon stimulation by plasticity-inducing events and might play a major role in learning (Voronin and Cherubini 2004). This supports the notion that connectivity rearrangement, in addition to LTP/LTD, underlies enhanced learning upon enrichment.

In conclusion, our study stresses the dramatic influence exerted by environment on brain plasticity, particularly in the hippocampus, a structure which plays a major role in learning and memory. Previous studies have already described how the length of exposure to EE can differentially affect several parameters such as growth factor expression (BDNF or IGF-1) (Vazquez-Sanroman et al. 2013; Baroncelli et al. 2010), neurogenesis (Deng et al. 2010) or behavior (Cao et al. 2010). The major contribution of our study is the integration of electrophysiological data together with morphological data that helps to unravel the processes that progressively occur as animals are kept for extended periods in an enriched environment. In addition, we show that a similar duration in EE (4 weeks) has different consequences in juvenile and young adult mice. Although some forms of plasticity, such as remodeling of synaptic contacts, still exists in young adults in response to enriched environment, the impact of EE on neurogenesis is no longer measurable at this age.

Acknowledgments We wish to thank Frederic Brau for help in microscopy and spine analysis, Lucien Relmy for animal care, Nicole Zsürger for help with the enriched environment setup, Franck Aguila for artwork, Thierry Coppola, Anouar Khayashi and Thomas Lorivel for fruitful discussions, Thomas Freret and Stéphane Martin for helpful comments on the manuscript and Joshua Levitz for his corrections and pertinent remarks on the manuscript. This study was financed by CNRS and the Plan Cancer 2009-13 ITMO. Salma Hosseiny was financed by Alexandria University, Egypt.

References

Artola A, von Frijtag JC, Fermont PC, Gispen WH, Schrama LH, Kamal A, Spruijt BM (2006) Long-lasting modulation of the induction of LTD and LTP in rat hippocampal CA1 by behavioural stress and environmental enrichment. Eur J Neurosci 23(1):261–272. doi:10.1111/j.1460-9568.2005.04552.x

Ashby MC, Maier SR, Nishimune A, Henley JM (2006) Lateral diffusion drives constitutive exchange of AMPA receptors at dendritic spines and is regulated by spine morphology. J Neurosci 26(26):7046–7055. doi:10.1523/JNEUROSCI.1235-06.2006

Baroncelli L, Braschi C, Spolidoro M, Begenisic T, Sale A, Maffei L (2010) Nurturing brain plasticity: impact of environmental enrichment. Cell Death Differ 17(7):1092–1103. doi:10.1038/cdd.2009.193

Bednarek E, Caroni P (2011) Beta-adducin is required for stable assembly of new synapses and improved memory upon environmental enrichment. Neuron 69(6):1132–1146. doi:10.1016/j.neuron.2011.02.034

Bennett EL, Diamond MC, Krech D, Rosenzweig MR (1996) Chemical and anatomical plasticity of brain 1964. J Neuropsychiatry Clin Neurosci 8(4):459–470

Bizon JL, Gallagher M (2003) Production of new cells in the rat dentate gyrus over the lifespan: relation to cognitive decline. Eur J Neurosci 18(1):215–219

Bliss TV, Collingridge GL (1993) A synaptic model of memory: long-term potentiation in the hippocampus. Nature 361(6407):31–39. doi:10.1038/361031a0

Bouet V, Freret T, Dutar P, Billard JM, Boulouard M (2011) Continuous enriched environment improves learning and memory in adult NMRI mice through theta burst-related-LTP independent mechanisms but is not efficient in advanced aged animals. Mech Ageing Dev 132(5):240–248. doi:10.1016/j.mad.2011.04.006

Cancedda L, Putignano E, Sale A, Viegi A, Berardi N, Maffei L (2004) Acceleration of visual system development by environmental enrichment. J Neurosci 24(20):4840–4848. doi:10.1523/JNEUROSCI.0845-04.2004

Cao L, Liu X, Lin EJ, Wang C, Choi EY, Riban V, Lin B, During MJ (2010) Environmental and genetic activation of a brain-adipocyte BDNF/leptin axis causes cancer remission and inhibition. Cell 142(1):52–64. doi:10.1016/j.cell.2010.05.029

Deng W, Aimone JB, Gage FH (2010) New neurons and new memories: how does adult hippocampal neurogenesis affect learning and memory? Nat Rev Neurosci 11(5):339–350. doi:10.1038/nrn2822

Eckert MJ, Bilkey DK, Abraham WC (2010) Altered plasticity in hippocampal CA1, but not dentate gyrus, following long-term environmental enrichment. J Neurophysiol 103(6):3320–3329. doi:10.1152/jn.01037.2009

Foster TC (2002) Regulation of synaptic plasticity in memory and memory decline with aging. Prog Brain Res 138:283–303. doi:10.1016/S0079-6123(02)38083-X

Foster TC, Dumas TC (2001) Mechanism for increased hippocampal synaptic strength following differential experience. J Neurophysiol 85(4):1377–1383

Guo N, Yoshizaki K, Kimura R, Suto F, Yanagawa Y, Osumi N (2013) A sensitive period for GABAergic interneurons in the dentate gyrus in modulating sensorimotor gating. J Neurosci 33(15):6691–6704. doi:10.1523/JNEUROSCI.0032-12.2013

Harris KM, Stevens JK (1989) Dendritic spines of CA 1 pyramidal cells in the rat hippocampus: serial electron microscopy with reference to their biophysical characteristics. J Neurosci 9(8):2982–2997

Henley JM, Wilkinson KA (2013) AMPA receptor trafficking and the mechanisms underlying synaptic plasticity and cognitive aging. Dialogues Clin Neurosci 15(1):11–27

Heurteaux C, Lucas G, Guy N, El Yacoubi M, Thummler S, Peng XD, Noble F, Blondeau N, Widmann C, Borsotto M, Gobbi G, Vaugeois JM, Debonnel G, Lazdunski M (2006) Deletion of the background potassium channel TREK-1 results in a depression-resistant phenotype. Nat Neurosci 9(9):1134–1141. doi:10.1038/nn1749

Hsia AY, Malenka RC, Nicoll RA (1998) Development of excitatory circuitry in the hippocampus. J Neurophysiol 79(4):2013–2024

Ilin Y, Richter-Levin G (2009) Enriched environment experience overcomes learning deficits and depressive-like behavior induced by juvenile stress. PLoS One 4(1):e4329. doi:10.1371/journal.pone.0004329

Jaskolski F, Mayo-Martin B, Jane D, Henley JM (2009) Dynamin-dependent membrane drift recruits AMPA receptors to dendritic spines. J Biol Chem 284(18):12491–12503. doi:10.1074/jbc.M808401200

Kandel ER, Dudai Y, Mayford MR (2014) The molecular and systems biology of memory. Cell 157(1):163–186. doi:10.1016/j.cell.2014.03.001

Kasai H, Fukuda M, Watanabe S, Hayashi-Takagi A, Noguchi J (2010) Structural dynamics of dendritic spines in memory and cognition. Trends Neurosci 33(3):121–129. doi:10.1016/j.tins.2010.01.001

Kempermann G, Kuhn HG, Gage FH (1997) More hippocampal neurons in adult mice living in an enriched environment. Nature 386(6624):493–495. doi:10.1038/386493a0

Kempermann G, Gast D, Gage FH (2002) Neuroplasticity in old age: sustained fivefold induction of hippocampal neurogenesis by long-term environmental enrichment. Ann Neurol 52(2):135–143. doi:10.1002/ana.10262

Lazic SE (2012) Modeling hippocampal neurogenesis across the lifespan in seven species. Neurobiol Aging 33(8):1664–1671. doi:10.1016/j.neurobiolaging.2011.03.008

Leger M, Bouet V, Freret T, Darmaillacq AS, Dacher M, Dauphin F, Boulouard M, Schumann-Bard P (2012) Environmental enrichment improves recent but not remote memory in association with a modified brain metabolic activation profile in adult mice. Behav Brain Res 228(1):22–29. doi:10.1016/j.bbr.2011.11.022

Malik R, Chattarji S (2012) Enhanced intrinsic excitability and EPSP-spike coupling accompany enriched environment-induced facilitation of LTP in hippocampal CA1 pyramidal neurons. J Neurophysiol 107(5):1366–1378. doi:10.1152/jn.01009.2011

Moser MB, Trommald M, Andersen P (1994) An increase in dendritic spine density on hippocampal CA1 pyramidal cells following spatial learning in adult rats suggests the formation of new synapses. Proc Natl Acad Sci USA 91(26):12673–12675

Nithianantharajah J, Hannan AJ (2006) Enriched environments, experience-dependent plasticity and disorders of the nervous system. Nat Rev Neurosci 7(9):697–709. doi:10.1038/nrn1970

Peters A, Kaiserman-Abramof IR (1970) The small pyramidal neuron of the rat cerebral cortex. The perikaryon, dendrites and spines. Am J Anat 127(4):321–355. doi:10.1002/aja.1001270402

Rampon C, Tang YP, Goodhouse J, Shimizu E, Kyin M, Tsien JZ (2000) Enrichment induces structural changes and recovery from nonspatial memory deficits in CA1 NMDAR1-knockout mice. Nat Neurosci 3(3):238–244. doi:10.1038/72945

Redolat R, Mesa-Gresa P (2012) Potential benefits and limitations of enriched environments and cognitive activity on age-related behavioural decline. Curr Top Behav Neurosci 10:293–316. doi:10.1007/7854_2011_134

Sale A, Berardi N, Maffei L (2009) Enrich the environment to empower the brain. Trends Neurosci 32(4):233–239

Sale A, Berardi N, Spolidoro M, Baroncelli L, Maffei L (2010) GABAergic inhibition in visual cortical plasticity. Front Cell Neurosci 4:10. doi:10.3389/fncel.2010.00010

Siddoway B, Hou H, Xia H (2013) Molecular mechanisms of homeostatic synaptic downscaling. Neuropharmacology. doi:10.1016/j.neuropharm.2013.07.009

Sisk CL, Zehr JL (2005) Pubertal hormones organize the adolescent brain and behavior. Front Neuroendocrinol 26(3–4):163–174. doi:10.1016/j.yfrne.2005.10.003

Spruston N (2008) Pyramidal neurons: dendritic structure and synaptic integration. Nat Rev Neurosci 9(3):206–221. doi:10.1038/nrn2286

Tada T, Sheng M (2006) Molecular mechanisms of dendritic spine morphogenesis. Curr Opin Neurobiol 16(1):95–101. doi:10.1016/j.conb.2005.12.001

Tang AC, Zou B (2002) Neonatal exposure to novelty enhances long-term potentiation in CA1 of the rat hippocampus. Hippocampus 12(3):398–404. doi:10.1002/hipo.10017

Vazquez-Sanroman D, Sanchis-Segura C, Toledo R, Hernandez ME, Manzo J, Miquel M (2013) The effects of enriched environment on BDNF expression in the mouse cerebellum depending on the length of exposure. Behav Brain Res 243:118–128. doi:10.1016/j.bbr.2012.12.047

Voronin LL, Cherubini E (2004) 'Deaf, mute and whispering' silent synapses: their role in synaptic plasticity. J Physiol 557(Pt 1):3–12. doi:10.1113/jphysiol.2003.058966

Waters NS, Klintsova AY, Foster TC (1997) Insensitivity of the hippocampus to environmental stimulation during postnatal development. J Neurosci 17(20):7967–7973

Young D, Lawlor PA, Leone P, Dragunow M, During MJ (1999) Environmental enrichment inhibits spontaneous apoptosis, prevents seizures and is neuroprotective. Nat Med 5(4):448–453. doi:10.1038/7449

Zito K, Scheuss V, Knott G, Hill T, Svoboda K (2009) Rapid functional maturation of nascent dendritic spines. Neuron 61(2):247–258. doi:10.1016/j.neuron.2008.10.054

Psychoneuroendocrinology (2015) 57, 72–83

Available online at www.sciencedirect.com

ScienceDirect

journal homepage: www.elsevier.com/locate/psyneuen

Neurogenesis-independent antidepressant-like effects of enriched environment is dependent on adiponectin

Sarah Nicolas[a,b], Julie Veyssière[a,b], Carine Gandin[a,b], Nicole Zsürger[a,b,1], Mariel Pietri[a,b], Catherine Heurteaux[a,b], Nicolas Glaichenhaus[a,b], Agnès Petit-Paitel[a,b], Joëlle Chabry[a,b,*]

[a] *Institut de Pharmacologie Moléculaire et Cellulaire, Unité Mixte de Recherche 7275, Centre National de la Recherche Scientifique 660, route des lucioles, 06560 Valbonne, France*
[b] *Université de Nice Sophia Antipolis, 28, avenue Valrose, 06103 Nice, France*

Received 8 December 2014; received in revised form 24 February 2015; accepted 21 March 2015

KEYWORDS
Adiponectin;
Anxiety;
Depression;
Enriched environment;
Behavior;
Neurogenesis

Summary Environmental enrichment (EE) that combines voluntary physical exercise, sensory and social stimuli, causes profound changes in rodent brain at molecular, anatomical and behavioral levels. Here, we show that EE efficiently reduces anxiety and depression-like behaviors in a mouse model of depression induced by long-term administration of corticosterone. Mechanisms underlying EE-related beneficial effects remain largely unexplored; however, our results point toward adiponectin, an adipocyte-secreted protein, as a main contributor. Indeed, adiponectin-deficient (adipo$^{-/-}$) mice did not benefit from all the EE-induced anxiolytic and antidepressant-like effects as evidenced by their differential responses in a series of behavioral tests. Conversely, a single intravenous injection of exogenous adiponectin restored the sensitivity of adipo$^{-/-}$ mice to EE-induced behavioral benefits. Interestingly, adiponectin depletion did not prevent the hippocampal neurogenesis induced by EE. Therefore, antidepressant properties of adiponectin are likely to be related to changes in signaling in the hypothalamus rather than through hippocampal-neurogenesis mechanisms. Additionally, EE did not modify the plasma levels of adiponectin but may favor the passage of adiponectin from the blood to the cerebrospinal fluid. Our findings provide advances in the understanding of the anxiolytic and antidepressant-like effects of EE and highlight adiponectin as a pivotal mediator.

* Corresponding author at: Institut de Pharmacologie Moléculaire et Cellulaire, 660 route des lucioles, Sophia Antipolis, 06560 Valbonne, France. Tel.: +33 4 93 95 77 48; fax: +33 4 93 95 77 08.
E-mail address: chabry@ipmc.cnrs.fr (J. Chabry).
[1] In memoriam to our friend and colleague.

http://dx.doi.org/10.1016/j.psyneuen.2015.03.017
0306-4530/

1. Introduction

In humans, psychologically stressful situations are major risk factors for appearance of anxiety and depression symptoms. Effective treatments mainly based on monoaminergic system regulation such as tricyclic antidepressants, monoamine oxidase inhibitors (MAOIs) and selective serotonin reuptake inhibitors (SSRIs) are available; however, about 40% of patients with depressive disorders are partially or completely resistant to treatments. Thus, identification of novel therapeutic targets is urgently needed.

Besides antidepressant drugs, other types of therapies for depression are frequently enforced including cognitive-behavioral therapies, dietary supplements and physical exercise. By themselves or in association with the usual medication, they can improve mood in people with mild to moderate depression and prevent relapse (Babyak et al., 2000). Little is known about the molecular basis underlying such beneficial effects. In animals, accumulating evidence indicates that environmental enrichment (EE) can mimic positive life experiences in humans. The EE model typically consists of housing rodents in enlarged groups in relatively spacious cages with a variety of objects frequently changed (e.g. running wheels, houses, tunnels, nesting material etc). EE causes an increase in hippocampal neurogenesis (Kempermann et al., 1997) and enhances learning and memory and neural plasticity (Hosseiny et al., 2014; Sale et al., 2009). EE also modulates the activity of the hypothalamo-pituitary-adrenal (HPA) axis through changes in neural circuitry in the hypothalamus (Cao et al., 2010). Recent studies demonstrated that EE reverses emotional disturbances in rodent models of neurological and psychiatric disorders including schizophrenia, depression and post-traumatic stress disorders (Takuma et al., 2011). Together, EE constitutes a suitable and relevant experimental model to decipher molecular events leading to specific and desirable changes and ultimately to the improvement of cerebral functions.

In rodents, EE has positive effects through alteration of numerous hormones and neurotransmitters including factors secreted by the adipose tissue, the adipokines (Cao et al., 2010). The most abundant adipokine, adiponectin, is released into the blood stream as full-length trimers, hexamers, high molecular weight (HMW) multimers and a globular fraction called globular adiponectin (Ouchi et al., 2003). It is primarily involved in inflammatory responses, energy expenditure and glucose and lipid homeostasis (Berg et al., 2002). Interestingly, adiponectin may have more widespread influence and functionality in the brain than previously thought (Arnoldussen et al., 2014). Indeed, the major isoforms of adiponectin receptors, adipoR1 and adipoR2, are expressed throughout the brain mainly in the hypothalamus, hippocampus and cortex (Kubota et al., 2007; Liu et al., 2012). Central actions of adiponectin have been reported including increase of oxygen consumption, thermogenesis (Qi et al., 2004) and regulation of food intake (Kubota et al., 2007). More recently, antidepressant-like properties have been ascribed to adiponectin likely through neurogenesis-dependent pathways (Liu et al., 2012; Yau et al., 2014).

Glucocorticoids are the most commonly prescribed anti-inflammatory/immunosuppressant medications worldwide; however, severe neuropsychiatric disorders including depression, suicide attempt, psychosis and panic disorder have been reported in association with glucocorticoid use (Judd et al., 2014). Hypercortisolism due to the unregulated activation of the hypothalamo-pituitary-adrenal (HPA) axis is thought to be involved in anxiety/depressive symptoms in humans. A wealth of information supports stress as a causal factor of depression, largely involving chronic stress-related HPA dysregulation and toxicity from excessive glucocorticoid release (Lupien et al., 2009). Other theories posit that a down regulation of hippocampal neurogenesis underlies the disorder (Kempermann and Kronenberg, 2003). David and coll. have established a relevant model of anxiety/depressive-like state that mimics HPA dysfunction (David et al., 2009); it consisted in a continuous input of glucocorticoid (corticosterone) in the drinking water of mice for several weeks. In this model, the abolishment of hippocampal neurogenesis blocked the efficacy of the antidepressant fluoxetine in some, but not all, behavioral paradigms, indicating that antidepressants may act through both neurogenesis-dependent and -independent mechanisms (David et al., 2009).

Here, we investigate the possible beneficial effects of EE on depression- and anxiety-relevant behaviors using the mouse model described above. We show that EE efficiently reverses anxiety/depressive-like state induced by long-term exposure to corticosterone as evaluated using a panel of behavioral tests (i.e. open-field (OF), light and dark (L&D), forced swim test (FST), novelty suppressed feeding (NSF) and learned helplessness (LH) tests). Our results point toward adiponectin as a main mediator of the ''positive stress'' since adiponectin depletion results in a partial insensitivity to beneficial effects of EE likely through neurogenesis-independent mechanisms. Antidepressant properties of adiponectin may be linked to changes in signaling in brain areas other than the hippocampus, as neuronal activation was detected only in the hypothalamus after intravenous (i.v.) injection of exogenous adiponectin.

2. Materials and methods

2.1. Materials

Globular adiponectin and corticosterone immunoassay were purchased from Enzo Life Sciences, BrdU, paraformaldehyde, corticosterone and β-cyclodextrine from Sigma.

2.2. Mice

Four week-old male wt or adiponectin knockout (adipo$^{-/-}$) mice with the same C57BL/6J genetic background were randomly assigned into different treatment groups and housed at 22 °C with a 12-h light-dark cycle (lights on at 07:00) with free access to beverage and chow (A04, SAFE). Mice housed either in standard ''SE'' (six/cage of $32L \times 17W \times 15H$ cm i.e. 91 cm^2/mouse) or enriched environment ''EE'' (twelve/cage of $57L \times 40W \times 20H$ cm i.e. 190 cm^2/mouse) received corticosterone (35 mg/l dissolved in tap water containing 4 g/l β-cyclodextrine) *ad libitum* or vehicle alone for six consecutive weeks. While the SE cages

contained sawdust only, the EE cages contained, in addition, two running wheels, tunnels, nests, scales, colored toys, hammocks and nesting materials; items were changed twice a week.

Animal procedures were conducted in compliance with the Institutional Animal Care and Use Committee of the University of Nice-Sophia Antipolis (permission number 010344.01 from the French ''Ministère de l'Enseignement Supérieur et de la Recherche'').

2.3. Behavioral studies

Before each trial, all devices were thoroughly cleaned with 70% ethanol and dried.

2.3.1. Open-field (OF) activity and light-dark (L&D) preference tests

Anxiety-like behavior was determined using the OF and L&D preference tests as previously described (Kinsey et al., 2007; Bailey et al., 2009; Wohleb et al., 2011). For the OF test, mice were placed in the corner of the test apparatus ($45L \times 45W \times 25H$ cm Plexiglas box) and activity was recorded for 5 min. Mice with anxiety-like behavior entered the center less often, delayed the first entry and spent less time in the center of the arena. For light and dark preference, the test apparatus ($40L \times 30W \times 25H$ cm) was divided into two equal zones with a doorway connecting the two sides. The light zone was very bright (200 lx) while the dark zone was protected from light by an opaque lid. To initiate testing, mice were placed into the light side and activity was recorded for 5 min. Anxiolytics have been found to increase time spent in the light zone.

2.3.2. Forced swim test (FST)

Mice were placed into glass buckets (20 cm diameter, 30 cm deep, filled with water 22 °C ± 0.5 °C). As described previously by (Porsolt et al., 1977), only the last 4 min were scored for immobility duration. A mouse was considered immobile when it remained floating in an upright position with only slight movements to keep its head above water (Pechnick et al., 2004).

2.3.3. Novelty suppressed feeding (NSF)

NSF is a conflict test that elicits competing motivations: the drive to eat and the fear of venturing into the center of the brightly lit arena. The testing apparatus consisted of a plastic box ($45L \times 45W \times 25H$ cm) with 2 cm of wooden bedding on the floor and a single pellet of food in the center. Mice were fasting for 20-h prior testing. At the time of testing, an animal was placed in a corner of the box, and the entire session was videotaped (i.e. 10 min period). The latency to eat (defined as the mouse sitting on its haunches and biting the pellet) was timed. Immediately after the test, food consumption was measured for 5 min as control for potential feeding differences.

2.3.4. Learned helplessness (LH)

Mice were placed into the shock chamber and exposed to inescapable shocks comprised of 360 footshocks (intensity: 0.3 mA, duration: 2 s, interval-episode: 10 s). The shock procedure was repeated four consecutive days. The fifth day, learned helplessness was assessed by testing shuttle box performance with footshocks in each trial as followed (intensity: 0.3 mA, duration: maximum 24 s, inter-trial interval: 60 s). The parameter ***escape latency*** was recorded as the time needed to shuttle into the other compartment after onset of footshocks, and ***failure*** when no attempt to escape was made. Total time of testing for helplessness lasted about 20—24 min, the exact time period depending on the animal's ability to learn the paradigm. Control animals underwent the same handling and contextual procedures without receiving the footshocks.

2.3.5. Rotarod

The motor coordination was assessed using the rotarod test. Mice were placed on a rotating wheel for two 5 min-habituation phases on fixed rod (4 rpm/min) 4 h apart. Twenty-four hours later, the latency to fall was recorded on accelerating rod (from 4 to 40 rpm/min). The retention duration on the rod was an index of motor coordination.

All behavioral tests and biological analyses of blood and fecal samples were done after a 6-week period of housing. Individual cohorts of mice were subjected to i—BrDU injections, ii—feces, blood sampling and tissue collection, iii—CSF sampling, iv—behavioral tests (one test *per* day, order of testing: L&D, OF, rotarod, NSF and FST), v—tail flick and LH.

2.4. Measurement of adiponectin in CSF and plasma

Mice were anesthetized with an i.p. injection of sodium pentobarbital; then CSF (2—5 μl) was obtained by cisternal puncture. Blood was collected simultaneously from the heart. Adiponectin concentration was measured using the ALPCO™ immunoassay ELISA according to the manufacturer's protocol.

2.5. I.c.v. and systemic and injections of adiponectin

For i.c.v. injections, wt mice were anesthetized with a ketamine (100 mg/kg) and xylazine (10 mg/kg) mixture. The mouse was fixed thanks to ear bars on a stereotaxic apparatus (Kopf) on heating mat and the skull was exposed, then i.c.v. injections (0.3 μg of adiponectin in 2 μl of NaCl 0.9% or vehicle alone) were performed using a Hamilton micro-syringe (cerebral lateral ventricle coordinates: −0.22 mm posterior and 1 mm lateral to the bregma; depth 2.0 mm) at 0.2 μl/min. To test the permeability of the BBB, globular adiponectin (1 mg/kg, 100 μl) or NaCl 0.9% (100 μl) was injected in the tail vein (i.v.) of vigil adipo$^{-/-}$ mice. Based on previous reports (Kubota et al., 2007; Qi et al., 2004), the behavioral tests were performed 2 h post-injection. Then, perfusions were performed by intracardiac puncture of saline solution following by fixation with 3.2% paraformaldehyde. Brains were collected and prepared for paraffin inclusion prior immunochemistry studies.

2.6. cFos immunohistochemistry

Coronal sections (8 μm) from fixed and parafin-included brains were cut with a microtome (Leica), and then cFos immunohistochemistry was performed on free-floating slices. Briefly, sections were dehydrated through successive ethanol bath, then incubated in Tris 50 mM pH 8 containing proteinase K (10 μg/ml) for 30 min at 37 °C. The slides were rinsed in PBS, treated in PBS H_2O_2 0.3% for 10 min, permeabilized in PBS Tween 0.3% for 10 min followed by a blocking step in PBS goat serum 2.5% for 2 h at room temperature prior incubation in the same buffer containing the rabbit anti-cFos antibody (1:150; Enzo) overnight at 4 °C. The sections were incubated in biotin-conjugated species-specific secondary antibodies (1:400; Vector Laboratories) for 2 h followed by a peroxidase—avidin complex solution according to the manufacturer's protocol. The peroxidase activity of immune complexes was visualized with DAB staining using the VectaStain ABC kit (Vector Laboratories). Sections through the hypothalamus from five mice *per* treatment were examined using an Olympus microscope.

2.7. Hippocampal neurogenesis assay

During the third week of housing in SE or EE, mice were i.p. injected with BrdU (50 mg/kg of body weight) once a day for five consecutive days. Twenty-one days after the last injection of BrdU, mice were euthanized and transcardially perfused with cold PBS then fixed with 3.2% paraformaldehyde. Serial coronal brain sections were cut (40 μm) throughout the hippocampus (from bregma 3.3 to 5.3) on a vibratome (Leica). Eight sections (one every fifth section) throughout the hippocampus were processed for BrdU immunohistochemistry. Briefly, floating slides were first incubated for 1 h at room temperature in PBS containing 2.5% horse serum, overnight at 4 °C with a mouse monoclonal anti-BrdU antibody (1:7500; Becton-Dickinson) and finally for 2 h in biotin-conjugated species-specific secondary antibodies. The DAB staining were performed as described above. BrdU-labeled cells in the subgranular layer (SGL) and granule cell layer (GCL) were counted in each section ($n = 5$ mice *per* group) at 40× magnification under a light microscope (Olympus). The total number of BrdU-positive cells per eight slices was multiplied by five to obtain the total number of cells *per* dentate gyrus.

2.8. Statistical analysis

Two-way analysis of variance (ANOVA) was performed using GraphPad Prism 4.0 software for treatment and environment effects, and when warranted, *post hoc* Bonferroni multiple comparisons were carried out. When the sample size was small ($n \leq 12$) and/or when a normal distribution cannot be assumed, the appropriate non-parametric Kruskal—Wallis analysis was applied followed by a Mann—Whitney test for comparisons between two independent groups. Due to the lack of normal distribution, the data from NSF test were analyzed by a Kaplan—Meier followed by a Wilcoxon-Peto-Peto test to evaluate difference between groups. Results from data analysis were expressed as mean ± standard error of the mean (SEM). Statistical significance was set at * $P < 0.05$ and ** $P < 0.01$, *** $P < 0.001$.

3. Results

3.1. Behavioral effects of EE in a stress-related mouse model of anxiety and depression

Several studies have confirmed that long-term exposure to glucocorticoids induces anxiety and depressive-like states in rodents (Murray et al., 2008; David et al., 2009). We sought to investigate the potential beneficial effects of housing in an enriched environment (EE) on anxiety and depression-like states. To do so, C57BL/6J mice housed either in "standard" (SE) or EE conditions were exposed continuously to a low dose of corticosterone in drinking water for six weeks. At the end of the treatment, a set of standardized behavioral tests routinely used to evaluate the anxiety and depressive-like states in mice (David et al., 2009) was performed. We first assessed the anxiety behavior of SE-housed mice in both open-field (OF) and light-dark (L&D) paradigms (Crawley, 2008) (Fig. 1A and 1B, *black bars*). As expected, corticosterone-treated mice exhibited reduced time spent (Fig. 1A *left*), enhanced latency of first entry in the center of the arena as well as reduced time spent in the aversive lighted chamber of the L&D device (Fig. 1B *right)* compared to vehicle-treated mice indicating that corticosterone treatment had a marked effect on anxiety parameters. Interestingly, the anxiety phenotype was reversed by EE housing in both vehicle- and corticosterone-treated groups. A significant main effect of interaction between environment and treatment was measured for the time spent in the center of the OF (Fig. 1A; environment: $F_{1,34} = 7.9$; $P = 0.01$; treatment: $F_{1,34} = 6.92$; $P = 0.012$, interaction: $F_{1,34} = 5.29$; $P = 0.03$). No significant difference in locomotor activity was found between groups as measured by total distance traveled in the OF paradigm (data not shown). Long-term treatment with corticosterone did not alter the motor coordination as assessed by the retention time in the rotarod test (Fig. 1.C *black bars;* interaction: $F_{1,34} = 0.09$; $P = 0.82$). Besides, EE-housed mice performed better in the rotarod since their retention time was higher than that of SE mice in both vehicle and corticosterone conditions (Fig. 1C). Altogether, we showed that EE housing prevents anxiety and strengthens motor coordination of mice in both basal and stress-induced conditions.

Second, we assessed the effect of chronic corticosterone treatment on depression-like behavior using the FST, the NSF and the LH paradigms. The FST is a well-standardized paradigm to evaluate resignation and despair states in mice. We found first that corticosterone treatment had no effect in the immobility duration in the FST (Fig. 1D, *black dots*), and second that EE led to a significant decrease of this parameter independently of the treatment (Fig. 1D, *white dots*; interaction: $F_{1,73} = 1.65$; $P = 0.2$). In the NSF test, we found that chronic corticosterone treatment led to a significant increase in the latency to feed (Fig. 1E, Kaplan—Meier survival analysis, Wilcoxon-Peto-Peto test, * $P < 0.05$). EE housing significantly decreased the latency to feed of both vehicle- and corticosterone-treated mice (Fig. 1E, *white dots*)

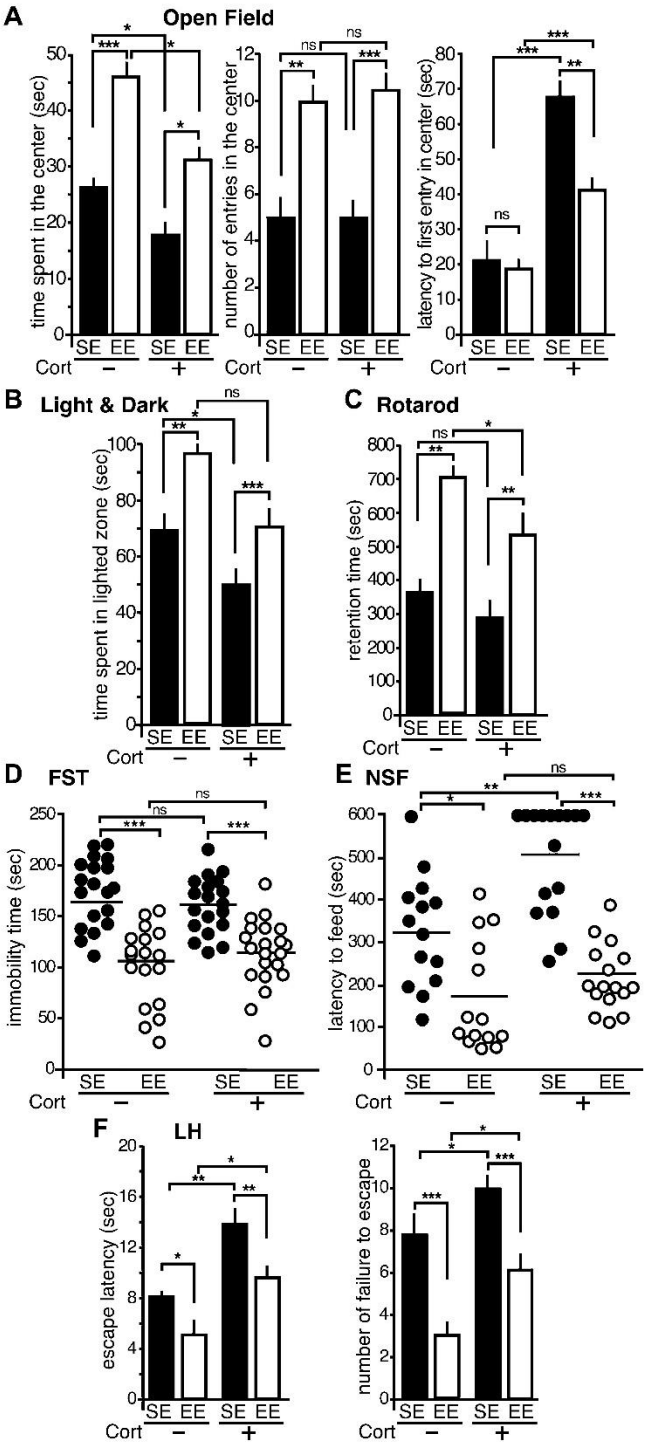

without affecting the home food consumption (Fig. S1). Mice were also tested in a learned helplessness (LH) paradigm, a depression model in which mice are exposed for four consecutive days to inescapable aversive electric footshocks (Chourbaji et al., 2005). On the day test, corticosterone-treated mice exhibited longer escape latency as compared to vehicle-treated mice housed in SE conditions (Fig. 1F, *left*). Over the time course of testing, EE housing shortened the latency to escape in corticosterone- and vehicle-treated groups (Fig. 1F, *left*, environment: $F_{1,44} = 74.9$; $P = 0.001$; treatment: $F_{1,44} = 89.2$; $P = 0.001$, interaction: $F_{1,44} = 4.3$; $P = 0.043$). Long-term exposure to corticosterone significantly increased the number of failure to escape (Fig. 1F, *right*). Importantly, EE housing efficiently reduced this parameter with or without corticosterone treatment (Fig. 1F, *right*). To rule out pain sensitivity as a confounding factor in the learned helplessness test, mice were submitted to the tail-flick test enabling an assessment of acute pain. No difference in the latency of tail withdrawal was found between groups in the tail-flick test indicating that the pain sensibility was not altered by the treatment (Fig. S2).

Altogether, our data suggest that high levels of sensory and motor stimuli provided by EE prevent anxiety and depression-like states in a mouse model of depression.

3.2. Variation of adiponectin levels in plasma and CSF as a function of environmental conditions

We sought to examine whether environmental conditions modify adiponectin concentrations in blood and CSF. Concentrations of the total, high and mid/low oligomeric complexes of adiponectin were assayed in the plasma and CSF of control and long-term exposed-corticosterone mice housed either in SE or EE (Fig. 2). Neither housing conditions nor treatment modified the plasma concentration of adiponectin (Fig. 2A). In marked contrast, EE housing led to a four-fold increase in the concentration of total, and among them, mid/low forms of adiponectin in CSF of mice challenged by chronic corticosterone (Fig. 2B, *white hatched bars*) whereas no difference was measured in the CSF of vehicle-treated mice (Fig. 2B). Neither corticosterone treatment nor housing conditions resulted in alterations of the CSF concentration of high molecular complexes of adiponectin (Fig. 2B).

Fig. 1 *Behavioral effects of a 6 week-period of EE housing in vehicle- and chronic corticosterone-treated wt mice.* (A) Anxiety behavior of vehicle- (−) and corticosterone-treated (+) mice housed for 6 weeks either in SE (*black*) or EE (*white*) were assessed in the open-field test. Measured features are the time spent in the aversive center of the arena (*left*), the number of entries in the centre (*middle*) and the latency to first entry (*right*). Values plotted are means ± SEM, $n = 16$–20 *per* group, (B) anxiety behavior was assessed in the light and dark paradigm by recording the time spent in the lighted aversive area. Data are the means ± SEM, $n = 16$–20 *per* group, (C) the motor coordination was assessed by the time of retention on the rotarod (means ± SEM, $n = 16$–20 *per* group). Anxiety and depressive-like phenotypes of vehicle- (−) and corticosterone-treated (+) mice housed either in SE or EE were assessed by the time of immobility in the FST (D) and the latency to feed in the NSF (E). The NSF test was stopped after a 10 min-period. Each dot represents an animal; the horizontal bars are means. (F) Depressive-like behavior of vehicle- and corticosterone-treated mice housed either in SE or EE was assessed by the latency to escape an inescapable footshock in the LH test. The latency to escape in seconds is the mean of data for 5 consecutive sessions (*left*), the number of failure to escape was represented (*right*). Values are means ± SEM ($n = 12$ *per* group). ns, non significant; * $P < 0.05$, ** $P < 0.01$; *** $P < 0.001$.

3.3. Behavioral effects of cerebral administration of exogenous adiponectin in the FST

We next investigated whether the direct administration of exogenous adiponectin into the brain could mimic the antidepressant-like effects of EE. I.c.v. injection of recombinant globular adiponectin to vehicle- and corticosterone-treated mice housed in SE significantly decreased immobility time in the FST suggesting an antidepressant-like effect (Fig. 2C). It is unlikely that the decrease of immobility time was due to an enhancement of locomotor activity because performances on rotarod were unchanged after i.c.v. injection of adiponectin (data not shown).

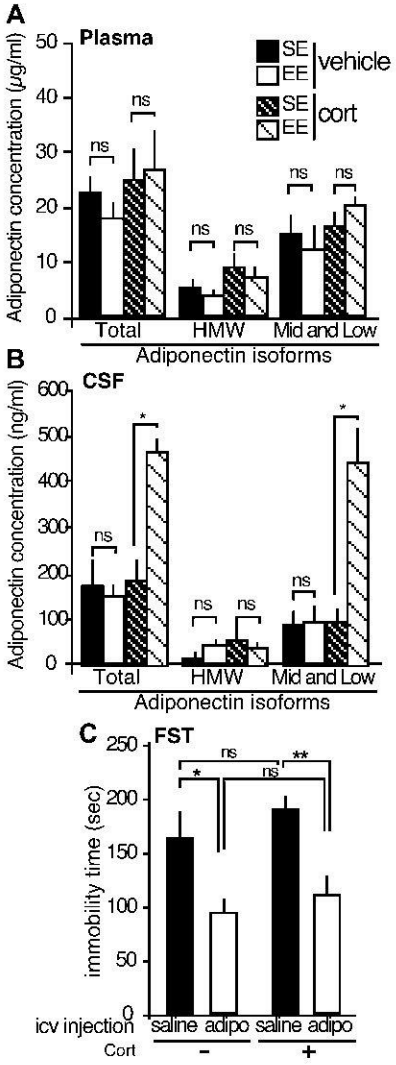

Fig. 2 *Variation of adiponectin levels in plasma and CSF as a function of housing conditions and effect of cerebral administration of exogenous adiponectin on depression-like behavior.* Concentrations of various forms of adiponectin in plasma (A) and CSF (B) of vehicle- and corticosterone-treated mice housed in SE or EE for 6 weeks. Values plotted are means ± SEM ($n = 10–12$ *per* group); ns, non significant; * $P < 0.05$. (C) Depression-like behavior was assessed by the immobility time in the FST after i.c.v. injection of 0.3 µg of globular adiponectin in vehicle- or corticosterone-treated mice housed in SE $N = 5–8$ *per* group; Mann–Whitney for comparison between two groups; ns, non significant; * $P < 0.05$; ** $P < 0.01$.

3.4. Behavioral characterization of adipo$^{-/-}$ mice as a function of corticosterone treatment and environmental housing conditions

To investigate whether adiponectin plays a role in the antidepressant-like effects of EE, adipo$^{-/-}$ mice housed either in SE or EE were challenged with chronic corticosterone administration. The corticosterone treatment significantly increased anxiety and depression-like behaviors of adipo$^{-/-}$ mice when assessed in the open field (time spent and latency of first entry in the center, Fig. 3A *left* and *right*, respectively), light and dark (Fig. 3B) and LH paradigms (Fig. 3F). Surprisingly, EE housing has no effect on the performances of adipo$^{-/-}$ mice in the open field (i.e. two-way ANOVA; time spent in the aversive area; interaction: $F_{1,44} = 0.63$; $P = 0.43$; the number of entries; interaction: $F_{1,44} = 2.09$; $P = 0.163$; latency to first entry in the center of the arena; interaction: $F_{1,44} = 0.08$; $P = 0.7$; Fig. 3A) and in the light and dark test (i.e. time spent in the light area, interaction: $F_{1,44} = 0.5$; $P = 0.48$; Fig. 3B) as compared to SE. EE-housed performed better in the rotarod test than SE-housed adipo$^{-/-}$ mice (Fig. 3C). Moreover, adipo$^{-/-}$ mice exhibited similar performances in FST whatever the housing and treatment conditions (Fig. 3D; two-way ANOVA, interaction: $F_{1,44} = 0.012$; $P = 0.9$). In contrast, EE housing significantly decreased latency to feed in the NSF test (Fig. 3E; Kaplan–Meier for SE *versus* EE groups; $P < 0.001$ and $P < 0.01$ for vehicle- and corticosterone, respectively). In the LH test, latency to escape and the number of failure to escape were decreased in EE conditions independently of the treatment. Two-way ANOVA analysis revealed the lack of significant main effect for these latter parameters (latency to escape, interaction: $F_{1,44} = 1.2$; $P = 0.23$; number of failure to escape, interaction: $F_{1,44} = 1.0$; $P = 0.31$). In the tail-flick test, latencies of tail withdrawal were similar between adipo$^{-/-}$ mouse groups (Fig. S2).

In summary, EE-housing prevented anxiety and depression-like behaviors in both wt and adipo$^{-/-}$ mice when assessed through the NSF and LH tests whereas it was found to be efficient only in wt mice when assessed through the open field, the light and dark and the FST (Table 1). These differences cannot be explained by differential metabolism of corticosterone between both mouse strains since fecal concentrations of corticosterone were similar in adipo$^{-/-}$ and wt mice whatever the housing conditions (Fig. S3; two-way ANOVA, interaction: $F_{1,36} = 0.21$; $P = 0.65$).

3.5. Adiponectin is not required for EE-induced hippocampal neurogenesis

To investigate the potential cellular mechanisms underlying the differential behavioral effects of EE in wt *versus* adipo$^{-/-}$ mice, we next evaluated changes in adult hippocampal neurogenesis and neuronal survival (i.e. 21 days post-BrdU injections) (Fig. 4). First, we found that chronic corticosterone treatment decreased the number of BrdU-positive hippocampal cells in the dentate gyrus of wt and

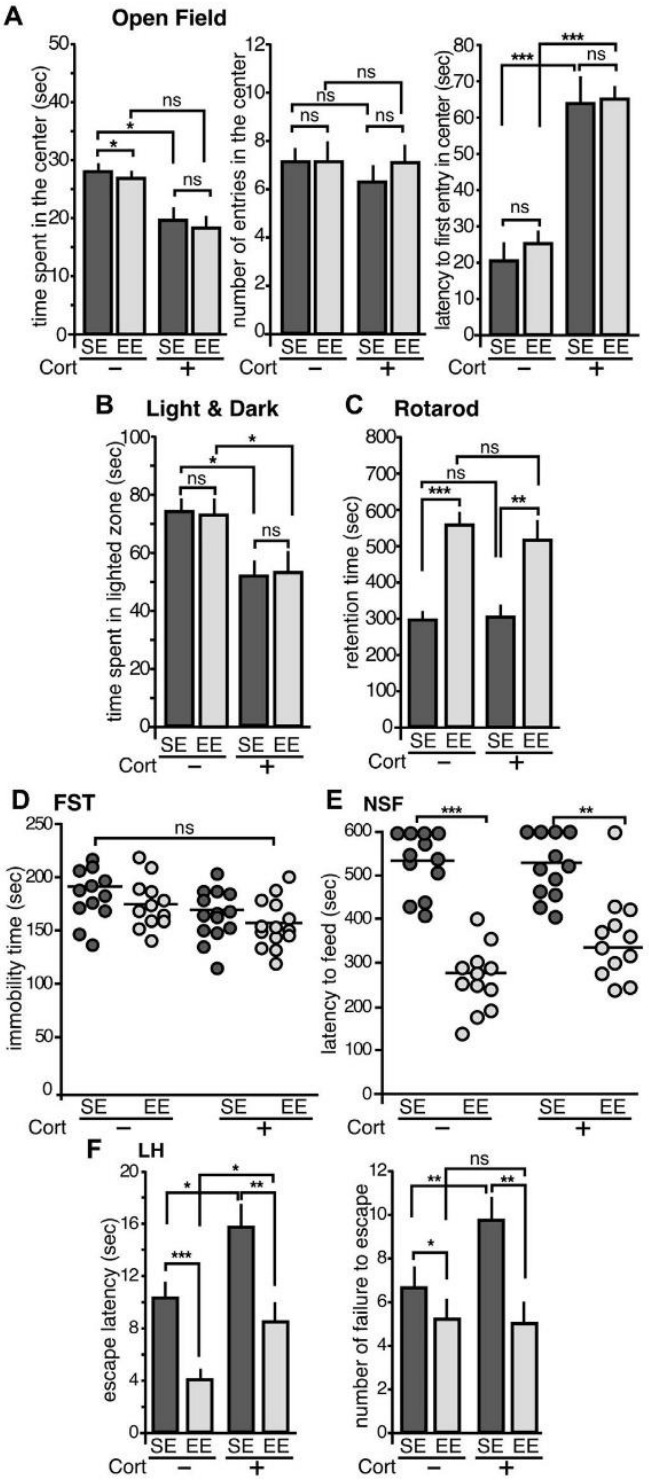

Fig. 3 *Role of adiponectin in mediating the behavioral effects of EE housing.* Control (−) and chronically corticosterone-treated (+) adipo$^{-/-}$ mice were submitted to a series of behavioral tests after a 6 week-period of SE (*dark grey*) or EE (*light grey*) housing in order to evaluate anxiety and depression-like phenotypes. (A) Measured features in the open field are the time spent in the aversive center of the arena (*left*), the number of entries (*middle*) and the latency to first entry in the centre (*right*). (B) Anxiety behavior was assessed by the time spent in the lighted aversive area of the light and dark paradigm. (C) The motor coordination was measured by the time of retention on the rotarod device. Depression-like behavior of adipo$^{-/-}$ mice was assessed by the immobility duration in the FST (D) and the latency to feed in the NSF (E). (F) Depression-like behavior of SE- and EE-housed adipo$^{-/-}$ mice was assessed by the latency to escape an inescapable footshock in the LH test upon chronic vehicle or corticosterone treatment. The escape latency is the mean of data for the entire session (*left*). The number of failure to escape during the entire session was represented (*right*). All values are mean ± SEM ($n = 12–14$ *per* group); ns, non significant; * $P < 0.05$, ** $P < 0.01$; *** $P < 0.001$.

adipo$^{-/-}$ mice (Fig. 4B; Mann–Whitney for vehicle *versus* cort groups; $P < 0.001$ and $P = 0.02$ for wt and adipo$^{-/-}$ mice, respectively). Upon corticosterone exposure as well as in basal conditions, EE-housed wt mice exhibited a number of BrdU-positive hippocampal cells significantly higher than SE-housed mice (Fig. 4B; Mann–Whitney for SE *versus* EE groups; $P < 0.01$). A similar result was found in adipo$^{-/-}$ mice (Fig. 4C; Mann–Whitney for SE *versus* EE groups; $P < 0.05$ and $P < 0.01$ for vehicle and cort groups, respectively). Therefore, adiponectin deficiency did not affect EE-enhanced neuronal survival and neurogenesis.

3.6. Adiponectin enters the CSF from the blood circulation differentially as a function of housing conditions and mediates EE-induced antidepressive-like properties

In order to investigate the influence of housing conditions on central actions of circulating adiponectin, SE- and EE-housed adipo$^{-/-}$ mice chronically treated with corticosterone were i.v. injected with exogenous adiponectin (Fig. 5). I.v. injection of adiponectin induced a significant decrease in the immobility time in EE-housed mice without major effects in SE-housed ones (Fig. 5A; Mann–Whitney for SE *versus* EE groups; ns, non significant for saline injections; $P < 0.01$ for adiponectin injections). Thus, a single systemic injection of adiponectin restored the sensitivity of adipo$^{-/-}$ to beneficial effects of EE in the FST. No significant effect of adiponectin was found on locomotor activity as measured by rotarod performance whatever the housing conditions (Fig. 5B; Mann–Whitney for SE *versus* EE groups; $P < 0.05$ for saline and adiponectin injections).

Then, we chose to target the hypothalamus, a brain area strongly involved in HPA axis regulation (20) and expressing adiponectin receptors (Liu et al., 2012). We compared potential targets of exogenous adiponectin in hypothalamus of adipo$^{-/-}$ mice using cFos immunohistochemistry. Three hours post adiponectin i.v. administration, cFos-positive cells were detectable in hypothalamus of adipo$^{-/-}$ mice housed in EE but not or, to a lesser extend in SE (Fig. 5C and D; Mann–Whitney for SE *versus* EE; ** $P < 0.01$). No cFos-positive immunoreactivity was observed in other brain area including hippocampus and cortex (data not shown). These results strongly suggest that plasma adiponectin enters the CSF differently depending on housing conditions and preferentially targets the hypothalamus.

4. Discussion

Here, we used a well-characterized model of anxiety/depressive-like model in mice consisting in a continuous input of glucocorticoids (David et al., 2009) in an attempt to further understanding and characterize the beneficial effects of EE. As a reliable readout of the anxiety/depression-like state, we performed a panel of behavioral tests generally used in the context of depression (FST, NSF and LH—David et al., 2009; Malberg and Duman, 2003; Revest et al., 2009; Santarelli et al., 2003) and anxiety studies (OF, L&D—David et al., 2009; Saxe et al., 2006). In all paradigms, a 6 week-period of EE housing successfully reversed the corticosterone-induced anxiety/depression in wt mice. The protocol of EE-housing set up appeared as efficient as antidepressant drugs like fluoxetine or imipramine when used in a similar anxiety/depression mouse model (David et al., 2009).

The FST is commonly used as a suitable assay for seeking antidepressants (Bogdanova et al., 2013); the immobility duration being an index of mouse ''despair'' or resignation (Porsolt et al., 1977). In agreement with a previous publication (Liu et al., 2012), we confirm the antidepressant properties of adiponectin since we show that a single i.c.v. injection of exogeneous adiponectin leads to a decrease in the immobility time in the FST test.

One of the major findings of our study is that adiponectin plays a pivotal role in mediating some but not all behavioral effects of EE. Both neurogenesis-dependent and -independent pathways are likely to be implemented to the achievement of antidepressant-like activity of EE. The current prevalent area in the depression research field largely focuses on ''the neurogenic hypothesis'', whereas little is known about the molecular mechanisms involved in the neurogenesis-independent pathways. However, because suppression of hippocampal neurogenesis does not always cause depression, it is still controversial whether new neurons are absolutely required for remission of the disease (Eisch and Petrik, 2012; Hanson et al., 2011). EE failed to produce anxiolytic and antidepressant actions in adipo$^{-/-}$ mice when assessed through OF, L&D and FST; however it remained efficient when assessed through NSF and LH (Table 1). The efficacy of antidepressants in NSF and LH requires chronic administration and has been reported to be neurogenesis dependent (David et al., 2009; Malberg, 2004; Malberg and Duman, 2003; Santarelli et al., 2003). In other hand, OF, L&D and FST are behavioral assays that do not involved hippocampal neurogenesis mechanisms (David et al., 2009; Saxe et al., 2006). Thus, it is tempting to postulate that adiponectin mediates antidepressant properties of EE through neurogenesis-independent pathways. In accordance to this assumption, we showed that EE enhances to similar extents neurogenesis and survival of neural progenitors in the dentate gyrus of wt and adipo$^{-/-}$ mice suggesting that adiponectin deficiency has no or minor impact on EE-induced neurogenesis. Our results may seem in disagreement with a recent publication showing that adiponectin may play a role in mediating the antidepressant effects of physical exercise through a neurogenesis-dependent pathway (Yau et al., 2014). However, although voluntary exercise is a major component of EE housing, this latter also provides high levels of sensory and exploratory stimuli as

Table 1 Behavioral effects of EE in wt and adipo$^{-/-}$ mice in basal and corticosterone conditions.

EE housing[a]		Open field			Light & dark	FST	NSF	LH		Rotarod
		Time spent	Number of entries	Latency to first entry	Time spent in the light	Immobility duration	Latency to feed	Latency to escape	Number of failures to escape	Retention duration
Vehicle	wt	↑	↑	0	↑	↓	↓	0	↓	↑
	adipo$^{-/-}$	0	0	0	0	0	↓	↓	↓	↑
Cort	wt	↑	↑	↓	↑	↓	↓	↓	↓	↑
	adipo$^{-/-}$	0	0	0	0	0	↓	↓	↓	↑

Summary of the effects assessed in multiple behavioral tests throughout the study. 0, no effect; ↑, increased parameter; ↓, decreased parameter.

[a] *Versus* the corresponding SE group.

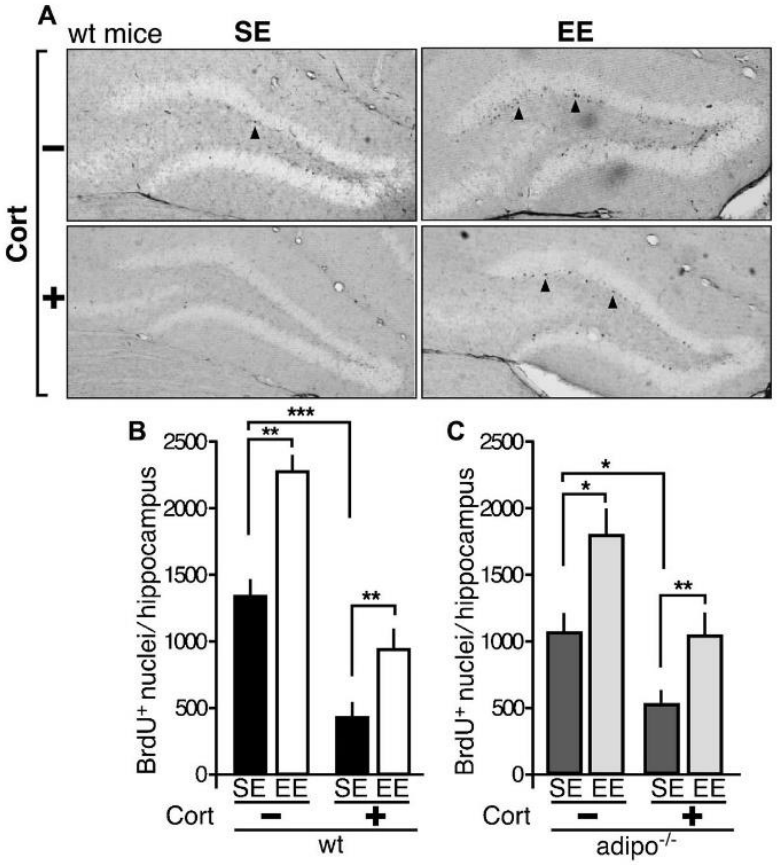

Fig. 4 *Neurogenesis in the dentate gyrus of the hippocampus is increased by EE in both adipo*$^{-/-}$ *and wt corticosterone-treated mice.* (A) Representative photomicrographs of BrdU-labeled nuclei (*arrowheads*) of dentate gyrus slices from mouse brains as a function of the treatment and the housing conditions. Histograms presenting the mean number of BrdU-positive nuclei (±SEM) counted in the dentate gyrus from vehicle- (−) and corticosterone-treated (+) wt (B) or adipo$^{-/-}$ mice (C) housed either in SE or EE. Mann–Whitney for comparison between groups; $n = 5$ mice *per* group; ns, non significant; * $P < 0.05$, ** $P < 0.001$, *** $P < 0.001$.

well as social interactions. In this context, one can imagine that in our experimental conditions, other molecules than adiponectin specifically regulated by EE may increase hippocampal neurogenesis and could account for such discrepancies.

EE housing may produce more complex and subtle biological changes in multiple brain areas compared to physical exercise alone. To explore the mechanism underlying the neurogenesis-independent effects of EE, we focused on the hypothalamus, a brain structure involved in antidepressant action of fluoxetine (David et al., 2009) as well as in EE-induced behaviors (Cao et al., 2010). The ability of adiponectin to target and activate hypothalamus cells has been demonstrated previously using cFos immunoreactivity as marker (Qi et al., 2004). We explored the distribution of cFos-positive cells throughout the brain of SE and EE-housed mice 3 h post i.v. injection of exogeneous globular adiponectin. We found that a single i.v. injection of adiponectin leads to a significant elevation of the number of adiponectin-activated neurons selectively in the hypothalamus from EE- compared to SE-housed adipo$^{-/-}$ mice. Interestingly, both adipoR1 and adipoR2 have been detected in various brain areas including hypothalamus (Kubota et al., 2007; Liu et al., 2012). While adipoR1 binds to globular adiponectin with high affinity, adipoR2 has an intermediate binding affinity for both globular and full-length adiponectin. The expression of adipoRs is regulated by numerous physiological and biological factors including circadian rhythm, feeding state, levels of circulating free fatty acids and insulin. Interestingly, voluntary exercise specifically up-regulates adipoR1 expression (Christiansen et al., 2010; Zeng et al., 2007). Nollet et al. (2012) suggested that the restoration of stress-related HPA axis defect by pharmacological blockade of the orexinergic system could induce antidepressant-like effects independently from a neurogenic action. Thus, one possibility is that adiponectin action may mediate the antidepressant-like effects of EE by modulating the activity of neural circuits in the hypothalamus rather than through a hippocampal neurogenesis-dependent pathway. By targeting hypothalamic cells, adiponectin could restore the functioning of the HPA axis and improve some depressive behaviors independently of hippocampal neurogenesis. Further experiments will be required to define whether and how adiponectin may modulate direct and/or indirect circuit connections between the hypothalamus and the brain areas implicated in mood disorders such as amygdala, hippocampus and dorsal raphe.

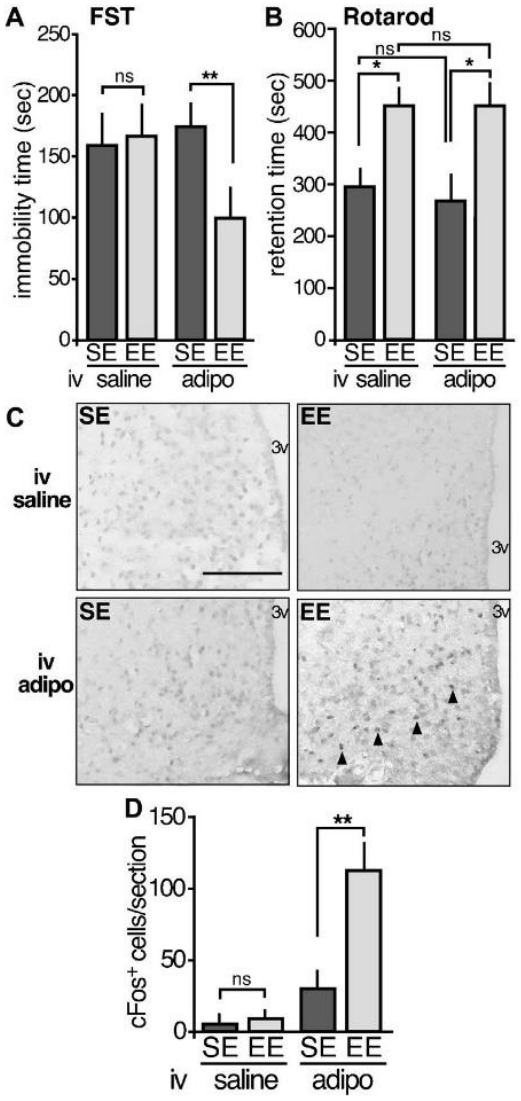

Fig. 5 *Effect of intravenous (i.v.) injections of exogenous adiponectin in depression-like behavior and cFos immunostaining in the hypothalamus of adipo$^{-/-}$ mice.* Depression-like behavior was assessed by the immobility time in the FST (A) and the motor coordination by the time of retention on the rotarod (B) 2 h after i.v. injection of NaCl 0.9% (saline) or globular adiponectin (1 mg/kg, 100 μl) in chronically corticosterone-treated adipo$^{-/-}$ mice housed either in SE or EE. $N = 6–7$ *per* group; Mann–Whitney for comparison between groups; ns, non significant; * $P < 0.05$; ** $P < 0.01$. Series of photomicrographs (C) and quantification (D) showing the distribution of adiponectin-induced cFos-immunoreactivity (*arrowheads*) in coronal sections of hypothalamus from corticosterone-treated SE- and EE-housed adipo$^{-/-}$ mice 3 h after i.v. injection of saline or adiponectin (1 mg/kg, 100 μl). 3v, third ventricle; scale bar, 100 μm. Means of 4 coronal sections of hypothalamus counted *per* mouse ± SEM; $n = 5$ mice *per* group; Mann–Whitney for comparison between groups; ** $P < 0.01$.

The adiponectin transport from the blood to the CSF seems to be modulated as a function of environmental conditions and/or psychological state. The fenestrated epithelium in close vicinity to the hypothalamus is a main site controlling the entry of molecules into the brain (Schwartz and Porte, 2005). EE profoundly alters the function of endothelial cells (During and Cao, 2006) thus may alter the blood brain barrier (BBB) permeability, but it could also affect features of the cerebral blood circulation and/or permeability of *glia limitans*. The enhancement of the transport of adiponectin to the brain parenchyma could constitute a mechanism aimed at counteracting the deleterious effects on behavior produced by corticosterone challenging and drastic conditions such as chronic stress and HPA dysfunction. Supporting this idea, i.v. injection of adiponectin induced a decrease of the immobility time in the FST paradigm in EE- but not SE-housed adipo$^{-/-}$ mice. This phenotype is unlikely to be caused by an indirect action of adiponectin on peripheral target tissues (e.g. muscles) since no change in locomotor activity performance was observed. Additionally, EE housing evoked an elevation of the low-MW adiponectin concentration in the CSF of EE-housed wt mice compared to SE. These data suggest that the enriched living conditions might favor the transport of low-MW adiponectin from the blood to the CSF.

Once synthesized and assembled in the secretory pathway of the adipocyte, adiponectin complexes circulate as biochemical distinct and stable entities with little evidence of interchange between the different forms including HMW species, hexamer (Mid MW), and trimer (Low MW) isoforms. The globular adiponectin, which forms only trimers, derives from the proteolytic cleavage of the full-length adiponectin. Whether or not the adiponectin and which species are able to cross the BBB remains a matter of controversy. In agreement with others (Qi et al., 2004), we showed that the mid/low adiponectin species are the only ones to be found in the CSF of wt mice. Moreover, we found that the level of total adiponectin was about 100 times lower in CSF than in the blood (Qi et al., 2004). Owing to possible blood contamination, the adiponectin concentration assay in brain areas is tricky and inconsistent. This reason prompted us to neglect this parameter despite previous report (Yau et al., 2014).

At odds with previous reports (Cao et al., 2010), no significant elevation of the blood adiponectin concentration was found in mice housed in EE *versus* SE. This could be explained by difference of diet, duration and/or age of mice at the onset of EE and alternatively by sensitivity of the adiponectin assays used. Nevertheless, the level of plasma adiponectin appears to be an unreliable biomarker of anxiety/depression state. It should be taken with caution, as it does not reflect faithfully the cerebral component of adiponectin. This may explain the discrepancies of the literature about plasma adiponectin concentration and anxiety/depression state in humans (Jeong et al., 2012; Diniz et al., 2012). Indeed, an association between circulating adiponectin levels and anxious and depressive symptoms has been proposed but so far with inconsistent results.

5. Conclusions

Altogether, our study defines adiponectin as a key molecule required for some of the anxiolytic and antidepressant effects of EE. Interestingly, our results also allow discriminating between adiponectin-independent antidepressant effects that involve hippocampal neurogenesis from other adiponectin-dependent effects of EE. These latter effects

could involve the modulation of neuronal activity in the neural circuits of hypothalamus. Development of selective hypothalamic adipoR agonists may represent a promising alternative therapeutic strategy to treat depressive disorders.

Role of funding source

Fundings were from the Centre national de la Recherche Scientifique.

Conflict of interest statement

No conflict of interest.

Acknowledgments

We are grateful to Dr S. Martin for critically reviewing the manuscript and C. Widman for help in statistical analysis. Special thanks are due to Drs A. Guyon and T. Lorivel for fruitful discussions all along the accomplishment of this study. We are also grateful to Dr V. Bouet (Université de Caen Basse-Normandie, France) for advices on EE housing setting up and L. Relmy for taking care of mice.

Appendix A. Supplementary data

Supplementary data associated with this article can be found, in the online version, at http://dx.doi.org/10.1016/j.psyneuen.2015.03.017.

References

Arnoldussen, I.A., Kiliaan, A.J., Gustafson, D.R., 2014. Obesity and dementia: adipokines interact with the brain. Eur. Neuropsychopharmacol. 24 (12), 1982—1999.

Babyak, M., Blumenthal, J.A., Herman, S., Khatri, P., Doraiswamy, M., Moore, K., Craighead, W.E., Baldewicz, T.T., Krishnan, K.R., 2000. Exercise treatment for major depression: maintenance of therapeutic benefit at 10 months. Psychosom. Med. 62, 633—638.

Bailey, M.T., Kinsey, S.G., Padgett, D.A., Sheridan, J.F., Leblebicioglu, B., 2009. Social stress enhances IL-1beta and TNF-alpha production by *Porphyromonas gingivalis* lipopolysaccharide-stimulated CD11b+ cells. Physiol. Behav. 98, 351—358.

Berg, A.H., Combs, T.P., Scherer, P.E., 2002. ACRP30/adiponectin: an adipokine regulating glucose and lipid metabolism. Trends Endocrinol. Metab. 13, 84—89.

Bogdanova, O.V., Kanekar, S., D'Anci, K.E., Renshaw, P.F., 2013. Factors influencing behavior in the forced swim test. Physiol. Behav. 118, 227—239.

Cao, L., Liu, X., Lin, E.J., Wang, C., Choi, E.Y., Riban, V., Lin, B., During, M.J., 2010. Environmental and genetic activation of a brain-adipocyte BDNF/leptin axis causes cancer remission and inhibition. Cell 142, 52—64.

Chourbaji, S., Zacher, C., Sanchis-Segura, C., Dormann, C., Vollmayr, B., Gass, P., 2005. Learned helplessness: validity and reliability of depressive-like states in mice. Brain Res. Brain Res. Protoc. 16, 70—78.

Christiansen, T., Paulsen, S.K., Bruun, J.M., Ploug, T., Pedersen, S.B., Richelsen, B., 2010. Diet-induced weight loss and exercise alone and in combination enhance the expression of adiponectin receptors in adipose tissue and skeletal muscle, but only diet-induced weight loss enhanced circulating adiponectin. J. Clin. Endocrinol. Metab. 95, 911—919.

Crawley, J.N., 2008. Behavioral phenotyping strategies for mutant mice. Neuron 57, 809—818.

David, D.J., Samuels, B.A., Rainer, Q., Wang, J.W., Marsteller, D., Mendez, I., Drew, M., Craig, D.A., Guiard, B.P., Guilloux, J.P., Artymyshyn, R.P., Gardier, A.M., Gerald, C., Antonijevic, I.A., Leonardo, E.D., Hen, R., 2009. Neurogenesis-dependent and -independent effects of fluoxetine in an animal model of anxiety/depression. Neuron 62, 479—493.

Diniz, B.S., Teixeira, A.L., Campos, A.C., Miranda, A.S., Rocha, N.P., Talib, L.L., Gattaz, W.F., Forlenza, O.V., 2012. Reduced serum levels of adiponectin in elderly patients with major depression. J. Psychiatr. Res. 46, 1081—1085.

During, M.J., Cao, L., 2006. VEGF, a mediator of the effect of experience on hippocampal neurogenesis. Curr. Alzheimer Res. 3, 29—33.

Eisch, A.J., Petrik, D., 2012. Depression and hippocampal neurogenesis: a road to remission? Science 338, 72—75.

Hanson, N.D., Owens, M.J., Nemeroff, C.B., 2011. Depression, antidepressants, and neurogenesis: a critical reappraisal. Neuropsychopharmacology 36, 2589—2602.

Hosseiny, S., Pietri, M., Petit-Paitel, A., Zarif, H., Heurteaux, C., Chabry, J., Guyon, A., 2014. Differential neuronal plasticity in mouse hippocampus associated with various periods of enriched environment during postnatal development. Brain Struct. Funct., http://dx.doi.org/10.1007/s00429-014-0865-y.

Jeong, H.G., Min, B.J., Lim, S., Kim, T.H., Lee, J.J., Park, J.H., Lee, S.B., Han, J.W., Choi, S.H., Park, Y.J., Jang, H.C., Kim, K.W., 2012. Plasma adiponectin elevation in elderly individuals with subsyndromal depression. Psychoneuroendocrinology 37, 948—955.

Judd, L.L., Schettler, P.J., Brown, E.S., Wolkowitz, O.M., Sternberg, E.M., Bender, B.G., Bulloch, K., Cidlowski, J.A., Ronald de Kloet, E., Fardet, L., Joels, M., Leung, D.Y., McEwen, B.S., Roozendaal, B., Van Rossum, E.F., Ahn, J., Brown, D.W., Plitt, A., Singh, G., 2014. Adverse consequences of glucocorticoid medication: psychological, cognitive, and behavioral effects. Am. J. Psychiatry 171, 1045—1051.

Kempermann, G., Kronenberg, G., 2003. Depressed new neurons—-adult hippocampal neurogenesis and a cellular plasticity hypothesis of major depression. Biol. Psychiatry 54, 499—503.

Kempermann, G., Kuhn, H.G., Gage, F.H., 1997. More hippocampal neurons in adult mice living in an enriched environment. Nature 386, 493—495.

Kinsey, S.G., Bailey, M.T., Sheridan, J.F., Padgett, D.A., Avitsur, R., 2007. Repeated social defeat causes increased anxiety-like behavior and alters splenocyte function in C57BL/6 and CD-1 mice. Brain Behav. Immun. 21, 458—466.

Kubota, N., Yano, W., Kubota, T., Yamauchi, T., Itoh, S., Kumagai, H., Kozono, H., Takamoto, I., Okamoto, S., Shiuchi, T., Suzuki, R., Satoh, H., Tsuchida, A., Moroi, M., Sugi, K., Noda, T., Ebinuma, H., Ueta, Y., Kondo, T., Araki, E., Ezaki, O., Nagai, R., Tobe, K., Terauchi, Y., Ueki, K., Minokoshi, Y., Kadowaki, T., 2007. Adiponectin stimulates AMP-activated protein kinase in the hypothalamus and increases food intake. Cell Metab. 6, 55—68.

Liu, J., Guo, M., Zhang, D., Cheng, S.Y., Liu, M., Ding, J., Scherer, P.E., Liu, F., Lu, X.Y., 2012. Adiponectin is critical in determining susceptibility to depressive behaviors and has antidepressant-like activity. Proc. Natl. Acad. Sci. U.S.A. 109, 12248—12253.

Lupien, S.J., McEwen, B.S., Gunnar, M.R., Heim, C., 2009. Effects of stress throughout the lifespan on the brain, behaviour and cognition. Nat. Rev. Neurosci. 10, 434—445.

Malberg, J.E., 2004. Implications of adult hippocampal neurogenesis in antidepressant action. J. Psychiatry Neurosci. 29, 196—205.

Malberg, J.E., Duman, R.S., 2003. Cell proliferation in adult hippocampus is decreased by inescapable stress: reversal by fluoxetine treatment. Neuropsychopharmacology 28, 1562—1571.

Murray, F., Smith, D.W., Hutson, P.H., 2008. Chronic low dose corticosterone exposure decreased hippocampal cell proliferation, volume and induced anxiety and depression like behaviours in mice. Eur J Pharmacol. 583 (1), 115—127.

Nollet, M., Gaillard, P., Tanti, A., Girault, V., Belzung, C., Leman, S., 2012. Neurogenesis-independent antidepressant-like effects on behavior and stress axis response of a dual orexin receptor antagonist in a rodent model of depression. Neuropsychopharmacology 37, 2210—2221.

Ouchi, N., Kihara, S., Funahashi, T., Nakamura, T., Nishida, M., Kumada, M., Okamoto, Y., Ohashi, K., Nagaretani, H., Kishida, K., Nishizawa, H., Maeda, N., Kobayashi, H., Hiraoka, H., Matsuzawa, Y., 2003. Reciprocal association of C-reactive protein with adiponectin in blood stream and adipose tissue. Circulation 107, 671—674.

Pechnick, R.N., Chesnokova, V.M., Kariagina, A., Price, S., Bresee, C.J., Poland, R.E., 2004. Reduced immobility in the forced swim test in mice with a targeted deletion of the leukemia inhibitory factor (LIF) gene. Neuropsychopharmacology 29, 770—776.

Porsolt, R.D., Le Pichon, M., Jalfre, M., 1977. Depression: a new animal model sensitive to antidepressant treatments. Nature 266, 730—732.

Qi, Y., Takahashi, N., Hileman, S.M., Patel, H.R., Berg, A.H., Pajvani, U.B., Scherer, P.E., Ahima, R.S., 2004. Adiponectin acts in the brain to decrease body weight. Nat. Med. 10, 524—529.

Revest, J.M., Dupret, D., Koehl, M., Funk-Reiter, C., Grosjean, N., Piazza, P.V., Abrous, D.N., 2009. Adult hippocampal neurogenesis is involved in anxiety-related behaviors. Mol. Psychiatry 14, 959—967.

Sale, A., Berardi, N., Maffei, L., 2009. Enrich the environment to empower the brain. Trends Neurosci. 32, 233—239.

Santarelli, L., Saxe, M., Gross, C., Surget, A., Battaglia, F., Dulawa, S., Weisstaub, N., Lee, J., Duman, R., Arancio, O., Belzung, C., Hen, R., 2003. Requirement of hippocampal neurogenesis for the behavioral effects of antidepressants. Science 301, 805—809.

Saxe, M.D., Battaglia, F., Wang, J.W., Malleret, G., David, D.J., Monckton, J.E., Garcia, A.D., Sofroniew, M.V., Kandel, E.R., Santarelli, L., Hen, R., Drew, M.R., 2006. Ablation of hippocampal neurogenesis impairs contextual fear conditioning and synaptic plasticity in the dentate gyrus. Proc. Natl. Acad. Sci. U.S.A. 103, 17501—17506.

Schwartz, M.W., Porte Jr., D., 2005. Diabetes, obesity, and the brain. Science 307, 375—379.

Takuma, K., Ago, Y., Matsuda, T., 2011. Preventive effects of an enriched environment on rodent psychiatric disorder models. J. Pharmacol. Sci. 117, 71—76.

Wohleb, E.S., Hanke, M.L., Corona, A.W., Powell, N.D., Stiner, L.M., Bailey, M.T., Nelson, R.J., Godbout, J., Sheridan, J.F., 2011. β-Adrenergic receptor antagonism prevents anxiety-like behavior and microglial reactivity induced by repeated social defeat. J. Neurosci. 31, 6277—6288.

Yau, S.Y., Li, A., Hoo, R.L., Ching, Y.P., Christie, B.R., Lee, T.M., Xu, A., So, K.F., 2014. Physical exercise-induced hippocampal neurogenesis and antidepressant effects are mediated by the adipocyte hormone adiponectin. Proc. Natl. Acad. Sci. U.S.A. 111, 15810—15815.

Zeng, Q., Isobe, K., Fu, L., Ohkoshi, N., Ohmori, H., Takekoshi, K., Kawakami, Y., 2007. Effects of exercise on adiponectin and adiponectin receptor levels in rats. Life Sci. 80, 454—459.

D- Article 7 : “Area-specific development of distinct projection neuron subclasses is regulated by postnatal epigenetic modifications”

Le cerveau est un organe complexe et nous sommes encore loin de comprendre la totalité des signaux à l’origine de son organisation en structures distinctes (hippocampe, amygdale, …). Le cortex, qui est une de ces structures, est impliqué dans de nombreux processus très variés tels que les mouvements ou la pensée « consciente ». Sa complexité est liée à son organisation particulière, non seulement en aires corticales (motrice, sensorielle, visuelle, …) mais également en couches neuronales bien distinctes (couches I à VI). Au cours du développement cortical, l'identité des principales classes de neurones de projection est établie par l'expression de déterminants moléculaires. Cependant, les mécanismes par lesquels les neurones de projection acquièrent leurs propriétés finales au cours des stades postnataux sont encore mal élucidés. Dans cette étude, nous avons montré que le nombre de neurones co-exprimant Ctip2 et Satb2, deux marqueurs respectivement impliqués dans la différenciation précoce des neurones de projections sous-cérébrales et callosales, augmente progressivement après la naissance dans le cortex somatosensoriel. Cette co-localisation postnatale de Ctip2/Satb2 caractérise deux sous-classes neuronales distinctes qui projettent non seulement vers le cortex contralatéral mais également vers le tronc cérébral. Cela suggère que si Ctip2 et Satb2 seuls sont des marqueurs d’identité neuronale, leur co-expression serait plutôt impliquée dans la modulation de leurs propriétés. Des approches de gain et perte de fonction ont ensuite révélé que l'adaptateur transcriptionnel Lmo4 est impliqué dans ce programme de maturation au travers de la modulation de mécanismes épigénétiques qu’il induit en fonction du temps et de la zone concernée.

En d’autres termes, cette analyse fournit les premières preuves directes d'un programme de développement commun qui oriente la maturation moléculaire, et donc cellulaire, des différents neurones de projection. Ce qui pourrait avoir des implications importantes dans l'étude du développement néocortical, puisque les " homologies sérielles " (i.e. : une connectivité ou des codes moléculaires similaires) entre les régions néocorticales pourraient donc être dues à des variations d’un " schéma commun ", plutôt qu'à de multiples programmes génétiques indépendants et spécifiques à une région donnée.

eLIFE elifesciences.org

RESEARCH ARTICLE

Area-specific development of distinct projection neuron subclasses is regulated by postnatal epigenetic modifications

Kawssar Harb[1,2,3], Elia Magrinelli[1,2,3], Céline S Nicolas[1,2,3], Nikita Lukianets[1,2,3], Laura Frangeul[4], Mariel Pietri[1,2,3], Tao Sun[5], Guillaume Sandoz[1,2,3], Franck Grammont[1,6], Denis Jabaudon[4], Michèle Studer[1,2,3*†], Christian Alfano[1,2,3*†]

[1]Institut de Biologie Valrose, University of Nice Sophia Antipolis, Nice, France; [2]Institut de Biologie Valrose, Institut national de la santé et de la recherche médicale, Nice, France; [3]Centre national de la recherche scientifique, Institut de Biologie Valrose, Nice, France; [4]Department of Basic Neurosciences, University of Geneva, Geneva, Switzerland; [5]Department of Cell and Developmental Biology, Weill Medical College of Cornell University, New York, United States; [6]Laboratoire J.A. Dieudonné, Nice, France

Abstract During cortical development, the identity of major classes of long-distance projection neurons is established by the expression of molecular determinants, which become gradually restricted and mutually exclusive. However, the mechanisms by which projection neurons acquire their final properties during postnatal stages are still poorly understood. In this study, we show that the number of neurons co-expressing Ctip2 and Satb2, respectively involved in the early specification of subcerebral and callosal projection neurons, progressively increases after birth in the somatosensory cortex. Ctip2/Satb2 postnatal co-localization defines two distinct neuronal subclasses projecting either to the contralateral cortex or to the brainstem suggesting that Ctip2/Satb2 co-expression may refine their properties rather than determine their identity. Gain- and loss-of-function approaches reveal that the transcriptional adaptor Lmo4 drives this maturation program through modulation of epigenetic mechanisms in a time- and area-specific manner, thereby indicating that a previously unknown genetic program postnatally promotes the acquisition of final subtype-specific features.
DOI: 10.7554/eLife.09531.001

***For correspondence:** michele.studer@unice.fr (MS); Christian.ALFANO@unice.fr (CA)

†These authors contributed equally to this work

Competing interests: The authors declare that no competing interests exist.

Funding: See page 22

Received: 18 June 2015
Accepted: 13 December 2015
Published: 27 January 2016

Reviewing editor: Jonathan A Cooper, Fred Hutchinson Cancer Research Center, United States

Introduction

The mammalian cerebral cortex is tangentially subdivided into several functional areas allowing effective interactions with the external world by organizing sensory information into a coherent perceptual model of the environment. All neocortical areas are radially organized into six neuronal layers that show prominent diversities in features and functions despite similarities in their laminar organization. This is mainly due to differences in the molecular identity, morphology and long-range connectivity of residing neurons (***Greig et al., 2013***; ***Huang, 2014***; ***O'Leary et al., 2007***). Cortical projection neurons (PNs) can be subdivided into three major classes: (i) the intra-telencephalic (IT) neurons projecting to ipsilateral and/or, through the corpus callosum, to contralateral regions of the telencephalon (i.e. callosal projection neurons – CPN); (ii) the cortico-thalamic (CT) neurons projecting to different dorsal thalamic nuclei; and (iii) the pyramidal-tract (PT) neurons, also defined as subcerebral projection neurons (SCPN), that innervate different subcerebral targets, such as the striatum, the brainstem, and the spinal cord (***Harris and Shepherd, 2015***; ***Shepherd, 2013***).

eLife digest The cerebral cortex is part of the outer layer of the mammalian brain, and it is important for a range of processes, including sensing, movement and conscious thought. The cerebral cortex is subdivided into several areas that are deputed to different functions. Each area is composed of an astounding variety of cells called projection neurons, which send information from the cerebral cortex to distant parts of the brain.

There are three main types of projection neurons, which each connect to a different brain region. However, when projection neurons first form in the embryo, they are all broadly similar. They then activate a combination of genes that determine their identity and behaviour through the activity of a vast range of transcription factors (proteins that control gene expression). At first, most of these transcription factors are active in more than one type of cortical neuron, but after the animal is born, these proteins become increasingly restricted to just one type of neuron. In this way, the major classes of projection neurons are specified. However, the mechanisms defining the remarkable variety of projection neuron subtypes in the cerebral cortex are still largely unknown.

Two of the transcription factors that act in the development of the major classes of projection neurons are called Satb2 and Ctip2. Satb2 prevents the activity of Ctip2, since the two proteins have opposite effects. However, some neurons in newborn animals produce both of these transcription factors.

Using mouse models, Harb et al. found that just after birth the number of projection neurons that express both Ctip2 and Satb2 increases in the cortical area that processes touch sense information – called the somatosensory cortex. These neurons are divided into two subclasses, each of which communicates with a different part of the brain. This suggests that Ctip2/Satb2 co-expression defines two subgroups of the major projection neuron classes rather than specifying new cell types.

Further investigations revealed that after birth Satb2 and Ctip2 are co-expressed in neurons due to another protein (called Lmo4) that modifies the structure of the DNA region that contains the Ctip2 gene. This prevents Satb2 from repressing Ctip2.

This work demonstrates that the great variety of projection neurons in the mammalian cerebral cortex is not due to the existence of several genetic programs directing the development of each single neuronal subtype. Instead, this variety is due to mechanisms that modify and refine, after birth, the processes that specify the major projection neuron classes. The main challenge in the future will be deciphering all the mechanisms that tilt the balance toward a given neuron subtype, and investigating whether and how this balance can be altered.

DOI: 10.7554/eLife.09531.002

Major molecular determinants of CPN and SCPN neuronal classes (***Greig et al., 2013***; ***Leone et al., 2008***; ***Molyneaux et al., 2007***; ***Srinivasan et al., 2012***) act by both promoting the identity of a given neuronal class and repressing alternative ones (***Fame et al., 2011***; ***Greig et al., 2013***; ***Kiritani et al., 2012***; ***Molnar and Cheung, 2006***; ***Molyneaux et al., 2007***; ***Reiner et al., 2010***; ***Sohur et al., 2014***). For example, Satb2, a chromatin remodeling protein, drives CPN specification and axonal pathfinding, and represses the expression of the transcription factor Ctip2 (gene name *Bcl11b*), which controls the connectivity of SCPN (***Alcamo et al., 2008***; ***Arlotta et al., 2005***; ***Baranek et al., 2012***; ***Britanova et al., 2008***; ***Srivatsa et al., 2014***). However, Satb2 was shown to control also subcerebral connectivity (***Leone et al., 2014***), indicating that the final acquisition of a given cell type is not based on the function of a unique transcriptional regulator but most probably on the combination of more determinants expressed at different levels. This is in agreement with observations performed on early embryonic stages, where neuronal types are not yet fully specified and factors with mutually exclusive functions largely overlap. Notably, expression of transcriptional determinants tends to segregate after birth in a cell- or time-specific manner when neurons differentiate and the major neocortical classes become more distinct from each other (reviewed in ***Greig et al., 2013***). Nevertheless, it is still not clear whether the transcriptional regulators acting during early stages of neuronal specification play any additional roles during postnatal maturation when PNs acquire their final properties. Even if antithetic factors promoting callosal or subcerebral PNs can co-localize in a small subset of neurons after birth (***Azim et al., 2009***; ***Baranek et al., 2012***;

Leone et al., 2008; *Tomassy et al., 2010*), it is not known whether their co-expression has a functional meaning, nor whether this hybrid molecular population corresponds to a permanent subgroup of cortical PNs. In particular, the persistence of few double Ctip2/Satb2-positive neurons at early postnatal stages of corticogenesis represents a conundrum, since Satb2 is a strong repressor of Ctip2 (*Alcamo et al., 2008*; *Baranek et al., 2012*; *Britanova et al., 2008*; *Leone et al., 2014*). Moreover, Satb2 and Ctip2 regulate the expression of two netrin1 receptors (Unc5C and DCC, respectively) with opposite effects on axon guidance (*Srivatsa et al., 2014*).

Here, we show that Ctip2/Satb2 co-expression does not delineate a transient stage of cortical development but instead distinct subpopulations of major PN classes, whose number progressively increases in the postnatal somatosensory mouse cortex. Double Ctip2/Satb2 (C/S+)-expressing cells define at least two neuronal subclasses, which project either to the brainstem or to the contralateral cortex and retain unique molecular, morphological, and electrophysiological features that distinguish them from single Ctip2- or Satb2-expressing cells. Moreover, we demonstrate that the transcriptional adaptor Lmo4 allows the co-localization of Ctip2 and Satb2 by competing with Satb2 for the binding to Hdac1, a histone deacetylase normally recruited by the Satb2-NuRD complex bound to the Ctip2 locus (*Alcamo et al., 2008*; *Britanova et al., 2008*). Notably, the distribution of both Lmo4+ and C/S+ cell populations in lower layers change over time in the cortical motor and somatosensory areas during postnatal stages of development.

Overall, we show that common molecular pathways may regulate different specification programs during postnatal maturation and/or refinement of functionally distinct classes of neocortical neurons (such as IT and PT neurons) in an area- and time-specific manner.

Results

A consistent subpopulation of cortical lower layer neurons postnatally co-expresses Ctip2 and Satb2

Previous studies reported transient embryonic Ctip2/Satb2 (C/S+) co-expression in the developing cortical plate; however, whether this co-expression persists at postnatal stages was still unclear (*Alcamo et al., 2008*; *Baranek et al., 2012*; *Britanova et al., 2008*; *Leone et al., 2014*). We thus examined the number and distribution of C/S+ cells from E14.5 to P21 to investigate whether they constitute a transient or rather a permanent population of cortical PNs. We first observed that while the number of single Ctip2+ and double C/S+ cells strongly decreases in the cortical plate from E14.5 to E16.5, as previously reported (*Leone et al., 2014*), double C/S+ (but not single Ctip2+) cells resurge between E16.5 and P0 (*Figure 1A and B*) and constitute 18% of lower layer (LL) neurons of the somatosensory cortex (S1) by P21 (*Figure 1B*). Then, to verify whether the postnatal increase of C/S+ neurons was due just to a general increment in Ctip2 and Satb2 expression, we calculated the percentage of C/S+ cells on the total of Ctip2+ or Satb2+ cells and found an increase with respect to both populations (*Figure 1C*).

Next, we investigated whether this population of C/S+ neurons was differentially distributed between frontal/motor (F/M) and parietal/somatosensory cortices. Interestingly, we observed that the highest percentage of C/S+ cells is primordially localized in layer V of the F/M cortex at P0, whereas the corresponding layer of the prospective somatosensory (pS) region has five times less double-positive cells (*Figure 1D*). When calculated on the total of Ctip2+ cells, the percentage of C/S+ neurons only slightly changes between F/M and pS, whereas it results four times higher in the F/M cortex with respect to the total of Satb2+ cells (*Figure 1—figure supplement 1A*). This trend is inverted at P7, where the highest percentage of double C/S+ cells in LL is localized in the primary somatosensory area (S1) (*Figure 1E* and *Figure 1—figure supplement 1B*), suggesting the existence of a time- and region-specific mechanism allowing Ctip2 expression in Satb2+ cells.

Taken together, our data reveal the progressive postnatal and area-specific development of a molecularly hybrid neuronal subpopulation co-expressing two transcriptional regulators with mutually exclusive functions in cortical development.

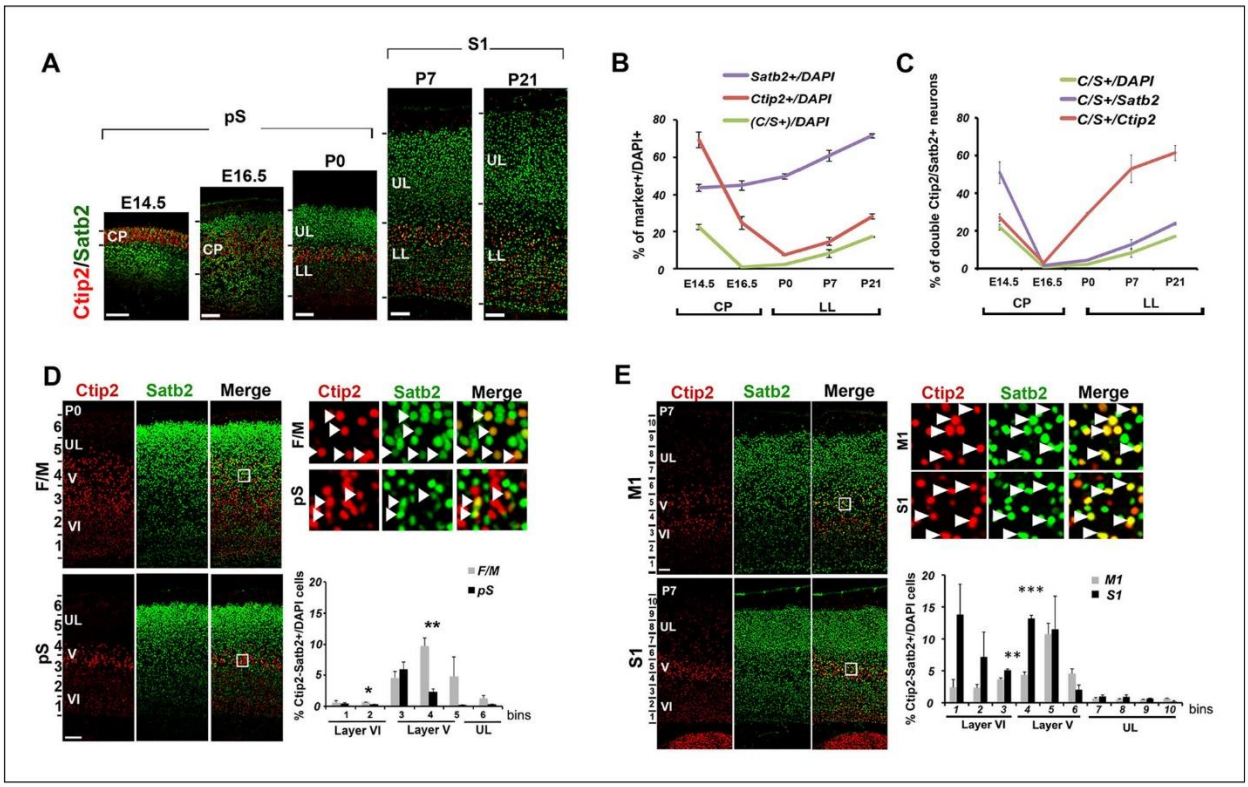

Figure 1. Temporal and areal distribution of Ctip2/Satb2+ neurons in the neocortex. (**A**). Coronal sections from prospective (pS) and primary (S1) somatosensory areas of E14.5, E16.5, P0, P7, and P21 cortices immunolabeled for Ctip2 and Satb2. (**B**). Percentage of Satb2+, Ctip2+, and double Ctip2/Satb2 (C/S+) neurons on the total number of DAPI+ neurons in the cerebral cortex at different ages. The counting was performed in the cortical plate (CP) from E14.5 to E16.5 and only in lower layers (LL) from P0 to P21. (**C**). Number of C/S+ neurons calculated as a percentage of DAPI+, Satb2+, and Ctip2+ cortical neurons at different ages. (**D**). Immunostaining for Satb2 and Ctip2 on P0 brain coronal sections from frontal/motor (F/M) and pS areas. Top right panels represent high-magnification views of boxes in layer V depicted in left panels. Arrowheads indicate C/S+ neurons. In bottom right panels, quantification and laminar distribution of double C/S+ neurons. (**E**). Immunostaining for Satb2 and Ctip2 on P7 brain coronal sections from primary motor (M1) and S1 cortices. Top right panels represent high-magnification views of boxes in layer V depicted in left panels. Arrowheads indicate C/S+ neurons. In bottom right panels, quantification and laminar distribution of double C/S+ neurons. Data are represented as means ± SEM. *p≤0.05, **p≤0.01, ***p≤0.001. SEM, standard error of the mean; UL, upper layers.Scale bars: A,D, E, 100 μm.

DOI: 10.7554/eLife.09531.003

The following figure supplement is available for figure 1:

Figure supplement 1. Time- and area-specific variations in the number and distribution of Ctip2/Satb2+ cells in early postnatal brains.

DOI: 10.7554/eLife.09531.004

Double Ctip2/Satb2+ neurons project to callosal and subcerebral targets

Since double C/S+ neurons are maintained at least until P21, we next investigated the molecular features and connectivity distinguishing these cells from single Ctip2+ or Satb2+ PNs. To analyze their connectivity, we injected cholera toxin subunit B (CTB)-conjugated fluorophores (***Conte et al., 2009***) into the cervical spinal cord, the rostral pontine region and ithe contralateral S1 cortex of P2/P3 pups (***Figure 2A–C***). Injections performed at the level of the spinal cord exclusively labeled corticospinal PNs (CSpPNs) (***Figure 2A***), whereas injections in the rostral pons marked all layer V subcerebral PNs (SCPN), including CSpPN, cortico-pontine (CpPN), and other cortico-brainstem (CBPN) neurons projecting through the pyramidal tract (***Figure 2B***). Immunolabeling of retrograde-traced cells at P7 revealed that C/S+ neurons constitute 31% of all subcerebral neurons; however, they do not reach the spinal cord indicating that C/S+ subcerebral neurons most probably project to the brainstem nuclei (***Figure 2A and B***). CTB injections in the contralateral S1 cortex labeled callosal projection neurons (CPN) and showed that 32% of these neurons co-expressed Ctip2 and Satb2 (***Figure 2C***).

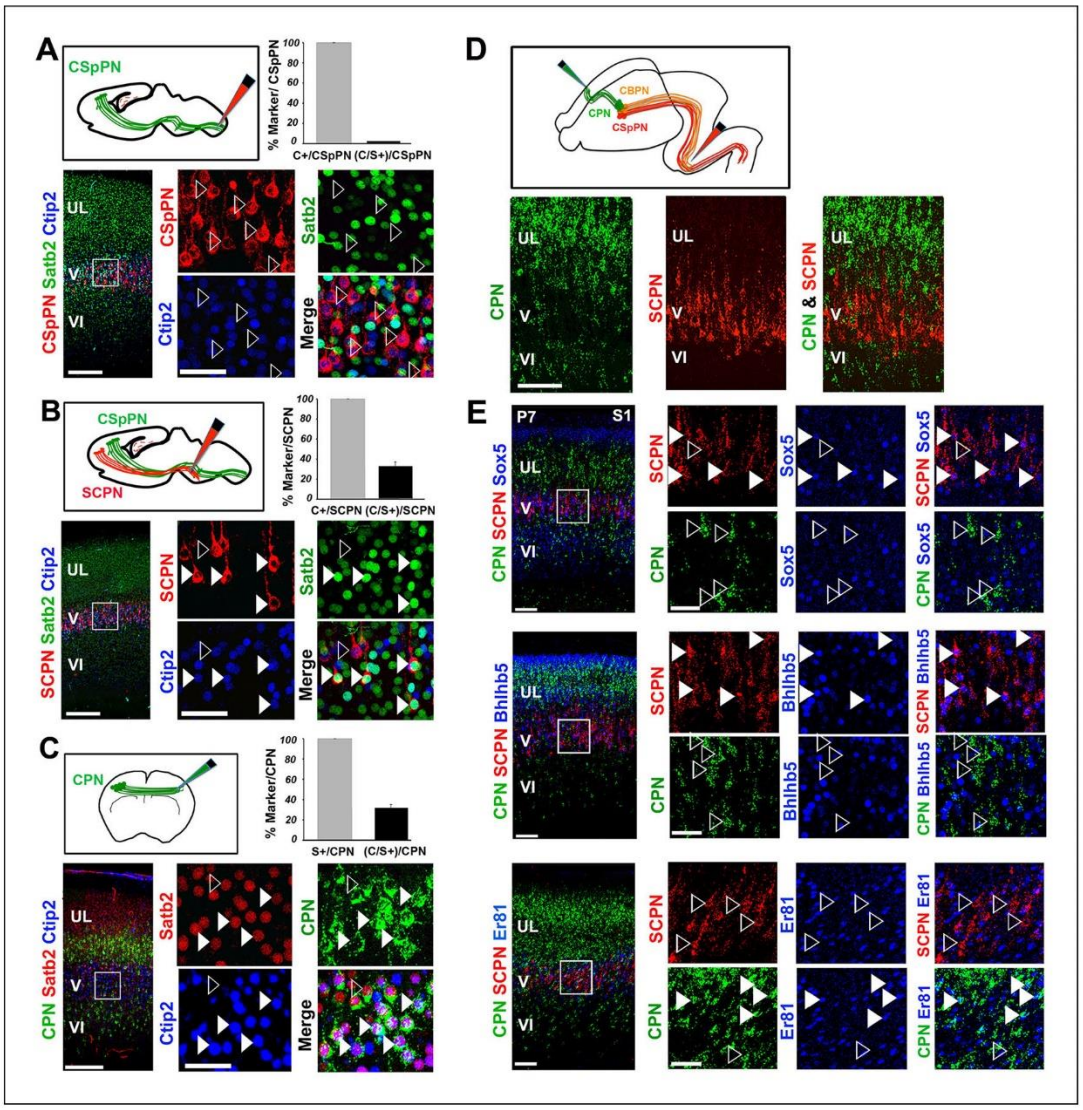

Figure 2. Ctip2 and Satb2 co-localization describes subgroups of cortico-brainstem and callosal projection neurons (**A-C**). Top left, schematic representations of cholera toxin subunit B (CTB) injections at cervical level to trace corticospinal projection neurons (CSpPNs) alone (**A**), at the midbrain/hindbrain junction to label subcerebral projection neurons (SCPN) including CSpPNs (**B**), and in the contralateral somatosensory cortex (S1) to label callosal projection neurons (CPN. (**C**). On bottom left of (**A-C**), immunostaining for Satb2 and Ctip2 on retrogradely labeled PNs of P7 S1 coronal sections. Squared panels in (**A-C**) represent high magnification views of boxes in layer V depicted in left panels. Filled arrowheads indicate retrogradely labeled neurons double labeled for Satb2 and Ctip2, while empty arrowheads indicate retrogradely labeled neurons labeled either for Ctip2 or Satb2. On top right of (**A-C**), quantification of Ctip2+ and double Ctip2/Satb2+ (C/S+) retrogradely labeled neurons on the total number of retrogradely labeled PNs in layer V. (**D**). On the top, schematic representation of the labeling paradigm to simultaneously double-label SCPN and CPN. Red retrobeads or Green IX retrobeads were injected into the midbrain/hindbrain junction at P2 and into the contralateral S1 at P3, respectively. On the bottom, panels representing labeled CPN (green) and SCPN (red) on P7 S1 coronal sections. (**E**). Left panel columns represent coronal sections traced for CPN and SCPN and immunostained for Sox5, Bhlhb5, and Er81. Panels on the right represent high-magnification views of boxes in layer V depicted in left panels. Filled white and yellow arrowheads indicate CPN or SCPN positive for the used marker, whereas empty arrowheads indicate negative staining. Scale bars: A,B,C, low-magnification images, 200 μm; D, E, low-magnification images, 100 μm; A,B,C,E, high magnifications, 50 μm. Data are represented as mean ± SEM. SEM, standard error of the mean.

DOI: 10.7554/eLife.09531.005

The following figure supplement is available for figure 2:

Figure supplement 1. Analysis of the molecular code of postnatal Ctip2/Satb2+ neurons.

DOI: 10.7554/eLife.09531.006

The observation that C/S+ neurons project to both contralateral and subcerebral targets raised the question of whether these cells constitute a hybrid population of dual-projecting neurons or two distinct subpopulations. To address this issue, CTB-coated beads were co-injected into the pons and the contralateral S1 of early postnatal brains (***Figure 2D***). No co-labeled callosal and subcerebral cells were observed in three independent experiments (***Figure 2D***), indicating that neurons co-expressing Ctip2 and Satb2 constitute two independent subpopulations: one projecting to the brainstem and the other to the contralateral hemisphere through the corpus callosum.

We then tested whether double C/S+ cells could be further distinguished by the expression of other molecular markers. We used the transcription factors Bhlhb5, highly expressed in CSpPNs of the sensorimotor cortex (***Joshi et al., 2008***), Sox5 present in the major classes of corticofugal PNs (subplate, corticothalamic and all subcerebral PNs) (***Lai et al., 2008***), and Er81(also named Etv1) expressed throughout layer V in both CPNs and SCPNs (***Molnar and Cheung, 2006***; ***Yoneshima et al., 2006***). Analyzing the distribution of these factors in C/S+ cells of P7 S1 cortices indicated that nearly 90% of C/S+ cells also express Bhlhb5, 58% Er81 and almost 70% Sox5 in layer V (***Figure 2—figure supplement 1A and B***). To further assess whether they are selective for callosal and/or subcerebral C/S+ cell subpopulations, we combined retrograde labeling with immunostaining for Bhlhb5, Er81, or Sox5 and found that Sox5 and Bhlhb5 are exclusively expressed in SCPNs, whereas Er81 solely labels CPNs in layer V (***Figure 2E***). Taken together, these data indicate that Ctip2/Satb2 co-expression describes at least two layer V subpopulations: callosal PNs co-expressing Er81, and cortico-brainstem PNs co-expressing Bhlhb5 and/or Sox5.

Morphological and electrophysiological characterization support distinct subpopulations of double Ctip2/Satb2+ neurons in S1 cortex

To unravel specific morphological and electrophysiological features of C/S+ cells, we exploited the *Thy1-eYFP-H* transgenic line, which labels layer Vb neurons from P14 onwards (***Feng et al., 2000***; ***Porrero et al., 2010***). We first verified that YFP+ neurons did express Ctip2 and Satb2 in the S1 area of P21 *Thy1-eYFP-H* cortices (***Figure 3—figure supplement 1A***). While 19.3% of GFP+ neurons resulted positive for Ctip2 but not for Satb2 (+/-) and 76.5% co-expressed Ctip2 and Satb2 (+/+), only 1.4% was positive for Satb2 alone (-/+) and 2.8% were negative for both markers (***Figure 3—figure supplement 1A and B***). In addition, YFP+/(C/S+) cells in layer V represent 55.7% of double C/S+ neurons, indicating overall that this mouse line represents an appropriate tool to undertake a detailed morphological and electrophysiological analysis of C/S+ neurons.

Comparison of different morphological features including soma shape, dendritic complexity, and apical dendrite length of YFP+ 3D-reconstructed neurons allowed the classification of C/S+ and single Ctip2+ neurons into two major subpopulations (***Figure 3A and B***). Overall, the soma of C/S+ neurons is significantly smaller in terms of diameter, area, and volume when compared to single Ctip2 neurons; moreover, it occupies on average deeper regions of layer Vand shows earlier bifurcation of the apical tuft. However, K-means clustering of all these parameters revealed that the C/S+ cells are constituted by at least three different subtypes, whereas Ctip2+ neurons by at least two (***Figure 3B–D***). Whereas subtype 1 (orange) is unique to C/S+ neurons, subtype 2 (magenta) and subtype 3 (green) are common to both groups, even if subtype 2 is prevalent in Ctip2+ cells and subtype 3 is mainly represented in C/S+ neurons. Thus, C/S+ and Ctip2+ neurons can be mainly subdivided into two distinct morphological subgroups in the P21 S1 cortex.

Since neurons with a large soma constituted broad fractions of both C/S+ and Ctip2+ populations (***Figure 3—figure supplement 1B***), we investigated whether they would differ for their respective electrophysiological characteristics. We recorded the activity of large soma YFP+ cells on P21 *Thy1-eYFP-H* brain slices and labeled recorded neurons with biocytin to subsequently test them for the expression of Ctip2 and/or Satb2 (***Figure 3E***, ***Figure 3—figure supplement 2A***). Steps of hyperpolarizing currents were first applied and the input resistance was measured, based on the I-V curves (***Figure 3F, G and G'***). Cells only expressing Ctip2 (n = 9) had a greater resistance compared to C/S + neurons (n = 23) (Ctip2+: Rpeak = 109.8 ± 11.7 MΩ and Rss = 84.8 ± 7.9 MΩ; C/S+: Rpeak = 73.3 ± 3,9 MΩ and Rss = 57.1 ± 2.3 MΩ; respectively; $p<0.05$) as well as a greater sag (difference between the voltage at peak and at steady-state: 4.6 ± 1.2 mV and 2.1 ± 0.3 mV, respectively, $p<0.05$) (***Figure 3F***), indicating that these two populations with large soma can be discriminated by their intrinsic electrical properties.

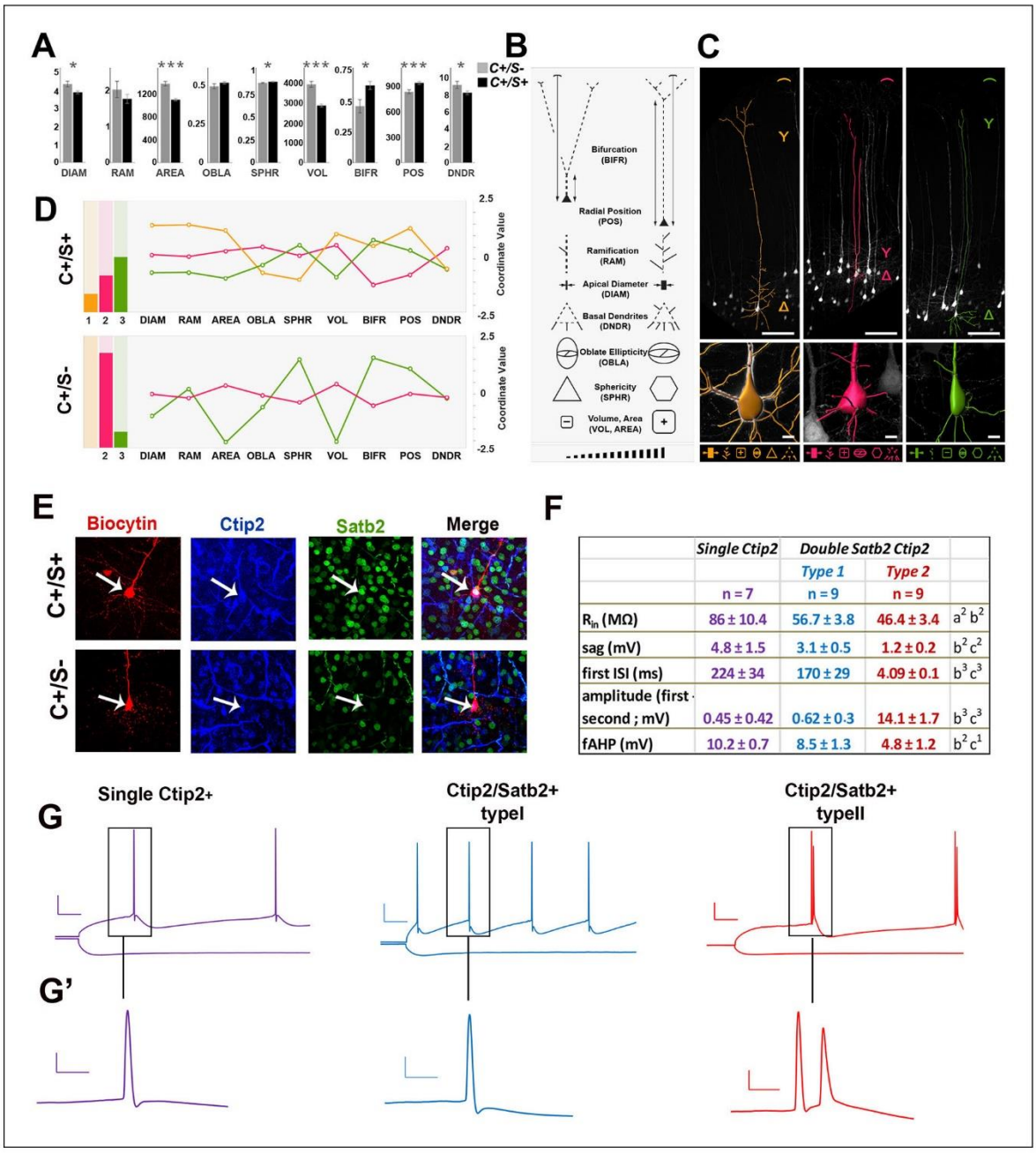

Figure 3. Morphometric and electrophysiological characterization of *Thy1-eYFP-H* layer V neurons. (**A**). The bar charts represent comparisons between double C/S+ (*black*) and single Ctip2+ (*grey*) neurons for different morphological features in YFP+ cells of P21 *Thy1-e-YFP-H* transgenic brains. The asterisks indicate statistical significance. *p≤0.05, **p≤0.01, ***p≤0.001. (**B**). Pictograms used to schematically illustrate morphological features and qualitative differences among YFP+ neurons. (**C**). 3D reconstructions of representative neurons of the three distinct morphological profiles. Upper part of the image illustrates length (expressed as soma distance from the pial surface) and bifurcation of the apical dendrite. The bottom part of the images indicates soma reconstruction and basal dendrite data. (**D**). The bar charts on the left represent the relative number of cells belonging to the morphological profiles identified by K-mean clustering analysis performed separately on each of the two molecular classes (double C/S+ and single Ctip2+ cells). The line graphs on the right represent morphological features for profile 1 (*orange*), unique to double C/S+ cells, profile 2 (*magenta*) and 3 (*green*), shared by both groups. (**E**). Immunofluorescence for Satb2, Ctip2, and biocytin on S1 coronal sections from P21 *Thy1-eYFP-H* transgenic cortices. (**F**). Table showing the input resistance (R_{in} reflecting the membrane resistance), the sag (difference of voltage between peak and steady-state potentials), the first interspike interval (ISI) and the difference of amplitude between the first and second action potential (AP), and the fast after-hyperpolarization (fAHP) of the three identified subpopulations. (**G**). Traces showing the variation in membrane potential when a hyperpolarizing current was injected (-0.2 nA; bottom) and the trains of action potentials when a depolarizing current was injected to the cell to reach the AP threshold (top).

Figure 3 continued on next page

Figure 3 continued

(G'). Magnifications of first and/or second APs. Scale bars: G, 20 mV - 50 ms; G', 20 mV - 5ms. Statistics (Mann-Whitney): a = difference between Ctip2+ and C/S+ type 1 cells; b = difference between Ctip2+ and C/S+ type 2; c = difference between C/S+ type 1 and type 2 cells. Data are represented as means ± SEM. [1]p<0.05; [2]p<0.01; [3]p<0.001. SEM, standard error of the mean. Scale bars: C, 10x mag., 100 μm; E, 40x mag., 10 μm.

DOI: 10.7554/eLife.09531.007

The following figure supplements are available for figure 3:

Figure supplement 1. Morphometric properties of YFP-positive neurons from the *Thy1-eYFP-H* transgenic line.

DOI: 10.7554/eLife.09531.008

Figure supplement 2. Electrophysiological analyses of YFP-positive neurons from the *Thy1-eYFP-H* transgenic line.

DOI: 10.7554/eLife.09531.009

Interestingly, the analysis of trains of action potentials generated by a step of depolarizing current distinguished again two distinct subpopulations within the C/S+ group. The first type of C/S+ neurons produces a train of single action potentials similar to those obtained in Ctip2+ cells, while the second type generates doublets or even triplets of action potentials (***Figure 3G,G'*** and ***Figure 3—figure supplement 2B***). Analysis from the I-V curves or from the action potentials generated at threshold showed further differences between the two types of C/S+ neurons, such as the cell resistance and size of the sag or the characteristics of action potentials and inter-spike intervals (***Figure 3F*** and ***Figure 3—figure supplement 2C***). Taken together, these data support the existence of two subtypes of C/S+ neurons that differ from Ctip2+ cells, and confirm that at P21 neurons co-expressing Ctip2 and Satb2 represent distinct subclasses of cortical PNs in layer V of the S1 cortex.

Dynamic expression of Lmo4 correlates with Ctip2/Satb2+ cell number and area-specific distribution

We next aimed at deciphering the mechanisms responsible for the co-expression of Ctip2 and Satb2 in the postnatal somatosensory cortex. Satb2 is known to repress Ctip2 expression by recruiting the Nucleosome Remodeling and Deacetylase (NuRD) complex, which in turn deacetylates the Ctip2 locus by interacting with the histone deacetylase 1 (Hdac1) (***Alcamo et al., 2008***; ***Britanova et al., 2008***). The protooncogene Ski was shown to play a key role in the Hdac1-NuRD complex interaction (***Baranek et al., 2012***); hence, we hypothesized that the resurgence of C/S+ cells at postnatal stages might be due to the down-regulation of Ski. On the contrary, Ski expression remained high from P0 to P21 and was observed also in several C/S+ cells after birth (***Figure 4—figure supplement 1A–C***), suggesting that a Ski-dependent mechanism is unlikely to contribute to the postnatal increase of C/S+ neurons in the S1 cortex.

Among other candidate genes that might interfere with the Satb2-mediated Ctip2 repression, we selected the transcriptional adaptor Lmo4. This factor interacts with several components of the NuRD complex, is highly expressed in the rostral F/M region, where C/S+ are more abundant, and only in scattered cells of the pS cortex at P0 (***Figure 4A***) (***Cederquist et al., 2013***; ***Gomez-Smith et al., 2010***; ***Huang et al., 2009***; ***Singh et al., 2005***). Lmo4 expression gradually increases in S1 at postnatal stages, reaching its peak in LL at P7, then in all layers at P21 (***Figure 4B***). The timing of Lmo4 expression is thus consistent with the increase of C/S+ cells in S1 from P0 to P21 (***Figure 1B-C*** and ***4B***), and accordingly, the number of triple Lmo4/Ctip2/Satb2-expressing cells progressively increases from P0 to P21 in layers V and VI (***Figure 4C***). Thus, the temporal and spatial dynamics of Lmo4 expression in C/S+ neurons indicate that this factor might favor their specification at peri- and postnatal stages of corticogenesis.

Lmo4 affects number and distribution of Ctip2/Satb2+ cells in S1 cortex

To determine whether Lmo4 is required in the specification of C/S+ cells, we first exploited a mouse mutant line (*Lmo4 CKO*), in which *Lmo4* is specifically inactivated in the cortex under the control of the *Emx1* promoter (***Huang et al., 2009***) (***Figure 4—figure supplement 2A***). We examined Ctip2 and Satb2 expression in P7 *Lmo4 CKO* cortices, when normally a high number of S1 lower layer cells and 92% of double C/S+ cells express Lmo4 (***Figure 4B and C***). Notably, the total number of both C/S+ and Ctip2+ cells is decreased in *Lmo4 CKO* S1 cortices (***Figure 4D and E***), whereas the number of Satb2-expressing cells is not particularly affected by the absence of Lmo4 (***Figure 4—figure***

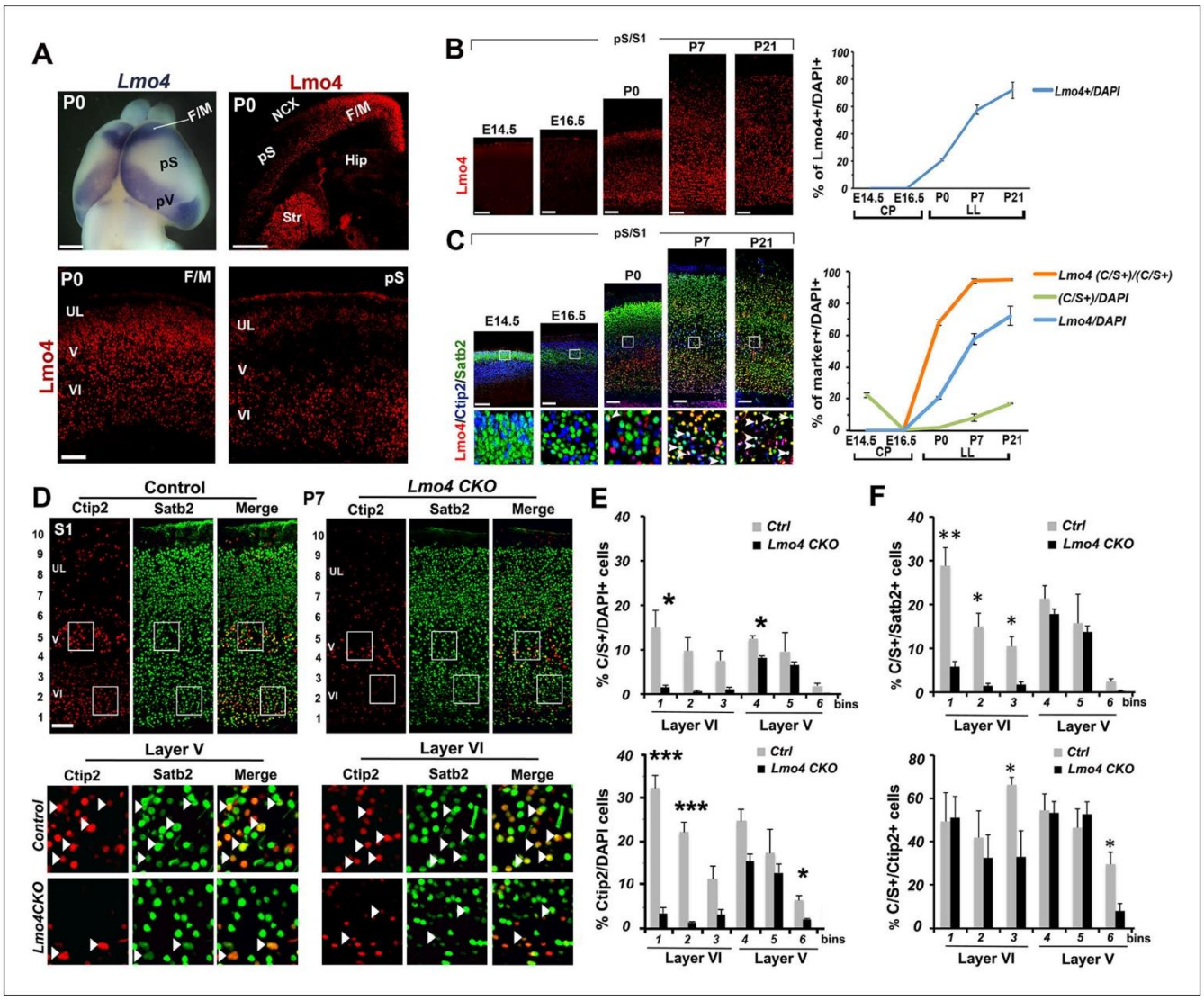

Figure 4. Lmo4 controls the number of Ctip2+ and double C/S+ neurons in the somatosensory cortex. (**A**). Whole-mount *in situ* hybridization for *Lmo4* on P0 brain (top left panel) and immunofluorescence for Lmo4 on coronal sections. (Below) Expression of Lmo4 in high-magnification views of frontal motor (F/M) and prospective somatosensory (pS) coronal sections. (**B**). Coronal sections from pS and primary somatosensory area (S1) of brains from E14.5 to P21 immunostained for Lmo4. On the right, time course of the percentage of Lmo4+ neurons on the total of DAPI+ cells (cortical plate -CP- for prenatal brains and lower layers –LL- for postnatal brains). (**C**). Triple immunostaining for Lmo4/Ctip2/Satb2 on coronal sections from pS and S1 E14.5 to P21 brains. Bottom squared panels represent high-magnification views of boxes in layer V depicted in top panels. On the right, quantification of Lmo4+ (*blue line*) and Ctip2/Satb2+ (C/S+) cells (*green line*) on the total of DAPI+ cortical cells, and of triple Lmo4/C/S+ cells (*orange*) on the total number of C/S+ neurons. (**D**). Double immunofluorescence for Satb2 and Ctip2 on coronal sections of P7 control and *Lmo4 CKO* somatosensory (S1) areas. Bottom squared panels represent high-magnification views of boxes in layers V and VI of top panels. Arrowheads point to double C/S+ neurons. (**E** and **F**) Quantification and layer distribution of double C/S+ or single Ctip2+ neurons on the total of DAPI+ cells (**E**), and of double C/S+ on the total of Satb2+ (top panel **F**) or Ctip2+ (bottom panel **F**) neurons. NCX: neocortex, pV: prospective visual, Hip: hippocampus, Str: striatum, UL, upper layer neurons. Scale bars: B, C, D and lower panels of A, 100 μm, upper panels of A, 1mm. Data are represented as means ± SEM. *p≤0.05, **p≤0.01, ***p≤0.001. SEM, standard error of the mean.

DOI: 10.7554/eLife.09531.010

The following figure supplements are available for figure 4:

Figure supplement 1. Ski is expressed by several C/S+ neurons at postnatal stages.

DOI: 10.7554/eLife.09531.011

Figure supplement 2. Unaltered distribution of Satb2+ neurons in the absence of Lmo4.

DOI: 10.7554/eLife.09531.012

supplement 2B). This might indicate that the alteration in C/S+ cells is mainly due to a general decrease in Ctip2 expression. However, the ratio of C/S+ cells decreased also compared to the total number of Ctip2+ (in upper layer V and VI) and Satb2+ cells (in layer VI) (*Figure 4F*). Since the number and distribution of Satb2+ cells does not significantly change, the reduced number of C/S+ cells is most probably due to an increased repression of Ctip2 in Satb2+ neurons.

Next, we investigated whether Lmo4 is cell-autonomously required in the specification of double C/S+ cells in layer V by overexpressing *Lmo4* in the S1 of WT cortices. To this aim, we cloned the coding sequence of *Lmo4* into the *pCdk5r1-IRES-EGFP* vector (*Figure 5A*), which drives the selective expression of a given transcript in postmitotic neurons (*Wang et al., 2007b*). To evaluate the efficacy of this new construct (*pCdk5r1-Lmo4-EGFP*), we electroporated mouse brains at E13.5 and analyzed the somatosensory cortex at P0 when Lmo4 is only faintly expressed (*Figure 4A*). Electroporated (GFP+) cells expressed high levels of Lmo4, whereas similar regions in the contralateral cortex contained just few Lmo4+ cells (*Figure 5B,C*).

The *pCdk5r1-Lmo4-EGFP* construct was then electroporated at E13.5, and brains were collected at P7, when the laminar specification of PNs is nearly completed (*Figure 5D*). Control (*pCdk5r1-EGFP* electroporated) cells were predominantly Satb2+ and Ctip2- in layer V (*Figure 5D*), whereas the overexpression of Lmo4 increased the ratio of Ctip2+ neurons among GFP+ cells from 7.6 ± 4.7% to 31.3 ± 3.8% (n = 3, p = 0.03) and the percentage of C/S+ neurons from 5.2 ± 3.4% to 16.4 ± 1.0% in LL (n = 3, p<0.05) (*Figure 5E*), supporting a cell-autonomous role for Lmo4 in inducing Ctip2 expression in both Satb2+ and Satb2- cells.

Overall, our Lmo4 loss- and gain-of-function approaches both demonstrate that Lmo4 acts in the specification of C/S+ cells primarily by modulating Ctip2 expression in layer V.

Upregulation of Lmo4 increases the number of double Ctip2/Satb2+ cells in *Nr2f1*-deficient somatosensory cortices

To further confirm that Lmo4 plays a role in the specification of C/S+ cells, we analyzed the distribution of these cells in mice lacking the transcription factor *Nr2f1* (also called *COUP-TFI*) in cortical neurons (*Nr2f1 fl/fl*$^{Emx1\text{-}Cre}$, from now on *Nr2f1 CKO*) (*Armentano et al., 2007*). *Nr2f1 CKOs* exhibit a remarkable upregulation of Lmo4 in layer V and in the lower part of UL of the somatosensory cortex at P0 (*Alfano et al., 2014*) (*Figure 6A–B*). In agreement with our previous studies (*Alfano et al., 2014*; *Tomassy et al., 2010*), the number of Ctip2+ cells is significantly increased in the mutant motorized somatosensory (mS) cortex, whereas Satb2+ cells are only slightly augmented (*Figure 6C–D* and *Figure 6—figure supplement 1A*). As expected, the number and distribution of C/S+ neurons are also increased on the total of cells and relative to the number of Satb2+ and Ctip2 + cells in *Nr2f1 CKOs* (*Figure 6C–D* and *Figure 6—figure supplement 1A*). Finally, mutant brains showed a much higher number of triple Lmo4/Ctip2/Satb2+ cells in layer V and upper layer VI than controls (*Figure 6—figure supplement 1C*). While 68% of C/S+ cells express Lmo4 in control cortices at P0, this ratio rises to 92% in mutant brains (*Figure 6—figure supplement 1D*), supporting a correlation between increased Lmo4 expression and higher number of C/S+ cells in LL of mutant cortices.

Next, we investigated whether ectopic Lmo4 expression and increased number of C/S+ cells in the mutant somatosensory cortex coincided with altered neuronal connectivity of layer V neurons. Previous work showed that corticospinal projection neurons (CSpPNs) were abnormally located in layer VIa of *Nr2f1 CKO* (*Tomassy et al., 2010*). By injecting CTB-coated beads either into the brainstem or the spinal cord regions of control and *Nr2f1* mutant brains, we observed an expansion of cortico-brainstem projection neurons (CBPNs) in layer Va and confirmed the mispositioning of the CSpPNs in upper layer VI of mutant cortices (*Figure 6E*). Interestingly, the highest percentage (66.4 ± 6.7%) of CBPNs co-expressing Ctip2 and Satb2 was in layer Va, whereas none of the labeled cells co-expressed these genes in layer VIa (*Figure 6F and G*). This suggests that Lmo4 increase may underlie both the strong increase in C/S+ cells and the shift of connectivity from corticospinal to corticobrainstem targets observed in mutant layer V.

Thus, to demonstrate that the upregulation of Lmo4 in the *Nr2f1 CKO* brains was directly involved in layer V Ctip2 radial expansion, we electroporated an *Lmo4-specific shRNA* construct (*Qin et al., 2012*) into E13.5 mutant brains and analyzed Lmo4 and Ctip2 laminar distribution in P0 electroporated mS1 cortices (*Figure 6—figure supplement 2*). While GFP+ control cells co-localize with Lmo4 and Ctip2 (*Figure 6—figure supplement 2A,B*), *Lmo4 shRNA*-expressing cells show a

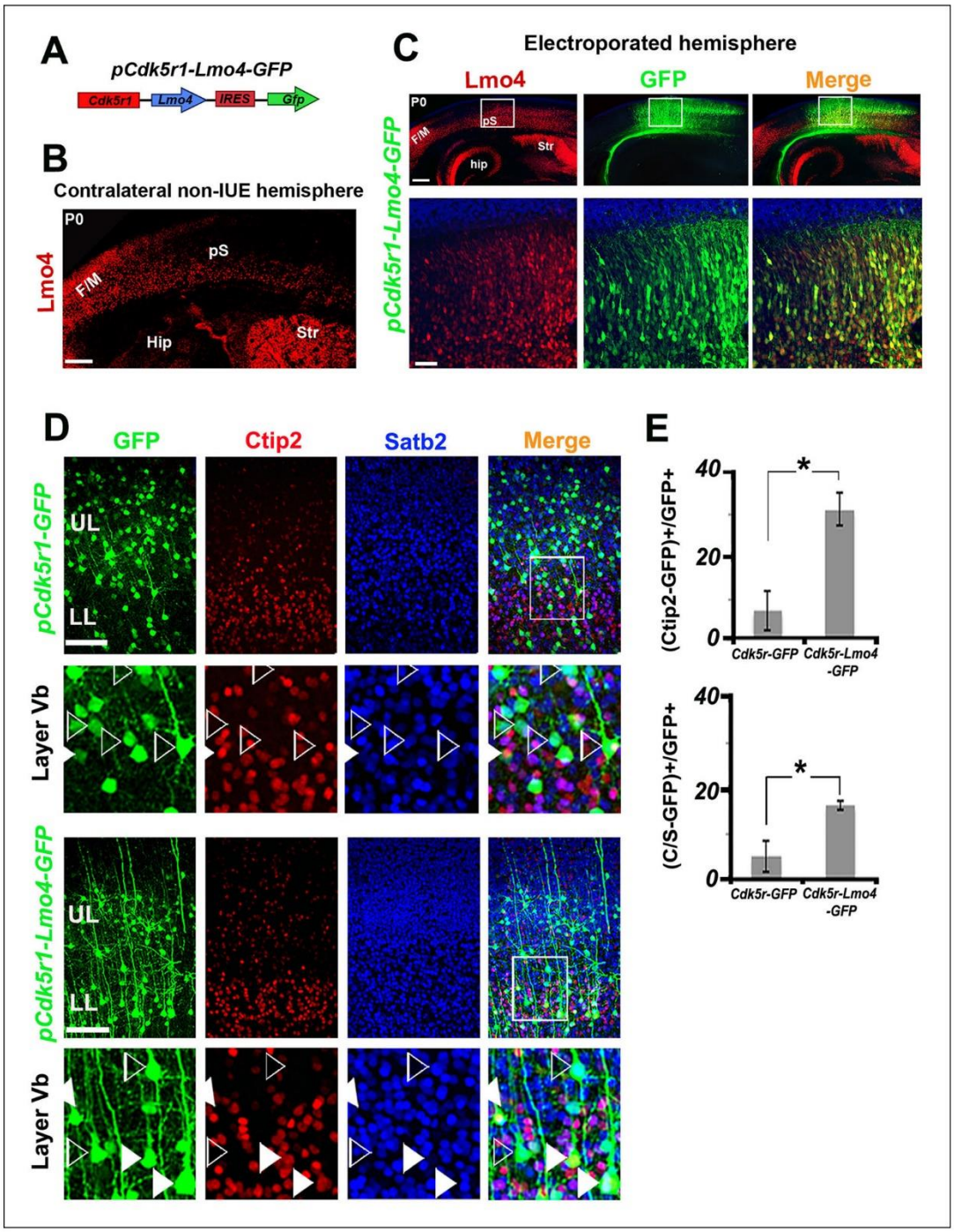

Figure 5. Lmo4 overexpression increases the number of Ctip2+ and C/S+ neurons in lower layers. (**A**). Schematic representation of the vector used to overexpress *Lmo4* in postmitotic neurons. (**B**). Immunostaining for Lmo4 on a coronal section of the contralateral (non-electroporated) hemisphere of P0 electroporated brains. (**C**). Coronal sections of a *pCdk5r1-Lmo4-IRES-GFP* electroporated E13.5 hemisphere immunolabeled for Lmo4 and GFP at P0. Bottom squared panels represent high-magnification views of boxes depicted in upper panels. (**D**). Immunostaining for Satb2, Ctip2, and GFP on coronal sections from P7 S1 cortices electroporated at E13.5 with *pCdk5r1-IRES-GFP* (on the top) or *pCdk5r1-Lmo4-IRES-GFP* (on the bottom). Squared panels represent high-magnification views of boxes depicted in top panels. Filled arrowheads indicate double C/S+ GFP+ cells, whereas empty arrowheads indicate GFP+ cells not expressing Ctip2. (**E**). Quantification of Ctip2+/GFP+ cells on the total number of GFP+ cells (on the top), and of (C/S+)/GFP+ cells on the total number of GFP+ cells (on the bottom) in layer V of electroporated brains. Data are represented as means ± SEM. *p≤0.05. (IUE) *In utero* electroporated; (Hip) hippocampus; (F/M) frontal motor area; (pS) prospective somatosensory area; SEM, standard error of the mean. Scale bars: **B**,**C** 300 μm; **C**, high magnification: 50 μm, **D**, 100 μm.

DOI: 10.7554/eLife.09531.013

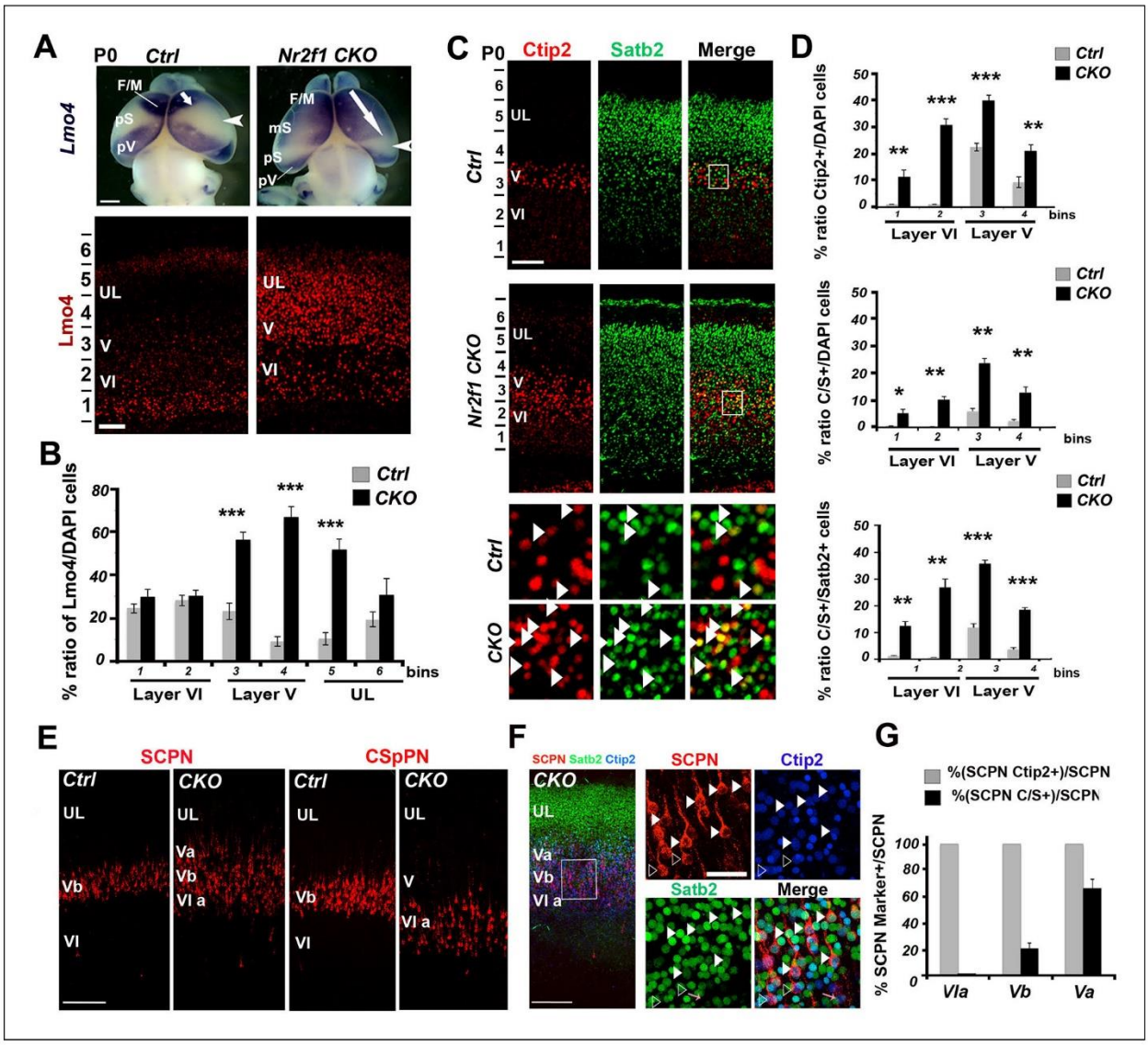

Figure 6. Increase of Lmo4- and double C/S-expressing neurons in the motorized somatosensory cortex of Nr2f1 CKO brains. (**A**). Whole-mount *in situ* hybridization for *Lmo4* (top panels) and Lmo4 immunofluorescence on coronal sections from the prospective somatosensory (pS) cortex (bottom panels) of P0 control and *Nr2f1 CKO* brains. (**B**). Quantification and layer distribution of Lmo4+ neurons in pS of P0 control and *Nr2f1 CKO* brains. (**C**). Coronal sections from the pS of P0 control and *Nr2f1 CKO* brains immunolabeled for Ctip2 and Satb2. Bottom squared panels represent high-magnification views of layer V neurons in boxes depicted in top panels. Arrowheads indicate C/S+ neurons. (**D**). Quantification of Ctip2+ and C/S+ neurons in the pS of P0 control and *Nr2f1 CKO* brains as a percentage of the total number of cells (DAPI+) or of Satb2+ neurons. (**E**). Coronal sections of S1 from controls and *Nr2f1 CKO* P7 brains retrogradely-labeled in the pontine region and in the cervical spinal cord. (**F**). Immunofluorescence for Satb2 and Ctip2 on P7 *Nr2f1 CKO* S1 retrogradely-labeled cortices. Filled arrowheads in high-magnification views indicate retrogradely-labeled subcerebral projection neurons (SCPNs) double positive for Satb2 and Ctip2, whereas empty arrowheads indicate retrogradely-labeled SCPNs positive for Ctip2. (**G**). Quantification of Ctip2+ and C/S+ retrogradelylabeled SCPNs on the total number of labeled PNs in layers Va, Vb, and VIa of *Nr2f1 CKO* brains. F/M, frontal motor area; pS, prospective primary somatosensory area; pV, prospective primary visual area; CSpPN, corticospinal projection neurons. UL, upper layers; VI, layer VI. Data are represented as means ± SEM. *p≤0.05, **p≤0.01, ***p≤0.001. SEM, standard error of the mean. Scale bars: A, 1 mm; lower panel A, C, 100 μm, E, F, 200 μm; high-magnification views in F, 50 μm.

DOI: 10.7554/eLife.09531.014

The following figure supplements are available for figure 6:

Figure supplement 1. Increase of double Ctip2/Satb2+ and triple Lmo4/Ctip2/Satb2+ neurons in the motorized *Nr2f1 CKO* somatosensory cortex.

DOI: 10.7554/eLife.09531.015

Figure supplement 2. Decrease of Ctip2 expression in the motorized *Nr2f1 CKO* somatosensory cortex after Lmo4 downregulation.

DOI: 10.7554/eLife.09531.016

drastic reduction not only in Lmo4 expression, as expected, but also in Ctip2 levels in layer Va (***Figure 6—figure supplement 2C,D***). This suggests that Ctip2 overexpression in layer Va is mainly due to Lmo4 increase and that *Nr2f1* loss not only upregulates Lmo4 levels but also favors its action on Ctip2 expression. In addition, cells electroporated with the control *shRNA* show a delayed migration to the apical region of the cortex, a phenotype that was already described in our previous publication (***Alfano et al., 2011***). Notably, downregulating *Lmo4* rescues the radial migratory defect and allows electroporated cells to reach the proper radial position in the upper regions of P0 cortices.

These data demonstrate that Lmo4 is functionally involved in the abnormal upregulation of layer V Ctip2 expression observed in the absence of Nr2f1, and more in general, support a key role for Lmo4 in Ctip2 de-repression.

Lmo4 de-represses Ctip2 by competing with Satb2 for Hdac1 binding

Next, we investigated whether Lmo4 was able to positively regulate Ctip2 by directly interfering with the molecular machinery underlying Satb2-mediated Ctip2 repression (***Alcamo et al., 2008***; ***Britanova et al., 2008***). Lmo4 was shown to bind Histone deacetylases 1 and 2 (Hdac1 and 2) to repress its downstream target genes (***Singh et al., 2005***). Since the Hdac1-NuRD-Satb2 complex assembly is fundamental for Ctip2 repression (***Alcamo et al., 2008***; ***Baranek et al., 2012***; ***Britanova et al., 2008***), we examined whether Lmo4 was able to compete with Satb2 for Hdac1 interaction. To this aim, we performed immunoprecipitation with Lmo4- and Satb2-specific antibodies on nuclear proteins extracted from control and *Nr2f1 CKO* P1 cortices, where Lmo4 and Ctip2 are strongly upregulated (***Figure 7A***). Immunoprecipitated protein fractions were analyzed by Western blot using an antibody specific for Hdac1 (***Alcamo et al., 2008***; ***Britanova et al., 2008***; ***Gyorgy et al., 2008***). Comparable levels of Hdac1 were co-immunoprecipitated (Co-IP) with Lmo4 and Satb2 antibodies in control conditions, whereas Hdac1-Lmo4 interaction increased at the expense of Hdac1-Satb2 in *Nr2f1 CKO* brains. These changes in the amount of each complex were not due to dramatic changes in the total amount of Satb2 and Lmo4 proteins between wt and *Nr2f1* mutant brains. Indeed, Satb2 protein levels resulted unaltered between the two conditions, whereas the amount of Lmo4 resulted only slightly increased in *Nr2f1* mutants (***Figure 7A***). Since the overall Lmo4 upregulation is not remarkable and takes place particularly in the mS1 cortex, the higher amount of Hdac1-Lmo4 complex in mutant Co-IP fractions might be due to a higher binding affinity between these factors in somatosensory regions. Accordingly, the number of C/S+ cells is remarkably higher in lower layers of S1 than in those of M1 in P7 wt brains (***Figure 1E***) despite similar Lmo4 levels between S1 and M1 areas (our data and (***Huang et al., 2009***).

Finally, we investigated whether Lmo4 binds Hdac1 by interacting with the Ski-Hdac1 complex and preventing its interaction with Satb2 (***Baranek et al., 2012***). To this aim, we analyzed the Lmo4-immunoprecipitated nuclear fractions from control and mutant cortices with the antibodies for Ski and Satb2. We found that Lmo4 binds Ski consistently, whereas it interacts very limitedly with Satb2, suggesting that Lmo4 normally interacts with Ski before it binds to the Satb2-NuRD complex. However, the increased Hdac1-Lmo4 binding does not seem to be related to higher interaction between Lmo4 and Ski, since the amount of bound Ski does not change in the mutant extracts (***Figure 7B***).

We next verified whether the chromatin state in the *Ctip2* genetic locus varies between control and mutant cortices (***Figure 7C***). We carried out a chromatin immunoprecipitation (ChIP) assay with the anti-Hdac1 antibody and with an antibody specific for the acetylated form of histone 4 (H4K12ac), whose levels are proportional to the rate of transcriptional activity. Immunoprecipitated chromatin fractions from P1 cortices were analyzed by semi-quantitative PCR and confirmed by QPCR using primers amplifying part of the matrix attachment region (MAR) in the *Ctip2* locus (***Britanova et al., 2008***). As a control, we used primers amplifying a sequence in the last intron of the *Rnd2* gene containing a previously described Nr2f1-binding site (***Alfano et al., 2011***). Our data show that a lower amount of Hdac1 binds the *Ctip2* locus, which accordingly appears more acetylated and thereby more active (***Figure 7C***). No Hdac1 binding and acetylation differences were observed with control primers, confirming specificity of its effect on the *Ctip2* locus (***Figure 7C***).

Since changes in the Hdac1-Satb2 interaction and in Ctip2 de-repression observed in *Nr2f1* mutant brains might be not only or not directly related to the observed Lmo4 increase in the mS1 region, we repeated the CoIP experiments by overexpressing Lmo4 and Satb2 in COS7 cells. To confirm the competition between Lmo4 and Satb2 for Hdac1 binding, COS7 cells were transfected with increasing quantities of a vector expressing *Lmo4* under the control a CMV enhancer (*pCIG2-*

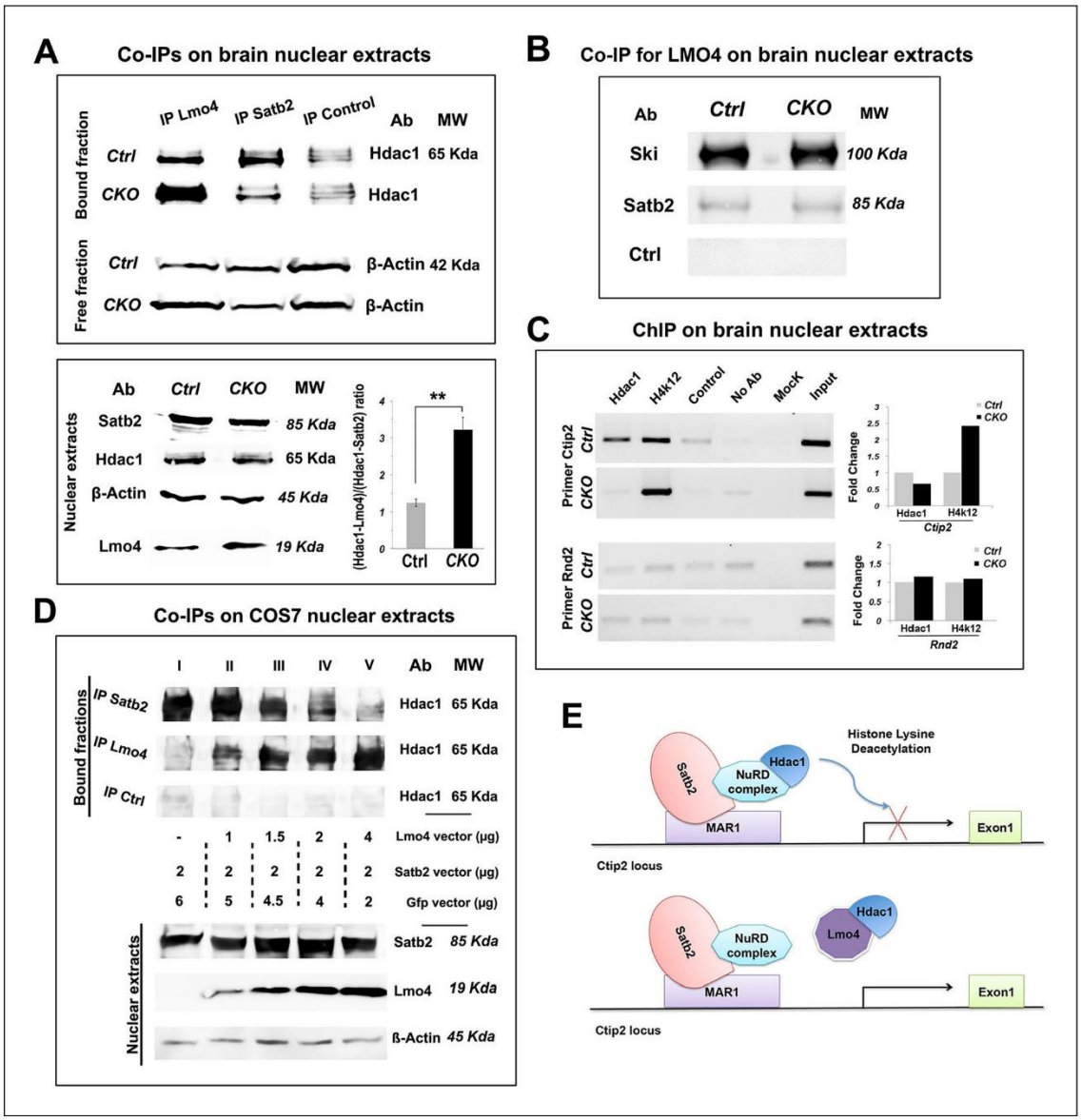

Figure 7. Lmo4 interacts with Hdac1 and prevents its binding to the Ctip2 locus. (**A**). On the top, Western blot on nuclear extracts from controls and *Nr2f1 CKO* P1 cortices immunoprecipitated with antibodies specific for Lmo4 (IP Lmo4), Satb2 (IP Satb2), or an unrelated epitope (IP control). IP fractions were analyzed using an antibody against Hdac1, whereas the corresponding input fractions were analyzed with an antibody specific for β-actin. On the bottom-left, Western blot on nuclear extracts from controls and *Nr2f1 CKO* P1 cortices for Satb2, Hdac1, Lmo4, and β-actin. To the right, ratio between Hdac1-Lmo4 and Hdac1-Satb2 complexes immunoprecipitated from control and *Nr2f1 CKO* extracts. (**B**). Western blot performed on nuclear extracts from controls and *Nr2f1 CKO* P1 cortices immunoprecipitated with specific antibody for Lmo4. IP fractions were analyzed using an antibody against Ski, Satb2 or an unrelated epitope (control). (**C**). On the left, semi-quantitative PCR performed on Chromatin-immunoprecipitation (ChIP) samples from controls and *Nr2f1 CKO* P1 cortices. The assay was performed using antibodies against Hdac1, the anti-Histone H4 (acetyl K12) (H4K12) and primers amplifying a MAR1 sequence on *Ctip2* and *Rnd2* loci. On the right, QPCR performed on ChIP samples from controls and *Nr2f1 CKO* cortices. (**D**). On the top, Western blot on nuclear extracts from COS7 cells transfected with an equal amount of Satb2- and an increasing amount of Lmo4-expressing vectors and immunoprecipitated with antibodies specific for Satb2 (IP Satb2), Lmo4 (IP Lmo4), or an unrelated epitope (IP control). IP fractions were analyzed using an antibody against Hdac1. On the bottom, Western blot on nuclear extracts from the transfected COS7 cells with specific antibodies for Satb2, Lmo4, and β-actin showing increase of Lmo4 and similar Satb2 and β-actin protein levels. (**E**). Schematic model of the putative mechanism by which Lmo4 de-represses Ctip2 expression. . **p≤0.01. MAR1: Matrix attachment region 1; NuRD complex: Nucleosome Remodeling and Deacetylase complex.

DOI: 10.7554/eLife.09531.017

Lmo4) together with a constant amount of the *pCAG-Satb2* plasmid (**Britanova et al., 2008**) (**Figure 7D**). Cell extracts, analyzed by immunoprecipitating proteins with an anti-Hdac1 antibody, showed a progressive increase in Hdac1-Lmo4 interaction, in line with the Lmo4 increase, at the expense of Hdac1-Satb2 binding (**Figure 7D**). This confirmed the competition model and put in direct relation the Lmo4 increase with the decreased Hdac1-Satb2 interaction.

Overall, our analysis indicates that Lmo4 progressively interferes with the Satb2-mediated Ctip2 repression by sequestering Hdac1 before it interacts with the Satb2-NuRD complex on the *Ctip2* locus and hence, favoring Ctip2 and Satb2 co-localization in cortical LL during postnatal stages of development (**Figure 7E**).

Discussion

This study shows that key developmental regulators with opposite functions during embryonic stages, such as Ctip2 and Satb2, can co-localize at postnatal stages and participate in generating the great diversity of PN subtypes in the young adult brain. The transcriptional adaptor Lmo4 epigenetically modifies the *Ctip2* locus and enables *Ctip2* expression in Satb2+ lower layer neurons by interfering with the Satb2-mediated deacetylation in a time- and area-specific manner. Double C/S+ neurons comprise at least two distinct neuronal subclasses with unique connectivity, morphology and electrophysiological profiles in the juvenile (P21) mouse brain.

Ctip2 and Satb2 co-expression correlates with several neuronal features

After birth, Satb2 and Ctip2 are not any more an exclusive hallmark of callosal (CPN) or subcerebral (SCPN) projection neurons, respectively, but are co-expressed in distinct subclasses of CPNs and SCPNs with specific connectivity profiles, morphological, and electrophysiological characteristics. In line with our results, Satb2 expression was shown to be associated with the SCPN markers Fezf2 and Sox5 in CPN populations of motor areas (**Sohur et al., 2014**; **Tantirigama et al., 2014**). In addition, Satb2 is not only required for CPNs but also for the proper differentiation and axon pathfinding of SCPNs (**Leone et al., 2014**). It is thus possible that early-born CPNs, which originate at a similar time as SCPNs and reach lower layers in S1, are more similar to subcerebral than late-born CPNs of upper layers.

We also show that C/S+ neurons expressing Er81 define a distinct subpopulation of CPNs residing in layer V of S1. This subpopulation is unlikely to project to the contralateral striatum, since callosal-striatal neurons are almost absent in S1 after P15 and fail to express Ctip2 but are instead positive for Sox5 (**Sohur et al., 2014**). Accordingly, none of the C/S+ CPNs identified here were positive for Sox5, whereas a group of C/S+ SCPNs clearly expressed Sox5. Our molecular analysis thus identified novel subclasses of SCPNs and CPNs major neuronal groups with distinct features, which can be specifically identified by Ctip2 andSatb2 co-expression.

The morphological and electrophysiological characterizations revealed hybrid but also unique features of C/S+ subpopulations compared to single Ctip2+ cells. Although a subset of both populations projects to subcerebral targets, the C/S+ neuronal axons do not reach the spinal cord and show typical morphological features of CPNs, such as a small soma, long, and thin apical dendrites and late bifurcation of the apical tuft (**Hattox and Nelson, 2007**). However, a small group of C/S+ neurons also share characteristics of SCPNs with single Ctip2+ cells, such as a large soma, high number of secondary dendrites, thick apical dendrites and an early bifurcation of the apical tuft (**De la Rossa et al., 2013**; **Hattox and Nelson, 2007**; **Tantirigama et al., 2014**). Thus, C/S+ cells include different subsets of PNs sharing some typical CPN and SCPN morphological features.

Electrophysiological recordings also revealed that C/S+ neurons exhibit a lower sag value than single Ctip2+ cells, indicating that C/S+ cells might acquire some UL electrical features, since normally these neurons have a lower hyperpolarization-activated current (Ih) than LL neurons (**De la Rossa et al., 2013**; **Sheets et al., 2011**). This is also reminiscent of the observations made in *Satb2* mutant or *Fezf2*-overexpressing brains, where UL neurons acquire electrical features of LL neurons (**De la Rossa et al., 2013**; **Leone et al., 2014**). Moreover, Ctip2+ neurons show higher ISI (first interspike interval) value than C/S+ cells. A similar variation in ISI values was previously described between UL and LL neurons (**De la Rossa et al., 2013**), suggesting that the co-expression of Satb2 in Ctip2+ layer V neurons may result in electrical features characteristic of UL neurons. Finally, since

these variations in electrophysiological properties were observed by analyzing cells with similar morphologies, C/S+ and Ctip2+ neurons might diverge in the expression of ion channels and pumps (***Oswald et al., 2013***; ***Staff et al., 2000***). In the future, it might be interesting to investigate eventual correlations between the expression of Satb2 and/or Lmo4 and the function/expression of specific ion channels in layer V neurons.

Lmo4 interferes with Satb2-mediated Ctip2 repression in the postnatal cortex

Our time-course analysis of C/S+ neurons confirms that only a small population of cells maintains the expression of these two antithetic factors during perinatal stages of corticogenesis (***Baranek et al., 2012***; ***Leone et al., 2014***) (***Figure 8***). This is consistent with the paradigm that competing molecular programs direct the differentiation of major PN classes during late embryonic stages of corticogenesis (reviewed in ***Greig et al., 2013***). However, we found that distinct subpopulations of C/S+ PNs are maintained and gradually increase postnatally in lower layers of the S1 cortex.

This study also demonstrates that Lmo4 progressively increases and co-localizes with double C/S + neurons after birth in the somatosensory area. Lmo4 is a widely expressed transcriptional modulator known to regulate several key biological processes, from cell growth to fate determination (***Sang et al., 2014***). It is well known that Lmo4 acts as a scaffolding protein for the assembly of multi-protein complexes and interacts with several co-factors of the NuRD complex (***Gomez-Smith et al., 2010***; ***Singh et al., 2005***; ***Wang et al., 2007a***).

Although other factors might be involved in Satb2/Ctip2 co-expression, our work demonstrates that Lmo4 de-represses Ctip2 by sequestering Hdac1, a critical component of the NuRD complex recruited by Satb2 on the *Ctip2* locus to inactivate its transcription. Overall, our data constitute first direct evidence that the control of epigenetic mechanisms may underlie area-specific variations in neuronal features. Most importantly, such processes take place after birth and seem to contribute to the maturation and refinement rather than to the initial specification of neuronal subtypes of the somatosensory area.

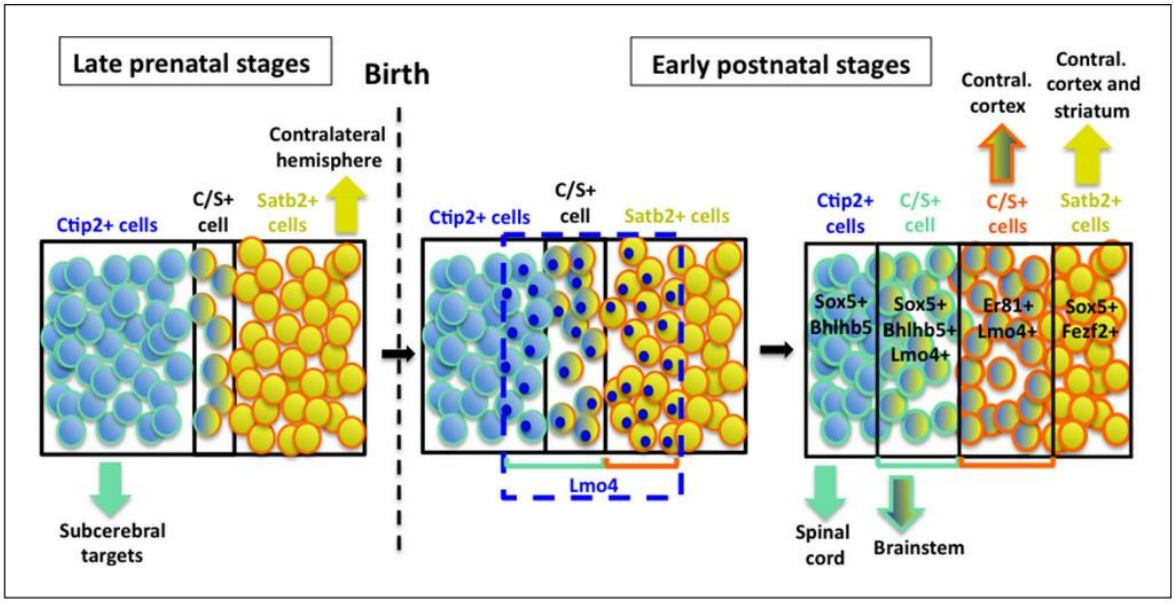

Figure 8. Hypothetical model of layer V neuronal subtype refinement. After birth, Lmo4 expression progressively increases in Satb2+ and in Ctip2+ cells of S1 cortex. Lmo4 de-represses Ctip2 expression in Satb2+ cells and probably Satb2 in Ctip2+ cells. According to the different dynamics leading to the refinement of distinct C/S+ subclasses, these cells will project either to subcerebral or to contralateral targets. Vertically oriented arrows indicate connectivity at postnatal stages. The blue dashed line and blue circles in different cells delimit territories of Lmo4 expression. Blue marine circles surrounding cells depict subcerebral projection neuron (SCPN) subpopulations, whereas orange ones delineate callosal neuron (CPN) subgroups. Black lines delimit different neuronal populations of the somatosensory cortex.

DOI: 10.7554/eLife.09531.018

Obviously, this study does not constitute an exhaustive investigation on the molecular mechanisms regulated by Lmo4, which seems to be also able to induce Satb2 expression in Ctip2-positive cells, since a notable portion of C/S+ cells seems to derive from a subpopulation of Ctip2+ cells (model in ***Figure 8***). This is not totally unexpected in light of previous reports that correlated Lmo4 expression with callosal (Satb2+) development (***Azim et al., 2009***; ***Molnar and Cheung, 2006***; ***Ye et al., 2015***). Accordingly, we found that the number of C/S+ cells decreased in *Lmo4* mutants not only on the total of the Satb2+ subpopulation but also on the total of the Ctip2+ one, suggesting that C/S+ cells may also derive from Lmo4-mediated de-repression (and/or activation) of Satb2 in Ctip2+ cells.

Finally, we noticed that Ctip2 was poorly upregulated in upper layers of *Nr2f1 CKO* motorized somatosensory cortices and of *Lmo4*-electroporated cortices. This could be explained by the presence of a laminar-specific transcription factor, which would act synergistically with Lmo4 to efficiently activate Ctip2 expression in lower layers. More experiments are required to test this hypothesis.

Possible mechanisms of action and interactors of Lmo4, Ctip2, and Satb2 during SCPN maturation in the somatosensory area

Lmo4 had already been implicated in specifying SCPN and CPN identities in the rostral motor cortex (***Cederquist et al., 2013***), but a similar function in sensory areas was not previously unveiled. Here, we show that Lmo4 acts preferentially in layers V and VI of the S1 cortex in which the majority of neurons (SCPN) projects subcerebrally and expresses Ctip2 at different levels. Lmo4 levels gradually increase from layer VI to upper layers at postnatal stages, together with the progressive specification of C/S+ cells.

Interestingly, we report that C/S+ neuron projections target the brainstem, but not the spinal cord. If Lmo4 and/or Satb2 and Ctip2 co-localization modulates axon targeting, what are their mechanisms of action? Ctip2 and Satb2 inhibit the expression of DCC and Unc5C, respectively, two receptors of the guidance cue Netrin-1 (***Srivatsa et al., 2014***). Since these receptors are involved in the midline crossing of corticospinal axons (***Finger et al., 2002***), one conceivable hypothesis would be that co-expression of Ctip2 and Satb2 inhibits both receptors, thus preventing subcerberal PNs to reach the spinal cord. Another explanation could be that Lmo4 inhibits neurite outgrowth by repressing the expression of the receptor tyrosine kinase Alk that plays key roles in neuritogenesis (***Lasek et al., 2011***). Alternatively, Lmo4 might interact with Lhx2, another LIM homeobox transcription factor known to regulate the expression of the guidance receptors Ephrin-A5 as well as Robo1 and 2, which in turn control different steps of corticospinal axon pathfinding (***Marcos-Mondejar et al., 2012***; ***Shetty et al., 2013***). Thus, either Lmo4 expression or Ctip2 and Satb2 co-expression might control several neuronal processes allowing the correct maturation and/or refinement of PT and IT subtypes during postnatal stages of corticogenesis. We envisage that also other transcription factors normally involved in determining distinct classes of PNs during development, might take a similar postnatal function during cortical maturation.

Conclusion

Overall, we show that area- and time-specific changes in common molecular mechanisms modulate the final features of both CPN and SCPN subpopulations in an area- and time-specific manner. More in general, our analysis provides first direct evidence of a common developmental program directing the molecular and cellular maturation of both IT and PT projection neurons. This might have important implications in the study of neocortical development, since 'serial homologies' (i.e. similar connectivity or molecular codes) among neocortical areas might be due to variations on a 'common theme', as previously suggested (***Harris and Shepherd, 2015***), rather than to multiple independent and area-specific genetic programs.

Materials and methods

Animals

All mouse experiments were conducted according to national and international guidelines and have been approved by the local ethical committee (CIEPAL NCE/2011-23). *Nr2f1 fl/fl* and *Lmo4 fl/fl* mice

were crossed to *Emx1-Cre* mice to inactivate either *Nr2f1* or *Lmo4* in cortical cells. WT, *Nr2f1 fl/fl*, or *Lmo4 fl/fl* were taken as controls. Mouse lines were genotyped as previously described (**Armentano et al., 2007**; **Armentano et al., 2006**; **Goebbels et al., 2006**; **Huang et al., 2009**). *Thy1-eYFP-H* mice were obtained from The Jackson Laboratory and genotyped as described in (**Feng et al., 2000**). Midday of the day of the vaginal plug was considered as embryonic day 0.5 (E0.5).

Postmortem tissue collection

Mice at P0, P7, and P21 were intracardially perfused with paraformaldehyde (PFA) 4%. Embryonic and postnatal brain samples were fixed either for 2 hr (for immunohistochemistry) or for over-night (for *in situ* hybridization [*ISH*]) at 4˚C in PFA 4%. Brain slices used for patch clamp experiments were fixed 4 hr at 4˚C in 4% PFA after recording. Samples were, then, either embedded in Optimal Cutting Temperature (OCT) medium (JUNG, Germany) after being equilibrated to 30% sucrose, and cut on a Leica cryostat, or gradually dehydrated to 96% ethanol for whole-mount *ISH*. Samples to be used for floating immunofluorescences and cholera toxin-injected brains were embedded in 4% agarose after fixation and then cut on a Leica vibratome at 200 µm. No samples were excluded in this study and for each experiment at least three animals from different litters were used.

Immunohistochemistry and immunofluorescence

Immunofluorescences on cryosections (CI) were performed as previously described (**Armentano et al., 2007**; **Armentano et al., 2006**). Floating immunofluorescence (FI) was performed on vibratome sections, which were blocked with 10% goat serum, 3% bovin serum albumin (BSA), and 0.3% triton X-100 over night at 4˚C. Primary and secondary antibodies were carried out over night at 4˚C. The following primary antibodies were used: mouse anti-Satb2 (dil. CI = 1:20, FI = 1:80, Abcam, UK), rat anti-Ctip2 (dil. CI = 1:300, FI = 1:400, Abcam), rabbit anti-Ctip2 (1:500, Abcam), rabbit anti-Sox5 (1:300, Gentaur, France), rabbit anti-Ski (1:50, Santa Cruz Biotechnology, Dallas, Texas), rat anti-Lmo4 (1:500, gift from Valsvader's lab), rabbit anti-Er81 (1:1000, gift from Arber's Lab), guinea pig anti-Bhlhb5 (1:50000, gift from Novitch's Lab), rabbit anti-GFP (1:1000, Molecular Probes, Eugene, Oregon), chicken anti-GFP (1:800, Abcam). The following secondary antibodies were used: goat anti-rabbit FC (488, 594, 633), goat anti-rat FC (488, 594, 633), goat anti-mouse FC (488, 594, 633), and goat anti-guinea pig FC (488, 594, 633) (dil. CI = 1:300, FI = 1:400, Life Technologies, Thermo Fisher Scientific, USA), goat anti-rabbit FC 350 (1:150, Life Technologies) and donkey anti-mouse FC 405 (1:300, Abcam). To reveal biocytin injected in patch-clamped cells, it was used Texas Red avidin D (1:500, Vector Laboratories, Burlingame, California). Slices were mounted with the following mounting solution: 80% glycerol, 2% N-propyl gallate, 1 µg/ml Hoechst (Invitrogen, Thermo Fisher Scientific, USA).

Whole-mount *In Situ* Hybridization (*ISH*)

Whole-mount *ISH* was performed as described in (**Alfano et al., 2014**; **Alfano et al., 2011**; **Armentano et al., 2007**). The antisense *Lmo4* RNA probe was labeled using the DIG RNA labelling Kit (Roche, Switzerland) following the manufacturer's instructions.

pCdk5r1-Lmo4-IRES-GFP and pCIG2-Lmo4-IRES-GFP plasmid construction

To synthesize the *pCdk5r1-Lmo4-IRES-GFP*, the Lmo4 ORF was amplified using available cDNA with the following primers: Mlu1-Lmo4.fw (5'GGACGCGTTGAGAGCAGCTC3') and MluI-Lmo4.rev (5'GGACGCGTTTCTGCATTACTC3'). These primers were designed with an Mlu1 restriction cassette at their 5' end. Once amplified, the Lmo4 amplicon was purified using the QIAGEN PCR Purification Kit (following manufacturer's protocols) and digested with Mlu1 (Biolabs, Ipswich, Massachusetts). The digested Lmo4 ORF was cloned into the empty ***pCdk5r1-IRES-GFP*** vector (digested as well with Mlu1). The plasmid was validated and sequenced using the following primer: pCDK5C.fw (5'-AGGACTAAACGCGTCGTGTCC-3').

To generate the *pCIG2-Lmo4-IRES-GFP*, the *Lmo4* variant 2 *mRNA* sequence was amplified using available P0 cDNA and the following primers: Lmo4_VAR2.FW (5'-GAAGTCCCCGAGCTGGTTTG-3') and Lmo4.REV (5'- CCATACTAGAGCAAATGTCTCTG-3'). Lmo4 amplicon was cloned into the

pCRII-TOPO vector (Invitrogen) according to manufacturer's instructions and, then, excised by using SpeI and EcoRV restriction enzymes (Biolabs). The SpeI ends was made blunt by fill-in with Klenow fragment (Biolabs). Finally, the Lmo4 fragment was cloned into a *pCIG2* plasmid (**Heng et al., 2008**) previously digested with SmaI (Biolabs). The *pCIG2 (pCAGGS-IRES-GFP2)* is a modified version of the *pCIG* vector (**Megason and McMahon, 2002**), which was obtained by inserting an IRES-GFP sequence into the *pCAGGS* vector (**Niwa et al., 1991**). Positive clones were amplified and purified by the QIAGEN Endofree Maxiprep Kit.

In utero electroporation

In utero electroporations of *pCdk5r1-IRES-EGFP, pCdk5r1-Lmo4-IRES-EGFP, control or Lmo4-specific shRNA* were performed as previously described (**Alfano et al., 2011**; **Tabata and Nakajima, 2001**). Briefly, after a 3-cm laparotomy on deeply anesthetized pregnant females and once extroflected *uteri*, the DNA mix (1 mg/ml) was injected into the lateral ventricle of E13.5 embryos using a Femtojet microinjector (Eppendorf, Germany). The electroporations were performed on whole heads using a Tweezertrode electrode (diameter 7 mm; BTX) connected to a NEPA21 electroporator (NEPAGENE, Japan) with the following parameters: four 37 V pulses, P(on) 50 ms, P(off) 1 s, 5% decay. Then *uteri* were reallocated in the abdominal cavity, and both peritoneum and abdominal skin were sewn with surgical sutures (B. Braun Surgical, Germany).

Transient transfection of COS cells

COS7 cells were cultured in DMEM (4.5 g/L; Invitrogen) containing 10% FCS. Transient transfections of Satb2 and Lmo4 were performed using Lipofectamine ^{TM} 2000 (Invitrogen) according to manufacturer's instructions at a cell confluence of 60-70%. An equal amount of *pCAG-Satb2* plasmid (gift from V. Tarabykin's lab) was added to the cells with increasing amount of *pCIG2-Lmo4-IRES-GFP plasmid*. A *pCIG2-IRES-GFP* plasmid was used to compensate any variations in the amount of the *pCIG2-Lmo4-IRES-GFP* by maintaining the total quantity of transfected DNA constant. Cells were harvested for co-immunoprecipitation and immunoblotting 48 hr after transfection.

Co-immunoprecipitation assayy

Co-immunoprecipitation was performed as described in (**Britanova et al., 2008**) with some modifications. Nuclear proteins were extracted from P1 control and *Nr2f1 CKO* cerebral cortices, or from harvested cells, using the NE-PER kit (Thermo Fisher Scientific) according to manufacturer's instructions. Nuclear extracts were then dialyzed against buffer D (20% glycerol, 20 mM HEPES (pH = 7.9), 100 mM KCl, 0.2 mM EDTA, 0.5 mM DTT, 0.5 mM PMSF, all from Sigma-Aldrich) in Slyde-A-Lyzer Mini Dialysis Units (3500 M.W.C.O. from Fisher Scientific, Thermo Fisher Scientific). For pre-clearing, 50 μg of the nuclear extracts were incubated with 100 μl Protein A Sepharose 50% bead slurry (Sigma-Aldrich). The pre-cleared nuclear extracts were then immunoprecipitated with either 2 μg of mouse anti-Satb2 (Abcam) or of rat anti-Lmo4 antibody (a gift from Jane Visvader's lab). A mouse anti-Brdu antibody (Sigma-Aldrich) was used as control. Immunocomplexes were collected by adding 100 μl of 50% Protein A-Sepharose bead slurry to the mix. The bound fraction was separated by pulse centrifugation and pelleted beads and input were re-suspended in 1x Nupage loading buffer (Invitrogen). Samples were loaded on a 10% SDS polyacrylamide gel and subjected to standard SDS-PAGE electrophoresis on Mini-Protean tetra cell (Biorad, Hercules, California). Then, immunocomplexes were transferred to Hybond-P membrane (Amersham, GE Healthcare, UK) via a Trans-Blot SD Semi-Dry Transfer Cell (Biorad). Immunoblotting on total nuclear extracts, bound and unbound fractions was performed with the following antibodies: rat anti-Lmo4 (1/500, gift from J. Visvader), rabbit anti-Hdac1 (1:500, Millipore, Merck, Germany), rabbit anti-Ski (1:50, Santa Cruz), mouse anti-Satb2 (1:50, Abcam), and rabbit anti-β-actin (1:500, Abcam). Primary antibodies were then detected by embedding the membrane in anti-rabbit, anti mouse or anti-rat biotinylated antibodies (1:500, Vector) and successively in ABC mix (Vector Laboratories). Revelation of the signals was performed by SuperSignal West Pico Chemiluminescent Kit (Thermo Scientific), and images were taken by Luminescent Image Analyzer LAS-3000 (Fujifilm, Japan).

Chromatin immunoprecipitation assay

Chromatin-immunoprecipitation (ChIP) assay on genomic DNA from controls and *Nr2f1 CKO* cortices was performed as described in (***Kuo and Allis, 1999***). Neocortices were dissected from 7 controls and *Nr2f1 CKO* P1 pups, and diced in ice cold Hanks Buffered Saline Solution. Proteins were crosslinked to DNA by adding 1% formaldehyde to the solution. The tissue was than disrupted by homogenization in lysis buffer (20 mM HEPES pH7.4, 1 mM EDTA, 150 mM NaCl, 1% SDS, 125 mM Glycine, PMSF 0.2 mg/ml). Nuclei were collected by centrifugation, re-suspended in sonication buffer (20 mM HEPES pH7.4, 1 mM EDTA, 150 mM NaCl, 0.4% SDS, PMSF 0.2mg/ml) and disrupted by 6 pulses of 10 μ amplitude in a Soniprep150 Sonicator (Sanyo). Before immunoprecipitation, samples were pre-cleared 1 hr in 50% ProteinA-Sepharose slurry and then incubated ON at 4°C with 3 μg of the following antibodies: rabbit anti-Hdac1 (Millipore), rabbit anti-H4K12 (Abcam), and a control antibody (rabbit anti-GFP, Molecular probe). An aliquot of DNA was not immunoprecipitated and used as a control; 0.5 μl of DNA from each sample were used to perform a PCR for semiquantitative analysis of the ChIP experiment using the following primers: for the *Ctip2* locus , Ctip2MAR.fw 5′-GCTTGGACTCAGTGTACCTC-3′ and Ctip2MAR.rev 5′-CAAGAAAGCACACACCGAGA-3′ and for the *Rnd2* locus, BsA.fw 5′-CGTTTGACCTTCCACCTTAG-3′ and BsA.rev: 5′-TCCCACTTGCTTGGCCAGC-3′. PCR bands were acquired by FUJI 3000 LAS intelligent dark box equipped with a CCD camera. Hdac1 and H4k12 fold enrichment on *Ctip2* and *Rnd2* loci were tested by QPCR analysis of ChIP samples using the *LightCycler 480* Real-Time PCR System (Roche) and the above-mentioned primers.

Retrograde labeling

For retrograde labeling, anesthetized P2 pups were placed on a stereotaxic apparatus and injected with the cholera toxin subunit B (CTB- 1 mg/ml; Invitrogen) conjugated fluorophores (Alexa Fluor, Thermo Fisher Scientific) in different brain regions. CPN in the somatosensory cortex were retrogradely labeled via injection of 92 nl of Alexa Fluor 488-conjugated CTB. Coordinates (in mm) were: AP: +1.2; and ML: 1.3 from the lambda; DV: 0.2 from the pial surface. Subcerebral injections were performed under ultrasound guidance using a Vevo 770 ultrasound backscatter microscopy system (Visual Sonics, Canada) at cervical vertebral level 1 (C1) to C2 to label corticospinal projection neurons (CSpPN), or at the midbrain-hindbrain junction to label subcerebral projection neurons (SCPN*via* 92 nl injections of Alexa Fluor 555-conjugated CTB. Dual retrograde labeling of SCPN and CPN was performed by injecting Red Retrobeads or Green IX Retrobeads (Lumafluor Inc, Durham, North Carolina), respectively, in P2 and P3 pups brains in the same regions described above. Injected pups were perfused at P7 and brains were collected as described in previous sections.

Imaging

Images of immunostained cryosections were acquired using a DM6000 microscope (Leica, Germany) equipped with LEICA DFC 310 FX camera, while images of immunofluorescences on floating-thick sections were taken with a Zeiss 710 confocal microscope. *ISH* and whole-mount *ISH* were acquired by a Zeiss Imager Z1 microscope equipped with AXIOCAM MRm camera and a Leica Spot microscope, respectively. Images from optical and confocal microscopes were then processed using Photoshop and Zen-lite 2012 softwares, respectively.

Counting and statistical analysis

Images of P0 coronal sections from the prospective somatosensory (pS) and the frontal/motor (F/M) regions were subdivided into 6 bins. Bins 1 and 2 represent layer VI, bins 3 and 4 represent layer V, while bins 5 and 6 represent the upper layers. At P7 the radial surface of analyzed brain regions was subdivided into 10 bins: bins 1–3 represent layer VI, bins 4–6 represent layer V, and bins 7–10 represent upper layers. Counting of single or double-labeled cells was normalized to the total number of DAPI cells in each bin. For triple immunofluorescences, the counting was performed on cortical images with a constant width of 600 μm. Each counting performed on electroporated and cholera-toxin-labeled neurons was normalized to the total number of GFP- or choleratoxin-labeled cells in the layer of interest.

All the data were statistically analyzed and graphically represented using Microsoft Office Excel software. The error bars represent the standard error of the mean (SEM). Two-tailed Student's t-test was used for the analysis of statistical significance (*$p \leq 0.05$, **$p \leq 0.01$, ***$p \leq 0.001$) between to different groups.

Morphological analysis

Neuron morphology was reconstructed in BitPlane Imaris from confocal 3D image stacks. Soma shape features were obtained using built-in Volume Rendering functionality on images with 40x magnification (criteria: surface background subtraction of 15 μm and detail smoothening of 2 μm). Extracted features of each soma shape include X, Y, and Z position of the center of mass, soma area, soma volume, oblate ellipticity, and sphericity. Calculation of these feature values was performed automatically as described in BitPlane Imaris technical documentation (http://www.bitplane.com/download/manuals/ReferenceManual6_1_0.pdf). Each soma was separated in a region of interest (ROI) of approximately 30 × 30 × 10 μm. In order to effectively render soma volume, the ROI was used to automatically compensate differences in local contrast. Limits of the soma volume were calculated automatically within ROI in most of the cases. For more detailed information, see the SI section.

Apical and basal dendrites features were obtained using Imaris Filament Tracer plugin. Features include apical dendrite diameter, total apical dendrite length (also referred as neuron radial position with respect to pial surface), number of basal dendrites, angle of each basal dendrite compared to apical one, apical dendrite ramification and bifurcation point. Apical dendrite diameter was measured at 5 μm from soma limit. Radial position and Bifurcation features were obtained from 10x image stacks. Radial position was measured as the total distance from the soma center to the pial membrane. Bifurcation was measured as the distance from the soma to the first bifurcation of the apical dendrite. Apical dendrite ramification was calculated on confocal Images of 40x as the number of secondary dendrites emerging from the apical dendrite, within a length of approximately 70 μm starting from the soma limit.

Statistical analysis of the distinctive morphological features

Ctip2+/Satb2+ and Ctip2+/Satb2- populations were compared using non-parametric Wilcoxon Mann–Whitney U-test. Comparison of populations, based on the data collected from 40x images, was performed on n = 145 neurons. Comparison based on Radial Position and Bifurcation was performed on n = 52 neurons (52 matched neurons on 10x and 40x images). Custom clustering analysis was performed using MATLAB and to diminish scale impact on clustering, z-scale standardization was applied across all feature variables. The unsupervised k-means++ clustering algorithm was applied using squared Euclidean as distance measure. The optimal number of clusters was defined by comparing the quality of cluster separation and neuron features similarity within each cluster. The silhouette values were calculated for outcomes for each testing cycle starting from k = 2 to k = 5. After the optimal cluster number has been defined, clustering was performed with large number of iterations (iterations = 1000). MATLAB Scripts and their dependencies are available for download at https://github.com/nikiluk/signalife-moo-clust/ and could be used according to their licensing terms.

Electrophysiology on acute slices

Whole-cell patch clamp recordings were performed on the soma of layer V YFP+ cortical neurons from 350 μm live slices of somatosensory cortices of the Thy1-eYFP-H transgenic brains. For whole-cell experiments, the slices (350 μm) were perfused with artificial cerebrospinal fluid (ACSF) which comprised (mM): 124 NaCl, 3 KCl, 26 $NaHCO_3$, 1.25 NaH_2PO_4, 2 $CaCl_2$, 1 $MgSO_4$, 15 D-glucose, 0.05 picrotoxin, 0.05 2-amino-5-phosphonovaleric acid (APV) and 0.02 6,7-dinitroquinoxaline-2,3-dione (DNQX), bubbled with O2:CO2: 95:5%. Visually guided, whole-cell recordings were obtained at 29°C from the soma of GFP-positive cortical neurons in layer V of somatosensory area, using patch electrodes (3–5 MΩ) filled with (in mM): 20 KCl, 100 Kgluconate, 10 HEPES, 4 Mg-ATP, 0.3 Na-GTP, 10 Na-phosphocreatine and 0.1% biocytin (Sigma Aldrich, Merck, Germany). Recordings were performed using an AxoPatch 200B amplifier (Axon Instruments, Foster City, CA), filtered at 10 kHz and were not corrected for liquid junction potentials. Data were collected using ClampEx software and analyses of recorded responses were performed using Clampfit. The cells usually had a holding

potential between -65 and -70 mV or were hold at these potentials. To calculate cell properties (resistance, time to peak, sag), currents from -200 pA to 80 pA were injected for 500 ms. The voltages were measured at the peak amplitude and at steady-state and the I-V curves were plotted. The slope of these curves corresponded to the resistance at peak (Rpeak) and at steady-state (Rss). The sag was measured as the difference of voltage at peak to the voltage at steady state when -200 pA was injected.

To measure firing and action potential properties, depolarasing currents were injected for 2 s by steps of 20 pA. The relationship between the amount of injected current and the firing frequency was then plotted. The ratio of the first interspike interval (ISI) to the last ISI was analyzed using responses recorded at two times the threshold current. To calculate action potential (AP) characteristics, we analyzed responses of cells at threshold current. Firing threshold is calculated as the interpolated membrane potential at which the derivative (dV/dt) equals 20 V/s. The firing threshold was set as the baseline to calculate characteristics of each AP (amplitude, half-width, duration, rise time). The fast afterhyperpolarization (fAHP) is the difference between the firing threshold and the minimum value found within 3 ms of the spike. The time of fAHP is the time between the peak of the spike and the fAHP. The depolarizing afterpolarization (DAP) following the fAHP (fDAP) is the difference between the maximum value obtained within 5 ms after the fAHP and the minimum value measured to calculate the fAHP. When bursts of 2 or 3 AP were fired at once, the threshold of the second AP was chosen as the maximum value to calculate the fDAP. The medium AHP (mAHP) is the difference between the threshold of AP and the minimum value found within 50 ms of the spike. The medium DAP (mDAP) is the difference between the maximum value found withnin 70 ms after the minimum value used to calculate the mAHP and this minimum value. When 2 or more APs were fired at once, the mAHP and mDAP were measured after the last AP of the burst.

Acknowledgements

We thank J Visvader for providing us the Lmo4 antibody, HH Chen for the *shRNA Lmo4* construct, Q Lu for the *pCdk5r1-Ires-GFP*, P Arlotta for the *pCdk5r1-Fezf2 IRES-GFP* and V Tarabykin for the *pCAG-Satb2* plasmids. We are also grateful to J Sanes for giving us the permission to use the *Thy1-eYFP-H* transgenic line. We thank N Elganfoud for technical help during this project and the PRISM Microscopy Facility for technical support. J Hazan and M Nieto for constructive suggestions on the manuscript, and the whole Studer lab for fruitful discussions. This work was supported by the "Agence Nationale de la Recherche" under grant reference # ANR-13-BSV4-0011, by the French Government (National Research Agency, ANR) through the "Investments for the Future" LABEX SIGNALIFE under program reference # ANR-11-LABX-0028-01, by the "Fondation Recherche Médicale; Equipe FRM 2011" #DEQ20110421321 and by the "Fondation Jérôme Lejeune" under n° R13098AA to MS. KH was funded by a CNRS from Lebanon and AFM fellowship from France and EM was funded by an AXA Research Fund fellowship.

Additional information

Funding

Funder	Grant reference number	Author
Agence Nationale de la Recherche	ANR-13-BSV4-0011	Michele Studer
Agence Nationale de la Recherche	ANR-11-LABX-0028-01	Michele Studer
CNRS Lebanon		Kawssar Harb
AFM-Téléthon		Kawssar Harb
AXA Research Fund		Elia Magrinelli
Fondation pour la Recherche Médicale	DEQ20110421321	Michele Studer
Fondation Jérôme Lejeune	R13098AA	Michele Studer

The funders had no role in study design, data collection and interpretation, or the decision to submit the work for publication.

Author contributions

KH, MS, CA, Conception and design, Acquisition of data, Analysis and interpretation of data, Drafting or revising the article, Contributed unpublished essential data or reagents; EM, CSN, Acquisition of data, Analysis and interpretation of data, Drafting or revising the article, Contributed unpublished essential data or reagents; NL, LF, TS, DJ, Analysis and interpretation of data, Drafting or revising the article, Contributed unpublished essential data or reagents; MP, Acquisition of data, Drafting or revising the article, Contributed unpublished essential data or reagents; GS, Conception and design, Drafting or revising the article, Contributed unpublished essential data or reagents; FG, Conception and design, Analysis and interpretation of data, Drafting or revising the article

Ethics

Animal experimentation: This study was performed in strict accordance with the recommendations in the Guide for the Care and Use of Laboratory Animals of the French Ministry of Research. All animal experiments were validated by our local ethical committees (IACUC registration number NCE2014-209).

References

Alcamo EA, Chirivella L, Dautzenberg M, Dobreva G, Fariñas I, Grosschedl R, McConnell SK. 2008. Satb2 regulates callosal projection neuron identity in the developing cerebral cortex. *Neuron* **57**:364–377. doi: 10.1016/j.neuron.2007.12.012

Alfano C, Viola L, Heng JI-T, Pirozzi M, Clarkson M, Flore G, De Maio A, Schedl A, Guillemot F, Studer M. 2011. COUP-TFI promotes radial migration and proper morphology of callosal projection neurons by repressing Rnd2 expression. *Development* **138**:4685–4697. doi: 10.1242/dev.068031

Alfano C, Magrinelli E, Harb K, Hevner RF, Studer M. 2014. Postmitotic control of sensory area specification during neocortical development. *Nature Communications* **5**:5632. doi: 10.1038/ncomms6632

Arlotta P, Molyneaux BJ, Chen J, Inoue J, Kominami R, Macklis JD. 2005. Neuronal subtype-specific genes that control corticospinal motor neuron development in vivo. *Neuron* **45**:207–221. doi: 10.1016/j.neuron.2004.12.036

Armentano M, Filosa A, Andolfi G, Studer M. 2006. COUP-TFI is required for the formation of commissural projections in the forebrain by regulating axonal growth. *Development* **133**:4151–4162. doi: 10.1242/dev.02600

Armentano M, Chou S-J, Srubek Tomassy G, Leingärtner A, O'Leary DDM, Studer M. 2007. COUP-TFI regulates the balance of cortical patterning between frontal/motor and sensory areas. *Nature Neuroscience* **10**:1277–1286. doi: 10.1038/nn1958

Azim E, Shnider SJ, Cederquist GY, Sohur US, Macklis JD. 2009. Lmo4 and Clim1 progressively delineate cortical projection neuron subtypes during development. *Cerebral Cortex* **19**:i62–i69. doi: 10.1093/cercor/bhp030

Baranek C, Dittrich M, Parthasarathy S, Bonnon CG, Britanova O, Lanshakov D, Boukhtouche F, Sommer JE, Colmenares C, Tarabykin V, Atanasoski S. 2012. Protooncogene ski cooperates with the chromatin-remodeling factor Satb2 in specifying callosal neurons. *Proceedings of the National Academy of Sciences of the United States of America* **109**:3546–3551. doi: 10.1073/pnas.1108718109

Britanova O, de Juan Romero C, Cheung A, Kwan KY, Schwark M, Gyorgy A, Vogel T, Akopov S, Mitkovski M, Agoston D, Šestan N, Molnár Z, Tarabykin V. 2008. Satb2 is a postmitotic determinant for upper-layer neuron specification in the neocortex. *Neuron* **57**:378–392. doi: 10.1016/j.neuron.2007.12.028

Cederquist GY, Azim E, Shnider SJ, Padmanabhan H, Macklis JD. 2013. Lmo4 establishes rostral motor cortex projection neuron subtype diversity. *Journal of Neuroscience* **33**:6321–6332. doi: 10.1523/JNEUROSCI.5140-12.2013

Conte WL, Kamishina H, Reep RL. 2009. Multiple neuroanatomical tract-tracing using fluorescent alexa fluor conjugates of cholera toxin subunit b in rats. *Nature Protocols* **4**:1157–1166. doi: 10.1038/nprot.2009.93

De la Rossa A, Bellone C, Golding B, Vitali I, Moss J, Toni N, Lüscher C, Jabaudon D. 2013. In vivo reprogramming of circuit connectivity in postmitotic neocortical neurons. *Nature Neuroscience* **16**:193–200. doi: 10.1038/nn.3299

Fame RM, MacDonald JL, Macklis JD. 2011. Development, specification, and diversity of callosal projection neurons. *Trends in Neurosciences* **34**:41–50. doi: 10.1016/j.tins.2010.10.002

Feng G, Mellor RH, Bernstein M, Keller-Peck C, Nguyen QT, Wallace M, Nerbonne JM, Lichtman JW, Sanes JR. 2000. Imaging neuronal subsets in transgenic mice expressing multiple spectral variants of GFP. *Neuron* **28**:41–51. doi: 10.1016/S0896-6273(00)00084-2

Finger JH, Bronson RT, Harris B, Johnson K, Przyborski SA, Ackerman SL. 2002. The netrin 1 receptors Unc5h3 and dcc are necessary at multiple choice points for the guidance of corticospinal tract axons. *The Journal of Neuroscience : The Official Journal of the Society for Neuroscience* **22**:10346–10356.

Goebbels S, Bormuth I, Bode U, Hermanson O, Schwab MH, Nave K-A. 2006. Genetic targeting of principal neurons in neocortex and hippocampus of NEX-cre mice. *Genesis* **44**:611–621. doi: 10.1002/dvg.20256

Gomez-Smith M, Qin Z, Zhou X, Schock SC, Chen H-H. 2010. LIM domain only 4 protein promotes granulocyte colony-stimulating factor-induced signaling in neurons. *Cellular and Molecular Life Sciences* **67**:949–957. doi: 10.1007/s00018-009-0223-z

Greig LC, Woodworth MB, Galazo MJ, Padmanabhan H, Macklis JD. 2013. Molecular logic of neocortical projection neuron specification, development and diversity. *Nature Reviews Neuroscience* **14**:755–769. doi: 10.1038/nrn3586

Gyorgy AB, Szemes M, de Juan Romero C, Tarabykin V, Agoston DV. 2008. SATB2 interacts with chromatin-remodeling molecules in differentiating cortical neurons. *European Journal of Neuroscience* **27**:865–873. doi: 10.1111/j.1460-9568.2008.06061.x

Harris KD, Shepherd GMG. 2015. The neocortical circuit: themes and variations. *Nature Neuroscience* **18**:170–181. doi: 10.1038/nn.3917

Hattox AM, Nelson SB. 2007. Layer v neurons in mouse cortex projecting to different targets have distinct physiological properties. *Journal of Neurophysiology* **98**:3330–3340. doi: 10.1152/jn.00397.2007

Heng JI-T, Nguyen L, Castro DS, Zimmer C, Wildner H, Armant O, Skowronska-Krawczyk D, Bedogni F, Matter J-M, Hevner R, Guillemot F. 2008. Neurogenin 2 controls cortical neuron migration through regulation of Rnd2. *Nature* **455**:114–118. doi: 10.1038/nature07198

Huang Z, Kawase-Koga Y, Zhang S, Visvader J, Toth M, Walsh CA, Sun T. 2009. Transcription factor Lmo4 defines the shape of functional areas in developing cortices and regulates sensorimotor control. *Developmental Biology* **327**:132–142. doi: 10.1016/j.ydbio.2008.12.003

Huang ZJ. 2014. Toward a genetic dissection of cortical circuits in the mouse. *Neuron* **83**:1284–1302. doi: 10.1016/j.neuron.2014.08.041

Joshi PS, Molyneaux BJ, Feng L, Xie X, Macklis JD, Gan L. 2008. Bhlhb5 regulates the postmitotic acquisition of area identities in layers II-v of the developing neocortex. *Neuron* **60**:258–272. doi: 10.1016/j.neuron.2008.08.006

Kiritani T, Wickersham IR, Seung HS, Shepherd GMG. 2012. Hierarchical connectivity and connection-specific dynamics in the corticospinal-corticostriatal microcircuit in mouse motor cortex. *Journal of Neuroscience* **32**:4992–5001. doi: 10.1523/JNEUROSCI.4759-11.2012

Kuo M-H, Allis CD. 1999. In vivo cross-linking and immunoprecipitation for studying dynamic Protein:DNA associations in a chromatin environment. *Methods* **19**:425–433. doi: 10.1006/meth.1999.0879

Lai T, Jabaudon D, Molyneaux BJ, Azim E, Arlotta P, Menezes JRL, Macklis JD. 2008. SOX5 controls the sequential generation of distinct corticofugal neuron subtypes. *Neuron* **57**:232–247. doi: 10.1016/j.neuron.2007.12.023

Lasek AW, Gesch J, Giorgetti F, Kharazia V, Heberlein U. 2011. Alk is a transcriptional target of LMO4 and ER that promotes cocaine sensitization and reward. *Journal of Neuroscience* **31**:14134–14141. doi: 10.1523/JNEUROSCI.3415-11.2011

Leone DP, Srinivasan K, Chen B, Alcamo E, McConnell SK. 2008. The determination of projection neuron identity in the developing cerebral cortex. *Current Opinion in Neurobiology* **18**:28–35. doi: 10.1016/j.conb.2008.05.006

Leone DP, Heavner WE, Ferenczi EA, Dobreva G, Huguenard JR, Grosschedl R, McConnell SK. 2015. Satb2 regulates the differentiation of both callosal and subcerebral projection neurons in the developing cerebral cortex. *Cerebral Cortex* **25**. doi: 10.1093/cercor/bhu156

Marcos-Mondejar P, Peregrin S, Li JY, Carlsson L, Tole S, Lopez-Bendito G. 2012. The Lhx2 transcription factor controls thalamocortical axonal guidance by specific regulation of Robo1 and Robo2 receptors. *Journal of Neuroscience* **32**:4372–4385. doi: 10.1523/JNEUROSCI.5851-11.2012

Megason SG, McMahon AP. 2002. A mitogen gradient of dorsal midline wnts organizes growth in the CNS. *Development (Cambridge, England)* **129**:2087–2098.

Molnár Z, Cheung AFP. 2006. Towards the classification of subpopulations of layer v pyramidal projection neurons. *Neuroscience Research* **55**:105–115. doi: 10.1016/j.neures.2006.02.008

Molyneaux BJ, Arlotta P, Menezes JRL, Macklis JD. 2007. Neuronal subtype specification in the cerebral cortex. *Nature Reviews Neuroscience* **8**:427–437. doi: 10.1038/nrn2151

Niwa H, Yamamura K, Miyazaki J. 1991. Efficient selection for high-expression transfectants with a novel eukaryotic vector. *Gene* **108**:193–199.

O'Leary DDM, Chou S-J, Sahara S. 2007. Area patterning of the mammalian cortex. *Neuron* **56**:252–269. doi: 10.1016/j.neuron.2007.10.010

Oswald MJ, Tantirigama MLS, Sonntag I, Hughes SM, Empson RM. 2013. Diversity of layer 5 projection neurons in the mouse motor cortex. *Frontiers in Cellular Neuroscience* **7**. doi: 10.3389/fncel.2013.00174

Porrero C, Rubio-Garrido P, Avendaño C, Clascá F. 2010. Mapping of fluorescent protein-expressing neurons and axon pathways in adult and developing Thy1-eYFP-h transgenic mice. *Brain Research* **1345**:59–72. doi: 10.1016/j.brainres.2010.05.061

Qin Z, Zhou X, Gomez-Smith M, Pandey NR, Lee KFH, Lagace DC, Beique J-C, Chen H-H. 2012. LIM domain only 4 (LMO4) regulates calcium-induced calcium release and synaptic plasticity in the hippocampus. *Journal of Neuroscience* **32**:4271–4283. doi: 10.1523/JNEUROSCI.6271-11.2012

Reiner A. 2010. Corticostriatal projection neurons – dichotomous types and dichotomous functions. *Frontiers in Neuroanatomy* **4**. doi: 10.3389/fnana.2010.00142

Sang M, Ma L, Sang M, Zhou X, Gao W, Geng C. 2014. LIM-domain-only proteins: multifunctional nuclear transcription coregulators that interacts with diverse proteins. *Molecular Biology Reports* **41**:1067–1073. doi: 10.1007/s11033-013-2952-1

Sheets PL, Suter BA, Kiritani T, Chan CS, Surmeier DJ, Shepherd GMG. 2011. Corticospinal-specific HCN expression in mouse motor cortex: ih-dependent synaptic integration as a candidate microcircuit mechanism involved in motor control. *Journal of Neurophysiology* **106**:2216–2231. doi: 10.1152/jn.00232.2011

Shepherd GMG. 2013. Corticostriatal connectivity and its role in disease. *Nature Reviews Neuroscience* **14**:278–291. doi: 10.1038/nrn3469

Shetty AS, Godbole G, Maheshwari U, Padmanabhan H, Chaudhary R, Muralidharan B, Hou P-S, Monuki ES, Kuo H-C, Rema V, Tole S. 2013. Lhx2 regulates a cortex-specific mechanism for barrel formation. *Proceedings of the National Academy of Sciences of the United States of America* **110**:E4913–E4921. doi: 10.1073/pnas.1311158110

Singh RR. 2005. Negative regulation of estrogen receptor transactivation functions by LIM domain only 4 protein. *Cancer Research* **65**:10594–10601. doi: 10.1158/0008-5472.CAN-05-2268

Sohur US, Padmanabhan HK, Kotchetkov IS, Menezes JRL, Macklis JD. 2014. Anatomic and molecular development of corticostriatal projection neurons in mice. *Cerebral Cortex* **24**:293–303. doi: 10.1093/cercor/bhs342

Srinivasan K, Leone DP, Bateson RK, Dobreva G, Kohwi Y, Kohwi-Shigematsu T, Grosschedl R, McConnell SK. 2012. A network of genetic repression and derepression specifies projection fates in the developing neocortex. *Proceedings of the National Academy of Sciences of the United States of America* **109**:19071–19078. doi: 10.1073/pnas.1216793109

Srivatsa S, Parthasarathy S, Britanova O, Bormuth I, Donahoo A-L, Ackerman SL, Richards LJ, Tarabykin V. 2014. Unc5C and DCC act downstream of Ctip2 and Satb2 and contribute to corpus callosum formation. *Nature Communications* **5**. doi: 10.1038/ncomms4708

Staff NP, Jung HY, Thiagarajan T, Yao M, Spruston N. 2000. Resting and active properties of pyramidal neurons in subiculum and CA1 of rat hippocampus. *Journal of Neurophysiology* **84**:2398–2408.

Tabata H, Nakajima K. 2001. Efficient in utero gene transfer system to the developing mouse brain using electroporation: visualization of neuronal migration in the developing cortex. *Neuroscience* **103**:865–872. doi: 10.1016/S0306-4522(01)00016-1

Tantirigama MLS, Oswald MJ, Duynstee C, Hughes SM, Empson RM. 2014. Expression of the developmental transcription factor Fezf2 identifies a distinct subpopulation of layer 5 intratelencephalic-projection neurons in mature mouse motor cortex. *Journal of Neuroscience* **34**:4303–4308. doi: 10.1523/JNEUROSCI.3111-13.2014

Tomassy GS, De Leonibus E, Jabaudon D, Lodato S, Alfano C, Mele A, Macklis JD, Studer M. 2010. Area-specific temporal control of corticospinal motor neuron differentiation by COUP-TFI. *Proceedings of the National Academy of Sciences of the United States of America* **107**:3576–3581. doi: 10.1073/pnas.0911792107

Wang N, Lin KK, Lu Z, Lam KS, Newton R, Xu X, Yu Z, Gill GN, Andersen B. 2007a. The LIM-only factor LMO4 regulates expression of the BMP7 gene through an HDAC2-dependent mechanism, and controls cell proliferation and apoptosis of mammary epithelial cells. *Oncogene* **26**:6431–6441. doi: 10.1038/sj.onc.1210465

Wang X, Qiu R, Tsark W, Lu Q. 2007b. Rapid promoter analysis in developing mouse brain and genetic labeling of young neurons by doublecortin-DsRed-express. *Journal of Neuroscience Research* **85**:3567–3573. doi: 10.1002/jnr.21440

Ye Z, Mostajo-Radji MA, Brown JR, Rouaux C, Tomassy GS, Hensch TK, Arlotta P. 2015. Instructing perisomatic inhibition by direct lineage reprogramming of neocortical projection neurons. *Neuron* **88**:475–483. doi: 10.1016/j.neuron.2015.10.006

Yoneshima H, Yamasaki S, Voelker CCJ, Molnár Z, Christophe E, Audinat E, Takemoto M, Nishiwaki M, Tsuji S, Fujita I, Yamamoto N. 2006. Er81 is expressed in a subpopulation of layer 5 neurons in rodent and primate neocortices. *Neuroscience* **137**:401–412. doi: 10.1016/j.neuroscience.2005.08.075